



LEARNING AND MEMORY - EDITOR'S PICK 2021

EDITED BY: Denise Manahan-Vaughan

PUBLISHED IN: Frontiers in Behavioral Neuroscience



frontiers

Frontiers eBook Copyright Statement

The copyright in the text of individual articles in this eBook is the property of their respective authors or their respective institutions or funders. The copyright in graphics and images within each article may be subject to copyright of other parties. In both cases this is subject to a license granted to Frontiers.

The compilation of articles constituting this eBook is the property of Frontiers.

Each article within this eBook, and the eBook itself, are published under the most recent version of the Creative Commons CC-BY licence.

The version current at the date of publication of this eBook is CC-BY 4.0. If the CC-BY licence is updated, the licence granted by Frontiers is automatically updated to the new version.

When exercising any right under the CC-BY licence, Frontiers must be attributed as the original publisher of the article or eBook, as applicable.

Authors have the responsibility of ensuring that any graphics or other materials which are the property of others may be included in the CC-BY licence, but this should be checked before relying on the CC-BY licence to reproduce those materials. Any copyright notices relating to those materials must be complied with.

Copyright and source acknowledgement notices may not be removed and must be displayed in any copy, derivative work or partial copy which includes the elements in question.

All copyright, and all rights therein, are protected by national and international copyright laws. The above represents a summary only. For further information please read Frontiers' Conditions for Website Use and Copyright Statement, and the applicable CC-BY licence.

ISSN 1664-8714

ISBN 978-2-88971-214-4

DOI 10.3389/978-2-88971-214-4

About Frontiers

Frontiers is more than just an open-access publisher of scholarly articles: it is a pioneering approach to the world of academia, radically improving the way scholarly research is managed. The grand vision of Frontiers is a world where all people have an equal opportunity to seek, share and generate knowledge. Frontiers provides immediate and permanent online open access to all its publications, but this alone is not enough to realize our grand goals.

Frontiers Journal Series

The Frontiers Journal Series is a multi-tier and interdisciplinary set of open-access, online journals, promising a paradigm shift from the current review, selection and dissemination processes in academic publishing. All Frontiers journals are driven by researchers for researchers; therefore, they constitute a service to the scholarly community. At the same time, the Frontiers Journal Series operates on a revolutionary invention, the tiered publishing system, initially addressing specific communities of scholars, and gradually climbing up to broader public understanding, thus serving the interests of the lay society, too.

Dedication to Quality

Each Frontiers article is a landmark of the highest quality, thanks to genuinely collaborative interactions between authors and review editors, who include some of the world's best academicians. Research must be certified by peers before entering a stream of knowledge that may eventually reach the public - and shape society; therefore, Frontiers only applies the most rigorous and unbiased reviews.

Frontiers revolutionizes research publishing by freely delivering the most outstanding research, evaluated with no bias from both the academic and social point of view. By applying the most advanced information technologies, Frontiers is catapulting scholarly publishing into a new generation.

What are Frontiers Research Topics?

Frontiers Research Topics are very popular trademarks of the Frontiers Journals Series: they are collections of at least ten articles, all centered on a particular subject. With their unique mix of varied contributions from Original Research to Review Articles, Frontiers Research Topics unify the most influential researchers, the latest key findings and historical advances in a hot research area! Find out more on how to host your own Frontiers Research Topic or contribute to one as an author by contacting the Frontiers Editorial Office: frontiersin.org/about/contact

LEARNING AND MEMORY - EDITOR'S PICK 2021

Topic Editor:

Denise Manahan-Vaughan, Ruhr University Bochum, Germany

Citation: Manahan-Vaughan, D., ed. (2021). Learning and Memory - Editor's Pick 2021. Lausanne: Frontiers Media SA. doi: 10.3389/978-2-88971-214-4

Table of Contents

- 04** ***Guidance of Navigating Honeybees by Learned Elongated Ground Structures***
Randolf Menzel, Lea Tison, Johannes Fischer-Nakai, James Cheeseman, Maria Sol Balbuena, Xiuxian Chen, Tim Landgraf, Julian Petrasch, Johannes Polster and Uwe Greggers
- 18** ***Learning and Its Neural Correlates in a Virtual Environment for Honeybees***
Hanna Zwaka, Ruth Bartels, Sophie Lehfeldt, Meida Jusyte, Sören Hantke, Simon Menzel, Jacob Gora, Rafael Alberdi and Randolf Menzel
- 38** ***A Specific Role of Hippocampal NMDA Receptors and Arc Protein in Rapid Encoding of Novel Environmental Representations and a More General Long-Term Consolidation Function***
Cameron M. Bye and Robert J. McDonald
- 58** ***Improving Hippocampal Memory Through the Experience of a Rich Minecraft Environment***
Gregory D. Clemenson, Caden M. Henningfield and Craig E. L. Stark
- 71** ***Somatostatin Serves a Modulatory Role in the Mouse Olfactory Bulb: Neuroanatomical and Behavioral Evidence***
Sonia Nocera, Axelle Simon, Oriane Fiquet, Ying Chen, Jean Gascuel, Frédérique Datiche, Nanette Schneider, Jacques Epelbaum and Cécile Viollet
- 91** ***Prolonged Cannabidiol Treatment Lacks on Detrimental Effects on Memory, Motor Performance and Anxiety in C57BL/6J Mice***
Eva M. Schleicher, Frederik W. Ott, Melanie Müller, Barbara Silcher, Marius E. Sichler, Maximilian J. Löw, Jannek M. Wagner and Yvonne Bouter
- 103** ***Acute Disruption of the Dorsal Hippocampus Impairs the Encoding and Retrieval of Trace Fear Memories***
Jacob H. Wilmot, Kyle Puhger and Brian J. Wiltgen
- 112** ***Social Memory and the Role of the Hippocampal CA2 Region***
Nikolaos Tzakis and Matthew R. Holahan
- 127** ***Memory Performance Correlates of Hippocampal Subfield Volume in Mild Cognitive Impairment Subtype***
Kathryn M. Broadhouse, Loren Mowszowski, Shantel Duffy, Isabella Leung, Nathan Cross, Michael J. Valenzuela and Sharon L. Naismith
- 140** ***Late Effects of ^1H + ^{16}O on Short-Term and Object Memory, Hippocampal Dendritic Morphology and Mutagenesis***
Frederico Kiffer, Tyler Alexander, Julie Anderson, Thomas Groves, Taylor McElroy, Jing Wang, Vijayalakshmi Sridharan, Michael Bauer, Marjan Boerma and Antiño Allen



Guidance of Navigating Honeybees by Learned Elongated Ground Structures

Randolf Menzel^{1*}, Lea Tison¹, Johannes Fischer-Nakai², James Cheeseman³, Maria Sol Balbuena⁴, Xiuxian Chen¹, Tim Landgraf⁵, Julian Petrasch⁵, Johannes Polster⁵ and Uwe Greggers¹

¹Institute of Biology, Freie Universität Berlin, Berlin, Germany, ²Fachbereich Biowissenschaften, Polytechnische Gesellschaft Frankfurt am Main, Institute für Bienenkunde, Goethe-Universität Frankfurt am Main, Frankfurt, Germany, ³Department of Anaesthesiology, Faculty of Medical and Health Science, The University of Auckland, Auckland, New Zealand, ⁴Laboratorio de Insectos Sociales, Departamento de Biodiversidad y Biología Experimental, Facultad de Ciencias Exactas y Naturales, Universidad de Buenos Aires, Instituto de Fisiología, Biología Molecular y Neurociencias (IFIBYNE), CONICET-Universidad de Buenos Aires, Buenos Aires, Argentina, ⁵Dahlem Center of Machine Learning and Robotics, Institute for Informatics, Freie Universität Berlin, Berlin, Germany

OPEN ACCESS

Edited by:

Martin Giurfa,
UMR5169 Centre de Recherches sur
la Cognition Animale (CRCA), France

Reviewed by:

Ryuichi Okada,
Kobe University, Japan
Franck Ruffier,
Aix-Marseille Université, France

*Correspondence:

Randolf Menzel
menzel@neurobiologie.fu-berlin.de

Received: 27 August 2018

Accepted: 07 December 2018

Published: 15 January 2019

Citation:

Menzel R, Tison L, Fischer-Nakai J, Cheeseman J, Balbuena MS, Chen X, Landgraf T, Petrasch J, Polster J and Greggers U (2019) Guidance of Navigating Honeybees by Learned Elongated Ground Structures. *Front. Behav. Neurosci.* 12:322. doi: 10.3389/fnbeh.2018.00322

Elongated landscape features like forest edges, rivers, roads or boundaries of fields are particularly salient landmarks for navigating animals. Here, we ask how honeybees learn such structures and how they are used during their homing flights after being released at an unexpected location (catch-and-release paradigm). The experiments were performed in two landscapes that differed with respect to their overall structure: a rather feature-less landscape, and one rich in close and far distant landmarks. We tested three different forms of learning: learning during orientation flights, learning during training to a feeding site, and learning during homing flights after release at an unexpected site within the explored area. We found that bees use elongated ground structures, e.g., a field boundary separating two pastures close to the hive (Experiment 1), an irrigation channel (Experiment 2), a hedgerow along which the bees were trained (Experiment 3), a gravel road close to the hive and the feeder (Experiment 4), a path along an irrigation channel with its vegetation close to the feeder (Experiment 5) and a gravel road along which bees performed their homing flights (Experiment 6). Discrimination and generalization between the learned linear landmarks and similar ones in the test area depend on their object properties (irrigation channel, gravel road, hedgerow) and their compass orientation. We conclude that elongated ground structures are embedded into multiple landscape features indicating that memory of these linear structures is one component of bee navigation. Elongated structures interact and compete with other references. Object identification is an important part of this process. The objects are characterized not only by their appearance but also by their alignment in the compass. Their salience is highest if both components are close to what had been learned. High similarity in appearance can compensate for (partial) compass misalignment, and vice versa.

Keywords: navigation, sun compass, guiding landmarks, object recognition, ground structures, compass alignment

INTRODUCTION

Elongated landscape features like edges of forests, hedgerows, rivers, roads or boundaries of fields are potentially salient landmarks because they keep essential components of their object properties beyond the area at which the animals may have perceived and learned them (Chan et al., 2012). Thus, they may be recognized as (partially) familiar and spatially related to the intended goal even at different locations and under different viewpoints. Since these objects stretch in a particular direction relative to a compass, they provide a directional component that together with their intrinsic polarity may support navigational tasks to be completed efficiently and reliably. Polarity of elongated landmarks result from view-dependent differences, e.g., at a forest edge. Two or more of such linear objects could potentially be bound together in a network of spatially extended objects characterizing many locations as unique in relation to many (or even any) other location. Following an elongated landmark may thus help the animal to reach a goal although the travel may even involve longer travel time and distances.

Navigating pigeons are known to be guided by roads (Guilford et al., 2004; Lipp et al., 2004); however, the effect may well depend on the structure of the overall landscape e.g., along the south-north stretching landscape and main roads of Italy, and may not be seen in other landscapes, e.g., Germany (Wiltschko et al., 2007; Schiffner et al., 2013). Bats are known to fly along fixed routes called “flyways” stretching along linear landscape elements (Heithaus et al., 1975) and integrate such flyways in their nightly navigation (Geva-Sagiv et al., 2015). Homing bumble bees (Osborne et al., 2013) and honeybees (Wolf et al., 2014) have also a tendency to follow field boundaries and other elongated ground structures. Young honeybees tend to fly along parallel linear mowing structures in an agricultural grassland on their first orientation flights (Degen et al., 2015). Honeybees have to learn the time-compensated sun compass in relation to the landscape structures. Elongated objects may be particularly important in this learning process. von Frisch and Lindauer (1954) discovered that bees read the sun compass direction from extended landmarks (edge of a forest) when the sky is overcast, an observation that was confirmed by Dyer and Gould (1981).

Here, we investigated how bees learn elongated landscape structures and which kind of memory results from this acquisition. These questions were studied under multiple test conditions in two different rural environments: a rather feature-less landscape and a landscape rich in local and far-distant features. The catch-and-release paradigm was applied to test the memory for these structures. Individually identified foraging bees familiar with the surroundings of the hive were trained to a feeding site and captured just as they were about to fly back to the hive. They were then transported to a release site within the explored area and equipped with a transponder that allowed the flight trajectory to be tracked by harmonic radar. Under these conditions the bee usually first performed a vector flight that resembled the direction and distance that would have brought it back to the hive had it not been transported to a

remote release site. The vector flight was followed by a search flight and then by a straight flight leading back to the hive during the final homing performance (Menzel et al., 2005, 2011; Menzel, 2013). Bees are known to use multiple learned landscape features during homing, and learned elongated landscape structures are expected to be one of several sources of information. Thus, it is particularly important to evaluate under which conditions such landscape structures are acquired and used. We found that this depends on how prominent these features are, how they had been learned, and with which other guiding information they compete.

MATERIALS AND METHODS

Experimental Areas

The experiments were performed at two rural locations termed area A and area B. Area A was a rather featureless, large open grass field close to Klein Lüben (Brandenburg, Germany, coordinates: N 52.97555, E 11.83677) displaying landmarks on the ground (patches of grass at different stages of growth, clover flowers, a boundary line formed between two meadows mown at different times, and two parallel irrigation channels). A row of bushes ran along the southern border of the test field. It was discernible over a distance of about 100 m to the north; the irrigation channels could be detected by the bees from approximately 30 m on both sides (Menzel and Greggers, 2015). Hives were located either at the boundary line in the middle of the field or 60 m to the east of the boundary line (Experiment 1), at an irrigation channel (Experiment 2), or at the row of bushes in the southwestern corner of the field (Experiment 3). The radar for tracking bees in flight was located at the southern edge of the field close to the row of bushes.

Area B was a highly structured agricultural landscape stretching to the east of the area scanned by the radar (50°48'51.9"N) with trees and bushes, pathways, creeks, and grass fields close to the village Großseelheim (Hessen, Germany, coordinates: 50°48'50.18"N, 8°52'21.01"E). The bee colony used for Experiments 4 and 5 was housed in a cabin close to the radar at the west edge of the study area and close to a gravel road running parallel to the east-facing edge of the village. The colony used for Experiment 6 was located at the southern edge of the study area at a distance of 520 m from the radar close to a road.

A realistic 3-dimensional virtual world was used to examine how the environment of area B appeared to the honeybee eye (Polster et al., 2018). A large 3-D world was reconstructed from aerial imagery and the imaging properties and distributions of ommatidia in both eyes were modeled following Giger (1996) and Stürzl et al. (2010). Using this model, panorama views were computed and used here to address the question whether the panorama at the three essential sites (hive, feeder, release site) contributed to the flight routes during homing. To quantify the amount of ground structure in each image, we calculated three metrics for sub-regions of the bee view, excluding all pixels above the horizon (**Supplementary Figures S1–S7**). The Michelson contrast was defined as the brightness difference of

the brightest and darkest pixel, divided by their sum. Hence, the maximum Michelson contrast was 1.0, the lowest 0.0. The mean Michelson contrast over all given bee views is 0.54 ± 0.15 . The Michelson contrast might be sensitive to outliers. We hence used the brightness standard deviation to estimate more robustly the image's information content. Let the maximum pixel brightness be 1.0, and 0.0 the minimum. The average brightness over all bee views was 0.38 ± 0.03 and the mean standard deviation was 0.07 ± 0.03 . The brightness variation can still be high in a strongly textured landscape with no elongated ground structures whatsoever. We therefore also counted the number of connected edge pixels using Canny's edge detector (Canny, 1986). Edge pixels are defined as strong image gradients. The gradient direction is then used to decide whether edge pixels belong to the same image structure such as a road or field ridge.

Radar Tracking

Tracking bees with a harmonic radar was achieved as previously described (Riley et al., 1996). Two harmonic radar set-ups were used. The one used in Experiment 1 was described in Riley et al. (1999, 2003), the one used in all other experiments was described in Menzel et al. (2005). In short, the technical details of the latter were as follows. The sending unit consisted of a 9.4 GHz radar transceiver (Raytheon Marine GmbH, Kiel, NSC 2525/7 XU) combined with a parabolic antenna providing approximately 44 dBi. The transponder fixed to the thorax of the bee consisted of a dipole antenna with a Low Barrier Schottky Diode HSCH-5340 of centered inductivity. The second harmonic component of the signal (18.8 GHz) was the target for the radar. The receiving unit consisted of an 18.8 GHz parabolic antenna, with a low-noise pre-amplifier directly coupled to a mixer (18.8 GHz oscillator), and a downstream amplifier with a 90 MHz ZF filter. A 60 MHz ZF signal was used for signal recognition. The transponder was 10.5 mg in weight and 11 mm in length. We used a silver or gold wire with a diameter of 0.33 mm and a loop inductance of 1.3 nH. Radar signals were updated every 3 s. The range of both harmonic radar systems was set to 0.5 nautic miles in most experiments. The improved performance of the radar system used in Experiments 4–6 allowed to set the range temporarily to 0.75 nm or 1.5 nm. The raw radar out-put was captured from the screen at a frequency of 1 Hz, stored as bitmap file and further analyzed off-line by a custom made program that detected and tracked radar signals, and converted circular coordinates into a Cartesian coordinates taking into account multiple calibration posts in the environment. Finally the radar signals were displayed in a calibrated geographic map created with the software Pix4D from aerial images (Strecha et al., 2012) taken with a commercial drone (DYI Inspire). If no signals were received from a bee for more than 30 s the flight trajectory was interrupted, and the last as well as the first signal before and after interruption was marked.

Experimental Design

The respective colonies were placed at their locations at least 3 weeks prior to the start of the experiments ensuring that

foragers were familiar with their respective landscapes. The experimental design followed the catch-and release procedure as applied in many of our previous navigation experiments (Menzel et al., 2005, 2011). A full protocol of all foragers coming to the feeder was established by marking each bee with a colored number tag. Single bees were captured in a small vial at the feeder when they prepared to return to the hive ("homing flight"). They were carried to a release site within the explored area in the dark and then released after a radar transponder had been fixed to their thorax. Usually, animals were tested for their homing flights only once, thus ensuring that they did not use any experience from previous homing flights. In Experiment 6, foragers were trained to a feeder close to the hive (5–10 m), caught when leaving the feeder and then transported to a release site as in the other experiments. Other than in the other experiments, these animals were released multiple times at different release sites and also tested in release sites where they were not released before.

Statistics

The variance of circular data in Experiment 1 was analyzed by means of the Wheeler Watson test using Igor Pro 7 circular statistics¹. The Fisher Exact Test was applied in Experiment 2 to examine the proportions of turns at the guiding landmark (irrigation channel) using STATISTICA (Statsoft, Inc., Tulsa, OK, USA). Circular data in Experiment 1 were analyzed used Oriana circular statistics².

RESULTS

Experiment 1: Hive Training, Field Boundary

In Experiment 1, we asked whether a rather weak elongated ground structure (a field boundary separating two meadows mown at different times) guided homing bees when they were released at sites that brought them close to this landscape feature during their search flights. To answer this question, we trained the bees to a feeder 200 m east of the hive (**Figure 1A**) and released them at various sites either to the north or to the south of the hive. During training the bees did not follow an elongated ground structure but instead flew over rather even grassland. In one test (**Figures 1A–D**), the hive was located directly at this boundary, in the second test (**Figures 1E–H**), the hive was located 60 m east of it. The data analyzed here derive from an experiment in which we studied homing behavior from release sites at various directions and distances from the hive in a rather feature-poor environment (Menzel et al., 2005; see, <https://doi.org/10.1073/pnas.0408550102>). The question addressed here was not analyzed in the published data. We selected those homing flights that brought the bees closer than 60 m to the right or left of the boundary during their vector flight or search flight component.

Fifty-five from 77 bees from the hive close to the boundary performed the correct turn towards the hive when getting close

¹Wavemetrics.com

²<https://www.rockware.com/product/oriana/>

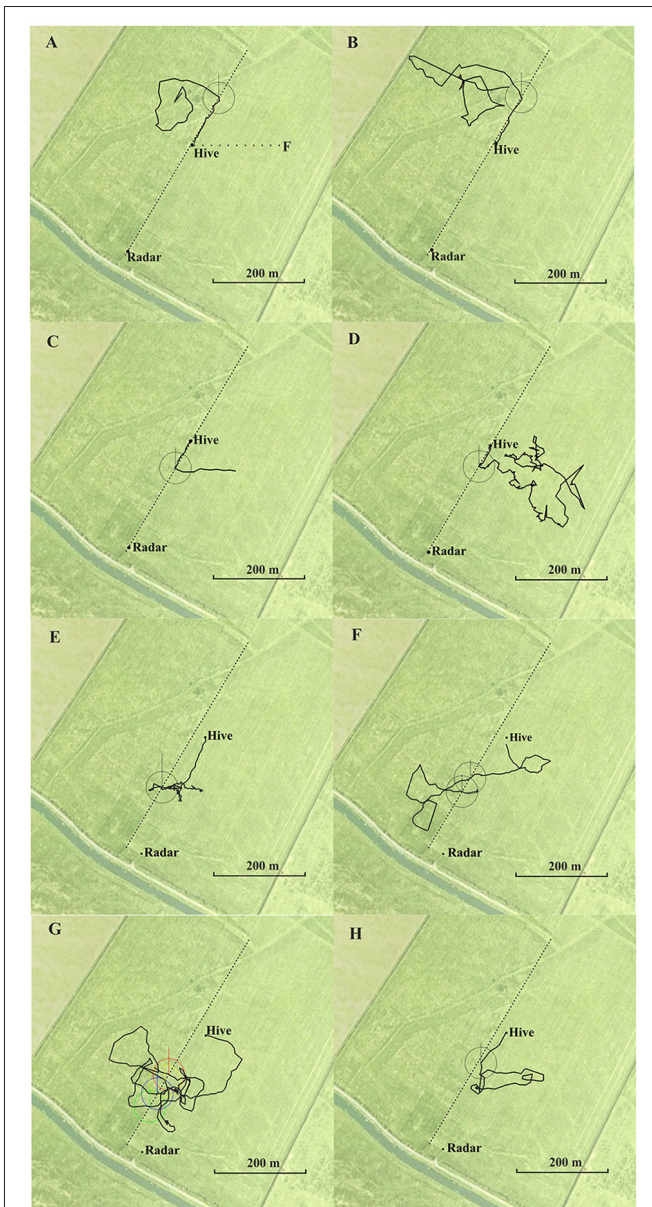


FIGURE 1 | Eight representative examples of flight trajectories of homing bees released at different release sites (**A,B** north, **C–G** south of the hive). The hive was located at the boundary between two meadows in (**A–E**), and 60 m east of the boundary in (**F,G**). The feeding site (F) and the flight route between hive and feeder (dotted line) is indicated in (**A**). The respective release site was the beginning of the trajectory. The trajectory ends at the hive. They first flew approximately 200 m to the west (vector flight; not recorded in **A**). The circles around each crossing are used to determine the angle of the flight trajectory after crossing the boundary relative to the direction to the hive and relative to north. Statistics for the angular turn when crossing the border line for the condition in which the hive was located at the boundary (**A–D**): angle to hive: mean vector μ : 2.8°, concentration: 77.3, circular variance 0.006, circular standard deviation 6.6°, standard error of mean 1.1°, 95% confidence interval \pm for 0.6°, 4.9°; angle to north: mean vector μ : 25.5°, concentration: 145, circular variance 0.415, circular standard deviation 59.4°, standard error of mean 10.5°, 95% confidence interval \pm for 4.84°, 46.1° (total $N = 35$ crossings in the south of the hive including multiple crossing of the same bee). Statistics of the angular turns when crossing the border line for the

(Continued)

FIGURE 1 | Continued

condition when the hive was located 60 m east of the boundary (**E–H**): angle to hive: mean vector μ : 9.5°, concentration: 224.6, circular variance 0.002, circular standard deviation 3.83°, standard error of mean 0.66°, 95% confidence interval \pm for 8.2°, 10.7°; angle to north: mean vector μ : 52.87°, concentration: 0.28, circular variance 0.864, circular standard deviation 114.4°, standard error of mean 50.79°, 95% confidence interval \pm for 313.3°, 152.5° ($N = 34$ crossings in the south of the hive including multiple crossing of the same bee). North is upwards.

to the boundary, 17 bees crossed it without turning, and five bees turned in the incorrect direction. From the 84 crossings made by the 55 bees, 74 were in the correct direction, 19 of them when the bees were already flying towards the hive. Exemplary trajectories are shown in **Figures 1A–D**. Bees from the hive 60 m east of the boundary flew significantly less frequently to the boundary (4 out of 34 came closer than ≤ 60 m) and returned home by trajectories that were more than 30 m further away from the boundary. These four bees followed the boundary in the correct direction towards the hive, and the 34 bees turned home equally well (exemplary flights in **Figures 1E–H**). We measured the angles when crossing the boundary as a measure of guidance towards the hive relative to the direction to the respective hive and relative to the north (see legend of **Figure 1**) and found that the angular distribution of bees from the hive at the boundary was significantly narrower than that of bees from the hive located further away from the boundary (angles relative to the respective hive: $P < 0.001$, angles to the north: $P < 0.001$; Wheeler Watson test). Thus, the boundary provided less guidance when the hive was not located directly at it, but it guided homing when the hive was located close to it.

Thus bees learned to use the boundary as a guiding structure when the hive was close to it. In contrast bees, did not use this elongated ground structure when they hive was not located at it although it would have been a useful landmark for bringing them close to their hive from the distance. The high proportion of correct turns towards the hive in the first case must have involved additional landmarks since this boundary was very similar along the whole stretch from SW to NE, and bees performed equally well when released north or south of the hive. These additional landmarks were obviously sufficient for successful homing in both experiments as bees from the hive at the boundary that did not get close to the boundary returned home equally well, and bees from the hive located 60 m east of the boundary also returned home equally well without following the boundary. These additional landmarks are likely to be other ground structures because no higher rising landmarks were in the vicinity and the horizon was flat within 2° visual angle. **Figure 1** shows additional ground structures (e.g., different grasses growing in a dip in the ground stretching from SW to NE and local patches of vegetation differing between the area SW and NE of the hives) that possibly indicated to the bees if they were south or north of their respective hive. Since the hive could not be seen beyond a distance of 60 m, beacon orientation towards the hive can also be excluded.

Experiment 2: Hive Training, Irrigation Channel

In Experiment 2 two hives were located close to a narrow irrigation channel in the NW corner of the experimental field in two successive years (2011, 2012, **Figure 2**). The respective feeding stations were located SE of the hives at an equal distance. The corresponding release sites in the catch-and-release experiment were selected so that the homing bees either reached the irrigation channel during their initial vector flights (in 2011), or the vector flights ended at about 80 m southeast of the irrigation channel (in 2012). The data analyzed here derive from data addressing the question of whether neonicotinoids effect bees' homing behavior (Fischer et al., 2014; see, <https://doi.org/10.1371/journal.pone.0091364>). The

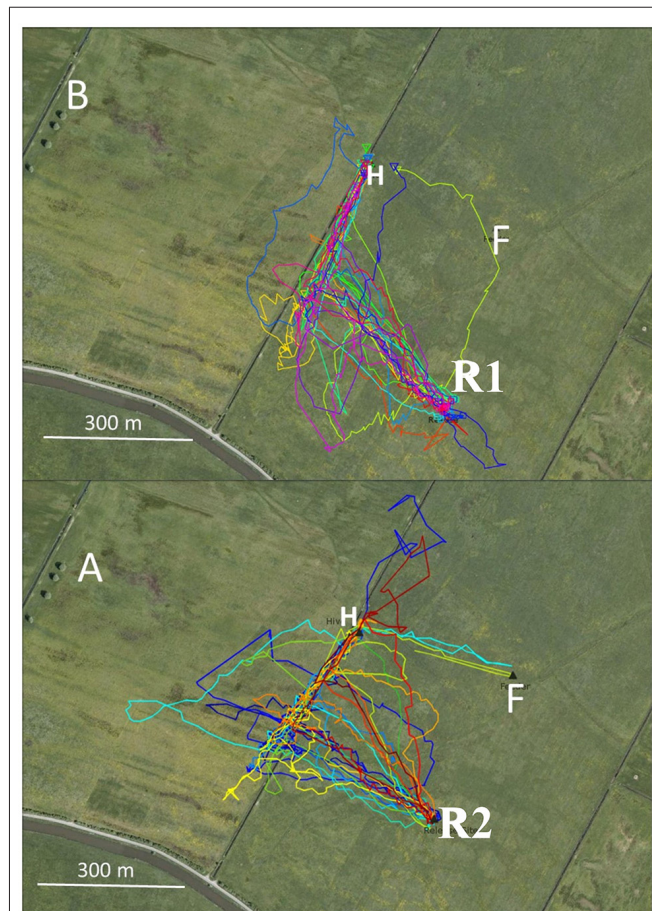


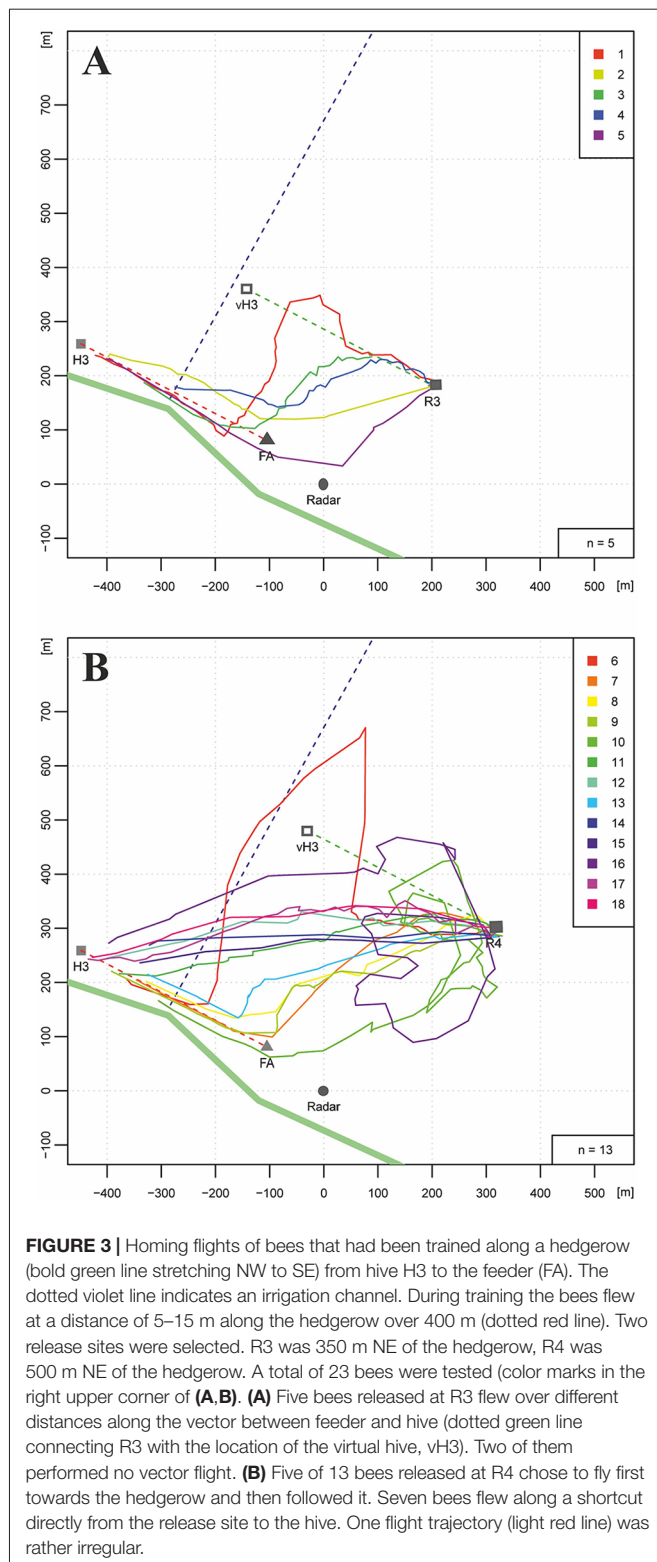
FIGURE 2 | Flight trajectories of homing bees that were trained from two hives (H) to respective feeders (F) in two consecutive years (2011: **B**, 2012: **A**). The hives were located close to an irrigation channel. The respective feeders (were equidistant from the hives. The release site R1 in 2011 was located at the same distance from the irrigation channel as the distance between the hive and the feeder. Therefore, the bees released at that site reached the irrigation channel at the end of their vector flight. In 2012, the release site R2 was further away from the channel leading to a termination of the vector flight before reaching the channel. These test conditions allowed us to ask if the irrigation channel was a necessary guiding structure for homing. Statistics: 2011 first turn correct: 22/25; 2012: 12/22, $P < 0.05$; multiple turns until reaching the hive: 2011: 3/25, 2012: 6/22, $P < 0.05$.

data used here correspond to the flight trajectories of the control groups that did not receive drugs and were not analyzed according to the question addressed here. In 2011, all 25 bees reached the channel and 22 turned towards the hive. Three bees crossed the channel and flew further to the NW aiming towards the hive on trajectories either close to (within 30 m) or further away (up to 100 m) from the channel to the W (**Figure 2**). Thus, each bee made only one turn that brought it to the hive. In 2012, none of 22 bees reached the channel during the initial vector flight (**Figure 2**). Thirteen out of the 22 bees turned to the hive either at the end of their vector flight or earlier without closely following the channel, six bees did not fly directly to the hive but did multiple turns, and three crossed the channel without turns. Four of six bees first turned away from the hive, then made a 180° turn within 100 m and then continued flying towards the hive. The precision of homing was significantly better in 2011 (see **Figure 2** caption). Since the two hive locations did not differ with respect to the irrigation channel, we can assume that the bees from both hives learned the spatial relation of their respective hives to the channel equally well. The only difference between the two groups was the distance between the respective release site and the channel. If the bees reached the channel at the end of their vector flight, they used it as a “highway” to reach the hive. If their vector flight ended before, they aimed towards the hive but less precisely.

Experiment 3: Hive and Feeder Training, Hedgerow

We trained bees along a hedgerow at the southern border of the same experimental field as in Experiments 1 and 2, and asked if the bees would use the hedgerow as a guiding structure when they were trained along it for 400 m and released at two different distances from the hedgerow (**Figures 3A,B**, R3: 350 m, R4: 500 m). The data presented here were obtained from a control experiment addressing the question of whether long-lasting anesthesia affects homing (Cheeseman et al., 2014b; see, <https://doi.org/10.1073/pnas.1201734109>). Data correspond to control, untreated bees, and were not analyzed with respect to the question addressed here. The distance of the release sites from the hedgerow was selected so that the hedgerow would appear at a visual angle $< 2^\circ$ from R4 (500 m), whereas it would be visible from R3 (350 m, 2.5°). We hypothesized that the hedgerow would compete as a guiding structure with the information used during the training flights, namely the memory of the hedgerow as seen during the flights between hive and feeder ($> 50^\circ$). If the vector memory dominated, the bees should aim towards the virtual hive location (**Figures 3A,B**: vH3). Yet, if the memory about the hedgerow dominated, the bees should fly directly to this structure and then continue along it towards the hive. The salience of the hedgerow as a guiding structure should depend on the distance of the release site; a larger distance (R4, 500 m) would correspond to a lower salience.

Figures 3A,B show the results for R3 and R4, respectively. The hedgerow was indeed a salient landmark either leading to a strong reduction in the vector flight length (flight trajectories



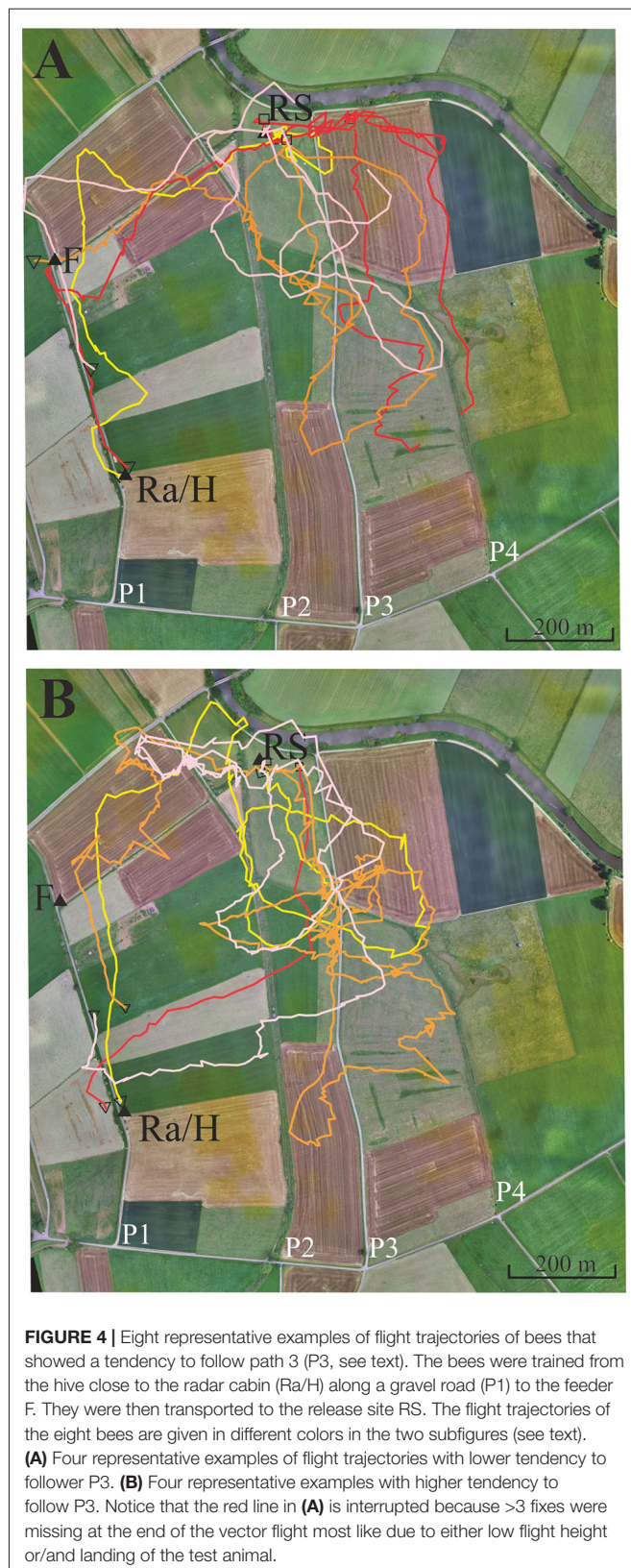
1, 3, 4, in **Figure 3A**) or to a complete absence of the vector flight (flight trajectories 2 and 5 in **Figure 3A**, and flight trajectories 8, 9, 10, 13 in **Figure 3B**). Most interestingly, 7 out of 11 flights in **Figure 3B** followed direct connections

between R4 and the hive. No such flights were found for the closer release site R3 indicating guidance by the hedgerow if it could be seen during the homing flights. Direct homing flights from the release site to the hive indicate a short-cut to the hive although it could not be seen from the release site. In these cases guidance is expected to derive from memory of ground structures as learned during orientation flights.

Experiment 4: Hive and Feeder Training, Gravel Road

Experiment 4, as well as Experiments 5 and 6, were performed in area B, a landscape rich in local and far distant landmarks. Several linear structures ran parallel to each other in approximately S-N direction (**Figure 4**, paths P1, P2, P3, P4). Other elongated structures running approximately E-W divided up pastures. A narrow road also followed the approximate direction E-W (see background of **Figures 4–6**, see also **Supplementary Figures S1, S2** showing the modeled bee eye views; Polster et al., 2018) together with the values of the Michelson contrast, lightness (including standard deviation), and the respective panoramas. The bees were trained to fly along path P1 to a feeder 400 m north of the hive. The data analyzed here come from an experiment aimed to examine the effect of the herbicide glyphosate on navigation (Balbuena et al., 2015; see, <https://doi.org/10.1242/jeb.117291>) and correspond to control, non-treated animals ($N = 71$). These data were not analyzed according to the question addressed here. The release site was chosen so that bees were likely to cross one of two (or both) S-N stretching paths (P2, P3). These paths ran approximately parallel to P1.

Four different homing strategies were observed: (1) bees first performed a vector flight leading to the virtual location of the hive and then reached the hive directly (37 out of 71, representative example trajectory in **Figure 4B**, red line); (2) they flew first to the feeder and then to the hive along the trained path P1 (12 out of 71, representative example in **Figure 4A**, yellow line); (3) bees first performed a vector flight leading to the virtual location of the hive and then flew to the hive *via* the feeder (14 out of 71, representative example in **Figure 4A**, red line); and (4) some bees (8 out of 71, **Figure 4**) followed path P3 running parallel to the trained P1 and then took a short cut to the hive. These eight trajectories belonged to 16 trajectories that got closer than 60 m to P3 and followed it to the south for a rather short stretch (>200 m). No bee followed P2 although 22 bees crossed it during the first 400 m, the length of the vector flight. P3 was rather similar in appearance to P1 as both were gravel roads, whereas P2 was overgrown with grass. It thus appears that only a small proportion of bees were attracted to a parallel path (P3) that mimicked important components of the linear ground structure they had learned during their foraging flights (P1), its S-N direction and appearance (gravel road). The road leading to the radar/hive is visible in the bee views at the feeder—and these views have a high Michelson contrast. No obvious panorama feature appeared to guide the bees



during their four different homing strategies (Supplementary Figures S1, S2).

Experiment 5: Feeder Training, Path, Irrigation Channel and Its Higher Rising Riverine Vegetation

In this experiment, we asked if bees learn an elongated landscape structure (path P2, see Figure 4) at the feeder and generalize it to a structure (path P3) that resembles components of P2 (see also Supplementary Figures S3, S4 showing the modeled bee eye views together with the values of the Michelson contrast, lightness (including standard deviation), and the respective panoramas). Two hives (A, B) were located in the radar cabin at P1. In the first test, bees from colony A were trained to feeder F1 in the NE at a 350 m distance, and bees of colony B were trained to a feeder F2 in the SE at a distance 340 m (Figure 5). In a second test, the training feeders were reversed. The two feeders differed with respect to the close surrounding landscape. F1 was located in the open landscape, and the bees could see path P2 and a parallel narrow irrigation channel with its higher rising riverine vegetation stretching S-N during their flights to the feeder both from the distance and during their final approach to it. Contrarily F2 was located under a group of trees and bushes. Bees trained to F2 were exposed to highly salient landmarks (trees, a EW stretching road, close-by bridge) and P2 was not seen as an elongated ground structure when the bees performed their final approach to the feeder located within the branches of the bushes. The data analyzed in this section come from experiments demonstrating the effect of thiacloprid, a neonicotinoid pesticide, on navigation and dance communication (Tison et al., 2016; see, <https://doi.org/10.1021/acs.est.6b02658>). They correspond to control, non-treated bees and have not been analyzed before with respect to the question addressed here, namely the guiding effect of elongated ground structures.

Foragers were collected when they left the respective feeders and were transported to the release site R5 at a 780 m distance to the hives. We analyzed the successful homing flights that reached P2 and P3. As expected the bees flew first along a vector that resembled in direction and distance the one they would have flown from the respective feeder to the hive (Figure 5). Most interestingly more than half of the foragers at F1 (43 out of 71) followed P3. Some bees did this several times (Figure 5). Foragers from F2, however, behaved differently. Only 5 out of 56 followed P3 (F1 vs. F2, Fischer exact test, $P < 0.0001$). The effect did not depend on which colony was trained to F1 or F2, but depended on the feeding site. Both groups of foragers came from colonies inside the same cabin and should have equal experience with the close P1. Thus, hive training to P1 cannot have caused the following of P3 since otherwise both groups of foragers should have shown the same behavior. Rather, this different behavior must result from the characteristics of their respective feeding sites. P2 and P3 run approximately parallel to each other but their appearance was rather different (P2: overgrown with grass, P3: gravel road). Furthermore, an irrigation channel that ran close and parallel to P2, was a feature lacking in P3. There was also no high-growing riverine vegetation along P3. We conclude that bees foraging at F1 but not those foraging at F2 associated the S-N stretching P2 and may have

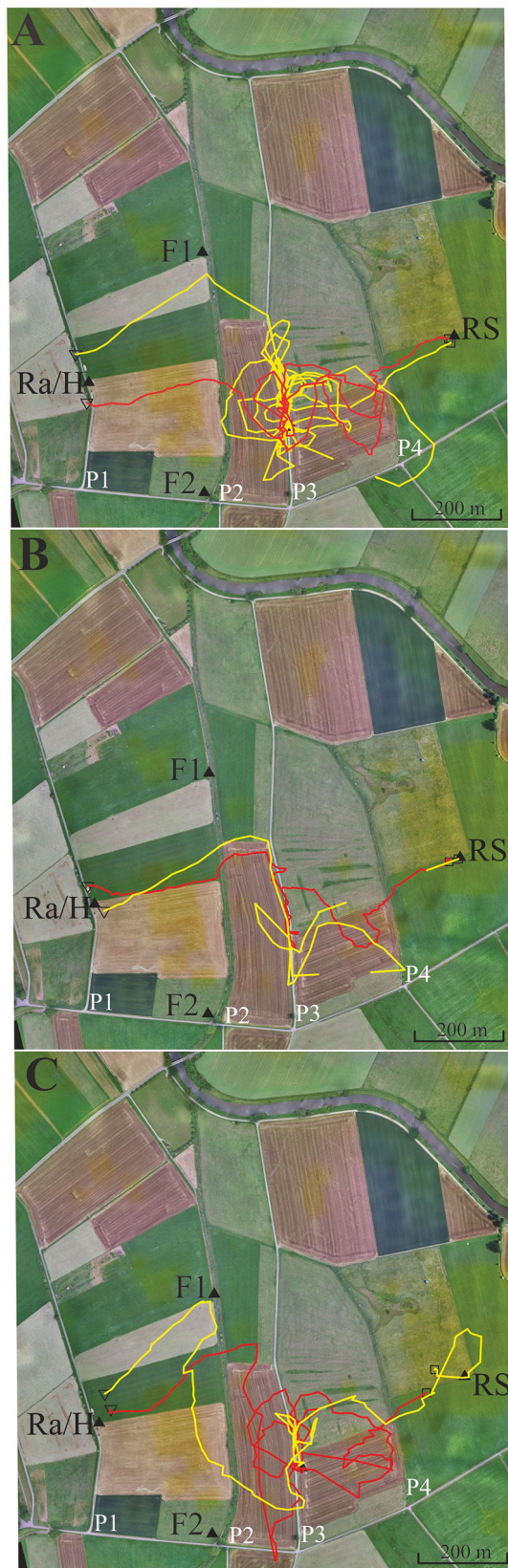


FIGURE 5 | (Continued)

FIGURE 5 | Six representative flight trajectories of bees that were distracted by path 3 (P3) on their homing flights from the release site RS to the hive. The bees were trained to feeder F1 (closed black triangle) and then released at RS 780 m east of the hive respectively marked with a closed black triangle. They passed P2 and P3, and in some cases even reached P4. **(A)** Two representative examples of high distraction by P3. **(B)** Two representative examples for low distraction by P3. **(C)** Two examples with different forms of distraction, one by a delayed effect leading to a distraction flight after passing P3. Trajectories were interrupted if no radar signals were recorded for more than 30 s. The black open square indicates the beginning of the flight, and the open black triangle the end of the flight as recorded by the harmonic radar.

mistaken P3 with P2 during their homing flights. The elongated character of P2 was visible to the bees only when they reached feeder F1.

The bee views at the hive, feeders and release site are shown in **Supplementary Figures S3, S4**. The respective views and the panorama could not be calculated for feeder F2 since it is below trees and bushes, and the necessary data could not be collected with the helicopter. The ground structures at the hive, feeder F1 and release site were very different, and so any matching directly at the release site was most unlikely. A similar argument applies to the fine structure of the respective panoramas, and a coarse resemblance of the panoramas did not exist making it very unlikely that panorama matching played a guiding role.

Experiment 6: Exploratory Learning, Gravel Road

Bees learn landmarks by exploration not only during their first orientation flights (Degen et al., 2016) but also during searching when homing from an unexpected release site. The learning effect is seen in repetitive releases from the same site (Menzel et al., 2005). In this experiment, we asked if bees released several times at an elongated ground structure (a gravel road, P3) learn to use this landmark for effective homing and prefer to fly along it rather than above unstructured grassland [**Supplementary Data** for Experiment 6 and also **Supplementary Figures S5–S7** showing the modeled bee eye views together with the values of the Michelson contrast, lightness (including standard deviation), and the respective panoramas. The model calculations could not be run for release site R1700m + 400 W because it was outside the virtual world]. The test procedure emphasizes exploratory learning along a constant compass direction (southwards towards the hive) and asks whether a highly salient elongated ground structure (gravel road running in the same direction) is used by the bees as an additional guide. The hive was located at the S border of the experimental field (**Figure 6**).

After the bees became familiar with the landscape and performed regular foraging flights, individually marked bees were trained to a feeding site very close to the hive (<10 m). Single bees were released multiple times at increasing distances from the hive in a north direction along path P3. Each test bee was first brought to release site R400 m (400 m north of the hive), then to R800 m, then to R1000 m, and finally to R1200 m. R1200 was not located at the S-N

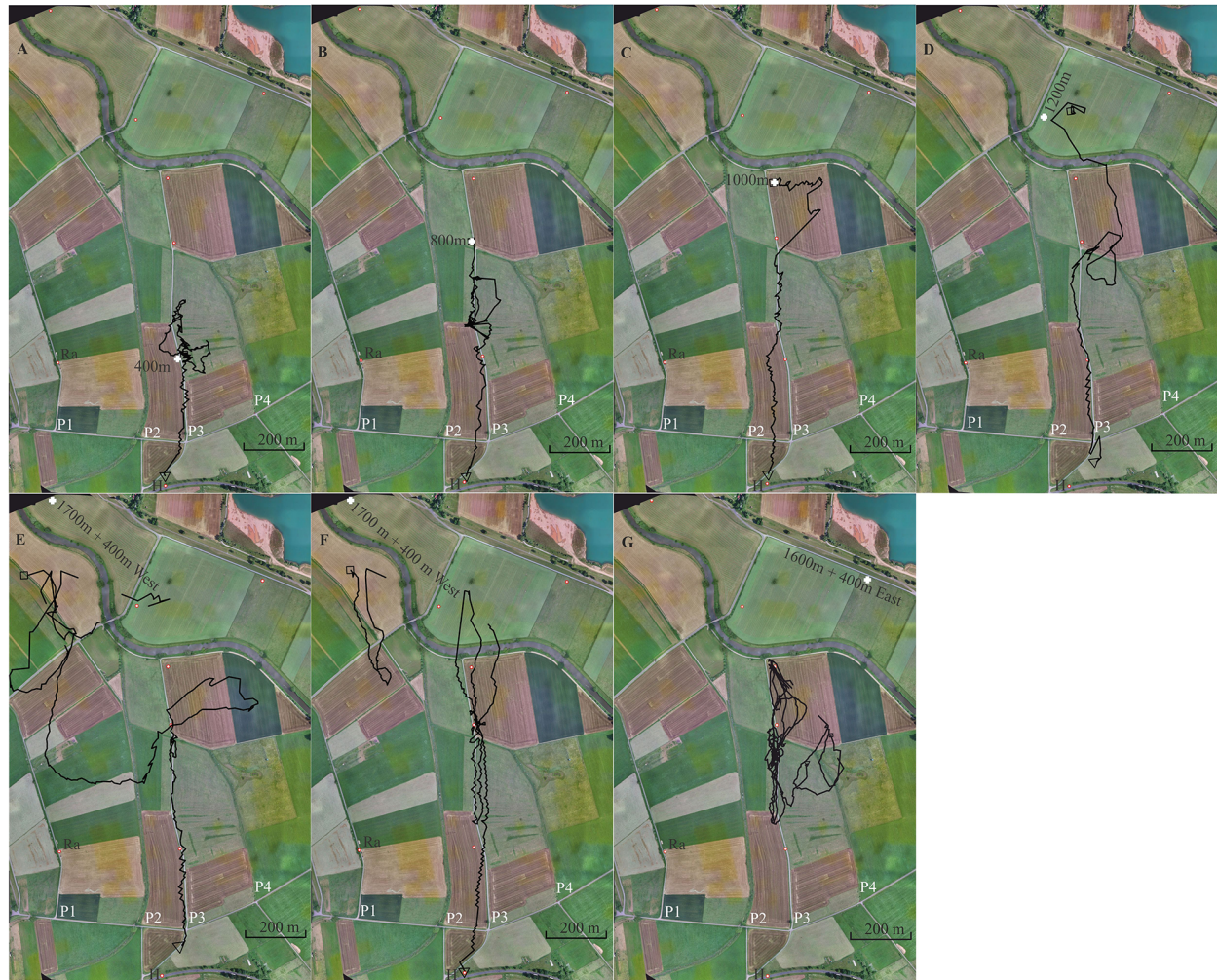


FIGURE 6 | Seven representative flight trajectories of bees released multiple times along a linear ground structure, a gravel road (P3). The first three release sites were at 400 m (A), 800 m (B) and 1,000 m (C) north of the hive (H), respectively. Further release sites were used as test sites at 1,200 m (D), 1,700 + 400 m W (E,F) and 1,600 + 400 m E (G). Each bee was released only once at these latter 3 release sites. The panels show in the background a section of the experimental area together with the respective release sites (white cross), and the S-N stretching elongated ground structures, paths 1, 2, 3 and 4 (P1, P2, P3, P4). P1 and P3 were gravel roads. P3 was the one along which the release sites were located. The open black square marks the beginning of the flight, and the black open triangle the end of the flight. Trajectories are interrupted if no radar signals were recorded for more than 30 s.

stretching gravel road but behind a group of trees at a small road stretching from SW to NE. Two additional release sites were chosen to test whether the bees searched for P3 and followed it during homing. These release sites were located 400 m E or W of P3 (R1600 m + 400 m E and R1700 m + 400 W). The radar signals were rather unreliable at distances >1,000 m and therefore the initial flight paths after releases at R1200, R1600 and R1700 were usually not seen (Figures 6E–G).

A total of 126 flights were tracked (see **Supplementary Data** for Experiment 6). **Figure 6** shows one representative trajectory for each release site (two for R1700 + 400 m W). Bees learned well to fly along P3. When they were released at R400 for the first time, they performed a few search flights that brought them back to the release site and then followed P3 to the S

reaching the hive. When released at R800 for the first time, they usually headed S along P3 immediately reaching R400 and then continued towards the hive. Sometimes the bees searched up and down along P3 over short distances (see **Figure 6B**). Path following was not always directly above the path but over the even grassland to the E or W. Releases at R1200 brought the bees E or W of P3 at its N end, as seen in **Figure 6D**. Some bees corrected their flights and followed P3, others continued their vector flight parallel to P3 at a distance of >60 m over the whole distance. Those that flew W of P3 possibly mistook P2 with P3 although these two ground structures appeared rather differently (see Experiment 5). At least some of these bees came closer than 100 m to P3 and even crossed it but ignored it as a guiding structure. When they were displaced by 400 m to the E or W and released further in the N, they first flew according

to the vector they had learned to the S. Since the radar's limited range did not allow us to record the flights beyond 1,200 m away from the radar (**Figures 6E–G**), we detected only the S ends of these vector flights. The bees then searched but showed a clear tendency to fly towards the E when released W of P3 and to the W when released E of P3. The straight homing flights started in 6 of the 7 animals when they reached P3 coming either from the W or the E. One animal released at R1600 + 400 east hit P3, traveled it up and down several times but was not seen flying back to the hive. The tight connections of these 6 trajectories to the path suggests that the bees were guided by P3 although they did not fly accurately above it but rather approximately ≤ 60 m to the W.

The gravel road appeared as a salient feature throughout all flights starting along it. There were no corresponding ground structures at the release sites 1,200 m and 1,600 + 400 W m. Since the gravel road was not seen by the bees at the hive entrance one can rule out that this elongated ground structure was learned at the hive. No obvious feature of the panoramas appeared at the various release sites, supporting the interpretation that the guiding structures were only those at the ground seen by the bees on their homing flights.

Exploratory learning during multiple homing trips along a constant compass direction leads to both learning of this compass direction and learning of an equally directed salient ground structure (gravel road, P3). The release sites E and W of the gravel road indicate a dominance of the memory for the compass direction and only partial generalization to similar elongated ground structures aligned with the compass direction. The learned path is chosen over these displaced similar ground structures and displaced other landscape structures indicating object identification.

DISCUSSION

An extended landmark like the edge of a forest or a linear boundary on the ground can function as unique guiding structure for a flying animal, with characters different from a localized single beacon associated with the goal or the panorama learned as a picture at the goal. The object's elongation keeps a stable relationship to a compass direction, a property that has been particularly well characterized for the honeybee in experiments by von Frisch and Lindauer (1954) and Dyer and Gould (1981) showing that bees read the compass direction from the edge direction of a forest under fully overcast sky. If the goal has been experienced as being close to the elongated landmark, an animal getting close to it at any other place will possibly be reminded about the learned object as a marker of the goal and may be guided towards the goal. Guidance to the correct direction can result either from the elongated structure's polarity (e.g., in the case of a forest edge) or from additional landmarks that inform the animal whether it is upstream or downstream of the goal along this elongated landmark. This alignment effect has been well studied in humans (McNamara et al., 2003; Valiquette et al., 2007) and requires a functional hippocampus possibly via multiple co-activated place cells (referred to as "boundary vector cells," Barry et al., 2006). Route directions taken by

animated navigation systems is also strongly supported by line-like landmarks allowing robots to navigate more efficiently (Se et al., 2005; Furlan et al., 2007). Bats use stereotypical routes ("flyways") along linear landmarks (Heithaus et al., 1975), and integrate such flyways in their navigation system (Geva-Sagiv et al., 2015). Both migratory birds and homing pigeons have also been observed to follow elongated ground structures like rivers (Geyr von Schweppenbug, 1933; Able, 1980). Guidance by such linear structures may become particularly obvious if the animal follows them to such an extent that even detours are made to keep tracking them, as has been observed in navigating pigeons in response to highways (Guilford et al., 2004; Lipp et al., 2004).

Navigation in bees, as in other animals, involves several sensory modalities, multiple sensory cues and different neural processes. Here, we focused on one environmental component, the presence of elongated structures in the environment, which could act as potentially salient guides for navigation. Guidance may be reflected by a "highway response" (following the elongated structure, Collett and Graham, 2015), by turns when hitting or crossing the structure leading the animals to a course along it, by attraction from the distance, by confusion with or generalization to similar landscape structures, and by the ways in which these structures are learned. We tried to overcome the problem of isolating the effect of one component over the other by comparing experimental data from different training regimes and different spatial relations between the particular elongated structures at the training as well as the test sites. We also varied the overall layout of the landscape under which these training sessions and tests were performed. One landscape was rather feature-less (Klein Lüben, Area A) while the other was rich in both local and distant features (Großseelheim, Area B). Other components of the experimental design were kept constant. The question asked was how these structures are learned as guideposts for their homing flights.

Experiment 1 proves that a linear landmark (a boundary between two pastures) was learned as a cue for the location of the hive. A strong innate tendency to follow such a linear structure was not seen when the hive was not located close to this ground structure. The correct turns towards the hive, both NE and SW of the boundary, emphasized the role and use of features of the boundary (e.g., its polarity although close to negligible) and additional local landmarks. In addition, orientation towards a beacon at the goal or by a view of the panorama was excluded based on the lack of spatial modulation given the resolution of the compound eyes of honeybees. This latter argument was questioned (Cheung et al., 2014) but emphasized by reference to the literature on spatial recognition of bees (Cheeseman et al., 2014a). Experiment 2 was set up to test whether a highly contrasting elongated landmark (an irrigation channel) leads to better homing performance if the bees reached it at the end of their vector flight as compared to a situation in which bees terminate their vector flight earlier and thus start their search flights before homing. No strong tendency was seen to follow the channel when bees terminated their vector flights before reaching the ground structure, but the bees

that followed the channel more closely were more precise in homing.

Experiment 3 introduced a different elongated landmark, a hedgerow along which bees flew between the hive and a feeder. Such an arrangement allowed us to study the guiding role of vector flights in competition with this elongated structure. Two release sites were located at different distances from the hedgerow so that they had a higher or lower influence on homing flights. Bees starting at the release site at a shorter distance from the hedgerow performed short or no vector flights indicating that the hedgerow exerted a strong guiding influence on them. When the release site was at a larger distance, bees performed either flights towards the hedgerow or along shortcuts from the release site to the hive. A shortcut may be a form of spatial reference based on a memory that stores the spatial relations of two locations, the release site and the hive. Under these conditions, the hedgerow would be one of several local features characterizing the location of a further distant release site in its spatial relation to the hive. A beacon at the hive can be excluded since the distance was too large for the bees to see the hive situated low down on the ground.

Experiment 4 addressed the question of whether homing bees generalize a well-trained elongated ground structure (P1) to other elongated structures of similar appearance and quite similar compass orientation. Two of them (P2 and P3) were in the range of the release site and both had a similar compass direction (S-N) as P1. P3 matched P1 more closely in terms of its texture (both were gravel roads) but it was further east while P2 differed in texture (path overgrown by grass). None of the bees followed P2, and only few followed P3 for short stretches; only one bee followed it extensively at some distance (red line in **Figure 4B**). Thus, even if such a highly contrasting elongated ground structure was well learned during foraging flights, its attractiveness as a guiding landmark was rather low. This suggests that similar but displaced structures are embedded in the landscape in such a way that they lose their attraction if their spatial relations to other landmarks (e.g., the panorama and local landmarks) do not fit. This argument is emphasized by the finding that the views at the respective sites (hive, feeder, release site) as modeled by a bee eye simulation and their corresponding panoramas did not uncover any specific guidance by the skyline or the distributions of local landmarks close by.

Experiment 5 proved that an elongated ground structure (P2) was learned as a landmark for the location of the feeder only if it was seen in the open as a bypassing linear landscape feature. We did not see any bee flying up and down P2 during training and during the foraging phase, suggesting that the compass direction of P2 was learned without scanning it. This landmark's compass direction appeared to be the dominant parameter but not its object characteristic, because the scanning flight behavior was triggered by P3, which differed greatly in its appearance (gravel road as compared to a path overgrown by grass with an irrigation channel running parallel). The memory for the S-N stretching structure became effective only after the vector flight was terminated, i.e., during a subsequent search period. This indicates the dominance of the vector memory

during the initial part of homing from an unexpected release site under these specific test conditions since there was no elongated ground structure matching the one at the feeder (P2) was visible at the release site. Furthermore, no guidance by the panorama was detectable, possibly because the skyline appeared not as a salient feature even in such a landscape rich in structure.

In Experiment 6, bees learned their homing flights by exploration. The three training sites were arranged along P3 aligned to a constant compass direction, and additional test sites (R1200 m, R1700 + 400 west or at R1600 + 400 east) were used for releasing the bees. Although there was a clear tendency to follow P3 as a highly contrasting linear ground structure and to correct displacements to the E or W, quite a few bees did not use it as a “highway” steering towards the S over rather unstructured grassland further away from it. The surrounding landscape contained multiple landmarks both at the horizon and on the ground providing the bees during their exploratory learning with additional spatial references. Guidance by P3 was, therefore, not the only reference for their homing behavior, and it is not surprising that they did not always follow it tightly. We interpret this result as a further indication that elongated landmarks are embedded in a spatial memory in which multiple landmarks and their spatial relationships are stored.

Taken together, the dominance of linear ground structures is not as high as expected because even rather salient extended directional cues (e.g., an irrigation channel or a gravel road) are selected for guidance only under certain conditions. The bee's aerial view of the landscape embeds elongated ground structures into multiple landscape features indicating that memory of these linear structures is one of several components in navigation. Elongated structures interact and compete with other references. Object identification is an important part of this process. The objects are characterized not only by their appearance but also by their compass direction. Their salience is highest if both components are close to what had been learned. High similarity in appearance (e.g., texture) can compensate for (partial) misalignment in the compass, and vice versa. These conditions need to be integrated in a concept of navigation memory that avoids isolating particular natural landscape features and this requires experimental approaches under natural conditions with natural dimensions. Several attempts in this direction aim to synthesize and integrate the multiple components of navigation memory, e.g., the navigation toolbox concept (Wiener et al., 2011) or the concept of the integrated map (Jacobs and Menzel, 2014). They share the understanding that the essence of navigation can be captured only if the multiple interacting components are understood as parts of a unified cognitive entity. Such a unifying entity may still be differently expressed by individual bees depending on their life history, experience and age. These circumstances may cause the varying behavior of test bees as we saw it in practically all experiments presented here and in particular in Experiment 4 and 5. So far we lack the data necessary to trace the individual differences to former experience, but experiments are on the way currently to collect such data.

Multiple elongated landmarks may support a dedicated system for processing object geometry. A laboratory test situation would be a rectangular box in which an animal has to decide between locations placed in a particular location relative to the overall geometry of the environment. Since the seminal results by Cheng (1986) indicating a “geometric module” additional data from several animal species (ants, fishes, birds, primates and humans) support this conclusion (Cheng and Newcombe, 2005). It might be questionable whether concepts developed from observations under highly restrictive laboratory conditions and for minimal space may be transferable to the natural environment with relevant species specific dimensions. However, one may also argue that model studies under restrictive conditions may capture at least partly cognitive processes that compose multiple elongated landmarks under natural conditions into a global spatial reference frame that represents the intrinsic geometry of discrete object locations (Chan et al., 2012). Interestingly, the encoding of such environmental geometry is related to the hippocampus in laboratory rodents and in humans, as is spatial memory, structured as a “cognitive map” (O’Keefe and Nadel, 1978; Moser and Moser, 2008).

Very little is known about the neural substrate of navigation in insects (Homborg et al., 2011; Seelig and Jayaraman, 2015), and no neural recordings were performed yet that simulate close to natural conditions of navigation in insects close to natural conditions. The central complex is likely to be involved in compass related visual computation, and the mushroom body in multi-perceptual coding, object recognition and memory formation. These two high order neuropils are likely to code two major components of navigation, spatial reference and object identification. Recently, a parsimonious spiking neural network model was proposed that enabled simulated agents to follow learned routes (Müller et al., 2018). We extended the model proposed by Ardin et al. (2016). This model evaluated route following in flying insects (in particular the honeybee) in different worlds with changing object densities. The model included associative learning of sensory input with a behavioral context tempting to simulate foraging and homing. The spiking neural network model used sparse stimulus representation in the mushroom body and reward-based synaptic plasticity in its output synapses. Simulated bees were able to navigate correctly even when panoramic cues were missing, and performance degraded due to both: (a) too many features; and (b) too sparse features like in the flat world. Context related learning enabled the agents to successfully discriminate even partly overlapping routes. The structure of the visual environment was found to be crucial for the success rate. The model failed to reach the goal more often in visually rich environments due to the overlap of features represented by the Kenyon cells. Reducing the landmark density improved the agents route following. In very sparse environments, extended landmarks, such as roads or field edges, were found to help the agent to stay on its route. It thus appears that rather simple route following can be successfully implemented in rather straight forward assumptions about the processing of ground structure features in high order neural processes of the insect brain. Additional components might

still be necessary for guidance and action selection while navigating along different memorized routes in complex natural environments.

Neural recording data are needed that examine how the central complex and the mushroom body interact, and whether one or the other of these two structures receive the output of the computations in the other structure. The sparse connections between central complex and mushroom body makes it likely that the central complex sends its compass information to the mushroom body because this information can be compressed in commands carrying low amount of information. The mushroom body in such a view (Menzel, 2014) would then treat this information together with the multiple perceptual inputs as one additional component characterizing objects and their spatial relations. In this interpretation the mammalian hippocampus and the mushroom body would have functional similarities possibly including a memory structure as a cognitive map.

DATA AVAILABILITY

Experiment 1: <https://doi.org/10.1073/pnas.0408550102>

Experiment 2: <https://doi.org/10.1371/journal.pone.0091364>

Experiment 3: <https://doi.org/10.1073/pnas.1201734109>

Experiment 4: <https://doi.org/10.1242/jeb.117291>

Experiment 5: <https://doi.org/10.1021/acs.est.6b02658>

Experiment 6: see **Supplementary Information**.

ETHICS STATEMENT

The animals used (Honeybees, *Apis mellifera*) were not exposed to any uncomfortable or unnatural conditions.

AUTHOR CONTRIBUTIONS

RM conceived the goal of the study. JC, JF-N, LT, MB, RM, UG designed and performed the experiments. TL and JPo developed the bee eye view model and made calculations. JPe, TL, XC, UG helped to analyze the data.

FUNDING

This work was supported by Deutsche Forschungsgemeinschaft Grant Me 365/32-1 and 365/34-2, grants from the Hertie Gemeinnützige Stiftung, Dr. Klaus Tschira Stiftung, the gGmbH OLIN, and the Joint Program Germany-New Zealand (Internationale Zusammenarbeit Neuseeland-Deutschland, 01DR12054), and Royal Society of New Zealand New Zealand-Germany S&T programme Grant FRG11-27 as well as the Marsden Fund Grant UOA 07/012.

ACKNOWLEDGMENTS

We highly appreciate the collaboration with Dr. J. Riley, A. D. Smith and D. R. Reynolds during Experiment 1. We are grateful to W. D. Haass and B. Fischer for constructing and building the harmonic radar device used in Experiments 4–6, to the farmers in Klein Lüben and Großseelheim who gave us access

to their grassland, and to Dr. Büchler for providing us with bee colonies at Großseelheim. We thank many students who helped us during the field experiments. We are also grateful to Anne Carney for her help with the English.

SUPPLEMENTARY MATERIAL

The Supplementary Material for this article can be found online at: <https://www.frontiersin.org/articles/10.3389/fnbeh.2018.00322/full#supplementary-material>

REFERENCES

- Able, K. P. (1980). "Mechanisms of orientation, navigation and homing," in *Animal Migration, Orientation, Navigation*, ed. S. A. Gauthreaux (New York, NY: Academic Press), 281–387.
- Ardin, P., Peng, F., Mangan, M., Lagogiannis, K., and Webb, B. (2016). Using an insect mushroom body circuit to encode route memory in complex natural environments. *PLoS Comput. Biol.* 12:e1004683. doi: 10.1371/journal.pcbi.1004683
- Balbuena, M. S., Tison, L., Hahn, M. L., Greggers, U., Menzel, R., and Farina, W. M. (2015). Effects of sub-lethal doses of glyphosate on honeybee navigation. *J. Exp. Biol.* 218, 2799–2805. doi: 10.1242/dev.117291
- Barry, C., Lever, C., Hayman, R., Hartley, T., Burton, S., O'Keefe, J., et al. (2006). The boundary vector cell model of place cell firing and spatial memory. *Rev. Neurosci.* 17, 71–97. doi: 10.1515/revneuro.2006.17.1-2.71
- Canny, J. (1986). A computational approach to edge detection. *IEEE Trans. Pattern Anal. Mach. Intell.* 8, 679–698. doi: 10.1016/b978-0-08-051581-6.50024-6
- Chan, E., Baumann, O., Bellgrove, M. A., and Mattingley, J. B. (2012). From objects to landmarks: the function of visual location information in spatial navigation. *Front. Psychol.* 3:304. doi: 10.3389/fpsyg.2012.00304
- Cheeseman, J. F., Millar, C. D., Greggers, U., Lehmann, K., Pawley, M. D., Gallistel, C. R., et al. (2014a). Reply to Cheung et al.: the cognitive map hypothesis remains the best interpretation of the data in honeybee navigation. *Proc. Natl. Acad. Sci. U S A* 111:E4398. doi: 10.1073/pnas.1415738111
- Cheeseman, J. F., Millar, C. D., Greggers, U., Lehmann, K., Pawley, M. D., Gallistel, C. R., et al. (2014b). Way-finding in displaced clock-shifted bees proves bees use a cognitive map. *Proc. Natl. Acad. Sci. U S A* 111, 8949–8954. doi: 10.1073/pnas.1408039111
- Cheng, K. (1986). A purely geometric module in the rat's spatial representation. *Cognition* 23, 149–178. doi: 10.1016/0010-0277(86)90041-7
- Cheng, K., and Newcombe, N. S. (2005). Is there a geometric module for spatial orientation? Squaring theory and evidence. *Psychon. Bull. Rev.* 12, 1–23. doi: 10.3758/bf03196346
- Cheung, A., Collett, M., Collett, T. S., Dewar, A., Dyer, F., Graham, P., et al. (2014). Still no convincing evidence for cognitive map use by honeybees. *Proc. Natl. Acad. Sci. U S A* 111, E4396–E4397. doi: 10.1073/pnas.1413581111
- Collett, T. S., and Graham, P. (2015). Insect navigation: do honeybees learn to follow highways? *Curr. Biol.* 25, R240–R242. doi: 10.1016/j.cub.2014.11.003
- Degen, J., Kirbach, A., Reiter, L., Lehmann, K., Norton, P., Storms, M., et al. (2015). Exploratory behaviour of honeybees during orientation flights. *Animal Behav.* 102, 45–57. doi: 10.1016/j.anbehav.2014.12.030
- Degen, J., Kirbach, A., Reiter, L., Lehmann, K., Norton, P., Storms, M., et al. (2016). Honeybees learn landscape features during exploratory orientation flights. *Current Biology* 26, 2800–2804. doi: 10.1016/j.cub.2016.08.013
- Dyer, F. C., and Gould, J. L. (1981). Honey bee orientation: a backup system for cloudy days. *Science* 214, 1041–1042. doi: 10.1126/science.214.4524.1041
- Fischer, J., Müller, T., Spatz, A. K., Greggers, U., Grünewald, B., and Menzel, R. (2014). Neonicotinoids interfere with specific components of navigation in honeybees. *PLoS One* 9:e91364. doi: 10.1371/journal.pone.0091364
- Furlan, A., Baldwin, T., and Klippel, A. (2007). "Landmark classification for route directions," in *Proceedings of the Fourth ACL-SIGSEM Workshop on Prepositions* (Prague: Association for Computational Linguistics), 9–16.
- Geva-Sagiv, M., Las, L., Yovel, Y., and Ulanovsky, N. (2015). Spatial cognition in bats and rats: from sensory acquisition to multiscale maps and navigation. *Nat. Rev. Neurosci.* 16, 94–108. doi: 10.1038/nrn3888
- Geyer von Schweppenburg, H. V. (1933). Zur theorie der leitlinie. *Ardea* 22, 83–92.
- Giger, G. (1996). *Honeybee Vision: Analysis of Pattern Orientation*. Canberra: Australian National University.
- Guilford, T., Roberts, S., Biro, D., and Rezek, I. (2004). Positional entropy during pigeon homing II: navigational interpretation of Bayesian latent state models. *J. Theor. Biol.* 227, 25–38. doi: 10.1016/j.jtbi.2003.07.003
- Heithaus, E. R., Fleming, T. H., and Opler, P. A. (1975). Foraging patterns and resource utilization in seven species of bats in a seasonal tropical forest. *Ecology* 56, 841–854. doi: 10.2307/1936295
- Homburg, U., Heinze, S., Pfeiffer, K., Kinoshita, M., and el Jundi, B. (2011). Central neural coding of sky polarization in insects. *Philos. Trans. R. Soc. Lond. B Biol. Sci.* 366, 680–687. doi: 10.1098/rstb.2010.0199
- Jacobs, L. F., and Menzel, R. (2014). Navigation outside of the box: what the lab can learn from the field and what the field can learn from the lab. *Mov. Ecol.* 2:3. doi: 10.1186/2051-3933-2-3
- Lipp, H.-P., Vyssotski, A. L., Wolfer, D. P., Renaudineau, S., Savini, M., Tröster, G., et al. (2004). Pigeon homing along highways and exits. *Curr. Biol.* 14, 1239–1249. doi: 10.1016/j.cub.2004.07.024
- McNamara, T. P., Rump, B., and Werner, S. (2003). Egocentric and geocentric frames of reference in memory of large-scale space. *Psychon. Bull. Rev.* 10, 589–595. doi: 10.3758/bf03196519
- Menzel, R. (2013). "The cognitive structure of visual navigation in honeybees," in *The New Visual Neuroscience*, eds J. S. Werner and L. M. Chalupa (Cambridge, MA: MIT Press), 1179–1189.
- Menzel, R. (2014). The insect mushroom body, an experience-dependent recoding device. *J. Physiol. Paris* 108, 84–95. doi: 10.1016/j.jphysparis.2014.07.004
- Menzel, R., and Greggers, U. (2015). The memory structure of navigation in honeybees. *J. Comp. Physiol. A Neuroethol. Sens. Neural Behav. Physiol.* 201, 547–561. doi: 10.1007/s00359-015-0987-6
- Menzel, R., Greggers, U., Smith, A., Berger, S., Brandt, R., Brunke, S., et al. (2005). Honey bees navigate according to a map-like spatial memory. *Proc. Natl. Acad. Sci. U S A* 102, 3040–3045. doi: 10.1073/pnas.0408550102
- Menzel, R., Kirbach, A., Haass, W.-D., Fischer, B., Fuchs, J., Koblofsky, M., et al. (2011). A common frame of reference for learned and communicated vectors in honeybee navigation. *Curr. Biol.* 21, 645–650. doi: 10.1016/j.cub.2011.02.039
- Moser, E. I., and Moser, M. B. (2008). A metric for space. *Hippocampus* 18, 1142–1156. doi: 10.1002/hipo.20483
- Müller, J., Nawrot, M., Menzel, R., and Landgraf, T. (2018). A neural network model for familiarity and context learning during honeybee foraging flights. *Biol. Cybern.* 112, 113–126. doi: 10.1007/s00422-017-0732-z
- O'Keefe, J., and Nadel, J. (1978). *The Hippocampus As A Cognitive Map*. New York, NY: Oxford University Press.
- Osborne, J. L., Smith, A., Clark, S. J., Reynolds, D. R., Barron, M. C., Lim, K. S., et al. (2013). The ontogeny of bumblebee flight trajectories: from naive explorers to experienced foragers. *PLoS One* 8:e78681. doi: 10.1371/journal.pone.0078681

FIGURE S1 | Supplemental Material A for **Figure 4** (panorama).

FIGURE S2 | Supplemental Material B for **Figure 4** (ground structures).

FIGURE S3 | Supplemental Material A for **Figure 5** (panorama).

FIGURE S4 | Supplemental Material A for **Figure 5** (ground structures).

FIGURE S5 | Supplemental Material A for **Figure 6** (panorama).

FIGURE S6 | Supplemental Material A for **Figure 6** (panorama).

FIGURE S7 | Supplemental Material A for **Figure 6** (ground structures).

- Polster, J., Petrasch, J., Menzel, R., and Landgraf, T. (2018). Reconstructing the visual perception of honey bees in complex 3-D worlds. *arXiv:1811.07560* [preprint].
- Riley, J. R., Greggers, U., Smith, A. D., Stach, S., Reynolds, D. R., Stollhoff, N., et al. (2003). The automatic pilot of honeybees. *Proc. Biol. Sci.* 270, 2421–2424. doi: 10.1098/rspb.2003.2542
- Riley, J. R., Reynolds, D. R., Smith, A. D., Edwards, A. S., Osborne, J. L., Williams, I. H., et al. (1999). Compensation for wind drift by bumble-bees. *Nature* 400:126. doi: 10.1038/22029
- Riley, J. R., Smith, A. D., Reynolds, D. R., Edwards, A. S., Osborne, J. L., Williams, I. H., et al. (1996). Tracking bees with harmonic radar. *Nature* 379, 29–30. doi: 10.1038/379029b0
- Schiffner, I., Fuhrmann, P., and Wiltschko, R. (2013). Homing flights of pigeons in the Frankfurt region: the effect of distance and local experience. *Anim. Behav.* 86, 291–307. doi: 10.1016/j.anbehav.2013.05.018
- Se, S., Lowe, D. G., and Little, J. J. (2005). Vision-based global localization and mapping for mobile robots. *IEEE Trans. Robot.* 21, 364–375. doi: 10.1109/tro.2004.839228
- Seelig, J. D., and Jayaraman, V. (2015). Neural dynamics for landmark orientation and angular path integration. *Nature* 521, 186–191. doi: 10.1038/nature14446
- Strecha, C., Küng, O., and Fua, P. (2012). Automatic mapping from ultra-light UAV imagery. *EuroCOW 2012*. No. EPFL-CONF-175351.
- Stürzl, W., Boeddeker, N., Dittmar, L., and Egelhaaf, M. (2010). Mimicking honeybee eyes with a 280 degrees field of view catadioptric imaging system. *Bioinspir. Biomim.* 5:036002. doi: 10.1088/1748-3182/5/3/036002
- Tison, L., Hahn, M. L., Holtz, S., Rößner, A., Greggers, U., Bischoff, G., et al. (2016). Honey bees' behavior is impaired by chronic exposure to the neonicotinoid thiacloprid in the field. *Environ. Sci. Technol.* 50, 7218–7227. doi: 10.1021/acs.est.6b02658
- Valiquette, C. M., McNamara, T. P., and Labrecque, J. S. (2007). Biased representations of the spatial structure of navigable environments. *Psychol. Res.* 71, 288–297. doi: 10.1007/s00426-006-0084-0
- von Frisch, K., and Lindauer, M. (1954). Himmel und erde in konkurrenz bei der orientierung der bienen. *Naturwissenschaften* 41, 245–253. doi: 10.1007/bf00634944
- Wiener, J., Shettleworth, S., Bingman, V. P., Cheng, K., Healy, S., Jacobs, L. F., et al. (2011). "Animal navigation, a synthesis," in *Animal Thinking: Contemporary Issues in Comparative Cognition*. Strüngmann Forum Reports, eds J. Menzel and J. Fischer (Cambridge, MA: MIT Press), 51–78.
- Wiltschko, R., Schiffner, I., and Sigmund, B. (2007). Homing flights of pigeons over familiar terrain. *Anim. Behav.* 74, 1229–1240. doi: 10.1016/j.anbehav.2007.01.028
- Wolf, S., McMahon, D. P., Lim, K. S., Pull, C. D., Clark, S. J., Paxton, R. J., et al. (2014). So near and yet so far: harmonic radar reveals reduced homing ability of Nosema infected honeybees. *PLoS One* 9:e103989. doi: 10.1371/journal.pone.0103989

Conflict of Interest Statement: The authors declare that the research was conducted in the absence of any commercial or financial relationships that could be construed as a potential conflict of interest.

Copyright © 2019 Menzel, Tison, Fischer-Nakai, Cheeseman, Balbuena, Chen, Landgraf, Petrasch, Polster and Greggers. This is an open-access article distributed under the terms of the Creative Commons Attribution License (CC BY). The use, distribution or reproduction in other forums is permitted, provided the original author(s) and the copyright owner(s) are credited and that the original publication in this journal is cited, in accordance with accepted academic practice. No use, distribution or reproduction is permitted which does not comply with these terms.



Learning and Its Neural Correlates in a Virtual Environment for Honeybees

Hanna Zwaka^{1,2*}, Ruth Bartels¹, Sophie Lehfeldt¹, Meida Jusyte¹, Sören Hantke¹, Simon Menzel¹, Jacob Gora¹, Rafael Alberdi¹ and Randolph Menzel^{1,3}

¹ Department of Biology and Neurobiology, Freie Universität Berlin, Berlin, Germany, ² Molecular and Cellular Biology, Harvard University, Cambridge, MA, United States, ³ Bernstein Center for Computational Neuroscience, Berlin, Germany

The search for neural correlates of operant and observational learning requires a combination of two (experimental) conditions that are very difficult to combine: stable recording from high order neurons and free movement of the animal in a rather natural environment. We developed a virtual environment (VE) that simulates a simplified 3D world for honeybees walking stationary on an air-supported spherical treadmill. We show that honeybees perceive the stimuli in the VE as meaningful by transferring learned information from free flight to the virtual world. In search for neural correlates of learning in the VE, mushroom body extrinsic neurons were recorded over days during learning. We found changes in the neural activity specific to the rewarded and unrewarded visual stimuli. Our results suggest an involvement of the mushroom body extrinsic neurons in operant learning in the honeybee (*Apis mellifera*).

Keywords: virtual environment (VE), learning and memory, mushroom body, honey bee, feedback neurons, GABA, operant learning, mushroom body extrinsic neurons

OPEN ACCESS

Edited by:

Etsuro Ito,

Waseda University, Japan

Reviewed by:

Makoto Mizunami,

Hokkaido University, Japan

Hiroyuki Ai,

Fukuoka University, Japan

*Correspondence:

Hanna Zwaka

zwaka@fas.harvard.edu

Received: 29 July 2018

Accepted: 30 October 2018

Published: 25 January 2019

Citation:

Zwaka H, Bartels R, Lehfeldt S, Jusyte M, Hantke S, Menzel S, Gora J, Alberdi R and Menzel R (2019) Learning and Its Neural Correlates in a Virtual Environment for Honeybees. *Front. Behav. Neurosci.* 12:279. doi: 10.3389/fnbeh.2018.00279

INTRODUCTION

In the past, two different approaches have been followed to search for neural correlates of operant learning and navigation: Monitoring neural activity of animals (usually rats) while navigating in a rather small space (O'Keefe and Nadel, 1978; McNaughton et al., 2006; Puryear et al., 2010; Ball et al., 2014), and animals navigating in a virtual environment [VE, (Mallot et al., 1998)]. The latter has the advantage that the simulated environment can be large and fully manipulated. Its disadvantages relate to compromised sensory feedback provided by the moving visual world and the stationary conditions of the animal. Nevertheless, animals and humans can learn and navigate in a virtual reality set-up that produces the relevant visual feedback to the intended movements (Gillner and Mallot, 1998; Holscher et al., 2005, design guidelines for VEs can be found at: <http://cogprints.org/3297/>). Such devices have been developed and combined with neural recordings of EEG, local field potentials and single neurons for humans (Gillner and Mallot, 1998; Araújo et al., 2002; Baumeister et al., 2010; Doeller et al., 2010) as well as for animals (Mizunami et al., 1998; Harvey et al., 2009, 2012; Dombeck et al., 2010; Takalo et al., 2012; Aronov and Tank, 2014).

Insects are particularly suitable for behavioral-neural analyses. Despite having small brains they perform complex tasks in their respective environments (Menzel, 2012) including multiple forms of learning like classical, operant and observational learning under natural conditions. These forms of learning have been studied extensively on a behavioral level (Srinivasan, 2010; Giurfa and Menzel, 2013). Laboratory learning tests have been developed to keep the stimulus conditions close to those under natural conditions. In cockroaches, neurons were successfully recorded in freely

moving animals (Mizunami et al., 1998; Bender et al., 2010). *Drosophila* flying in a simple VE has helped to elucidate a range of visual performances and visual learning at multiple levels of analysis (Heisenberg and Wolf, 1979; Wolf and Heisenberg, 1984; Peng et al., 2007). However, combining flight behavior in a VE with neural recordings has turned out to be rather difficult in *Drosophila* leading to correlations between turning behavior and local field potentials (van Swinderen and Greenspan, 2003) and to correlates of the fly's heading direction (Kim et al., 2017). Walking *Drosophila* are suitable for studying neural correlates of seemingly more complex behaviors like operant and observational learning (Fiala, 2007) and landmark orientation (Seelig and Jayaraman, 2015; Turner-Evans et al., 2017). These experiments allow researchers to combine the potential of molecular genetic tools with behavioral tests.

Honeybees are capable of a variety of complex learning tasks that go beyond classical and operant conditioning including non-elemental learning (Giurfa, 2003). So far, the search for neural correlates of learning, memory formation and memory retrieval in honeybees was limited to olfactory conditioning of restrained animals (Okada et al., 2007; Denker et al., 2010; Strube-Bloss et al., 2011; Menzel, 2014; Filla and Menzel, 2015). Past experiments have shown that honeybees can be trained to discriminate colors in a virtual environment (Buatois et al., 2017, 2018; Rusch et al., 2017; Schultheiss et al., 2017). Here we set out to train bees to visual stimuli in a virtual reality environment while recording simultaneously from higher order brain centers. In the future, this might enable us to record neural correlates of complex learning tasks in the virtual environment.

We developed a VE that consists of an air-supported spherical treadmill allowing the stationary walking honeybee (*Apis mellifera*) in closed-loop to control a visual environment projected onto a cone-shaped screen from above. This set-up gives us the opportunity to combine stable extracellular recordings over many hours with rather free moving animals. The honeybee can actively select a visual stimulus while we record from what are most likely A3 mushroom body extrinsic neurons that are known to change their response properties during classical olfactory conditioning (Haehnel and Menzel, 2010; Filla and Menzel, 2015). These neurons receive input from Kenyon cells, the intrinsic neurons of the mushroom body. They are sensitive to combinations of multiple sensory modalities including visual stimuli (Homberg and Erber, 1979; Schildberger, 1981; Grünewald, 1999).

Here, we also show that honeybees that were trained in free flight transfer the learned information to the VE.

After training in the VE, we found significant changes in neural activity to the rewarded and unrewarded colors in the VE.

EXPERIMENTAL PROCEDURES

Spherical Treadmill, Geometry of the Virtual Environment and Overall Set-Up

The virtual environment (VE) was an advanced version of the VE described in deCamp (2013). The treadmill consisted of a Styrofoam sphere (10 cm diameter) placed in a half-spherical

plastic cup with several symmetrically located holes through which a laminar airflow passed and let the sphere float on air.

The projector (Epson EMP-TW 700, Suwa, Japan, digital scanning frequency: pixel clock: 13.5–81 MHz, horizontal sweep: 15–60 kHz, vertical sweep: 50–85 Hz) was positioned above a Faraday cage and illuminated the inner surface of a cone-shaped screen (height 60 cm, bottom diameter 7 cm, top diameter 75 cm) via a large surface mirror and a Perspex window (Figure 2). The inner surface of the cone consisted of white paper. The shape of the patterns projected onto this screen were adjusted so that they appeared undistorted to the bee. During an experiment, the Faraday cage was closed. A web camera (c920, Logitech, Morges Gesellschaft, Switzerland) positioned above it imaged the head of the animal via a 500 mirror objective allowing observation of the animal during the experiment. The light from the projector, which fell directly on the upper view of the animal, was blocked by a screen.

Control of the Virtual Environment and Experimental Procedure

The virtual environment and the recognition of the bee's movement was under the control of the custom program BeeWorld. It was implemented in Java by using OpenGL-Bindings for Java (LWJGL). Two optical high precision computer mice (Imperator, Razer Europe GmbH, Hamburg, Germany; G500, Logitech Europe S.A.) detected the movement of the sphere, initiated by the walking bee. The mice were accurately positioned under 90° at the equator of the Styrofoam sphere and precisely aligned to the optimal distance with x/y micro drives. The readings of the optical mice were precisely calibrated by rotating the sphere around the vertical axes. Thus, it was possible to convert ticks produced by the mice to forward movement, horizontal movement and rotatory movement of the bee in inch. Rotatory movement was obtained by calculating the mean of the movement along the x-axes of both mice. This redundancy is making the signal more reliable. The translational component of the movement results from the differences between the ticks of the y-axes of both mice. Both y-signals were multiplied with their position vectors and summed up. The resulting vector gives the translational components of the movement (Figure 2C):

$$Translation = x_1 * \begin{pmatrix} -0.707 \\ -0.707 \end{pmatrix} + x_2 * \begin{pmatrix} 0.707 \\ -0.707 \end{pmatrix}$$

To obtain the new position of the bee after a move, the translational vector was added in the direction the bee was virtually orientated:

$$\begin{aligned} T.x * \cos(O) + T.y * \sin(O) &= x \\ T.y * \cos(O) + T.x * \sin(O) &= y \end{aligned}$$

T is the translation vector. O is the orientation.

The data from the mice was read at a frequency of 500 Hz by the computer. The bee was able to control the virtual scenery by rotatory and translatory movements of the sphere. Multiple scenarios were designed and stored as xml files. These files were

loaded by the custom program BeeWorld. They contained the positions, widths, and colors (RGB) of a variable number of vertically oriented stripes or other structures. In order to improve the feedback to the bee about the rotatory components, every scenario had a checkerboard pattern projected onto the ground immediately in front of the bee, and gray stripes of different height at the background simulating a far-distant skyline. The rotation and translation of the checkerboard pattern was coupled one-to-one to the intended movement of the animal and the rotation of the skyline was set to a lower angular velocity simulating further distance by motion parallax. The angular velocities of these patterns as well as that of all objects in between could be separately adjusted.

The field of view in OpenGL was limited to 179° , the scenarios projected onto the screen, however, simulated a 360° view. To solve this, four 90° views were combined and transformed to fit the cone-shaped screen. In addition to the 360° view, the checkerboard pattern was projected in the middle of the screen. Movement and rotation speed of our 360° skyline and the checkerboard ground pattern was set relative to the rotation speed of the stripes in the scenarios. The depth components between virtual objects seemingly in the background and virtual objects closer to the animal were simulated by occlusion, size of the objects, and motion parallax that changed with movement of the animal.

Data from walking traces were synchronized with the data from spike recordings as collected with an analog/digital converter (micro3, CED, Cambridge Electronic Design, Cambridge, UK, 20 KHz sampling frequency per channel). A photodiode directed at the projector detected a short light signal under the control of the BeeWorld program and fed it into the ADC input of the analog/digital converter for synchronization. The scenario used in all experiments here consisted of one blue and one yellow vertically oriented stripe with an angular width of 30° , the horizontal checkerboard pattern immediately in front of the bee and the gray skyline pattern in the background. The angular rotation of the checkerboard pattern was equal to the angular movement of the sphere simulating a respective movement of the floor directly below and in front of the bee. The angular rotation of the stripe pattern was set to 75% of the checkerboard pattern, and a skyline pattern projected onto the screen together with the stripe pattern moved with 50% of the checkerboard pattern. Thus, these three patterns simulated different distances to the honeybee.

T-Maze Experimental Design

Free-flying bees were trained in a T-maze (70 cm long until T-junction, about 5 cm in width, 4 cm high with a 55 cm long head side, see **Figure 3**) with one color (either blue or yellow) rewarded with 30% sucrose and another color punished with a 0.5 M potassium chloride solution. To attract foragers, a feeding station offering 1–10% sucrose solution was placed near the experimental set-up. During the first foraging flights, animals were actively induced into the entrance of the T-maze with a help of a sucrose-containing syringe. Individual foragers were marked, and all T-maze approaches were noted. Only one bee was tested

at a time. Bees could fly into the T-maze but had to walk until a point of decision and decide for one side. In the beginning, sucrose droplets in the entrance of the maze showed the direction to the point of decision. The experimental set-up consisted of a plastic T-maze covered with UV-transparent Plexiglas to ensure daylight conditions within the maze. Little doors inside the maze ensured that the bee had to walk in one direction after the point of decision and could not turn back in order to perceive the colors again. The animals were trained over 25 trials.

Afterwards, they flew back to their hives or—in case of a wrong decision—could enter again. To avoid side preferences, we switched the sides of reward and punishment. Subsequently the animals were transferred to the virtual environment and tested in a scenario similar to the T-maze situation without reward.

Animals

Worker honeybees (*Apis mellifera carnica*) were caught at the hive entrance during summertime. In winter, sugar water foraging animals flying in an indoor flight room were collected at the feeding sites. The bees were immobilized by cooling, mounted in Plexiglas tubes, and kept in a high humidity chamber. During the night, bees were held on Styrofoam spheres and were able to move freely on the spheres. All animals were fed to saturation after capture and on each subsequent day at 4 p.m. with 16 μ l of 30% sucrose solution.

Treadmill Training

During the night, bees were on Styrofoam spheres held in an apparatus to measure walking activity that only allowed the animal to walk forward and backward. The animals were able to move on the spheres held by balances, which kept the animal on the spherical treadmill with its own weight. This balance allowed the animal to also change the distance to the surface of the treadmill during walking. Walking activity was detected by means of walking distance. The walking distance was measured with light barriers that assessed the light shining through a wheel connected to the moving sphere with differently colored (black, gray, or transparent) subdivision. The percentage of measured light gave information about the turning direction and speed when measured over time. A connected Arduino microprocessor sent counted subdivision crosses per time to a computer that analyzed the data. Animals that performed well were later transferred to the VE.

Virtual Environment Experimental Design

To study conditioning in the VE we allowed the animal to walk freely through the VE. Two different training paradigms were used in the VE. Either a color was rewarded (color-only) or a color was rewarded in combination with an odor (color-odor).

The animal was rewarded with 30% sucrose solution in the acquisition phase in both paradigms after arriving at a previously determined color. The colored stripe had to have a particular size and location in front of the animal to be rewarded (rewarding site). When the animal walked toward one stripe, the stripe turned in front of it depending on the rotatory movement of

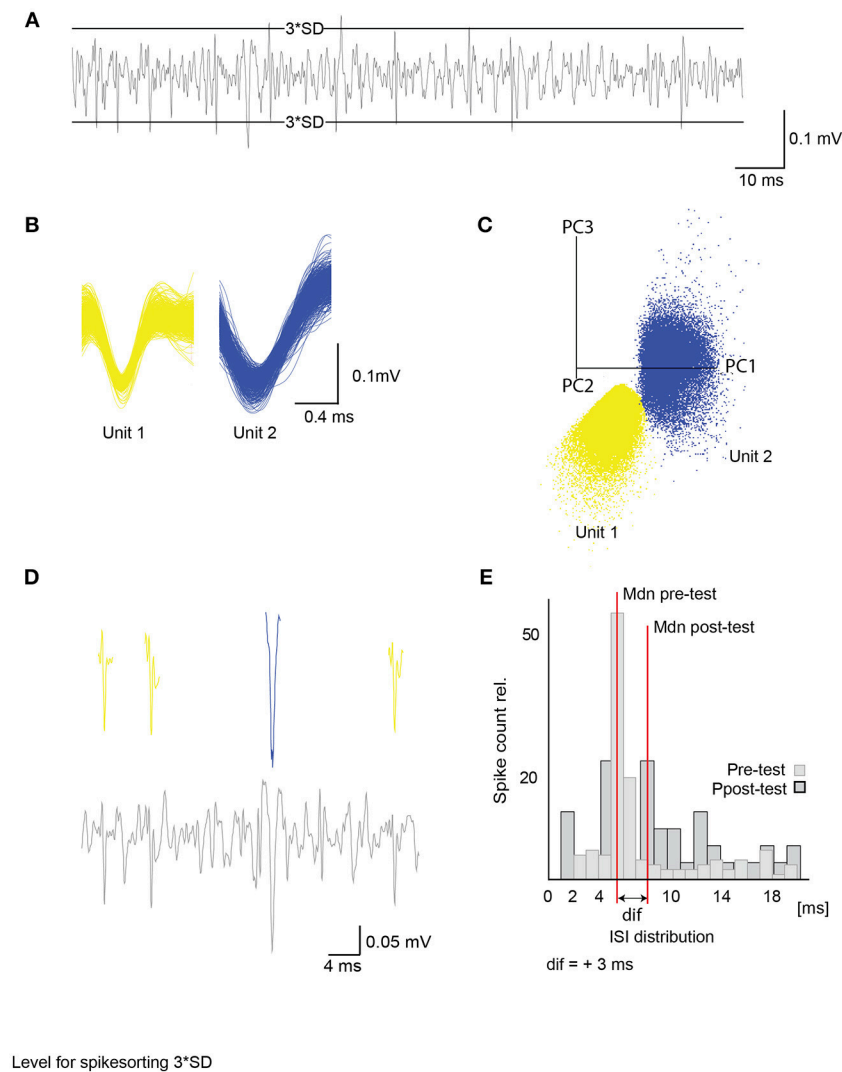


FIGURE 1 | Unit activity extracted from raw data and inter-spoke interval analysis. **(A)** Differential extracellular recording with a 3 times standard deviation (3*SD) level for spike sorting. Only activity crossing the levels was considered in spike detection. **(B)** Example of two single unit waveforms (500 events) with their corresponding principal component analysis. Axes give first 3 principal components **(C)**. **(D)** Example of a filtered extracellular recording channel (lower panel) with detected units from **(B)** (upper panel). **(E)** Example of a single unit inter-spoke interval distribution for 600 ms after stimulus onset with relative spike count and inter-spoke interval in milliseconds (ms). Median (Mdn) depicted in red is used to compare ISI before and after acquisition of single units with a Wilcoxon signed-rank test (see **Figure 9**). ISI, inter-spoke interval; SD, standard deviation.

the spherical treadmill. When it kept walking toward the stripe (translatory movement of the sphere), it got bigger, simulating the object getting closer, and when it reached it, it covered 180° of the screen. Arriving at one color (10 cm walking distance) was counted as a decision. A custom-built rewarding device automatically turned toward the animal. This device consisted of a metal arm with an angle bracket at the end, holding a droplet of sucrose solution. Via Spike2 a digital command was sent to an analog-digital converter that sent a five-volt signal to a rotating motor (XFLY 400, Motraxx, Burghann, Germany) that turned the arm toward the animal, so that it could reach the droplet. The honeybee could lick the sucrose solution for 10 s, either

in combination with an odor or without. Afterwards the arm turned back automatically. Only in the color-odor paradigm, was the odor presented during the rewarded color for 4 s followed by a sucrose reward for 10 s with an overlap of 1 s. The odor was switched on when the animal reached the rewarding site. Spike2 controlled the odor stimulation, marked the time and sent a digital command, which triggered a relay board that in turn controlled the valves for odor stimulation. The odor pulse lasted for 4 s. In both designs, the color was switched off simultaneously with the ending of the reward. The reward lasted for 10 s. When the animal walked toward the unrewarded color (C-) nothing happened, and it could continue walking in the VE until it

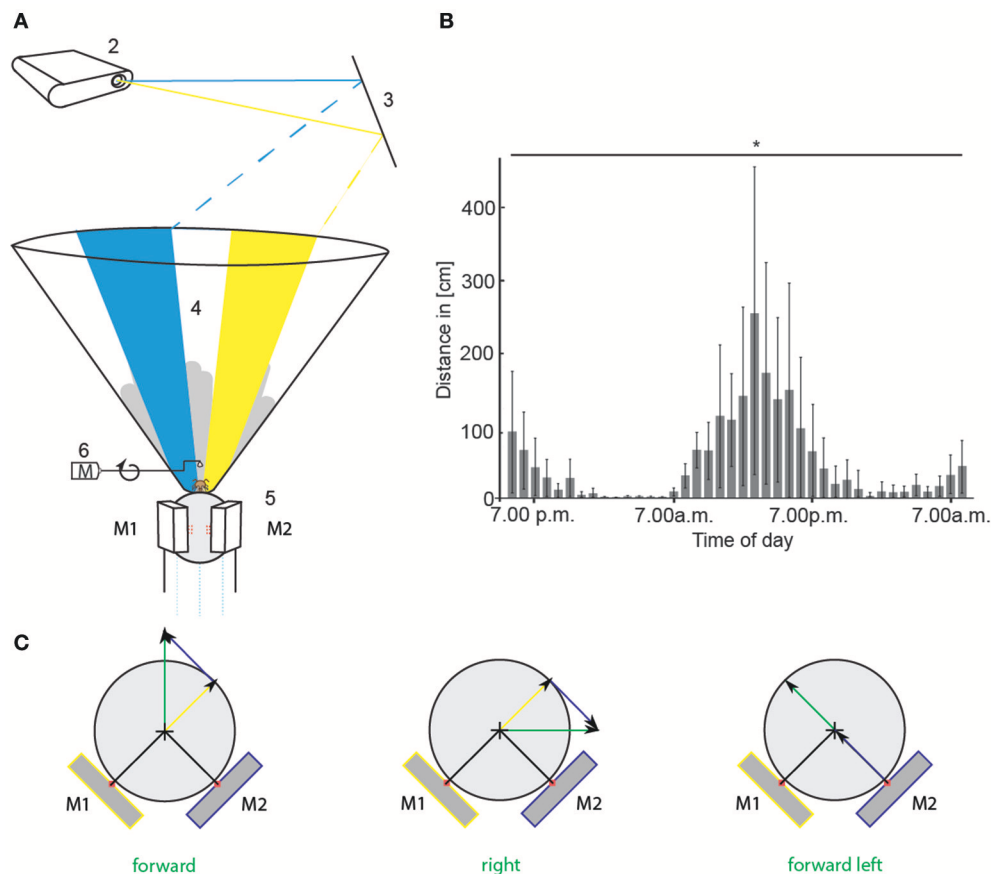


FIGURE 2 | Virtual environment experimental set-up and circadian walking activity. **(A)** A honeybee was placed in the center of the VE set-up and ran on a Styrofoam sphere floating on air (1). An LCD projector (2) projected a scenario consisting of two colored stripes (blue and yellow), and a skyline via a mirror (3) onto the inner surface of cone-shaped screen (4). Two optical mice (5, M1 and M2) recorded the movement of the sphere when the bee walked. The scenario in the VE moved accordingly (closed-loop). The gray skyline in the background moved with different parallaxes than the colored stripes to mimic far-distant objects. A checkerboard projected directly on the sphere in front of the animal moved with the bee's walking speed providing direct visual-motor feedback. The scenario at the starting point of every operant learning trial is shown here. Two colored stripes were present. We call this stimulus color choice (CC). When the animal walked toward one stripe, the stripe moved in front of it. When it kept walking toward the stripe, it got bigger, simulating the object getting closer. Upon reaching it, it covered 180° of the screen. A rewarding device (6) turned toward the animal. It consisted of a metal arm on a motor (M) with an angle bracket at the end, holding a droplet of sucrose solution. **(B)** Circadian walking activity of 16 bees that were held on similar spheres as in the VE for 40 h. Walking distance in cm per 1 h is plotted against daytime. Walking distances differed significantly between the hours [ANOVA, $F_{(39,600)} = 2.3$, $p < 0.0001$]. Bars indicate standard deviation (SD). **(C)** Sketch of translatory input to computer mice (M1, M2) for different walking directions of the bee (green arrow). Depicted are the two mice in yellow and blue and their respective input in yellow and blue. Input of each mouse is used to calculate vectors (yellow and blue arrow) for reconstruction of the bee's walking trajectory (green arrow). VE, virtual environment. Asterisks indicate statistical significance.

reached the rewarded color (C+). If the animals stopped walking for more than 20 min during the experiment, we switched to a different acquisition trial presenting the CS+ color, the odor and the US. All animals received at least eight acquisition trials including one to eight trials actively walking. The inter-trial interval was 10 min. For every animal, at least five trials were successful rewarded trials. Thus, we used the minimum of five trials for comparison between animals.

In a pre-test before the acquisition started, the naïve responses toward the stimuli were tested three times. Five stimuli were presented independently (see also **Figure 5**) in a pseudo-random fashion with an inter-trial interval of 1 min independent of the animal's movement.

The following terminology was used for the various training and test conditions:

- **CC:** We presented a stimulus for 14 s consisting of a blue and a yellow colored stripe. The stimulus was equal to the scenario that was presented at the starting point in every acquisition trial. This was the moment when the bee could walk toward one or the other color. Therefore, we will call this stimulus CC for color choice.
- **C+:** In this situation we showed the rewarded color (C+) alone for 14 s to the animal. In the test situation no reward was presented.
- **C-:** Here we presented the unrewarded color (C-) alone to the honeybee for 14 s. If the animal

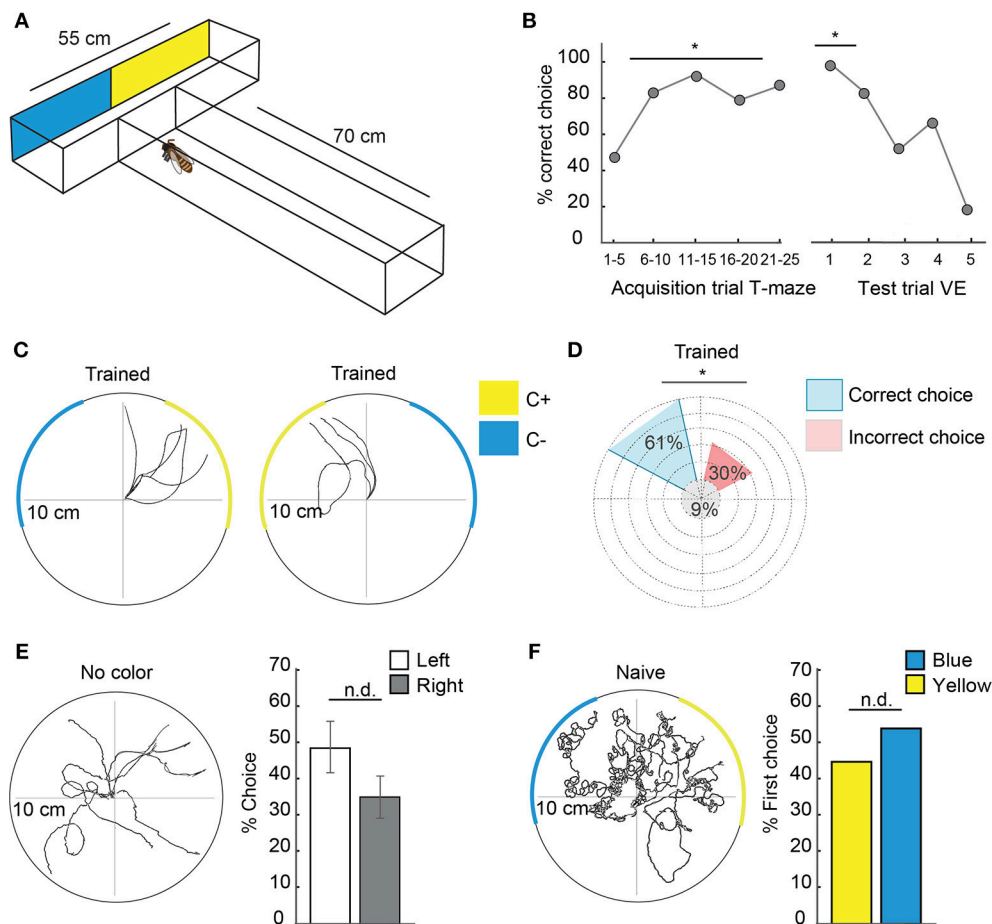


FIGURE 3 | Honeybees transferred learned information from free flight experiments to the virtual environment. **(A)** T-maze experimental set-up for free-flying honeybees. The T-maze consisted of a 70 cm long tunnel, 5 cm in width and 4 cm high with a 55 cm long head side. At the end of the legs, one of the colors (yellow or blue) was rewarded with sucrose whereas the other was punished with potassium chloride solution. Bees flew toward the entrance of the T-maze, walked until the point of decision and decided for one side. Afterwards they flew back to their hive or in case of a wrong decision could enter again. Sides were changed in a pseudo-random fashion to avoid side preferences. After acquisition they were transferred to the VE and were tested in a scenario similar to the T-maze without reward (see also **Figure 2A**). **(B)** Left side: Acquisition curve of correct choices ($N = 6$ animals) in the T-maze with five trials depicted together from trial 1 to 25. 50% of correct choice equals chance. Right side: extinction curve of choices in the VE with the first five tests in the VE. In the VE, the same bees as in A ($N = 6$ animals) were faced with a similar situation to the T-maze and could choose one or the other color by walking toward it. Arriving at one color (10 cm distance) was counted as a decision. Afterwards the scenario was set back to CC and they could choose again. No reward was presented during the test. Sides were changed to avoid side preference dependent choices. In the first trial, all bees chose the previously rewarded color over the unrewarded. The first test trial differed significantly from chance (binomial test $p = 0.015$). **(C)**: Walking trajectories in the VE during representative test situations in a bee trained to yellow in the T-maze. Reaching the rewarded color was counted as correct choice in **(B)**. After 30 s, the colors switched sides. **(D)** Percentage of correct and incorrect choices in the VE with trained colors (yellow or blue) after acquisition in the T-maze pooled for all bees ($N = 6$ animals, $n = 150$ choices). Significantly more choices were delivered to the previous C+ over the C- (binomial test $p = 0.0001$). **(E)** Walking trajectories of a bee trained in the T-maze in a VE scenario without colored stripes but with skyline and checkerboard. Comparison of percentage choices for left and right in the VE shows no significant side differences ($N = 6$, $n = 114$ choices, Two one-sided t -test, $p = 0.03$). **(F)** Walking trajectories of naive bees in a scenario with colored stripes, skyline, and checkerboard. No preferences for one of the colors was found (Two one-sided t -test, $p = 0.018$, $N = 12$ animals, $n = 12$ choices). VE, virtual environment. Asterisks indicate statistical significance.

approached this color it experienced “no reward.” This happened both during acquisition and during the test.

- **US:** Additionally, we presented the sucrose reward alone (US) three times for 10 s to the animal.
- **O:** We presented the odor alone (O) three times in the pre-test for 4 s.

During training, the odor was only present when the animal approached the rewarded color. The odor was paired with the sucrose reward for 1 s.

In a memory test on the day after the acquisition (post-test), all color stimuli (CC, C+, and C-), the reward alone (US) and the odor alone (O) were presented to the honeybee again. This remained the only test situation in the experiment.

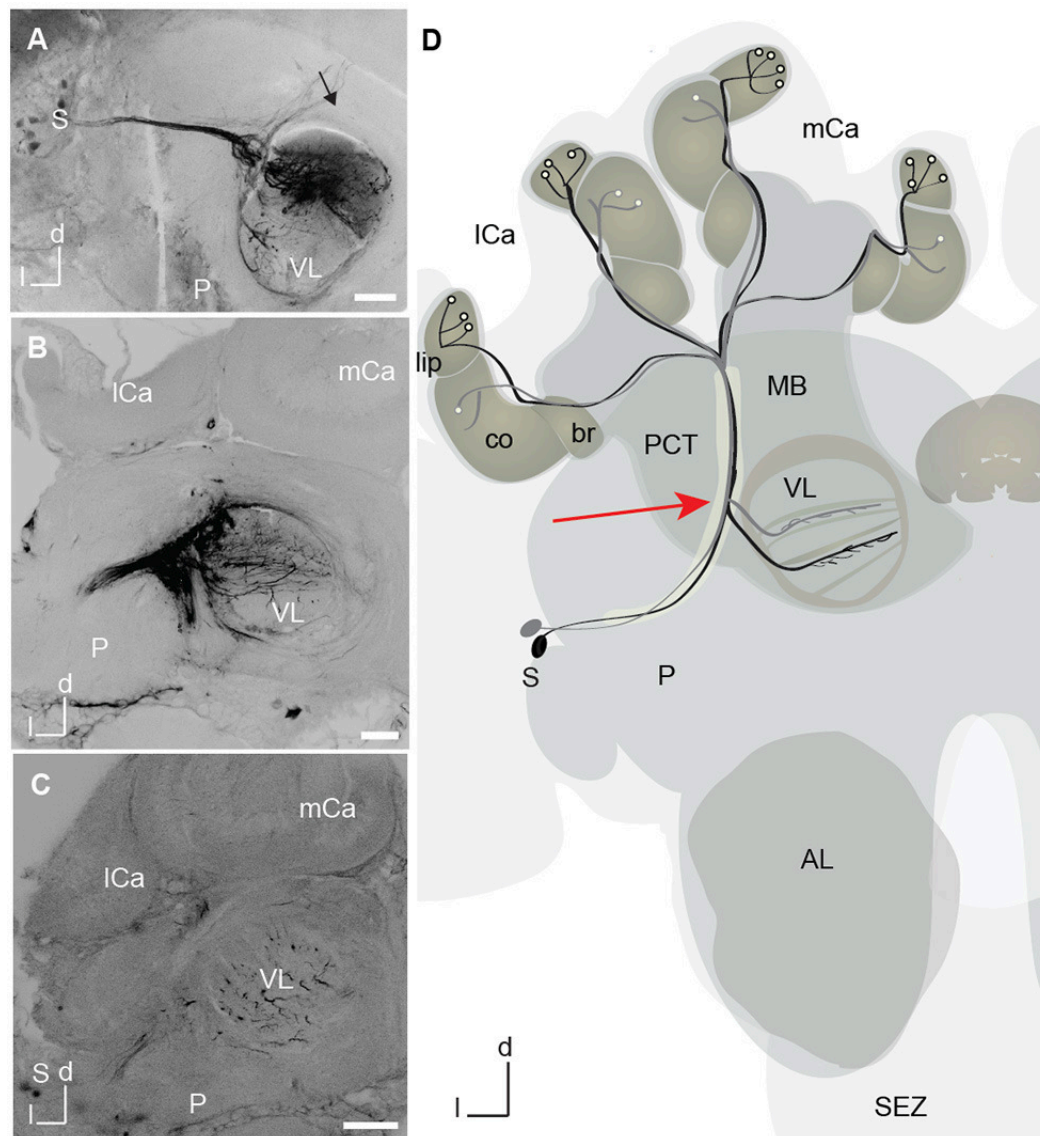


FIGURE 4 | A3 mushroom body extrinsic neurons marked with dye at the tip of the recording electrode. **(A)** Projection view of a mass-fill of A3 dorsal neurons after electrode injection with MicroRuby on the tip of the electrode. Tracts of the dorsal somata cluster and the horizontal layers in the vertical lobe (VL) are visible. Axons project toward the calyx in the protocerebral calyx tract (PCT, black arrow) revealing A3 neurons. **(B)** Projection view of a different mass-fill of A3 neurons after electrode injection with MicroRuby on the tip of the electrode. Again, tracts of A3 dorsal (d) neurons are visible together with a horizontal layer in the VL. **(C)** Projection view of a mass fill of A3d neurons with arborizations in the VL. **(D)** Schematic drawing of two different innervation types of A3 feedback neurons. In black A3 neuron connecting lip and corresponding layer in the VL, in gray A3 connecting collar and corresponding layer in the VL. A3 neurons were also found to connect the basal ring and the corresponding basal ring layer in the VL. All types connect to the medial lobe. Another class-A3 lobe connecting neurons—do not innervate the calyx (not shown) (Zwaka et al., 2018). The red arrow points to the recording site. AL, antennal lobes; br, basal ring; CB, central body; co, collar; d, dorsal; P, protocerebrum; I, lateral; ICa, lateral calyx; MB, mushroom bodies; mCa, medial calyx; PCT, proto cerebral calyx tract; SEZ, subesophageal zone; S, Soma; VL, vertical lobe.

Learning Performance in the VE During Extracellular Recording

The behavioral response evaluated as a measure of learning was the approach to the rewarded color or color/odor combination. The time until the animal reached the rewarded color was the measure of the learning effect (**Figure 6A**). As not all animals received five operant acquisition trials, we excluded one animal from the analysis.

Electrophysiology Extracellular Recording

For extracellular recordings, custom-made tetrodes consisting of four polyurethane-insulated copper wires were used (15 μ m diameter, Elektrisola, Germany). The wires were twisted and glued together with superglue or by short exposure to 210°C. The tips were cut and electroplated, reducing the impedance to 80–150 k Ω (Ferguson et al.,

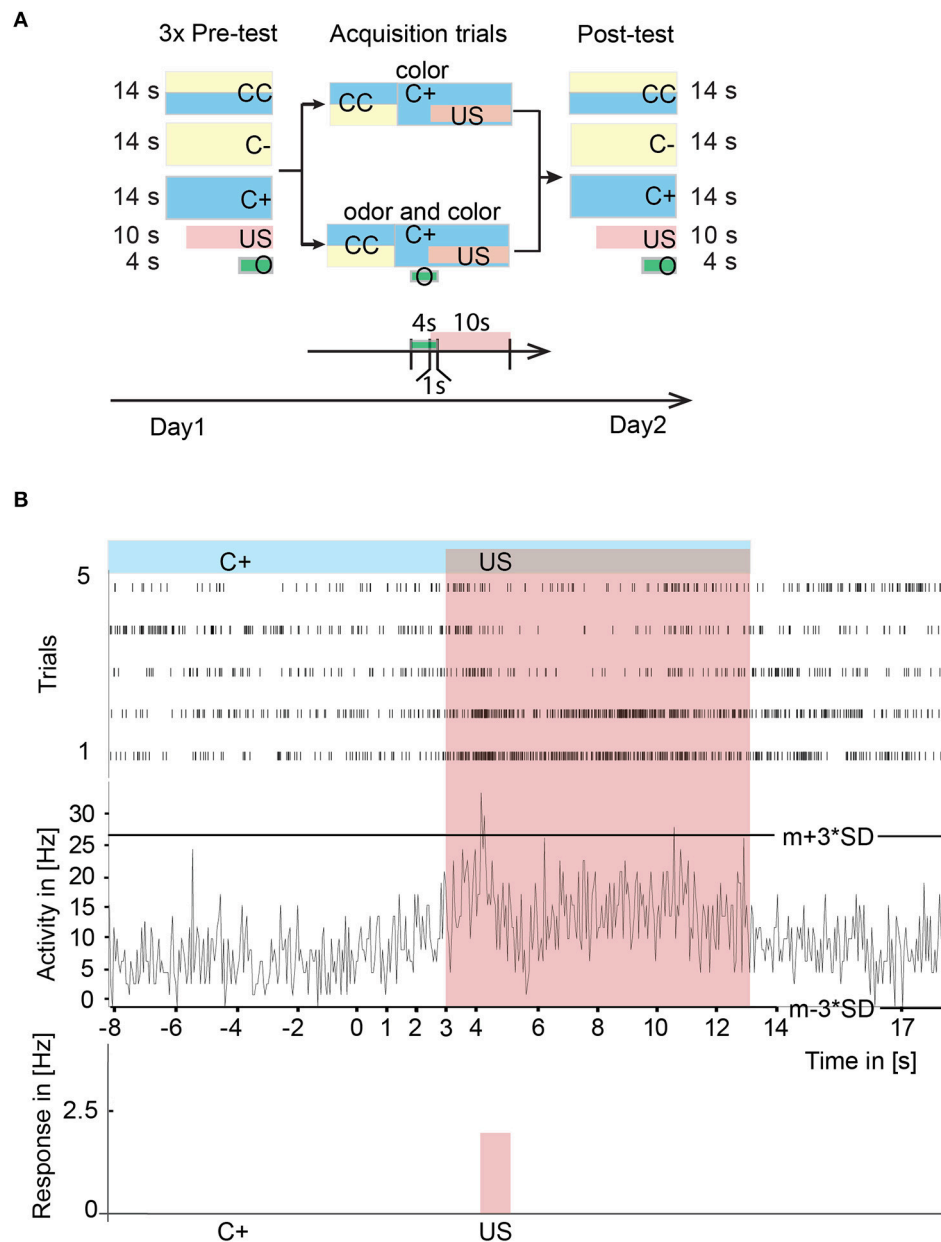
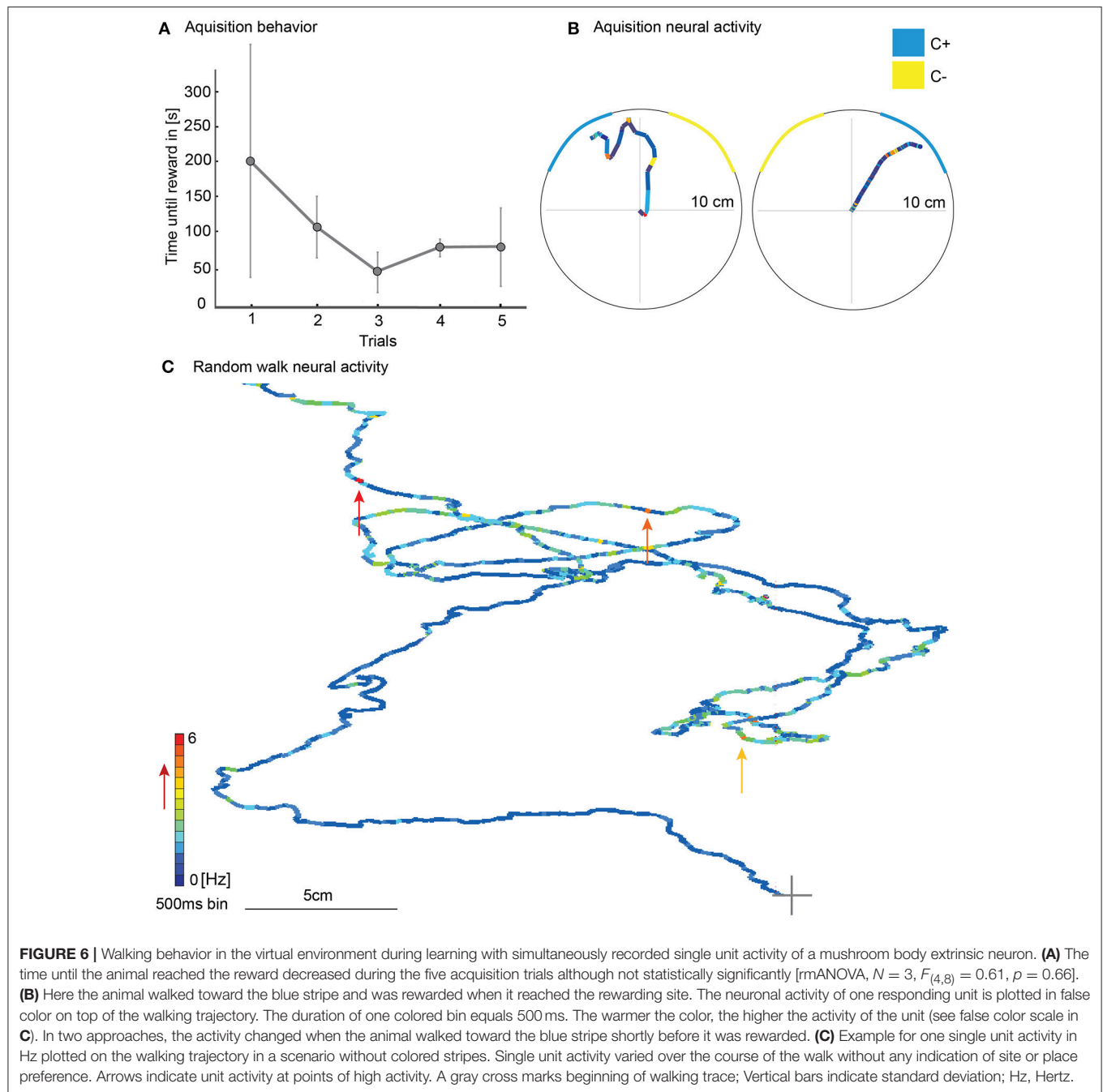


FIGURE 5 | Experimental paradigms and neural correlates of A3 neurons of stimuli during learning in the virtual environment. **(A)** Experimental design for operant learning in the VE. On the first day in a pre-test, we presented a scenario with two colored stripes (CC) and two scenarios with only one color (C+, C-), each three times in a pseudo-random fashion for 14 s with an inter trial interval of 1 min. Additionally, we presented the sucrose reward (US) three times alone. In experiments with odor presentation in the VE, we additionally tested an odor three times for 4 s in the pre-test. During acquisition, the animal could walk freely in the VE with two stripes (CC) one of which (C+) was rewarded and one was unrewarded (C-). After reaching C+, in the color-only paradigm the US was presented to the animal for 10 s. Afterwards, the C+ was switched off simultaneously with the US. In the color-odor paradigm, a 4 s lasting odor and subsequently the US was presented after reaching C+. In the post-test situation on the day after the acquisition, CC, C+, C-, the US, and the odor were presented to the honeybee again. **(B)** Peri-stimulus time histogram over five acquisition trials of single unit activity in the upper panel and mean trial activity in the middle panel. Activity exceeding a three-standard deviation plus mean threshold ($m+3*SD$) or falling below $m-3*SD$ threshold was noted as a response to the stimulus. The sum of the responses was divided by the duration of the stimulus and noted as a significant response in Hz (lower panel). Here, a significant increase in response to the US has been detected. CC, rewarded and unrewarded colored stripes; C+, rewarded color; C-, unrewarded color; O, conditioned stimulus (odor); US, unconditioned stimulus (reward); VE, virtual environment.

2009) (Redish Lab, University of Minnesota) using the electroplating device NanoZ (Neuralynx, Bozeman, Montana).

Preparation of the Animals

A small piece of copier transparency film was fixed with dental wax on the thorax as a holder for the stationary



running animal on the treadmill. Dissection started by opening the head capsule. Bee Ringer [NaCl (130 mM), KCl (6 mM), MgCl_2 (4 mM), CaCl_2 (5 mM), glucose (25 mM), sucrose (170 mM, pH 6.7)] was applied to the brain when necessary to avoid drying of the brain surface. The tip of the electrode was dipped in a 5% tetramethylrhodamine-biotin solution (TMR, Microruby, MoBiTec, Göttingen, Germany) in 0.2 and 1 M potassium acetate. After recording, the recording site was verified in the dissected brain. Only animals with recordings from the desired recording site were admitted to the analysis.

The tip of the electrode was mounted on an external micromanipulator as described in Duer et al. (2015). The electrodes were inserted at the rim of the vertical lobe at a depth of 40–100 μm , where A3 neurons bifurcate and enter the vertical lobe. A silver-wire reference was coiled with the electrode, bent as a hook, and placed gently on the brain surface. After placing the electrodes in the selected brain area (ventral aspect of the mushroom body) under visual control, the electrode was fixed with non-toxic two-component silicon (kwik-sil, WPI, Sarasota) in the brain. After hardening of the kwik-sil, the electrode was released from the micromanipulator and the bee was transferred

to the virtual environment set-up and carefully adjusted on the floating sphere. The electrode holder consisted of a small balance that kept the animal on the treadmill with its own weight. This balance also allowed the animal to change the distance to the surface of the treadmill during walking. The direct light from the LCD projector was shaded to prevent direct illumination of the dorsal regions of the compound eye and the ocelli. A manipulator made it possible to precisely center the animal on the spherical treadmill.

Analysis

Only animals that completed the whole experiment including pre-test and acquisition on the first day and a memory post-test on the second day were analyzed.

Single unit activity in extracellular recordings is not equivalent to neuronal activity as for example from single cells in intracellular recordings. In such an analysis, false-positive spikes might be detected, as there is always a potential risk of misclassification. False-positive errors are events that are wrongly classified and belong for example to a different cell. Contrarily false-negative errors are events that are misclassified as noise. Thus not all spikes from one cell are in one group (Harris et al., 2000; Joshua et al., 2007). However, automatic or semi-automatic spike sorting algorithms as used in this study reduce these errors close to an optimum between 0 and 8% (Harris et al., 2000).

The data acquisition-and-analysis software Spike2 was used for the semi-automated template-matching spike sorting. All channels were recorded at a sampling rate of 20,000 Hz and low-pass filtered. One channel was differentially recorded from two electrodes, and two channels were single-ended electrodes. Before analysis, the data was filtered with a band-pass FIR-filter (350–2,500 Hz). The channel with the best signal-to-noise ratio was used for further analysis. Subsequently, the mean activity and standard deviation (SD) were calculated and used as a threshold for computing templates. Only events that either exceeded three SD or dropped below three SD were used for template matching (Figure 1A). In addition to this restrain, after sorting, all results were visually controlled for sorting quality and additionally checked by the first three components of each unit using a principal component analysis (PCA) provided by Spike2 (Figures 1B,C, Figure S1). Sorting results were improved using the K-means clustering approach provided by Spike2. Units that were present at the beginning of the experiment but decreased drastically until vanishing in the following 16 h were excluded from further analysis.

To identify rate changes to a stimulus in single unit activity we constructed peri-stimulus time histograms from all trials using a bin size of 50 ms. Afterwards we calculated the mean and the standard deviation (SD) from 20 s before stimulus onset. Rate changes that either exceeded the mean plus three times SD or dropped below the mean minus three times SD were considered an effect (Strube-Bloss et al., 2011).

In addition to changes in unit activity to the stimulus, we compared activity of single units in pre-tests, training, and 16 h tests. Thus, we analyzed changes in spike firing

rates (SFR) from pre-test to acquisition and from pre-test to test toward the tested stimuli (Figures 9A,B). We calculated the Δ SFR using the activity extracted from the analysis for single unit changes toward the stimulus (compare Figure 5) exceeding the $3 \times \text{SD}$ threshold in the PSTHs. The spike activity was normalized by taking the ratio between stimuli response in pre-test and training or pre-test and test. Thus, we defined Δ SFR as the change in spike firing rate from e.g., pre-test to test toward a stimulus divided by total response:

$$\Delta \text{SFR} = \frac{\text{SFR}_{\text{test}} - \text{SFR}_{\text{pre}}}{\text{SFR}_{\text{test}} + \text{SFR}_{\text{pre}}}$$

A positive Δ SFR means an increase in neuronal firing, a negative Δ SFR means decreased neuronal firing, and Δ SFR of 0 means no change in neuronal firing due to the stimulus (Hussaini and Menzel, 2013). Δ SFR was calculated for every single unit. Δ SFRs of all units were analyzed together. We performed a Wilcoxon signed-rank test against a hypothetical change of zero.

To detect subtle excitatory or inhibitory rate changes that extend over several 100 ms to a stimulus, we compared the inter-spike interval (ISI) in the pre-test in a response window of 600 ms after stimulus onset- to the ISI in the post-test in a response window of 600 ms after stimulus (Figure 1D). The same was done during acquisition from stimulus to stimulus to search for ISI changes. We tested for significant differences in the median of the ISI distributions in all trials using a Wilcoxon signed-rank test. These approaches were adapted from an analysis of MB extrinsic neurons in Strube-Bloss et al. (2011). For depiction of the change, we subtracted the median ISI in the post-test from the median ISI in the pre-test for every single unit.

Histochemistry

Brains were fixed with 4% paraformaldehyde (PFA, Roth, Karlsruhe, Germany) or a mixture of 1.3% PFA and 0.7% glutaraldehyde (GA, Sigma-Aldrich, Munich, Germany) for at least 4 h. Subsequently, brains were washed three times in phosphate buffered saline [PBS; NaCl (37 mM), KCl (2.7 mM), Na_2HPO_4 (8 mM), KH_2PO_4 (1.4 mM), pH 7.2] for 10 min each, dehydrated in an ascending alcohol series (50, 70, 90, 99, and 100% each 10 min), cleared in methylsalicylate (Roth, Karlsruhe, Germany) for 10 min, and mounted on a special object slide (a metal plate of 0.5 mm thickness with a central hole and cover slips on both sides) in methylsalicylate.

Confocal Imaging

Confocal image stacks of the whole brains were acquired using a confocal laser scanning microscope (Leica TCS SP2, Wetzlar, Germany) using a 40×0.4 IMM lens objective or a 20×0.5 water lens objective. Per stack, around 400 sections were scanned with a resolution of 1024×1024 voxels each, and with a voxel size of $0.61 \times 0.61 \times 1.3 \mu\text{m}$ or $0.73 \times 0.73 \times 1.1 \mu\text{m}$. Stained neurons were scanned at 633 nm. Linear intensity compensation was used to adjust differences in brightness depending on scanning-depth.

Statistics

For statistical analysis of multiple comparison, a Wilcoxon signed-rank test was performed (Statistica version 8.0, StatSoft, Inc., Tulsa, OK, USA). For normally distributed data, a two-way ANOVA was used to analyze the interaction between two variables (Statistica version 8.0, StatSoft, Inc., Tulsa, OK, USA) with an additional Fisher LSD *post-hoc* test. For comparison of nominal paired data, a McNemar test was performed (R Core Team, 2017) as well as a binomial test. A two one-sided *t*-test (TOST) for equivalence was performed in (R Core Team, 2017) using the equivalence package for a paired sample with epsilon for small sample size = difference in standard deviations. In all tests, differences were considered significant if $p \leq 0.05$.

Terminology

The terms used to describe structural components of the honeybee brain have been adapted according to the nomenclature system of the Insect Brain Name Working Group (Ito et al., 2014).

RESULTS

The Virtual Environment

The virtual environment (VE) simulated a simplified 3D world for a honeybee walking stationary at the center of an air-supported spherical treadmill (**Figure 2A**). An LCD projector projected the visual patterns from above via a mirror into the inner surface of a cone. The distortion of the patterns caused by the projection on the inner surface of the cone were compensated for by the design of projected patterns. The depth components were simulated by occlusion, size, and motion parallax. The rotatory and translatory movements of the treadmill were translated into respective changes of the visual patterns. Different scenarios were written in a custom program implemented in Java by using OpenGL-Bindings for Java (LWJGL). We used a simple set of stimuli consisting of two colored stripes (blue and yellow) appearing in front of a structured gray skyline in the background, which moved with different parallaxes mimicking far-distant objects. To simulate the movement with the bee's actual walking speed, the animal walked on a checkerboard pattern projected directly onto the sphere in front of it, thus providing a direct visual-motor feedback by the ground over which the animals walked. Two optical mice recorded the movement of the sphere. To adapt to the walking situation, the experimental animals were held on similar spherical treadmills during the night. Animals on the spherical treadmills showed circadian activity (**Figure 2B**). All data reported here came from experiments at times of the day at which free-flying honeybees usually performed foraging behavior and accordingly the highest activity on the treadmill.

Animals Transferred Learned Behavior From Free Flight to the Virtual Environment

To analyze whether animals perceived the visual stimuli in the VE and recognized them as meaningful stimuli, we performed a transfer experiment. Free-flying bees were trained to enter a T-maze (**Figure 3A**) in which they ran toward a T-junction with two differently colored legs. Approaching one color was rewarded

with sucrose and approaching the other color was punished with potassium chloride solution. After leaving the T-maze, they flew back to their hive or -in case of a wrong decision- could enter again. To avoid side preferences, we switched the sides of reward and no-reward in a pseudo-random fashion. Subsequently the animals were transferred to the VE and tested in a scenario similar to that in the T-maze (**Video S1**). Here, no reward was presented. The acquisition curve of correct choices in the T-maze shows that the honeybees learned to make the correct turn toward the rewarded color (C+) and discriminated it from the unrewarded color (C-, **Figure 3B**, from trial 5 onwards: binomial test $p < 0.01$). After the transfer into the VE, the same bees were faced with a similar situation as in the T-maze (**Figure 3A**). They could choose between the two colors that they had discriminated in the T-maze by walking toward one of them. At the starting point of the test two colored stripes were presented, similar to the point of decision in the T-maze experiments. Here and in the following experiments this stimulus situation is called color choice (CC). When the animal walked toward one stripe, the stripe moved toward it by increasing its visual angle in front of it simulating the object to get closer. When the animal reached it, the color covered 180° of the screen. Arriving at one color (10 cm walking distance) was counted as a decision. Afterwards the scenario was set back to CC and the animal could choose again (**Figure 3C**). To avoid side preferences, the sides of the colors were changed every 30 s. Each animal ($N = 6$) was tested for 5 min. In the first trial, all bees chose the previous C+ over the C- (**Figure 3B**, binomial test $p = 0.015$). Significantly more decisions were made for C+ in all decisions (**Figure 3D**, $N = 6$ animals, $n = 150$ choices, binomial test $p = 0.0001$). A comparison of the percentage of choices demonstrates that there was no side preferences for left or right in the VE without colored stripes present [**Figure 3E**, $N = 6$ animals, $n = 114$ choices, two one-sided *t*-test (TOST), $p = 0.03$, TOST test analyzes data for equivalence (Walker and Nowacki, 2011)]. Naïve bees introduced into the VE for the first time showed no difference in choosing between blue and yellow (**Figure 3F**, $N = 12$ animals, $n = 12$ choices, TOST test, $p = 0.018$).

Neuronal Recordings During Learning in the Virtual Environment

The search for neural correlates of learning in a VE requires the combination of stable recording from central neurons and free movement of an animal. We performed 24-h lasting extracellular recordings from the area where A3 mushroom body extrinsic neurons bifurcate (**Figure 4**). The recording site could be well selected visually by placing the recording electrodes at the lateral rim of the vertical lobe (red arrow in **Figure 4D**). After the experiment, the recording site was verified by dye marking via the tip of the recording electrode (**Figures 4A–C**).

To study operant learning in the VE we allowed the animal to walk freely through the VE. Two different training paradigms were used in the VE: Either only a color was rewarded (color-only) or the rewarded color was paired with an odor (color-odor, **Figure 5A**). Each bee was trained only in one paradigm. At the beginning of each acquisition trial, two colored stripes

were presented and the bee walked toward one of the two colors such that it reached a particular size and location in front of the animal. This size and location equaled 10 cm walking distance from the starting point toward the center of the stripe thus covering 180° of the screen (rewarding site). After arriving at a previously determined color (blue or yellow, randomly selected by the experimenter), the animal was rewarded with 30% sucrose solution (rewarded color, C+). When this situation was reached a rewarding device turned toward the animal, and the animal could lick the sucrose solution for 10 s. Sides were switched to distinguish between side and color effects on unit activity.

Single unit activity was analyzed (for sorting procedure see **Figure 1**) in peri-stimulus time histograms with a bin size of 50 ms in all trials (**Figure 5B**). Activity exceeding the mean plus three standard deviations (from activity before stimulus onset) threshold ($m+3*SD$) or falling below $m-3*SD$ threshold was noted as an excitatory or inhibitory response to the stimulus, respectively. The response strength in Hz to the stimulus was calculated with the sum of the unit's activity divided by the duration of the particular stimulus in seconds.

We performed pre-tests to get the neural responses of the respective naïve animal toward the stimuli that were tested in a pseudo-random fashion before operant training started: (1) both a blue and a yellow stripe (CC) for 14 s. In this moment, the bee could walk toward the C+ or C- (called CC for color choice), (2) C+ (later the to be rewarded color) alone for 14 s, (3) C- (later the not to be rewarded color) alone for 14 s, (4) US three times for 10 s each. (5) In the color-odor paradigm, we additionally tested the odor three times in the pre-test for 4 s.

In a memory test on the day after acquisition (post-test), all color stimuli (CC, C+, and C-), the US, and the odor were presented again, separately. This remained the only extinction tests in the experiment.

Comparing all bees, there were only two points in time that were fixed: The time the color was switched on and the time the reward was delivered. Therefore, we analyzed the neural activity when C+, C-, or CC was switched on, during the time the animal had arrived at C+ shortly before the reward (US) was switched on, and during the US. We compared the activity of the single units to the stimuli prior to acquisition (pre-test), during acquisition (acquisition) and in a memory test after acquisition (post-test) without a reward. No significant inhibitory responses were determined, most likely due to the rather low spike activity and the high criterion for the significant test (mean minus three standard deviation). Only animals that received all pre-tests, acquisition trials and post-test with a stable extracellular recording over two consecutive days were analyzed ($N = 29$ Units).

During the five acquisition trials of the color-only training, the mean of the time until the animals reached the reward decreased although not significantly [**Figure 6A**, $N = 3$; rmANOVA, $N = 3$, $F_{(4,8)} = 0.61$, $p = 0.66$]. Walking traces from acquisition trials with corresponding unit activity showed changes in neural activity (**Figure 6B**). During random walk without any colored stripes in the VE, the single unit activity varied over the course of the walk and showed no indication of a place preference (**Figure 6C**).

Response Rate Changes to the Rewarded Stimuli During Learning Color-Only Experiments

Twelve units were recorded while the bees were trained in the VE to approach one of two colors (blue or yellow) that was subsequently rewarded. Almost all units changed their responses during the experiment with both an increase in the number of responding units and an increase in the spike frequency to C+ (**Figure 7**). First, we analyzed the changes in the number of units responding to the stimuli during the pre-test and the post-test and found higher response activity for the C+ (**Figure 7A**, McNemar test, $p = 0.04$). Such a global analysis may, however, not uncover learning-related plasticity in single units due to opposing changes, e.g., units being recruited or units dropping out. Recruitment in this case relates to a neuron, which had not responded to the stimulus before and started to respond after acquisition or in the test (after memory formation). Likewise, a neuron that responded to a stimulus before acquisition and did not respond in the acquisition or post-test situation anymore is regarded as dropping out. An analysis revealed that single units were recruited and dropped (**Figure 7B**).

When we compared responses to all stimuli (CC, C+, and C-) during pre-test and post-test (**Figure 7C**), we found that in sum 10 out of 12 units (Units 1, 2, 3, 4, 6, 7, 8, 9, 10, 12) respond to at least one more stimulus (CC, C+, and C-) after learning in the post-test than in the pre-test. One unit gained a response to the US (Unit 5).

Color-Odor Experiments

Sixteen units were recorded while the bees were trained in the VE to approach one of two colors (blue or yellow) that was subsequently paired with an odor and the reward (compare **Figure 5**). As in the previous experiment, we compared the activity of the single units to the stimuli prior to acquisition (pre-test), during acquisition (acquisition) and in a memory test after acquisition on the next day (post-test) without a reward. In these color-odor experiments, we additionally analyzed the activity during the odor presentation. We hypothesize that the odor stimulus preceding the reward may become salient and thus indicative in uncovering learning-related plasticity.

When we compared the pre-test to the post-test no significant changes were found in the percentage of responding units (McNemar test > 0.05 , **Figure 8A**). However, analyzing the percentage of units that changed their responses to the stimuli revealed that an equal number of units was recruited and dropped out. More units were recruited than dropped during C- stimulation. These changes are not significant (**Figure 8B**, McNemar test $p > 0.05$). During acquisition, only two units (Units 13, 18) responded to the C+. Comparing responses to stimuli during post-test and pre-test (**Figure 8C**) showed that nine units (Units 13, 14, 17, 20, 21, 23, 24, 25, 26) responded to at least one more stimulus in the post-test than in the pre-test, whereas six lowered their response activity to stimuli (Units 15, 16, 18, 19, 22, 27). Two units did not change their responses (Units 28 and 29).

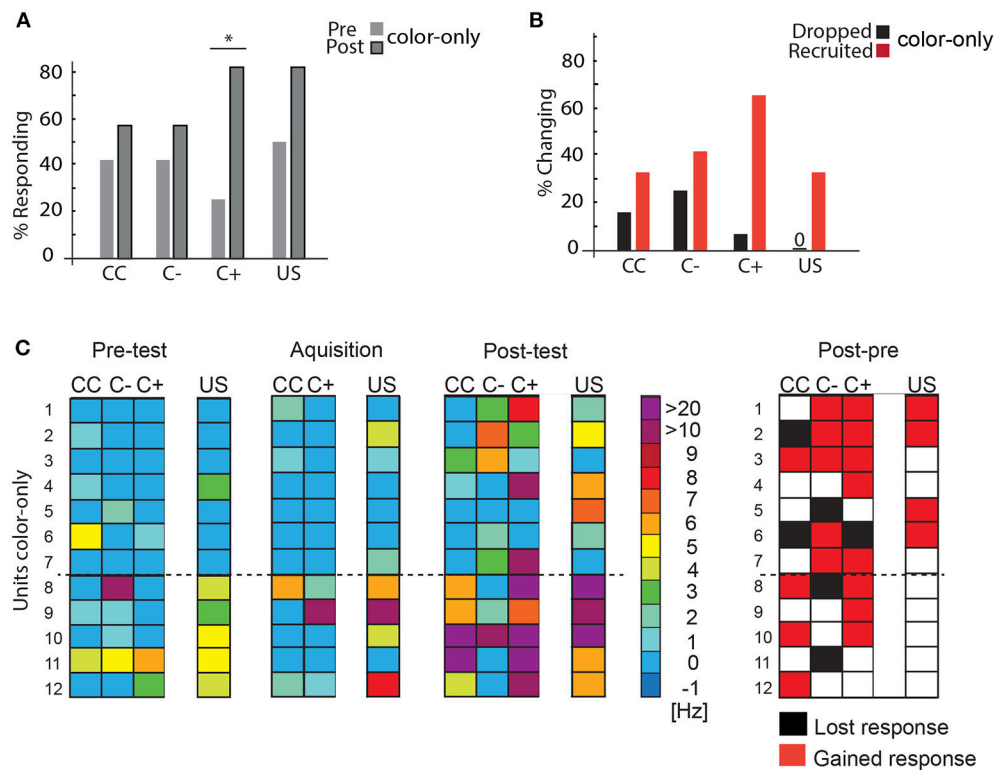


FIGURE 7 | Learning-related plasticity during the color-only paradigm. **(A)** Percentage of responding units to the C+ increased significantly from the pre-test to the post-test (McNemar test, $p = 0.04$). **(B)** Percentage of changing responses categorized as being recruited and dropping out as measured for the different stimulus conditions. **(C)** Left side: Single unit responses in the pre-test, during acquisition and in the post-test for the different stimulus conditions. Excitatory responses are marked in warm colors. The warmer the color, the higher the change in the respective activity. No change in activity compared to before is marked in blue. No inhibitory responses were found during the analysis most likely due to the rather low spike activity and the high criterion for the significant test (mean minus three standard deviation) ($N = 12$). The single unit activity changed from the pre-test to the post-test and during the acquisition. Right side: Summary of recruited or dropped units after learning. Here, dropped and recruited refers to post-test compared to the pre-test for all stimuli. Black indicates that the unit responded less to the respective stimulus in the post-test than in the pre-test, red indicates that the unit responded more than in the pre-test, white indicates no change; US, unconditioned stimulus (reward). CC, response during the color choice with both colors blue and yellow present; C+, response to the rewarded color; C-, response to the unrewarded color; US, response to the sucrose reward. Asterisks indicate statistical significance.

Spike Rates Change of Units During Learning

After analyzing the changes in the absolute number of units responding to the stimuli, we next analyzed the changes in spike firing rates (SFR) to the respective stimuli. Even though the absolute number of units responding might not be different, this analysis helps us detect an increase or a decrease in firing rate to a stimulus. We compared the conditions during the pre-tests with those during acquisition, and during the pre-tests with those during the post-test for all tested stimuli. We calculated the Δ SFR using the changes of spike rates during stimulation as compared to the spontaneous spike rate 20 s before, including only those data in which the changes exceeded the $3 \times \text{SD}$ threshold in the PSTHs. The spike activity was normalized by taking the ratio between stimuli response in pre-test and training or pre-training and test (see Experimental Procedures). Thus, Δ SFR defines the change in spike firing rate from e.g., pre-test to test toward a stimulus divided by total response. A positive Δ SFR indicates an increase in firing rate, a negative Δ SFR a decrease, and Δ SFR of

0 indicates no change (Hussaini and Menzel, 2013). Δ SFRs of all units were analyzed together applying the Wilcoxon signed-rank test against a hypothetical change of zero. Again, we shall deal with the color-only paradigm first and then with the color-odor paradigm.

Firing rate decreased significantly for US during color-only training (Figure 9A, training as compared to pre-test, Wilcoxon signed-rank test, $N = 12$, US: $p = 0.04$) but increased during the test (Figure 9A, Wilcoxon signed-rank test, $N = 12$, $p < 0.0001$). Similarly firing rate increased significantly to both the rewarded and unrewarded color (Figure 9B, Wilcoxon signed-rank test, $N = 12$, C-: $p = 0.02$, C+: $p = 0.04$). A significant increase was found for the rewarded odor (Wilcoxon signed-rank test, $N = 17$, O+: $p < 0.00046$) during color-odor training but not for the rewarded color (C+). The post-tests revealed a significant increase in firing rate for the non-rewarded color C- (Wilcoxon signed-rank test, $N = 17$, C-: $p = 0.016$). Again, a very different pattern of learning-related plasticity was found between the two paradigms, color-only and color-odor. These

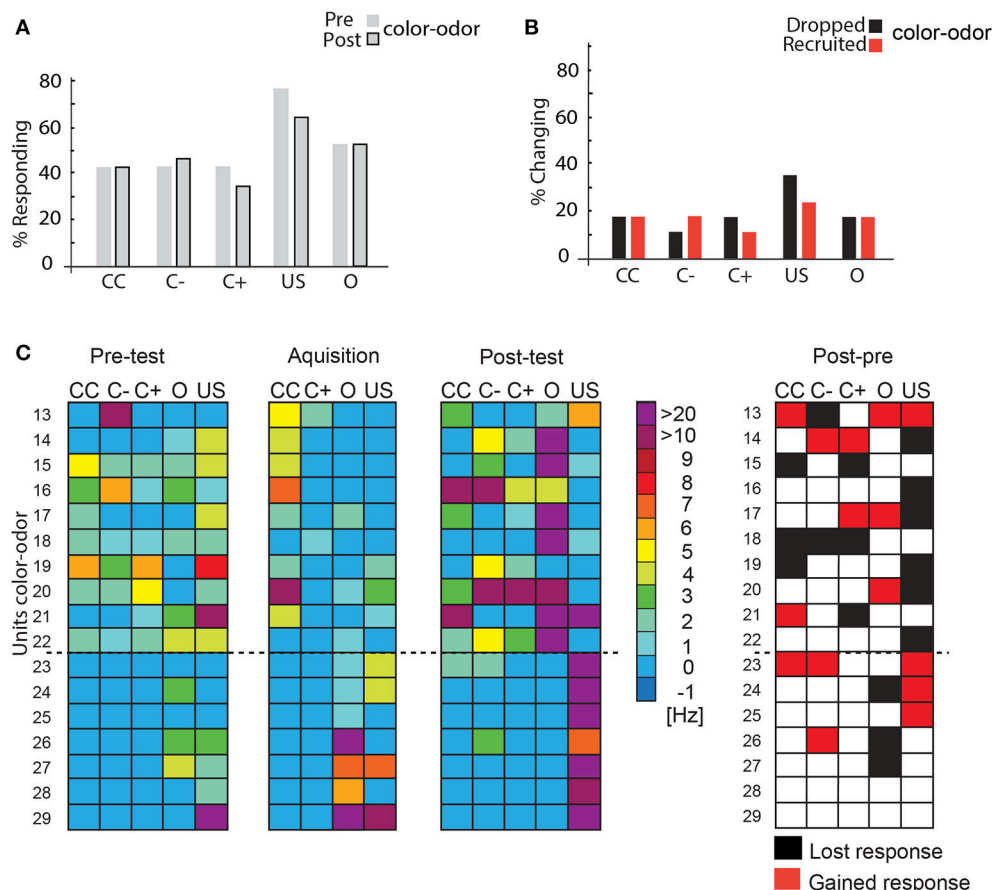


FIGURE 8 | Learning-related plasticity during the color-odor paradigm. **(A)** No significant changes occurred in the percentage of responding units from the pre- test to the post- test (McNemar test, $p > 0.5$). **(B)** Percentage of changing responses categorized as being recruited and dropping out as measured for the different stimulus conditions. **(C)** Left side: Single unit response in the pre- test, during the acquisition and in the post- test for the different stimulus conditions. Excitatory responses are marked in warm colors. The warmer the color, the higher the change in the respective activity. No change in activity compared to before is marked in blue. No inhibitory responses were found during the analysis most likely due to the rather low spike activity and the high criterion for the significant test (mean minus three standard deviation) $N = 17$. Right side: Summary of recruited or dropped units after learning. Here, dropped and recruited refers to post- test compared to the pre- test. Black indicates that the unit responded less to the respective stimulus in the post- test than in the pre- test, red indicates that the unit responded more than in the pre- test, white indicates no change; US, unconditioned stimulus (reward). Only two units did not change their responses (number 28 and 29). CC, response during the color choice with both colors blue and yellow present; C+, response to the rewarded color; C-, response to the unrewarded color; US, response to the sucrose reward.

results indicate changes in spike firing to the stimuli in the range of short-term memory (training) but also changes in neuronal activity that persist until the next day (post-test).

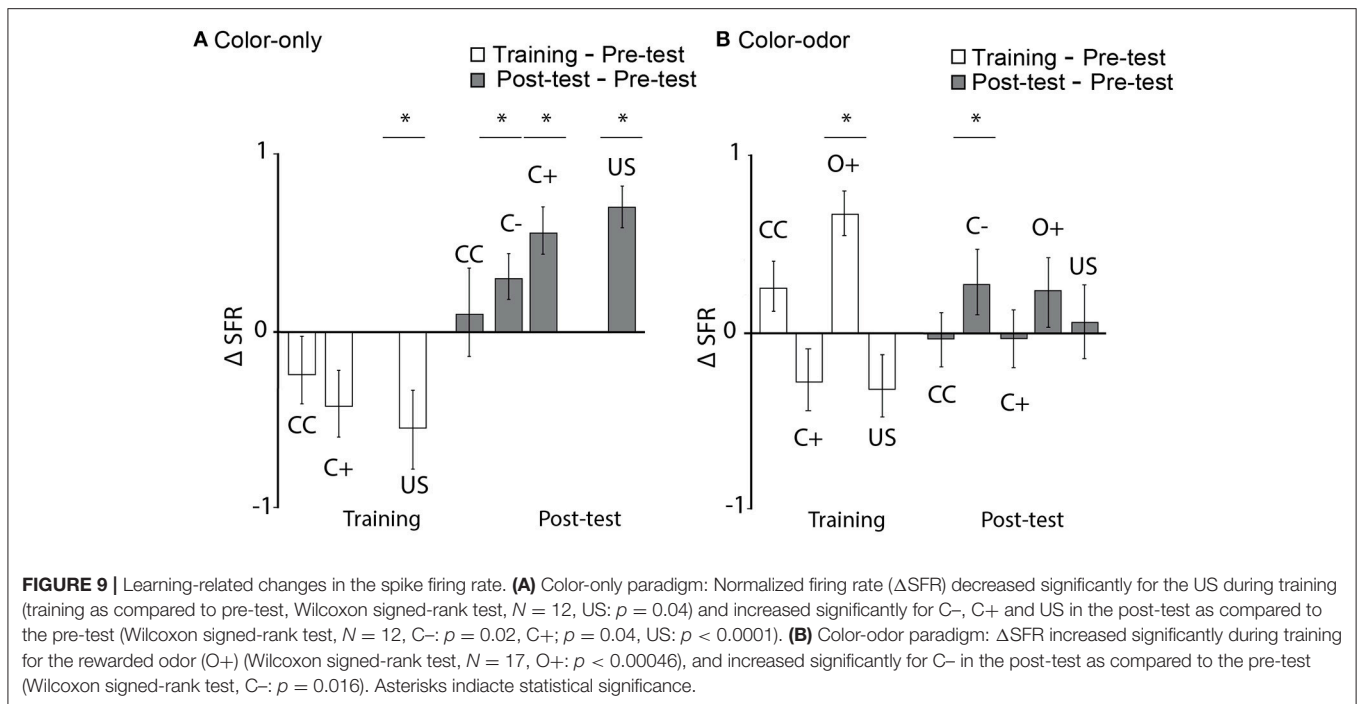
Temporal Dynamics of Spiking Rate Changes During Learning

We found learning-related spike rate changes for several stimuli, but not for the CC situation. Animals saw both colors appearing at the same time and walked toward one or the other color during the CC scenario in order to get a reward (compare **Figure 2A**). It seems surprising that no neural response changes were observed during the CC condition. To detect fast spike rate changes that are not detected by our global analyses during stimulation, we compared the time courses of spiking by inter-spike interval (ISI) analysis during pre-test, acquisition, and post-test, and focused on the time window directly after stimulus onset (600 ms). This

method detects subtle excitatory or inhibitory rate changes that extend over several 100 ms during stimulation (Strube-Bloss et al., 2011). Additionally, we analyzed the ISI that occurred during acquisition by comparing median ISI during onset of C+ to median ISI during US onset. The medians of the pre-test and the post-test- ISI was extracted and statistically analyzed for every unit using a Wilcoxon signed-rank test (see also **Figure 1** for median ISI). We subtracted the median ISI in the post-test from the median ISI in the pre-test for every unit separately for depicting the changes.

No significant differences in the changes of ISI medians were found for any tested conditions for animals trained in the color-only paradigm (**Figure 10A**, $N = 12$, Wilcoxon signed-rank test, $p > 0.05$).

However, significant differences appeared for the CC situation in animals trained in the color-odor paradigm (**Figure 10B** right



side, Wilcoxon signed-rank test, $N = 17$, $p = 0.046$). The changes in ISI medians indicate that learning lead to higher spike frequencies in the CC test conditions immediately after stimulus onset. Furthermore, the ISI medians became significantly shorter at color onset as compared to sugar onset during acquisition (**Figure 10B** left side, Wilcoxon signed-rank test, $p = 0.005$). The ISI medians did not change significantly from pre-test to post-test for the C+ and C-, the odor and the US (data not shown, Wilcoxon signed-rank test $p > 0.05$). As a control we analyzed the ISI over the whole time of the experiment. ISI did also not change significantly when we compared the ISI of the time before the pre-test without stimulation with the ISI of the time before the post-test without stimulation (Wilcoxon signed-rank test $p > 0.05$).

These results show that even though no changes for the CC were found when comparing the spike rate changes over the whole stimulus (**Figure 9**), fast changes indeed occurred within 600 ms after stimulus onset in one of our paradigms, the color-odor training but not the color-only training marking the operant conditions of this experimental conditions.

DISCUSSION

We developed a virtual environment (VE) for honeybees that allowed us to combine stable recordings from mushroom body (MB) extrinsic neurons with a learning assay. The VE is suitable for testing bees both after operant color learning of free-flying bees, and de-novo color-only or color-odor training inside the VE. MB extrinsic neurons (ENs) changed their responses both to the rewarded color (C+) and unrewarded the color (C-). For the first time, we found evidence for an involvement of A3 neurons in operant learning in the honeybee.

In operant learning, animals establish an association between an external stimulus and their behavioral responses by trial and error. This form of learning is also called instrumental, because the animal's own behavior is instrumental to obtaining some outcome (Wynne and Udel, 2013). The requirement is an external stimulus that is only present if the animal performs a certain behavior. This stimulus can be positive or negative and subsequently alters the associated behavior (Mackintosh, 1974; Spencer et al., 1999). A VE provides us with the opportunity to study operant learning while the corresponding brain activity is monitored. Although operant learning in freely moving invertebrates has been widely studied (Giurfa and Menzel, 2013; Perry et al., 2013; Hawkins and Byrne, 2015) the underlying neural mechanisms are still largely unknown. Evidence for neural correlates of operant learning in invertebrates comes from *Drosophila*, *Aplysia* and *Lymnae*. These studies suggest that different cellular and network mechanisms underlie classical and operant conditioning (Brembs et al., 2002; Hawkins et al., 2006; Hawkins and Byrne, 2015). In the honeybee, mushroom body extrinsic neurons (MB ENs) were extensively studied in classical conditioning paradigms and found to change their response properties during olfactory conditioning (Mauelshagen, 1993; Grünewald, 1999; Okada et al., 2007; Haehnel and Menzel, 2010; Strube-Bloss et al., 2011; Hussaini and Menzel, 2013; Menzel, 2014; Filla and Menzel, 2015). A3 MB ENs are particularly interesting in this context because it is known that they change their responses during context-dependent classical conditioning with learning-related neural changes both for the visual context and the olfactory cue (Filla and Menzel, 2015). These data suggested a multisensory and value-integrating pathway specifically designed for action selection comparable to neurons in the mammalian prefrontal cortex.

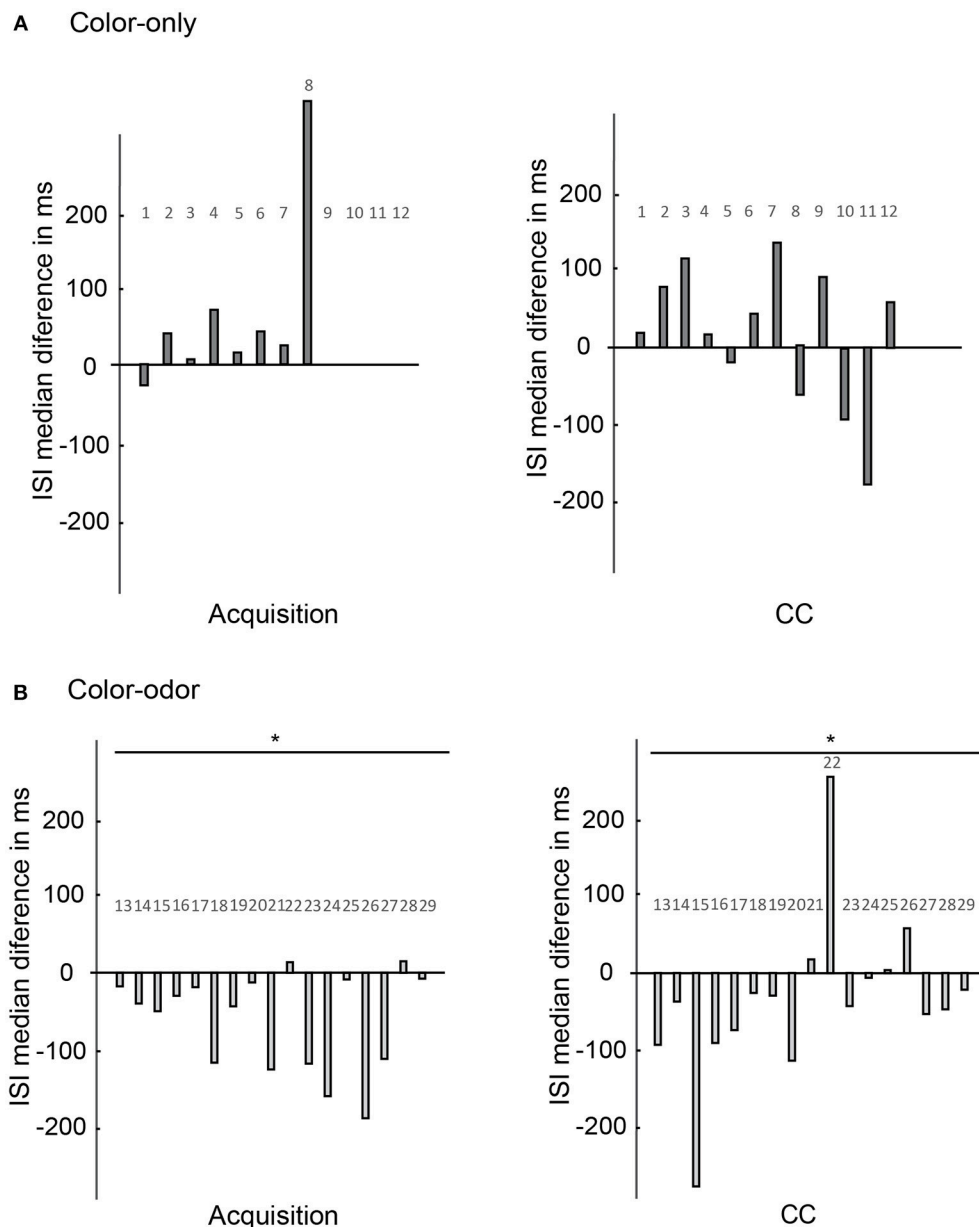


FIGURE 10 | Changes of the ISI medians as compared for the acquisition and the CC phase. Changes of ISI medians of the units (x-axis) are calculated for the 600 ms after stimulus onset in the pre-test and in the post-test (y-axis). **(A)** Color-only paradigm: ISI medians of 12 units (x-axis) during the acquisition phase and the CC phase. The changes of ISI medians are not significantly different for color onset as compared to reward onset ($N = 12$, Wilcoxon signed-rank test, $p > 0.05$). No significant changes are found for the CC phase comparing the pre-test and post-test ($N = 12$, Wilcoxon signed-rank test, $p > 0.05$). **(B)** Color-odor paradigm: Changes in ISI medians are significantly different during the acquisition for the color and the reward onset ($N = 17$, Wilcoxon signed-rank test, $p = 0.005$). The changes of ISI medians are also significantly different for the CC for the pre-test and post-test comparison ($N = 17$, Wilcoxon signed-rank test, $p = 0.046$). Asterisks indicate statistical significance.

We applied two different learning paradigms where the active selection and approach had to be performed for either a colored target (color-only) or for a color that was subsequently combined with an odor (color-odor). It is known from behavioral studies with freely flying bees and bees conditioned to the proboscis extension response that odors are particularly salient stimuli (Menzel, 1990). In our context, studies in *Drosophila*

are notable documenting an involvement of the mushroom bodies in complex stimulus learning and decision making (Zhang et al., 2007; Xi et al., 2008; Yi et al., 2013; Solanki et al., 2015).

Neural activity in the color-only paradigm changed significantly for the rewarded color C+ (Figure 7A). About 70% of the units were recruited and only few stopped responding

to the C+. In response to the unrewarded color C– units were recruited and dropped to a more equal amount (**Figure 7B**). These findings resemble those found in other MB ENs (A1/A2) during differential olfactory classical conditioning (Strube-Bloss et al., 2011). Resembling classical conditioning, however might be explained due to the fact that our operant conditioning paradigm is not purely operant as possible for example in *Drosophila*. These results corroborate the conclusion that MB ENs appear to code learning-related plasticity for the CS+ by a dominance of response increase. A different strategy might be involved in coding responses to the unrewarded stimulus CS– by keeping the overall excitation level rather constant increasing and decreasing the neural responses in participating neurons.

Response changes in the color-odor paradigm differed partly from those found in differential olfactory classical conditioning mentioned above. In a classical conditioning experiment where a color context announced the rewarded odor cue, the number of A3 neurons and their discharges increased for the odor cue (Filla and Menzel, 2015). In our learning paradigm however, the number of units responding to the C+ did not change significantly (**Figure 8A**), and a similar number of units were recruited and dropped out for all stimuli (**Figure 8B**). However, during training, we observed a significant enhanced spike rate to the rewarded odor (**Figure 9B**) and a tendency for a reduced rate to the color during training. This observation fits previously reported changes in the PE1 neuron (Okada et al., 2007; Hussaini and Menzel, 2013). This single identified MB EN, decreased its response to a classically conditioned odor (Okada et al., 2007; Hussaini and Menzel, 2013) and increased it to a rewarded context (Hussaini and Menzel, 2013). As this cell is

thought to get inhibitory input from PCT (or A3) cells (Rybak and Menzel, 1998), its response changes fit very well to our data.

Differences between classical conditioning and operant learning can also be found in other experiments with MB ENs. A1/A2 ENs, for example, develop their learning-related spike rate changes during the 3 h after classical conditioning (Strube-Bloss et al., 2011). We found such changes in what are most likely A3 neurons, already during the training process (**Figure 10**). We conclude from our verified recording site (see Experimental Procedures) and the physiological properties of the recorded cells that the analyzed spikes are A3 neurons, at least to a large part. In our experiments 25 out of 29 units changed their spiking frequency before training toward the presentation of an odor, a color or the sucrose reward. A3 neurons typically react with an increase toward a sucrose stimulation (Grünwald, 1999) and a change in the spiking activity toward odors and colors (Grünwald, 1999; Filla and Menzel, 2015).

In the search for neural correlates of operant learning, one would like to analyze the point of decision where the animal initiates a walk toward one of the two colors. Unfortunately, such decision points were not obvious since every walking trajectory included several turns or stops making it impossible to isolate attempts to walk toward the color. Thus, we decided to examine fixed points in every acquisition trial for all bees and selected two specific moments in which the scenario with both colors showed up (CC). This is the starting point for each acquisition trial. Therefore, one might expect changes in neural responses at this point when the animal responds behaviorally and starts to walk toward the C+ to get the reward.

TABLE 1 | Comparison of changes in neural activity after learning in VE and classical conditioning.

Experimental result color-only	Similar to classical conditioning	Different from classical conditioning
Change in neural activity for the rewarded color C+ after conditioning. About 70% recruited units and only few that dropped out (Figures 7A,B).	Around 50% of MB ENs change their odor response after differential olfactory classical conditioning dominated by CS+ odor recruitment (Strube-Bloss et al., 2011).	
Recruited and dropped out units in response to the unrewarded color C– after conditioning (Figure 7B).	Recruited and dropped units to the CS– odor after conditioning (Strube-Bloss et al., 2011).	Less responding units to the CS– odor after conditioning compared to before, more units dropped than recruited (Strube-Bloss et al., 2011).
Experimental result color-odor	Similar to classical conditioning	Different from classical conditioning
No significant change in the number of units responding to the C+ after conditioning (Figure 8A). Similar number of recruited and dropped out units for all stimuli (Figure 8B).	Recruited and dropped units to the CS– odor after conditioning (Strube-Bloss et al., 2011).	Increased number of A3 neurons and their discharges for the CS+ odor where a particular color context announced the particular rewarded CS+ odor (Filla and Menzel, 2015).
Significantly enhanced spike rate during training to the rewarded odor (Figure 9B) and a tendency for a reduced rate to the color during training.	PE1 neuron decreased its response to a classically conditioned odor (Okada et al., 2007; Hussaini and Menzel, 2013) and increased it to a rewarded context (Hussaini and Menzel, 2013). PE1 is thought to get inhibitory input from or A3 cells (Rybak and Menzel, 1998).	
Changes in neuron response during the training process (Figure 10B).		A1/A2 ENs develop learning-related spike rate changes after classical conditioning (Strube-Bloss et al., 2011).

Indeed, in the color-odor paradigm, the inter-spike interval (ISI) during the CC was significantly lowered after training (**Figure 10B**). Filla and Menzel (2015) showed that after visual pre-training the presence of a visual context induces an attention effect, reflected in faster response to the reward odor than testing the reward odor alone. The increased ISI to CC might reflect such an attentional effect. After the onset of the CC a behavioral response from the animal is needed to gain the reward.

In summary, the VE for honeybees allowed us to search for neural correlates of learning while animals navigated in an environment that responded to their actions. We demonstrate that honeybees transfer learned information from free flight learning experiments to the VE, documenting its suitability for testing operant behavior. Previously, this transfer has been reported to be unpredictable most likely due to the constrained movement and impaired active vision in the VE (Buatois et al., 2018). The VE also enabled us to study neural correlates of learning over several hours. We found significant changes in neural activity after learning to both the rewarded and unrewarded colors in the color-only paradigm. These forms of neural plasticity resemble processes found in classical conditioning experiments with honeybees. Learning-related neural plasticity differed in the color-odor paradigm from those reported in classical conditioning (**Table 1**). These forms of neural plasticity can be interpreted as indicating attentional effects. Our results suggest the involvement of the MB in operant learning.

AUTHOR CONTRIBUTIONS

HZ: conception and design, acquisition of data, analysis and interpretation, writing the article; RB: conception and design, revising the article; SL and MJ: acquisition of data; SH, JG, and RA: writing custom program for virtual environment and

analysis software; SM: building virtual environment set-up; RM: conception and design, writing and revising the article; SL and MJ: acquisition and analysis of data.

FUNDING

Funding provided by the German Ministry for Education and Research (BMBF) via 01GQ0941 is appreciated.

ACKNOWLEDGMENTS

Funding provided by the Deutsche Forschungsgemeinschaft (DFG) via ME 365/41-1 is appreciated. We would like to thank Sebastian Hausmann for training bees in the T-maze, and Benjamin Paffhausen for help with micro-processors. The authors have no conflict of interest to declare.

SUPPLEMENTARY MATERIAL

The Supplementary Material for this article can be found online at: <https://www.frontiersin.org/articles/10.3389/fnbeh.2018.00279/full#supplementary-material>

Video S1 | Video shows a honeybee walking in the virtual environment. The free-flying bee was trained in a T-maze to associate yellow with a sucrose reward and blue with a potassium chloride punishment. Subsequently the animal was transferred to the VE and tested in a scenario similar to the point of decision in the T-maze. When the animal walked toward one stripe, the stripe turned in front of it depending on the rotatory movement of the spherical treadmill. When it kept walking toward the stripe, it got bigger, simulating the object getting closer, and stopped, when it reached it. Afterwards the scenario set back to the decision point and the animal could choose again. Sides were switched in a pseudo-random fashion to avoid side preferences. The bee in the video repeatedly chooses to walk toward yellow.

Figure S1 | **(A)** Example of all single unit waveforms (500 events) for one animal with their corresponding principal component analysis **(B)**. **(B)** Upper panel: Three dimensional plot of principal component analysis for all units in **(A)**. Lower panel: all units crossing minus three standard deviations lower left panel and crossing plus three standard deviations lower right panel. PCA is rotate in 3D for better display.

REFERENCES

- Araújo, D. B., Baffa, O., and Wakai, R. T. (2002). Theta oscillations and human navigation: a magnetoencephalography study. *J. Cogn. Neurosci.* 14, 70–78. doi: 10.1162/089892902317205339
- Aronov, D., and Tank, D. W. (2014). Engagement of neural circuits underlying 2D spatial navigation in a rodent virtual reality system. *Neuron* 84, 442–456. doi: 10.1016/j.neuron.2014.08.042
- Ball, D., Kliebe, R., Windels, F., Nolan, C., Stratton, P., Sah, P., et al. (2014). Rodent scope: a user-configurable digital wireless telemetry system for freely behaving animals. *PLoS ONE* 9:e89949. doi: 10.1371/journal.pone.0089949
- Baumeister, J., Reinecke, K., Cordes, M., Lerch, C., and Weiss, M. (2010). Brain activity in goal-directed movements in a real compared to a virtual environment using the Nintendo Wii. *Neurosci. Lett.* 481, 47–50. doi: 10.1016/j.neulet.2010.06.051
- Bender, J. A., Pollack, A. J., and Ritzmann, R. E. (2010). Neural activity in the central complex of the insect brain is linked to locomotor changes. *Curr. Biol.* 20, 921–926. doi: 10.1016/j.cub.2010.03.054
- Brembs, B., Lorenzetti, F. D., Reyes, F. D., Baxter, D. A., and Byrne, J. H. (2002). Operant reward learning in aplysia: neuronal correlates and mechanisms. *Science* 296, 1706–1709. doi: 10.1126/science.1069434
- Buatois, A., Flumian, C., Schultheiss, P., Avarguès-Weber, A., and Giurfa, M. (2018). Transfer of visual learning between a virtual and a real environment in honey bees: the role of active vision. *Front. Behav. Neurosci.* 12:139. doi: 10.3389/fnbeh.2018.00139
- Buatois, A., Pichot, C., Schultheiss, P., Sandoz, J.-C., Lazzari, C. R., Chittka, L., et al. (2017). Associative visual learning by tethered bees in a controlled visual environment. *Sci. Rep.* 7:12903. doi: 10.1038/s41598-017-12631-w
- deCamp, N. V. (2013). *Extracellular Long Term Recordings in the Mushroom Body of Social Insects During Real and Virtual Navigation*. Berlin: Freie Universität.
- Denker, M., Finke, R., Schaupp, F., Grün, S., and Menzel, R. (2010). Neural correlates of odor learning in the honeybee antennal lobe. *Eur. J. Neurosci.* 31, 119–133. doi: 10.1111/j.1460-9568.2009.07046.x
- Doeller, C. F., Barry, C., and Burgess, N. (2010). Evidence for grid cells in a human memory network. *Nature* 463, 657–661. doi: 10.1038/nature08704
- Dombeck, D. A., Harvey, C. D., Tian, L., Looger, L. L., and Tank, D. W. (2010). Functional imaging of hippocampal place cells at cellular resolution during virtual navigation. *Nat. Neurosci.* 13, 1433–1440. doi: 10.1038/nn.2648

- Duer, A., Paffhausen, B. H., and Menzel, R. (2015). High order neural correlates of social behavior in the honeybee brain. *J. Neurosci. Methods* 254, 1–9. doi: 10.1016/j.jneumeth.2015.07.004
- Ferguson, J. E., Boldt, C., and Redish, A. D. (2009). Creating low-impedance tetrodes by electroplating with additives. *Sens. Actu. A Phys.* 156, 388–393. doi: 10.1016/j.sna.2009.10.001
- Fiala, A. (2007). Olfaction and olfactory learning in *Drosophila*: recent progress. *Curr. Opin. Neurobiol.* 17, 720–726. doi: 10.1016/j.conb.2007.11.009
- Filla, I., and Menzel, R. (2015). Mushroom body extrinsic neurons in the honeybee (*Apis mellifera*) brain integrate context and cue values upon attentional stimulus selection. *J. Neurophysiol.* 114, 2005–2014. doi: 10.1152/jn.00776.2014
- Gillner, S., and Mallot, H. A. (1998). Navigation and acquisition of spatial knowledge in a virtual maze. *J. Cogn. Neurosci.* 10, 445–463. doi: 10.1162/089892998562861
- Giurfa, M. (2003). Cognitive neuroethology: dissecting non-elemental learning in a honeybee brain. *Curr. Opin. Neurobiol.* 13, 726–735. doi: 10.1016/j.conb.2003.10.015
- Giurfa, M., and Menzel, R. (2013). “Cognitive components of insect behavior,” in *Handbook of Behavioral Neuroscience* eds R. Menzel and P. R. Benjamin (London, UK: Elsevier), 14–25.
- Grünwald, B. (1999). Physiological properties and response modulations of mushroom body feedback neurons during olfactory learning in the honeybee, *Apis mellifera*. *J. Comp. Physiol. A* 185, 565–576. doi: 10.1007/s003590050417
- Haehnel, M., and Menzel, R. (2010). Sensory representation and learning-related plasticity in mushroom body extrinsic feedback neurons of the protocerebral tract. *Front. Syst. Neurosci.* 4:161. doi: 10.3389/fnsys.2010.00161
- Harris, K. D., Henze, D. A., Csicsvari, J., Hirase, H., and Buzsáki, G. (2000). Accuracy of tetrode spike separation as determined by simultaneous intracellular and extracellular measurements. *J. Neurophysiol.* 84, 401–414. doi: 10.1152/jn.2000.84.1.401
- Harvey, C. D., Coen, P., and Tank, D. W. (2012). Choice-specific sequences in parietal cortex during a virtual-navigation decision task. *Nature* 484, 62–68. doi: 10.1038/nature10918
- Harvey, C. D., Collman, F., Dombeck, D. A., and Tank, D. W. (2009). Intracellular dynamics of hippocampal place cells during virtual navigation. *Nature* 461, 941–946. doi: 10.1038/nature08499
- Hawkins, R. D., and Byrne, J. H. (2015). Associative learning in invertebrates. *Cold Spring Harb. Perspect. Biol.* 7:a021709. doi: 10.1101/cshperspect.a021709
- Hawkins, R. D., Kandel, E. R., and Bailey, C. H. (2006). Molecular mechanisms of memory storage in aplysia. *Biol. Bull.* 210, 174–191. doi: 10.2307/4134556
- Heisenberg, M., and Wolf, R. (1979). On the fine structure of yaw torque in visual flight orientation of *Drosophila melanogaster*. *J. Comp. Physiol.* 130, 113–130. doi: 10.1007/BF00611046
- Holscher, C., Schnee, A., Dahmen, H., Setia, L., and Mallot, H. A. (2005). Rats are able to navigate in virtual environments. *J. Exp. Biol.* 208, 561–569. doi: 10.1242/jeb.01371
- Homberg, U., and Erber, J. (1979). Response characteristics and identification of extrinsic mushroom body neurons of the bee. *Z. Für Naturforschung C* 34, 612–615. doi: 10.1515/znc-1979-7-820
- Hussaini, S. A., and Menzel, R. (2013). Mushroom body extrinsic neurons in the honeybee brain encode cues and contexts differently. *J. Neurosci.* 33, 7154–7164. doi: 10.1523/JNEUROSCI.1331-12.2013
- Ito, K., Shinomiya, K., Ito, M., Armstrong, J. D., Boyan, G., Hartenstein, V., et al. (2014). A systematic nomenclature for the insect brain. *Neuron* 81, 755–765. doi: 10.1016/j.neuron.2013.12.017
- Joshua, M., Elias, S., Levine, O., and Bergman, H. (2007). Quantifying the isolation quality of extracellularly recorded action potentials. *J. Neurosci. Methods* 163, 267–282. doi: 10.1016/j.jneumeth.2007.03.012
- Kim, S. S., Rouault, H., Druckmann, S., and Jayaraman, V. (2017). Ring attractor dynamics in the *Drosophila* central brain. *Science* 356, 849–853. doi: 10.1126/science.aal4835
- Mackintosh, N. (1974). *The Psychology of Animal Learning*. Oxford: Academic Press.
- Mallot, H. A., Gillner, S., van Veen, H. A. H. C., and Bühlhoff, H. H. (1998). “Behavioral experiments in spatial cognition using virtual reality,” in *Spatial Cognition*, eds C. Freksa, C. Habel, and K.F. Wender (Berlin: Springer Berlin Heidelberg), 447–467.
- Mauelshagen, J. (1993). Neural correlates of olfactory learning paradigms in an identified neuron in the honeybee brain. *J. Neurophysiol.* 69, 609–625. doi: 10.1152/jn.1993.69.2.609
- McNaughton, B. L., Battaglia, F. P., Jensen, O., Moser, E. I., and Moser, M.-B. (2006). Path integration and the neural basis of the “cognitive map”. *Nat. Rev. Neurosci.* 7, 663–678. doi: 10.1038/nrn1932
- Menzel, R. (1990). “Learning, memory, and “cognition” in honey bees,” in *Neurobiology of Comparative Cognition* eds D. S. Olton and R. P. Kesner (Hillsdale, NJ: Lawrence Erlbaum Associates, Inc.), 237–292.
- Menzel, R. (2012). The honeybee as a model for understanding the basis of cognition. *Nat. Rev. Neurosci.* 13, 758–768. doi: 10.1038/nrn3357
- Menzel, R. (2014). The insect mushroom body, an experience-dependent recoding device. *J. Physiol.* 108, 84–95. doi: 10.1016/j.jphysparis.2014.07.004
- Mizunami, M., Okada, R., Li, Y., and Strausfeld, N. J. (1998). Mushroom bodies of the cockroach: activity and identities of neurons recorded in freely moving animals. *J. Comp. Neurol.* 402, 501–519.
- Okada, R., Rybak, J., Manz, G., and Menzel, R. (2007). Learning-related plasticity in PE1 and other mushroom body-extrinsic neurons in the honeybee brain. *J. Neurosci.* 27, 11736–11747. doi: 10.1523/JNEUROSCI.2216-07.2007
- O’keefe, J., and Nadel, L. (1978). *The Hippocampus as a Cognitive Map*. Oxford: Clarendon Press.
- Peng, Y., Xi, W., Zhang, W., Zhang, K., and Guo, A. (2007). Experience improves feature extraction in *Drosophila*. *J. Neurosci.* 27, 5139–5145. doi: 10.1523/JNEUROSCI.0472-07.2007
- Perry, C. J., Barron, A. B., and Cheng, K. (2013). Invertebrate learning and cognition: relating phenomena to neural substrate. *Wiley Interdiscip. Rev. Cogn. Sci.* 4, 561–582. doi: 10.1002/wcs.1248
- Puryear, C. B., Kim, M. J., and Mizumori, S. J. Y. (2010). Conjunctive encoding of movement and reward by ventral tegmental area neurons in the freely navigating rodent. *Behav. Neurosci.* 124, 234–247. doi: 10.1037/a0018865
- R Core Team (2017). *R: A Language and Environment for Statistical Computing*. Vienna: R Foundation for Statistical Computing.
- Rusch, C., Roth, E., Vinauger, C., and Riffell, J. A. (2017). Honeybees in a virtual reality environment learn unique combinations of colour and shape. *J. Exp. Biol.* 220 (Pt 19), 3478–3487. doi: 10.1242/jeb.164731
- Rybak, J., and Menzel, R. (1998). Integrative properties of the Pe1 neuron, a unique mushroom body output neuron. *Learn. Mem.* 5, 133–145.
- Schildberger, K. (1981). Some physiological features of mushroom-body linked fibers in the house cricket brain. *Naturwissenschaften* 68, 623–624. doi: 10.1007/BF00398621
- Schultheiss, P., Buatois, A., Avarguès-Weber, A., and Giurfa, M. (2017). Using virtual reality to study visual performances of honeybees. *Curr. Opin. Insect Sci.* 24, 43–50. doi: 10.1016/j.cois.2017.08.003
- Seelig, J. D., and Jayaraman, V. (2015). Neural dynamics for landmark orientation and angular path integration. *Nature* 521, 186–191. doi: 10.1038/nature14446
- Solanki, N., Wolf, R., and Heisenberg, M. (2015). Central complex and mushroom bodies mediate novelty choice behavior in *Drosophila*. *J. Neurogenet.* 29, 30–37. doi: 10.3109/01677063.2014.1002661
- Spencer, G. E., Syed, N. I., and Lukowiak, K. (1999). Neural changes after operant conditioning of the aerial respiratory behavior in *Lymanaea stagnalis*. *J. Neurosci.* 19, 1836–1843. doi: 10.1523/JNEUROSCI.19-05-01836.1999
- Srinivasan, M. V. (2010). Honey bees as a model for vision, perception, and cognition. *Annu. Rev. Entomol.* 55, 267–284. doi: 10.1146/annurev.ento.010908.164537
- Strube-Bloss, M. F., Nawrot, M. P., and Menzel, R. (2011). Mushroom body output neurons encode odor-reward associations. *J. Neurosci.* 31, 3129–3140. doi: 10.1523/JNEUROSCI.2583-10.2011
- Takalo, J., Piironen, A., Honkanen, A., Lempeä, M., Aikio, M., Tuukkanen, T., et al. (2012). A fast and flexible panoramic virtual reality system for behavioural and electrophysiological experiments. *Sci. Rep.* 2:324. doi: 10.1038/srep00324
- Turner-Evans, D., Wegener, S., Rouault, H., Franconville, R., Wolff, T., Seelig, J. D., et al. (2017). Angular velocity integration in a fly heading circuit. *eLife* 6:e23496. doi: 10.7554/eLife.23496
- van Swinderen, B., and Greenspan, R. J. (2003). Salience modulates 20–30 Hz brain activity in *Drosophila*. *Nat. Neurosci.* 6, 579–586. doi: 10.1038/nn1054

- Walker, E., and Nowacki, A. S. (2011). Understanding equivalence and noninferiority testing. *J. Gen. Intern. Med.* 26, 192–196. doi: 10.1007/s11606-010-1513-8
- Wolf, R., and Heisenberg, M. (1984). *Vision in Drosophila: Genetics of Microbehavior*. (Berlin; Heidelberg; New York, NY; Tokyo: Springer).
- Wynne, C. D. L., and Udell, M. A. R. (2013). *Animal Cognition: Evolution, Behavior and Cognition*. (Basingstoke: Palgrave Macmillan).
- Xi, W., Peng, Y., Guo, J., Ye, Y., Zhang, K., Yu, F., et al. (2008). Mushroom bodies modulate salience-based selective fixation behavior in *Drosophila*. *Eur. J. Neurosci.* 27, 1441–1451. doi: 10.1111/j.1460-9568.2008.06114.x
- Yi, W., Zhang, Y., Tian, Y., Guo, J., Li, Y., and Guo, A. (2013). A subset of cholinergic mushroom body neurons requires Go signaling to regulate sleep in *Drosophila*. *Sleep* 36, 1809–1821. doi: 10.5665/sleep.3206
- Zhang, K., Guo, J. Z., Peng, Y., Xi, W., and Guo, A. (2007). Dopamine-mushroom body circuit regulates saliency-based decision-making in *Drosophila*. *Science* 316, 1901–1904. doi: 10.1126/science.1137357
- Zwaka, H., Bartels, R., Grünewald, B., and Menzel, R. (2018). Neural organization of A3 mushroom body extrinsic neurons in the honeybee brain. *Front. Neuroanat.* 12:57. doi: 10.3389/fnana.2018.00057

Conflict of Interest Statement: The authors declare that the research was conducted in the absence of any commercial or financial relationships that could be construed as a potential conflict of interest.

Copyright © 2019 Zwaka, Bartels, Lehfeldt, Jusyte, Hantke, Menzel, Gora, Alberdi and Menzel. This is an open-access article distributed under the terms of the Creative Commons Attribution License (CC BY). The use, distribution or reproduction in other forums is permitted, provided the original author(s) and the copyright owner(s) are credited and that the original publication in this journal is cited, in accordance with accepted academic practice. No use, distribution or reproduction is permitted which does not comply with these terms.



A Specific Role of Hippocampal NMDA Receptors and Arc Protein in Rapid Encoding of Novel Environmental Representations and a More General Long-Term Consolidation Function

Cameron M. Bye and Robert J. McDonald*

Canadian Centre for Behavioural Neuroscience, University of Lethbridge, Lethbridge, AB, Canada

OPEN ACCESS

Edited by:

Bruno Poucet,
Center for the National Scientific
Research (CNRS), France

Reviewed by:

Xavier De Jaeger,
Ceva Santé Animale, France
Bruno Truchet,
Aix-Marseille Université, France

*Correspondence:

Robert J. McDonald
r.mcdonald@uleth.ca

Received: 29 May 2018

Accepted: 14 January 2019

Published: 26 February 2019

Citation:

Bye CM and McDonald RJ (2019)
A Specific Role of Hippocampal
NMDA Receptors and Arc Protein
in Rapid Encoding of Novel
Environmental Representations
and a More General Long-Term
Consolidation Function.
Front. Behav. Neurosci. 13:8.
doi: 10.3389/fnbeh.2019.00008

Activation of the NMDA receptor (NMDAR) has been proposed to be a key event responsible for the structural changes that occur in neurons during learning and memory formation. It has been extensively studied yet no consensus has been reached on its mnemonic role as both NMDAR dependent and independent forms of learning have been observed. We investigated the role that hippocampal NMDAR have in rapid spatial learning and memory across training environments. Hippocampal NMDAR was blocked via intra-hippocampal injection of the competitive antagonist CPP. Groups of rats were pre-trained on a spatial version of the Morris water task, and then mass reversal training under NMDAR blockade occurred in the same or different training environments as pre-training. We measured expression of Arc protein throughout the main hippocampal subfields, CA1, CA3, and dentate gyrus, after mass-training. We observed that NMDAR blockade allowed for rapid spatial learning, but not consolidation, when the SUBJECTS used previously acquired environmental information. Interestingly, NMDAR blockade impaired rapid spatial learning when rats were mass-trained in a novel context. Arc protein expression in the dentate gyrus followed this pattern of NMDAR dependent spatial behavior, with high levels of expression observed after being trained in the new environment, and low levels when trained in the same environment. CPP significantly reduced Arc expression in the dentate gyrus. These results implicate dentate NMDAR in the acquisition of novel environmental information.

Keywords: NMDA receptor, hippocampus, spatial learning, consolidation, Morris water maze

INTRODUCTION

The plasticity and the neurobiological mechanisms underlying memory-based behavior mediated by the hippocampus and related networks is complex and not completely understood. One neural property proposed to support the formation of memories is synaptic plasticity. Synaptic plasticity is the strengthening or weakening of synaptic connections between neurons via long-term potentiation (LTP) and long-term depression (LTD), respectively. LTP is an amplification of

the excitatory post synaptic potential as a result of high frequency inputs (Bliss and Lomo, 1973; Levy and Steward, 1979). Typically, LTP is induced artificially through electrical stimulation but some of the biomarkers for LTP have been found in freely learning animals (Whitlock et al., 2006).

N-methyl-D-aspartate receptors (NMDAR) are a class of postsynaptic glutamate receptors located in many regions of the brain including the hippocampus (Dingledine, 1983). Although not necessary for normal synaptic transmission, the NMDAR plays an important role in mediating synaptic plasticity (Collingridge et al., 1983; Harris et al., 1984). By manipulating extracellular ion concentrations involved in NMDAR function like calcium or magnesium, LTP can be inhibited (Dunwiddie and Lynch, 1979; Herron et al., 1985). LTP can also be inhibited with NMDAR antagonists that block the receptor (Herron et al., 1986; Abraham and Kairiss, 1988). Genetic knockouts for the NMDAR in mice have also been associated with reduced synaptic plasticity and LTP in the hippocampus (Sakimura et al., 1995). A significant body of evidence over the past decades has shown a strong relationship between the expression of LTP and the NMDAR.

In a breakthrough study linking NMDAR function, LTP, and hippocampal based memory, Morris et al. (1986) bilaterally infused an NMDAR antagonist (APV) into the ventricles of rats that blocked LTP in the hippocampus. When trained on the Morris water task (MWT) that requires the rats to locate and learn the position of a hidden platform under a pool of opaque water, they failed to accurately find the hidden escape platform location. These results are similar to those of rats with hippocampal lesions (Sutherland et al., 1983). NMDAR inactivation has been associated with impairments in other learning tasks as well (Tonkiss et al., 1988; Ward et al., 1990). NMDAR antagonists have not been found to influence the retrieval of already formed memories (Shapiro and Caramanos, 1990). This early research has generated the popular theory that these receptors are critical for inducing synaptic plasticity, and therefore are critical for the encoding of experiences and memories (Collingridge and Bliss, 1987).

However, separate lines of research suggest that this story is not as straightforward as it might seem. NMDAR antagonists may have multiple effects on behavior because when administered intraperitoneally or intraventricularly (Morris et al., 1986; Morris, 1989; Ward et al., 1990) NMDARs are blocked throughout the entire brain (Monaghan and Cotman, 1985). Not all brain regions are primarily involved in memory functions and so blocking NMDARs in these areas may produce confounding behavioral effects. NMDAR antagonists have been shown to induce a wide variety of electrophysiological and behavioral impairments involving sensory (Salt, 1986), motor, (Cain et al., 1996), and anxiolytic responses (Stephens et al., 1986). For example, in the MWT motor impairments can severely limit the rats' ability to learn (Cain et al., 1996). On top of all this, NMDAR independent LTP has also been found (Grover and Teyler, 1990).

Several behavioral methodologies have been proposed to avoid these potential confounds. Non-spatial visual discrimination tasks can be used to dissociate the effects that NMDAR antagonists might have on sensorimotor processes from their effects on learning. Typically, rats with NMDARs blocked are

impaired on the MWT but successful at the visual discrimination task (Morris, 1989). More surprisingly, pre-training rats on the MWT has been shown to eliminate the learning deficits associated with NMDAR antagonists (Bannerman et al., 1995; Saucier and Cain, 1995). Briefly, if a rat is procedurally trained to learn the MWT, prior to drug administration and standard training, the rat is capable of learning new spatial information independent of NMDAR function at control levels. This pre-training is thought to diminish the potential impacts of the antagonist on sensory or motor functions.

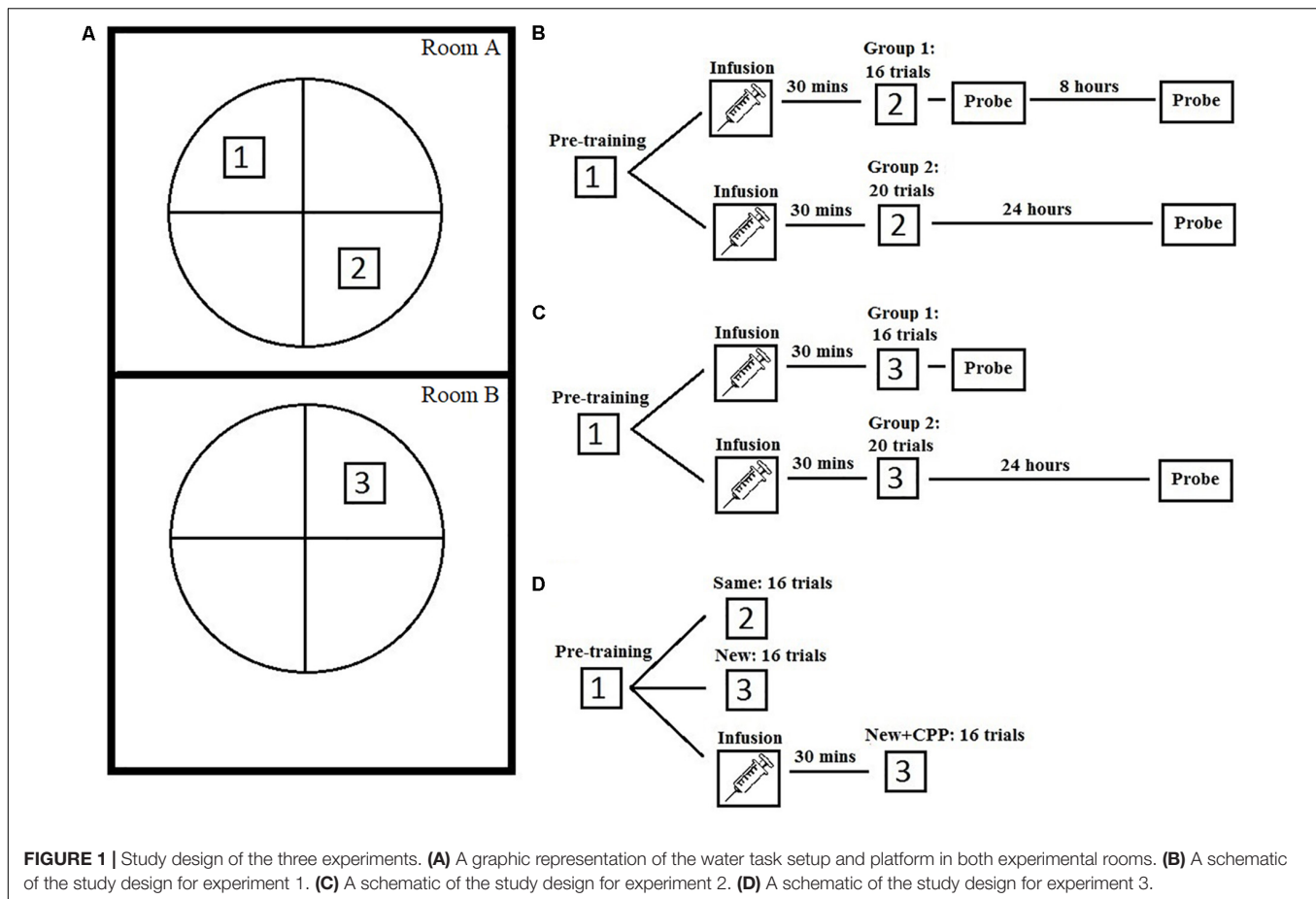
Pre-training can take the form of standard training involving finding a hidden platform (McDonald et al., 2005), training in an entirely different context (Bannerman et al., 1995) or navigating the pool in a non-spatial way with either curtains drawn or a non-fixed platform position (Cain et al., 1996; Hoh et al., 1999). Studies utilizing pre-training have produced results very different from the earlier research and suggest that the proposed role of NMDAR in the acquisition of information may be incorrect.

Much of the spatial training that rats undergo while being administered NMDAR antagonist occurs over multiple days, however, if training occurs rapidly within a short time period then the rats may be able to acquire the spatial information (McDonald et al., 2005). Research using time delays suggests that the NMDARs role in memory may be in the consolidation of that information as opposed to its acquisition, a process that occurs later in time. The distinction between rapidly acquired information versus information that is acquired over days may explain the inability of rats to learn in several NMDAR antagonist studies. Indeed, the majority of research showing learning impairments following blockade of NMDAR in spatial memory are done over several days of drug administration (Morris, 1989; Robinson et al., 1989; Inglis et al., 2013).

Critical support for the consolidation idea came from Kentros et al. (1998). They examined the effects that a NMDAR antagonist would have on the formation and stability of place fields in the hippocampus. They found that NMDAR blockade did not prevent the formation of new place field representations in the hippocampus when the rat was located in a new environment and the representation lasted for approximately 1.5 h. The antagonist did, however, prevent the long-term stability of the representation. This study provided important electrophysiological support for the idea that the acquisition of new spatial information is possibly independent of NMDAR function.

Further support came from McDonald et al. (2005) who pre-trained rats to find a hidden location in the MWT, then later rapidly trained to a new location while given intraperitoneal or intra-hippocampal injections of a NMDAR antagonist. The rats successfully learned the new location during the training period showing acquisition without NMDAR function. When tested 24 h later, the rats did not remember what they had learned suggesting that their ability to learn was intact while their ability to consolidate the information into long-term memory was impaired.

The goal of the present work is to further assess the role of NMDARs in hippocampal-based learning and memory functions. An outline of these experiments can be found



in **Figure 1**. Experiment 1 was an extension of the work done by McDonald et al. (2005) in which an NMDAR antagonist was only administered to the dorsal hippocampus, leaving the ventral portion most likely unaffected although the exact drug diffusion is unknown. It is possible that ventral hippocampal NMDA-based plasticity could support place learning which could account for the lack of effect in this study. From an experimental design perspective, intra-cranial injections of NMDA directly into the entire hippocampus is also important because this procedure leaves NMDARs in other brain regions unaffected allowing the isolation of the mnemonic effects of this manipulation from any other potential behavioral effects.

For Experiment 1, rats were given 4 days of spatial pre-training, followed by NMDAR antagonist drug infusion (2-carboxypiperazin-4-yl)-propyl-1-phosphonic acid (CPP) and mass spatial training to a new platform location. This was followed by a series of probe tests, one immediately after training to test the hypothesis that hippocampal NMDARs are necessary for the acquisition of novel spatial information, and two others done 8 h and 24 h later to examine the effect of NMDAR blockade on short-term memory consolidation. Based on our previous results we hypothesized that rats should be able to acquire new information without the use of NMDARs, but that this information would

not be consolidated and would disappear after a short period of time.

MATERIALS AND METHODS

Subjects, Acclimation, and Handling

Subjects were male Long Evans rats aged 90 days upon arrival to the facility ($n = 16$). The weight range at the start of the experiment was between 300 and 350 g. They were housed in pairs and were kept on a 12 h light/12 h dark cycle with lights turning on at 7:30 and turning off at 19:30. The rats had *ad libitum* access to both water and food. Rats were allowed 7 days of acclimatization in their home cages to reduce stress induced from travel. After this period, all rats from each experiment were handled for 5 min a day for 5 days to familiarize them with the experimenters and being manipulated. All procedures were in accordance with the regulations set out by the Canadian Council of Animal Care and approved by the University of Lethbridge Animal Care Committee.

Training Room/Apparatus

A large white circular fibreglass pool 46 cm in height and 127 cm in diameter was used. The pool was placed roughly in the center of the room. The pool was filled with water low enough that the

rats could not escape by climbing onto the walls but high enough that the rats could see the extra maze cues on the laboratory walls. Water was made non-transparent with non-toxic white paint. The pool was emptied, cleaned, and refilled with fresh water daily. The escape platform was located approximately 2 cm below the surface of the water. It was a white plastic circle 13 cm in diameter and made up approximately 1% of the total surface area of the pool. It had several small holes drilled into the surface for grip. Posters of simple colored geometric shapes were placed on the walls of the laboratory room to serve as visual cues along with the computer, experimenter, a large black shelf, and a door.

Surgery

Permanent guide cannulae were implanted bilaterally into the hippocampus of all rats. Rats received subcutaneous injections of buprenorphine (Temgesic®, Schering-Plough) at 0.03 mg/kg prior to surgery to offer post-surgical analgesia. Rats were anesthetized using 4% isoflurane gas (Benson Medical Industries, Inc.) in oxygen with a flow of 1.5 l/min. Surgical anesthetic plane was maintained using 1–2% isoflurane throughout surgery. The rats were positioned in a stereotaxic apparatus (Kopf Instruments). An incision was made in the scalp, the skin retracted, and seven 0.7 mm holes were drilled into the skull. Three pilot holes were drilled for anchor screws (Small Parts, United States), and four holes for guide cannulae. Two 23-gauge stainless steel guide cannulae were lowered bilaterally into the dorsal (A/P –3.5, M/L: ± 2.0 , D/V: –3.2) and ventral (A/P: –5.8, M/L: ± 5.2 , D/V: –6.0) hippocampus and were held in position using dental acrylic. The guide cannulae were plugged using 30-gauge wire obturators, which stayed inside until infusion. Following surgery, rats were injected with Metacam®, 5 mg/ml, 0.5 mg/kg (Boehringer Ingelheim) and monitored for 24 h, then returned to their home cages.

Data Collection and Statistical Analysis

Data were collected with a movement tracking software (Noldus Ethovision 3.1) and a ceiling mounted camera. Statistical analysis was performed using IBM SPSS 34 Statistic Version 22. Acquisition and probe test data were analyzed with two-way repeated measures ANOVA. When a significant interaction occurred, planned *post hoc* pair wise comparisons were done between the pre- and mass trained quadrants on the trial 1 and immediate probes as we expected differences to occur. Planned *post hoc* pairwise comparisons were done for the consolidation probes comparing % time spent in the pre- vs. mass trained quadrants.

Training/Testing

The training procedure consisted of a three phase version of the MWT. All training and testing occurred in the same room and occurred between 07:00 and 12:00, except for phase 3. Two groups of rats were run in this experiment, differing only in the amount of training and time between phases.

Phase 1

Rats were brought into the testing room in individual cages on a wheeled cart and placed into the NE corner of the room. Animals

were run in squads of 4, one right after the other. For this phase, all rats were trained to find a hidden platform located in the SW quadrant of the pool. Each rat was given eight trials a day for 4 days, for a total of 32 trials. The starting position of each trial was randomly assigned to arbitrarily equidistant points. The sequence of start points varied each day. The rat was placed in the pool at one of the start positions facing the pool wall and allowed to swim until they reached the hidden platform or until 60 s had elapsed. If after 60 s the rat had not found the platform it would be led there by hand. After every trial the rat would be left on the platform for 10 s, removed and placed back in its transport cage. No drugs were administered during this phase of training. Each training session took approximately 30–40 min with an average inter-trial interval of 5 min.

Phase 2

Twenty-four hours after completing phase 1 rats began phase 2 of training. The platform was moved to the NE quadrant, opposite to that of phase 1. For group 1, training consisted of 16 trials within a 2-h period, all on day 5. For group 2, training was 20 trials. Similar to phase 1, rats were placed in the pool at one of the cardinal positions in random order, were allowed 60 s to find the platform, and remained on it for 10 s. The NE starting point was eliminated during phase 2 because it was closest to the platform. Prior to training, rats were brought into a novel room and assigned to either the treatment group or a control group. The assignment to treatment groups was designed in such a way that there was no difference in the pre-training acquisition between pre-treatment groups. The treatment group (group 1: $n = 6$, group 2: $n = 7$) received bilateral hippocampal infusion CPP in artificial cerebral spinal fluid (0.32 ng/ μ l). The control group (group 1: $n = 7$, group 2: $n = 7$) received just artificial cerebral spinal fluid. Obturators were removed and infusions were done at a rate of 0.25 μ l/min for 4 min, for a total of 1 μ l per infusion site. This dose is the same used in the McDonald et al. (2005) study and is a dose that has been shown to impair spatial performance (Riekkinen and Riekkinen, 1997).

The infusion cannulae were left inside the permanent guide cannula for an extra minute to allow for diffusion of the drug. After this 5-min procedure, new obturators were placed into the permanent guide cannula and rats were returned to their home cage. Training began 30 min after infusion.

For group 1, the platform was removed after the 16 massed training trials and a 30-s probe test was given. The interval between the last trial and the probe test was 5 min. Group 2 did not receive a probe test during this time. All training occurred within a 2-h period, a time frame that CPP has been shown to block prime-burst potentiation in the hippocampus (Kentros et al., 1998).

Phase 3

Eight hours after completing the phase 2 probe test, group 1 received a second probe test. This was done to determine if what was learned during mass training would be remembered. The rat was placed in the pool in the exact same way, in the same start location, as the prior probe test. After 30 s the rat was removed from the pool. Group 2 received a probe test 24 h after completing

phase 2. This difference in the two groups was used to examine potential differences in periods of consolidation.

Perfusion

The day after phase 3 the rats were euthanized with an intraperitoneal injection of sodium pentobarbital (300 mg/kg) and then transcardially perfused with 4% paraformaldehyde solution and 5% phosphate buffered ACSF. The tissue was left in the 4% paraformaldehyde solution for 24 h for cryoprotection, then placed into a 30% sucrose + 0.2% sodium azide solution for 5 days. Brain tissue was sliced on a freezing microtome and sections of the hippocampus were stained with a cresyl violet stain. Proper cannulation placement was analyzed and all subjects with cannulation points outside of the hippocampus were excluded from analysis.

RESULTS

Experiment 1

An outline of Experiment 1 can be found in **Figure 1**.

Results Group 1

The primary measure of learning and memory used during acquisition was latency to find the platform. Path length was also recorded with identical results across all experiments and so were not included for sake of space. However, they can be found in the **Supplementary Material**. Pre-training was analyzed in four trial average blocks. **Figure 2A** clearly shows that over the 4-day pre-training period, all rats from both groups learned the escape platform position in the pool. Two-way repeated measures ANOVA showed that there was a significant effect of Trial ($F_{7,77} = 63.307$, $P < 0.001$) on latency but no effect of Group ($F_{1,11} = 0.016$, $P > 0.05$) and no interaction ($F_{7,77} = 1.571$, $P > 0.05$). Pre-training data were reliably identical across groups and experiments and so will only be presented as a graph once (**Figure 2A**).

Figure 2B shows that with or without hippocampal NMDAR function, rats successfully learned a new platform position over a 2-h training period. Mass-training was analyzed in two trial average blocks. Despite the initial difference in escape latency, a two-way repeated measures ANOVA revealed a significant effect of Trial on latency ($F_{7,77} = 22.829$, $P < 0.001$) but not of Group ($F_{1,11} = 4.008$, $P > 0.05$) and no interaction ($F_{7,77} = 1.984$, $P > 0.05$).

To determine if the rats had successfully acquired a spatial memory during pre-training, as well as test the effects of CPP on the expression of already formed memories, the first trial of mass training was analyzed as a probe trial (**Figure 2C**). Comparisons were made between the percentage of time spent in the target quadrant where rats were trained during pre-training and an average of the percentage of time spent in the other three quadrants. Because the platform was present during this trial, not all animals had equal latencies on trial one of mass-training and so not all animals spent an equal amount of time searching within the pool. The percent of time spent in each quadrant given the total time each animal spent in the pool was

used. Controls spent an average 39.6% search time in the target quadrant and 20.1% in all other quadrants. CPP infused rats spent an average 37.8% search time in the target quadrant and an average of 20.7% in all other quadrants. Two-way repeated ANOVA revealed that there was a significant effect of quadrant ($F_{1,11} = 55.660$, $P < 0.001$) but not of Group ($F_{1,11} = 0.247$, $P > 0.05$) and no interaction ($F_{1,11} = 0.227$, $P > 0.05$). These data show that rats had developed a spatial memory during pre-training and that CPP did not interfere with the expression of this memory. Cannulation placements for this experiment can be seen in **Figure 2D**.

After 16 trials of mass-training to the new quadrant location, the platform was removed, and rats were put through a 30-s probe test to determine if a new spatial preference had been learned (**Figure 3A**). Comparisons were made between the percentage of time spent in the new target quadrant where rats were trained during mass training and an average of the percentage of time spent in the other three quadrants. ACSF infused controls spent an average of 42% in the new target quadrant and 19.3% in the all other quadrants. CPP infused rats spent an average of 36.1% in the new target quadrant and 21.2% in all others. Two-way repeated measures ANOVA revealed a significant effect of quadrant ($F_{1,11} = 52.568$, $P < 0.001$) but not of Group ($F_{1,11} = 2.289$, $P > 0.05$) with no interaction ($F_{1,11} = 2.280$, $P > 0.05$). These results indicate that both groups had learned a new spatial preference following mass-training.

Probe data were also analyzed comparing percentage of time spent in a small region surrounding the platform covering 2% of the total surface area of the pool (annulus), to contrast with the 25% surface area of the quadrant. This type of analysis provides information about the spatial specificity of what was learned during mass training, as the region of interest is limited to the area immediately surrounding the platform location. Controls spent an average of 10.2% in the new annulus and an average of 1.5% in the pre-trained location. CPP infused rats spent an average of 7.9% in the new annulus quadrant and an average of 2.2% in all others (**Figure 3B**). Two-way repeated measures ANOVA revealed a significant effect of quadrant ($F_{2,22} = 51.402$, $P < 0.001$) but not of Group ($F_{1,12} = 0.355$, $P > 0.05$) with no interaction ($F_{2,22} = 2.090$, $P > 0.05$). This shows that the spatial preference rats learned over training was specific to the platform location.

Previous work has shown that hippocampal NMDARs may have a critical role in the consolidation of newly acquired memories (McDonald et al., 2005; Roesler et al., 2005). To assess this claim, for group 1, a probe test was administered 8 h after the end of mass training to determine if what was learned during mass-training would remain or be forgotten due to a lack of consolidation.

The percentage of time spent in the two trained target quadrants, pre-training and mass training, as well as the average percentage of time spent in the other two non-trained quadrants, were compared within and between groups (**Figure 3C**). Two-way repeated measures ANOVA, showed no effect of quadrant ($F_{2,22} = 2.043$, $P > 0.05$), no effect of Group ($F_{1,11} = 11.373$, $P > 0.05$), but a significant Group \times Quadrant interaction ($F_{2,22} = 7.256$, $P < 0.05$). *Post hoc* pairwise comparisons using

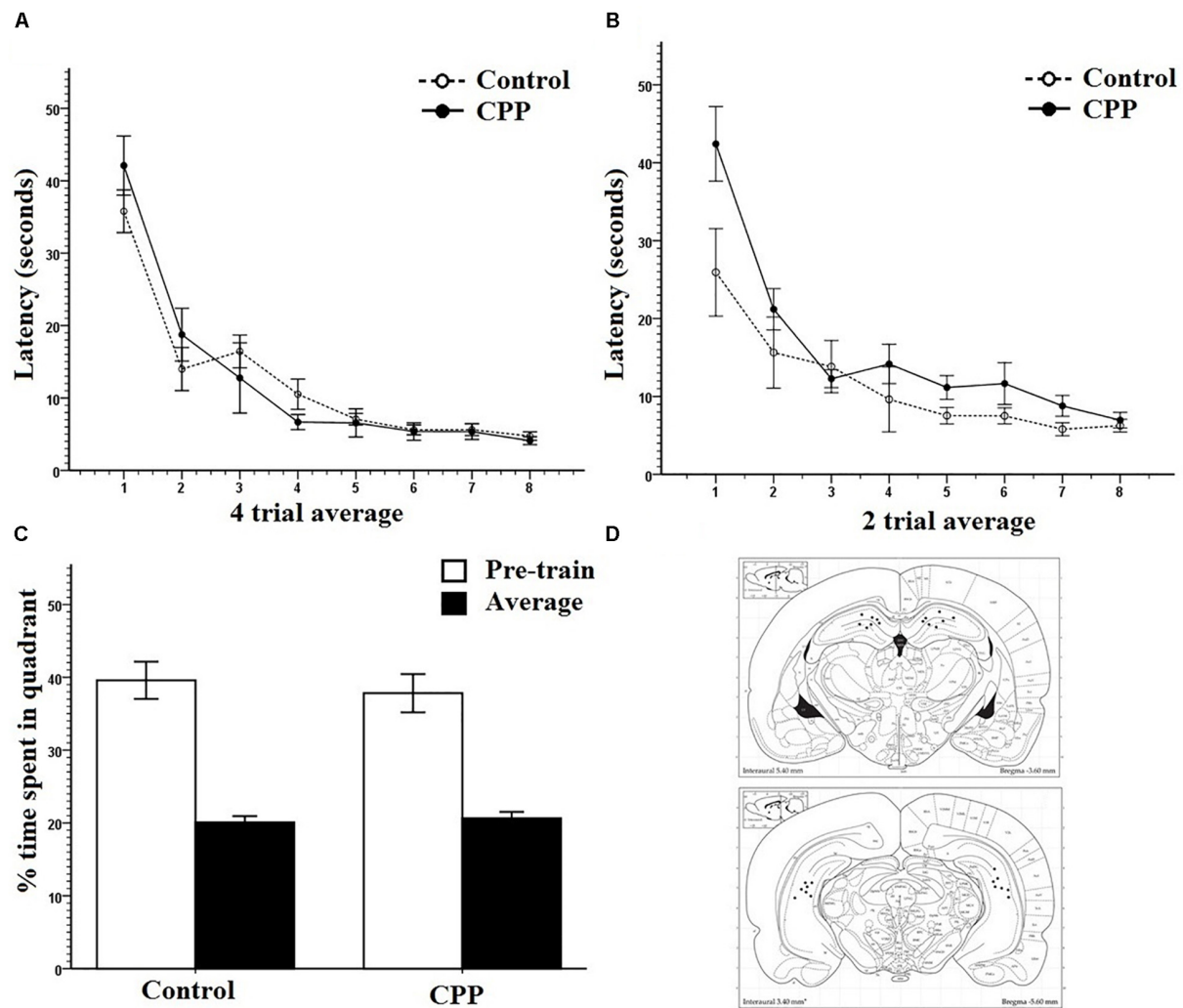


FIGURE 2 | (A) Pretraining for group 1 in Experiment 1. Four trial averages of the latency in seconds to find the platform over training 4 days/eight trials per day. Both controls and pre-CPP rats successfully learn over training. **(B)** Mass training for group 1 in Experiment 1. Two trial averages of the latency in seconds to find the new platform over training 2 h/16 trials. Both controls and CPP rats learn over training. **(C)** A probe test of trial 1 mass training in group 1 of Experiment 1. The percentage of time spent of the trial length in the pre-training quadrant versus an average of the other three. Both controls and CPP rats display a preference for the pre-trained quadrant. **(D)** Dorsal and ventral hippocampal cannulation locations for the CPP rats of group 1 in Experiment 1. Error bars $1 \pm$ SE.

LSD revealed a significant difference within the CPP group with these rats spending more time in the pre-trained quadrant (Avg = 37.35%) than in the mass trained quadrant (Avg = 17.18%) ($P = 0.03$). No difference was found within the control group between any of the quadrants.

These results indicate that the effect of mass training did not last 8 h in the rats given CPP, and that their spatial preference reverted back to the pre-trained quadrant. The control probe data seems harder to interpret. On the surface this quadrant preference result would suggest that the control rats had forgotten the mass-trained target platform position. However, we do not think this is the case. We were concerned that the 30-s probe trial performed immediately following mass training might have resulted in some extinction and provided the subjects with the knowledge that the platform

might be located nowhere (probe trial) or elsewhere (mass training). The combination of this new knowledge and some extinction could have resulted in a somewhat contaminated competition test. We were intrigued by the idea that the control rats might have swam to the target annulus but did not persevere there because of this new knowledge and some extinction. Importantly, this probe trial was not part of any of the experiments reported in McDonald et al. (2005) in which the control rats always showed a quadrant preference for the mass-trained location in different groups of rats over many experiments. One possibility was that the rats did search the mass-trained location but did not persevere there for long.

To test this idea, we analyzed the 8-h probe trial in another way. This probe data was analyzed comparing percentage

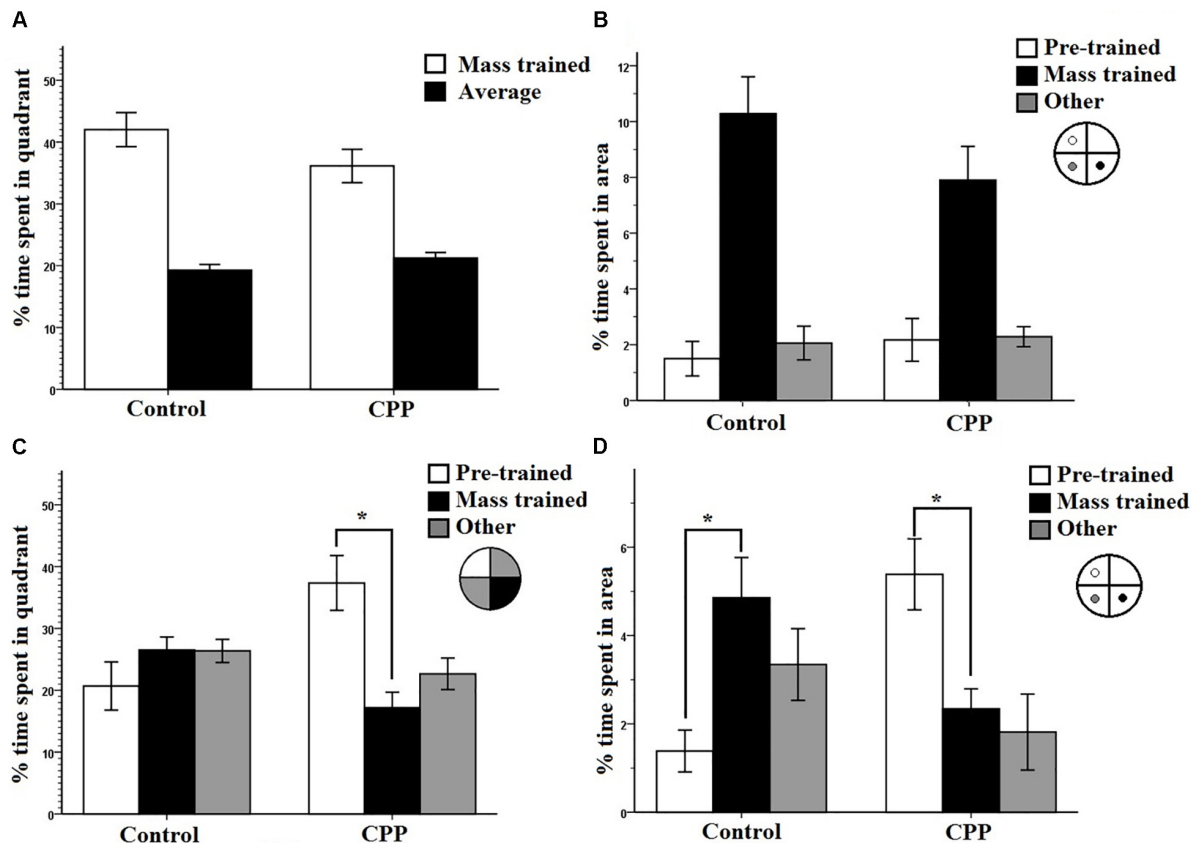


FIGURE 3 | (A) A 30-s probe test immediately after mass training for group 1 in Experiment 1. The percentage of time spent in the mass trained quadrant versus an average of the other three was compared. Both controls and CPP rats displayed a preference for the mass trained quadrant. **(B)** A 30-s probe test immediately after mass training for group 1 in Experiment 1. The percentage of time spent in the region immediately surrounding the platform locations during pre-training, mass training, and a non-trained area were compared. Both controls and CPP rats displayed a preference for the area surrounding the mass trained platform. **(C)** A 30-s probe test 8 h after mass training for group 1 in Experiment 1. The percentage of time spent in the pre-trained quadrant, mass trained quadrant and the average of the other two was compared. Controls displayed no preference whereas CPP rats displayed a preference for the pre-trained quadrant. **(D)** A 30-s probe test 8 h after mass training for group 1 in Experiment 1. The percentage of time spent in the region immediately surrounding the platform locations during pre-trained, mass trained and a non-trained area were compared. Controls displayed a preference for the area immediately surrounding the mass trained platform whereas CPP rats displayed a preference for the area surrounding the pre-trained platform. Error bars $1 \pm \text{SE}$, $*p < 0.05$.

of time spent in the annulus of the pre-trained and mass-trained platform locations. Probe data for the 8-h consolidation probe was analyzed comparing percentage of time spent in the annulus of the pre-trained and mass trained platform locations. Controls spent an average of 4.8% in the mass trained annulus and an average of 1.3% in the pre-trained annulus. However, CPP infused rats spent an average of 2.3% in the pre-trained annulus and an average of 5.4% in the mass trained annulus (**Figure 3D**). Two-way repeated measures ANOVA revealed no significant effect of quadrant ($F_{2,24} = 1.029$, $P < 0.001$) and not of Group ($F_{1,12} = 0.001$, $P > 0.05$). However, there was a significant interaction ($F_{2,22} = 10.936$, $P < 0.001$). *Post hoc* pairwise comparisons using LSD revealed a significant difference within the CPP group, rats spending more time in the pre-trained location than in the mass trained location ($P = 0.012$). Control rats spent significantly more time in the mass trained location than in the pre-trained location ($P = 0.006$).

These results indicate that rats given CPP reversed their spatial preference compared to controls 8 h after mass-training suggesting that the CPP rats did not consolidate the representation guiding them to the mass training location. Although it appeared that the control rats did not remember the mass-training escape location based on the quadrant preference data, they clearly expressed a memory for the correct location and this memory was highly specific to the correct annulus providing direct evidence that they retained the mass-training representation for at least 8 h.

Results Group 2

Figure 1 shows the experimental design for Group 2. As in Group 1, latency and various measures of spatial specificity of behavior during probe trials were analyzed Group 2. For the initial acquisition data a two-way repeated measures ANOVA showed that there was a significant effect of Trial ($F_{7,84} = 26.965$, $P < 0.001$) on latency but no effect of Group ($F_{1,12} = 0.925$,

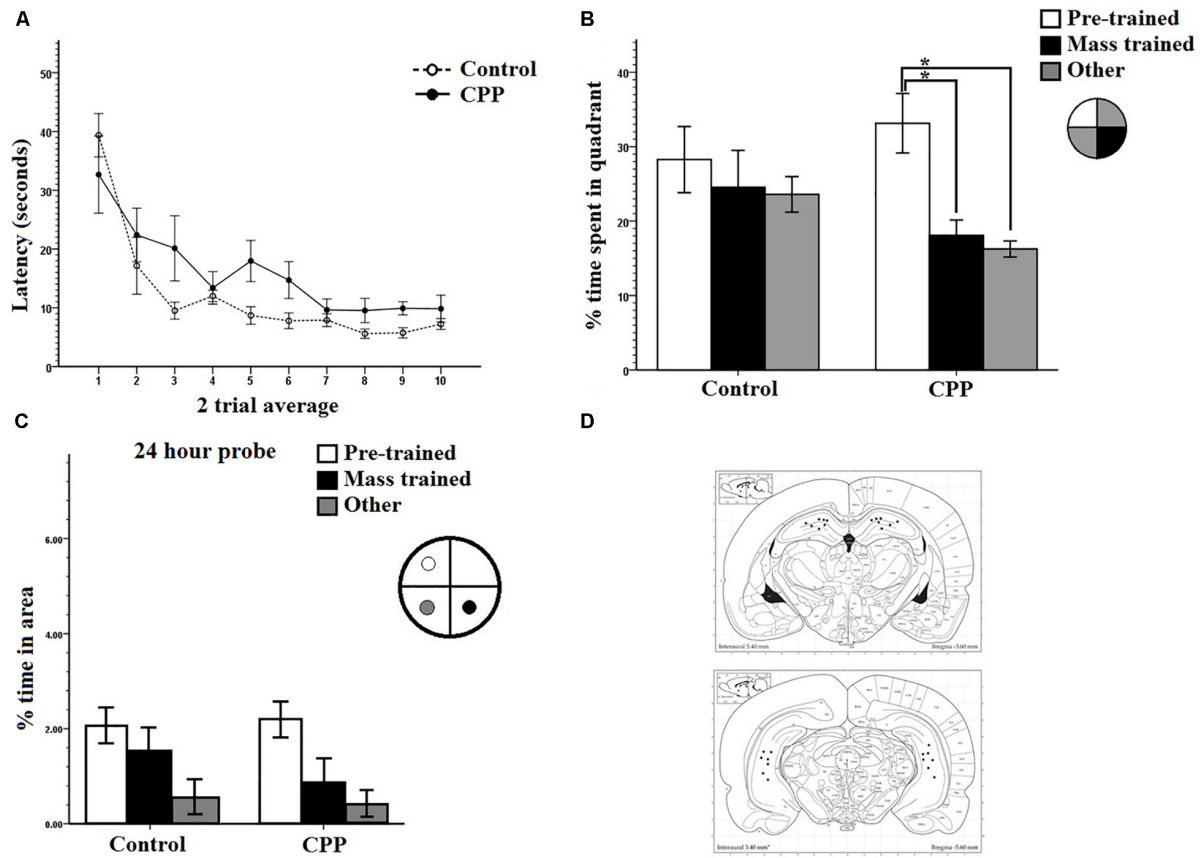


FIGURE 4 | (A) Mass training for group 2 in Experiment 1. Two trial averages of the latency in seconds to find the new platform over training 2 h/20 trials. Both controls and CPP rats learn over training. **(B)** A 30-s probe test 24 h after mass training for group 1 in Experiment 1. The percentage of time spent in the pre-trained quadrant, mass trained quadrant and the average of the other two was compared. Controls displayed no preference whereas CPP rats displayed a preference for the pre-trained quadrant. **(C)** A 30-s probe test 24 h after mass training for group 2 in Experiment 1. The percentage of time spent in the region immediately surrounding the platform locations during pre-trained, mass trained and a non-trained area were compared. **(D)** Dorsal and ventral hippocampal cannulation locations for the CPP rats of group 2 in Experiment 1. Error bars $1 \pm \text{SE}$. $*p < 0.05$.

$P > 0.05$) and no interaction ($F_{7,84} = 0.537$, $P > 0.05$). Over the 4-day pre-training period, all rats from both groups learned the platform position in the pool.

The data from the massed training day for Group 2 is shown in **Figure 4A**. As can be seen, rats with or without hippocampal NMDAR function could successfully learn a new platform position in the same training context over a 2-h period. Consistent with these observations, a two-way repeated measures ANOVA revealed a significant effect of Trial on latency ($F_{9,108} = 17.898$, $P < 0.001$) but not of Group ($F_{1,12} = 4.106$, $P > 0.05$) and no interaction ($F_{9,108} = 1.412$, $P > 0.05$). Cannulation placements for this experiment can be seen in **Figure 4D**.

For Group 2, the probe test for memory retention was done 24 h after completion of mass-training. The percentage of time spent in the two trained target quadrants, pre-training and mass-training, as well as the average percentage of time spent in the other two non-trained quadrants, were compared within and between groups (**Figure 4B**). Two-way repeated measures ANOVA, showed a significant effect of quadrant

($F_{2,24} = 4.408$, $P < 0.05$), a significant effect of Group ($F_{1,12} = 7.681$, $P < 0.05$), and no Group \times Quadrant interaction ($F_{2,24} = 1.366$, $P > 0.05$). *Post hoc* pairwise comparisons using LSD revealed a significant difference within the CPP group, rats in this group spent more time in the pre-trained quadrant (Avg = 33.1%) than in the mass-trained quadrant (Avg = 18.1%) ($P = 0.05$) as well as the average of the other two quadrants (16.3%) ($P = 0.009$). No differences were found within any of the control group percentages or between groups.

Just like for group 1, the control rats from group 2 did not appear to remember the rapidly acquired new location when tested later. For group 2, the subjects were tested 24 h later. Interestingly, when we did an alternative analysis of the 8-h probe data for group 1 in which we assessed the spatial specificity of the probe trial we found evidence that the controls did remember the precise location of newly acquired escape platform (spending more time in the new platform annulus versus the old platform annulus) whereas the CPP rats spent more time in the old platform annulus.

We did this same analysis for the 24-h probe groups and the results suggest that both the control and CPP rats did not remember the newly acquired location 24-h later (**Figure 4C**) but the CPP rats did seem to prefer the old annulus location. An ANOVA with repeated measures on location indicated a significant effect of swim location ($F_{2,24} = 7.6401$, $P < 0.0027$), but no Group ($F_{1,12} = 0.7531$, $P = 0.4$) or interaction effect ($F_{2,24} = 0.4261$, $P = 0.6$). A *post hoc* pairwise comparisons using LSD indicated significant differences between the old and new platform location ($p < 0.03$), and the old and other location ($p < 0.001$).

We completed one final analysis of this data set looking at what annulus area each subject entered first during the probe trial. In the test of first annulus area entered for the 24-h probe, most of the controls swam to the mass trained annulus over the pre-trained annulus location (**Figure 5**) and the CPP rats first swam to the pre-trained escape annulus. We employed a chi-square analysis of this data set with the knowledge that this statistic requires high sample sizes to have enough power. Despite this caveat, the control preference was marginally significant ($5/6$, $X^2 = 5.6$, $df = 2$, $P = 0.060$), whereas analysis of the CPP rats that swam to the pre-trained over the mass trained annulus was significant ($6/7$, $X^2 = 7.4$, $df = 2$, $P = 0.025$).

The 24-h probe results are similar to those found in group 1 and indicate that rats with hippocampal NMDARs blocked can rapidly learn a new spatial position during mass training, they do not maintain this preference over a 24-h period. Control rats showed evidence that they did remember the new spatial position 24 h later by entering the new platform position first providing further evidence that hippocampal NMDARs are involved the consolidation of spatial memory.

Discussion

In this experiment, rats with bilateral hippocampal cannulations were pre-trained on the spatial version of the MWT, given either intra-hippocampal CPP or ACSF and then mass-trained to a new platform location.

The general pattern of results showed that rats with hippocampal NMDAR blockade were able to rapidly acquire information to help them navigate to a new spatial location in a pool in which pre-training to a different location had occurred. Probe trial data suggested that although this representation was acquired the CPP rats, it was not consolidated properly.

These results provide three insights into the role of NMDAR in learning and memory. Firstly, NMDAR are not necessary for the expression of previously acquired memories, and the blockade of NMDAR does not extinguish or alter previously acquired memories (Shapiro and Caramanos, 1990; Kim et al., 1991; Matus-Amat et al., 2007). Second, NMDAR are not necessary for the rapid acquisition of novel information. This effect has been explored in different ways in the past (Bannerman et al., 1995; Otnæss et al., 1999; Inglis et al., 2013) and compliments the previous work done in our lab (Holahan et al., 2005; McDonald et al., 2005). Third, NMDARs have a role in the consolidation of recently acquired memory (Kesner and Dakis, 1995; Santini et al., 2001).

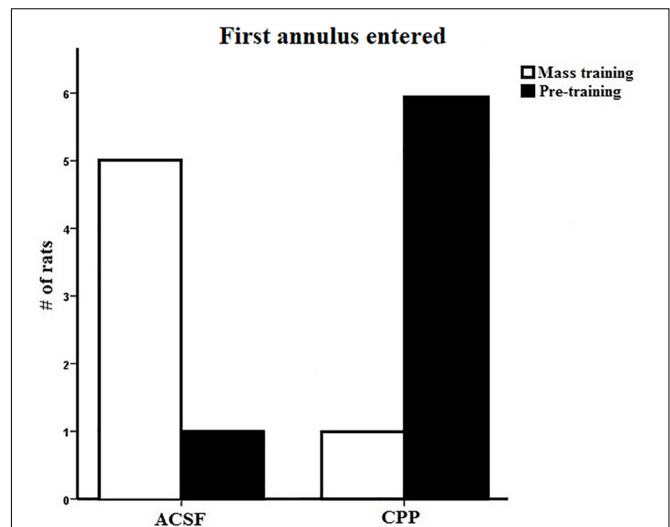


FIGURE 5 | First annulus entered during the 24-h probe test for group 2 in Experiment 1. Five out of the six control rats first swam to the mass trained annulus where as six out of the seven CPP rats first swam to the pre-trained annulus.

Experiment 2

It has been argued that in studies where the same training context is used for both pre-training and standard training (Hoh et al., 1999; McDonald et al., 2005), most of the learning that is crucial for completing the task occurs during the pre-training phase and that later training in the task can be completed without engaging plasticity mechanisms in the hippocampus. This means that even though the platform is in a different position during regular training, the rat can locate and “learn” the new position without needing hippocampal plasticity mediated by NMDARs and may either rely on previously acquired hippocampal memories or cortical plasticity (Inglis et al., 2013). However, even when two completely different contexts are used (Bannerman et al., 1995), replications have failed to reproduce identical results (Inglis et al., 2013). To determine whether NMDARs only encode novel spatial information, and not further learning dependent on previously acquired spatial information, a second version of Experiment 1 was completed but using two different contexts for pre-training and mass training.

Methods

In the multiple room version of the rapid acquisition MWT procedure, animals were pre-trained in room A: a separate room at the other end of the facility, with distinct extra maze cues and relationships between these cues. These included the door, posters, computer, and experimenter. This training consisted of 4 days of training, eight trials a day, to the same platform location each day, similar to Experiment 1. For the second phase, animals were mass-trained to a new platform location in room B over 2 h. Room B was the same room used in Experiment 1. The animals were brought to the room in a different style of transport cage between pre-training and mass-training phase. The drug administration process was identical to Experiment 1, either CPP

or ASCF was infused bilaterally into the hippocampus 30 min prior to mass training in room B. A depiction of the two rooms and experimental design can be seen in **Figure 1**.

Two groups of rats were trained on this task. For group 1 ($n = 13$), mass-training consisted of 16 trials in room B. In group 2 ($n = 11$), mass training was 20 trials. Trial one of mass training was analyzed in a similar way as Experiment 1 to assess if spatial pre-training in room A had any effects on novel spatial navigation. Previous work from our lab has shown that some aspects of spatial navigation can transfer between training environments (Clark et al., 2015). Group 1 received a 30-s probe test immediately after mass training to assess whether mass training induced a spatial preference. For group 2, a 30-s probe test was run 24 h after mass-training to determine if what was learned during mass-training was consolidated into long-term memory.

Surgical procedure, data analysis, and histology was identical to that of Experiment 1.

Results Group 1

Similar to the results of Experiment 1, both groups of rats successfully learned to navigate to the hidden platform location over the course of pre-training. A two-way repeated measures ANOVA showed that there was a significant effect of Trial ($F_{7,63} = 39.969$, $P < 0.001$) on latency but no effect of Group ($F_{1,9} = 0.704$, $P > 0.05$) and no interaction ($F_{7,63} = 0.704$, $P > 0.05$). **Figure 6A** shows the mass-training data and clearly indicates that the control group learned the new location of the escape platform while the CPP group did not learn the new location over the course of training. A two-way repeated measures ANOVA revealed a significant effect of Trial on latency ($F_{7,63} = 3.599$, $P < 0.05$) and of Group ($F_{1,9} = 19.872$, $P < 0.05$) but no interaction ($F_{7,63} = 1.856$, $P > 0.05$).

The probe test run immediately after mass training showed that control rats spent more time in the quadrant that the new platform position was previously located while the CPP rats did not show this quadrant preference (**Figure 6B**). Control rats spent more time in the target quadrant (35.2%) than in the average of the other three (21.6%) (**Figure 6B**). This was not the case for the CPP rats who spent relatively equal time in each (21.6% and 20.5%). Consistent with these observations two-way repeated measures ANOVA revealed a significant effect of quadrant ($F_{1,9} = 5.811$, $P < 0.05$) and of Group ($F_{1,9} = 15.975$, $P < 0.05$) but no interaction ($F_{1,9} = 4.179$, $P > 0.05$). This pattern of results show that NMDAR blockade impairs rats' ability to learn a spatial location when the available environmental information is novel.

Results Group 2

Both groups of rats successfully learned to navigate to the escape platform position during pre-training. For this data set, a two-way repeated measures ANOVA showed that there was a significant effect of Trial ($F_{7,77} = 47.696$, $P < 0.001$) on latency but no effect of Group ($F_{1,11} = 0.423$, $P > 0.05$) and no interaction ($F_{7,77} = 0.587$, $P > 0.05$). **Figure 6C** shows the mass training data and clearly shows that control rats learned the new escape platform position over the course of mass training whereas rats

given intra-hippocampal CPP injections were severely impaired. Statistical analysis of this data set using a two-way repeated measures ANOVA revealed a significant effect of Trial on latency ($F_{9,99} = 4.192$, $P < 0.001$) and of Group ($F_{1,11} = 11.5$, $P < 0.05$) but no interaction ($F_{9,99} = 1.842$, $P > 0.05$).

For the 24-h probe, the percentage time swam in the quadrant where the platform was located during mass-training was compared to an average of the other three quadrants (**Figure 6D**). As can be seen (**Figure 6D**) both groups did not spend more time in the mass-trained quadrant compared to the other quadrants. A two-way repeated measures ANOVA revealed an effect of quadrant ($F_{1,11} = 8.565$, $P < 0.05$) but not of Group ($F_{1,11} = 0.414$, $P > 0.05$) and no interaction ($F_{1,11} = 0.074$, $P > 0.05$). These results suggest that mass training to a new location in a new room was not retained 24 h after training in either groups. The implication of this pattern of results will be discussed below.

Cannulation placements can be seen in **Figures 6E,F**.

Discussion

When rats were given intra-hippocampal CPP injections they were incapable of acquiring novel spatial information in room B, despite spatial pre-training in room A. Probe tests revealed that controls acquired a spatial preference for the pool quadrant where the platform was located, CPP rats did not. This contrasts with Experiment 1 in which rats were capable of temporarily acquiring new spatial information under hippocampal NMDAR blockade in the same room as pre-training. The only factor that differed from these two experiments was the spatial information available to the rats during mass training.

The results of Experiment 2 indicate that hippocampal NMDAR may be necessary for the acquisition of spatial information during MWT training (the arrangement and type of extra-maze cues, room and maze geometry). Presumably, this environmental information would be learned during pre-training in room A. Once this has been learned, however, hippocampal NMDARs would not be necessary for using this same information in learning new things, such as learning to navigate to a new platform location. When brought to a novel room, however, rats without hippocampal NMDAR function could not perform at the level of controls, indicating their importance in novel spatial learning.

When brought to training room B, both CPP and ASCF controls displayed a spatial preference for one of the pool quadrants during trial 1 of mass-training, despite having never been in room B before. This means that some information learned during pre-training in room A carried over to room B. It has been shown that some components of spatial navigation, namely heading direction, can be transferred between spatially distinct environments (Dudchenko and Zinyuk, 2005; Clark et al., 2015). Head direction cell orientation is often controlled by environmental boundaries and maze shape (Hamilton et al., 2007; Clark et al., 2012). Indeed, in this experiment the overall shape of the testing rooms were similar, but opposite in orientation and different in dimension, (room A: width: 10 ft., length: 20 ft.; room B: width: 10 ft., length: 15 ft.) as well as using an identical pool. Based on Clark et al. (2015), which used the exact same rooms and

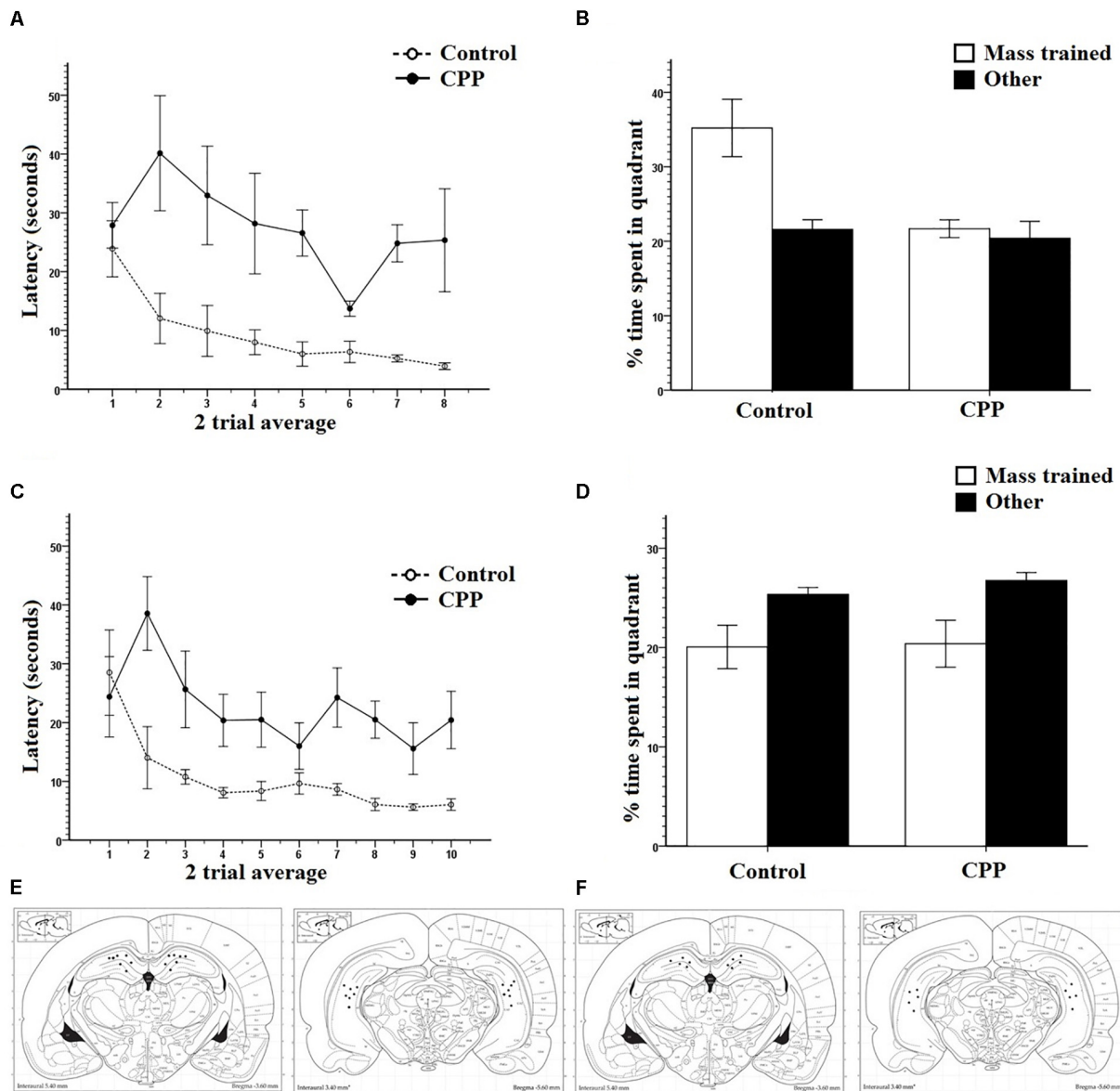


FIGURE 6 | (A) Mass training for group 1 in Experiment 2 in room B after being pre-trained in room A. Two trial averages of the latency in seconds to find the new platform over training 2 h/16 trials. Control rats learned over training whereas as CPP rats did not. **(B)** A 30-s probe test immediately after mass training for group 1 in Experiment 2. The percentage of time spent in the mass trained quadrant versus an average of the other three was compared. Control rats displayed a preference for the mass trained quadrant whereas the CPP rats did not. **(C)** Mass training for group 2 in Experiment 2 in room B after being pre-trained in room A. Two trial averages of the latency in seconds to find the new platform over training 2 h/20 trials. Control rats learned over training whereas as CPP rats did not. **(D)** A 30-s probe test 24 h after mass training for group 1 in Experiment 2. The percentage of time spent in the mass trained quadrant versus an average of the other three was compared. No group of rats displayed a preference for mass trained quadrant. **(E)** Dorsal and ventral hippocampal cannulation locations for the CPP rats of group 1 in Experiment 2. **(F)** Dorsal and ventral hippocampal cannulation locations for the CPP rats of group 2 in Experiment 2. Error bars $1 \pm SE$.

pools as in this experiment, although with different extra-maze cues, it is very possible that head direction information from room A influenced trial 1 of mass training in room B. Despite this initial effect, it was not maintained throughout training, and rats treated with CPP failed to learn the new platform location. This also provides further evidence that NMDAR blockade does not interfere with previously acquired memories.

Experiment 3

IEG activity is a molecular product of learning and memory related behaviors. Spatial memory tasks such as the water maze have been shown to induce expression of Arc, an IEG, in the hippocampus (Guzowski et al., 2001). IEGs such as Arc are thought to mediate the molecular consolidation of memory because of their time course of action and the types of

subsequent molecular mechanisms they induce. When applied to hippocampal tissue, Arc antisense will allow for the induction of LTP, yet its long-term maintenance will disappear (Guzowski et al., 2001). Arc knockout mice similarly express heightened early phase LTP and reduced late phase LTP (Plath et al., 2006). In a fear conditioning paradigm, Czerniawski et al. (2011) showed that an NMDAR antagonist could prevent arc expression in both the dorsal and ventral hippocampus and that arc antisense would impair memory consolidation but spare initial learning, linking NMDARs, Arc, and memory consolidation. Taken together, these electrophysiological, molecular, and behavioral data, all suggest a role for IEGs, and NMDAR dependent Arc in particular, in the long-term consolidation of memory.

For the final experiment, we were interested in assessing immediate early gene (IEG) activity in the hippocampus immediately following mass training in the same versus different rooms. The prediction was that IEGs in hippocampus will be selectively activated in the new room but not the same room condition. We also included a group of rats given mass training in the new room condition but with NMDAR blockade. The prediction is this group would not show the elevations of IEG activity, thus linking NMDAR function and rapid new spatial learning in a new environment.

Methods

The design of Experiment 3 is depicted in **Figure 1**. Behavioral training and testing was very similar to that of Experiments 1 and 2. Pre-training was done in context A for all groups except cage controls. There were four groups in this experiment, differing only in how their mass training was done in reference to pre-training: Same room, New room, New room + CPP, and cage controls ($n = 5$). For the Same room group ($n = 5$), mass reversal training consisted of 16 trials and was performed identically to Experiment 1. For the New room group ($n = 5$) and New room + CPP group ($n = 5$) mass training consisted of 16 trials and was identical to Experiment 2. Drug infusion for the New room + CPP rats was done 30 min before mass training and was performed identical to the CPP group in Experiment 2. The rats were run one at a time during mass training to avoid variation in timing of procedures. After completing mass training, rats were brought back to their home cage until perfusion. Perfusion occurred approximately 70–80 min after trial 8 of mass training. This is a time period in which IEG protein expression after learning is active (Lonergan et al., 2010). Euthanization and perfusion procedures were identical to Experiments 1 and 2.

Tissue collection and immunohistochemistry

After extraction, the brains were placed in 4% PFA solution for 24 h, at which point they were then placed in a 30% sucrose + sodium azide solution for a 3-day period of cryoprotection. The brains were then sliced on a freezing microtome in 12 series, to include the entire hippocampal formation. Tissue was stained using a 3-day immunohistochemical protocol that fluorescently stained Arc protein.

On day 1, tissue was pre-washed in 1% PBS solution, 3×10 min. Tissue was then placed in 2 ml of a 0.3% triton

and PBS solution with a 1:1000 ratio of primary antibody. For Arc protein staining, Arc (c-7) sc-17839 mouse monoclonal IgG (Santa Cruz Biotechnologies) was used. The tissue well was placed on a rotating belly dancer and left to incubate for 24 h. On day 2, the tissue went through a second wash in 1% PBS solution, 3×7 min. After the wash, the tissue was placed in a 1:500 solution of PBS and Alexa fluor 488 donkey anti-mouse IgG (H + L) (Thermo Fisher Scientific). The tissue well was then covered in tin foil to prevent light from affecting the staining process. The well was placed back on the belly dancer and the room light turned off and left for a second 24-h incubation period. On day 3, the tissue was put through another 1% PBS wash, 3×7 min and then wet mounted onto 1% gelatin and 0.2% chromatin coated slides. The slides were covered and placed in a refrigerator at 3°C for 24 h.

Microscopy and cell counts

Cell counts were done on a Zeiss AxioImager M1 microscope (Zeiss, Jena, Germany) using the program Stereo Investigator® (MicroBrightField Inc., 2013, Version 10). A constant light intensity exposure was set at 50%. Light was projected through a FITC filter. A $20\times$ magnification was used when counting cells. All labeled granule cells were individually counted in the granule cell layer of the dentate gyrus. All labeled pyramidal cells were individually counted in the pyramidal cell layers of areas CA1 and CA3. Cell counts in each hippocampal slice for each animal were summed and multiplied by 12 (12 series sections were sliced) to get an approximation of total cell number in each region. Tissue photographs were taken and colored with ImageJ® (Rasband, 2012). For cell count data, *post hoc* pairwise comparisons were done between groups with Bonferroni correction.

Behavioral Results

Over the 4-day pre-training period, the latency for each group followed identical patterns and indicated that all rats from all three groups learned the platform position in the pool. Consistent with this claim, a two-way repeated measures ANOVA showed that there was a significant effect of Trial on latency ($F_{7,84} = 47.373$, $P < 0.001$), no effect of Group ($F_{2,12} = 3.636$, $P > 0.05$) but there was an interaction ($F_{7,14} = 2.312$, $P < 0.05$).

Mass-training was analyzed in two trial average blocks (**Figure 7A**). As can be seen, the average latency of the first trial block was high, at 34.8 s for the Same room rats, 25.9 s for the New room rats, and 34.6 s for the New + CPP rats. By the end of mass training the average latency for the last trial block reduced to 7.0 s for Same room rats, 4.7 s for New room rats, but stayed high at 32.0 s for New + CPP rats. Two-way repeated measures ANOVA revealed a significant effect of Trial on latency ($F_{7,84} = 4.861$, $P < 0.001$) as well as Group ($F_{2,12} = 7.967$, $P < 0.05$) and no interaction ($F_{7,14} = 1.139$, $P > 0.05$). Collectively, these results indicate that both Same room and New room rats successfully learned the platform locations over the course of mass-training while the New + CPP rats did not.

Immunohistochemistry Results

Cell counting was done for all rats in areas CA1, CA3, and dentate gyrus. **Figure 7B** shows that new room rats expressed more Arc positive cells than cage controls, same room rats and

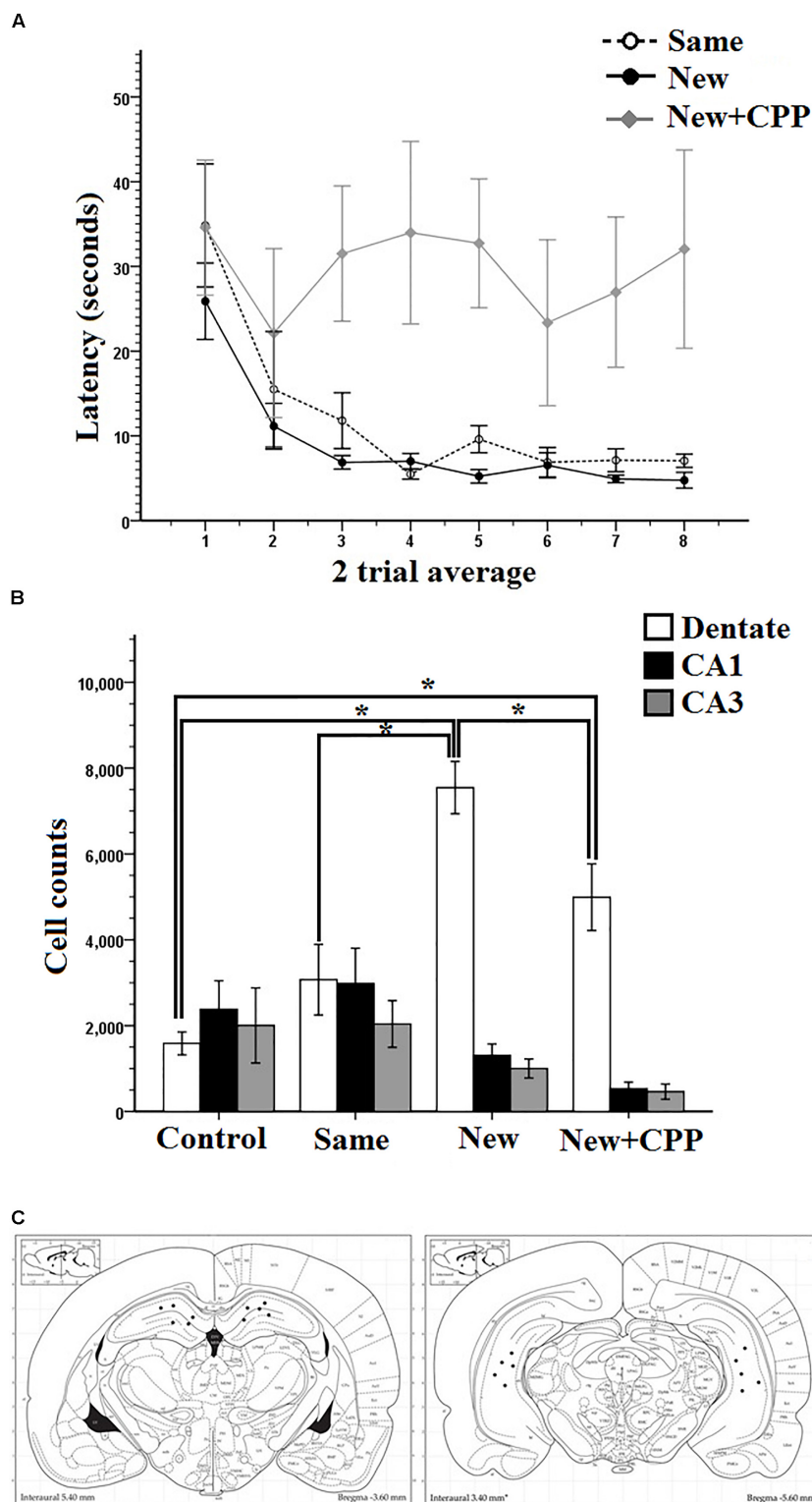


FIGURE 7 | (A) Mass training for Experiment 3 after being pre-trained in room A. Same rats were mass trained in room A, New and New + CPP rats were mass trained in room B. Two trial averages of the latency in seconds to find the new platform over training 2 h/16 trials. Same and New rats learned whereas New + CPP rats failed to learn over the course of training. **(B)** Hippocampal cell counts of Arc positive cells in the dentate gyrus, CA1, and CA3, 70–80 min after trial 8 of massed training in Experiment 3. New rats displayed the significantly more Arc in the dentate gyrus than any other group. CPP significantly reduced the expression of Arc in the dentate gyrus in rats mass trained in the room B. **(C)** Dorsal and ventral hippocampal cannulation locations for the CPP rats of group 2 in Experiment 2. Error bars $1 \pm \text{SE}$. * $p < 0.05$.

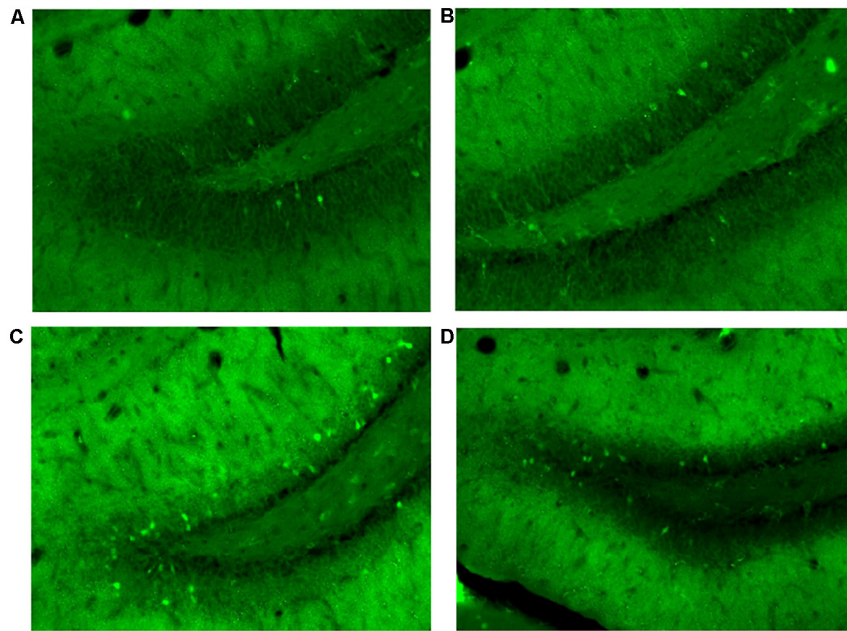


FIGURE 8 | Granule cells in the dorsal dentate gyrus stained positive for Arc protein 70–80 min after mass training in Experiment 3. **(A)** Cage controls. **(B)** Same room. **(C)** New room. **(D)** New + CPP.

New + CPP rats. All three areas were compared between all four behavior groups (**Figure 7B**). Repeated measures ANOVAs were completed on the data and there were significant effects of area ($F_{2,32} = 29.428$, $P < 0.001$), of Group ($F_{1,16} = 3.435$, $P < 0.001$) as well as an interaction ($F_{6,32} = 10.712$, $P < 0.001$). *Post hoc* pairwise comparisons were made between all the groups and areas. Significant differences were found between cell counts in the dentate gyrus of the New room rats. New room rats expressed more Arc positive cells than cage controls ($P < 0.001$), same room rats ($P < 0.001$), and New + CPP rats as well ($P < 0.05$). The New + CPP rats also expressed more Arc positive granule cells than cage controls ($P < 0.05$) but did not differ from Same room rats. For area CA1 and CA3, no significant differences were found between any of the groups. This indicates that New room training induces more dentate Arc expression than Same room and cage controls, and that intra-hippocampal NMDAR blockade diminishes this effect.

Cannulation placement for this experiment can be seen in **Figure 7C**. Images of the tissue can be seen in **Figure 8**.

Discussion

In this experiment, rats were trained in a version of the MWT that involved multiple training rooms. The effect of the NMDAR antagonist CPP on Arc protein expression in hippocampal sub-regions in response to learning experiences was examined. When pre-trained in the MWT in room A, rats could easily learn a new platform position in room A or in room B. However, when CPP was infused into hippocampus prior to the second training phase, rats could not learn a platform position in room B, despite pre-training. These results are identical to those found in Experiment 2. They further support the idea that hippocampal

NMDARs are critical for the acquisition of novel environmental information used in spatial navigation.

The expression of the protein for the immediate early gene Arc differed between group and region, depending on the training conditions. In the dentate gyrus, expression was high for the New group compared to the equally low cage controls and Same room group. When CPP was given, this corresponded with both a reduction in dentate Arc expression and an impairment in learning compared to the New room group. No significant differences were observed for either area CA1 or CA3 between any of the groups.

Despite a lack of a defined pattern of behavior related activity in areas CA1 and CA3, the pattern of Arc expression in the dentate gyrus fits with the behaviors exhibited by the rats in their respective learning conditions. Learning a new spatial platform location in the same environment as pre-training, dentate arc expression was not significantly different from cage controls. Learning in the new room, however, produced a large increase in dentate Arc expression. This would indicate that if Arc is necessarily tied to learning and plasticity, that the same room reversal training in the MWT is not the same as novel room training, behaviorally or molecularly.

GENERAL DISCUSSION

In these experiments, we assessed the role that hippocampal NMDARs have in spatial memory and the molecular processes associated with it. Without the use of NMDAR function in the hippocampus, rats were capable of expressing what they had learned previously, and they could also learn new spatial

information in the same environment as pre-training. When brought to a completely novel training environment, rats could not learn new spatial information at all without the use of hippocampal NMDARs. These results lead to the conclusion that NMDARs mediate the acquisition of novel environmental information to be used in spatial navigation.

This type of NMDAR dependent behavior was also found to induce specific patterns of Arc expression in the hippocampus, namely the dentate gyrus. Expression was low in the NMDAR independent task (same room), and high in the NMDAR dependent task (new room). CPP both blocked learning and reduced Arc expression in animals trained in the new room. This pattern of results points to a link between these three phenomena: NMDAR function, Arc expression, and novel spatial learning. The relationship between these will be explored below.

NMDAR Blockade in the Dorsal Versus Full Hippocampus

The inspiration and design of the current experiments came from McDonald et al. (2005). In that series of experiments only the dorsal hippocampus was blocked for the intracranial experiments and no effect of NMDAR blockade on mass-training of a new spatial position was reported. Experiment 1, from the current work, was completed to determine if the pattern of results observed in the McDonald et al. (2005) study was due to functional NMDARs in the ventral hippocampus. The ventral portion of the hippocampus has been shown to support certain aspects of spatial learning (Ferbinteanu et al., 2003). Very few MWT studies have been done with full hippocampal NMDAR blockade (Steele and Morris, 1999; Inglis et al., 2013). Both the experiments cited above utilized pre-training procedures followed by further training under receptor blockade, and both experiments resulted in successful spatial learning under specific circumstances, despite full blockade. These experiments will be explained in more detail below.

As a stated hypothesis in Experiment 1, the full hippocampal NMDAR blockade discounts the possibility that the reason why animals were capable of learning novel spatial locations in the McDonald et al. (2005) study was due to a functional ventral hippocampus.

One important difference between the results reported in Experiment 1 and those from the McDonald et al. (2005) study was the 8- and 24-h probe results. In the original study, control rats show a clear quadrant preference for the new platform location 24 h later while CPP rats did not. In the present study, the strength of the representation following these delays seemed to have been compromised somewhat. This difference from the McDonald et al. (2005) paper might be because we instituted, in the present set of experiments, the 30-s probe trial immediately after mass training. This did not happen in the original 2005 study. This probe can lead to some extinction and provides the subjects with the knowledge that the platform might be located nowhere (probe trial) or elsewhere (mass training). It is possible that the controls transition from new location, old location, and other quadrants more quickly which could negatively affect the

quadrant preference measure. Further research is required to confirm this hypothesis.

NMDARs and Memory Retrieval

The lack of NMDAR involvement in memory retrieval has long been accepted after several experiments outlining rats' ability to use previously acquired information during NMDAR blockade (Shapiro and Caramanos, 1990; Bast et al., 2005). Biologically this would make sense, if NMDARs are necessary for LTP induction and learning based plasticity, then once the circuit connections representing the memory have been formed and consolidated, plasticity mechanisms should not be involved in simple circuit activation during retrieval. However, recent evidence has shown the contrary; that NMDAR blockade can prevent the expression of previously established fear memories (Lopez et al., 2015). Our results in Experiment 1 further support the claim that NMDARs are not involved in memory retrieval and expression. When analyzed as a probe, trial 1 of mass training revealed that rats from both groups displayed a spatial preference for the pre-training platform location, indicating that it was both successfully learned and retrieved.

NMDARs and Spatial Learning

Starting with Bannerman et al. (1995) and Saucier and Cain (1995), the idea of NMDAR independent learning began to be explored. Novel MWT training in the presence of NMDAR antagonist drugs resulted in learning impairments, but by changing certain parameters of the task, these impairments could be eliminated. Since then, many studies have examined this phenomenon, through NMDAR independent extinction (Santini et al., 2001), place cell formation (Kentros et al., 1998), LTP (Grover and Teyler, 1990), and molecular cascades associated with learning and plasticity (Moosmang et al., 2005). How exactly learning processes can be made NMDAR independent is not certain. Some have shown that behavioral strategies are learned once, and then can be applied across multiple learning scenarios independent of NMDAR plasticity (Hoh et al., 1999). Others have argued that where in the brain learning takes place changes over training (Inglis et al., 2013).

Almost all studies examining NMDAR independent spatial learning have done so using pre-training, in some form or another. A review of the literature on experiments using NMDAR blockade, pre-training, and spatial learning reveals two overall findings. The first is spatial learning can be made NMDAR independent when done with the same information available to prior learning and is also done rapidly. This is made most clear by Steele and Morris (1999) where rats were pre-trained in the MWT on a version that involved a new platform location every day. After several days, rats continued training in the same room but with hippocampal NMDAR blockade. The manipulated variable was inter-trial interval, and it was found that when it was kept short at 15 s rats learned successfully. However, when it was lengthened to 20 min, they failed to learn. This means that rapid learning was possible while learning over longer periods of time was not. Because the platform changes every day, the effect of receptor blockade on long-term training cannot be assessed.

Work done by Saucier and Cain (1995) and Hoh et al. (1999) have shown that non-spatial pre-training (NSP) can lead to rapid NMDAR independent spatial learning. The argument put forth by these researchers is that NSP allows for behavioral search strategies to be developed prior to spatial training and that this is what leads to NMDAR independence later on. However, behavioral search strategies themselves were also found to be learned independent of NMDAR. This contrasts with earlier work done (Morris et al., 1990) in which NSP led to impairments in same room spatial training that was done over the course of several days. NSP is performed with a curtain around the pool and so may potentially conflict with our explanation of previously learned environmental information hypothesis. However, the complete environmental repertoire that contributes to spatial navigation behaviors goes beyond wall cues like posters.

The MWT environment can be divided into two separate spaces: the intra-maze (local) environment which contains everything inside the pool walls, and the extra-maze (global) environment which contains everything outside the pool walls but inside the experiment room. Some evidence shows that aspects of spatial navigation can even transfer between multiple contexts and so would constitute potentially larger, environment independent navigation strategies as well, such as heading direction (Taube and Burton, 1995; Clark et al., 2015). Given the continued use of the maze and global location of the maze throughout training, NSP does not necessarily mean that no usable environmental information is used to learn the platform location. With this in mind, in the studies using NSP, rats successfully learn the MWT when trained rapidly (Saucier and Cain, 1995; Hoh et al., 1999).

Our work reinforces these conclusions. It shows that in the absence of NMDAR function in the hippocampus, rapid learning is possible when the extra-maze, environmental information used to learn a new escape location is identical to what has been previously learned. After both an 8-h and a 24-h retention period, everything that was learned during mass training was forgotten. Our specific pattern of results indicates that whatever was learned was not consolidated. A lack of consolidation may explain why rats in these types of tasks can learn rapidly but not with increased ITIs or over several days. NMDAR involvement in memory consolidation has been shown on multiple occasions (Santini et al., 2001; McDonald et al., 2005).

The second finding, in the literature, is that novel spatial learning can be made NMDAR independent when done over several days. This comes primarily from two experiments. Bannerman et al. (1995) was able to get rats to learn the MWT in a room different from that of pre-training, and did so over multiple training days. A similar effect was found in that experiments replication (Inglis et al., 2013). In the Bannerman et al. (1995) study, a NSP experiment was also done, and when done in room 1, it did not allow for spatial learning in room 2 across multiple days. NSP is a very specific type of pre-training that eliminates extra-maze cues. Given that there is no visual environmental information outside of the pool, it is possible that the rats given NSP pre-training treated room 2 in the Bannerman study in the same way that the rats in the Cain and Hoh studies treated their respective training rooms. Stated differently, without previous

environmental information to compare to new information, all information is new, and so new training done in a different or same room will not matter. A similar intra-maze environment and lack of extra-maze specific cues means that there is no such thing as same room or different room (dependent on extra-maze cues) following NSP, and that all subsequent spatial training will follow the same principles. This would also explain the multiple day learning impairments observed in Morris et al. (1990).

However, multiple day NMDAR independent learning does not apply to naïve rats in the MWT. This may be because novel MWT training does not just involve spatial learning but also developing successful motor patterns for swimming, trying out search strategies, as well as reducing fear. The MWT is an aversive learning task and given NMDAR involvement in motor function and anxiety, some have argued that learning deficits cannot be dissociated from other types of effects (Keith and Rudy, 1990; Ahlander et al., 1999). Because of the ubiquitous nature of the NMDAR, it may have a role in many neural and behavioral processes outside of spatial navigation and learning. This is why pre-training is used, it allows for specific aspects of the task to be isolated and examined.

In all of the work involving MWT training that relies on previously learned environmental information, NMDAR independent learning is successful when done rapidly but not when done with increased ITIs or over several days. However, when training is done with novel environmental information and the potentially confounding influence of behavioral strategies, anxiety, and sensori-motor impairments are removed, learning may be NMDAR independent when done over several days, but not rapidly. To our knowledge, no one has examined the role of NMDAR in rapid novel spatial learning after pre-training. Our work provides support for these conclusions by showing that when transferred to a new room with novel environmental cues rats without NMDAR function cannot rapidly learn.

The shift in NMDAR dependence may have to do with the requirements of the task. Reversal learning in the MWT consists of fundamentally different task parameters and learning requirements than novel learning. When put through the MWT for the first time, rats must learn many things ranging from behavioral search strategies, spatial locations, and interacting with the maze, the experimenter, and the environment. These include, but are not limited to, swimming away from the pool wall, the size and stability of the hidden platform, the arrangement of extra-maze cues, etc. One of the main reasons why pre-training procedures are used is to limit the type of learning that must occur in subsequent training procedures for successful maze navigation. When put through reversal learning in the same spatial context after a pre-training procedure, the only thing required for the rat to learn is a new platform position. The dimensions and details of the maze and room, as well as a successful search strategy, have already been learned. Also, rats have to extinguish the previously learned spatial information, so that reversal doesn't just involve new learning, but extinction as well. The rat must do this using information and strategies it is already familiar with.

Further training with a completely new set of information such as in Experiment 2 is also different from both naïve

training and same room reversal. Several components of training are already familiar to the rat such as swimming and an expectation of the rules of further training. Yet some things are completely unfamiliar like where the animal is and what exists in its environment. In this way, three different stages of MWT training, naïve, new room, same room reversal, all have increasing amounts of familiarity to them, respectively.

This means that all three stages of training may involve different search strategies, or the same strategies but based on different types of available information. Given the different task requirements during each stage, it is not unlikely that the role plasticity has will vary across stages of training. Our own results, as well as a review of the relevant literature, reveal that NMDARs in the hippocampus will be heavily involved in several neural and behavioral processes outside of learning during naïve MWT training, resulting in an inability to dissociate between learning, anxiety, and sensori-motor processes just from behavioral data alone. After extensive pre-training and task-familiarization, NMDARs consolidate changes to existing spatial information. And that when processing completely novel environmental information, are necessary for its rapid learning.

Immediate Early Genes and the Dentate Gyrus

The use of IEGs in neuroscience research is commonly used to map behaviorally relevant neural activity. The IEG Arc is thought to be dependent on LTP related activity and so is used to map neurobiological mechanisms of learning and memory. Learning and memory behaviors are known to reliably induce Arc mRNA and protein expression in behaviorally relevant brain regions. Activation of the NMDAR has been identified as a critical mechanism that leads to Arc expression. Blocking NMDARs with antagonist drugs reduces behavior induced Arc mRNA (Czerniawski et al., 2011). Furthermore, NMDAR hypofunction leads to reduced Arc expression (Balu and Coyle, 2014). The links between learning, NMDAR, LTP, and Arc activity is well supported by research (Guzowski et al., 2001; Shepherd and Bear, 2011).

The results from Experiment 3 show that in one version of a MWT that did not require NMDARs to learn, Arc protein expression was not significantly different from cage controls. In a version of the task that did require NMDARs to learn, Arc protein expression was high compared to cage controls and the NMDAR independent task. When an NMDAR antagonist was introduced to the hippocampus, it impaired learning as well as reduced Arc protein expression. The level of expression in the CPP group was significantly below the New room group but also significantly higher than the cage control group. No observable patterns emerged in areas CA1 or CA3, however, the pattern of expression described above was observed in the dentate gyrus.

Two important conclusions can be reached from these results. One is that NMDAR dependent learning of novel environmental information activates Arc in the dentate gyrus. The other is that NMDAR blockade reduces Arc expression in the dentate gyrus. Because we did not determine the binding efficacy of CPP administered, it is impossible to know if the heightened Arc

expression seen in the CPP + New group relative to cage controls was because of NMDAR independent processes or due to some residual NMDAR function. We believe the latter is the most likely explanation, which likely indicates that the intra-hippocampal CPP injections resulted in extensive but not complete NMDAR block. Further research is required to assess this and other potential explanations.

Given the specific pattern of results our experiments produced, as well as the contributions of other work on this topic, we can also make hypotheses regarding the function of dentate gyrus plasticity as it pertains to spatial learning.

Dentate specific lesions of granule cells using Colchicine injections (Sutherland and Rudy, 1988) have been shown to impair both reference memory across training days and working memory within training days in spatial water tasks (McNaughton et al., 1989; Xavier et al., 1999). Selective genetic knockout of NMDAR NR1 subunit exclusively in the dentate gyrus of mice produces working memory impairments while maintaining reference memory in an 8-arm radial maze (Niewoehner et al., 2007). Similarly, McHugh et al. (2007) produced a dentate specific knockout mouse that could learn context fear conditioning. However, the mice could not learn context discrimination, supporting the dentate's proposed role in pattern separation (Leutgeb et al., 2007; Kesner, 2013). Chen et al. (2009) produced a mutant mouse with reduced GluN1R subunit expression in the dentate gyrus. The behavioral phenotype of these mice was that of impaired MWT performance over multiple days, as well as impaired same room reversal learning over multiple days. The results from lesion and knockout experiments points to three functions of the dentate gyrus: (1) its role in the hippocampal circuits mediating spatial learning; (2) a role in both working memory with a sparing of reference memory; and (3) supporting discriminations between multiple learned environments. Interestingly, genetic experiments show a very specific type of behavioral learning deficit after NMDAR manipulation in the dentate gyrus, namely, the inability to discriminate environmental information and learn rapidly where as in our experiment, rapid novel environmental learning resulted in NMDAR dependent activity in the dentate gyrus. The previous work produces behavioral effects after the molecular manipulation, our work shows a possible molecular effect after similar behavioral manipulations. Although, more work would necessarily have to be done to prove it, this bidirectional effect demonstrates a link between NMDAR plasticity in the dentate gyrus and the rapid learning of novel environmental information.

Potential Limitations

One potential caveat when interpreting the pattern of effects from the current experiments is trying to differentiate between memory consolidation versus extinction effects of the NMDAR manipulation. Rats given CPP during mass-training in the same room showed a spatial preference for the pre-trained platform location during the 24-h probe. It could be argued that this happens because NMDAR blockade prevented extinction learning from occurring toward the original platform. When learning a new platform location after pre-training, presumably two types of learning are going on: new spatial learning and

extinction learning for the old platform position. However, it is very unlikely that rats would be able to learn a new spatial location during training while also not being able to learn extinction for an old spatial location at the same time since the mechanisms underlying cellular consolidation of extinction memories are proposed to be very similar to the cellular consolidation of other memories (Santini et al., 2001; Quirk and Mueller, 2008).

Another potential limitation with our claim of a role of NMDAR receptors in hippocampal memory consolidation is that the results of the 8- and 24-h probes in Experiment 1 may be due to state dependent learning during mass training. The fact that CPP rats in Experiment 1 behaved differently 24 h after mass training compared to immediately after could be due to the fact that the immediate probe happened while CPP was still active in these rats, and not 24 h later. However, prior work investigating NMDAR involvement in consolidation suggests that it is not state dependent (Kentros et al., 1998; Santini et al., 2001; McDonald et al., 2005).

Many studies examining the effects of spatial learning on IEG expression have found it in all three sub-regions of the hippocampus proper: Dentate gyrus, CA1, and CA3 (Guzowski et al., 1999, 2001). However, in our experiment, same room reversal training did not induce Arc expression any different from cage controls. New room training did induce higher Arc expression but was limited to the dentate gyrus. An alternative explanation of this effect could be the time course of protein action. It is possible, although has not been explored to our knowledge, that IEG protein expression varies throughout the hippocampus after MWT training in a time dependent manner. For example, using our paradigm, if animals were euthanized 70 min after mass training trial 1 versus after trial 16, then sub-region expression differences may be seen. Consistent with this idea, it has been shown that rats change their search strategies throughout the course of training (Graziano et al., 2003). Different strategies may induce activity in different hippocampal sub-regions depending on what the animal is learning. However, given the robust time course of Arc protein action (30–90 min), sub-region activation dependent on training time would likely be observed regardless of which trial the rat was perfused in our experimental design.

Contributions of the Present Work

The novel contributions of this work center on three main findings. The first is that hippocampal blockade across both dorsal/ventral aspects results in similar behavioral patterns in the MWT as a dorsal-limited blockade. This suggests that the lack

of an impairment of NMDAR dorsal hippocampal blockade on rapid acquisition of a new spatial location, reported in McDonald et al. (2005) was not due to intact ventral hippocampal NMDA function. Second, NMDARs appear to be necessary for encoding and consolidation of new environmental information that will be utilized for spatial navigational behaviors but not new spatial navigational behaviors in a previously trained context. Finally, NMDAR dependent Arc activation occurs in the dentate gyrus after rapid spatial learning in a new environment. These three novel contributions to the understanding of the neurobiology of learning and memory will hopefully lead to more discoveries in the future.

AUTHOR CONTRIBUTIONS

RJM was the principal investigator, provided study design and funded the research with his grants, and wrote the article. CB provided study design, collected the data, performed the statistical analysis, rodent surgery, microscopy, and wrote the article.

FUNDING

This work was funded by the NSERC Discovery grant and the NSERC Discovery accelerator Supplement awarded to RJM. CB was supported by the NSERC Create Grant Scholarship.

SUPPLEMENTARY MATERIAL

The Supplementary Material for this article can be found online at: <https://www.frontiersin.org/articles/10.3389/fnbeh.2019.00008/full#supplementary-material>

FIGURE S1 | Pretraining for groups 1 and 2 in Experiment 1. Four trial averages of the Path length in meters to find the platform over training 4 days/eight trials per day. Both controls and pre-CPP rats successfully learn over training. Also shows mass training for groups 1 and 2 in Experiment 1. Two trial averages of the Path lengths in meters to find the new platform over training 2 h/16 trials. Both controls and CPP rats learn over training.

FIGURE S2 | Pretraining for groups 1 and 2 in Experiment 2. Four trial averages of the Path length in meters to find the platform over training 4 days/eight trials per day. Both controls and pre-CPP rats successfully learn over training. Also shows mass training for groups 1 and 2 in Experiment 2. Two trial averages of the Path lengths in meters to find the new platform over training 2 h/20 trials. CPP rats fail to learn over mass training.

REFERENCES

- Abraham, W. C., and Kairiss, E. W. (1988). Effects of the NMDA antagonist 2AP5 on complex spike discharge by hippocampal pyramidal cells. *Neurosci. Lett.* 89, 36–42. doi: 10.1016/0304-3940(88)90477-6
- Ahlander, M., Misane, I., Schött, P. A., and Ögren, S. O. (1999). A behavioral analysis of the spatial learning deficit induced by the NMDA receptor antagonist MK-801 (dizocilpine) in the rat. *Neuropsychopharmacology* 21, 414–426. doi: 10.1016/S0893-133X(98)00116-X
- Balu, D. T., and Coyle, J. T. (2014). Chronic D-serine reverses arc expression and partially rescues dendritic abnormalities in a mouse model of NMDA receptor hypofunction. *Neurochem. Int.* 75, 76–78. doi: 10.1016/j.neuint.2014.05.015
- Bannerman, D. M., Good, M. A., Butcher, S. P., Ramsay, M., and Morris, R. G. M. (1995). Distinct components of spatial learning revealed by prior training and NMDA receptor blockade. *Nature* 378, 182–186. doi: 10.1038/378182a0
- Bast, T., da Silva, B. M., and Morris, R. G. (2005). Distinct contributions of hippocampal NMDA and AMPA receptors to encoding and retrieval of one-trial place memory. *J. Neurosci.* 25, 5845–5856. doi: 10.1523/JNEUROSCI.0698-05.2005

- Bliss, T. V., and Lomo, T. (1973). Long-lasting potentiation of synaptic transmission in the dentate area of the anaesthetized rabbit following stimulation of the perforant path. *J. Physiol.* 232, 331–356. doi: 10.1113/jphysiol.1973.sp010273
- Cain, D. P., Saucier, D., Hall, J., Hargreaves, E. L., and Boon, F. (1996). Detailed behavioral analysis of water maze acquisition under APV or CNQX: contribution of sensorimotor disturbances to drug induced acquisition deficits. *Behav. Neurosci.* 110, 86–102. doi: 10.1037/0735-7044.110.1.86
- Chen, P. E., Errington, M. L., Kneussel, M., Chen, G., Annala, A. J., Rudhard, Y. H., et al. (2009). Behavioral deficits and subregion-specific suppression of LTP in mice expressing a population of mutant NMDA receptors throughout the hippocampus. *Learn. Mem.* 16, 635–644. doi: 10.1101/lm.1316909
- Clark, B. J., Harris, M. J., and Taube, J. S. (2012). Control of anterodorsal thalamic head direction cells by environmental boundaries: comparison with conflicting distal landmarks. *Hippocampus* 22, 172–187. doi: 10.1002/hipo.20880
- Clark, B. J., Hong, N. S., Bettenson, D. J., Woolford, J., Horwood, L., and McDonald, R. J. (2015). Maintained directional navigation across environments in the Morris water task is dependent on vestibular cues. *J. Exp. Psychol.* 41, 301–308. doi: 10.1037/xan0000066
- Collingridge, G. L., and Bliss, T. V. P. (1987). NMDA receptors-their role in long-term potentiation. *Trends Neurosci.* 10, 288–293. doi: 10.1016/0166-2236(87)90175-5
- Collingridge, G. L., Kehl, S. J., and McLennan, H. (1983). The antagonism of amino acid induced excitations of rat hippocampal CA1 neurones *in vitro*. *J. Physiol.* 334, 19–31. doi: 10.1113/jphysiol.1983.sp014477
- Czerniawski, J., Ree, F., Chia, C., Ramamoorthi, K., Kumata, Y., and Otto, T. A. (2011). The importance of having Arc: expression of the immediate-early gene Arc is required for hippocampus-dependent fear conditioning and blocked by NMDA receptor antagonism. *J. Neurosci.* 31, 11200–11207. doi: 10.1523/JNEUROSCI.2211-11.2011
- Dingledine, R. (1983). N-methyl aspartate activates voltage-dependent calcium conductance in rat hippocampal pyramidal cells. *J. Physiol.* 343, 385.
- Dudchenko, P. A., and Zinyuk, L. E. (2005). The formation of cognitive maps of adjacent environments: evidence from the head direction cell system. *Behav. Neurosci.* 119, 1511–1523. doi: 10.1037/0735-7044.119.6.1511
- Dunwiddie, T. V., and Lynch, G. (1979). The relationship between extracellular calcium concentrations and the induction of hippocampal long-term potentiation. *Brain Res.* 169, 103–110. doi: 10.1016/0006-8993(79)90377-9
- Ferbinteanu, J., Ray, C., and McDonald, R. J. (2003). Both dorsal and ventral hippocampus contribute to spatial learning in Long-Evans rats. *Neurosci. Lett.* 345, 131–135. doi: 10.1016/S0304-3940(03)00473-7
- Graziano, A., Petrosini, L., and Bartoletti, A. (2003). Automatic recognition of explorative strategies in the Morris water maze. *J. Neurosci. Methods* 130:3344. doi: 10.1016/S0165-0270(03)00187-0
- Grover, L. M., and Teyler, T. J. (1990). Two components of long-term potentiation induced by different patterns of afferent activation. *Nature* 347, 477. doi: 10.1038/347477a0
- Guzowski, J. F., McNaughton, B. L., Barnes, C. A., and Worley, P. F. (1999). Environment specific expression of the immediate-early gene Arc in hippocampal neuronal ensembles. *Nat. Neurosci.* 2, 1120–1124. doi: 10.1038/16046
- Guzowski, J. F., Setlow, B., Wagner, E. K., and McGaugh, J. L. (2001). Experience-dependent gene expression in the rat hippocampus after spatial learning: a comparison of the immediate-early genes Arc, c-fos, and zif268. *J. Neurosci.* 21:50895098.
- Hamilton, D. A., Akers, K. G., Weisend, M. P., and Sutherland, R. J. (2007). How do room an apparatus cues control navigation in the Morris water task? Evidence for distinct contributions to a movement vector. *J. Exp. Psychol.* 33:100.
- Harris, E. W., Ganong, A. H., and Cotman, C. W. (1984). Long-term potentiation in the hippocampus involves activation of N-methyl-D-aspartate receptors. *Brain Res.* 323, 132–137. doi: 10.1016/0006-8993(84)90275-0
- Herron, C. E., Lester, R. A., Coan, E. J., and Collingridge, G. L. (1986). Frequency dependent involvement of NMDA receptors in the hippocampus: a novel synaptic mechanism. *Nature* 322, 265–268. doi: 10.1038/322265a0
- Herron, C. E., Lester, R. A. J., Coan, E. J., and Collingridge, G. L. (1985). Intracellular demonstration of an N-methyl-D-aspartate receptor mediated component of synaptic transmission in the rat hippocampus. *Neurosci. Lett.* 60, 19–23. doi: 10.1016/0304-3940(85)90375-1
- Hoh, T., Beiko, J., Boon, F., Weiss, S., and Cain, D. P. (1999). Complex behavioral strategy and reversal learning in the water maze without NMDA receptor-dependent long-term potentiation. *J. Neurosci.* 19:RC2.
- Holahan, M. R., Taverna, F. A., Emrich, S. M., Louis, M., Muller, R. U., Roder, J. C., et al. (2005). Impairment in long-term retention but not short-term performance on a water maze reversal task following hippocampal or mediodorsal striatal N methyl-D-aspartate receptor blockade. *Behav. Neurosci.* 119:1563. doi: 10.1037/0735-7044.119.6.1563
- Inglis, J., Martin, S. J., and Morris, R. G. (2013). Upstairs/downstairs revisited: spatial pre-training induced rescue of normal spatial learning during selective blockade of hippocampal N methyl-d-aspartate receptors. *Eur. J. Neurosci.* 37, 718–727. doi: 10.1111/ejn.12087
- Keith, J. R., and Rudy, J. W. (1990). Why NMDA-receptor-dependent long-term potentiation may not be a mechanism of learning and memory: reappraisal of the NMDA-receptor blockade strategy. *Psychobiology* 18, 251–257.
- Kentros, C., Hargreaves, E., Hawkins, R. D., Kandel, E. R., Shapiro, M., and Muller, R. V. (1998). Abolition of long-term stability of new hippocampal place cell maps by NMDA receptor blockade. *Science* 280, 2121–2126. doi: 10.1126/science.280.5372.2121
- Kesner, R. P. (2013). An analysis of the dentate gyrus function. *Behav. Brain Res.* 254, 1–7. doi: 10.1016/j.bbr.2013.01.012
- Kesner, R. P., and Dakis, M. (1995). Phencyclidine injections into the dorsal hippocampus disrupt long-but not short-term memory within a spatial learning task. *Psychopharmacology* 120, 203–208. doi: 10.1007/BF02246194
- Kim, J. J., DeCola, J. P., Landeira-Fernandez, J., and Fanselow, M. S. (1991). N-methyl-D aspartate receptor antagonist APV blocks acquisition but not expression of fear conditioning. *Behav. Neurosci.* 105, 126–133. doi: 10.1037/0735-7044.105.1.126
- Leutgeb, J. K., Leutgeb, S., Moser, M. B., and Moser, E. I. (2007). Pattern separation in the dentate gyrus and CA3 of the hippocampus. *Science* 315, 961–966. doi: 10.1126/science.1135801
- Levy, W. B., and Steward, O. (1979). Synapses as associative memory elements in the hippocampal formation. *Brain Res.* 175, 233–245. doi: 10.1016/0006-8993(79)91003-5
- Loneragan, M. E., Gafford, G. M., Jarome, T. J., and Helmstetter, F. J. (2010). Time-dependent expression of Arc and zif268 after acquisition of fear conditioning. *Neural Plast.* 2010:139891. doi: 10.1155/2010/139891
- Lopez, J., Gamache, K., Schneider, R., and Nader, K. (2015). Memory retrieval requires ongoing protein synthesis and NMDA receptor activity-mediated AMPA receptor trafficking. *J. Neurosci.* 35, 2465–2475. doi: 10.1523/JNEUROSCI.0735-14.2015
- Matus-Amat, P., Higgins, E. A., Sprunger, D., Wright-Hardesty, K., and Rudy, J. W. (2007). The role of dorsal hippocampus and basolateral amygdala NMDA receptors in the acquisition and retrieval of context and contextual fear memories. *Behav. Neurosci.* 121, 721–731. doi: 10.1037/0735-7044.121.4.721
- McDonald, R. J., Hong, N. S., Craig, L. A., Holahan, M. R., Louis, M., and Muller, R. U. (2005). NMDA receptor blockade by CPP impairs post-training consolidation of a rapidly acquired spatial representation in rat hippocampus. *Eur. J. Neurosci.* 22, 1201–1213. doi: 10.1111/j.1460-9568.2005.04272.x
- McHugh, T. J., Jones, M. W., Quinn, J. J., Balthasar, N., Coppari, R., Elmquist, J. K., et al. (2007). Dentate gyrus NMDA receptors mediate rapid pattern separation in the hippocampal network. *Science* 317, 94–99. doi: 10.1126/science.1140263
- McNaughton, B. L., Barnes, C. A., Meltzer, J., and Sutherland, R. J. (1989). Hippocampal granule cells are necessary for normal spatial learning but not for spatially-selective pyramidal cell discharge. *Exp. Brain Res.* 76, 485–496. doi: 10.1007/BF00248904
- MicroBrightField Inc. (2013). *Stereo Investigator®*, Version 10. Williston, VT: MicroBrightField Inc.
- Monaghan, D. T., and Cotman, C. W. (1985). Distribution of N-methyl-D-aspartate-sensitive L [3H] glutamate-binding sites in rat brain. *J. Neurosci.* 5, 2909–2919. doi: 10.1523/JNEUROSCI.05-11-02909.1985
- Moosmang, S., Haider, N., Klugbauer, N., Adelsberger, H., Langwieser, N., Müller, J., et al. (2005). Role of hippocampal Cav1.2 Ca²⁺ channels in NMDA receptor independent synaptic plasticity and spatial memory. *J. Neurosci.* 25, 9883–9892. doi: 10.1523/JNEUROSCI.1531-05.2005

- Morris, R. G. (1989). Synaptic plasticity and learning: selective impairment of learning rats and blockade of long-term potentiation in vivo by the N-methyl-D-aspartate receptor antagonist AP5. *J. Neurosci.* 9, 3040–3057. doi: 10.1523/JNEUROSCI.09-09-03040.1989
- Morris, R. G. M., Anderson, E., Lynch, G. A., and Baudry, M. (1986). Selective impairment of learning and blockade of long-term potentiation by an N-methyl-D-aspartate receptor antagonist, AP 5. *Nature* 319, 774–776. doi: 10.1038/319774a0
- Morris, R. G. M., Davis, S., and Butcher, S. P. (1990). Hippocampal synaptic plasticity and NMDA receptors: a role in information storage? *Philos. Trans. R. Soc. Lond. B* 329, 187–204. doi: 10.1098/rstb.1990.0164
- Niewoehner, B., Single, F. N., Hvalby, Ø., Jensen, V., Meyer zum Alten Borgloh, S., Seeburg, P. H., et al. (2007). Impaired spatial working memory but spared spatial reference memory following functional loss of NMDA receptors in the dentate gyrus. *Eur. J. Neurosci.* 25, 837–846. doi: 10.1111/j.1460-9568.2007.05312.x
- Otnæss, M. K., Brun, V. H., Moser, M. B., and Moser, E. I. (1999). Pre-training prevents spatial learning impairment after saturation of hippocampal long-term potentiation. *J. Neurosci.* 19, 1–5. doi: 10.1523/JNEUROSCI.19-24-j0007.1999
- Plath, N., Ohana, O., Dammermann, B., Errington, M. L., Schmitz, D., Gross, C., et al. (2006). Arc/Arg3.1 is essential for the consolidation of synaptic plasticity and memories. *Neuron* 52, 437–444. doi: 10.1016/j.neuron.2006.08.024
- Quirk, G. J., and Mueller, D. (2008). Neural mechanisms of extinction learning and retrieval. *Neuropsychopharmacology* 33, 56–72. doi: 10.1038/sj.npp.1301555
- Rasband, W. S. (2012). *ImageJ*. Bethesda, MD: National Institutes of Health.
- Riekkinen, M., and Riekkinen, P. Jr. (1997). Dorsal hippocampal muscarinic acetylcholine and NMDA receptors disrupt water maze navigation. *Neuroreport* 8, 645–648. doi: 10.1097/00001756-199702100-00013
- Robinson, G. S. Jr., Crooks, G. B. Jr., Shinkman, P. G., and Gallagher, M. (1989). Behavioral effects of MK 801 mimic deficits associated with hippocampal damage. *Psychobiology* 17, 156–164.
- Roesler, R., Reolon, G. K., Luft, T., Martins, M. R., Schröder, N., Vianna, M. R., et al. (2005). NMDA receptors mediate consolidation of contextual memory in the hippocampus after context preexposure. *Neurochem. Res.* 30, 1407–1411. doi: 10.1007/s11064-005-8509-5
- Sakimura, K., Kutsuwada, T., Ito, I., and Manabe, T. (1995). Reduced hippocampal LTP and spatial learning in mice lacking NMDA receptor epsilon1 subunit. *Nature* 373, 151–155. doi: 10.1038/373151a0
- Salt, T. E. (1986). Mediation of thalamic sensory input by both NMDA receptors and non NMDA receptors. *Nature* 322, 263–265. doi: 10.1038/322263a0
- Santini, E., Muller, R. U., and Quirk, G. J. (2001). Consolidation of extinction learning involves transfer from NMDA-independent to NMDA-dependent memory. *J. Neurosci.* 21, 9009–9017. doi: 10.1523/JNEUROSCI.21-22-09009.2001
- Saucier, D., and Cain, D. P. (1995). Spatial learning without NMDA receptor-dependent long-term potentiation. *Nature* 378, 186–189. doi: 10.1038/378186a0
- Shapiro, M. L., and Caramanos, Z. (1990). NMDA antagonist MK-801 impairs acquisition but not performance of spatial working and reference memory. *Psychobiology* 18, 231–243.
- Shepherd, J. D., and Bear, M. F. (2011). New views of Arc, a master regulator of synaptic plasticity. *Nat. Neurosci.* 14, 279–284. doi: 10.1038/nn.2708
- Steele, R. J., and Morris, R. G. M. (1999). Delay-dependent impairment of a matching-to-place task with chronic and intrahippocampal infusion of the NMDA-antagonist D-AP5. *Hippocampus* 9, 118–136. doi: 10.1002/(SICI)1098-1063(1999)9:2<118::AID-HIPO4>3.0.CO;2-8
- Stephens, D. N., Meldrum, B. S., Weidmann, R., Schneider, C., and Grützner, M. (1986). Does the excitatory amino acid receptor antagonist 2-APH exhibit anxiolytic activity? *Psychopharmacology* 90, 166–169.
- Sutherland, R. J., and Rudy, J. W. (1988). Place learning in the Morris place navigation task is impaired by damage to the hippocampal formation even if the temporal demands are reduced. *Psychobiology* 16, 157–163.
- Sutherland, R. J., Whishaw, I. Q., and Kolb, B. (1983). A behavioural analysis of spatial localization following electrolytic, kainate-or colchicine-induced damage to the hippocampal formation in the rat. *Behav. Brain Res.* 7, 133–153. doi: 10.1016/0166-4328(83)90188-2
- Taube, J. S., and Burton, H. L. (1995). Head direction cell activity monitored in a novel environment and during a cue conflict situation. *J. Neurophysiol.* 74, 1953–1971. doi: 10.1152/jn.1995.74.5.1953
- Tonkiss, J., Morris, R. G. M., and Rawlins, J. N. P. (1988). Intra-ventricular infusion of the NMDA antagonist AP5 impairs performance on a non-spatial operant DRL task in the rat. *Exp. Brain Res.* 73, 181–188. doi: 10.1007/BF00279671
- Ward, L., Mason, S. E., and Abraham, W. C. (1990). Effects of the NMDA antagonists CPP and MK 801 on radial arm maze performance in rats. *Pharmacol. Biochem. Behav.* 35, 785–790. doi: 10.1016/0091-3057(90)90359-P
- Whitlock, J. R., Heynen, A. J., Shuler, M. G., and Bear, M. F. (2006). Learning induces long-term potentiation in the hippocampus. *Science* 313, 1093–1097. doi: 10.1126/science.1128134
- Xavier, G. F., Oliveira-Filho, F. J., and Santos, A. M. (1999). Dentate gyrus-selective colchicine lesion and disruption of performance in spatial tasks: difficulties in “place strategy” because of a lack of flexibility in the use of environmental cues? *Hippocampus* 9, 668–681. doi: 10.1002/(SICI)1098-1063(1999)9:6<668::AID-HIPO8>3.0.CO;2-9

Conflict of Interest Statement: The authors declare that the research was conducted in the absence of any commercial or financial relationships that could be construed as a potential conflict of interest.

Copyright © 2019 Bye and McDonald. This is an open-access article distributed under the terms of the Creative Commons Attribution License (CC BY). The use, distribution or reproduction in other forums is permitted, provided the original author(s) and the copyright owner(s) are credited and that the original publication in this journal is cited, in accordance with accepted academic practice. No use, distribution or reproduction is permitted which does not comply with these terms.



Improving Hippocampal Memory Through the Experience of a Rich Minecraft Environment

Gregory D. Clemenson, Caden M. Henningfield and Craig E. L. Stark*

Department of Neurobiology and Behavior, University of California, Irvine, Irvine, CA, United States

OPEN ACCESS

Edited by:

Denise Manahan-Vaughan,
Ruhr University Bochum, Germany

Reviewed by:

Magdalena Mendez-Lopez,
University of Zaragoza, Spain

Inah Lee,
Seoul National University,
South Korea

*Correspondence:

Craig E. L. Stark
cestark@uci.edu

Received: 08 January 2019

Accepted: 06 March 2019

Published: 21 March 2019

Citation:

Clemenson GD, Henningfield CM and Stark CEL (2019) Improving Hippocampal Memory Through the Experience of a Rich Minecraft Environment.
Front. Behav. Neurosci. 13:57.
doi: 10.3389/fnbeh.2019.00057

It is well known that the brain changes in response to the surrounding environment. The hippocampus has been shown to be particularly susceptible to environmental enrichment, with effects ranging from the generation of new hippocampal neurons and synapses to an increased expression of neurotrophic factors. While many of these changes in the hippocampus are well documented in animals, our understanding of how environmental enrichment can apply to humans is more ambiguous. In animals, spatial exploration has been shown to be a clear way to elicit the effects of environmental enrichment and considering the role of the hippocampus in spatial navigation, which has been shown in both animal models and humans, it suggests a viable avenue for translation of environmental enrichment to humans. Here, we test the hypothesis that the spatial exploration of a virtual video game environment, can impact the hippocampus and lead to an improvement in hippocampal-dependent memory. Using the video game Minecraft, we tested four groups of participants, each playing on custom servers and focusing on different aspects of Minecraft to test the effects of both building and exploration over the course of 2 weeks. We found an improvement in hippocampus-associated memory from pre-test to post-test and that the degree of improvement was tied to both the amount of exploration of the Minecraft world and the complexity of the structures built within Minecraft. Thus, the number of enrichment participants engaged in while playing Minecraft was directly correlated with improvements in hippocampal-dependent memory outside of the game.

Keywords: environmental enrichment, hippocampus, spatial exploration, video games, Minecraft

INTRODUCTION

The effects of environmental enrichment on the hippocampus have been well studied in animals. Simply exposing animals to an enriching experience that promotes sensory, physical, spatial, and cognitive stimulation can have an extremely positive impact on the hippocampus (Clemenson et al., 2018). While there is a vast amount of literature demonstrating the powerful influence of environmental enrichment in animals, how this manipulation applies to humans is less clear. Isolated factors such as exercise have been directly applied to humans with some success (Pereira et al., 2007; Erickson et al., 2009, 2010, 2011; Bugg and Head, 2011), but far less has been done in the area of spatial exploration. Studies in humans have shown that not only is the hippocampus active during spatial navigation like the rodent (Ekstrom et al., 2003; Jacobs et al., 2013), but structural changes can occur in the hippocampus with spatial training and expertise (Maguire et al., 1998, 2000; Woollett et al., 2009; Woollett and Maguire, 2011). Work in our lab and others has even shown that spatial

training, in the form of playing immersive 3D video games, can alter hippocampal-dependent memory (Clemenson and Stark, 2015) and volume (West et al., 2017, 2018). Here, we show that focusing on specific aspects of the video game Minecraft can lead to improvements in hippocampal memory. Using custom servers to control the experience and record movement and interactions with the surrounding Minecraft environment, we found that this improvement is specifically correlated with the amount of spatial exploration and the complexity of structures built within the Minecraft world.

Exposing animals to an enriched environment can lead to increased hippocampal neurogenesis (Kempermann et al., 1997, 2002), synaptogenesis (Rampon et al., 2000; Gogolla et al., 2009), dendritic density and complexity (Moser et al., 1994; Faherty et al., 2003; Gonçalves et al., 2016), enhanced long-term potentiation (LTP; van Praag et al., 1999; Farmer et al., 2004), and increased expression of synaptic proteins and neurotrophic factors (Fabel et al., 2003; Nithianantharajah et al., 2004; Bekinshtein et al., 2011). Ultimately, these changes to the hippocampal circuitry lead to robust improvements in hippocampus-dependent cognition, including spatial learning and memory (Kempermann et al., 1997; Nilsson et al., 1999; van Praag et al., 1999, 2002; Sampedro-Piquero et al., 2013; Mora-Gallegos et al., 2015; Garthe et al., 2016) and pattern separation (Creer et al., 2010; Clemenson et al., 2015; Wu et al., 2015). Pattern separation is a computation designed to reduce interference between items in memory and thought to rely heavily on the dentate gyrus subfield of the hippocampus (McClelland et al., 1995; Yassa and Stark, 2011). Importantly, there is a clear and consistent positive relationship between hippocampal neurogenesis and pattern separation (França et al., 2017). In humans, we use the Mnemonic Similarity Task (MST; Kirwan and Stark, 2007; Stark et al., 2013) which was designed to index pattern separation by assessing behavioral responses to highly similar lure items after an initial study exposure. In addition, environmental enrichment has been shown to ameliorate many of the cognitive and functional deficits associated with rodent models of aging and other neurodegenerative disorders (Kempermann et al., 2002; Segovia et al., 2006; Leal-Galicia et al., 2008; Darmopil et al., 2009; Speisman et al., 2013).

In animal models, both exercise (van Praag et al., 1999; Kobil et al., 2011; Mustroph et al., 2012; Vivar et al., 2013) and spatial exploration (Freund et al., 2013; Clemenson et al., 2015) have been shown to be core aspects of enrichment. For example, using radio frequency identification tags to track animal location, one study examined the exploratory behaviors of mice living in an enriched environment for 3 months (Freund et al., 2013). Mice exhibiting low spatial exploration tended to move back and forth between a few locations within the enrichment cage (e.g., between the nesting location and food location) whereas mice exhibiting greater spatial exploration tended to move unpredictably around the entire enrichment cage. Despite all mice were genetically identical, exploratory behaviors varied greatly amongst individual mice and further analysis revealed that individual exploratory behaviors positively correlated with hippocampal neurogenesis.

Given the relationship between the hippocampus in spatial navigation and memory in both humans and animals alike, we propose that the spatial exploration of a virtual video game environment is a human correlate of environmental enrichment and can lead to improvements in hippocampal function. Immersive 3D video game environments allow us to tease apart the contribution of spatial exploration with other elements of enrichment, such as exercise. Consistent with this hypothesis, we previously showed that playing the 3D video game Super Mario 3D World for 2 weeks could improve hippocampus-associated memory (Clemenson and Stark, 2015). Video games such as Super Mario 3D World often revolve around rich and immersive open-world environments for users to explore. Success in these games requires an awareness of the surrounding environment and a keen map knowledge to complete quests and find objectives. While the improvements we observed in hippocampus-associated memory correlated with video game performance there were several limitations of our study, many of which are common to most video game studies, that make it difficult to understand what about the experience led to the effect. First, our active control group played an entirely different game than our experimental group (Angry Birds vs. Super Mario 3D World). Although Angry Birds can still be considered an “engaging” game, it is inherently less spatial and therefore less complex and quite possibly less “enriching” than Super Mario 3D World. Second, the mechanics of each of these games are fundamentally different. Angry Birds is relatively simple and requires the user to launch a bird into a structure, while Super Mario 3D World requires several skills including problem-solving, jumping puzzles (specifically the timing of multiple jumps), and even interacting with enemies. Third, although our hypothesis revolves around the exploration of a virtual environment, it is difficult to quantify the spatial exploration of an individual while playing Super Mario 3D World as path data are not available. Collectible items within Super Mario 3D World are spread throughout the world and may provide a crude exploration metric, but these measures are magnitudes less sensitive than those used in animals (Freund et al., 2013).

While spatial exploration has clear relevance to enrichment and the hippocampus, the building aspect of Minecraft is more ambiguous. Despite no direct correlate of building in enrichment studies of humans or animals, there are several aspects of building that may be relevant to enrichment. First, enriched environments provide a certain amount of novelty to animals and although this has not been explicitly tested within the context of an enriched environment, we do know that the hippocampus plays a role in novelty recognition (Cohen and Stackman, 2015) and is greatly responsive to the exposure of a novel environment (Vazdarjanova and Guzowski, 2004; Tashiro et al., 2007). In building new structures, participants are constantly exposing themselves to this novelty and giving themselves rich episodes for the hippocampus to encode. In addition, they are learning a new cognitive skill of how to build potentially very complex structures. Thus, there is a great deal of non-spatial episodic information present in this condition. We should note, however, that while not explicitly spatial, the active process of building

inherently becomes more spatial as building progresses. As the hippocampus plays a role in spatial mental imagery, including the ability to perceive objects or scenes from different perspectives (Hassabis et al., 2007; Bird et al., 2010; Summerfield et al., 2010) which may depend on the complexity of the scene or objects (Kim et al., 2013; Rungratsameetaweemana and Squire, 2018; Urgolites et al., 2018), the building condition should not be considered purely “non-spatial.” But, it has many rich non-spatial components and the scale of spatial involvement is certainly different than open-world exploration, giving us a different means within the same gaming environment of assessing whether enrichment, broadly defined, might have an impact on memory.

Here, we used the video game Minecraft and show that the spatial exploration of a virtual environment can improve hippocampus-associated memory. Minecraft is a sandbox game, which means that users are not restricted by game rules about the order of play. There is no right or wrong or winning or losing. It is a simple, endless, open world filled with mountains, deserts, forests, and oceans, for users to explore, create, and make their own. While all of our groups played Minecraft, they each focused on different combinations of the two main aspects of Minecraft: building and exploration. By creating completely custom Minecraft servers for every individual, we altered the focus of each group to promote building, exploration, or both. In addition, by being able to control their experience, we could manipulate the degree of sustained engagement in learning new aspects related to their activity (i.e., learning new skills or expanding their exploration of the world). Custom Minecraft servers also granted us the ability and control to track all movement as well as record the structures built in each world. Using the exact same metric of spatial exploration, our results parallel those in animals (Freund et al., 2013) and are consistent with our hypothesis that spatial exploration can improve hippocampus-associated memory. In addition, we found that the building of complex structures also influenced hippocampus-associated memory, suggesting that alternate novel, learning experiences found within Minecraft can be beneficial.

MATERIALS AND METHODS

Participants

In total, 82 individuals (53 female, 29 male; mean age = 19.83, SD = 1.08) participated in the study. Participants played Minecraft at the UCI Esports Arena for 2 weeks (Monday-Friday), for a maximum of 45 min/day (7.5 h), however the actual time spent in the video game was slightly less (mean: 7.02 h, SD = 0.75) due to training, daily setup, and irregularities in participant schedules. All participants were recruited through advertisements posted around the UC Irvine campus and received compensation of \$60, paid at the completion of the study. The advertisement specifically asked for participants with little to no experience with the video game Minecraft and did not reveal any details about the design or intention of the study, only that participants would play Minecraft for 2 weeks. All participants were screened for general video game experience, with an abbreviated version of the video

game questionnaire used previously (Clemenson and Stark, 2015) including questions aimed at addressing both prior and current video game experience. We specifically screened against participants with prior Minecraft experience and knowledge. While many participants had prior experience with video games at one point in time, none of them actively played (<1 h/week) at the time of participation (within 3 months). This study was carried out in accordance with the recommendations of the Institutional Review Board (IRB) of the University of California at Irvine with written informed consent from all subjects. All subjects gave written informed consent in accordance with the Declaration of Helsinki. The protocol was approved by the Institutional Review Board (IRB) of the University of California at Irvine.

UC Irvine Esports Arena

All Minecraft training took place at the UC Irvine Esports Arena located on the UC Irvine campus. The Esports Arena is home to 80 + high-end PCs, which were used by the participants to play Minecraft. Once the participants were trained on Minecraft, they were free to make their own hours and able to visit the arena anytime in the morning, between 9 am and 12 pm (when the Esports Arena was closed to the public), to continue their training. An experimenter was present at all times during training, to monitor progress and answer questions.

Minecraft

Minecraft is a popular sandbox, or open-world, style video game that is practically infinite and is procedurally generated as the player explores. The entire Minecraft world is made up of different biomes (plains, jungles, deserts, forests, mountains, oceans, etc. . .) that are composed of different types of blocks, all of which can be manipulated by the player. There are no specific goals to the game and no right or wrong ways to play it. Minecraft is simply intended to be a video game world that players can creatively make their own.

All Minecraft participants played on individual custom servers, which were hosted on a local server in our lab. Custom servers were created using SpigotMC¹ and a custom mod, Tracker (created by GDC), was added to track spatial locations of individuals and information about the world they created (e.g., blocks placed, current biome, time spent underground, etc.). All Minecraft participants within each group played on the exact same map but individually. The starting location was the same for every individual, ensuring that all participants received the same starting experience. All servers were set to “peaceful” which removed enemies and kept players health at full. Although difficult, it was still possible for players to die if they decided to swim in lava or fall off a mountain. Upon player death, they respawned at the initial starting point.

Participants were randomly assigned to one of four Minecraft groups in a 2 × 2 design focusing on building vs. exploring activities (to vary the type of enrichment) and undirected vs. directed activities (to vary the degree of enrichment): Free Building (11 females, 10 males; mean age = 20.4,

¹www.spigotmc.org

SD = 1.27; low exploration, low building enrichment), Directed Building (13 females, six males; mean age = 19.4, SD = 0.61; low exploration, high building enrichment), Free Exploration (16 females, seven males; mean age = 19.88, SD = 1.22; high exploration, no building enrichment), and Explore and Build (13 females, six males; mean age = 19.58, SD = 0.84; high exploration, mid building enrichment; **Figures 1A,B**). While participants knew that they were going to play Minecraft, they were not told any details about the study and were blind to the group they were in. To prevent participants from observing other individuals from other groups, each Minecraft group was split into two cohorts and each cohort played in the UCI Esports Arena during the same 2 weeks. A Minecraft tutorial was given to all study participants, with instructions on how to build a house, which ultimately became their “home.” While all Minecraft groups were given the same instructions for PC controls and taught the basics of Minecraft, each group was told to focus on a different aspect of Minecraft: building or exploring. In addition, they differed in how goal-oriented these aspects were and, as a result, the degree of engagement in pursuing new challenges in the area.

The Free Building and Directed Building groups were asked to focus on the building aspect of Minecraft. Both groups played on a completely flat world (no biomes, no mountains, no lakes, no caves, etc.) with no animal or vegetation spawns. While both groups focused on building, the main difference between the Free Building and the Directed Building groups was that the Directed Building group was given challenges to continuously expose them to new aspects of building and thereby provide a potentially higher level of enrichment. We did so by directing them to build complex structures found on grabcraft² such as an AT-AT Walker (**Figure 1A** lower left box, 3,785 blocks) and Spongebob’s House (3,486 blocks). Once a structure was chosen, the necessary blocks to build the structure were placed into a chest in the world. During the first week, participants in the Directed Building group were limited to pre-selected structures to ensure they had a grasp on the controls and mechanics of Minecraft. During the second week, they were allowed free choice of structure. In contrast, the Free Building group was given chests full of blocks but were not given any specific direction as to what they could or should build. During the second week, to maintain engagement, participants in the Free Building group were given new items to build with redstone—Minecraft’s tool for powering items and creating circuits.

The Free Exploration group played Minecraft in the most traditional sense. All participants played on individual servers, using the exact same map [seed: 1932176428914146755, starting point (x, y, z): -312, 73, -420] with easy access to resources. After creating their “home” at the starting spawn location, participants were told they could play Minecraft however they wished. The only rule was that at the end of their training session, they had to end up at their “home.” This encouraged participants to learn about the surrounding area and preventing anyone from walking in a straight line endlessly for the duration of the study. Thus, they were allowed to engage in as much or as little spatial

exploration as they wished and therefore have as much or as little potential enrichment as they wished. To maintain engagement, at the beginning of the second week, participants were given a scavenger hunt list of objects and places to find to encourage further exploration of the Minecraft world. This scavenger hunt list included flowers, gems, resources, waterfalls, villages, and other objects/locations that were in the local areas.

The Explore and Build group was designed to bring in both potential avenues of enrichment by combining the two activities. The first week was the same as the first week of the Free Exploration in which they explored and learned the spatial layout of their area. The second week was modeled on the Directed Building, but rather than providing them with free access to all needed materials for their structure of choice, participants had to find these materials in the world themselves. Therefore, this pushed heavily on both learning complex construction techniques and on spatial exploration as they searched for the needed materials.

Mnemonic Similarity Task (MST)

One of our primary outcome variables was the lure discrimination index (LDI) of the MST (Kirwan and Stark, 2007; Stark et al., 2013), which was designed to behaviorally index pattern separation and hippocampal function. The MST is now a widely used behavioral task and has been repeatedly shown to be sensitive to age-related memory decline and to hippocampal connectivity (Yassa et al., 2010a, 2011b; Bennett and Stark, 2015; Bennett et al., 2015) and function (Bakker et al., 2008, 2012, 2015; Yassa et al., 2010b, 2011a,b) and even to the alteration of hippocampal function following treatment for MCI with Levetiracetam (Bakker et al., 2012, 2015). There are two phases of the MST (**Figure 2A**). The first phase is an implicit encoding phase in which participants are shown pictures of everyday objects and asked to make a simple “indoor/outdoor” judgment. The second phase is an explicit test phase in which participants are shown everyday objects that are either the same (target), similar (lure), or different (foil) to the items encoded in the first phase. Participants then make “old/similar/new” judgments for each of these objects. Two metrics are used during the analysis. The LDI is the metric that has been shown to be sensitive to DG/CA3 activity and is defined as the probability of correctly identifying a lure item as “similar,” correcting for any response bias using the probability of incorrectly identifying a foil item as “similar”: $p(\text{similar}|\text{lure}) - p(\text{similar}|\text{foil})$. The recognition index (REC) is a standard object recognition memory score, defined as the probability of correctly identifying a target item as “old” minus the probability of incorrectly identifying a foil item as “old”: $p(\text{old}|\text{target}) - p(\text{old}|\text{foil})$.

Roaming Entropy (RE)

Roaming entropy (RE) is a measure of spatial exploration that was previously used to measure the exploratory behavior of mice living in an enriched environment (Freund et al., 2013). In the equation below, p_{ij} is the probability of participant i being at location j . The RE is defined as the Shannon entropy of the roaming distribution of participant i , where k is the total number

²www.grabcraft.com

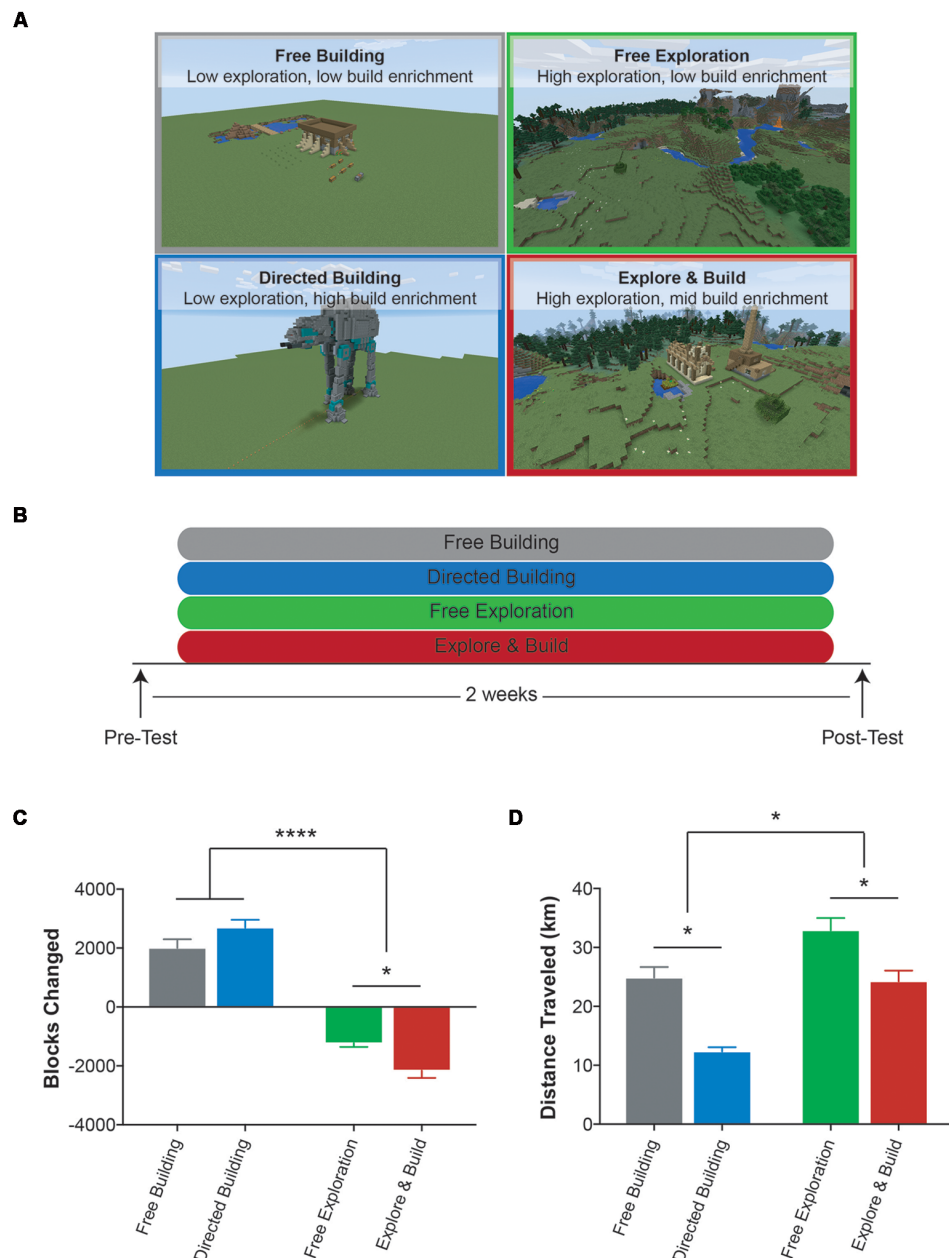


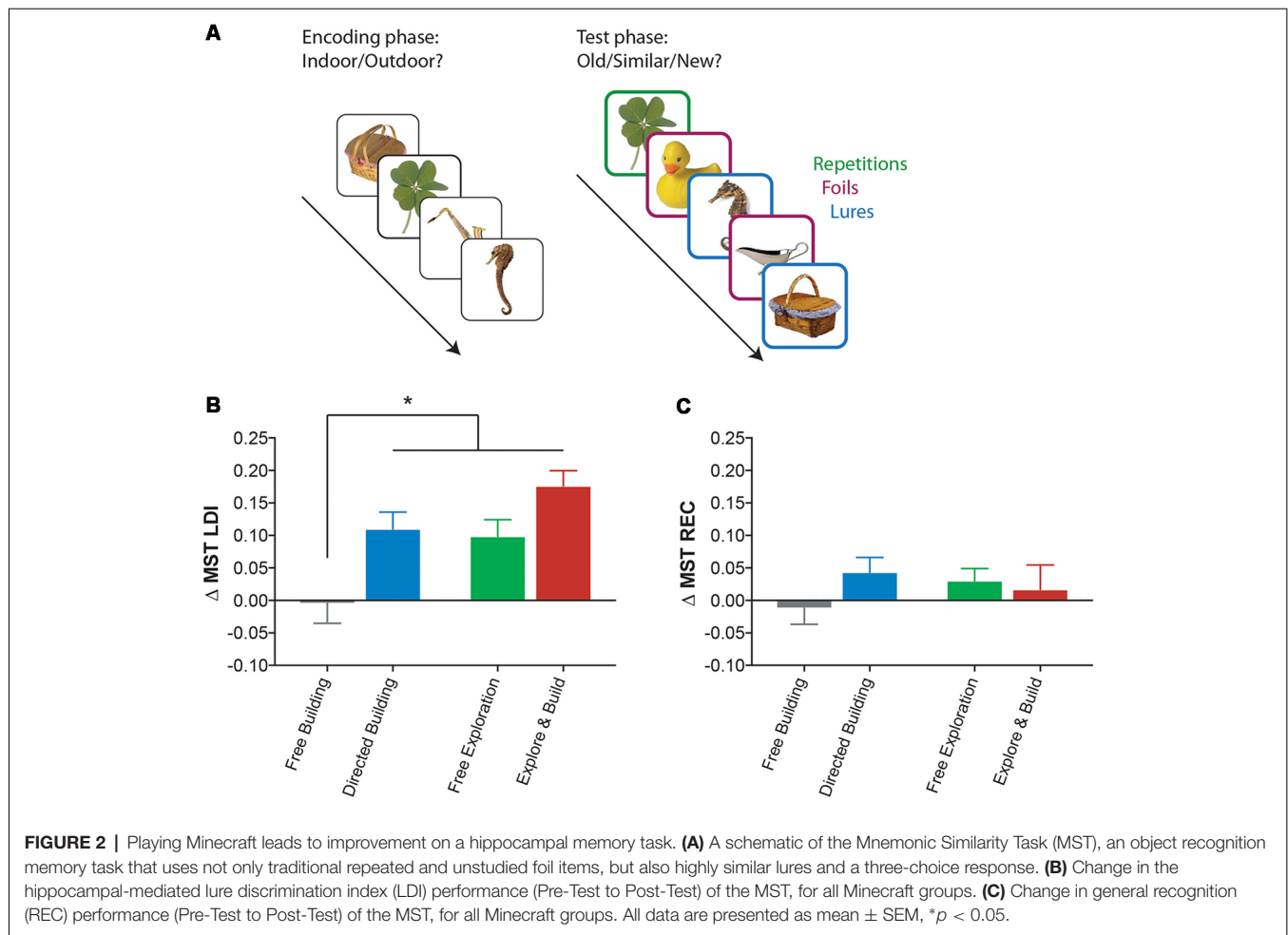
FIGURE 1 | Description of the Minecraft groups and experimental design. **(A)** Example images of the four Minecraft groups used in this study: Free Building (gray), Directed Building (blue), Free Exploration (green) and Explore and Build (red). **(B)** Experimental design. **(C)** The average total number of blocks changed for each Minecraft group over the course of the study. A positive number indicates an overall addition of blocks to the world and a negative number indicates an overall subtraction of blocks from the world. **(D)** The average total distance (km) traveled by each Minecraft group over the course of the study. All data are presented as mean \pm SEM, * $p < 0.05$, **** $p < 0.0001$.

of possible locations. Dividing by $\log(k)$ scales the range from 0 to 1.

$$RE_i = \sum_{j=1}^k (p_{i,j} \log(p_{i,j})) / \log(k)$$

In the mouse study (Freund et al., 2013), mice were tagged with radio frequency ID tags and were monitored by

antennas placed around the enriched environment. Essentially, RE is a measure of how likely a mouse would be located at each target location (antenna), at any given time. A lower RE value reflects that animal's movements were more predictable, and therefore exhibited less exploration, and a higher RE value reflects that the animal's movements were less predictable, and therefore exhibited more exploration. In our study, we used the same RE measure to assess the spatial



exploration of participants as they explored Minecraft. A virtual location was placed every 10 meters in the x-, y-, and z-axes (mirroring the antennae locations). We calculated the probability that an individual would be at each location at any given time, summed across all locations in the world that could have been visited in the allotted time. A lower RE value indicates that a participant's position was more predictable (lower spatial exploration) whereas a higher RE value means a participant's position was less predictable (higher spatial exploration).

Principal Components Analysis (PCA)

We performed a principal components analysis (PCA; MATLAB_R2018a) on the spatial location data collected from each participant as he or she moved through the world to determine the amount of variance each variable (x-, y-, and z-) contributed to the overall variance. Participant's total coordinate data was split into 60-s chunks and each 60-s dataset was entered into a PCA, providing a vector describing the relationship of the three variables (x-, y-, and z-). Using the coefficients for each variable (individual values that make up the normalized vector of each principal component), we first averaged within the subject (across 60 s blocks) and then across all subjects in a

group. We then calculated the percent variance contributed by the y variable $\left(\frac{y}{x+y+z}\right)$.

Statistical Analyses

Statistical analyses were conducted using Prism 7 (GraphPad Prism). Planned comparisons between groups were performed using two-way analysis of variances (ANOVAs), without repeated measures, and Sidak correction for multiple comparisons. General linear regression models (GLMs) were used to analyze correlations between group metrics. Shapiro-Wilk normality test revealed that distributions did not significantly deviate from the normal distribution. A significance value of 0.05 was used for all statistical analyses.

RESULTS

All Four Groups Focused on Different Aspects of Minecraft

Participants were randomly assigned to one of four groups that varied in both the central activity (exploring vs. building) and the amount of engagement in that activity (Figures 1A,B). The two groups that focused on building, Free Building and

Directed Building, were placed in a flat and featureless world and simply asked to build. While the Free Building group was given limitless resources and little guidance, the Directed Building group was instructed on how to build progressively more complex structures. The Free Exploration and Explore and Build groups both played on rich, computer-generated worlds typical of Minecraft and were simply asked to explore the world. The Explore and Build group was a combination of building and exploring. While the first week was the same as the Free Exploration group, during the second week of training, they were required to scavenge for resources needed to build a complex structure.

In analyzing their behavior within the game, as expected, the four groups differed in the most basic measures of building and exploration. The Free Building and Directed Building groups focused on building far more than exploring, while the Free Exploration and Explore and Build groups focused heavily on exploring, with the Explore and Build partaking in both (Figures 1C,D). For each participant, we used the number of blocks changed in the world as a measure of the amount of building (Figure 1C; a positive value is a cumulative addition of blocks to the world and a negative value is a cumulative subtraction of blocks from the world) and analyzed the scores using a 2×2 ANOVA with factors for the type of activity (building vs. exploring) and whether the activity was directed or not (free vs. directed). We found a significant main effect of type of activity (two-way ANOVA: $F_{(1,78)} = 285.8$, $p < 0.0001$) with building groups placing more blocks in the environment and the active exploring groups removing more blocks from the world (removing blocks is often necessary to explore and find resources in the world) and a significant interaction (two-way ANOVA: $F_{(1,78)} = 11.44$, $p < 0.01$). A *post hoc* analysis (Sidak correction for multiple comparisons at $p < 0.05$) revealed that while there was no difference between building groups (Free Building vs. Directed Building), the Explore and Build removed significantly more blocks from the world when compared to the Free Exploration group, consistent with their need to harvest the necessary resources to build a structure during the second week.

As an initial measure of the amount of exploration, we calculated the total distance that individuals walked while playing Minecraft (Figure 1D). Here, we found a significant main effect of activity type with the exploring groups walking more than the building groups (two-way ANOVA: $F_{(1,78)} = 31.05$, $p < 0.0001$) and a main effect of amount of engagement with the free groups walking more than the directed groups (two-way ANOVA: $F_{(1,78)} = 35.07$, $p < 0.0001$). A *post hoc* analysis (Sidak correction for multiple comparisons at $p < 0.05$) revealed that the Free Building and Explore and Build groups were similar, but all other comparisons differed reliably. It is interesting to note that in terms of distance, the Free Building group traveled more than the Directed Building group and a similar amount to the Explore and Build group. One source of this is that the Free Building group had to continually return to the chest in order to retrieve resources to build. Unlike the Directed Building group, which had a specific plan for building, the building process of the Free Building group was unconstrained. Without a specific goal in mind, this free-form building group was apparently far less

efficient in their trips to and from the supply chest. Regardless, when combined with the data above on building, it is clear that all four Minecraft groups were different in how they interacted with the environment.

All but the Free Building Group Showed Improvements in Hippocampus-Associated Memory

Our initial question was whether playing Minecraft, focusing on either building, exploring or both, can improve hippocampus associated memory. Using the change in the MST's LDI (post-test minus pre-test, Figure 2B) as a measure of change in hippocampal function, we found a significant main effect of activity type (two-way ANOVA: $F_{(1,78)} = 10$, $p < 0.01$) and amount of engagement (two-way ANOVA: $F_{(1,78)} = 12.89$, $p < 0.001$). A *post hoc* analysis (Sidak correction for multiple comparisons at $p < 0.05$) revealed that not only were the Directed Building, Free Exploration, and Explore and Build groups all showing reliable changes in the LDI score, but all three groups showed reliably greater improvements than the Free Building group (which did not differ from zero, one-sample *t*-test $t_{(20)} = 0.15$, $p = 0.87$). While there was some evidence for an additive effect in the Explore and Build condition relative to the Directed Building ($p = 0.06$, uncorrected) and Free Exploration ($p = 0.03$, uncorrected), these did not survive corrections for multiple comparisons. Importantly, there was no change in general recognition memory measure in the MST (Figure 2C), indicating a specific improvement in the highly hippocampal-dependent lure discrimination metric.

LDI Improvement Correlated With Spatial Exploration of the Minecraft World but Not Total Distance Traveled

One of our main hypotheses was that environmental enrichment via the exploration of the Minecraft world would be important for the observed improvement in hippocampal behavior. Similar to spatial exploration found in mice (Freund et al., 2013) we found that our human participants varied greatly in their exploratory behavior (Figure 3A). Even within a group, some explored the world far more than others. As in the rodent work, we used RE to measure the amount of exploration (see "Materials and Methods" section). Participants with lower exploration RE scores (e.g., Figure 3A, left) tended to focus their exploration around the spawn area (where their house was built), whereas participants with higher exploration RE scores (e.g., Figure 3A, right) were more likely to adventure further in all directions. As expected, we found a main effect of activity type with the exploring groups (Free Exploration and Explore and Build) showing higher RE values than the building groups (two-way ANOVA: $F_{(1,78)} = 170.2$, $p < 0.0001$; data not shown).

More important than this simple group effect, however, is the relationship between the amount an individual explored the world and their subsequent memory improvement. When examined individually, we found a significant correlation between RE and Δ LDI in both exploring groups (Free Exploration: $R^2 = 0.17$, $p < 0.05$; Explore and Build: $R^2 = 0.21$,

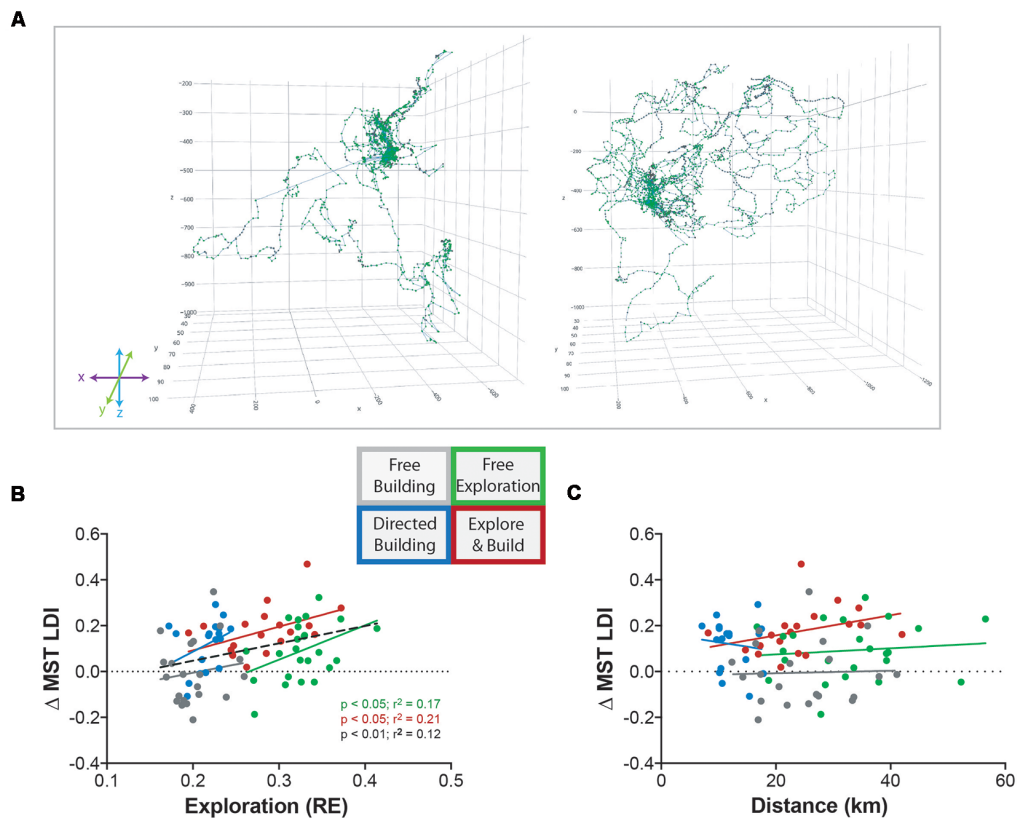


FIGURE 3 | Exploration of Minecraft correlates with improvement in hippocampal memory. **(A)** Example path traces of low exploration (left) and high exploration (right) individuals from the Free Exploration group. **(B)** The relationship between the change in MST LDI performance (Pre-Test to Post-Test) and the amount of exploration roaming entropy (RE). Colors correspond to the Minecraft group indicated by the diagram: Free Building (gray), Directed Building (blue), Free Exploration (green), and Explore and Build (red). The black dotted line represents the combination of all four Minecraft groups together. Significant statistics are denoted by group color including black for all groups. **(C)** The relationship between the change in MST LDI performance (Pre-Test to Post-Test) and the total distance traveled (km). Colors correspond to the groups as previously described.

$p < 0.05$; **Figure 3B**), with effects in the two building groups not being reliable on their own. Importantly, in no group was the total amount of distance covered correlated with Δ LDI (**Figure 3C**), indicating that the quality of exploration was important for the improvement in LDI. Further supporting this conclusion, when analyzing the relationship between RE and Δ LDI across all groups, there was not only a reliable correlation ($R^2 = 0.012$, $p < 0.01$), but when testing whether a single slope fits all datasets or whether the slope differed, we found no evidence for the use of differing slopes (Extra sum of squares $F_{(4,154)}$, $p = 0.8$) suggesting a common relationship between the amount of exploration and improvement in memory regardless of condition.

LDI Improvement Correlated With Active Building More Complex Structures

The Directed Building demonstrated a clear and significant improvement in LDI performance when compared to Free Building, who also focused on building. We wanted to better understand the structures that both Directed Building and Free Building created. One clear difference between these two groups was that the structures the Directed Building created were denser

and seemingly more complex, with the Directed Building adding more blocks to the environment (**Figure 1C**) and walking less (**Figure 1D**) than all other groups. Assessing “complexity” of their building activity is not as straightforward as measuring something like RE as there is no established metric of building activity or complexity. Furthermore, building is an active process with a constant exchange between the placement and removal of blocks, a factor that we cannot reasonably address with our current dataset. What we would like to capture is whether their building is a simple structure or something more challenging that required more planning to physically construct (e.g., building stairs or scaffolds to reach locations during construction). Here, we use three different measures to address building activity in Minecraft.

Perhaps the simplest metric that could capture this complexity is the block-change density, or the number of blocks changed per square kilometer. Using this metric, we found a significant main effect of activity type (two-way ANOVA: $F_{(1,78)} = 259.4$, $p < 0.0001$; data not shown), amount of engagement ($F_{(1,78)} = 13.13$, $p = 0.0005$), and an interaction ($F_{(1,78)} = 53.2$, $p < 0.0001$). A *post hoc* analysis (Sidak correction for multiple comparisons at $p < 0.05$) revealed that the Directed

Building group had a higher block-change density than all other groups and that the Free Building group had a higher block-change density than the two exploring groups. As building complex structures in Minecraft (e.g., **Figure 4C**) typically requires significant movement vertically (to place blocks more than one unit above you, you must build some form of stairs to reach that level), block-change density is only a very rough, indirect measure of this complexity. We created two metrics to assess the degree of variance along the vertical (y) axis.

First, using the previous measure of spatial exploration (RE), we calculated a RE value for each individual axis, which allowed us to individually quantify the predictability of movement along each axis. We predicted that if Directed Building were in fact building taller structures, they would spend more time exploring the vertical axis (i.e., greater unpredictability) compared to the other groups. Using this measure, we created an index score to measure the amount of vertical-axis bias ($\frac{yRE}{xRE+zRE}$) for all individuals (**Figure 4A**). We found no evidence for an effect of activity type, but a significant main effect of amount of engagement (two-way ANOVA: $F_{(1,78)} = 22.92$, $p < 0.0001$) and a significant interaction between activity type and amount of direction (two-way ANOVA: $F_{(1,78)} = 4.976$, $p < 0.05$) with the directed groups (Directed Building and Explore and Build) scoring significantly higher on this index compared to both exploring groups (Free Building and Free Exploration). A *post hoc* analysis (Sidak correction for multiple comparisons at $p < 0.05$) revealed Directed Building scoring reliably higher than both Free Building and Free Exploration whereas Explore and Build only scored reliably higher than Free Building. Furthermore, a positive correlation was found in Directed Building between the y-axis bias index score and ΔLDI in Directed Building ($R^2 = 0.22$, $p < 0.05$) but not in other groups (**Figure 4B**).

Second, we used PCA to measure how much of the variability of movement was contributed by the movement along the vertical axis. Each coordinate data set was split into 1-min blocks and PCA was used to characterize the variance in location within that time and determine how much the total motion was driven by motion along each axis (x, y, and z). The resulting coefficients from the three PCs were first averaged within the subject (across 1-min blocks) and then across all subjects in a group. The first principal component (PC1) accounted for 83%–89% (across groups) of the variance in motion and was heavily dominated by movement along the horizontal plane (x and z axes; **Figure 4D**). Despite the high degree of similarity, we found a significant main effect of activity type (two-way ANOVA: $F_{(1,78)} = 10.85$, $p < 0.01$; data not shown) with the building groups (Free Building and Directed Building) having a higher contribution of y-axis movement (~8%) to PC1 than the exploring groups (Free Exploration and Explore and Build, ~4%). The second PC (PC2) accounted for 10%–15% of the variance and showed main effects of both activity type (two-way ANOVA: $F_{(1,78)} = 45.45$, $p < 0.0001$) and amount of engagement (two-way ANOVA: $F_{(1,78)} = 61.85$, $p < 0.0001$) along with a significant interaction between the two (two-way ANOVA: $F_{(1,78)} = 43.72$, $p < 0.0001$; **Figure 4E**). Much of the observed

effects can be attributed to the Directed Building as a *post hoc* analysis (Sidak correction for multiple comparisons at $p < 0.05$) revealed a highly significant difference between the Directed Building and all other groups. Their movement along the y-axis contributed to ~30% of the total variance in PC2 compared to ~11% for all other groups. There was a clear and positive correlation between y-axis variance of Directed Building and ΔLDI ($R^2 = 0.2$, $p = 0.05$; **Figure 4F**). Lastly, although PC3 only accounted for ~1% of the total variance, the y-axis variable contributed to significantly more of the variance in the Free Building, Free Exploration and Explore and Build groups than the Directed Building (Multiple comparisons: $p < 0.0001$ for all groups; data not shown; **Figure 4D**). These data indicate that the y-axis variable plays a bigger role in the Directed Building than in all other groups.

DISCUSSION

We set out to replicate and improve upon our prior report that video games may act as human analogs for environmental enrichment (Clemenson and Stark, 2015) and to explore the effects of the kind of enrichment and the amount of enrichment had on memory ability. Using the video game Minecraft, we constrained the environment to encourage participants to focus on either spatial exploration or building and we promoted greater levels of engagement in new, more challenging forms of each activity by use of directed, or guided activities within the game. We again observed improvements in a hippocampal-dependent memory task, unrelated to the video game activity, following 2 weeks of gameplay (**Figure 2B**) with results indicating that both the kind of enrichment activity and the degree of engagement in the activity were correlated with the amount of improvement.

Even without directed activities to enhance engagement, we found that the spatial exploration of a Minecraft environment led to greater improvements in hippocampal cognition. In animals, spatial exploration of an enriched environment has been tied to hippocampal neuroplasticity (Freund et al., 2013). Using Minecraft as our enriched environment, we translated this animal study to humans and found similar results. Using the exact same methodology and equation for exploration (RE), we found that higher spatial exploration, but not overall distance walked, led to greater improvements on a hippocampal memory task. As expected, the two groups that focused on the exploring aspect of Minecraft (Free Exploration and Explore and Build) scored the highest on our exploration metric. However, it is important to note that when all four groups were combined (**Figure 3B**), we observed a highly significant correlation with hippocampal memory which suggests an important notion about building in Minecraft. Although Free Building and Directed Building were on the lower end of the exploration metric, participants were still able to explore an environment regardless of how simple it might be. While we tried to limit spatial exploration of both Free Building and Directed Building, their environments became progressively more spatial as they began to build structures and added to the uniqueness of their own individual worlds. With more time, Free Building and Directed

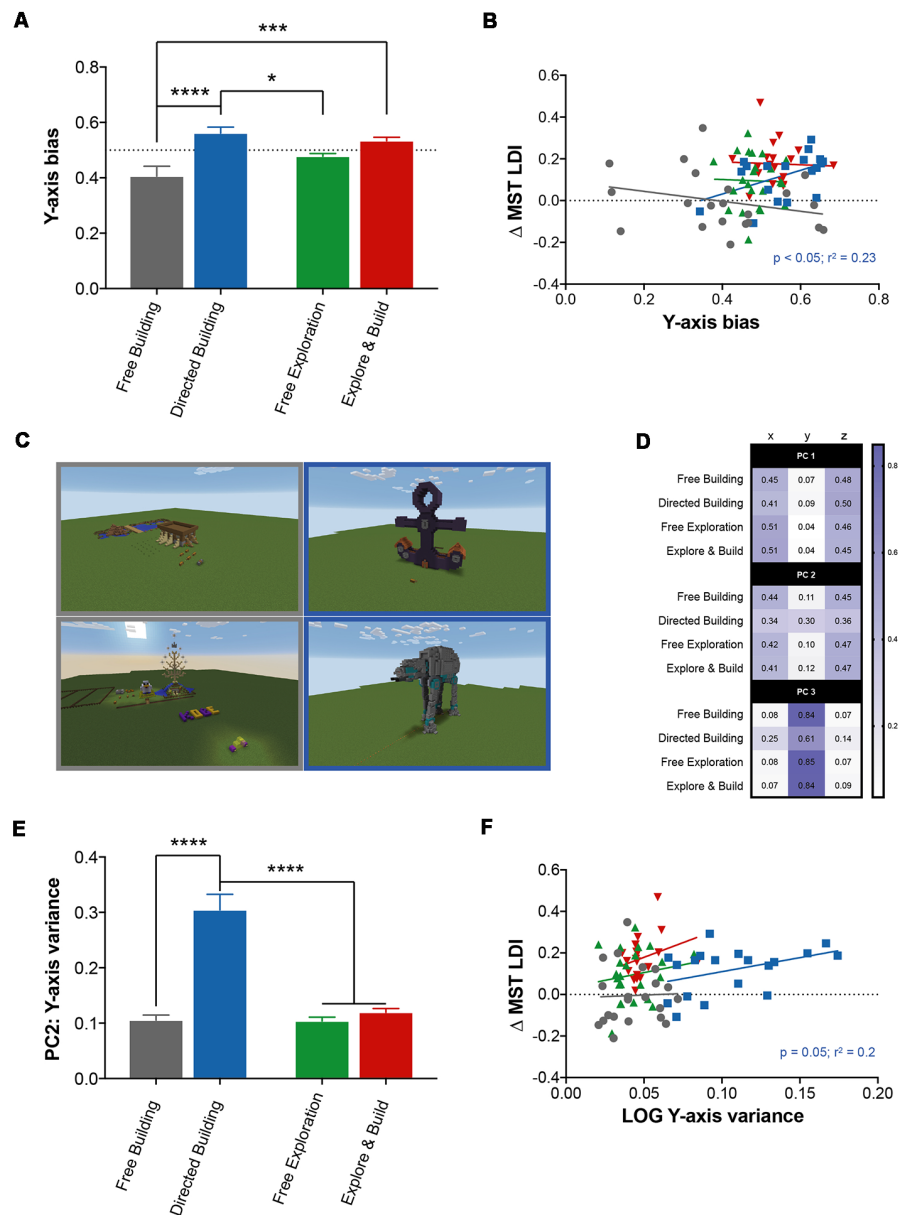


FIGURE 4 | Building in Minecraft correlates with improvement in hippocampal memory. **(A)** The y-axis bias score represents the amount of spatial exploration (RE) along the vertical axis (y axis) compared to the horizontal axes (x- and z-axes) for all Minecraft groups. The dotted line represents a value where exploration along the vertical axis is equal to exploration along the horizontal axes. **(B)** The relationship between the change in MST LDI performance (Pre-Test to Post-Test) and the y-axis bias score. Minecraft groups are represented by their corresponding colors with significant statistics denoted by group color. **(C)** Example images from the Free Building (left column) and Directed Building (right column) groups. **(D)** Overview of the principal components analysis (PCA) for all Minecraft groups. Each value represents the amount of variance explained by the variable (column) for each Minecraft group (row), for all three principal components (PC1, PC2, and PC3). **(E)** The amount of variance explained by the y variable of all Minecraft groups for the second principal component. **(F)** The relationship between the change in MST LDI performance (Pre-Test to Post-Test) and the LOG of the y-axis variance of the second principal component. All data are presented as mean \pm SEM, * $p < 0.05$, *** $p < 0.001$, **** $p < 0.0001$.

Building might naturally increase their exploratory behaviors as they build and make their environment more spatial. In addition, this correlation highlights the fact that, similar to the animal studies, spatial exploration is a powerful factor driving our observed results and that its effects may be independent of other factors underlying enrichment's effects.

In addition to spatial exploration, our results showed that building within Minecraft can also lead to improvements in hippocampal-based memory. The effects were less robust as simply giving people the world to explore (Free Exploration) led to reliable effects, while simply giving people the resources needed to build structures (Free Building) was insufficient. For

the building to be effective at improving memory, participants needed to be directed towards building activities that had them build new, more complex structures (Directed Building). While the Directed Building consistently placed higher in all three metrics of building activity, results from the other groups (Free Building, Free Exploration and Explore and Build) were mixed. Since building is an active process, it is possible that we are only capturing a portion of building complexity. Further analyses are necessary to better understand the contribution of the building process. The environmental enrichment literature strongly implicates spatial exploration as a powerful means to induce the effects on the hippocampus (as observed here as well), but the translation of the building aspect of Minecraft is less clear. In part, this may be because there simply are not analogous experiments in the rodent. However, several explanations recapitulate a common question in the hippocampal literature: whether the observed results stem from spatial aspects of the Directed Building group, such as spatial mental imagery, or whether they are the result of non-spatial forms of novelty and learning, building in Minecraft allows users to create their own unique, complex and spatial environments. As mentioned previously, building is a way to change the surrounding environment and inherently makes an environment more spatial. After all, cities are a product of building within our own environments and the complex structures and the spatial nature of modern cities require maps to navigate. In fact, many studies in humans specifically use city environments to understand the role of the hippocampus in navigation. However, building new items and structures in Minecraft, and learning how to build them, is a novel learning experience for participants outside of anything spatial *per se*. While we cannot be resolute on this matter as the interpretations discussed here are merely speculation, it was the case that being pushed to learn to create new, complex structures (Directed Building) had as big an effect on memory improvement as free exploration of the world (Free Exploration) despite far lower amounts of exploration (RE), supporting the notion that at least some of the observed effect was likely non-spatial. In addition, the Explore and Build group showed roughly twice the improvement in memory that the Free Exploration group showed, despite having half of the exploration-driven gameplay directed towards learning to build new structures. Thus, we conclude that spatial exploration alone has a clear effect, but that learning new skills (directed groups) can have a similar effect, possibly non-spatial in nature.

Here, we show that playing the video game Minecraft can positively impact hippocampal function in the form of improved memory performance on tasks unrelated to activities in the game itself. Both spatial exploration and building were at least partly responsible for this observed improvement. Whether these aspects are able to improve performance on other hippocampus-related behaviors is still unknown, however, we did observe an improvement in a virtual water maze task in our previous study using video game enrichment. We would predict similar results given that the exploration of a virtual environment like Minecraft has more direct relevance to a virtual water maze than the MST task. While we previously demonstrated that 3D video games can have an influence on hippocampal function

using the video game Super Mario 3D World (Clemenson and Stark, 2015), this study improves upon the previous study for several critical reasons. First and foremost, while Minecraft is not completely open-source, it is customizable which affords great flexibility and freedom to create environments on private servers where we can entice users to focus on distinct aspects of the game, while still being able to both track player movement and the addition/removal of blocks from the world. Second, this control over the environment and ability to track participants allowed us to implement the same metrics of spatial exploration as in rodent studies, giving us a better understanding of how environmental enrichment relates to humans. Lastly, all groups in this study played Minecraft. Several studies have explored the effects of video games on brain function, however, a major caveat of many of these studies is the fact that the controls and experimental groups play entirely different games. All video games differ on several levels, including game mechanics, game dynamics, visual and audio features, engagement, etc. These inherent differences add a level of uncertainty and can reduce the reliability of the interpretations. Often, this simply cannot be helped as commercial video games are stuck with a set of rules that make it difficult to deviate from. The video game Minecraft can address these limitations and sets itself apart as a platform for video game research.

It is well understood that the hippocampus is a region of great neuroplasticity and is constantly shaped by environmental experiences. Results from this study are consistent with animal research and support the idea that video games can act as a form of environmental enrichment in humans. While specific aspects of the enrichment manipulations used in animals are simply not present in video games, the virtual worlds found in modern video games provide a rich and complex environment for people to experience and offer a real opportunity for intervention in humans.

DATA AVAILABILITY

The datasets generated for this study are available on request to the corresponding author.

AUTHOR CONTRIBUTIONS

GC and CS designed the experiment, analyzed the data and wrote the article. GC and CH collected the data.

FUNDING

This work was supported by the DANA Foundation and National Institutes of Health (NIH) R21 AG056145.

ACKNOWLEDGMENTS

We would like to thank UCI Esports, especially Mark Deppe, Kathy Chiang, and Samantha Anton, for their help, time and generosity. We would also like to thank Olayemi Osibowale and Sean Kil for helping with data collection and Shauna Stark for helpful discussions.

REFERENCES

- Bakker, A., Albert, M. S., Krauss, G., Speck, C. L., and Gallagher, M. (2015). Response of the medial temporal lobe network in amnesic mild cognitive impairment to therapeutic intervention assessed by fMRI and memory task performance. *Neuroimage Clin.* 7, 688–698. doi: 10.1016/j.nicl.2015.02.009
- Bakker, A., Krauss, G. L., Albert, M. S., Speck, C. L., Jones, L. R., Stark, C. E., et al. (2012). Reduction of hippocampal hyperactivity improves cognition in amnesic mild cognitive impairment. *Neuron* 74, 467–474. doi: 10.1016/j.neuron.2012.03.023
- Bakker, A., Kirwan, C. B., Miller, N. I., and Stark, C. E. L. (2008). Pattern separation in the human hippocampal CA3 and dentate gyrus. *Science* 319, 1640–1642. doi: 10.1126/science.1152882
- Bekinschtein, P., Oomen, C. A., Saksida, L. M., and Bussey, T. J. (2011). Effects of environmental enrichment and voluntary exercise on neurogenesis, learning, and memory and pattern separation: BDNF as a critical variable? *Semin. Cell Dev. Biol.* 22, 536–542. doi: 10.1016/j.semcdb.2011.07.002
- Bennett, I. J., Huffman, D. J., and Stark, C. E. L. (2015). Limbic tract integrity contributes to pattern separation performance across the lifespan. *Cereb. Cortex* 25, 2988–2999. doi: 10.1093/cercor/bhu093
- Bennett, I. J., and Stark, C. E. L. (2015). Mnemonic discrimination relates to perforant path integrity: an ultra-high resolution diffusion tensor imaging study. *Neurobiol. Learn. Mem.* 129, 107–112. doi: 10.1016/j.nlm.2015.06.014
- Bird, C. M., Capponi, C., King, J. A., Doeller, C. F., and Burgess, N. (2010). Establishing the boundaries: the hippocampal contribution to imagining scenes. *J. Neurosci.* 30, 11688–11695. doi: 10.1523/JNEUROSCI.0723-10.2010
- Bugg, J. M., and Head, D. (2011). Exercise moderates age-related atrophy of the medial temporal lobe. *Neurobiol. Aging* 32, 506–514. doi: 10.1016/j.neurobiolaging.2009.03.008
- Clemenson, G. D., Gage, F. H., and Stark, C. E. L. (2018). “Environmental enrichment and neuronal plasticity,” in *The Oxford Handbook of Developmental Neural Plasticity*, ed. M. Chao (New York, NY: Oxford University Press). doi: 10.1093/oxfordhb/9780190635374.013.13
- Clemenson, G. D., Lee, S. W., Deng, W., Barrera, V. R., Iwamoto, K. S., Fanselow, M. S., et al. (2015). Enrichment rescues contextual discrimination deficit associated with immediate shock. *Hippocampus* 25, 385–392. doi: 10.1002/hipo.22380
- Clemenson, G. D., and Stark, C. E. L. (2015). Virtual environmental enrichment through video games improves hippocampal-associated memory. *J. Neurosci.* 35, 16116–16125. doi: 10.1523/JNEUROSCI.2580-15.2015
- Cohen, S. J., and Stackman, R. W. (2015). Assessing rodent hippocampal involvement in the novel object recognition task. A review. *Behav. Brain Res.* 285, 105–117. doi: 10.1016/j.bbr.2014.08.002
- Creer, D. J., Romberg, C., Saksida, L. M., van Praag, H., and Bussey, T. J. (2010). Running enhances spatial pattern separation in mice. *Proc. Natl. Acad. Sci. U S A* 107, 2367–2372. doi: 10.1073/pnas.0911725107
- Darmopil, S., Petanjek, Z., Mohammed, A. H., and Bogdanović, N. (2009). Environmental enrichment alters dentate granule cell morphology in oldest-old rat. *J. Cell. Mol. Med.* 13, 1845–1856. doi: 10.1111/j.1582-4934.2008.00560.x
- Ekstrom, A. D., Kahana, M. J., Caplan, J. B., Fields, T. A., Isham, E. A., Newman, E. L., et al. (2003). Cellular networks underlying human spatial navigation. *Nature* 425, 184–188. doi: 10.1038/nature01964
- Erickson, K. I., Prakash, R. S., Voss, M. W., Chaddock, L., Hu, L., Morris, K. S., et al. (2009). Aerobic fitness is associated with hippocampal volume in elderly humans. *Hippocampus* 19, 1030–1039. doi: 10.1002/hipo.20547
- Erickson, K. I., Raji, C. A., Lopez, O. L., Becker, J. T., Rosano, C., Newman, A. B., et al. (2010). Physical activity predicts gray matter volume in late adulthood: the Cardiovascular Health Study. *Neurology* 75, 1415–1422. doi: 10.1212/WNL.0b013e3181f88359
- Erickson, K. I., Voss, M. W., Prakash, R. S., Basak, C., Szabo, A., Chaddock, L., et al. (2011). Exercise training increases size of hippocampus and improves memory. *Proc. Natl. Acad. Sci. U S A* 108, 3017–3022. doi: 10.1073/pnas.1015950108
- Fabel, K., Fabel, K., Tam, B., Kaufer, D., Baiker, A., Simmons, N., et al. (2003). VEGF is necessary for exercise-induced adult hippocampal neurogenesis. *Eur. J. Neurosci.* 18, 2803–2812. doi: 10.1111/j.1460-9568.2003.03041.x
- Faherty, C. J., Kerley, D., and Smeys, R. J. (2003). A Golgi-Cox morphological analysis of neuronal changes induced by environmental enrichment. *Dev. Brain Res.* 141, 55–61. doi: 10.1016/s0165-3806(02)00642-9
- Farmer, J., Zhao, X., van Praag, H., Wodtke, K., Gage, F. H., and Christie, B. R. (2004). Effects of voluntary exercise on synaptic plasticity and gene expression in the dentate gyrus of adult male Sprague-Dawley rats *in vivo*. *Neuroscience* 124, 71–79. doi: 10.1016/j.neuroscience.2003.09.029
- França, T. F. A., Bitencourt, A. M., Maximilla, N. R., Barros, D. M., and Monserrat, J. M. (2017). Hippocampal neurogenesis and pattern separation: a meta-analysis of behavioral data. *Hippocampus* 27, 937–950. doi: 10.1002/hipo.22746
- Freund, J., Brandmaier, A. M., Lewejohann, L., Kirste, I., Kritzer, M., Krüger, A., et al. (2013). Emergence of individuality in genetically identical mice. *Science* 340, 756–759. doi: 10.1126/science.1235294
- Garthe, A., Roeder, I., and Kempermann, G. (2016). Mice in an enriched environment learn more flexibly because of adult hippocampal neurogenesis. *Hippocampus* 26, 261–271. doi: 10.1002/hipo.22520
- Gogolla, N., Galimberti, I., Deguchi, Y., and Caroni, P. (2009). Wnt signaling mediates experience-related regulation of synapse numbers and mossy fiber connectivities in the adult hippocampus. *Neuron* 62, 510–525. doi: 10.1016/j.neuron.2009.04.022
- Gonçalves, J. T., Schafer, S. T., and Gage, F. H. (2016). Adult neurogenesis in the hippocampus: from stem cells to behavior. *Cell* 167, 897–914. doi: 10.1016/j.cell.2016.10.021
- Hassabis, D., Kumaran, D., and Maguire, E. A. (2007). Using imagination to understand the neural basis of episodic memory. *J. Neurosci.* 27, 14365–14374. doi: 10.1523/JNEUROSCI.4549-07.2007
- Jacobs, J., Weidemann, C. T., Miller, J. F., Solway, A., Burke, J. F., Wei, X. X., et al. (2013). Direct recordings of grid-like neuronal activity in human spatial navigation. *Nat. Neurosci.* 16, 1188–1190. doi: 10.1038/nn.3466
- Kempermann, G., Gast, D., and Gage, F. H. (2002). Neuroplasticity in old age: sustained fivefold induction of hippocampal neurogenesis by long-term environmental enrichment. *Ann. Neurol.* 52, 135–143. doi: 10.1002/ana.10262
- Kempermann, G., Kuhn, H. G., and Gage, F. H. (1997). More hippocampal neurons in adult mice living in an enriched environment. *Nature* 386, 493–495. doi: 10.1038/386493a0
- Kim, S., Borst, G., Thompson, W. L., Hopkins, R. O., Kosslyn, S. M., and Squire, L. R. (2013). Sparing of spatial mental imagery in patients with hippocampal lesions. *Learn. Mem.* 20, 657–663. doi: 10.1101/lm.031633.113
- Kirwan, C. B., and Stark, C. E. L. (2007). Overcoming interference: an fMRI investigation of pattern separation in the medial temporal lobe. *Learn. Mem.* 14, 625–633. doi: 10.1101/lm.663507
- Kobilo, T., Liu, Q. R., Gandhi, K., Mughal, M., Shaham, Y., and van Praag, H. (2011). Running is the neurogenic and neurotrophic stimulus in environmental enrichment. *Learn. Mem.* 18, 605–609. doi: 10.1101/lm.2283011
- Leal-Galicia, P., Castañeda-Bueno, M., Quiroz-Baez, R., and Arias, C. (2008). Long-term exposure to environmental enrichment since youth prevents recognition memory decline and increases synaptic plasticity markers in aging. *Neurobiol. Learn. Mem.* 90, 511–518. doi: 10.1016/j.nlm.2008.07.005
- Maguire, E. A., Burgess, N., Donnett, J. G., Frackowiak, R. S., Frith, C. D., and O’Keefe, J. (1998). Knowing where and getting there: a human navigation network. *Science* 280, 921–924. doi: 10.1126/science.280.5365.921
- Maguire, E. A., Gadian, D. G., Johnsrude, I. S., Good, C. D., Ashburner, J., Frackowiak, R. S., et al. (2000). Navigation-related structural change in the hippocampi of taxi drivers. *Proc. Natl. Acad. Sci. U S A* 97, 4398–4403. doi: 10.1073/pnas.070039597
- McClelland, J. L., McNaughton, B. L., and O’Reilly, R. C. (1995). Why there are complementary learning systems in the hippocampus and neocortex: insights from the successes and failures of connectionist models of learning and memory. *Psychol. Rev.* 102, 419–457. doi: 10.1037/0033-295X.102.3.419
- Mora-Gallegos, A., Rojas-Carvajal, M., Salas, S., Saborio-Arce, A., Fornaguera-Trias, J., and Brenes, J. C. (2015). Age-dependent effects of environmental enrichment on spatial memory and neurochemistry. *Neurobiol. Learn. Mem.* 118, 96–104. doi: 10.1016/j.nlm.2014.11.012
- Moser, M. B., Trommald, M., and Andersen, P. (1994). An increase in dendritic spine density on hippocampal CA1 pyramidal cells following spatial learning in adult rats suggests the formation of new synapses. *Proc. Natl. Acad. Sci. U S A* 91, 12673–12675. doi: 10.1073/pnas.91.26.12673
- Mustroph, M. L., Chen, S., Desai, S. C., Cay, E. B., DeYoung, E. K., and Rhodes, J. S. (2012). Aerobic exercise is the critical variable in an enriched environment that increases hippocampal neurogenesis and water maze learning in male

- C57BL/6J mice. *Neuroscience* 219, 62–71. doi: 10.1016/j.neuroscience.2012.06.007
- Nilsson, M., Perfilieva, E., Johansson, U., Orwar, O., and Eriksson, P. S. (1999). Enriched environment increases neurogenesis in the adult rat dentate gyrus and improves spatial memory. *J. Neurobiol.* 39, 569–578. doi: 10.1002/(sici)1097-4695(19990615)39:4<569::aid-neu10>3.0.co;2-f
- Nithianantharajah, J., Levis, H., and Murphy, M. (2004). Environmental enrichment results in cortical and subcortical changes in levels of synaptophysin and PSD-95 proteins. *Neurobiol. Learn. Mem.* 81, 200–210. doi: 10.1016/j.nlm.2004.02.002
- Pereira, A. C., Huddleston, D. E., Brickman, A. M., Sosunov, A. A., Hen, R., McKhann, G. M., et al. (2007). An *in vivo* correlate of exercise-induced neurogenesis in the adult dentate gyrus. *Proc. Natl. Acad. Sci. U S A* 104, 5638–5643. doi: 10.1073/pnas.0611721104
- Rampon, C., Jiang, C. H., Dong, H., Tang, Y. P., Lockhart, D. J., Schultz, P. G., et al. (2000). Effects of environmental enrichment on gene expression in the brain. *Proc. Natl. Acad. Sci. U S A* 97, 12880–12884. doi: 10.1073/pnas.97.23.12880
- Rungratsameetaaweemana, N., and Squire, L. R. (2018). Preserved capacity for scene construction and shifts in perspective after hippocampal lesions. *Learn. Mem.* 25, 347–351. doi: 10.1101/lm.047340.118
- Sampedro-Piquero, P., Begega, A., Zancada-Menendez, C., Cuesta, M., and Arias, J. L. (2013). Age-dependent effects of environmental enrichment on brain networks and spatial memory in Wistar rats. *Neuroscience* 248, 43–53. doi: 10.1016/j.neuroscience.2013.06.003
- Segovia, G., Yagüe, A. G., García-Verdugo, J. M., and Mora, F. (2006). Environmental enrichment promotes neurogenesis and changes the extracellular concentrations of glutamate and GABA in the hippocampus of aged rats. *Brain Res. Bull.* 70, 8–14. doi: 10.1016/j.brainresbull.2005.11.005
- Speisman, R. B., Kumar, A., Rani, A., Pastoriza, J. M., Severance, J. E., Foster, T. C., et al. (2013). Environmental enrichment restores neurogenesis and rapid acquisition in aged rats. *Neurobiol. Aging* 34, 263–274. doi: 10.1016/j.neurobiolaging.2012.05.023
- Stark, S. M., Yassa, M. A., Lacy, J. W., and Stark, C. E. (2013). A task to assess behavioral pattern separation (BPS) in humans: data from healthy aging and mild cognitive impairment. *Neuropsychologia* 51, 2442–2449. doi: 10.1016/j.neuropsychologia.2012.12.014
- Summerfield, J. J., Hassabis, D., and Maguire, E. A. (2010). Differential engagement of brain regions within a ‘core’ network during scene construction. *Neuropsychologia* 48, 1501–1509. doi: 10.1016/j.neuropsychologia.2010.01.022
- Tashiro, A., Makino, H., and Gage, F. H. (2007). Experience-specific functional modification of the dentate gyrus through adult neurogenesis: a critical period during an immature stage. *J. Neurosci.* 27, 3252–3259. doi: 10.1523/JNEUROSCI.4941-06.2007
- Urgolites, Z. J., Levy, D. A., Hopkins, R. O., and Squire, L. R. (2018). Spared perception of object geometry and object components after hippocampal damage. *Learn. Mem.* 25, 330–334. doi: 10.1101/lm.047464.118
- van Praag, H., Christie, B. R., Sejnowski, T. J., and Gage, F. H. (1999). Running enhances neurogenesis, learning, and long-term potentiation in mice. *Proc. Natl. Acad. Sci. U S A* 96, 13427–13431. doi: 10.1073/pnas.96.23.13427
- van Praag, H., Schinder, A. F., Christie, B. R., Toni, N., Palmer, T. D., and Gage, F. H. (2002). Functional neurogenesis in the adult hippocampus. *Nature* 415, 1030–1034. doi: 10.1038/4151030a
- Vazdarjanova, A., and Guzowski, J. F. (2004). Differences in hippocampal neuronal population responses to modifications of an environmental context: evidence for distinct, yet complementary, functions of CA3 and CA1 ensembles. *J. Neurosci.* 24, 6489–6496. doi: 10.1523/JNEUROSCI.0350-04.2004
- Vivar, C., Potter, M. C., and van Praag, H. (2013). All about running: synaptic plasticity, growth factors and adult hippocampal neurogenesis. *Curr. Top. Behav. Neurosci.* 15, 189–210. doi: 10.1007/7854_2012_220
- West, G. L., Konishi, K., Diarra, M., Benady-Chorney, J., Drisdelle, B. L., Dahmani, L., et al. (2018). Impact of video games on plasticity of the hippocampus. *Mol. Psychiatry* 23, 1566–1574. doi: 10.1038/mp.2017.155
- West, G. L., Zendel, B. R., Konishi, K., Benady-Chorney, J., Bohbot, V. D., Peretz, I., et al. (2017). Playing Super Mario 64 increases hippocampal grey matter in older adults. *PLoS One* 12:e0187779. doi: 10.1371/journal.pone.0187779
- Woollett, K., and Maguire, E. A. (2011). Acquiring ‘the Knowledge’ of London’s layout drives structural brain changes. *Curr. Biol.* 21, 2109–2114. doi: 10.1016/j.cub.2011.11.018
- Woollett, K., Spiers, H. J., and Maguire, E. A. (2009). Talent in the taxi: a model system for exploring expertise. *Philos. Trans. R. Soc. Lond. B Biol. Sci.* 364, 1407–1416. doi: 10.1098/rstb.2008.0288
- Wu, M. V., Luna, V. M., and Hen, R. (2015). Running rescues a fear-based contextual discrimination deficit in aged mice. *Front. Syst. Neurosci.* 9:114. doi: 10.3389/fnsys.2015.00114
- Yassa, M. A., Lacy, J. W., Stark, S. M., Albert, M. S., Gallagher, M., and Stark, C. E. (2011a). Pattern separation deficits associated with increased hippocampal CA3 and dentate gyrus activity in nondemented older adults. *Hippocampus* 21, 968–979. doi: 10.1002/hipo.20808
- Yassa, M. A., Mattfeld, A. T., Stark, S. M., and Stark, C. E. L. (2011b). Age-related memory deficits linked to circuit-specific disruptions in the hippocampus. *Proc. Natl. Acad. Sci. U S A* 108, 8873–8878. doi: 10.1073/pnas.1101567108
- Yassa, M. A., Muftuler, L. T., and Stark, C. E. L. (2010a). Ultrahigh-resolution microstructural diffusion tensor imaging reveals perforant path degradation in aged humans *in vivo*. *Proc. Natl. Acad. Sci. U S A* 107, 12687–12691. doi: 10.1073/pnas.1002113107
- Yassa, M. A., Stark, S. M., Bakker, A., Albert, M. S., Gallagher, M., and Stark, C. E. (2010b). High-resolution structural and functional MRI of hippocampal CA3 and dentate gyrus in patients with amnesic Mild Cognitive Impairment. *Neuroimage* 51, 1242–1252. doi: 10.1016/j.neuroimage.2010.03.040
- Yassa, M. A., and Stark, C. E. (2011). Pattern separation in the hippocampus. *Trends Neurosci.* 34, 515–525. doi: 10.1016/j.tins.2011.06.006

Conflict of Interest Statement: The authors declare that the research was conducted in the absence of any commercial or financial relationships that could be construed as a potential conflict of interest.

Copyright © 2019 Clemenson, Henningfield and Stark. This is an open-access article distributed under the terms of the Creative Commons Attribution License (CC BY). The use, distribution or reproduction in other forums is permitted, provided the original author(s) and the copyright owner(s) are credited and that the original publication in this journal is cited, in accordance with accepted academic practice. No use, distribution or reproduction is permitted which does not comply with these terms.



OPEN ACCESS

Edited by:

Nadine Ravel,
INSERM U1028 Centre de
Recherche en Neurosciences de
Lyon, France

Reviewed by:

Daniel W. Wesson,
University of Florida, United States
Malgorzata Maria Kossut,
Nencki Institute of Experimental
Biology (PAS), Poland

*Correspondence:

Cécile Viollet
cecile.viollet@inserm.fr

[†]These authors have contributed
equally to this work

*Present address:

Sonia Nocera,
Grupo de Neurobiología del
Desarrollo, Cajal Institute,
Madrid, Spain
Axelle Simon,
INSERM, UMR1266-Institute of
Psychiatry and Neuroscience of
Paris, Paris, France
Jacques Epelbaum,
UMR CNRS/MNHN 7179, Muséum
National d'Histoire Naturelle,
Brunoy, France
Cécile Viollet,
INSERM, UMR1266-Institute of
Psychiatry and Neuroscience of
Paris, Paris, France

Received: 03 October 2018

Accepted: 12 March 2019

Published: 09 April 2019

Citation:

Nocera S, Simon A, Fiquet O,
Chen Y, Gascuel J, Datiche F,
Schneider N, Epelbaum J and
Viollet C (2019) Somatostatin Serves
a Modulatory Role in the Mouse
Olfactory Bulb: Neuroanatomical and
Behavioral Evidence.
Front. Behav. Neurosci. 13:61.
doi: 10.3389/fnbeh.2019.00061

Somatostatin Serves a Modulatory Role in the Mouse Olfactory Bulb: Neuroanatomical and Behavioral Evidence

Sonia Nocera^{1,2†}, Axelle Simon^{1,2†}, Oriane Fiquet^{1,2}, Ying Chen^{1,2}, Jean Gascuel³,
Frédérique Datiche³, Nanette Schneider³, Jacques Epelbaum^{1,2} and Cécile Viollet^{1,2*}

¹INSERM, UMR 894-Center for Psychiatry and Neuroscience (CPN), Paris, France, ²Université Paris Descartes-Sorbonne
Paris Cité, Paris, France, ³CNRS UMR 6265—Centre des Sciences du Goût et de l'Alimentation (CSGA), Dijon, France

Somatostatin (SOM) and somatostatin receptors (SSTR1–4) are present in all olfactory structures, including the olfactory bulb (OB), where SOM modulates physiological gamma rhythms and olfactory discrimination responses. In this work, histological, viral tracing and transgenic approaches were used to characterize SOM cellular targets in the murine OB. We demonstrate that SOM targets all levels of mitral dendritic processes in the OB with somatostatin receptor 2 (SSTR2) detected in the dendrites of previously uncharacterized mitral-like cells. We show that inhibitory interneurons of the glomerular layer (GL) express SSTR4 while SSTR3 is confined to the granule cell layer (GCL). Furthermore, SOM cells in the OB receive synaptic inputs from olfactory cortical afferents. Behavioral studies demonstrate that genetic deletion of SSTR4, SSTR2 or SOM differentially affects olfactory performance. SOM or SSTR4 deletion have no major effect on olfactory behavioral performances while SSTR2 deletion impacts olfactory detection and discrimination behaviors. Altogether, these results describe novel anatomical and behavioral contributions of SOM, SSTR2 and SSTR4 receptors in olfactory processing.

Keywords: somatostatin receptor, mitral cells, interneurons, olfaction, SSTR3, SSTR2, SSTR4, knockout mice

INTRODUCTION

The neuropeptide somatostatin (SOM, encoded by the *sst* gene) is found in most regions of the central nervous system. It is expressed both in local interneurons and long-projecting neurons that connect distant brain regions. SOM is known to exert neuromodulatory actions on cognitive, emotional and sensory behaviors through the activation of specific receptors (SSTR1–4 in the central nervous system, SSTR5 in the periphery; Martel et al., 2012; Liguz-Leczna et al., 2016). SOM receptors are localized in dendritic domains of principal cells or interneurons in most brain regions where they contribute to the fine-tuning of neuronal activity, shaping synaptic activity and plasticity of the central nervous system (Large et al., 2016). In addition to the large set of literature related to the cortical and hippocampal distribution of SOM neuronal networks, several studies have described SOM distribution in human and rodent olfactory processing pathways

Abbreviations: AON, anterior olfactory nucleus; BTC, blocks to criterion; Ent, entorhinal cortex; EPL, external plexiform layer; GL, glomerular layer; GCL, granule cell layer; OB, olfactory bulb; Pir, piriform cortex; Post, posterior; SOM, somatostatin; SSTR, somatostatin receptor.

(Videau et al., 2003; Lepousez et al., 2010a; Brunjes et al., 2011; Martel et al., 2012; De La Rosa-Prieto et al., 2016; Large et al., 2016; Saiz-Sanchez et al., 2016). The recent description of different combinations of SSTR subtypes in each olfactory structure from the bulb to the olfactory cortex (Martel et al., 2015) suggests that the SOM peptide modulates different stages of olfactory processing. Pharmacological and behavioral data support this hypothesis, showing that activation or blockade of somatostatin receptor 2 (SSTR2) transduction in the murine olfactory bulb (OB) respectively increases or decreases olfactory fine discrimination as well as basal gamma oscillations in the OB (Lepousez et al., 2010b).

The OB is the first telencephalic relay in olfactory processing and it shows a typical cytoarchitecture: each concentric bulbar layer contains distinct interneuron cell populations with specific neurochemical and anatomical features that participate in the local synaptic shaping of the olfactory signal driven by the mitral and tufted cells, the principal neurons of the OB (for review, see Nagayama et al., 2014). Apical primary dendrites of the principal cells receive afferent synaptic inputs from olfactory neurons that project from the olfactory epithelium into the peripheral glomerular layer (GL). Their long axonal projections relay the signal to the anterior olfactory nucleus (AON) and to downstream structures of the olfactory cortex, i.e., olfactory tubercle for tufted cells, piriform cortex and entorhinal cortex and limbic regions for mitral cells. In between, major synaptic interactions take place in each OB layer. In the GL, intrinsic inhibitory circuits control both gain and strength of the sensory inputs in a spatial and temporal manner (Wilson et al., 2014; Linster and Cleland, 2016; Chong and Rinberg, 2018). In the external plexiform layer (EPL), dendro-dendritic reciprocal synapses occur between lateral dendrites of the mitral cells and dendrites of granule cell interneurons, the main inhibitory population of the OB, whose somata are located in deepest layer, the granule cell layer (GCL). These reciprocal synaptic interactions induce local field potential oscillations, including gamma oscillations which are involved in fast discrimination between close stimuli in the OB (Frederick et al., 2016) and feed-forward transmission of the signal to downstream associational regions of the olfactory cortex (Kay, 2014). Finally, retrograde afferents from the olfactory cortex and other brain structures also target the OB (Shipley and Ennis, 1996; Lepousez and Lledo, 2013; Kay, 2014; Wilson et al., 2014; Diodato et al., 2016; Case et al., 2017), and modify local synaptic activity (Balu et al., 2007; Boyd et al., 2012; Devore and Linster, 2012; Markopoulos et al., 2012; Soria-Gómez et al., 2014; Brunert et al., 2016; Sanz Diez et al., 2017).

In mouse OB, SOM is predominantly expressed in calretinin-expressing GABAergic interneurons of the inner EPL and in sparse GABAergic deep short-axon cells and fibers in the GCL (Lepousez et al., 2010a). It is hardly detected in the GL (Lepousez et al., 2010a; De La Rosa-Prieto et al., 2016; Burton et al., 2017). Recent anatomical and physiological data revealed that EPL interneurons, including those expressing SOM, interact with mitral cell dendrites via dendro-dendritic reciprocal synapses (Hamilton et al., 2005; Lepousez et al., 2010a; Huang et al., 2013),

similar to granule cells. This anatomically supports the tonic regulation by endogenous SOM of basal gamma oscillations in the OB and olfactory behavior (Lepousez et al., 2010b).

Besides the peptide itself, SOM receptors are strongly expressed in the OB (Videau et al., 2003; Martel et al., 2015). The present study was undertaken to: (i) precisely identify their cellular localization using reliable immunohistochemical tools and transgenic models; (ii) determine the neural afferents targeting OB SOM neurons using viral tracing; and (iii) study how genetically impairing SOM transduction impacts olfactory performance. Our results show that SSTR4 and SSTR3 receptors are expressed in distinct inhibitory interneuronal populations, respectively located in GL and GCL. SSTR2 receptors are clearly expressed in a subpopulation of mitral cell-like neurons. Furthermore, we show that local SOM-expressing neurons receive feedback projections from downstream regulatory regions of the olfactory cortex. This indicates that endogenous and centrifugal SOM can specifically target all the key dendritic regulation sites of the olfactory mitral cell-mediated transmission in the OB. Genetic ablation of SOM, SSTR2 or SSTR4 show limited effects on olfactory behavioral performances, with no major impact on olfactory learning or memory. Olfactory detection and discrimination performances are impaired in SSTR2 KO mice as compared to WT but SSTR4 KO and SOM KO do not show such changes. These differential results suggest a multimodal somatostatinergic control of olfactory processing, pointing to different cellular and behavioral contributions of each SSTR subtype.

MATERIALS AND METHODS

Animals

All procedures were approved by a local ethics committee (French Ministry of Health and Research Authorization N° 00618.04 and APAFIS#5670-2016120716328268) in accordance with the European Communities Council Directive (86/609/EU) and the European Union guidelines. Mice were bred and housed in the CPN animal facility on a 12 h light/dark cycle with *ad libitum* access to food and water except during behavioral experiments. Control (WT) and transgenic littermates from constitutive knock-out (KO) transgenic lines, *sst* KO (referred as SOM KO in the text; Low et al., 2001), *sstr2* KO (SSTR2 KO, Viollet et al., 2000) and *sstr4* KO (SSTR4 KO, Helyes et al., 2009) as well as SSTR2 KO-LacZ KI (Allen et al., 2003) and Kv3.1-EYFP animals (Metzger et al., 2002) were used for immunohistochemical studies. Five to 8-week-old SOM-IRES-Cre heterozygous males (Taniguchi et al., 2011) were used for viral studies. Three independent cohorts of eight age-matched transgenic and control (WT) male mice (3–5 months) from SOM, SSTR2 or SSTR4 KO transgenic lines were used for the behavioral sequences. Animals which did not perform all operant tasks were excluded from statistical analysis (1 WT and 1 SOM KO mice, 1 SSTR2 KO mouse, 1 WT and 1 SSTR4 KO mice). Experimenters were blind to the genotype of the animals during both experiments and analysis.

TABLE 1 | Primary antibodies used in this study.

Primary antibody	Species (mono, polyclonal)	Dilution use	Source/Reference
Arl13b	Mouse (monoclonal)	1:500	#73-287, Antibodies Inc
Beta-Galactosidase (β -Gal)	Chicken (polyclonal)	1:2,500	# ab9361, Abcam
Calretinin (CR)	Goat (polyclonal)	1:4,000	#AB1550, Chemicon
GAD67	Mouse (monoclonal)	1:400	#MAB5406, Millipore
Green fluorescent protein (GFP)	Chicken (polyclonal)	1:1,000	#Ab 13970, Abcam
Neuronal nitric oxide synthase (nNOS)	Rabbit (polyclonal)	1:800	#61-7000, Invitrogen
Olfactory marker protein (OMP)	Goat (polyclonal)	1:20,000	# 544-10001, Wako
Parvalbumin (PV)	Mouse (monoclonal)	1:500	#P3088, Sigma
Reelin	Mouse (monoclonal)	1:500	#MAB5364, Millipore
Somatostatin	Goat (polyclonal)	1:500	#D20, sc-7819 Santa Cruz
Somatostatin receptor 2 (SSTR2)	Rabbit (monoclonal)	1:2,000	#ab134152, Abcam
Somatostatin receptor 3 (SSTR3)	Rabbit (polyclonal)	1:2,000	#PA3-207, Thermo Scientific

Immunohistochemistry

Mouse Samples

Mice (at least three per group) were deeply anesthetized with an intraperitoneal injection of ketamine/xylazine mixture (100 mg/kg/7 mg/kg in saline) and then transcardially perfused with 4% paraformaldehyde (PFA) in 0.1 M phosphate buffer pH 7.4. Brains were quickly removed, post-fixed for 2 h in 4% PFA, cryoprotected (30% sucrose in PBS), fast-frozen at -40°C in isopentane and sectioned in 40 μm coronal sections using a microtome (Leica). After several washing steps in Tris buffer saline (TBS), sections were incubated for 30 min at room temperature in the blocking solution (10% normal donkey serum (NDS), 0.3% Triton X100 in TBS) then primary antibodies were incubated for 24 h (4 days for Arl13b staining; see **Table 1**) in 2% NDS, 0.3% Triton X100 in TBS. After three washes in TBS, sections were incubated for 2 h with appropriate Alexa488-, Cy3- and Cy5-conjugated donkey secondary antibodies (Jackson ImmunoResearch, respective dilutions: 1/500, 1/1,000, 1/200) in the same buffer. After three TBS rinses, sections were mounted beneath coverslips with Fluoromount G mounting medium onto glass slides (Southern Biolabs). For Arl13b, reelin or GAD67, sections were incubated 1 h in "Mouse On Mouse" solution (Vector Labs) before the blocking step. For GAD67 staining, sections were incubated during the whole procedure in Triton-free buffer including 0.1% sodium azide and with the primary antibodies for 7 days.

Sections were analyzed under a confocal laser scanning microscope (TCS SP5, Leica) under a 40 \times oil-immersion objective. Images were sequentially acquired for A488 and Cy5 or Cy3 fluorescent signals using single excitation beams (Ar laser at 488 nm wavelength, laser diode at 561 nm and HeNe laser at 633 nm). Displayed images correspond to 1.64–24.8 μm -thick stacks along the z-axis (0.4 μm step). Enlarged illustrations (**Figures 2E,F, 3**) correspond to 0.4 and 0.51 μm -thick stacks, respectively.

For cell density measurements, fluorescent immunostaining for SOM and SSTR2 performed on WT serial 40 μm coronal OB sections was imaged at constant light settings using a Lamina slide scanner (Perkin Elmer, $\times 20$ objective) equipped with GFP and Cy3 filter sets. Each two-channel image was extracted using

Pannoramic Viewer software and exported into Image J using Bio-Format importer plug-in. Six anterior anatomic levels (every 250 μm from Bregma 4.25) were analyzed with Image J with a dedicated macro transforming SSTR2 and SOM staining into masks in order to count the labeled cells or area in each region of interest (GL, EPL and GCL). Data were averaged from three to four mice per level.

Viral Tracing

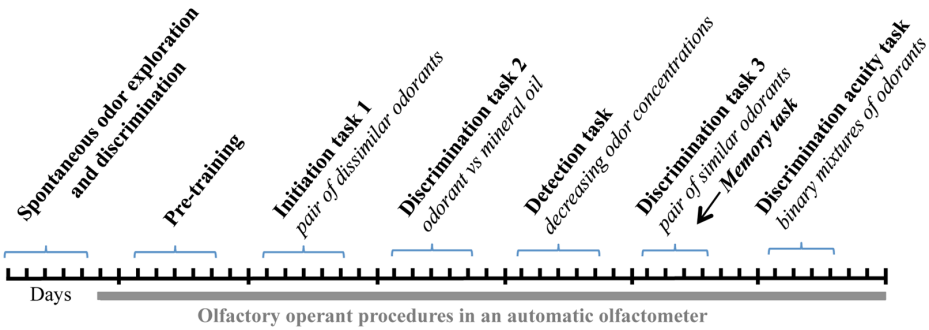
Polytrans-synaptic tracing was performed using PRVBa2001 virus, an attenuated Cre-dependent pseudorabies virus. This virus encodes a green fluorescent protein marker and replicates only in neurons that express cre recombinase and their presynaptic neurons, allowing the identification of neural inputs in a retrograde manner (DeFalco et al., 2001). PRVBa2001 solution titer was 3.10^9 PFU/ml of culture media. Trace of fluorospheres (1 μm diameter, blue 365/415; 1:100 solution in 0.9% NaCl, Molecular Probes) was co-injected with PRVBa2001 (1/10 ratio) to localize the injection site.

Mice were injected in a stereotaxic frame using validated procedures under isoflurane gaseous anesthesia. A hole was drilled in the skull above the medial OB (Bregma 4 A-P axis and 0.8 M-L) to insert a 34-gauge blunt needle (World Precision Instruments) 1.7 mm deep. One-hundred nanoliter of the injection solution (PRVBa2001 virus + fluorospheres) was injected at 20 nl/min and left in place for 15 min to ensure proper injection and diffusion. Injection sites were checked *a posteriori* using detection of fluorospheres.

Mice were sacrificed 3–5 days post-injection in order to trace PRVBa2001 virus progression. Brains were then fixed as previously described and 2D reconstructions of serial anteroposterior coronal sections (50 μm thick, every 300 μm) were prepared and analyzed using Zeiss Axiovision software on a Zeiss Imager M2 epifluorescence microscope (10 \times magnification). The neuroanatomical location of the positive labeled cells was determined using *the mouse brain in stereotaxic coordinates atlas* (Paxinos and Franklin, 2008).

Behavior

Three separate sets of experiments were undertaken in order to determine the contribution of constitutively SOM, SSTR2 and SSTR4 knockout on olfaction. The details of the behavioral

TABLE 2 | Details of the sequence of behavioral tests.


	SOM KO	SSTR2 KO	SSTR4 KO
Habituation/dishabituation task	H: 1% pentanal, C+1: 1% hexanal, C+3: 1% octanal		
Operant procedures			
Initiation task	S+: 1% anisole S–: 1% cineole		S+: 1% hexanal S–: 1% heptanal
Discrimination task 2	S+: 1% isoamylacetate S–: mineral oil		S+: 1% (+) carvone S–: mineral oil
Detection task	S+: isoamylacetate dilutions S–: mineral oil		S+: (+) carvone dilutions S–: mineral Oil
Discrimination task 3		S+: 1% (+) carvone S–: 1% (–) carvone	
Discrimination acuity task		S+: (+) carvone/(–) carvone binary mixtures S–: (+) carvone/(–) carvone inverse binary mixtures	
Memory task (21d)	S+: 1% anisole S–: 1% cineole		S+: 1% hexanal S–: 1% heptanal

procedures are described in **Table 2** (top). Each test was performed with a cohort of transgenic and WT littermate animals in a well-ventilated room by an experimenter blind to genotype. To reduce the duration of the water-restriction period, there was no interval between the tests.

Spontaneous Odor Exploration and Discrimination in a Habituation-Dishabituation Protocol

Mice were tested in custom-built open plexiglass boxes (25 × 40 × 15 cm) made so that odorant stimuli (10 µl centered on a 5 cm diameter filter paper, Whatman) could be inserted at various places beneath a grid floor. Three different odorants (Sigma-Aldrich, 1% vol/vol in mineral oil) were used: the habituation odor pentanal (H) and two test odors of variable similarity, hexanal with one additional carbon chain (C+1) and octanal with three additional carbon chains (C+3). One week before the experiment, mice were housed individually and handled daily. Two days prior to the experiment, animals were habituated to the testing box for 20 min. Except for SOM cohort, mice were water-deprived the night before the test in order to increase motivation. The day of the experiment, mice were tested successively with freshly prepared odors: mice explored the box for 5 min before the habituation odor (H) was presented four consecutive times (H₁ to H₄ trials, 2 min each). Mice were then exposed for 2 min successively to C+1 test odor, again to the habituation odor (H₅) and finally to C+3 test odor. Each odor presentation was followed by a 5 min inter-trial interval and the box was cleaned with water and alcohol between each session. Odor exploration, i.e., the time spent investigating the filter area,

was recorded offline by an experimenter blind to the genotype of the mice. H₁ to H₄ data were analyzed to test the formation of a memory and habituation. Comparison between H and test odor trials (H₄ vs. C₊₁, H₅ vs. C₊₃) tested the ability to discriminate between the habituation odor and the test odor.

Olfactory Operant Conditioning

Mice were trained using custom-built computer-controlled four-channel olfactometers as previously described (Martel et al., 2015). Odorants (Sigma-Aldrich) were prepared daily and diluted vol/vol with odorless mineral oil (Sigma-Aldrich). Odors were generated by bubbling charcoal-filtered air in 10 ml of odorant in a 40 ml glass tube. The odorant vapor was mixed with clean air before its introduction into the sampling port (ratio 1:20).

Mice were first trained to the go/no-go procedure during five pre-training sessions to learn the operant procedure (for details, see Martel et al., 2015). Then mice were trained to respond to the presence of an odor (positive stimulus, S+) by licking the water port and to refrain from responding to the presence of another odor (negative stimulus, S–; **Figure 10A**). In each trial, a single stimulus (positive or negative) was presented. If the response criterion was met in S+ trials, a droplet of water (3 µl) was given as a reward and the trial was scored as a hit. Failing to lick in S– trial was scored as a correct rejection. S+ and S– trials were presented in a pseudo-random order, each block contained 10 S+ and 10 S– trials, never presented more than three times consecutively. The percentage of correct responses was determined for each block of 20 trials ((hits +

correct rejections)/20 × 100) and scored for the 10 consecutive blocks of each session. Scores ≥ 85% implied that mice had correctly learned to assign the reward value of the S+ and the non-reward value of the S−. The number of blocks necessary to reach the 85% learning criterion (Blocks to criterion or BTC) was used to compare individual learning per group. To calculate BTCs, mice which did not reach the criterion were arbitrarily assigned one extra block. The three last blocks of the learning task were averaged to score the final performance level reached for each group.

Mice were submitted to an initiation task where they had to learn the rule and discriminate between dissimilar odorants (Table 2). This initial task is difficult for the mice and required between 30 and 35 blocks with anisole/cineole odor pair and 50 blocks with hexanal/heptanal odor pair to increase performances. The longer training with hexanal/heptanal is probably due to the close similarity of those latter chemicals, which increased the complexity of the task for the animals. This odor pair of the initiation task was later changed to anisole/cineole pair for SOM and SSTR2 experiments. One SSTR2 WT mouse was trained for 30 blocks instead of 35 and will not appear on Figure 10B, even if it reached the 85% criterion ($n = 6$ for this graph only).

Mice were then trained to discriminate between a novel odorant and odorless mineral oil (Discrimination Task 2). Once the 85% criterion was reached, they were tested for detection thresholds using decreasing concentrations of the odorant diluted in mineral oil as S+ (one concentration per day for 10 blocks), mineral oil serving as S−. The concentrations of odorant used in these tasks were 1%, 0.1%, 0.01%, 0.001% and 0.0001% (vol/vol). Two odorants were used: (+) carvone for SSTR4 cohort and isoamylacetate for SOM and SSTR2 cohorts.

Next, animals were trained to discriminate between mixtures with increasing complexity to evaluate discrimination acuity. Mice were first trained to distinguish between two similar odorants [(+) and (−) carvone enantiomers], (+) carvone being used as S+. Then, animals had to discriminate between progressively closer binary mixtures of enantiomers where (+) carvone proportion in S+ was progressively decreased from 80% to 52.5%. Thus, the concentration of (+) carvone/(−) carvone enantiomers in the mixture was sequentially equalized in separate sessions (one session per day, 10 blocks per session) to 80/20, 60/40 and 52.5/47.5 for S+ vs. 20/80, 40/60 and 47.5/52.5 for S−, respectively.

Twenty-one days after the initiation task, in addition to Discrimination 3, mice were tested for olfactory memory of the initiation discrimination task. The 20 trials of each block were composed of 16 trials for the enantiomer discrimination and four trials for the olfactory memory in which no reward was given (two hexanal and two heptanal for SSTR4 cohort, two anisole and two cineole for SOM and SSTR2 cohorts). Memory performance was calculated from the averaged performances in these four trials.

Data were expressed as mean percentage of correct response for each training block. Five-block data were averaged to analyze learning performances. The performances of the last three blocks

of a training session were averaged and this mean value was used as a discrimination score for each group.

Statistical Analysis

All results are expressed as mean ± standard error of the mean (SEM). The degree of statistical significance was calculated using STATVIEW software (SAS Institute, Cary, NC, USA). For SSTR2 distribution, two-way repeated-measures analysis of variance (r-m ANOVA) with cellular layer as an in-between factor and anteroposterior levels as a within-subjects factor with Bonferroni correction was used.

Statistical analyses for behavioral data can be found in Supplementary data. Raw data of the habituation-dishabituation protocol were analyzed, respectively between H1 and H4 trials, H4 and C₊₁ trials and H5 and C₊₃ trials using two-way r-m ANOVA with the group as in-between subjects factor and trials as within-subjects factor. For multiple comparisons, a Bonferroni *post hoc* test was performed.

For olfactory operant behavioral protocols, BTC, memory and final performance data (mean of the last three blocks) were analyzed using one-way ANOVA with the group as a between-subjects factor. Learning or session performances were analyzed using two-way r-m ANOVA with the group as between-subjects factor and trials, blocks as within-subjects factors. The effect of concentration (or complexity) on performances was analyzed using three-way r-m ANOVA using S+ concentration (or mixture) as an additional within-subjects factor. For multiple comparisons, a Bonferroni *post hoc* test was performed.

RESULTS

Cellular Distribution of SOM Systems in the Main Olfactory Bulb

Since molecular and binding studies had shown the abundance of SSTR1-SSTR4 subtypes in mouse OB, we validated and used a combination of immunological tools (Table 1) and transgenic mice models to study the cellular localizations of SOM peptide, SSTR2, SSTR3 and SSTR4 receptors (Figure 1). SSTR1 distribution was not attempted because poor specificity was found for the available SSTR1 antibodies using SSTR1 knockout mice (Kreienkamp et al., 1999), see also <https://www.abcam.com/Somatostatin-Receptor-1-antibody-ab100881/reviews/39250>). As previously reported in Lepousez et al. (2010a), SOM is mainly expressed in interneurons of the inner part of the EPL, as well as running fibers and sparse deep short axon cells in the GCL (Figures 1A–C). Interestingly, SSTR2, SSTR3 or Beta-galactosidase (β-Gal)-mediated SSTR4 patterns delineated distinct bulbar layers, from the GCL to the peripheral GL (see Figures 1A–C and Figures 5B,E,H).

Monoclonal anti-SSTR2 antibody mainly labeled small neurons located in the mitral cell layer (MCL) with typical dendrite-like projections crossing the EPL and projecting into the GL (magenta, Figures 1A, 2). Most cells showed small round cell bodies (mean diameter $9.25 \pm 0.19 \mu\text{m}$, $n = 232$ cells, $N = 2$) but colocalization was not found with SOM (Figures 1A, 5C) or

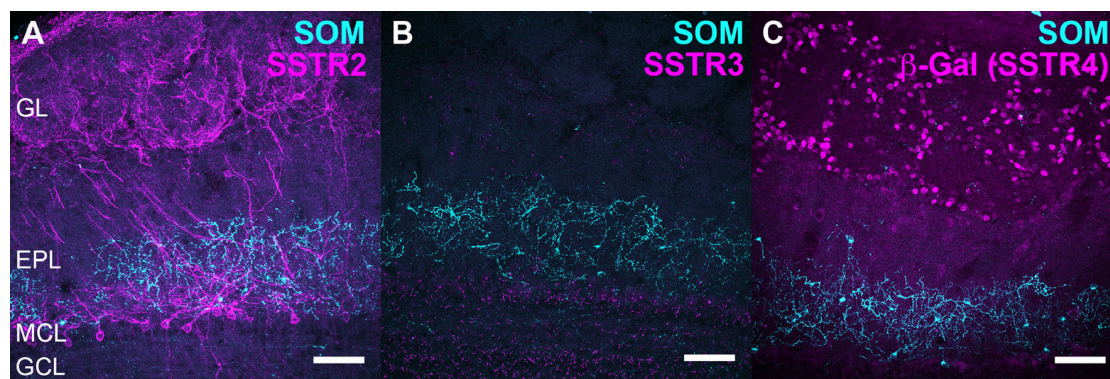


FIGURE 1 | Relative distribution of somatostatin (SOM) and somatostatin receptor 2 (SSTR2), SSTR3 and SSTR4 receptors in the olfactory bulb (OB). **(A–C)** Double labeling of SOM (cyan) with SSTR2 **(A)**, SSTR3 **(B)** or SSTR4 **(C)**, evidenced by nuclear β -Galactosidase immunoreactivity, (SSTR2 KO and SSTR2 magenta) in the mouse OB. Brain sections from wild-type **(A,B)** or SSTR4 KO-lacZ KI heterozygous **(C)** mice were used. **(A–C)** 45, 52, 35 confocal planes (0.41 μ m) stacked for each illustration. EPL, external plexiform layer; GCL, granule cell layer; GL, glomerular layer; MCL, mitral cell layer; SSTR, somatostatin receptor. Scale bars: 50 μ m.

with interneuron markers parvalbumin (**Figure 2A**) or calretinin (**Figures 2B, 3A–C**). SSTR2-positive cells were intermingled with the mitral cells, recognizable by their large pear-shaped somata (mean diameter $16.97 \pm 1.30 \mu\text{m}$) and thick primary dendrites (**Figures 2D,G**). SSTR2-positive cells never co-expressed the mitral cell markers reelin, Tbx21 or Kv3.1-EYFP markers (**Figures 2D,G**, enlarged in **Figures 2E, 3D–F**). Reelin also labels tufted cells in the outer EPL, but no SSTR2-labeled cells were found at this level (**Figures 2D,G**). We cannot exclude a minimal expression of reelin in some MCL SSTR2 cells since a faint signal was occasionally detected (**Figures 2E, 3E,F**). At any rate, SSTR2 labeling did not colocalize with GAD67 fibers and cell bodies (**Figures 2I, 3G–I**), suggesting that OB SSTR2 neurons are not GABAergic. SSTR2 projections delineated glomeruli, some of them being strongly labeled, and overlapped with OMP labeling without colocalization (**Figure 2C**, enlarged in **Figure 2F**). SSTR2 density significantly decreased along the anteroposterior axis (sampled every 250 μm caudally until Bregma 4.25; percent SSTR2 stained area: GL $F_{(5,17)} = 3.070$, $P = 0.037$, EPL $F_{(5,17)} = 3.702$, $P = 0.019$, GCL $F_{(5,16)} = 0.204$, $P = 0.96$) showing enrichment in SSTR2 glomeruli in the rostral part of the bulb while SOM density did not significantly change (percent SOM stained area: GL $F_{(5,16)} = 0.303$, EPL $F_{(5,16)} = 0.989$, GCL $F_{(5,16)} = 0.564$, $P_s > 0.4$; **Figure 4**). In the inner layers IPL (internal plexiform layer, just below the MCL) and GCL, a dense and fine network of SSTR2 fibers was observed (**Figures 1A, 2A–D**). Occasionally some SSTR2-positive cells in the IPL had lateral dendritic projections, and strongly labeled superficial short-axon-like cells were observed in the GCL. A similar pattern (**Figure 5A**) was observed after β -Gal labeling in homozygous SSTR2 KO-lacZ KI mice (**Figure 5I**), and SSTR2 labeling totally disappeared in SSTR2 KO and SSTR2 KO-LacZ KI homozygous animals (**Figures 5D,G**).

SSTR3 antibody labeled typical primary cilia patterns in the OB, as reported in many brain regions (O'Connor et al., 2013), SSTR3 signals were sparse in the GL and highly concentrated in the IPL and GCL mirroring the dense distribution of cells (mostly granule cells) in these layers (**Figures 1B, 6A**). In the

GCL, all SSTR3-positive cilia were also labeled with the ciliary marker Arl13b antibody (**Figure 6A**, zoom in **Figure 6B**). As a comparison, primary cilia positive for the ciliary marker adenylyl cyclase III was more abundant in the GL and EPL layers (**Figure 6C**).

Since no commercially available SSTR4 antibody showed reliable specificity, β -Gal expression was used to localize SSTR4-expressing cells in heterozygous or homozygous SSTR4 KO-LacZ KI mice (Helyes et al., 2009). β -Gal nuclear expression was predominantly found in cells surrounding the glomeruli in the GL and sparsely disseminated in the GCL (**Figures 1C, 6D**). Among the main known periglomerular cell populations (Nagayama et al., 2014), β -Gal antibody specifically labeled the nuclei of approximately a third of the calretinin-positive population (**Figure 3E**, $32.5\% \pm 1.7$, $n = N = 48$ sections for four animals) and did not colocalize with TH, calbindin nor parvalbumin (not shown). Among calretinin-positive cells, β -Gal nuclear staining was associated with nNOS-expressing neurons (**Figures 6F, 3J–L**). Both double staining of β -Gal with CR or nNOS antibody showed predominant intraglomerular projections (**Figures 6E,F**).

Main Afferents to Bulbar Somatostatinergic Populations

Since retrograde afferents are known to modulate bulbar synaptic activity, we decided to map the neural afferents targeting bulbar somatostatinergic cells. A conditional pseudorabies virus expressing GFP (PRVBa2001, DeFalco et al., 2001) was injected in the OB of SOM-Ires-Cre heterozygous mice, together with fluorescent beads to visualize the injection site. Mice were sacrificed 3–5 days after infection and the pattern of GFP expression was examined in serial sections of the whole brain at 3 days post-injection (3 dpi; **Figure 7**). GFP-expressing cells were mainly found in the olfactory cortical area, i.e., the AON, piriform and entorhinal cortex, with rare cells occurring in the dorsal tenia tecta (DTT), and the posteromedial cortical amygdala (PMCo). The number of labeled neurons increased with time in these regions (see **Figures 7, 8**), which send

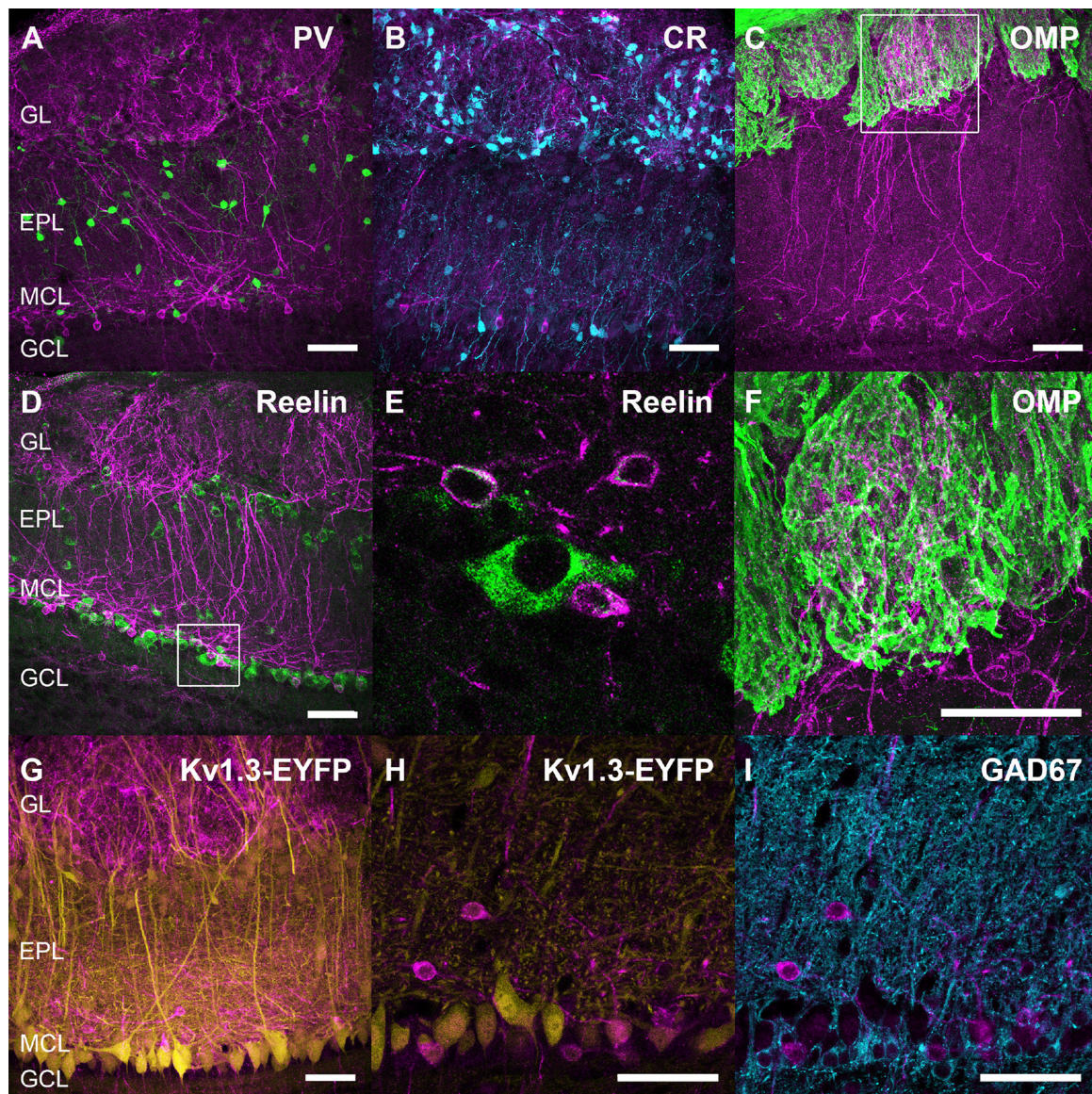


FIGURE 2 | Neurochemical characterization of SSTR2-expressing neurons. Double labeling of SSTR2 (magenta) with parvalbumin (PV, green, **A**), calretinin (CR, cyan, **B**), olfactory marker protein (OMP, green, **C**, zoomed on a single $0.4\ \mu\text{m}$ confocal plane in **F**), reelin (green, **D**, zoomed on two confocal planes in **E**) or GAD67 (cyan, **I**). Brain sections from wild-type (**A–F,I**) and Kv3.1-EYFP (**G,H**) heterozygous mice were used. Respective number of confocal planes stacked for each illustration: (**A–D,G**) 43, 60, 46, 45, 60, (**H,I**) $0.41\ \mu\text{m}$ ($3 \times 0.17\ \mu\text{m}$). EPL, external plexiform layer; GCL, granule cell layer; GL, glomerular layer; MCL, mitral cell layer; SSTR, somatostatin receptor. Scale bars: $50\ \mu\text{m}$.

monosynaptic inputs to the OB (Shipley and Ennis, 1996; Mohedano-Moriano et al., 2012; De La Rosa-Prieto et al., 2015; Diodato et al., 2016). Stronger retrograde infection by the virus appeared after 5 dpi in extra-olfactory regions, the ventral CA1 of the hippocampus, the claustrum, the paraventricular nucleus of the hypothalamus (not shown), the agranular insular cortex, the basolateral amygdala (BLA) and the locus coeruleus (LC; **Figure 8**). Except for the LC (Shipley and Ennis, 1996; Schwarz et al., 2015), these regions have not been identified as direct projection areas to the OB (Shipley and Ennis, 1996; Diodato et al., 2016) and the late detection of GFP suggests

that they are second- or higher-order projection neurons to the OB (**Figure 8**), consistent with results using different tracing methods (Shipley and Ennis, 1996; Mohedano-Moriano et al., 2012; De La Rosa-Prieto et al., 2015; Diodato et al., 2016). These data suggest that higher cortical centers modulate SOM signaling in the OB.

Impact of SOM Transduction Impairment on Olfactory Performances

The olfactory performances of WT and KO mutant littermates were compared using a sequence of behavioral tests (**Table 2**).

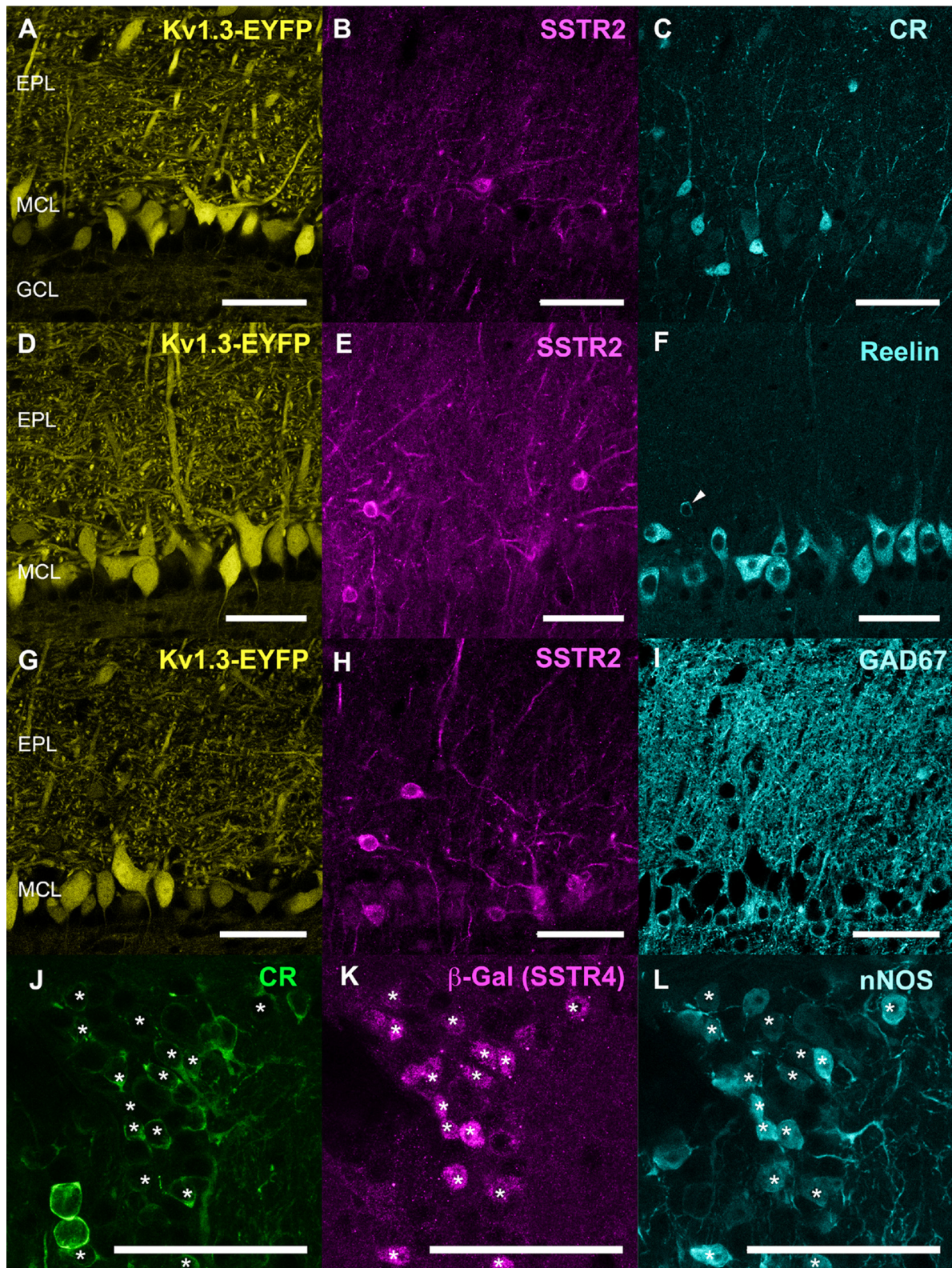


FIGURE 3 | (A–I) Respective distribution of Kv3.1-EYFP, SSTR2 and CR (**A–C**), Kv3.1-EYFP, SSTR2 and reelin (**D–F**), Kv3.1-EYFP, SSTR2 and GAD67 (**G–I**). Three confocal planes (0.4 μm step) were stacked for each illustration. (**J–L**) Colocalization (star) of calretinin (CR, green), β (write with a “beta” like in **Figure 1**)-Galactosidase (magenta) and nNOS (cyan) in the GL of SSTR4 KO-LacZ KI heterozygous mice (**J–L** on two stacked 0.4 μm confocal plane). Scale bars: 50 μm.

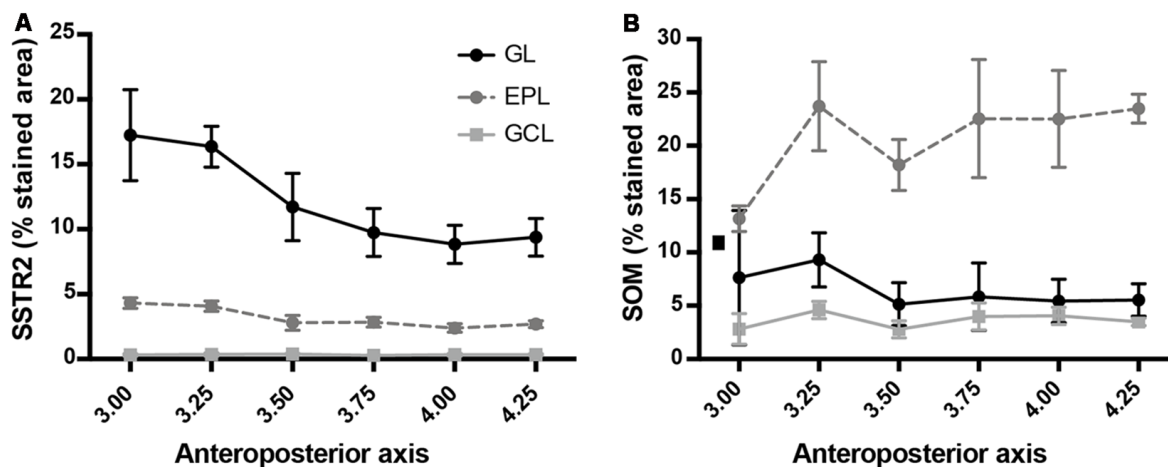


FIGURE 4 | SSTR2 (A) and SOM (B) cell density along the anteroposterior axis of the main OB. Horizontal scale: Bregma levels.

The respective impact of SOM, SSTR2 and SSTR4 removal was studied separately, using dedicated transgenic mice cohorts.

In the habituation/dishabituation protocol, mice were exposed four times to a first odorant stimulus (habituation odor H), then sequentially to test odors of variable similarity with respectively one ($C+1$) or three ($C+3$) additional carbon chains.

In the SOM cohort (**Figure 9A**), odor exploration significantly decreased over time between H1 and H4 trials ($F_{(3,36)} = 16.95$, $P < 0.0001$, r-m ANOVA) suggesting global odor habituation since no significant group effect or trial \times group interaction were found (group: $F_{(1,12)} = 0.67$, $P > 0.05$; trial \times group interaction $F_{(3,36)} = 0.17$, $P > 0.05$). Exploration time increased between H4 and C_{+1} trials ($F_{(1,12)} = 10.29$, $P < 0.01$) and between H5 and C_{+3} trials ($F_{(1,12)} = 68.25$, $P < 0.0001$), indicating that mice discriminate between the habituated odor and the test odors. No significant group effect or trial \times group interaction was found regardless of test odor (H4 vs. C_{+1} : group ($F_{(1,12)} = 0.80$, trial \times group interaction $F_{(1,12)} = 0.12$; H5 vs. C_{+3} : group: $F_{(1,12)} = 3.75$, trial \times group interaction $F_{(1,12)} = 0.20$, all P s > 0.05).

In the SSTR2 cohort (**Figure 9B**) exploration globally decreased between H1 and H4 trial in all mice (Trial: $F_{(3,39)} = 6.19$, $P < 0.01$) similarly in WT and SSTR2 KO groups (Group: $F_{(1,12)} = 0.67$, $P > 0.05$, no group \times trial interaction) suggesting odor habituation. Mice investigated more the habituated odor than the test odors (Trial H4 vs. C_{+1} : $F_{(1,13)} = 6.68$, $P < 0.05$, Trial H5 vs. C_{+3} $F_{(1,13)} = 4.69$, $P < 0.05$) but no significant group effect was found (Group: H4 vs. C_{+1} $F_{(1,13)} = 0.37$, $P = 0.55$, H5 vs. C_{+3} $F_{(1,13)} = 3.04$ $P = 0.10$, P s > 0.05).

In the SSTR4 cohort (**Figure 9C**) odor exploration strongly decreased between H1 and H4 for WT and SSTR2 KO groups (trial: $F_{(3,42)} = 38.66$, $P < 0.0001$), indicating habituation in both groups (Group $F_{(1,14)} = 2.480$, $P = 0.14$). Mice investigated more C_{+1} than H4 (Trial: H4 vs. C_{+1} $F_{(1,14)} = 84.38$, $P < 0.0001$), SSTR4 KO mice exploring significantly longer than WT (group: $F_{(1,14)} = 5.26$, $P < 0.05$). Between H5 and C_{+3} , odor exploration

time increased similarly in both groups (Trial: $F_{(1,14)} = 40.17$, $P < 0.0001$, group: $F_{(1,14)} = 0.06$, $P > 0.05$).

Next, WT and KO littermates were submitted to olfactory operant conditioning to compare their fine olfactory performances (see **Table 2** for details). During this task, the mice have to lick when presented with a rewarding odor S+ and not to lick when the non-rewarding odorant S− is presented (correct responses). For the sake of clarity, results independently obtained for each cohort are reported together, task per task.

Mice were first taught to learn the rule and to discriminate dissimilar odor pairs in an initiation task (**Table 2**). As illustrated in **Figure 10A**, performances progressively increased with training showing that mice learned to correctly discriminate the anisole-cineole odor pair (5-block: SOM cohort, $F_{(6,66)} = 24.08$, $P < 0.0001$ $n = 6-7$; SSTR2 cohort, $F_{(5,65)} = 60.06$, $P < 0.0001$, $n = 7-8$). No group effect was observed (group: SOM cohort $F_{(1,11)} = 1.35$, SSTR2 cohort $F_{(1,13)} = 0.72$, P s > 0.05). SSTR4 mice required 50 blocks to improve their performances with hexanal/heptanal odor pair (5-blocks: $F_{(9,108)} = 17.29$, $P < 0.0001$, $n = 7$), similarly in WT and SSTR4 KO (group: $F_{(1,12)} = 2.16$, $P > 0.05$). The number of blocks necessary to reach the 85% learning criterion (BTC) was not significantly different between WT and KO mice for each cohort (**Figure 10B**), suggesting that learning the rule was not affected in any mutant mice (group: SOM cohort $F_{(1,12)} = 2.19$, SSTR2 cohort $F_{(1,13)} = 0.52$, SSTR4 cohort $F_{(1,12)} = 1.84$, all P s > 0.05 , Bonferroni-corrected ANOVA, $n = 7-8$). In each cohort, performances after learning (mean of the last three blocks) were similar in WT and KO mice (group: SOM cohort: WT = 84.29 ± 2.83 , SOM KO = 85.23 ± 3.09 , $F_{(1,12)} = 0.02$; SSTR2 cohort: WT = 86.45 ± 2.63 , SSTR2 KO = 89.05 ± 2.00 , $F_{(1,13)} = 0.27$; SSTR4 cohort: WT = 75.00 ± 3.93 , KO = 84.52 ± 3.68 , $F_{(1,12)} = 1.04$, all P s > 0.05 , Bonferroni-corrected ANOVA, $n = 7-8$). Twenty-one days after completion of the task, mice were tested for memory of this initial discrimination (**Figure 10C**). In each cohort, no significant difference was found

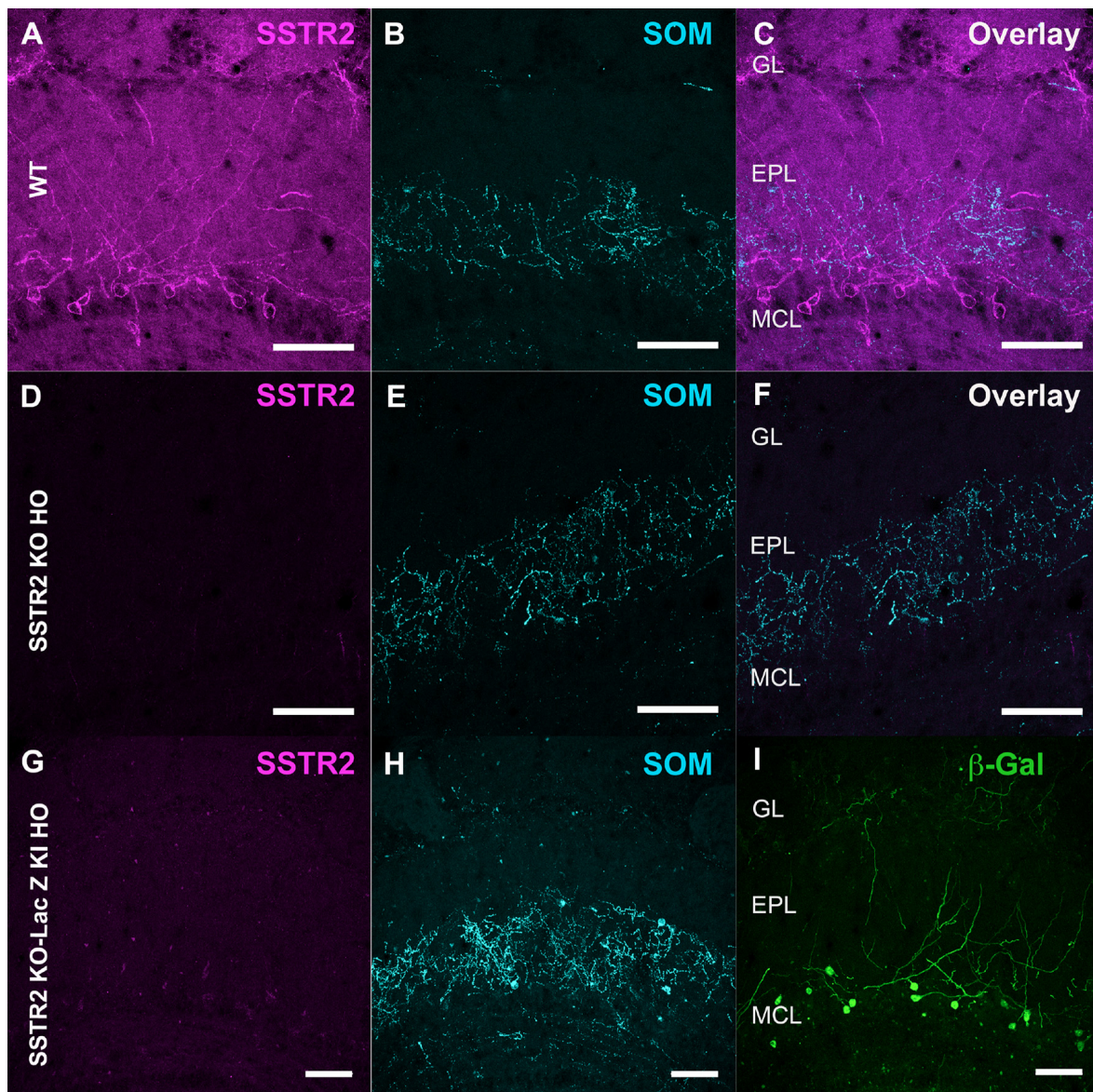


FIGURE 5 | Specificity of SSTR2 labeling. **(A–F)** Immunolabeling of SSTR2 **(A, magenta)** and SOM **(B, cyan)** in WT **(A,B)** and homozygous SSTR2 KO mice **(D,E)**. Panels **(C,F)** show overlay (47 confocal planes). **(G–I)** Immunolabeling of SSTR2 **(G, magenta)**, SOM **(H, cyan)** and β -Galactosidase **(I, green)** in homozygous SSTR2 KO-LacZ KI mice (67 confocal planes). Scale bars: 50 μ m.

between WT and KO mice (group: SOM cohort $F_{(1,12)} = 0.06$; SSTR2 cohort $F_{(1,13)} = 1.14$; SSTR4 cohort $F_{(1,12)} = 0.19$; all P s > 0.05, Bonferroni-corrected ANOVA, $n = 7-8$), suggesting that SOM, SSTR2 or SSTR4 deletion did not affect olfactory memory after a 3-week delay.

Next, olfactory detection was evaluated by measuring how mice discriminate serial dilutions of an odorant. Mice were first trained to discriminate a novel S+ odor from its solvent (mineral oil; **Table 2**) until they reached the 85% learning criterion. WT and KO mice reached similar performances at the end of the task in each cohort (mean of the last three blocks: group: SOM cohort WT = $93.6 \pm 2.2\%$, SOM KO = $81.9 \pm 5.4\%$, $F_{(1,12)} = 0.26$, $n = 7$;

SSTR2 cohort WT = $90.8 \pm 4.9\%$, SSTR2 KO = $85.2 \pm 6.1\%$, $F_{(1,13)} = 2.56$, $n = 8-7$; SSTR4 cohort WT = $92.4 \pm 1.5\%$, SSTR4 KO = $90.9 \pm 2.9\%$, $F_{(1,12)} = 0.19$, $n = 7$; all P s > 0.05, Bonferroni-corrected ANOVA). Then mice were exposed to decreasing series of S+.

In the SOM cohort (**Figure 10D₁**), ANOVA performed on all training sessions showed a significant effect of concentration on performance ($F_{(4,48)} = 9.13$, $P < 0.0001$), suggesting that performances decreased over concentrations in both WT and SOM KO mice with no group effect (group: $F_{(1,12)} = 1.54$, $P > 0.5$) but a significant concentration \times group interaction ($F_{(4,48)} = 4.023$, $P < 0.01$). ANOVA performed

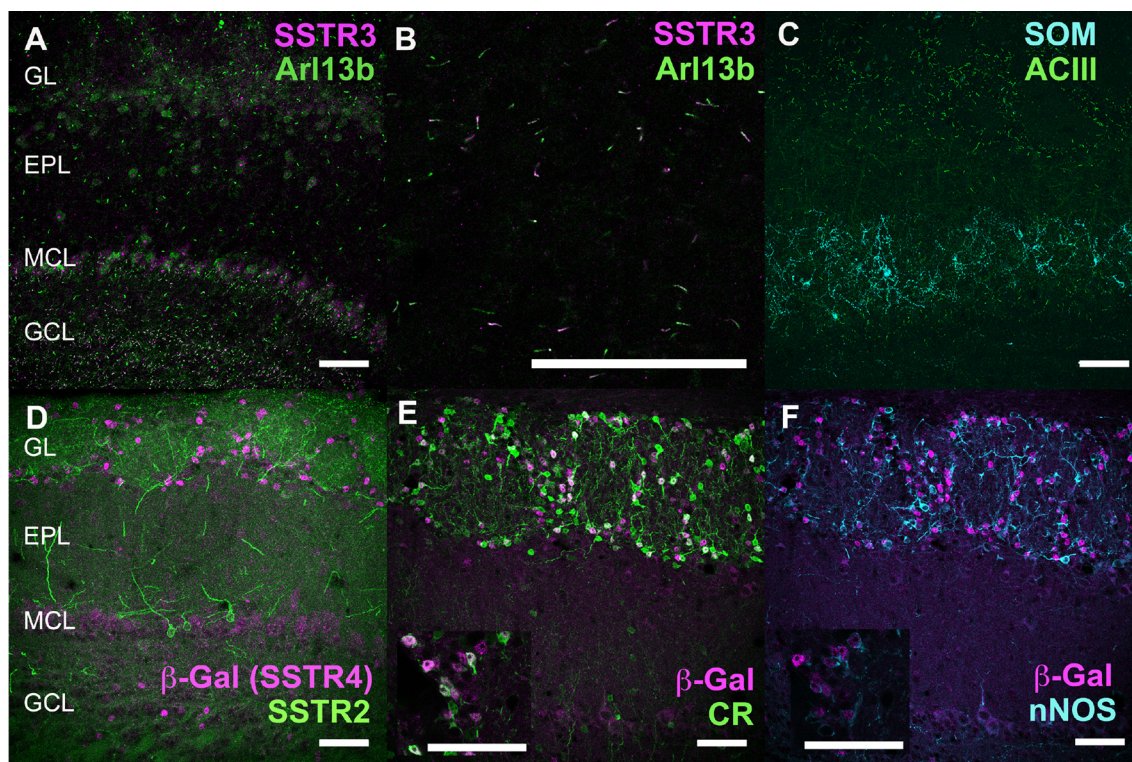


FIGURE 6 | Neurochemical mapping of SSTR3 and SSTR4 in the OB. **(A–C)** Double labeling of SSTR3 (magenta) with Arl13b (green) primary cilia marker in the OB. **(B)** Higher magnification of Arl13b labeling superimposed to all SSTR3-labeled primary cilia in the IPL (arrows). **(C)** Double labeling of SOM (cyan) with Adenylyl cyclase 3 (ACIII, green, **C**). **(D–F)** Double-labeling of β -Galactosidase (magenta, visualizing SSTR4 expression) with SSTR2 (green, **D**), calretinin (CR, green, **E**), or neuronal nitric oxide synthase (nNOS, cyan, **F**) in the OB. Embedding of nuclear β -Gal signals in CR-labeled cells (**E**) and nNOS-labeled cells (**F**) is shown on a single 0.4 μ m confocal plane in the respective inserts. Brain sections from wild-type **(A–C)** or SSTR4 KO-lacZ KI **(D–F)** mice were used. Respective number of planes stacked for each illustration **(A,C–F)**: 20, 40, 31, 15, 15 (0.4 μ m). EPL, external plexiform layer; GCL, granule cell layer; GL, glomerular layer; MCL, mitral cell layer; RMS, rostral migratory stream. Scale bars: 50 μ m.

on each training session did not show any significance between groups ($P_s > 0.05$). Analysis of the last three blocks (**Figure 10E₁**) showed that averaged performance significantly decreased with S+ concentration (concentration: $F_{(4,48)} = 52.64$, $P < 0.0001$), WT performing always better than SOM KO mice (group: $F_{(1,12)} = 4.90$, $P = 0.05$, no significant interaction).

In the SSTR2 cohort (**Figure 10D₂**), ANOVA performed on all training sessions showed a significant effect of concentration on performance ($F_{(4,52)} = 22.39$, $P < 0.0001$) and no significant group effect ($F_{(1,13)} = 4.58$, $P = 0.052$) or significant interaction. Analysis of the mean of the last three blocks (**Figure 10E₂**) showed significant concentration and group effects (concentration: $F_{(4,52)} = 11.33$, $P < 0.0001$, group: $F_{(1,13)} = 4.86$, $P < 0.05$) and a significant concentration \times group interaction ($F_{(4,52)} = 2.90$, $P < 0.05$) indicating that performances of WT and SSTR2 KO mice evolved differentially over S+ dilutions. *Post hoc* analysis showed that SSTR2 KO mice scores were significantly lower than WT at 0.1%, 0.01% and 0.001% (group: $F_{(1,13)} = 9.62$, $P < 0.01$, $F_{(1,13)} = 5.95$, $P < 0.05$, $F_{(1,13)} = 11.41$, $P < 0.01$, respectively) but not at 1% ($F_{(1,13)} = 0.53$, $P > 0.05$) or 0.0001% ($F_{(1,13)} = 0.06$, $P > 0.05$, **Figure 10E₂**).

In the SSTR4 cohort, ANOVA performed on all training sessions showed a significant effect of concentration ($F_{(3,36)} = 58.52$, $P < 0.0001$) without any group effect ($F_{(1,12)} = 0.0003$, $P > 0.05$) or significant interaction, indicating that performances globally decreased for both groups. Mean of the last three blocks (**Figure 10E₃**) decreased with concentration ($F_{(3,36)} = 60.48$, $P < 0.0001$) similarly in WT and SSTR4 KO mice (group: $F_{(1,12)} = 0.01$, $P > 0.05$, group \times concentration interaction $F_{(3,36)} = 0.40$, $P > 0.05$).

In summary, while SOM KO showed lower performances than WT, only SSTR2 KO mice showed significantly impaired detection responses in our experimental conditions.

Finally, olfactory discrimination acuity was evaluated by increasing the complexity of the task using binary mixtures of two enantiomers, (+) carvone and (–) carvone (**Table 2**). Mice first learned to discriminate between pure carvone enantiomers (1% vol/vol). In each cohort, WT and KO mice reached similar performances at completion of the task (averaged last three blocks: group: SOM cohort WT = $86.3 \pm 6.2\%$, SOM KO $84.8 \pm 7.6\%$, $F_{(1,12)} = 0.05$, $n = 7$; SSTR2 cohort WT $94.4 \pm 1.5\%$, SSTR2 KO $86.7 \pm 2.7\%$, $F_{(1,13)} = 2.97$, $n = 8–7$; SSTR4 cohort WT $95.7 \pm 1.3\%$, SSTR4 KO $92.9 \pm 1.8\%$, $F_{(1,12)} = 0.93$,

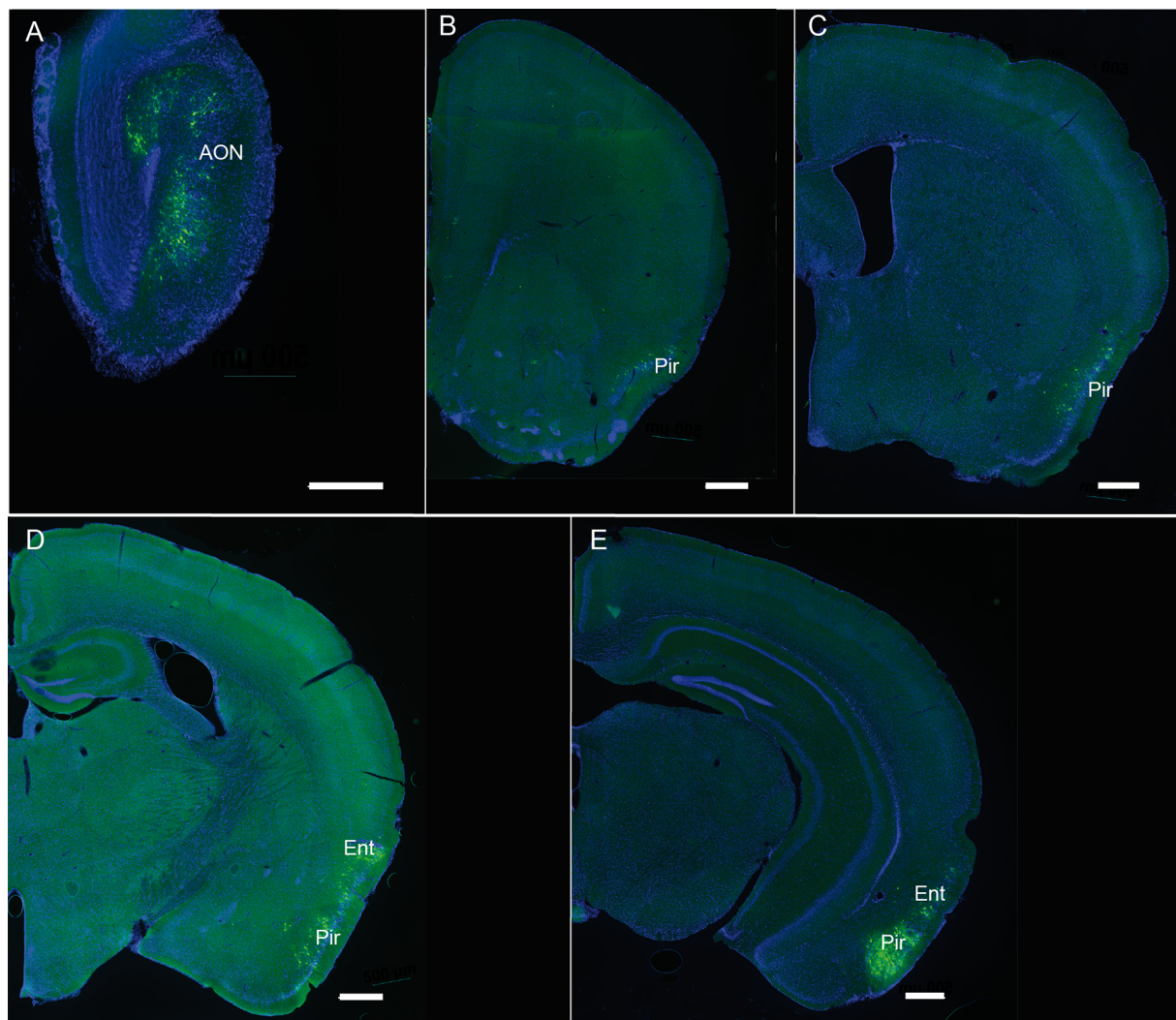


FIGURE 7 | (A–E) Representative pictures showing the retrograde labeling observed ipsilaterally 3 days after injection of PRV Ba2001 Cre-dependent pseudorabies virus in the OB of heterozygous SOM-IRES-Cre mice. The following Bregma levels are illustrated: 3.17 **(A)**, 1.41 **(B)**, –0.11 **(C)**, –2.03 **(D)**, –2.79 **(E)**. AON, anterior olfactory nucleus; Pir, piriform cortex; Ent, entorhinal cortex; Green: GFP; blue: DAPI. Scale bars: 500 μ m.

$n = 7$, all P s > 0.05). All groups reached the criterion, showing that they discriminate the two odorants. Mice were then expected to progressively discriminate between 100/0, 80/20, 60/40, 55/45 and 52.5/47.5 binary mixtures of 1% (+) carvone and 1% (–) carvone, such as the difficulty of the discrimination task increased over sessions.

In the SOM cohort (**Figure 10F₁**). ANOVA on all training sessions showed that WT and KO discrimination performances globally decreased with task complexity (mixture: $F_{(3,36)} = 30.93$, $P < 0.0001$), similarly in both groups (group: $F_{(1,12)} = 0.01$, $P > 0.05$, no significant interaction). Analysis of the averaged last three blocks (**Figure 10G₁**) confirmed that discrimination performances significantly decreased with task difficulty (mixture: $F_{(3,36)} = 29.02$, $P < 0.0001$) similarly in both groups (group: $F_{(1,12)} = 0.001$, $P > 0.05$, no significant interaction).

In the SSTR2 cohort (**Figure 10F₂**), ANOVA on all training sessions showed that global performances decreased with task complexity (mixture: $F_{(3,39)} = 66.52$, $P < 0.0001$) with a significant group effect ($F_{(1,13)} = 5.20$, $P < 0.05$, no significant interaction). Analysis of each session showed that SSTR2 KO performed significantly lower than WT at 80/20 and 60/40 mixtures (group: $F_{(1,13)} = 5.51$, $P < 0.05$ and $F_{(1,13)} = 5.26$, $P < 0.05$). Mean of the last three blocks (**Figure 10G₂**) analysis showed that final performances decreased with task complexity (mixtures: $F_{(3,39)} = 32.27$, $P < 0.0001$) in both groups (group: $F_{(1,13)} = 9.68$, $P < 0.01$, no significant interaction). Analysis of each session showed that SSTR2 KO mice performed significantly lower than WT at 80/20 ($F_{(1,13)} = 7.12$, $P < 0.05$) and 60/40 ($F_{(1,13)} = 5.25$, $P < 0.05$; **Figure 10G₂**) while there was no group difference at 100/0 and 55/45 (P s > 0.05).

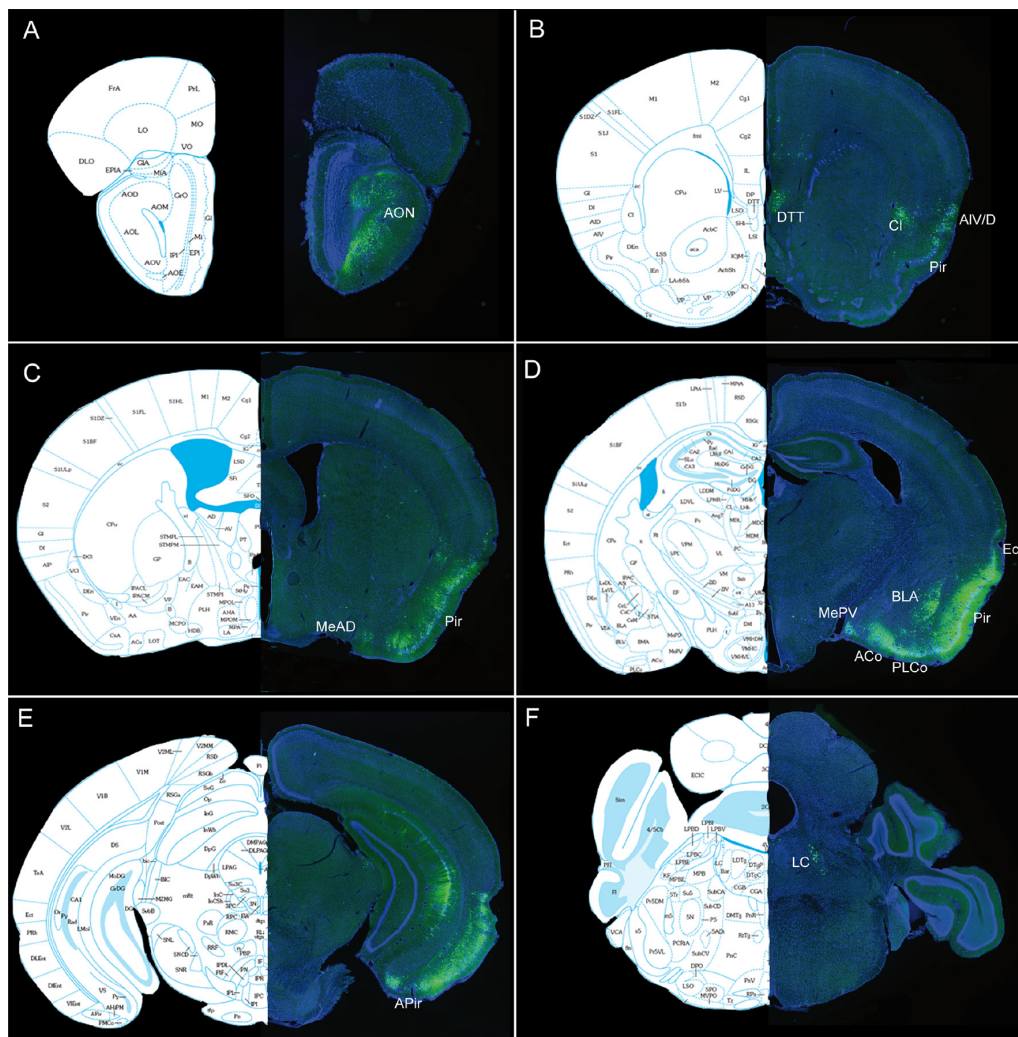


FIGURE 8 | (A–F) Representative pictures showing PRVBa2001-infected neurons expressing GFP ipsilaterally 3 days after injection in the OB of heterozygous SOM-IRES-Cre mice. The following Bregma levels are illustrated: 3.56 **(A)**, 1.94 **(B)**, 0.02 **(C)**, -1.36 **(D)**, -3.51 **(E)**, -5.34 **(F)**. Aco Anterior cortical nucleus of amygdala, AIV/D agranular insular area, AON: anterior olfactory nucleus, BLA basolateral amygdala, APir : anterior piriform cortex, Cl claustrum, DTT dorsal tenia tecta, Ect ectothinal cortex, Ent entorhinal cortex, MeAD medial nucleus of amygdala, MePV medial amygdaloid nucleus, Pir piriform cortex, LC locus coeruleus, PLCo posterolateral cortical amygdaloid area. Atlas pictures are based on Paxinos and Franklin (2008).

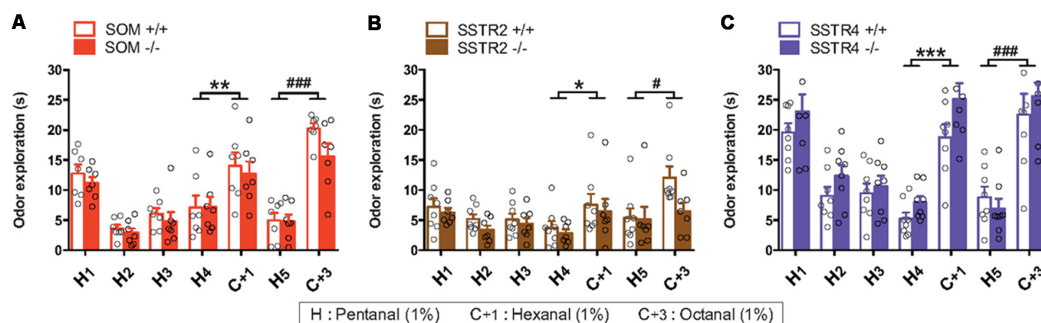


FIGURE 9 | Spontaneous olfactory discrimination for SOM **(A)**, SSTR2 **(B)** and SSTR4 **(C)** transgenic mice cohorts using a habituation/dishabituation task. H, hexanal; C₊₁, heptanal; C₊₃, octanal. WT mice: empty bars, KO mice: plain bars. $n = 7-8$ mice per group. Inter-Trial Interval: 5 min. Open circles indicate individual values, error bars indicate SEM. Odor exploration **(A–C)**, trial effect: H₄ vs. C₊₁ * $P < 0.05$, ** $P < 0.01$, *** $P < 0.001$, H₅ vs. C₊₃ # $P < 0.05$, ### $P < 0.001$, two-way r-m ANOVA.

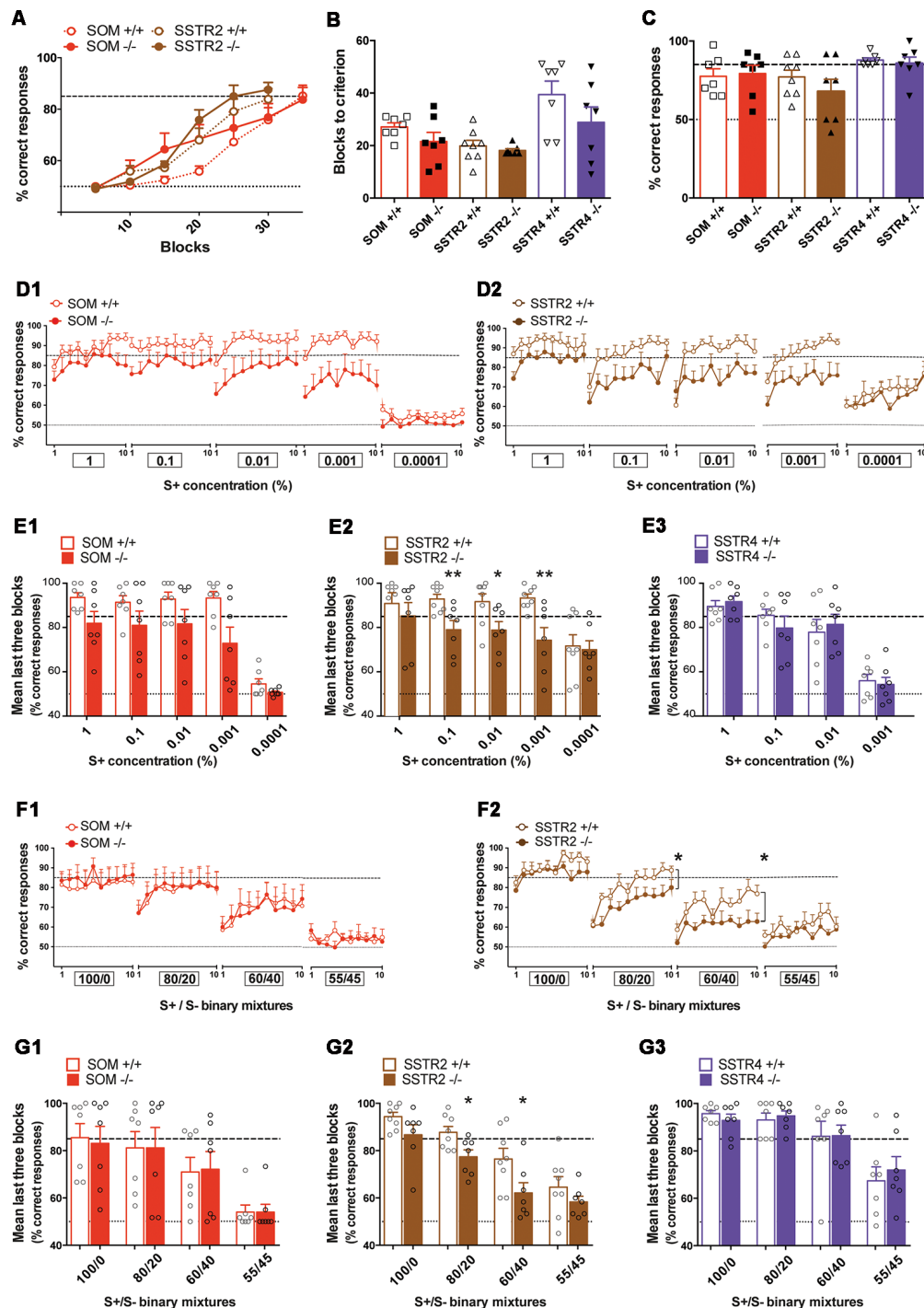


FIGURE 10 | Olfactory performances of SOM KO and SSTR2 KO mice cohorts evaluated using operant tasks. **(A)** Learning curves for SOM and SSTR2 cohorts (Initiation task, odor pair: anisole/cineole). **(B)** Mean blocks to criterion (BTC) number for WT and KO groups in the initiation task. **(C)** Olfactory memory performances 21 days after completion of the initiation task. **(B,C)** Symbols show individual values. **(D)** Mean percentage of correct responses for each training session in the olfactory detection task. **(D1)** SOM cohort ($n = 7$), **(D2)** SSTR2 cohort ($n = 7-8$). Ten blocks per session, boxes indicate S+ concentrations (%). **(E)** Mean performance of the last three blocks in the olfactory detection task. **(E1)** SOM cohort ($n = 7$), **(E2)** SSTR2 cohort ($n = 7-8$), **(E3)** SSTR4 cohort ($n = 7$). Open circles indicate individual values. $*P < 0.05$, $**P < 0.01$ vs. WT, Bonferroni-corrected ANOVA. **(F)** Mean percentage of correct responses for each training session in the olfactory discrimination task. **(F1)** SOM cohort ($n = 7$), **(F2)** SSTR2 cohort ($n = 7-8$). Ten blocks per session, boxes indicate S+/S- mixtures. Group: $*P < 0.05$, r -m ANOVA. **(G)** Mean performance of the last three blocks in the discrimination task. **(G1)** SOM cohort ($n = 7$), **(G2)** SSTR2 cohort ($n = 7-8$), **(G3)** SSTR4 cohort ($n = 7$). $*P < 0.05$ vs. WT, Bonferroni-corrected ANOVA. Red: SOM cohort, Brown: SSTR2 cohort, Purple: SSTR4 cohort. WT mice: open symbols/bars, KO mice: filled symbols/bars. Black dashed line: 85% success criterion, gray dashed line: 50% chance level. Error bars indicate SEM.

In the SSTR4 cohort, discrimination performances also globally decreased with task complexity (mixture: $F_{(3,36)} = 40.28$, $P < 0.0001$) without significant difference between WT and KO mice (group: $F_{(1,12)} = 0.32$, $P > 0.05$, no significant interaction). Averaged last three blocks performance (Figure 10G₃) showed that WT and SSTR4 KO discrimination scores similarly decreased in both groups (mixture: $F_{(3,36)} = 22.66$, $P < 0.0001$, group: $F_{(1,12)} = 0.041$, $P > 0.05$, no significant interaction).

In summary, SSTR2 KO mice showed impaired discrimination performances as compared to WT when the discrimination task was getting difficult in our experimental conditions.

DISCUSSION

In this work we combined histological, viral tracing and transgenic approaches to characterize the cellular targets of SOM in the murine OB. We demonstrate that SOM targets all levels of mitral dendritic processing in the OB with SSTR2 being expressed on the soma and dendrites of previously uncharacterized mitral-like cells, SSTR4 being associated with inhibitory periglomerular cells in the GL and SSTR3 restricted to neuronal cilia concentrated in the GCL. Genetic deletion of SSTR4, SSTR2 or SOM differentially affected olfactory performances. SSTR4 deletion did not impact the olfactory phenotype. Olfactory detection was differentially impaired in SOM KO and SSTR2 KO mice while only SSTR2 KO mice showed impaired fine discrimination. These data bring novel neuroanatomical and functional arguments in favor of the fine modulation of olfactory functions by SOM and call for future studies dissecting the respective origin and contribution of each SSTR subtype in the cellular and physiological responses to the peptide during olfactory processing.

One important finding was the identification of an atypical mitral cell-like neuronal population identified by SSTR2 expression. Using a specific monoclonal SSTR2 antibody, we show that SSTR2 labels a subpopulation of ovoid cells of the MCL layer projecting a single thick dendrite toward the GL. These cells are intermingled with the large typical mitral cells recognizable with their pear-shaped soma ($>20\ \mu\text{m}$, Nagayama et al., 2014) and thick primary dendrites labeled with Kv3.1 or Tbx21 antibodies. Further, SSTR2 is not detected in tufted cells. Some SSTR2-expressing neurons faintly express reelin in their soma, a marker of mitral and tufted cells in the OB while no colocalization was found with GABAergic or interneuron markers. SSTR2-positive cells strongly innervate glomeruli in the GL and interact with OMP-positive compartments (Nagayama et al., 2014). Thin labeled axon-like neurites are visible in the GCL, but the lateral olfactory tract is not labeled, suggesting that SSTR2 is mainly localized in somatic and dendritic compartments of principal cells, as previously reported in most forebrain structures (Csaba and Dournaud, 2001; Viollet et al., 2008; Liguz-Lecznar et al., 2016). Our study thus biochemically identifies the SSTR2-positive cells previously observed after agonist internalization using a polyclonal anti-SSTR2 antibody (Lepousez et al., 2010a). In this latter study, SSTR2 labeling

colocalized with dextran staining after retrograde injection of the retrograde tracer into the GL, showing that SSTR2-positive cells did project to the GL, consistent with the labeling of large dendrites in the EPL during ligand internalization (Lepousez et al., 2010b). Altogether, our data strongly suggest that SSTR2 labeling reveals a subpopulation of non-GABAergic mitral-like cells, not yet reported (Nagayama et al., 2014). Additionally, we found some SSTR2-positive cells in the IPL with lateral dendritic projections, and strongly labeled superficial short axon-like cells in the GCL. Such a SSTR2 immunohistochemical distribution in the OB is found in WT mice as well as in SSTR2KO-lacZ-KI mutant labeled with β -Gal antibody (Allen et al., 2003) and it disappears in homozygous SSTR2 KO or SSTR2 KO-LacZ KI mutant mice as expected.

Interestingly, not only SSTR2 but also SSTR1, SSTR3 and SSTR4 subtypes are highly expressed in the OB and display distinct binding patterns, each being associated to a given OB layer (Videau et al., 2003; Martel et al., 2015). We confirm here that SSTR3 and SSTR4 are associated to GCL and GL layers, respectively. SSTR3 is associated to the primary cilium, considered as a chemical sensor due to its concentration of many GPCRs and associated transduction pathways. Its loss leads to major cognitive and physiological defects (Louvi and Grove, 2011). In the OB, SSTR3 colocalizes with the ciliary marker Arl13b whose staining reflects nuclear density in all layers. SSTR3-labeled cilia are dense in the GCL, suggesting they may be associated with packed inhibitory granule cells which constitute 90% of OB neurons. We cannot exclude that they also label glial cells, but SSTR3 staining was associated with NeuN-positive cells in most brain telencephalic regions when studied in detail (Sipos et al., 2018). Recent studies in striatal interneurons has indicated that the major role of ciliary SSTR3 is in the maintenance of cellular connectivity and synaptic activity (Guo et al., 2017), showing that ligand-receptor interaction has crucial consequences for cellular function (Green et al., 2016; Nager et al., 2017). Furthermore, pharmacological and genetic evidence has demonstrated that knocking-out *ssstr3* gene in the hippocampus affects synaptic plasticity and recognition memory (Einstein et al., 2010). Since granule cells are major actors in the synaptic modulation of the olfactory signal in the OB through the reciprocal dendritic regulation of mitral cells, SSTR3 activation may directly influence their synaptic activity as well as their responses to local inhibition (Nusser et al., 2001) or afferent modulatory inputs (Nunez-Parra et al., 2013) which are proposed to control oscillatory states (David et al., 2015).

An intriguing finding was also that SSTR4 labeling is mostly associated to the GL in a nNOS-positive calretinin-positive subpopulation of GABAergic periglomerular cells (Kosaka and Kosaka, 2005; Nagayama et al., 2014). Due to technical constraints including a lack of specific SSTR4 antibody and nuclear expression of beta-galactosidase in the SSTR4 KO-LacZ KI (Helyes et al., 2009), we relied on nNOS immunohistochemical properties to conclude that cells bearing SSTR4 mainly project to the intraglomerular domain (Crespo

et al., 2003; Nagayama et al., 2014). In such a way, SSTR4 SOM receptors are positioned to modulate early synaptic stages of olfactory processing, either directly or through the release of nNOS, a potent neuromodulator in other brain structures (Vasilaki et al., 2002; Mastrodimou et al., 2006; Pavesi et al., 2013; Liguz-Leczna et al., 2016). Furthermore, a functional interaction occurs between two compartment-based SSTR2 and SSTR4 receptor subtypes in the mouse hippocampus (Moneta et al., 2002; Gastambide et al., 2010). In the OB, SSTR4-expressing cells surround glomeruli labeled by SSTR2-positive terminals suggesting a similar mechanism. The physiological conditions requiring SSTR4 activation remain obscure. One hypothesis would be that SSTR4 plays a role in the olfactory control of emotional behavior, since several studies have consistently reported anatomical, physiological and behavioral evidence that deleting *sstr4* gene induces stress responses in mice (Scheich et al., 2016; Prévôt et al., 2017). The local or extra-bulbar origin of the ligand targeting these receptors remains an open question since, no major SOM immunostaining was detected in the GL or OSNs, as previously reported (Lepousez et al., 2010a; De La Rosa-Prieto et al., 2016). Only rare somata and parts of SOM neurites were occasionally labeled in the GL, in accordance to *in situ hybridization* data in the GL from Allen Brain Atlas¹. However, it remains possible that under special conditions a surge in SOM release is triggered to activate SSTR4 receptors. Another possibility involves cortistatin, a peptide homologous to SOM which binds to SSTR receptors with equivalent affinities (Martel et al., 2012). Cortistatin has a more restricted brain distribution than SOM (de Lecea, 2008) and has been described in rat and mouse OB where it is expressed at low levels, like SOM (Martel et al., 2015). *In situ hybridization* data² and distribution of Cre or GFP tracers in cortistatin transgenic model mice³ confirm that CST is mainly expressed in MCL and outer GCL cells which project to the outer border of the EPL, providing an appropriate alternate source of SOM-like ligand in the OB.

Finally, SSTR1 is highly expressed in the OB (Martel et al., 2015) suggesting that SSTR1 may add another modulatory level, including an autoreceptor function as previously described in other forebrain structures (Thermos et al., 2006; De Bundel et al., 2010; Martel et al., 2012). No home-made or commercial SSTR1 antibody tested could be properly validated using an SSTR1 KO strain (Kreienkamp et al., 1999, data not shown) to be used to map the cells expressing this subtype in the OB.

According to that scheme, SSTR subtypes are differentially expressed in neurons involved in distinct inhibitory circuits regulating the dendritic excitability of the mitral cells in the OB. SOM cells may thus constitute a core of a sub-circuit in the OB, where the peptide exerts neuromodulatory influences through the dendritic regulation of afferent and recurrent excitation in principal cells and/or inhibition in GABAergic interneurons, as previously shown in piriform and neocortical

circuits (Sturgill and Isaacson, 2015; Large et al., 2016). SOM neuromodulation may partly result from centrifugal influence occurring through GCL (and occasionally GL) SOM fibers, originating from AON as shown here or from the medial raphe nucleus (Araneda et al., 1999), and the piriform cortex (Diodato et al., 2016). Comparison of rabies-based Cre-dependent retrograde viral infection in SOM-Ires-Cre mice with published evidence reporting monosynaptic inputs to the OB (Shipley and Ennis, 1996; Diodato et al., 2016) shows that OB SOM populations themselves receive direct centrifugal projections from a restricted number of central structures. Discrete groups of GFP-labeled neurons are found after 3 dpi in the AON, dorsal tenia tecta (DTT), piriform and entorhinal cortex, medial amygdala and ventral CA1 of the hippocampus, all structures involved in olfactory and emotional processing and previously reported to send back projections to the OB (Hintiryan et al., 2012; Miyamichi et al., 2013; Diodato et al., 2016). Most centrifugal projections are glutamatergic but basal forebrain nuclei send cholinergic fibers as well as GABAergic fibers to the OB (Nunez-Parra et al., 2013; Case et al., 2017; Sanz Diez et al., 2017) which may mediate disinhibition of the principal cells (Gracia-Llanes et al., 2010). Progressively, GFP infected neurons appear in the hypothalamic paraventricular nucleus, claustrum and BLA, suggesting that the virus retrogradely infects second- or third-order neurons. Indeed these regions, except the LC, are not known as direct projection areas to the OB (Shipley and Ennis, 1996; Mohedano-Moriano et al., 2012; De La Rosa-Prieto et al., 2015; Diodato et al., 2016). In conclusion, SOM populations in the mouse OB are tightly contacted by top-down afferents, most of them coming from regions involved in olfactory and emotional processes.

Such occurrence of centrifugal afferents on somatostatinergeric modulation in the OB may explain why the genetic deletion of SSTR2 or SSTR4 receptor or SOM peptide, which are expressed at key levels of olfactory processing in the OB, leads to contrasted phenotypes after olfactory evaluation. A consistent set of data suggests that the OB is the primary site for odor detection and recognition (Uchida and Mainen, 2003; Wesson et al., 2008), filtering the information coming from olfactory sensory neurons. In mice, a single respiratory sniff allows the discrimination of a novel odor, based on immediate glomerular activation (Chong and Rinberg, 2018) and local changes in principal cells activity (Sirotin et al., 2015). A coordinated firing of many neurons across the OB would mediate local gamma oscillations, whose power is correlated to fine discrimination performances (Kay, 2014) and integrative properties of neuronal ensembles with intracortical associational synapses in the piriform cortex are involved in the decoding of odor features. The piriform cortex is involved in the discrimination of simple tasks, based on spike timing and synchrony of local field potentials oscillations in the gamma band but also in the beta band which emerge with learning and experience in every part of the olfactory system (Kay, 2014; Wilson et al., 2014). More difficult discrimination between close or complex odors would mainly engage top-down inputs from the entorhinal cortex, responsible

¹<http://mouse.brain-map.org/gene/show/20366>

²<http://mouse.brain-map.org/experiment/show?id=72472766>

³<http://www.gensat.org/imagenavigator.jsp?imageID=66192>

for pattern separation processes (Chapuis et al., 2013; Wilson et al., 2014). Finally, afferents from the orbitofrontal cortex seem preferentially involved in the reward-value of an odor and long-term memory encoding in the piriform cortex (Wilson et al., 2014).

Using a spontaneous olfactory discrimination task, we found that WT and KO mice behaved similarly in SOM, SSTR2 and SSTR4 cohorts concerning the habituation to an odor or the discrimination of a novel odorant (H_5 vs. C_{+3}), suggesting that deleting these genes has no major impact on short-term olfactory memory formation or odor discrimination abilities in our conditions. Complementary experiments varying odorants at lower concentrations may reveal specific roles, if any, of SOM, SSTR2 and SSTR4 on short-term memory.

Concerning SSTR2, we had previously shown that its pharmacological blockade or activation in the OB respectively impaired or improved fine olfactory discrimination. Discrimination performances were correlated with power changes in gamma oscillations recorded in the OB of awake mice (Lepousez et al., 2010b). We show here that SSTR2 gene deletion affects olfactory performances in an operant task, since the mice fail to reach the discrimination criterion earlier than WT when the difficulty of the task increases. In line with our previous pharmacological data, this supports the hypothesis involving SSTR2 receptors and endogenous SOM in the modulation of olfactory discrimination and basal gamma oscillations in the OB. Since gamma oscillations rely on dendrodendritic synaptic interactions between mitral and granule cells, SSTR2 receptors may mediate a potent endogenous somatostatinergic tone on the mitral-like cells of the OB described herein. Reciprocal synapses between SOM interneurons and mitral dendrites have been previously reported (Lepousez et al., 2010a), but the ultrastructural localization of SSTR2 receptors at this level has not been described yet. Furthermore, since the SSTR2 KO mouse line is a constitutive transgenic line, we cannot exclude that the removal of SSTR2, present at all levels of the olfactory pathway, especially in both piriform and entorhinal cortex (Allen et al., 2003; Martel et al., 2015) also impacts the discrimination of very similar odors. Interestingly we show here that SSTR2 deletion also impairs olfactory detection abilities in an operant task. Alteration of both fine discrimination and detection was previously reported in mice lacking mitral but not tufted cells (Díaz et al., 2012), in agreement with the exclusive detection of SSTR2 in mitral-like cells in the OB. In comparison, removing SOM has few effects on olfactory detection (and no effect on discrimination) in our experimental conditions. It is somehow counterintuitive that removing the peptide has less effect than removing one single receptor out of four in the OB. This may be due to a global redistribution of the receptors, since a massive up-regulation of SOM binding sites is observed in SOM KO mice (Videau et al., 2003) and *in vivo* and *in vitro* data showed that intracellular localization and trafficking of all SSTR except SSTR4 is strongly dependent on SOM release in physiological or pathophysiological conditions (Csaba and Dournaud, 2001; Le Verche et al., 2009; Csaba et al., 2012). Another explanation

would rely on the extent of redundancy between SOM and cortistatin peptides in the olfactory pathway since both peptides exert distinct cellular and functional effects in the cortex (de Lecea, 2008).

Finally, SSTR4 KO and WT animals displayed similar olfactory behavioral responses in our experimental conditions. This was unexpected considering the abundance of SSTR4 binding sites (Martel et al., 2015) and SSTR4-expressing periglomerular cells at the first synaptic crossroad in the OB where odor detection and contrast enhancement takes place (Wilson et al., 2014; Chong and Rinberg, 2018). No major change in habituation, learning, detection or discrimination abilities was observed in the SSTR4 KO mice when compared to WT littermates. Since this receptor induces hyperpolarizing synaptic effects (Qiu et al., 2008), periglomerular SSTR4 may be required in given physiological conditions inducing a strong local release of somatostatinergic ligands (SOM or cortistatin). The question of the physiological conditions requiring SSTR4 activity remains to be addressed.

In conclusion, this anatomical and behavioral study opens novel perspectives concerning the modulatory roles of SOM in mouse OB. Previous pharmacological results (Lepousez et al., 2010b) and the transgenic data included here show that bulbar SOM, either endogenous or released from centrifugal afferents, exerts a tonic control on the activity of SSTR2-positive mitral cells in the OB. It also suggests more complex regulations involving different SSTR subtypes and additional olfactory regions. Physiological studies with opto- and chemogenetic models are now clearly required to dissect the contribution of each peptide and SSTR subtype in the synaptic modulatory effects of SOM in olfactory processing.

AUTHOR CONTRIBUTIONS

CV and JE designed research. AS and SN performed immunohistochemistry. JG, FD and NS viral tracing. SN, OF, YC and CV behavioral experiments. CV prepared the manuscript.

FUNDING

This work was supported by Institut National de la Santé et de la Recherche Médicale (INSERM), ANR Research Grant (ANR-10-MALZ-003-01 SOMADOLF to JE and CV) and Erasmus fellowship (SN).

ACKNOWLEDGMENTS

The authors thank Drs M. Alonso, G. Lepousez and S. Wagner (UMR3571 CNRS—Unité Perception et Mémoire, Institut Pasteur) for olfactometer technical support, Dr Yoshihara (RIKEN, Japan), Dr C. Adori (Karolinska Institute, Stockholm, Sweden) and Dr J. Diaz (CPN, Paris) for providing Tbx21, secretagogin and Arl13b antibodies, respectively, Dr D. de Saint Jan (INC, Strasbourg, France) for providing Kv3.1-EYFP brains, Dr S. Schulz (Jena University, Germany) for providing SSTR2 KO-lacZ KI brains. PRVBa2001 was generously provided by

Prof. Enquist (Princeton University). The authors thank animal experimentation facilities of the CPN (Paris) and CSGA (Dijon), CPN and HISTIM imaging (Institut Cochin, Paris) facilities, as well as D. Gény (CPN) and S. Chaudy (CSGA) for technical help and R.A. Piskorowski (IPNP) for manuscript editing.

REFERENCES

- Allen, J. P., Hathway, G. J., Clarke, N. J., Jowett, M. I., Topps, S., Kendrick, K. M., et al. (2003). Somatostatin receptor 2 knockout/lacZ knockin mice show impaired motor coordination and reveal sites of somatostatin action within the striatum. *Eur. J. Neurosci.* 17, 1881–1895. doi: 10.1046/j.1460-9568.2003.02629.x
- Araneda, S., Gysling, K., and Calas, A. (1999). Raphe serotonergic neurons projecting to the olfactory bulb contain galanin or somatostatin but not neuropeptide Y. *Brain Res. Bull.* 49, 209–214. doi: 10.1016/s0304-9230(99)00055-6
- Balu, R., Pressler, R. T., and Strowbridge, B. W. (2007). Multiple modes of synaptic excitation of olfactory bulb granule cells. *J. Neurosci.* 27, 5621–5632. doi: 10.1523/JNEUROSCI.4630-06.2007
- Boyd, A. M., Sturgill, J. F., Poo, C., and Isaacson, J. S. (2012). Cortical feedback control of olfactory bulb circuits. *Neuron* 76, 1161–1174. doi: 10.1016/j.neuron.2012.10.020
- Brunert, D., Tsuno, Y., Rothermel, M., Shipley, M. T., and Wachowiak, M. (2016). Cell-type-specific modulation of sensory responses in olfactory bulb circuits by serotonergic projections from the raphe nuclei. *J. Neurosci.* 36, 6820–6835. doi: 10.1523/JNEUROSCI.3667-15.2016
- Brunjes, P. C., Kay, R. B., and Arrivillaga, J. P. (2011). The mouse olfactory peduncle. *J. Comp. Neurol.* 519, 2870–2886. doi: 10.1002/cne.22662
- Burton, S. D., LaRocca, G., Liu, A., Cheetham, C. E., and Urban, N. N. (2017). Olfactory bulb deep short-axon cells mediate widespread inhibition of tufted cell apical dendrites. *J. Neurosci.* 37, 1117–1138. doi: 10.1523/JNEUROSCI.2880-16.2016
- Case, D. T., Burton, S. D., Gedeon, J. Y., Williams, S. G., Urban, N. N., and Seal, R. P. (2017). Layer- and cell type-selective co-transmission by a basal forebrain cholinergic projection to the olfactory bulb. *Nat. Commun.* 8:652. doi: 10.1038/s41467-017-00765-4
- Chapuis, J., Cohen, Y., He, X., Zhang, Z., Jin, S., Xu, F., et al. (2013). Lateral entorhinal modulation of piriform cortical activity and fine odor discrimination. *J. Neurosci.* 33, 13449–13459. doi: 10.1523/JNEUROSCI.1387-13.2013
- Chong, E., and Rinberg, D. (2018). Behavioral readout of spatio-temporal codes in olfaction. *Curr. Opin. Neurobiol.* 52, 18–24. doi: 10.1016/j.conb.2018.04.008
- Crespo, C., Gracia-Llanes, F. J., Blasco-Ibáñez, J. M., Gutiérrez-Mecinas, M., Marques-Mari, A. I., and Martínez-Guijarro, F. J. (2003). Nitric oxide synthase containing periglomerular cells are GABAergic in the rat olfactory bulb. *Neurosci. Lett.* 349, 151–154. doi: 10.1016/s0304-3940(03)00819-x
- Csaba, Z., and Dournaud, P. (2001). Cellular biology of somatostatin receptors. *Neuropeptides* 35, 1–23. doi: 10.1054/npep.2001.0848
- Csaba, Z., Peineau, S., and Dournaud, P. (2012). Molecular mechanisms of somatostatin receptor trafficking. *J. Mol. Endocrinol.* 48, R1–R12. doi: 10.1530/jme-11-0121
- David, F., Courtiol, E., Buonviso, N., and Fourcaud-Trocmé, N. (2015). Competing mechanisms of γ and β oscillations in the olfactory bulb based on multimodal inhibition of mitral cells over a respiratory cycle. *eNeuro* 2:ENEURO.0018-15.2015. doi: 10.1523/eneuro.0018-15.2015
- De Bundel, D., Aourz, N., Kiagiadakis, F., Clinckers, R., Hoyer, D., Kastellakis, A., et al. (2010). Hippocampal sst1 receptors are autoreceptors and do not affect seizures in rats. *Neuroreport* 21, 254–258. doi: 10.1097/wnr.0b013e3283353a64
- De La Rosa-Prieto, C., De Moya-Pinilla, M., Saiz-Sanchez, D., Ubeda-Banon, I., Arzate, D. M., Flores-Cuadrado, A., et al. (2015). Olfactory and cortical projections to bulbar and hippocampal adult-born neurons. *Front. Neuroanat.* 9:4. doi: 10.3389/fnana.2015.00004
- De La Rosa-Prieto, C., Saiz-Sanchez, D., Ubeda-Banon, I., Flores-Cuadrado, A., and Martínez-Marcos, A. (2016). Neurogenesis, neurodegeneration, interneuron vulnerability, and amyloid- β in the olfactory bulb of APP/PS1 mouse model of Alzheimer's disease. *Front. Neurosci.* 10:227. doi: 10.3389/fnins.2016.00227
- de Lecea, L. (2008). Cortistatin—functions in the central nervous system. *Mol. Cell. Endocrinol.* 286, 88–95. doi: 10.1016/j.mce.2007.12.014
- DeFalco, J., Tomishima, M., Liu, H., Zhao, C., Cai, X., Marth, J. D., et al. (2001). Virus-assisted mapping of neural inputs to a feeding center in the hypothalamus. *Science* 291, 2608–2613. doi: 10.1126/science.1056602
- Devore, S., and Linster, C. (2012). Noradrenergic and cholinergic modulation of olfactory bulb sensory processing. *Front. Behav. Neurosci.* 6:52. doi: 10.3389/fnbeh.2012.00052
- Díaz, D., Lepousez, G., Gheusi, G., Alonso, J. R., Lledo, P. M., and Weruaga, E. (2012). Bone marrow cell transplantation restores olfaction in the degenerated olfactory bulb. *J. Neurosci.* 32, 9053–9058. doi: 10.1523/JNEUROSCI.0260-12.2012
- Diodato, A., Ruinart De Brimont, M., Yim, Y. S., Derian, N., Perrin, S., Pouch, J., et al. (2016). Molecular signatures of neural connectivity in the olfactory cortex. *Nat. Commun.* 7:12238. doi: 10.1038/ncomms12238
- Einstein, E. B., Patterson, C. A., Hon, B. J., Regan, K. A., Reddi, J., Melnikoff, D. E., et al. (2010). Somatostatin signaling in neuronal cilia is critical for object recognition memory. *J. Neurosci.* 30, 4306–4314. doi: 10.1523/JNEUROSCI.5295-09.2010
- Frederick, D. E., Brown, A., Brim, E., Mehta, N., Vujovic, M., and Kay, L. M. (2016). γ and β oscillations define a sequence of neurocognitive modes present in odor processing. *J. Neurosci.* 36, 7750–7767. doi: 10.1523/JNEUROSCI.0569-16.2016
- Gastambide, F., Lepousez, G., Viollet, C., Loudes, C., Epelbaum, J., and Guillou, J. L. (2010). Cooperation between hippocampal somatostatin receptor subtypes 4 and 2: functional relevance in interactive memory systems. *Hippocampus* 20, 745–757. doi: 10.1002/hipo.20680
- Gracia-Llanes, F. J., Crespo, C., Blasco-Ibáñez, J. M., Nacher, J., Varea, E., Rovira-Esteban, L., et al. (2010). GABAergic basal forebrain afferents innervate selectively GABAergic targets in the main olfactory bulb. *Neuroscience* 170, 913–922. doi: 10.1016/j.neuroscience.2010.07.046
- Green, J. A., Schmid, C. L., Bley, E., Monsma, P. C., Brown, A., Bohn, L. M., et al. (2016). Recruitment of β -arrestin into neuronal cilia modulates somatostatin receptor subtype 3 ciliary localization. *Mol. Cell. Biol.* 36, 223–235. doi: 10.1128/MCB.00765-15
- Guo, J., Otis, J. M., Higginbotham, H., Monckton, C., Cheng, J., Asokan, A., et al. (2017). Primary cilia signaling shapes the development of interneuronal connectivity. *Dev. Cell* 42, 286.e4–300.e4. doi: 10.1016/j.devcel.2017.07.010
- Hamilton, K. A., Heinbockel, T., Ennis, M., Szabó, G., Erdélyi, F., and Hayar, A. (2005). Properties of external plexiform layer interneurons in mouse olfactory bulb slices. *Neuroscience* 133, 819–829. doi: 10.1016/j.neuroscience.2005.03.008
- Helyes, Z., Pintér, E., Sándor, K., Elekes, K., Bánvölgyi, A., Keszthelyi, D., et al. (2009). Impaired defense mechanism against inflammation, hyperalgesia, and airway hyperreactivity in somatostatin 4 receptor gene-deleted mice. *Proc. Natl. Acad. Sci. U S A* 106, 13088–13093. doi: 10.1073/pnas.0900681106
- Hintiryan, H., Gou, L., Zingg, B., Yamashita, S., Lyden, H. M., Song, M. Y., et al. (2012). Comprehensive connectivity of the mouse main olfactory bulb: analysis and online digital atlas. *Front. Neuroanat.* 6:30. doi: 10.3389/fnana.2012.00030
- Huang, L., Garcia, I., Jen, H. I., and Arenkiel, B. R. (2013). Reciprocal connectivity between mitral cells and external plexiform layer interneurons in the mouse olfactory bulb. *Front. Neural Circuits* 7:32. doi: 10.3389/fncir.2013.00032
- Kay, L. M. (2014). Circuit oscillations in odor perception and memory. *Prog. Brain Res.* 208, 223–251. doi: 10.1016/b978-0-444-63350-7.00009-7
- Kosaka, K., and Kosaka, T. (2005). Synaptic organization of the glomerulus in the main olfactory bulb: compartments of the glomerulus and heterogeneity of the

SUPPLEMENTARY MATERIAL

The Supplementary Material for this article can be found online at: <https://www.frontiersin.org/articles/10.3389/fnbeh.2019.00061/full#supplementary-material>

- periglomerular cells. *Anat. Sci. Int.* 80, 80–90. doi: 10.1111/j.1447-073x.2005.00092.x
- Kreienkamp, H. J., Akgün, E., Baumeister, H., Meyerhof, W., and Richter, D. (1999). Somatostatin receptor subtype 1 modulates basal inhibition of growth hormone release in somatotrophs. *FEBS Lett.* 462, 464–466. doi: 10.1016/s0014-5793(99)01582-3
- Large, A. M., Kunz, N. A., Mielo, S. L., and Oswald, A. M. (2016). Inhibition by somatostatin interneurons in olfactory cortex. *Front. Neural Circuits* 10:62. doi: 10.3389/fncir.2016.00062
- Lepousez, G., Csaba, Z., Bernard, V., Loudes, C., Videau, C., Lacombe, J., et al. (2010a). Somatostatin interneurons delineate the inner part of the external plexiform layer in the mouse main olfactory bulb. *J. Comp. Neurol.* 518, 1976–1994. doi: 10.1002/cne.22317
- Lepousez, G., and Lledo, P.-M. (2013). Odor discrimination requires proper olfactory fast oscillations in awake mice. *Neuron* 80, 1010–1024. doi: 10.1016/j.neuron.2013.07.025
- Lepousez, G., Mouret, A., Loudes, C., Epelbaum, J., and Viollet, C. (2010b). Somatostatin contributes to *in vivo* γ oscillation modulation and odor discrimination in the olfactory bulb. *J. Neurosci.* 30, 870–875. doi: 10.1523/JNEUROSCI.4958-09.2010
- Le Verche, V., Kaindl, A. M., Verney, C., Csaba, Z., Peineau, S., Olivier, P., et al. (2009). The somatostatin 2A receptor is enriched in migrating neurons during rat and human brain development and stimulates migration and axonal outgrowth. *PLoS One* 4:e5509. doi: 10.1371/journal.pone.0005509
- Liguz-Leczna, M., Urban-Ciecko, J., and Kossut, M. (2016). Somatostatin and somatostatin-containing neurons in shaping neuronal activity and plasticity. *Front. Neural Circuits* 10:48. doi: 10.3389/fncir.2016.00048
- Linster, C., and Cleland, T. A. (2016). Neuromodulation of olfactory transformations. *Curr. Opin. Neurobiol.* 40, 170–177. doi: 10.1016/j.conb.2016.07.006
- Louvi, A., and Grove, E. A. (2011). Cilia in the CNS: the quiet organelle claims center stage. *Neuron* 69, 1046–1060. doi: 10.1016/j.neuron.2011.03.002
- Low, M. J., Otero-Corchon, V., Parlow, A. F., Ramirez, J. L., Kumar, U., Patel, Y. C., et al. (2001). Somatostatin is required for masculinization of growth hormone-regulated hepatic gene expression but not of somatic growth. *J. Clin. Invest.* 107, 1571–1580. doi: 10.1172/jci11941
- Markopoulos, F., Rokni, D., Gire, D. H., and Murthy, V. N. (2012). Functional properties of cortical feedback projections to the olfactory bulb. *Neuron* 76, 1175–1188. doi: 10.1016/j.neuron.2012.10.028
- Martel, G., Dutar, P., Epelbaum, J., and Viollet, C. (2012). Somatostatinergic systems: an update on brain functions in normal and pathological aging. *Front. Endocrinol.* 3:154. doi: 10.3389/fendo.2012.00154
- Martel, G., Simon, A., Nocera, S., Kalainathan, S., Pidoux, L., Blum, D., et al. (2015). Aging, but not tau pathology, impacts olfactory performances and somatostatin systems in THY-Tau22 mice. *Neurobiol. Aging* 36, 1013–1028. doi: 10.1016/j.neurobiolaging.2014.10.033
- Mastrodimo, N., Vasilaki, A., Papadioti, A., Low, M. J., Hoyer, D., and Thermos, K. (2006). Somatostatin receptors in wildtype and somatostatin deficient mice and their involvement in nitric oxide physiology in the retina. *Neuropeptides* 40, 365–373. doi: 10.1016/j.npep.2006.07.002
- Metzger, F., Repunte-Canonigo, V., Matsushita, S., Akemann, W., Diez-Garcia, J., Ho, C. S., et al. (2002). Transgenic mice expressing a pH and Cl⁻ sensing yellow-fluorescent protein under the control of a potassium channel promoter. *Eur. J. Neurosci.* 15, 40–50. doi: 10.1046/j.0953-816x.2001.01837.x
- Miyamichi, K., Shlomai-Fuchs, Y., Shu, M., Weissbourd, B. C., Luo, L., and Mizrahi, A. (2013). Dissecting local circuits: parvalbumin interneurons underlie broad feedback control of olfactory bulb output. *Neuron* 80, 1232–1245. doi: 10.1016/j.neuron.2013.08.027
- Mohedano-Moriano, A., de la Rosa-Prieto, C., Saiz-Sanchez, D., Ubeda-Bañon, I., Pro-Sistiaga, P., De Moya-Pinilla, M., et al. (2012). Centrifugal telencephalic afferent connections to the main and accessory olfactory bulbs. *Front. Neuroanat.* 6:19. doi: 10.3389/fnana.2012.00019
- Moneta, D., Richichi, C., Aliprandi, M., Dournaud, P., Dutar, P., Billard, J. M., et al. (2002). Somatostatin receptor subtypes 2 and 4 affect seizure susceptibility and hippocampal excitatory neurotransmission in mice. *Eur. J. Neurosci.* 16, 843–849. doi: 10.1046/j.1460-9568.2002.02146.x
- Nagayama, S., Homma, R., and Imamura, F. (2014). Neuronal organization of olfactory bulb circuits. *Front. Neural Circuits* 8:98. doi: 10.3389/fncir.2014.00098
- Nager, A. R., Goldstein, J. S., Herranz-Perez, V., Portran, D., Ye, F., Garcia-Verdugo, J. M., et al. (2017). An actin network dispatches ciliary GPCRs into extracellular vesicles to modulate signaling. *Cell* 168, 252.e14–263.e14. doi: 10.1016/j.cell.2016.11.036
- Nunez-Parra, A., Maurer, R. K., Krahe, K., Smith, R. S., and Araneda, R. C. (2013). Disruption of centrifugal inhibition to olfactory bulb granule cells impairs olfactory discrimination. *Proc. Natl. Acad. Sci. U S A* 110, 14777–14782. doi: 10.1073/pnas.1310686110
- Nusser, Z., Kay, L. M., Laurent, G., Homanics, G. E., and Mody, I. (2001). Disruption of GABA_A receptors on GABAergic interneurons leads to increased oscillatory power in the olfactory bulb network. *J. Neurophysiol.* 86, 2823–2833. doi: 10.1152/jn.2001.86.6.2823
- O'Connor, A. K., Malarkey, E. B., Berbari, N. F., Croyle, M. J., Haycraft, C. J., Bell, P. D., et al. (2013). An inducible CiliaGFP mouse model for *in vivo* visualization and analysis of cilia in live tissue. *Cilia* 2:8. doi: 10.1186/2046-2530-2-8
- Pavesi, E., Heldt, S. A., and Fletcher, M. L. (2013). Neuronal nitric-oxide synthase deficiency impairs the long-term memory of olfactory fear learning and increases odor generalization. *Learn. Mem.* 20, 482–490. doi: 10.1101/lm.031450.113
- Paxinos, G., and Franklin, K. (2008). *The Mouse Brain in Stereotaxic Coordinates*. Academic Press, Elsevier.
- Prévôt, T. D., Gastambide, F., Viollet, C., Henkous, N., Martel, G., Epelbaum, J., et al. (2017). Roles of hippocampal somatostatin receptor subtypes in stress response and emotionality. *Neuropsychopharmacology* 42, 1647–1656. doi: 10.1038/npp.2016.281
- Qiu, C., Zeyda, T., Johnson, B., Hochgeschwender, U., de Lecea, L., and Tallent, M. K. (2008). Somatostatin receptor subtype 4 couples to the M-current to regulate seizures. *J. Neurosci.* 28, 3567–3576. doi: 10.1523/JNEUROSCI.4679-07.2008
- Saiz-Sanchez, D., Flores-Cuadrado, A., Ubeda-Bañon, I., de la Rosa-Prieto, C., and Martinez-Marcos, A. (2016). Interneurons in the human olfactory system in Alzheimer's disease. *Exp. Neurol.* 276, 13–21. doi: 10.1016/j.expneurol.2015.11.009
- Sanz Diez, A., Najac, M., and de Saint Jan, D. (2017). Basal forebrain control of olfactory bulb interneurons. *bioRxiv [Preprint]*. doi: 10.1101/216259
- Scheich, B., Gaszner, B., Kormos, V., László, K., Ádori, C., Borbély, É., et al. (2016). Somatostatin receptor subtype 4 activation is involved in anxiety and depression-like behavior in mouse models. *Neuropharmacology* 101, 204–215. doi: 10.1016/j.neuropharm.2015.09.021
- Schwarz, L. A., Miyamichi, K., Gao, X. J., Beier, K. T., Weissbourd, B., Deloach, K. E., et al. (2015). Viral-genetic tracing of the input-output organization of a central noradrenaline circuit. *Nature* 524, 88–92. doi: 10.1038/nature14600
- Shipley, M. T., and Ennis, M. (1996). Functional organization of olfactory system. *J. Neurobiol.* 30, 123–176. doi: 10.1002/(sici)1097-4695(199605)30:1<123::aid-neu11>3.0.co;2-n
- Sipos, É., Komoly, S., and Ács, P. (2018). Quantitative comparison of primary cilia marker expression and length in the mouse brain. *J. Mol. Neurosci.* 64, 397–409. doi: 10.1007/s12031-018-1036-z
- Sirotni, Y. B., Shusterman, R., and Rinberg, D. (2015). Neural coding of perceived odor intensity. *eNeuro* 2:ENEURO.0083-15.2015. doi: 10.1523/eneuro.0083-15.2015
- Soria-Gómez, E., Bellocchio, L., Reguero, L., Lepousez, G., Martin, C., Bendahmane, M., et al. (2014). The endocannabinoid system controls food intake via olfactory processes. *Nat. Neurosci.* 17, 407–415. doi: 10.1038/nn.3647
- Sturgill, J. F., and Isaacson, J. S. (2015). Somatostatin cells regulate sensory response fidelity via subtractive inhibition in olfactory cortex. *Nat. Neurosci.* 18, 531–535. doi: 10.1038/nn.3971
- Taniguchi, H., He, M., Wu, P., Kim, S., Paik, R., Sugino, K., et al. (2011). A resource of Cre driver lines for genetic targeting of GABAergic neurons in cerebral cortex. *Neuron* 71, 995–1013. doi: 10.1016/j.neuron.2011.07.026
- Thermos, K., Bagnoli, P., Epelbaum, J., and Hoyer, D. (2006). The somatostatin sst1 receptor: an autoreceptor for somatostatin in brain and retina? *Pharmacol. Ther.* 110, 455–464. doi: 10.1016/j.pharmthera.2005.09.003

- Uchida, N., and Mainen, Z. F. (2003). Speed and accuracy of olfactory discrimination in the rat. *Nat. Neurosci.* 6, 1224–1229. doi: 10.1038/nn1142
- Vasilaki, A., Mouratidou, M., Schulz, S., and Thermos, K. (2002). Somatostatin mediates nitric oxide production by activating sst(2) receptors in the rat retina. *Neuropharmacology* 43, 899–909. doi: 10.1016/s0028-3908(02)00181-8
- Videau, C., Hochgeschwender, U., Kreienkamp, H. J., Brennan, M. B., Viollet, C., Richter, D., et al. (2003). Characterisation of [125I]-Tyr0DTrp8-somatostatin binding in sst1- to sst4- and SRIF-gene-invalidated mouse brain. *Naunyn Schmiedeberg's Arch. Pharmacol.* 367, 562–571. doi: 10.1007/s00210-003-0758-8
- Viollet, C., Lepousez, G., Loudes, C., Videau, C., Simon, A., and Epelbaum, J. (2008). Somatostatinergic systems in brain: networks and functions. *Mol. Cell. Endocrinol.* 286, 75–87. doi: 10.1016/j.mce.2007.09.007
- Viollet, C., Vaillend, C., Videau, C., Bluet-Pajot, M. T., Ungerer, A., L'Héritier, A., et al. (2000). Involvement of sst2 somatostatin receptor in locomotor, exploratory activity and emotional reactivity in mice. *Eur. J. Neurosci.* 12, 3761–3770. doi: 10.1046/j.1460-9568.2000.00249.x
- Wesson, D. W., Carey, R. M., Verhagen, J. V., and Wachowiak, M. (2008). Rapid encoding and perception of novel odors in the rat. *PLoS Biol.* 6:e82. doi: 10.1371/journal.pbio.0060082
- Wilson, D. A., Xu, W., Sadrian, B., Courtiol, E., Cohen, Y., and Barnes, D. C. (2014). Cortical odor processing in health and disease. *Prog. Brain Res.* 208, 275–305. doi: 10.1016/b978-0-444-63350-7.00011-5

Conflict of Interest Statement: The authors declare that the research was conducted in the absence of any commercial or financial relationships that could be construed as a potential conflict of interest.

Copyright © 2019 Nocera, Simon, Fiquet, Chen, Gascuel, Datiche, Schneider, Epelbaum and Viollet. This is an open-access article distributed under the terms of the Creative Commons Attribution License (CC BY). The use, distribution or reproduction in other forums is permitted, provided the original author(s) and the copyright owner(s) are credited and that the original publication in this journal is cited, in accordance with accepted academic practice. No use, distribution or reproduction is permitted which does not comply with these terms.



Prolonged Cannabidiol Treatment Lacks on Detrimental Effects on Memory, Motor Performance and Anxiety in C57BL/6J Mice

Eva M. Schleicher[†], Frederik W. Ott[†], Melanie Müller, Barbara Silcher, Marius E. Sichler, Maximilian J. Löw, Jannek M. Wagner and Yvonne Bouter*

Department of Psychiatry and Psychotherapy, Division of Molecular Psychiatry, University Medical Center Goettingen (UMG), Georg-August-University, Goettingen, Germany

OPEN ACCESS

Edited by:

Carlos Tomaz,
Universidade Ceuma, Brazil

Reviewed by:

Vincenzo Micale,
Università degli Studi di Catania, Italy
Carmen Pedraza,
University of Málaga, Spain

*Correspondence:

Yvonne Bouter
yvonne.bouter@med.uni-goettingen.de;
yvonne_bout@gmx.de

[†]These authors have contributed
equally to this work

Received: 15 February 2019

Accepted: 17 April 2019

Published: 07 May 2019

Citation:

Schleicher EM, Ott FW, Müller M, Silcher B, Sichler ME, Löw MJ, Wagner JM and Bouter Y (2019) Prolonged Cannabidiol Treatment Lacks on Detrimental Effects on Memory, Motor Performance and Anxiety in C57BL/6J Mice. *Front. Behav. Neurosci.* 13:94. doi: 10.3389/fnbeh.2019.00094

The Cannabis plant contains more than 100 currently known phytocannabinoids. Regarding the rising consumption of the non-psychotropic phytocannabinoid cannabidiol (CBD) in people's everyday life (e.g., beauty products, food and beverages), the importance of studies on the influence of CBD on healthy humans and rodents is evident. Therefore, the behavioral profile of CBD was investigated with a battery of behavioral tests, including motor, anxiety, and memory tests after prolonged CBD treatment. Adult C57BL/6J wildtype (WT) mice were daily intraperitoneally injected with 20 mg/kg CBD for 6 weeks starting at two different points of ages (3 months and 5 months) to compare the influence of prolonged CBD treatment with a washout period (former group) to the effects of long term CBD treatment (current group). Our results show that CBD treatment does not influence motor performance on an accelerating Rotarod test, while it also results in a lower locomotor activity in the open field (OF). No influence of CBD on spatial learning and long term memory in the Morris Water Maze (MWM) was observed. Memory in the Novel Object Recognition test (NORT) was unaffected by CBD treatment. Two different anxiety tests revealed that CBD does not affect anxiety behavior in the Dark-Light Box (DLB) and OF test. Although, anxiety is altered by current CBD treatment in the Elevated Plus Maze (EPM). Moreover, CBD-treated C57BL/6J mice showed an unaltered acoustic startle response (ASR) compared to vehicle-treated mice. However, current CBD treatment impairs prepulse inhibition (PPI), a test to analyze sensorimotor gating. Furthermore, prolonged CBD treatment did not affect the hippocampal neuron number. Our results demonstrate that prolonged CBD treatment has no negative effect on the behavior of adult C57BL/6J mice.

Keywords: cannabidiol, behavior, morris water maze, anxiety, cannabinoid system, cannabis

INTRODUCTION

Over the last years, there has been growing interest in the therapeutic potential of the phytocannabinoid cannabidiol (CBD) occurring naturally in the plant *Cannabis sativa/indica*, commonly known as marijuana. Several studies showed that CBD is involved, among others, in immunomodulatory, anti-inflammatory, antiemetic, anticonvulsant, anxiolytic, antipsychotic,

muscle relaxant and neuroprotective processes (Atakan, 2012; Burstein, 2015; Watt and Karl, 2017). Interestingly, the interest in studying CBD initially came through its interaction with the probably most commonly recognized constituent of the cannabis plant, 9-Tetrahydrocannabinol (THC). CBD was first isolated by Adams et al. (1940) in 1940 and its structure was elucidated 23 years later (Cunha et al., 1980). The pharmacological mechanisms of THC are the most well understood among the more than 100 other currently known phytocannabinoids (Mechoulam et al., 2014). Whereas THC is dependent from CB1-, and CB2-receptor binding, the mechanism of action for CBD is still not fully understood (De Petrocellis and Di Marzo, 2010). There are several other receptors that appear to be involved in the therapeutic effect of CBD, such as TRPV1-, PPAR γ -, 5-HT1A-, and GPR55-Receptors (Zygmunt et al., 1999; Bouaboula et al., 2005; Russo et al., 2005; O'Sullivan, 2007; Ryberg et al., 2007).

Beneficial impacts of CBD on multiple diseases, such as multiple sclerosis (Mecha et al., 2013), brain ischemia (Schiavon et al., 2014; Mori et al., 2017) and epilepsy (Patra et al., 2019) have been shown in animal models.

Several studies support the beneficial effects of CBD for treating neuropsychiatric disorders, particularly affective disturbances as anxiety, depression and schizophrenia (Micale et al., 2013; Kucerovala et al., 2014; Blessing et al., 2015). An anxiolytic effect has also been observed in healthy humans (Cunha et al., 1980). Recently, Stark et al. (2019) showed that early treatment with CBD can even prevent the appearance of schizophrenia-like deficits.

Surprisingly, few studies have examined the possible effects of prolonged CBD treatment on healthy mice. Studies of CBD effects have been mostly restricted to its acute effect and less is known about the efficiency after chronic CBD treatment. Therefore, the purpose of this study was to investigate the consequences of prolonged CBD treatment on the behavior of healthy C57BL/6J animals. In addition, we analyzed the effects of CBD on behavior after a washout period.

MATERIALS AND METHODS

Animals and Drug Treatment

C57BL/6J mice (Jackson Laboratories, Bar Harbor, ME, USA) were used in this study with an equal distribution of male

and female mice. All animals were handled according to the guidelines of the Federation of European Laboratory Animal Science Association (FELASA) and approved by the "Lower Saxony State Office for Consumer Protection and Food Safety" (LAVES). Mice were kept in individually ventilated cages (IVC, 32 × 16 × 14 cm; Tecniplast, Hohenpeißenberg, Germany) in groups up to five. Water and food were available *ad libitum*.

Powdered CBD (THC Pharm GmbH, Frankfurt/Main, Germany) was dissolved in equal amounts of 2.5 ml Tween 80 (Carl Roth GmbH, Karlsruhe, Germany) and 2.5 ml 100% ethanol and diluted in 45 ml of 0.9% NaCl solution. A vehicle control treatment group was set up in the exact same way, with the exception of CBD. Mice were assigned to either CBD or vehicle-treated groups and treated daily with an intraperitoneal injection containing the injection volume of 10 ml/kg body weight for 6 weeks starting at the age of 3 months (in the following called "former") or 5 months (in the following called "current"; Figure 1). Mice were treated with 20 mg/kg body weight of CBD. Mice were weighed weekly and the injection volume was adjusted accordingly. In the current group, treatment continued during behavioral testing and lasted until the day of sacrifice. Behavioral testing started for all mice at the age of 6 months and mice were sacrificed with 26 weeks.

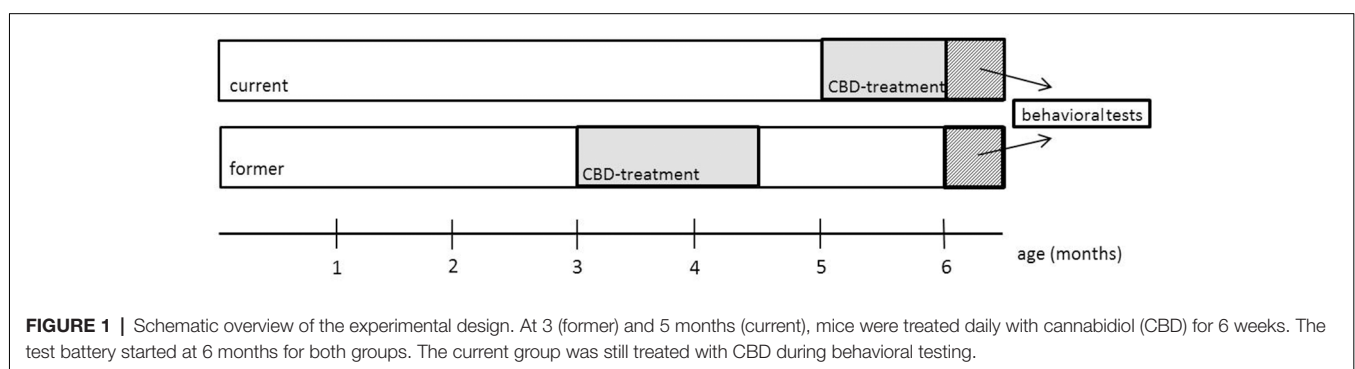
Behavior Testing

To detect possible behavioral and cognitive alterations due to prolonged CBD treatment, C57BL/6J mice were tested in a battery of anxiety-, motor and memory-tests ($n = 14-18$). All mice were tested at the age of 6 months and testing lasted 18 days. Mice were sacrificed after the last day of testing.

Mice were kept on a 12 h/12 h inverted light cycle. All behavior experiments were performed during the dark phase between 7 a.m. and 7 p.m. Ambient illumination was 624 lx in the light chamber and 3 lx in the dark chamber. Red light illumination was 173 lx.

Accelerating Rotarod

To analyze motor performance and motor skill learning in CBD-treated mice the accelerating Rotarod test (RotaRod 3375-5, TSE Systems GmbH, Bad Homburg, Germany) was used (Shiotsuki et al., 2010). C57BL/6J mice were placed face forwards



on the rod (\pm 30 mm, 60 mm width per mouse), suspended above a grid floor at a height of 14.7 cm, high enough to create avoidance of falling and to prevent the mice deliberately jumping off the rod. Mice performed four trials per day on two consecutive days. To keep the mice focused on the task, the test was performed under red light. The rod accelerated from 4 to 40 revolutions per minute (rpm) over a time period of 300 s with an average inter-trial interval (ITI) of 15 min before the next trial started. For each trial, the time on the rod was recorded.

Morris Water Maze

The Morris Water Maze test (MWM; Morris, 1984) was used to evaluate spatial reference memory in CBD-treated C57BL/6J mice as previously described (Bouter et al., 2014). In brief, the test relies on spatial cues to locate a submerged hidden platform (10 cm diameter) in a circular pool filled with non-transparent tap water. For spatial coordination, the pool was divided into four virtual quadrants that were defined based on their spatial relationship to the platform: left, right, opposite and target quadrant, which contains the goal platform.

During the cued training the platform was marked with a triangular flag and both, platform and starting position were changed in the four trials per day with an ITI of 15 min.

During acquisition training, spatial visual cues were fixed on the edge of the pool and the triangular flag was removed from the platform. This testing phase consisted of four trials per day over five consecutive days. Same trial procedures as for cued training were conducted.

The probe trial started 24 h after the last day of acquisition training to assess spatial reference memory at the end of the learning period. During the probe trial, the platform was removed from the pool and the mice were allowed to swim freely for 60 s.

To record escape latency, swimming speed and quadrant preference, ANY-Maze video tracking software (Stoelting Co., Wood Dale, IL, USA) was used.

Open Field and Novel Object Recognition

The open field (OF) test was used to assess locomotor activity and exploratory behavior as described by Jawhar et al. (2012). During the OF test, mice were placed into a square box where they could freely explore the area for 5 min. ANY-Maze video tracking software was used to record the percentage of time spent in the central part vs. total time and total distance traveled during a single 5-min trial.

Twenty-four hours after later, Novel Object Recognition Test (NORT) was performed in the same box, now containing two identical objects during the first testing day. The NORT is a widely used test to assess memory and preference for novelty in rodents (Antunes and Biala, 2012). Mice were allowed to explore freely for 5 min. On day two of NORT, one of the objects was replaced by a novel object and the test time stayed the same. ANY-Maze video tracking software (Stoelting Co., Wood Dale, IL, USA) was used to record the distance traveled, percentage of time spent in the center and the exploration time of each object.

The percentage of exploration time for the novel object was calculated as follows:

$$\text{Novel Object [\%]} = \left(\frac{\text{Novel Object}}{\text{Novel Object} + \text{Familiar Object}} * 100 \right)$$

Dark Light Box

The Dark Light Box (DLB) was used to test for possible anxiolytic- or anxiogenic-like effects of prolonged CBD in C57BL/6J mice. This test is based on the innate aversion of rodents to brightly illuminated areas and on the spontaneous exploratory behavior of rodents in response to mild stressors, such as a novel environment and light (Bourin and Hascoët, 2003). The test was performed using a gray plastic box (73 cm \times 25 cm \times 32 cm), which was divided into two areas: a smaller dark area (31 cm \times 25 cm), covered by a black sheet made of plexiglass, and a larger light area (42 cm \times 31 cm), which was not covered. These two areas were separated by a gray wall with a small opening (5 cm \times 5 cm), allowing the mice to move freely from one compartment to the other. Each mouse was introduced into the light area facing the wall opposite of the small opening and was allowed to explore the space freely for 300 s. ANY-Maze video tracking software (Stoelting Co., Wood Dale, IL, USA) was used to record the time spent in each compartment and the number of line crossings.

Elevated Plus Maze

The Elevated Plus Maze (EPM) test was used to assess anxiety-related behavior in C57BL/6J mice as previously described (Jawhar et al., 2012). The apparatus with a shape of a “+” consisted of four arms and a central area raised 75 cm above a padded surface.

Mice were placed in the center facing one of the two likewise oppositely positioned open arms and were allowed to freely explore the maze for 300 s. Distance traveled and the time spent in the open arms were recorded using ANY-Maze video tracking software (Stoelting Co., Wood Dale, IL, USA). Anxiety-like behavior can be measured by the time spent in the open arms as lower anxiety levels correspond to longer time spent in open arms (Karl et al., 2003).

Prepulse Inhibition

The prepulse inhibition (PPI) was used as a test for sensorimotor gating (Pouzet et al., 1999). Each mouse was placed individually in a small metal grid cage (90 mm \times 40 mm \times 40 mm) to restrict exploratory behavior and major movements. The cage was equipped with a movable platform floor attached to a sensor recording vertical movements of the floor. The cage was placed in a sound-attenuating isolation cabinet (TSE GmbH, Bad Homburg, Germany). Each experimental session started with a 3 min habituation period to 65 dB background white noise (continuous throughout the session) followed by a 2-min baseline recording. Loudspeakers on both sides of the cage were used to induce startle reflexes by acoustic stimuli. A startle reaction to an acoustic stimulus including body muscle contractions and jumping causes movement of the platform. A transient force resulting from this movement was recorded during a time window of 100 ms beginning with the onset of the acoustic stimulus.

Six pulse-alone trials using startle stimuli of 120 dB and 40 ms were applied after the baseline recording. PPI was tested applying the 120 dB 40 ms startle pulse alone or preceded by a prepulse 20 ms stimulus of 70-, 75- or 80 dB. An interval of 100 ms with background noise was applied between each prepulse and pulse stimulus. Ten trials of startle response alone, no stimulus trials and pulse preceded by a 70-, 75- or 80 dB prepulse were applied in a pseudorandom order with ITIs from 8 to 22 s. Maximum amplitudes for all types of trials were averaged for every mouse. PPIs at each sound level were calculated using the following formula:

$$\text{Prepulse inhibition [\%]} = \left(1 - \frac{\text{average startle amplitude after prepulse and pulse}}{\text{average startle amplitude after pulse alone}} * 100 \right)$$

Quantification of Neuron Numbers Using Unbiased Stereology

Stereological analysis was used to obtain the overall neuron number in the CA1 region of hippocampus as previously described (Bouter et al., 2013). Briefly, the hemisphere was cut into coronal sections of 30 μm thickness, of which every tenth was systematically collected and stained with cresyl violet. The stereological analysis required a working station (Olympus BX51 with a motorized specimen stage for automatic sampling, StereoInvestigator 7; Microbrightfield, Williston, VT, USA). The CA1 region of sections from Bregma -1.34 mm to -3.80 mm were counted in, using a $100\times$ oil lens (NA = 1.35). Neurons were counted with the optical dissector method; consequently, the total number of neurons was estimated by the optical fractionator method using a 2 μm top guard zone (West et al., 1991). The volume was calculated following Cavalieri's principle (Rosen and Harry, 1990).

Statistical Analysis

Differences between groups were tested with one-way and two-way analysis of variance (ANOVA) followed by Bonferroni multiple comparison or unpaired *t*-test as indicated. All data presented as mean \pm standard error of the mean (SEM). Significance levels are set as follows: *****p* < 0.0001; ****p* < 0.001; ***p* < 0.01; **p* < 0.05. All statistics were calculated using GraphPad Prism version 6.07 for Windows (GraphPad Software, San Diego, CA, USA).

RESULTS

Cannabidiol Treatment Does Not Affect Motor Performance of C57BL/6J Mice

No significant treatment effect was found in either former or current group (Figures 2A,C; two-way repeated measures ANOVA: *treatment* former: $F_{(1,27)} = 1.792$, *p* = 0.1919; *treatment* current: $F_{(1,36)} = 0.7475$, *p* = 0.393). Both vehicle and CBD-treated animals of the former and current treated groups showed a significant increase in motor performance over the eight trials (two-way repeated measures ANOVA: *trials* former:

$F_{(7,189)} = 23.02$, *p* < 0.0001; *trials* current: $F_{(7,252)} = 21.10$, *p* < 0.0001).

Cannabidiol Treatment Has No Influence on Body Weight

Former and current CBD-treated mice displayed similar weight compared to same-aged vehicle-treated mice over the 6 weeks of treatment (Figures 2B,D; two-way repeated measures ANOVA, *treatment* former: $F_{(1,27)} = 1.045$, *p* = 0.32; *treatment* current: $F_{(1,36)} = 0.627$, *p* = 0.434).

Cannabidiol Treatment Does Not Alter Spatial Memory

In the cued training period, for both, former and current groups, vehicle and CBD-treated mice showed a significant decline in escape latency over time (Figures 3A,E; two-way repeated measures ANOVA, *days* former: $F_{(2,81)} = 25.78$, *p* < 0.0001; *days* current: $F_{(2,107)} = 85.89$, *p* < 0.0001). CBD-treated mice of the current group required significantly more time to find the platform only on day one than vehicle-treated mice (Figure 3E; two-way repeated measures ANOVA followed by Bonferroni multiple comparisons, *treatment* day 1: *p* < 0.0001). No overall differences in swimming speed could be detected between the age and treatment groups (data not shown; two-way repeated measures ANOVA, *treatment*). The cued training period revealed that all mice had an intact vision and the motoric abilities to swim.

Across the 5 days of acquisition training all animals, irrespective of treatment showed a significant decrease in the escape latencies (Figures 3B,F; two-way repeated measures ANOVA, *days* former: $F_{(4,134)} = 17.49$, *p* < 0.0001; *days* current: $F_{(4,174)} = 29.65$, *p* < 0.0001). During acquisition training no significant difference in swimming speed between the groups could be detected (data not shown; two-way repeated measures ANOVA, *treatment*).

Cannabidiol Treatment Does Not Affect Spatial Reference Memory

Twenty-four hours after the last acquisition trial, a probe trial was performed to assess spatial reference memory. Both the vehicle- and CBD-treated mice of the former group displayed a significantly higher preference for the target quadrant, as indicated by the relative time spent in the different quadrants of the pool (Figure 3C; one-way repeated measures ANOVA followed by Bonferroni multiple comparisons, *former* vehicle: $F_{(3,52)} = 59.81$, *p* < 0.0001; Bonferroni for target quadrant vs. left, vs. right and vs. opposite quadrant: *p* < 0.0001; *former* CBD: $F_{(3,56)} = 62.72$, *p* < 0.0001, Bonferroni target quadrant vs. left, vs. right and vs. opposite quadrant: *p* < 0.0001). The swimming speed of the former group revealed no differences between the groups (Figure 3D; *former*: unpaired *t*-test, $F_{(14,13)} = 1.29$, *p* = 0.367).

In the same way, mice of the current CBD treatment group showed a significant preference for the target quadrant (Figure 3G; one-way repeated measures ANOVA followed by Bonferroni multiple comparisons *current* vehicle: $F_{(3,72)} = 25.73$, *p* < 0.0001, Bonferroni for target quadrant vs. left, vs. right and

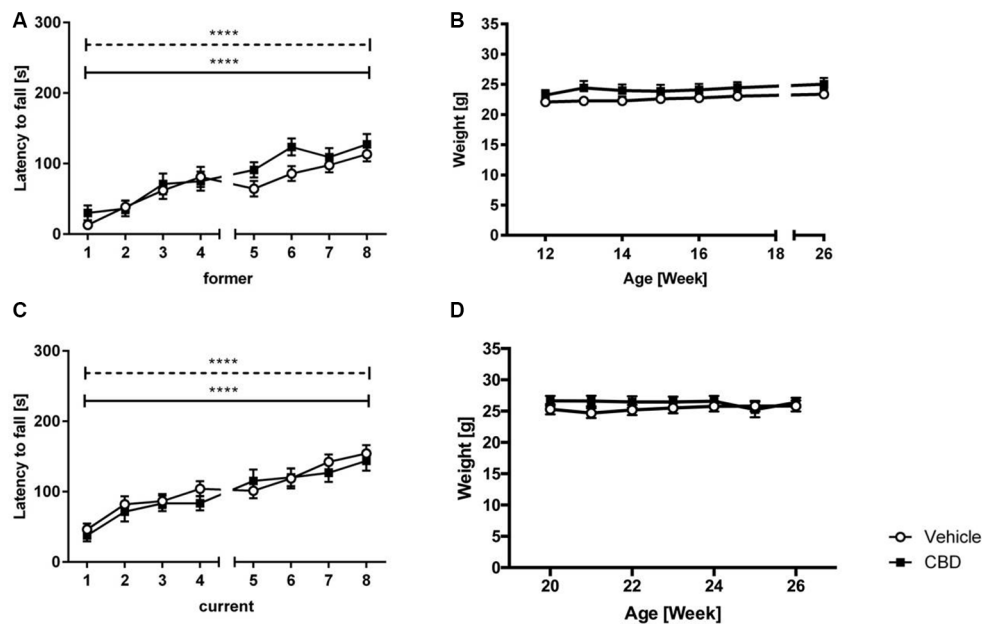


FIGURE 2 | CBD treatment does not influence motor performance of C57BL/6J mice. Latency to fall (A) and weight (B) for former CBD-treated C57BL/6J mice. No significant treatment effect between vehicle and CBD in the current treated group (C). Both groups showed an increased latency to fall over the training trials. No significant difference in weight in the current treatment group (D). s = seconds, $n = 14-19$, **** $p < 0.0001$; two-way repeated measures analysis of variance (ANOVA) followed by Bonferroni multiple comparisons. Data presented as mean \pm SEM.

vs. opposite quadrant: $p < 0.0001$; *current* CBD: $F_{(3,72)} = 20.88$, $p < 0.0001$, Bonferroni target quadrant vs. left, vs. right and vs. opposite quadrant: $p < 0.0001$). No difference in swimming speed was found among the current treatment groups (Figure 3H; *current*: unpaired t -test, $F_{(18,19)} = 1.88$, $p = 0.368$).

Our results show that prolonged CBD treatment does not impair spatial learning in C57BL/6J mice compared to vehicle-treated C57BL/6J mice, irrespective of the treatment time.

Cannabidiol Does Not Affect Memory in the Novel Object Recognition Test

In the former treatment group, CBD-treated mice showed a clear preference for the novel object (Figure 3I; *former* CBD: paired t -test, $p = 0.0002$), which is seen in vehicle-treated mice, too (Figure 3I; *former* vehicle: paired t -test, $p = 0.0263$). In the current treatment group, CBD-treated mice showed a trend towards a preference for the novel object (Figure 3J; *current* CBD: paired t -test, $p = 0.0684$), whereas current vehicle-treated mice did not (Figure 3J; *current* vehicle: paired t -test, $p = 0.7866$).

Cannabidiol Does Not Affect Anxiety Behavior in the Dark Light Box

In both, the former and current treatment group, CBD-treated mice did not explore the light box longer than the vehicle-treated mice (Figure 4A; *former*: unpaired t -tests; $F_{(12,14)} = 1.502$, $p = 0.101$; Figure 4G; *current*: unpaired t -tests: $F_{(18,17)} = 1.44$, $p = 0.464$). Regarding the former group, CBD-treated mice crossed the line slightly more often than vehicle mice (Figure 4B; *former*: unpaired t -test, $F_{(13,13)} = 2.03$, $p = 0.672$). In the

current treatment group, there was no difference measured in the number of line crossings observed between CBD and vehicle-treated mice (Figure 4H; *current*: unpaired t -test, $F_{(18,17)} = 2.47$, $p = 0.095$).

Current Cannabidiol Treatment Alters Anxiety Behavior in the Elevated Plus Maze

Former CBD-treated animals did not show a significant difference in the amount of time spent in the open arms compared to vehicle-treated controls (Figure 4C; *former*: unpaired t -test, $F_{(14,13)} = 3.759$, $p = 0.2856$). In contrast, current CBD-treated mice showed a significant decrease in the time spent in the open arms vs. vehicle-treated control mice (Figure 4I; *current*: unpaired t -test, $F_{(18,19)} = 3.344$, $p = 0.0134$). The distance traveled was investigated to assess the confounding factor of movement. No significant difference in the distance traveled could be observed between the two different treatment groups, either with former or current treatment (Figure 4D; *former*: unpaired t -test $F_{(14,13)} = 1.247$, $p = 0.2642$; Figure 4J; *current*: unpaired t -test $F_{(18,19)} = 2.850$, $p = 0.0969$).

Prolonged Cannabidiol Treatment Results in Lower Locomotor Activity in the Open Field

No significant difference between former vehicle and CBD-treated groups in regard to the time spent in the center could be detected (Figure 4E; *former*: unpaired t -test, $F_{(14,12)} = 2.890$, $p = 0.4435$). However, there was a significant difference in the distance traveled for a former treated vehicle

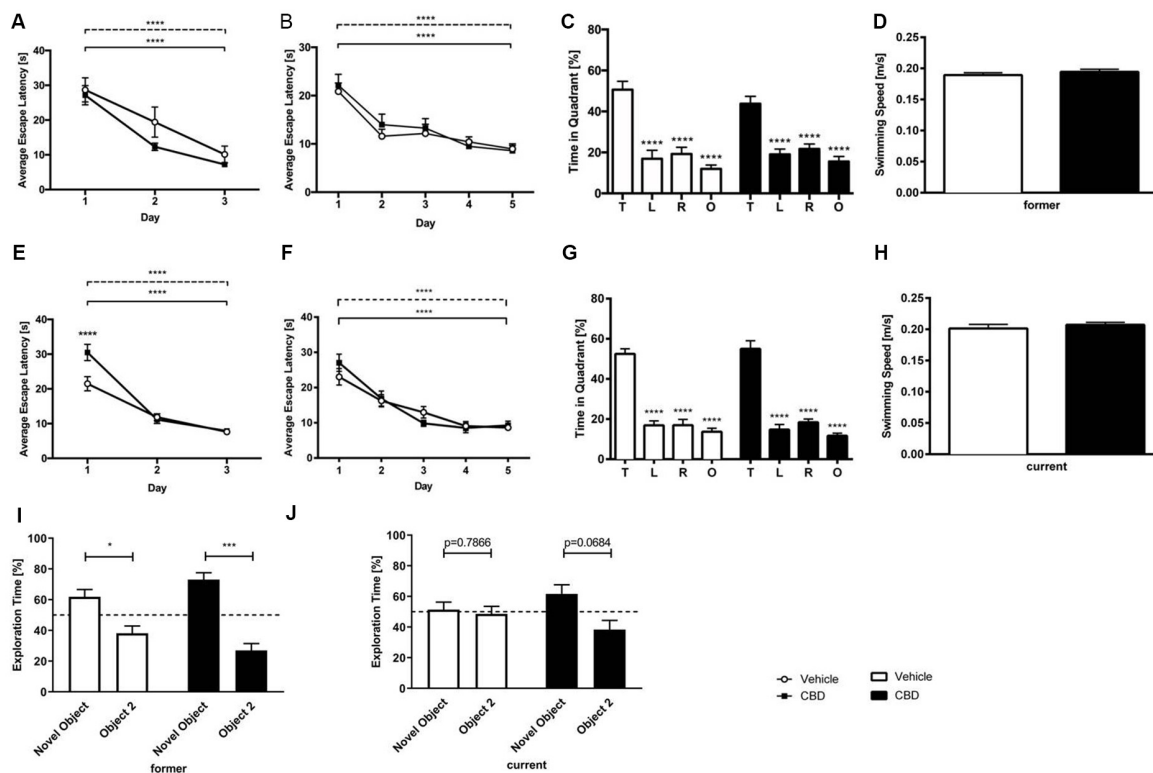


FIGURE 3 | CBD treatment does not affect spatial learning and long term memory. CBD-treated and control mice of the former group displayed intact motor and visual performance in the Morris Water Maze (MWM; **A**). No impairment of spatial learning due to CBD treatment in acquisition training was seen in former treated mice (**B**). The probe trial revealed that the long term memory was not affected by prolonged CBD treatment in C57BL/6J mice of the former group as they spent significantly more time in the target quadrant compared to the other quadrants of the maze (**C**). The swimming speed during probe trial was not affected (**D**). Current treated mice proved visual and motor abilities to swim in cued training (**E**). Spatial learning was not altered as mice of the current group improved significantly during acquisition training (**F**). In probe trial, current CBD-treated mice and vehicle-control mice displayed a clear preference for the target quadrant (**G**). The swimming speed of the mice of the current group during probe trial did not differ significantly (**H**). Furthermore, CBD treatment did not affect memory in novel object recognition (NOR) in the former group (**I**). Whereas current CBD-treated mice (**J**) showed a trend towards novelty preference, former treated mice showed clear preferences for the novel object. Fifty percent chance level is indicated by a dashed line. Two-way (**A,B,E,F**) and one-way (**C,G**) ANOVA followed by Bonferroni multiple comparisons, unpaired *t*-test (**D,H**), paired *t*-test (**I,J**); $n = 14-19$, **** $p < 0.0001$; *** $p < 0.001$; * $p < 0.05$. Data presented as mean \pm SEM.

vs. the CBD-treated group (Figure 4F; *former*: unpaired *t*-test, $F_{(13,14)} = 1.441$, $p = 0.0081$).

Similarly, current vehicle-treated mice traveled significantly more than CBD-treated mice (Figure 4L; *current*: unpaired *t*-test, $F_{(19,18)} = 3.861$, $p = 0.0258$), but did not spend significantly more time in the center than current vehicle-treated mice (Figure 4K; *current*: unpaired *t*-test, $F_{(19,18)} = 1.235$, $p = 0.4084$).

Cannabidiol Treatment Does Not Alter Acoustic Startle Response in C57BL/6J Mice

The acoustic startle response (ASR) to the startle stimulus alone was measured in CBD- and vehicle-treated C57BL/6J animals (Figure 5). Former (Figure 5A) and current (Figure 5D) CBD-treated C57BL/6J mice showed an unaltered startle response compared to same-aged vehicle C57BL/6J mice (*former*: unpaired *t*-test, $F_{(14,11)} = 1.960$, $p = 0.2672$; *current*: unpaired *t*-test, $F_{(14,14)} = 1.754$, $p = 0.3048$). Furthermore, the latency to startle was comparable between CBD and vehicle-treated

animals (Figure 5B *former*: unpaired *t*-test, $F_{(14,11)} = 2.124$, $p = 0.8995$; Figure 5E *current*: unpaired *t*-test, $F_{(14,14)} = 1.547$, $p = 0.801$).

Current Cannabidiol Treatment Impairs Prepulse Inhibition in C57BL/6J Mice

Current CBD wildtype (WT) treated mice displayed a significantly lower PPI compared to same-aged WT animals at 75 dB and 80 dB (Figure 5F; two-way repeated measures ANOVA: *treatment* *current*: $F_{(1,28)} = 10.95$, $p = 0.0026$; Bonferroni multiple comparison, vehicle vs. CBD: 75 dB $p < 0.05$ and 80 dB: $p < 0.01$). In contrast, former CBD treatment did not affect PPI (Figure 5C; two-way repeated measures ANOVA, *treatment* *former*: $F_{(1,25)} = 0.5182$, $p = 0.4783$).

No Adverse Effect of CBD on Hippocampal Neuron Number

Design-based stereological analysis revealed that the hippocampal neuron numbers of the CA1 region did not

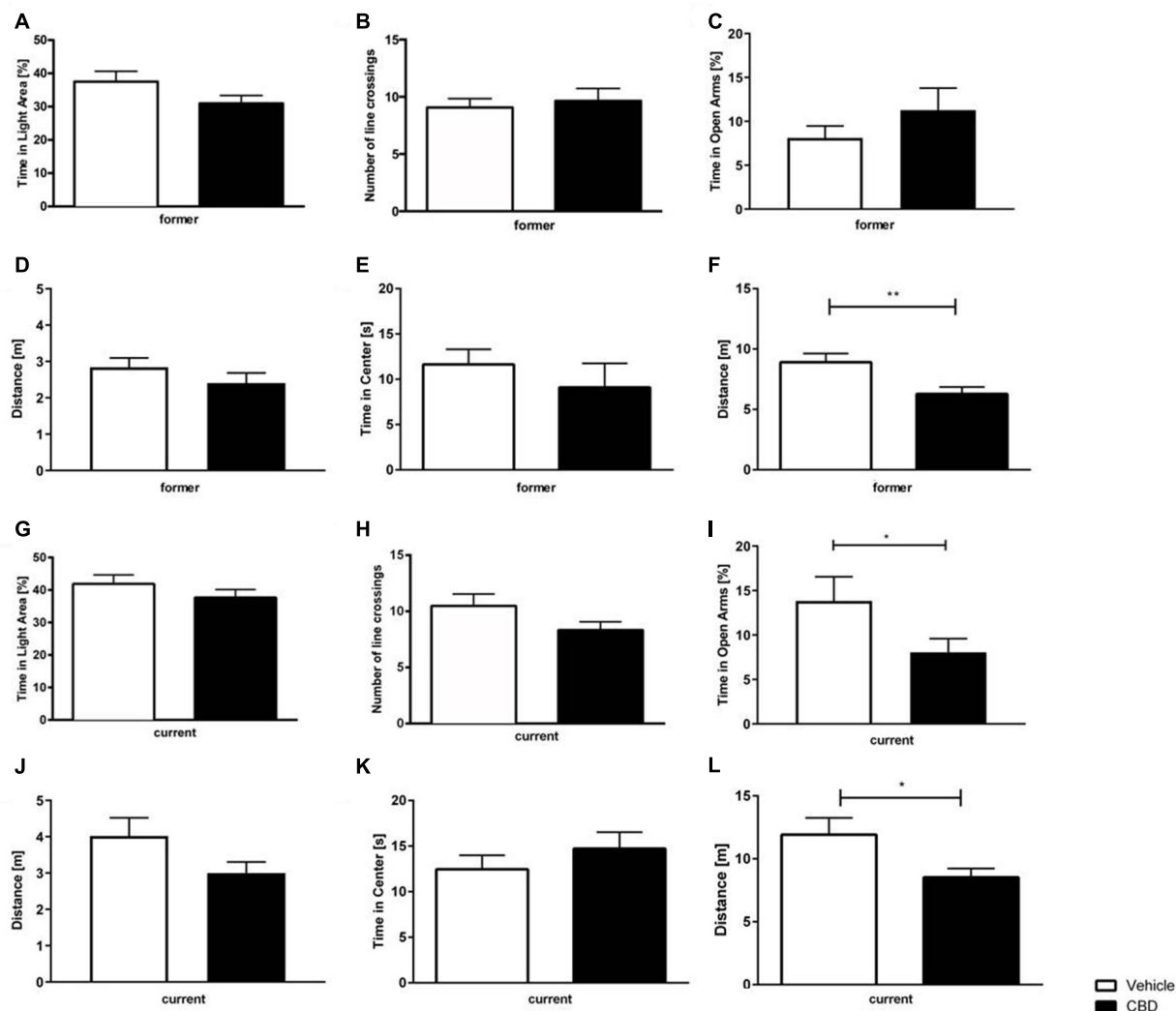


FIGURE 4 | Effects of prolonged CBD treatment on anxiety-related behavior. No significant difference in time spent in the light area in former CBD-treated mice (**A**). Number of line crossings as a confounding factor of mobility in the dark light box (DLB) did not significantly differ for the former treated group (**B**). Time spent in the open arms expressed as a percentage of total time spent in the maze (**C**) and traveled distance in the elevated plus maze (EPM) for former treated mice (**D**). In the open field (OF), there was no significant difference in time spent in the center of the box in former treatment group (**E**). Thus, a higher locomotor activity for vehicle-treated mice was found in the former CBD-treated mice (**F**). The time spent in the light area in current CBD-treated mice did not differ (**G**), as well as the number of line crossings in the DLB (**H**). Current CBD-treated mice showed a significant decrease in time spent in the open arms (**I**) but no difference in the distance traveled in the EPM (**J**). No significant difference between current CBD-treated mice and their vehicle-treated littermates in the time in the center (**K**), thus current CBD-treated mice traveled less distance in the OF (**L**). Unpaired *t*-test; *n* = 14–19, ***p* < 0.01; **p* < 0.05. Data presented as mean ± SEM.

significantly differ after former and current prolonged CBD treatment compared to the vehicle-treated mice (**Figure 6A**, one-way repeated measures ANOVA, $F_{(3,36)} = 0.224$, $p = 0.879$, former vehicle = $254,750 \pm 11,038$, former CBD = $255,240 \pm 10,437$; current vehicle = $260,663 \pm 9,635$, current CBD = $247,134 \pm 14,129$).

Likewise, no significant difference in volume of hippocampal CA1 region could be observed in the former or current group (**Figure 6B**; one-way repeated measures ANOVA, $F_{(3,36)} = 1.198$, $p = 0.324$; former: vehicle = $2.869 \times 10^8 \pm 1.806 \times 10^7$, CBD = $2.655 \times 10^8 \pm 1.005 \times 10^7$; current: vehicle = $2.965 \times 10^8 \pm 6.610 \times 10^6$, CBD = $2.967 \times 10^8 \pm 1.634 \times 10^7$).

The average number of sections counted was nine with a base of $196 \mu\text{m}$ and an optical dissector height of $5 \mu\text{m}$. The average number of sections counted was nine with a base of $196 \mu\text{m}$ and an optical dissector height of $5 \mu\text{m}$. The average predicted coefficient of error of the estimated total number of neurons was as followed: former vehicle: 0.056; former CBD: 0.056; current vehicle: 0.051; current CBD: 0.054.

DISCUSSION

CBD has been discussed as a therapy for neurodegenerative diseases including multiple sclerosis as well as diseases known

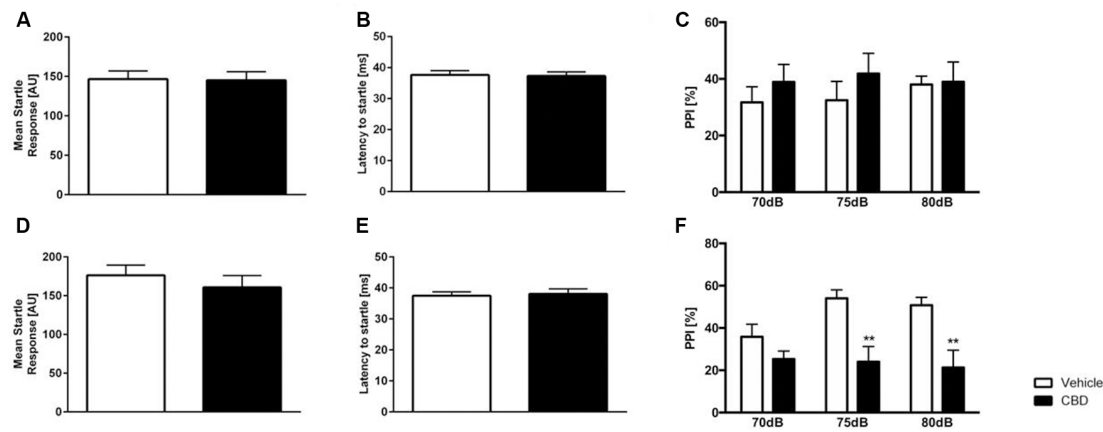


FIGURE 5 | Altered prepulse inhibition (PPI) in CBD-treated C57BL/6J mice. Former (A) and current (D) CBD-treated C57BL/6J mice showed an unaltered acoustic startle response (ASR) and latency to startle (B,E). PPI (PPI%) was unaltered in former CBD-treated C57BL/6J (C). PPI was significantly altered in current treated CBD C57BL/6J mice at 75 dB and 80 dB (F). Two-way ANOVA, $n = 12-15$, $**p < 0.01$. Data presented as mean \pm SEM.

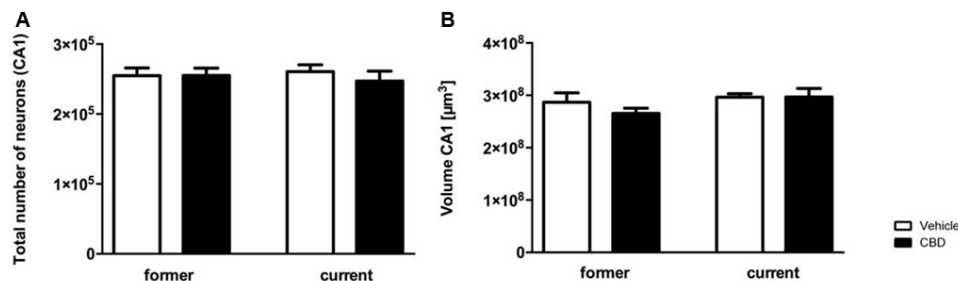


FIGURE 6 | Prolonged CBD treatment does not affect hippocampal neuron numbers and volumes in C57BL/6J mice. The CA1 region was counted from Bregma -1.34 mm to -3.80 mm. Former as well as current CBD treatment had no influence on the total number of neurons in the CA1 region (A). The CA1 volumes of the CBD and vehicle-treated mice in the former and the current group did not differ significantly (B). One-way ANOVA (A,B); $n = 9-11$. All data presented as mean \pm SEM.

for involving activation of the immune system and associated with oxidative stress (Iuvone et al., 2009; Krishnan et al., 2009; Scuderi et al., 2009; Booz, 2011). While most studies concentrate on THC, only a few studies investigate CBD treatment in healthy mice. However, there is evidence for many positive effects of prolonged CBD treatment on several brain-associated diseases like brain ischemia and epilepsy. Interestingly, positive effects of CBD treatment could be shown in mice with multiple sclerosis. CBD-treated mice with a dose of 5 mg/kg for 7–10 days reduced infiltration of leukocytes and the expression of cytokines (Mecha et al., 2013). Similarly, Patra et al. (2019) demonstrated a reduction of seizure burden as well as seizure severity in epilepsy models of rats and mice treated with CBD. In contrast to the probably most known constituent of the cannabis plant, THC, the mechanism of action for CBD remains still unclear, mainly because it involves several pharmacological targets (De Petrocellis and Di Marzo, 2010). Regarding the rising amount of CBD-containing lifestyle products (e.g., cosmetics, energy bars, drinks) more and more people consume CBD in their everyday life. This emphasizes the importance of studies in healthy rodents and humans.

Our study examines the influence of prolonged CBD treatment on healthy adult C57BL/6J mice and its consequences on behavior and hippocampal neuron numbers. Mice were divided into two treatment groups: a former treatment group and a current treatment group. The former treatment group received daily intraperitoneal injections of 20 mg/kg CBD-solution or vehicle-solution starting at the age of 3 months, while the current treatment group got the same treatment but started at the age of 5 months. Both groups started behavior testing at 6 months age. The aim of our study was to compare the influence of prolonged CBD treatment (current group) to the effects of prolonged CBD treatment with a washout period (former group) in adult mice.

It is described that there are sex differences in the modulation and expression of the endocannabinoid system. Cannabinoid exposure during adolescence has been shown to have long term consequences on brain and behavior (Andersen, 2003). Using cannabinoids during adolescence is more concerning because the endocannabinoid system is developed especially in this lifetime period and thus more vulnerable to exogenous insults as exposure of cannabinoids (Rice and Barone, 2000). It is known that gonadal hormones modulate the effects in cannabinoids in

adult rodents, which were used in our study (Marusich et al., 2015). Several studies suggested that female rodents are more sensitive to the effects of THC than males (Craft et al., 2012; Marusich et al., 2014). Nevertheless, there is no evidence about the effects of CBD on the modulation of the endocannabinoid system. In our study, there was no gender difference regarding behavior (data not shown).

To evaluate the effect of chronic CBD treatment on reference and spatial memory, mice performed the MWM. No effect on spatial memory and long term memory could be observed. These findings correlate with the results of Fadda et al. (2004) who found no spatial learning impairments in CBD-treated rats in the MWM. Even at doses of up to 50 mg/kg CBD treatment had no effect on spatial working memory in these rats. Interestingly, research in a pharmacological mouse model of Alzheimer's disease revealed positive effects of 20 mg/kg CBD treatment in the MWM (Martín-Moreno et al., 2011).

Learning in the MWM is highly dependent on the hippocampus (D'Hooze and De Deyn, 2001), therefore, the effect of CBD treatment on the neuron number in the CA1-region of the hippocampus was analyzed. No significant difference in the number of neurons or the volume of the hippocampus was detected after CBD treatment. Interestingly, Schiavon et al. (2014) showed that CBD treatment reduced MWM deficits and hippocampal neurodegeneration in response to brain ischemia in mice in a dose-dependent way. Likewise, Mori et al. (2017) observed a protective effect of acute treatment with 10 mg/kg CBD 30 min before and 3, 24 and 48 h after operation induced brain ischemia on neurodegeneration in the hippocampus. In a recently performed MRI study with regular cannabis users there was, in accordance to our findings, no difference in total hippocampal volume observed after treatment with CBD, while left subicular complex volume significantly increased from baseline to post-treatment, indicating a restorative effect of CBD on the subicular and CA1 subfields in cannabis users (Beale et al., 2018).

Similar to our findings in the MWM, there is no significant difference for NORT, concerning non-spatial learning and memory in C57BL/6J mice after prolonged CBD treatment. Both vehicle- and CBD-treated groups of former treatment showed a clear preference to the novel object. Our results are in line with Fagherazzi et al. (2012) who showed that CBD (5 mg/kg or 10 mg/kg for 14 days) does not affect memory of male adult rats in the NORT, neither were general parameters of behavior such as exploratory activity, locomotion and anxiety affected. Interestingly, their study also provides evidence that CBD might rescue memory impairments associated with brain disorder. This is in line with the results of Pazos et al. (2012) after hypoxic-ischemic injury via electrocoagulation.

Although CBD-treated mice traveled less distance in the OF test, they still had a clear preference to the novel object which excludes the confounding factor of locomotion. This stands in contrast with the findings of Viudez-Martínez et al. (2018) that CBD does not alter motor behavior 12 h after its administration of 30 mg/kg for 6 days in the OF test.

While CBD-treated mice showed an altered locomotion their motor performance in the Rotarod test was intact.

Interestingly, Navarrete et al. (2018) observed a normalization of cannabis motoric withdrawal behavior signs in adult male C57BL/6J mice. This effect is similar to the observation in healthy volunteers where CBD blocked the anxiety produced by THC (Zuardi et al., 1982).

Considering the significance of the endocannabinoid system for energy metabolism and feeding behavior, we examined the effects of prolonged CBD administration on body weight gain in C57BL/6J mice. In the current study, long term CBD administration did not affect the food uptake and appetite of mice as CBD-treated mice displayed similar weight compared to same-aged vehicle-treated mice. These results are in contrast with previous findings from Riedel and colleagues who reported that acute CBD treatment (10 mg/kg, one injection) induced a small although non-significant reduction in food intake and weight gain (Riedel et al., 2009). Furthermore, CBD treatment was shown to decrease the weight gain in rats (5 mg/kg for 14 days; Ignatowska-Jankowska et al., 2011). In adult male rats, oral administration of CBD (4.4 mg/kg) induced a significant reduction in total food intake over 4 h of test time (Farrimond et al., 2012). As we treated our mice for 42 days, these different findings may be the result of a habituation of the mice to the longer treatment time with CBD. To our knowledge, there is no data about the influence of CBD for human weight and stimulation of appetite, which makes further studies much more necessary. In contrast, there is evidence that synthetic THC (Dronabinol) is associated with an increase in weight when compared to placebo in HIV positive humans (Whiting et al., 2015).

A significance towards less distance traveled by CBD-treated mice in former and current treatment group could be observed in the OF, whereas the number of line crossings as a comparable parameter for distance in the DLB differed between current and former treatment. The OF test is a common measure of exploratory behavior and general activity with less focus on anxiety than the EPM. Increased anxiety probably results in less locomotion and in the OF test in the preference to stay in the periphery of the box (Ennaceur, 2014). Regarding the results of both tests, an increased anxiety behavior could be discussed as it is significantly shown in the current CBD-treated group compared to their vehicle-treated littermates. A moderate anxiolytic-like effect in the OF test in C57BL/6J mice at 50 mg/kg dose of CBD daily treated for 3 weeks, was observed by Long et al. (2010), whereas even a dose of 1 mg/kg significantly increased the time spent in the light compartment. After observing effects in chronic CBD treatment, Long et al. (2010) investigated the acute behavioral effects of CBD (1 mg/kg; 50 mg/kg) but no significant anxiolytic effects in the EPM could be found. In contrast to those findings, the current CBD-treated group in our study showed a significant decrease in the time spent in the open arms. Therefore, there is an anxiogenic-like effect of the current group in the EPM. Rats treated with lower doses of CBD (2.5, 5, 10 mg/kg) showed a significant increase in the entry ratio (open/total numbers of entries) which can be seen as an anxiolytic effect (Guimarães et al., 1990). Whereas a dose of 20 mg/kg had no effect compared to vehicle-treated male Wistar rats. This finding indicates that there is a limited range of

anxiolytic doses and that the application and the following results are different in mice and rats. While CBD can be beneficial for treating anxiety, the beginning and the duration of the treatment is crucial and has to be considered and discussed in every treatment approach.

CBD treatment did not alter ASR in WT mice. Sensory gating describes the inhibition of a stimulus-related neuronal response if the stimulus is preceded by a subthreshold warning stimulus (Ally et al., 2006). Sensory gating can be measured using PPI, a method that can be studied with similar procedures in humans and rodents and reflects the ability to exclude sensory information from processing (Braff and Geyer, 1990). Current CBD altered sensorimotor gating, whereas former treated mice did not affect PPI. Our findings are well in line with the findings of Long et al. (2010) that there was no effect of CBD in ASR independent from the different acute treatment doses (1, 5, 10 or 50 mg/kg), although acute and chronic (1 mg/kg) CBD treatment altered PPI. In Swiss mice, CBD treatment with 5 mg/kg had no effect on PPI but dose-dependently increased the startle response and reversed a MK-801-induced PPI deficit (Long et al., 2006).

Interestingly, altered sensory gating has been well documented in different psychiatric conditions including schizophrenia (Gjini et al., 2011; Rohleder et al., 2016). However, the influences of CBD on ASR and PPI in animal models of schizophrenia have been inconsistent. CBD treatment reversed PPI disruptive effects of MK-801 and amphetamine in mice, while CBD had no effect in rats treated with MK-801 (Gururajan et al., 2011; Gomes et al., 2014; Pedrazzi et al., 2015).

The effects of CBD on startle response and PPI seem to be highly species-, strain- and dose-dependent. However, the mechanism involved in CBD action on PPI is not yet understood, highlighting the need for more studies to clarify the relationship between CBD and PPI.

To summarize our findings, no side effects in C57BL/6J mice were evident regarding memory, motoric abilities or anxiety behavior after long term CBD treatment. Based on these results

it can be speculated that prolonged CBD treatment could be beneficial and safe for the treatment of a variety of conditions.

DATA AVAILABILITY

The datasets generated for this study are available on request to the corresponding author.

ETHICS STATEMENT

All animals were handled according to the guidelines of the Federation of European Laboratory Animal Science Association (FELASA) and approved by the “Lower Saxony State Office for Consumer Protection and Food Safety” (LAVES).

AUTHOR CONTRIBUTIONS

ES and FO performed experiments, analyzed data and wrote the manuscript. MS, JW, BS, MM and ML performed experiments. YB conceived and designed the project, performed experiments, analyzed data and wrote the manuscript. All authors contributed to revising the manuscript and approved the final version.

FUNDING

This work was supported by the German Research Foundation (CNMPB) to YB. This study was also supported by the Jacob-Henle-Program for Experimental Medicine of the University Medicine Goettingen to ML and JW. MS is supported by Helios Kliniken GmbH. We acknowledge the support by the Open Access Publication Funds of the Göttingen University.

ACKNOWLEDGMENTS

We thank Prof. Thomas A. Bayer for fruitful discussions.

REFERENCES

- Adams, R., Hunt, M., and Clark, J. H. (1940). Structure of cannabidiol, a product isolated from the marihuana extract of minnesota wild hemp. I. *J. Am. Chem. Soc.* 62, 196–200. doi: 10.1021/ja01858a058
- Ally, B. A., Jones, G. E., Cole, J. A., and Budson, A. E. (2006). Sensory gating in patients with Alzheimer's disease and their biological children. *Am. J. Alzheimers Dis. Other Dement.* 21, 439–447. doi: 10.1177/1533317506292282
- Andersen, S. L. (2003). Trajectories of brain development: point of vulnerability or window of opportunity? *Neurosci. Biobehav. Rev.* 27, 3–18. doi: 10.1016/s0149-7634(03)00005-8
- Antunes, M., and Biala, G. (2012). The novel object recognition memory: neurobiology, test procedure, and its modifications. *Cogn. Process.* 13, 93–110. doi: 10.1007/s10339-011-0430-z
- Atakan, Z. (2012). Cannabis, a complex plant: different compounds and different effects on individuals. *Ther. Adv. Psychopharmacol.* 2, 241–254. doi: 10.1177/2045125312457586
- Beale, C., Broyd, S. J., Chye, Y., Suo, C., Schira, M., Galettis, P., et al. (2018). Prolonged cannabidiol treatment effects on hippocampal subfield volumes in current cannabis users. *Cannabis Cannabinoid Res.* 3, 94–107. doi: 10.1089/can.2017.0047
- Blessing, E. M., Steenkamp, M. M., Manzanares, J., and Marmar, C. R. (2015). Cannabidiol as a potential treatment for anxiety disorders. *Neurotherapeutics* 12, 825–836. doi: 10.1007/s13311-015-0387-1
- Booz, G. W. (2011). Cannabidiol as an emergent therapeutic strategy for lessening the impact of inflammation on oxidative stress. *Free Radic. Biol. Med.* 51, 1054–1061. doi: 10.1016/j.freeradbiomed.2011.01.007
- Bouaboula, M., Hilairt, S., Marchand, J., Fajas, L., Le Fur, G., and Casellas, P. (2005). Anandamide induced PPAR γ transcriptional activation and 3T3-L1 preadipocyte differentiation. *Eur. J. Pharmacol.* 517, 174–181. doi: 10.1016/j.ejphar.2005.05.032
- Bourin, M., and Hascoët, M. (2003). The mouse light/dark box test. *Eur. J. Pharmacol.* 463, 55–65. doi: 10.1016/s0014-2999(03)01274-3
- Bouter, Y., Dietrich, K., Wittnam, J. L., Rezaei-Ghaleh, N., Pillot, T., Papot-Couturier, S., et al. (2013). N-truncated amyloid β (A β) 4–42 forms stable aggregates and induces acute and long-lasting behavioral deficits. *Acta Neuropathol.* 126, 189–205. doi: 10.1007/s00401-013-1129-2
- Bouter, Y., Kacprowski, T., Weissmann, R., Dietrich, K., Borgers, H., Brauf, A., et al. (2014). Deciphering the molecular profile of plaques, memory decline and neuron loss in two mouse models for Alzheimer's disease by deep sequencing. *Front. Aging Neurosci.* 6:75. doi: 10.3389/fnagi.2014.00075

- Braff, D. L., and Geyer, M. A. (1990). Sensorimotor gating and schizophrenia. Human and animal model studies. *Arch. Gen. Psychiatry* 47, 181–188. doi: 10.1001/archpsyc.1990.01810140081011
- Burstein, S. (2015). Cannabidiol (CBD) and its analogs: a review of their effects on inflammation. *Bioorg. Med. Chem.* 23, 1377–1385. doi: 10.1016/j.bmc.2015.01.059
- Craft, R. M., Wakley, A. A., Tsutsui, K. T., and Laggart, J. D. (2012). Sex differences in cannabinoid 1 vs. cannabinoid 2 receptor-selective antagonism of antinociception produced by delta9-tetrahydrocannabinol and CP55,940 in the rat. *J. Pharmacol. Exp. Ther.* 340, 787–800. doi: 10.1124/jpet.111.188540
- Cunha, J. M., Carlini, E. A., Pereira, A. E., Ramos, O. L., Pimentel, C., Gagliardi, R., et al. (1980). Chronic administration of cannabidiol to healthy volunteers and epileptic patients. *Pharmacology* 21, 175–185. doi: 10.1159/000137430
- De Petrocellis, L., and Di Marzo, V. (2010). Non-CB1, non-CB2 receptors for endocannabinoids, plant cannabinoids, and synthetic cannabimimetics: focus on G-protein-coupled receptors and transient receptor potential channels. *J. Neuroimmune Pharmacol.* 5, 103–121. doi: 10.1007/s11481-009-9177-z
- D'Hooge, R., and De Deyn, P. P. (2001). Applications of the Morris water maze in the study of learning and memory. *Brain Res. Rev.* 36, 60–90. doi: 10.1016/S0165-0173(01)00067-4
- Ennaceur, A. (2014). Tests of unconditioned anxiety—pitfalls and disappointments. *Physiol. Behav.* 135, 55–71. doi: 10.1016/j.physbeh.2014.05.032
- Fadda, P., Robinson, L., Fratta, W., Pertwee, R. G., and Riedel, G. (2004). Differential effects of THC- or CBD-rich cannabis extracts on working memory in rats. *Neuropharmacology* 47, 1170–1179. doi: 10.1016/j.neuropharm.2004.08.009
- Fagherazzi, E. V., Garcia, V. A., Maurmann, N., Bervanger, T., Halmenschlager, L. H., Busato, S. B., et al. (2012). Memory-rescuing effects of cannabidiol in an animal model of cognitive impairment relevant to neurodegenerative disorders. *Psychopharmacology* 219, 1133–1140. doi: 10.1007/s00213-011-2449-3
- Farrimond, J. A., Whalley, B. J., and Williams, C. M. (2012). Cannabinol and cannabidiol exert opposing effects on rat feeding patterns. *Psychopharmacology* 223, 117–129. doi: 10.1007/s00213-012-2697-x
- Gjini, K., Burroughs, S., and Boutros, N. N. (2011). Relevance of attention in auditory sensory gating paradigms in schizophrenia A pilot study. *J. Psychophysiol.* 25, 60–66. doi: 10.1027/0269-8803/a000042
- Gomes, F. V., Issy, A. C., Ferreira, F. R., Viveros, M. P., Del Bel, E. A., and Guimarães, F. S. (2014). Cannabidiol attenuates sensorimotor gating disruption and molecular changes induced by chronic antagonism of NMDA receptors in mice. *Int. J. Neuropsychopharmacol.* 18:pyu041. doi: 10.1093/ijnp/pty041
- Guimarães, F. S., Chiaretti, T. M., Graeff, F. G., and Zuardi, A. W. (1990). Antianxiety effect of cannabidiol in the elevated plus-maze. *Psychopharmacology* 100, 558–559. doi: 10.1007/bf02244012
- Gururajan, A., Taylor, D. A., and Malone, D. T. (2011). Effect of cannabidiol in a MK-801-rodent model of aspects of schizophrenia. *Behav. Brain Res.* 222, 299–308. doi: 10.1016/j.bbr.2011.03.053
- Ignatowska-Jankowska, B., Jankowski, M. M., and Swiergiel, A. H. (2011). Cannabidiol decreases body weight gain in rats: involvement of CB2 receptors. *Neurosci. Lett.* 490, 82–84. doi: 10.1016/j.neulet.2010.12.031
- Iuvone, T., Esposito, G., De Filippis, D., Scuderi, C., and Steardo, L. (2009). Cannabidiol: a promising drug for neurodegenerative disorders? *CNS Neurosci. Ther.* 15, 65–75. doi: 10.1111/j.1755-5949.2008.00065.x
- Jawhar, S., Trawicka, A., Jenneckens, C., Bayer, T. A., and Wirths, O. (2012). Motor deficits, neuron loss and reduced anxiety coinciding with axonal degeneration and intraneuronal A β aggregation in the 5XFAD mouse model of Alzheimer's disease. *Neurobiol. Aging* 33, 196.e29–196.e40. doi: 10.1016/j.neurobiolaging.2010.05.027
- Karl, T., Pabst, R., and von Hörsten, S. (2003). Behavioral phenotyping of mice in pharmacological and toxicological research. *Exp. Toxicol. Pathol.* 55, 69–83. doi: 10.1078/0940-2993-00301
- Krishnan, S., Cairns, R., and Howard, R. (2009). Cannabinoids for the treatment of dementia. *Cochrane Database Syst. Rev.* 2:CD007204. doi: 10.1002/14651858.cd007204.pub2
- Kucerova, J., Tabiova, K., Drago, F., and Micale, V. (2014). Therapeutic potential of cannabinoids in schizophrenia. *Recent Pat. CNS Drug Discov.* 9, 13–25. doi: 10.2174/1574889809666140307115532
- Long, L. E., Malone, D. T., and Taylor, D. A. (2006). Cannabidiol reverses MK-801-induced disruption of prepulse inhibition in mice. *Neuropsychopharmacology* 31, 795–803. doi: 10.1038/sj.npp.1300838
- Long, L. E., Chesworth, R., Huang, X.-F., McGregor, I. S., Arnold, J. C., and Karl, T. (2010). A behavioural comparison of acute and chronic Delta9-tetrahydrocannabinol and cannabidiol in C57BL/6JArc mice. *Int. J. Neuropsychopharmacol.* 13, 861–876. doi: 10.1017/s1461145709990605
- Martín-Moreno, A. M., Reigada, D., Ramírez, B. G., Mechoulam, R., Innamorato, N., Cuadrado, A., et al. (2011). Cannabidiol and other cannabinoids reduce microglial activation *in vitro* and *in vivo*: relevance to Alzheimer's disease. *Mol. Pharmacol.* 79, 964–973. doi: 10.1124/mol.111.071290
- Marusich, J. A., Craft, R. M., Lefever, T. W., and Wiley, J. L. (2015). The impact of gonadal hormones on cannabinoid dependence. *Exp. Clin. Psychopharmacol.* 23, 206–216. doi: 10.1037/pha0000027
- Marusich, J. A., Lefever, T. W., Antonazzo, K. R., Craft, R. M., and Wiley, J. L. (2014). Evaluation of sex differences in cannabinoid dependence. *Drug Alcohol Depend.* 137, 20–28. doi: 10.1016/j.drugalcdep.2014.01.019
- Mecha, M., Feliú, A., Iñigo, P. M., Mestre, L., Carrillo-Salinas, F. J., and Guaza, C. (2013). Cannabidiol provides long-lasting protection against the deleterious effects of inflammation in a viral model of multiple sclerosis: a role for A2A receptors. *Neurobiol. Dis.* 59, 141–150. doi: 10.1016/j.nbd.2013.06.016
- Mechoulam, R., Hanuš, L. O., Pertwee, R., and Howlett, A. C. (2014). Early phytocannabinoid chemistry to endocannabinoids and beyond. *Nat. Rev. Neurosci.* 15, 757–764. doi: 10.1038/nrn3811
- Micale, V., Di Marzo, V., Sulcova, A., Wotjak, C. T., and Drago, F. (2013). Endocannabinoid system and mood disorders: priming a target for new therapies. *Pharmacol. Ther.* 138, 18–37. doi: 10.1016/j.pharmthera.2012.12.002
- Mori, M. A., Meyer, E., Soares, L. M., Milani, H., Guimarães, F. S., and de Oliveira, R. M. W. (2017). Cannabidiol reduces neuroinflammation and promotes neuroplasticity and functional recovery after brain ischemia. *Prog. Neuropsychopharmacol. Biol. Psychiatry* 75, 94–105. doi: 10.1016/j.pnpbp.2016.11.005
- Morris, R. (1984). Developments of a water-maze procedure for studying spatial learning in the rat. *J. Neurosci. Methods* 11, 47–60. doi: 10.1016/0165-0270(84)90007-4
- Navarrete, F., Aracil-Fernández, A., and Manzanares, J. (2018). Cannabidiol regulates behavioural alterations and gene expression changes induced by spontaneous cannabinoid withdrawal. *Br. J. Pharmacol.* 175, 2676–2688. doi: 10.1111/bph.14226
- O'Sullivan, S. E. (2007). Cannabinoids go nuclear: evidence for activation of peroxisome proliferator-activated receptors. *Br. J. Pharmacol.* 152, 576–582. doi: 10.1038/sj.bjp.0707423
- Patra, P. H., Barker-Haliski, M., White, H. S., Whalley, B. J., Glyn, S., Sandhu, H., et al. (2019). Cannabidiol reduces seizures and associated behavioral comorbidities in a range of animal seizure and epilepsy models. *Epilepsia* 60, 303–314. doi: 10.1111/epi.14629
- Pazos, M. R., Cinquina, V., Gómez, A., Layunta, R., Santos, M., Fernández-Ruiz, J., et al. (2012). Cannabidiol administration after hypoxia-ischemia to newborn rats reduces long-term brain injury and restores neurobehavioral function. *Neuropharmacology* 63, 776–783. doi: 10.1016/j.neuropharm.2012.05.034
- Pedraza, J. F., Issy, A. C., Gomes, F. V., Guimarães, F. S., and Del-Bel, E. A. (2015). Cannabidiol effects in the prepulse inhibition disruption induced by amphetamine. *Psychopharmacology* 232, 3057–3065. doi: 10.1007/s00213-015-3945-7
- Pouzet, B., Feldon, J., Veenman, C. L., Yee, B. K., Richmond, M., Rawlins, J. N. P., et al. (1999). The effects of hippocampal and fimbria-fornix lesions on prepulse inhibition. *Behav. Neurosci.* 113, 968–981. doi: 10.1037/0735-7044.113.5.968
- Rice, D., and Barone, S. Jr. (2000). Critical periods of vulnerability for the developing nervous system: evidence from humans and animal models. *Environ. Health Perspect.* 108, 511–533. doi: 10.2307/3454543
- Riedel, G., Fadda, P., McKillop-Smith, S., Pertwee, R. G., Platt, B., and Robinson, L. (2009). Synthetic and plant-derived cannabinoid receptor antagonists show

- hypophagic properties in fasted and non-fasted mice. *Br. J. Pharmacol.* 156, 1154–1166. doi: 10.1111/j.1476-5381.2008.00107.x
- Rohleder, C., Müller, J. K., Lange, B., and Leweke, F. M. (2016). Cannabidiol as a potential new type of an antipsychotic. A critical review of the evidence. *Front. Pharmacol.* 7:422. doi: 10.3389/fphar.2016.00422
- Rosen, G. D., and Harry, J. D. (1990). Brain volume estimation from serial section measurements: a comparison of methodologies. *J. Neurosci. Methods* 35, 115–124. doi: 10.1016/0165-0270(90)90101-k
- Russo, E. B., Burnett, A., Hall, B., and Parker, K. K. (2005). Agonistic properties of cannabidiol at 5-HT_{1A} receptors. *Neurochem. Res.* 30, 1037–1043. doi: 10.1007/s11064-005-6978-1
- Ryberg, E., Larsson, N., Sjögren, S., Hjorth, S., Hermansson, N.-O., Leonova, J., et al. (2007). The orphan receptor GPR55 is a novel cannabinoid receptor. *Br. J. Pharmacol.* 152, 1092–1101. doi: 10.1038/sj.bjp.0707460
- Schiavon, A. P., Soares, L. M., Bonato, J. M., Milani, H., Guimarães, F. S., and Weffort de Oliveira, R. M. (2014). Protective effects of cannabidiol against hippocampal cell death and cognitive impairment induced by bilateral common carotid artery occlusion in mice. *Neurotox. Res.* 26, 307–316. doi: 10.1007/s12640-014-9457-0
- Scuderi, C., Filippis, D. D., Iuvone, T., Blasio, A., Steardo, A., and Esposito, G. (2009). Cannabidiol in medicine: a review of its therapeutic potential in CNS disorders. *Phytother. Res.* 23, 597–602. doi: 10.1002/ptr.2625
- Shiotsuki, H., Yoshimi, K., Shimo, Y., Funayama, M., Takamatsu, Y., Ikeda, K., et al. (2010). A rotarod test for evaluation of motor skill learning. *J. Neurosci. Methods* 189, 180–185. doi: 10.1016/j.jneumeth.2010.03.026
- Stark, T., Ruda-Kucerova, J., Iannotti, F. A., D'Addario, C., Di Marco, R., Pekarik, V., et al. (2019). Peripubertal cannabidiol treatment rescues behavioral and neurochemical abnormalities in the MAM model of schizophrenia. *Neuropharmacology* 146, 212–221. doi: 10.1016/j.neuropharm.2018.11.035
- Viudez-Martínez, A., García-Gutiérrez, M. S., Medrano-Relinque, J., Navarrón, C. M., Navarrete, F., and Manzanares, J. (2018). *Cannabidiol Does Not Display Drug Abuse Potential in Mice Behavior*. Available online at: <https://www.nature.com/articles/s41401-018-0032-8>. Accessed December 05, 2018.
- Watt, G., and Karl, T. (2017). *In vivo* evidence for therapeutic properties of cannabidiol (CBD) for Alzheimer's disease. *Front. Pharmacol.* 8:20. doi: 10.3389/fphar.2017.00020
- West, M. J., Slomianka, L., and Gundersen, H. J. (1991). Unbiased stereological estimation of the total number of neurons in the subdivisions of the rat hippocampus using the optical fractionator. *Anat. Rec.* 231, 482–497. doi: 10.1002/ar.1092310411
- Whiting, P. F., Wolff, R. F., Deshpande, S., Di Nisio, M., Duffy, S., Hernandez, A. V., et al. (2015). Cannabinoids for medical use: a systematic review and meta-analysis. *JAMA* 313, 2456–2473. doi: 10.1001/jama.2015.6358
- Zuardi, A. W., Shirakawa, I., Finkelfarb, E., and Karniol, I. G. (1982). Action of cannabidiol on the anxiety and other effects produced by delta 9-THC in normal subjects. *Psychopharmacology* 76, 245–250. doi: 10.1007/bf00432554
- Zygmunt, P. M., Petersson, J., Andersson, D. A., Chuang, H., Sörgård, M., Di Marzo, V., et al. (1999). Vanilloid receptors on sensory nerves mediate the vasodilator action of anandamide. *Nature* 400, 452–457. doi: 10.1038/22761

Conflict of Interest Statement: The authors declare that the research was conducted in the absence of any commercial or financial relationships that could be construed as a potential conflict of interest.

Copyright © 2019 Schleicher, Ott, Müller, Silcher, Sichler, Löw, Wagner and Bouter. This is an open-access article distributed under the terms of the Creative Commons Attribution License (CC BY). The use, distribution or reproduction in other forums is permitted, provided the original author(s) and the copyright owner(s) are credited and that the original publication in this journal is cited, in accordance with accepted academic practice. No use, distribution or reproduction is permitted which does not comply with these terms.



Acute Disruption of the Dorsal Hippocampus Impairs the Encoding and Retrieval of Trace Fear Memories

Jacob H. Wilmot^{1,2†}, Kyle Puhger^{1,2†} and Brian J. Wiltgen^{1,2*}

¹Department of Psychology, University of California, Davis, Davis, CA, United States, ²Center for Neuroscience, University of California, Davis, Davis, CA, United States

OPEN ACCESS

Edited by:

Jeansok J. Kim,
University of Washington,
United States

Reviewed by:

Stephen Maren,
Texas A&M University, United States
Kaori Takehara-Nishiuchi,
University of Toronto, Canada

*Correspondence:

Brian J. Wiltgen
bjwiltgen@ucdavis.edu

[†]These authors have contributed
equally to this work

Received: 19 April 2019

Accepted: 16 May 2019

Published: 29 May 2019

Citation:

Wilmot JH, Puhger K and Wiltgen BJ
(2019) Acute Disruption of the Dorsal
Hippocampus Impairs the Encoding
and Retrieval of Trace Fear Memories.
Front. Behav. Neurosci. 13:116.
doi: 10.3389/fnbeh.2019.00116

A major function of the hippocampus is to link discontinuous events in memory. This process can be studied in animals using Pavlovian trace conditioning, a procedure where the conditional stimulus (CS) and unconditional stimulus (US) are separated in time. While the majority of studies have found that trace conditioning requires the dorsal segment of the hippocampus, others have not. This variability could be due to the use of lesion and pharmacological techniques, which lack cell specificity and temporal precision. More recent studies using optogenetic tools find that trace fear acquisition is disrupted by decreases in dorsal CA1 (dCA1) activity while increases lead to learning enhancements. However, comparing these results is difficult given that some studies manipulated the activity of CA1 pyramidal neurons directly and others did so indirectly (e.g., via stimulation of entorhinal cortex inputs). The goal of the current experiments, therefore, was to compare the effects of direct CA1 excitation and inhibition on the encoding and expression of trace fear memories. Our data indicates that stimulation of ArchT in dCA1 pyramidal neurons reduces activity and impairs both the acquisition and retrieval of trace fear. Unlike previous work, direct stimulation of CA1 with ChR2 increases activity and produces deficits in trace fear learning and expression. We hypothesize that this is due to the artificial nature of optogenetic stimulation, which could disrupt processing throughout the hippocampus and in downstream structures.

Keywords: learning, memory, optogenetics, context fear, mice

INTRODUCTION

The hippocampus integrates spatial and temporal information to form complex memory representations. These include episodic memories in humans and contextual memories in animals (Eichenbaum, 2017). Simple associations, in contrast, can typically be learned without this structure. For example, rodents with damage to the hippocampus can acquire fear to an auditory cue that is immediately followed by shock (Chowdhury et al., 2005; Esclassan et al., 2009). However, if the shock is presented several seconds after the cue has ended, the same animals cannot form an association between them. This suggests that an important function of the hippocampus is to link discontinuous events—a property that allows it to encode sequences and form spatial maps, both of which involve associations between stimuli that are separated in time.

The ability to learn temporal associations can be studied in animals using trace conditioning. This is a Pavlovian procedure where a gap is inserted between the termination of the conditional stimulus (CS) and the onset of the unconditional stimulus (US). The majority of studies have found that the acquisition and retrieval of trace conditioning require the dorsal hippocampus (Chowdhury et al., 2005; Raybuck and Lattal, 2011, for review Raybuck and Lattal, 2014) although there are exceptions (Yoon and Otto, 2007; Czerniawski et al., 2009; Cox et al., 2013). This variability could be attributed to the use of lesion and pharmacological techniques, both of which lack cell specificity and temporal precision. More recent studies have utilized optogenetic tools to directly manipulate hippocampal neurons or alter their activity indirectly by stimulating entorhinal inputs. When CA1 activity was decreased during learning, deficits in trace fear conditioning were observed (Kitamura et al., 2014). In contrast, activation of CA1 neurons enhanced learning in young mice and ameliorated aging deficits in older animals (Kitamura et al., 2014; Sellami et al., 2017).

The goal of the current study was to directly compare the effects of CA1 stimulation on the acquisition and retrieval of trace fear memories. Based on previous work, we predicted that activation of dorsal CA1 (dCA1) pyramidal neurons would enhance learning while inhibition would impair both encoding and retrieval. The effect of CA1 activation on memory expression was less clear. Although it is possible to drive the retrieval of contextual fear memories by stimulating neurons in the dentate gyrus (Liu et al., 2012), the same procedure is far less effective in CA1 (Ramirez et al., 2013; Ryan et al., 2015). In addition, optogenetic activation of ventral CA1 has been shown to impair the retrieval of contextual fear (Jimenez et al., 2018). Accordingly, we predicted that direct stimulation of dCA1 neurons would either impair or have no effect on the expression of trace fear.

MATERIALS AND METHODS

Subjects

Subjects in this study were 2–4-month-old male and female C57BL/6J mice (Jackson Labs). Mice were maintained on a 12 h light/12 h dark cycle with *ad libitum* access to food and water. All experiments were performed during the light portion (7 a.m.–7 p.m.) of the light/dark cycle. Mice were group housed until surgery, at which point they were single housed for the rest of the experiment.

Surgery

Stereotaxic surgery was performed 2–3 weeks before behavioral experiments began. Mice were anesthetized with isoflurane (5% induction, 2% maintenance) and placed into a stereotaxic frame (Kopf Instruments). An incision was made in the scalp and the skull was adjusted to place bregma and lambda in the same horizontal plane. Small craniotomies were made above the desired injection site in each hemisphere. AAV was delivered at a rate of 2 nl/s to dCA1 (AP -2.0 mm and ML ± 1.5 mm from bregma; DV -1.25 mm from dura)

through a glass pipette using a microsyringe pump (UMP3, World Precision Instruments). For stimulation experiments, the AAVs used were AAV9-CaMKIIa-hChR2(H134R)-eYFP (250 nl/hemisphere, titer: 8.96×10^{13} , Penn Vector Core) and AAV9-CaMKIIa-eGFP (250 nl/hemisphere, titer: 3.49×10^{13} , Penn Vector Core). For inhibition experiments, the constructs were AAV5-CaMKIIa-ArchT-GFP (350 nl/hemisphere, titer: 5.2×10^{12} , UNC Vector Core) and AAV5-CaMKIIa-GFP (350 nl/hemisphere, titer: 5.3×10^{12} , UNC Vector Core). After AAV infusions, an optical fiber (200 μ m diameter, Thorlabs) was implanted above dCA1 in each hemisphere (AP -2.0 mm and ML ± 1.5 mm from bregma; DV -1.0 mm from dura). The fiber implants were secured to the skull using dental adhesive (C&B Metabond, Parkell) and dental acrylic (Bosworth Company).

Apparatus

The behavioral apparatus has been described previously (Tayler et al., 2011). Briefly, fear conditioning occurred in a conditioning chamber (30.5 cm \times 24.1 cm \times 21.0 cm) within a sound-attenuating box (Med Associates). The chamber consisted of a front-mounted scanning charge-coupled device video camera, stainless steel grid floor, a stainless steel drop pan, and overhead LED lighting capable of providing broad spectrum and infrared light. For context A, the conditioning chamber was lit with both broad spectrum and infrared light and scented with 95% ethanol. For context B, a smooth white plastic insert was placed over the grid floor and a curved white wall was inserted into the chamber. Additionally, the room lights were changed to red light, only infrared lighting was present in the conditioning chamber, and the chamber was cleaned and scented with disinfectant wipes (PDI Sani-Cloth Plus). In both contexts, background noise (65 dB) was generated with a fan in the chamber and HEPA filter in the room.

Trace Fear Conditioning Procedure

All behavioral testing occurred during the light portion of the light/dark cycle. Mice were habituated to handling and optical fiber connection for 5 min/day for 5 days before the beginning of behavior. Then, the mice were habituated to context B with one 5-min session of free exploration each day for 2 days. Next, the mice underwent trace fear conditioning in context A. During training, mice were allowed to explore the conditioning chamber for 3 min before receiving six conditioning trials. Each trial consisted of a 20 s pure tone (85 dB, 3,000 Hz) and a 2 s shock (0.9 mA) separated by a 20 s stimulus-free trace interval. The intertrial interval (ITI) was 120 s. Mice were removed from the chamber 120 s after the last trial. Twenty-four hours later, the mice were placed in context B for a tone test consisting of a 3 min baseline period followed by six 20-s tone presentations separated by a 140 s ITI. Freezing behavior was used to index fear and measured automatically using VideoFreeze software (Med Associates). The next day, mice were placed back in the original conditioning chamber (context A) for either a 12- or 20-min context test, depending on the experiment.

Experiment-Specific Methods

Experiment 1-ArchT Inhibition During Fear Memory Retrieval

Continuous green light (531 nm, 12 mW at fiber tip) illumination was delivered to dCA1 of mice expressing ArchT ($n = 6$) or eYFP ($n = 6$) during the tone and context testing periods. In the tone test, light onset was simultaneous with tone onset and lasted 40 s. The context test was 20 min and green light was delivered throughout the test in order to ensure c-Fos expression would be representative of neural activity that occurred while the laser was on.

Experiment 2-ChR2 Stimulation During Fear Memory Retrieval

Blue light (465 nm, 12 mW measured at fiber tip) was delivered (20 Hz, 15 ms pulse width) to dCA1 of mice expressing ChR2 ($n = 5$) or eGFP ($n = 4$) during the tone test and the context test. In the tone test, light onset was simultaneous with tone onset and lasted 40 s. The context test consisted of four 3-min epochs. The light was off for the first 3 min and on for the next 3 min; then, this sequence was repeated one time. Mice were sacrificed 90 min following the end of the context test in order to quantify c-Fos expression.

Experiment 3-ChR2 Stimulation During Trace Fear Encoding

As in Experiment 2, blue light was delivered to dCA1 of ChR2 ($n = 6$) and eGFP ($n = 6$) mice in 42 s epochs during the training session. Light onset was simultaneous with onset of the tone and the light coterminated with the shock. No light was delivered during the tone or context tests. The context test was 20 min.

Experiment 4-ArchT Inhibition During Trace Fear Encoding

As in Experiment 1, green light illumination was delivered to dCA1 of ArchT ($n = 5$) and eYFP ($n = 7$) mice during training in the same 42 s epochs described for Experiment 3. Light was not present during testing and the context test was 20 min.

Immunohistochemistry

Ninety minutes after behavioral testing, mice were transcardially perfused with 4% PFA. Following 24 h of post-fixation, 40 μ m coronal sections were cut and stained for c-Fos. Slices were washed three times in 1 \times phosphate buffered saline (PBS) at the beginning of the procedure and after all antibody and counterstaining steps. All antibodies and counterstains were diluted in a blocking solution containing 0.2% Triton-X and 2% normal donkey serum in 1 \times PBS, unless otherwise indicated. First, sections were incubated for 15 min in the blocking solution. Then, slices were incubated for 24 h at 4 $^{\circ}$ in anti-c-Fos rabbit primary antibody (1:5,000, ABE457, Millipore). Next, slices were placed in biotinylated donkey anti-rabbit secondary antibody (1:500, Jackson ImmunoResearch) for 60 min at room temperature, followed by Streptavidin-Cy3 (1:500, Jackson ImmunoResearch) for 45 min. Finally, sections were stained with DAPI (1:10,000 in PBS, Life Technologies) for 10 min, mounted on slides, and coverslipped with Vectashield anti-fade mounting media (Vector Labs).

Image Acquisition and Cell Quantification

Images were acquired at 20 \times magnification using a fluorescence slide scanner (BX61VS, Olympus). After acquisition, images were cropped to contain approximately 30,000–40,000 μ m² of dCA1. A blinded experimenter performed cell counts on 3–4 sections from each animal (6–8 hemispheres). c-Fos+ cells were counted using the multi-point tool in ImageJ. Cell counts were averaged across slices to obtain one value per animal.

Statistical Analysis

For analysis of behavioral data from training and tone test sessions, freezing scores in each phase type (baseline, tone, trace) were averaged for each animal. All behavioral data were analyzed using two-way repeated-measures ANOVA followed by Bonferroni-corrected *post hoc* comparisons when necessary. Cell count data was converted to a percent change score for each animal. Percent control was calculated by first dividing the number of c-fos+ cells/mm² in each animal by the mean number of c-fos+ cells/mm² in the control group. These values were then multiplied by 100 to convert them to a percent change. These scores were analyzed using unpaired *t*-tests. A threshold of $p < 0.05$ was used to determine statistical significance. All data are shown as mean \pm SEM. All data were analyzed with GraphPad Prism (v8) and all figures were generated using Prism and BioRender.

RESULTS

Inhibition of dCA1 Impairs Trace Fear Memory Retrieval

To silence dCA1 during retrieval, we expressed the inhibitory opsin ArchT in pyramidal neurons using the α CaMKII promoter. Animals then received six trace fear conditioning trials in the absence of laser stimulation (**Figure 1A**). Each trial consisted of a 20-s auditory CS followed by a 20-s trace interval and then a 2 s footshock. The ITI was 120 s. As expected, freezing increased during the tone and trace interval relative to the baseline period and there were no differences between ArchT mice and eYFP control animals (Main effect of stimulus period $F_{(2,20)} = 122$, $p < 0.05$; No effect of group, $F_{(1,10)} = 0.48$, $p > 0.05$, No stimulus period \times group interaction $F_{(2,20)} = 0.49$, $p > 0.05$; **Figure 1B**).

The next day, animals received a tone test in a novel environment. The test was identical to training except that no shocks were presented and continuous green light was delivered to dCA1 during the tone and trace intervals (**Figure 1A**). Group differences were not observed at baseline (BL); however, ArchT stimulation significantly reduced freezing during the tone and trace intervals [Group \times stimulus period interaction $F_{(2,20)} = 10.9$, $p < 0.05$; Bonferroni *post hoc* tests, BL ($p > 0.05$), tone and trace ($p < 0.05$; **Figure 1C**)]. The following day, mice were placed back in the original training environment for 20-min to assess context fear. Continuous green light was delivered to dCA1 during the entire test (**Figure 1A**). Similar to the trace fear data, stimulation of ArchT significantly reduced freezing to the context (Main effect of group $F_{(1,10)} = 23.81$, $p < 0.05$; Main effect of time $F_{(3,30)} = 10.48$, $p < 0.05$; No group \times time interaction $F_{(3,30)} = 1.73$, $p > 0.05$; **Figure 1D**).

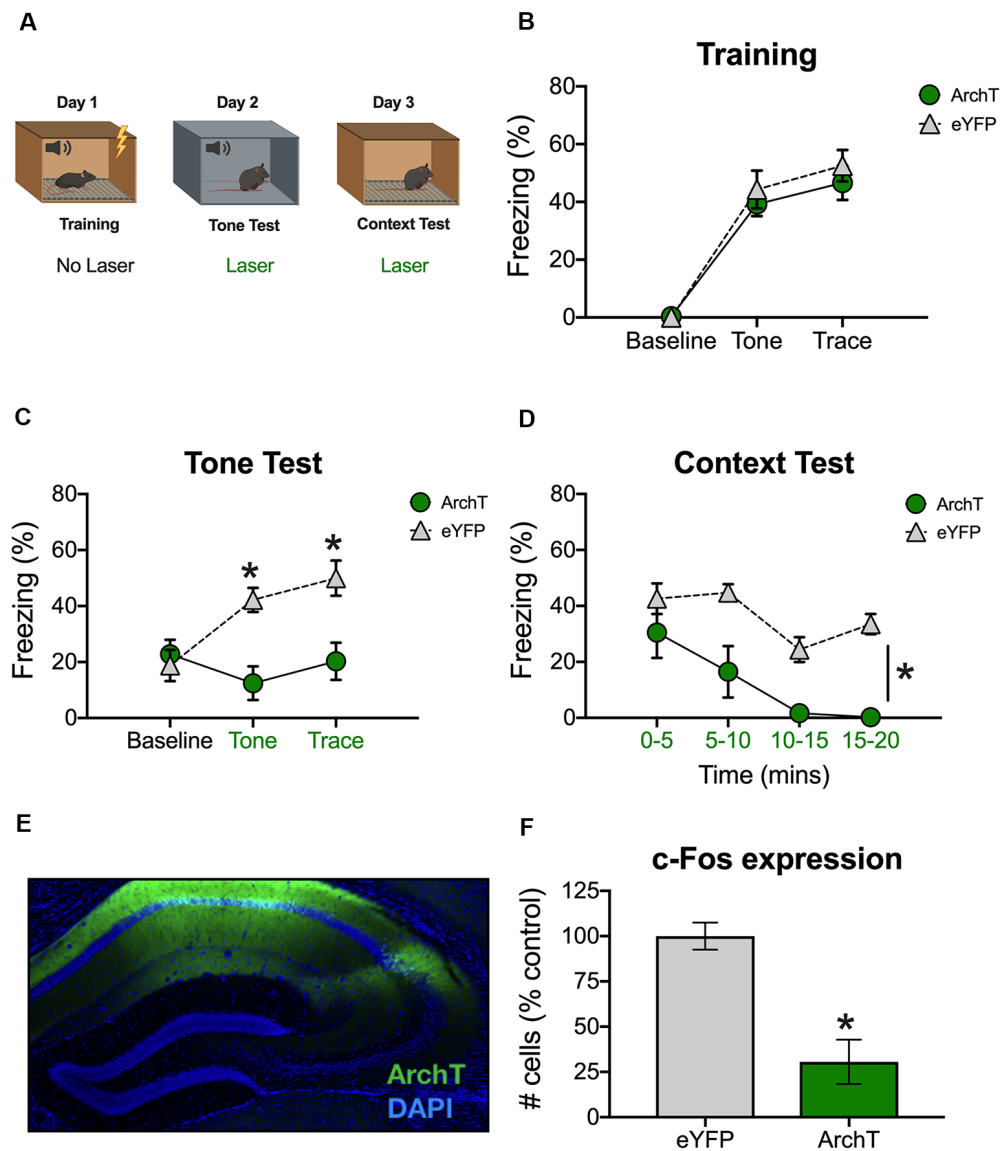


FIGURE 1 | Inhibition of dCA1 impairs trace fear memory retrieval. **(A)** Schematic of behavioral paradigm. On day 1, animals underwent trace fear conditioning without laser stimulation. The next day, mice underwent a tone memory test in a novel context with green light delivered to dorsal CA1 (dCA1) during each trial. Twenty-four hours later, mice were placed back in the conditioning environment for a context memory test. Green light was delivered to dCA1 during the entire context test. **(B)** Freezing during the training phase of trace fear conditioning (Mean \pm SEM). **(C)** Freezing during the tone test (Mean \pm SEM). **(D)** Freezing during the context test (Mean \pm SEM). **(E)** Example of virus expression. Green, ArchT; Blue, DAPI. **(F)** c-Fos expression in eYFP and ArchT mice after the context test. Green x-axis labels denote periods during which the laser was delivered. In all panels, green represents the ArchT group and gray represents the control group. * $p < 0.05$ relative to control.

To confirm that ArchT was expressed in dCA1 and that laser stimulation reduced neural activity, mice were sacrificed 90-min after the context test. We observed strong bilateral expression of ArchT and eYFP throughout the dCA1 (Figure 1E). We also found reduced expression of the immediate early gene c-Fos in ArchT mice relative to eYFP controls, indicating that our manipulation successfully reduced neural activity ($t_{(10)} = 4.83$, $p < 0.05$; Figure 1F). Together, these data demonstrate that reduced activity in dCA1 impairs the retrieval of both trace and context fear memories.

Stimulation of dCA1 Impairs Trace Fear Memory Retrieval

To examine the effects of dCA1 stimulation on retrieval, we expressed the excitatory opsin ChR2 in pyramidal neurons under control of the α CaMKII promoter. Animals were trained and tested using the same procedure described in the previous experiment (Figure 2A). During training, freezing increased during the tone and trace intervals relative to the baseline period and no differences were observed between ChR2 and eGFP groups (Main effect of stimulus period $F_{(2,14)} = 59.71$,

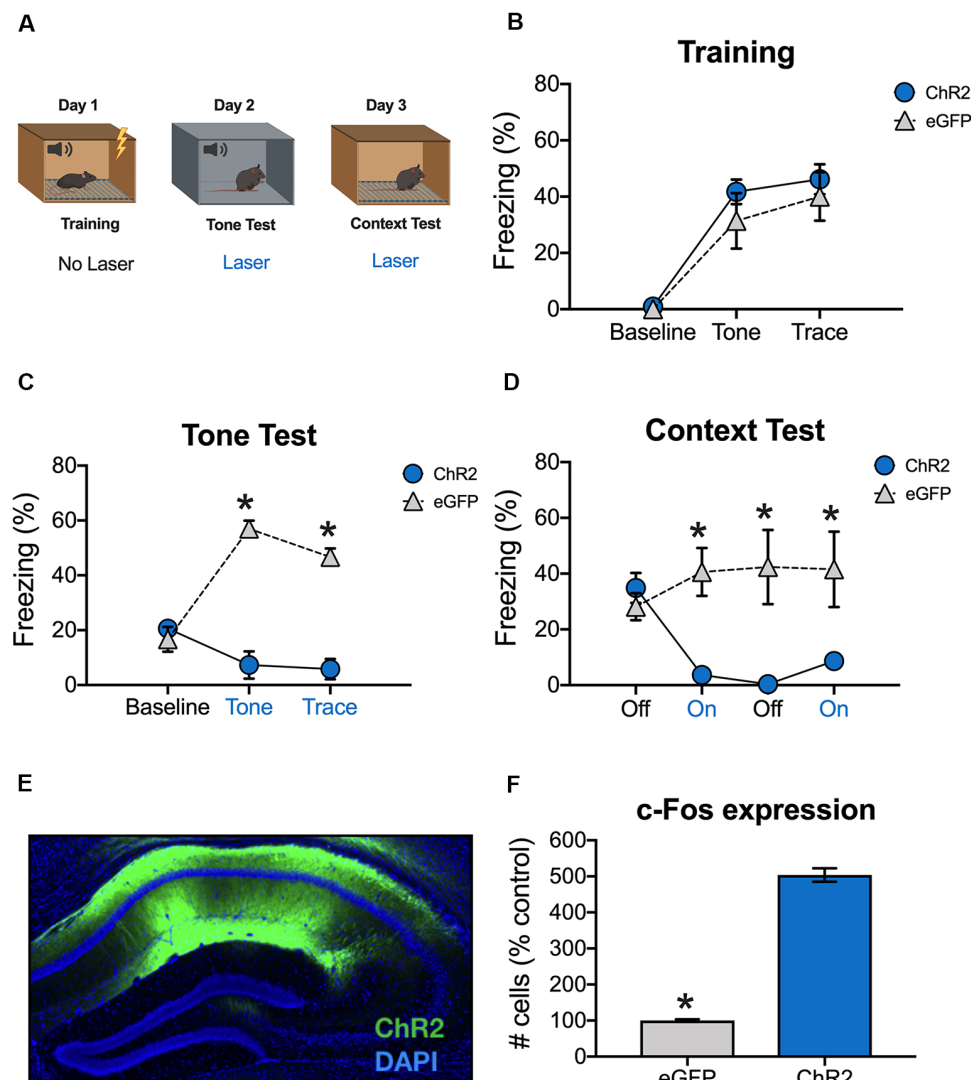


FIGURE 2 | Stimulation of dCA1 impairs trace fear memory retrieval. **(A)** Schematic of behavioral paradigm. On day 1, animals underwent trace fear conditioning without laser stimulation. The next day, mice underwent a tone memory test in a novel context with blue light delivered (20 Hz) to dCA1 during each trial. Twenty-four hours later, mice were placed back in the conditioning environment for a context memory test. The laser was not turned on for the first 3 min of the context test. Then, blue light was delivered to dCA1 for the next 3 min, followed by another 3 min laser off period, and a last 3-min laser on epoch. **(B)** Freezing during the training phase of trace fear conditioning (Mean \pm SEM). **(C)** Freezing during the tone test (Mean \pm SEM). **(D)** Freezing during the context test (Mean \pm SEM). **(E)** Example of virus expression. Green, ChR2; Blue, DAPI. **(F)** c-Fos expression in eGFP and ChR2 mice after the context test. Blue x-axis labels denote periods during which the laser was delivered. In all panels, blue represents the ChR2 group and gray represents the control group. * $p < 0.05$ relative to control.

$p < 0.05$; No effect of group, $F_{(1,7)} = 0.82$, $p > 0.05$, No stimulus period \times group interaction $F_{(2,14)} = 0.63$, $p > 0.05$; **Figure 2B**).

Animals received a tone test the next day, during which blue light (20 Hz) was delivered to dCA1 during the tone and trace intervals (**Figure 2A**). There were no group differences at baseline, but ChR2 stimulation significantly reduced freezing during the subsequent tone and trace intervals [Group \times stimulus period interaction $F_{(2,14)} = 43.7$, $p < 0.05$; Bonferroni *post hoc* tests, BL ($p > 0.05$), tone and trace ($p < 0.05$; **Figure 2C**)]. Twenty-four hours later, the mice were put back in the original training environment to assess context fear. This test began with a 3-min laser off period (BL) followed by 3-min of

blue light stimulation and 3-min of no stimulation. It ended with a second 3-min period of blue light stimulation. During BL, the groups froze at similar levels indicating that both had acquired context fear memories. However, when dCA1 was stimulated, freezing was significantly reduced in ChR2 mice relative to eGFP controls. Freezing remained low in this group after the laser turned off and did not recover for the remainder of the test session [Group \times stimulus period interaction $F_{(3,21)} = 12.34$, $p < 0.05$; Bonferroni *post hoc* tests, BL ($p > 0.05$) all subsequent laser on and laser off periods ($p < 0.05$; **Figure 2D**)].

To examine virus expression and determine the effects of dCA1 stimulation on neural activity, mice were perfused

90 min after the context test. As expected, we observed robust expression of ChR2 (**Figure 2E**) and stimulation produced a large increase in the number c-Fos positive dCA1 neurons relative to eGFP controls ($t_{(7)} = 18.78$, $p < 0.05$; **Figure 2F**). These data demonstrate that stimulation of dCA1 neurons impairs the retrieval of both trace and context fear memories.

Stimulation of dCA1 Impairs the Acquisition of Trace Fear Conditioning

We next determined the effects of stimulation on encoding by delivering blue light to dCA1 during each training trial (tone-trace interval-shock; **Figure 3A**). There were no group differences during the baseline period, but ChR2 stimulation significantly reduced freezing during the tone and trace intervals [Group \times stimulus period interaction $F_{(2,20)} = 18.2$, $p < 0.05$; Bonferroni *post hoc* tests, BL ($p > 0.05$), tone and trace ($p < 0.05$; **Figure 3B**)]. The same effects were observed the next day when mice received a tone test in the absence of blue light stimulation [Group \times stimulus period interaction $F_{(2,20)} = 8.09$, $p < 0.05$; Bonferroni *post hoc* tests, BL ($p > 0.05$), tone and trace ($p < 0.05$; **Figure 3C**)]. Twenty-four hours after the tone test, context memory was assessed by returning the mice to the training context. Blue light was not delivered during this session. Similar to the tone test data, context fear was significantly reduced in

ChR2 mice relative to eGFP controls (Main effect of group $F_{(1,10)} = 14.52$, $p < 0.05$; Main effect of time $F_{(3,30)} = 1.07$, $p < 0.05$; No group \times time interaction $F_{(3,30)} = 0.96$, $p > 0.05$; **Figure 3D**). Together, these data demonstrate that both trace and context fear memories are disrupted when dCA1 is stimulated during encoding.

Inhibition of dCA1 Impairs the Acquisition of Trace Fear Conditioning

In our last experiment, we examined the effects of inhibition on trace fear encoding by stimulating ArchT during training (**Figure 4A**). As in the previous experiment, light was delivered to dCA1 during each conditioning trial (tone-trace interval-shock). Surprisingly, there were no differences between the ArchT and eYFP groups during the baseline period or during the tone and trace intervals (No effect of group $F_{(1,10)} = 2.77$, $p > 0.05$; Main effect of stimulus period $F_{(2,20)} = 60.7$, $p < 0.05$; No Group \times stimulus period interaction $F_{(2,20)} = 2.07$, $p > 0.05$; **Figure 4B**). However, when memory was tested the next day (in the absence of light stimulation) ArchT animals froze significantly less than eYFP controls during all stimulus periods (Main effect of group $F_{(1,10)} = 29.74$, $p < 0.05$; Main effect of stimulus period $F_{(2,20)} = 41.33$, $p < 0.05$; No Group \times stimulus period interaction $F_{(2,20)} = 0.29$, $p > 0.05$; **Figure 4C**).

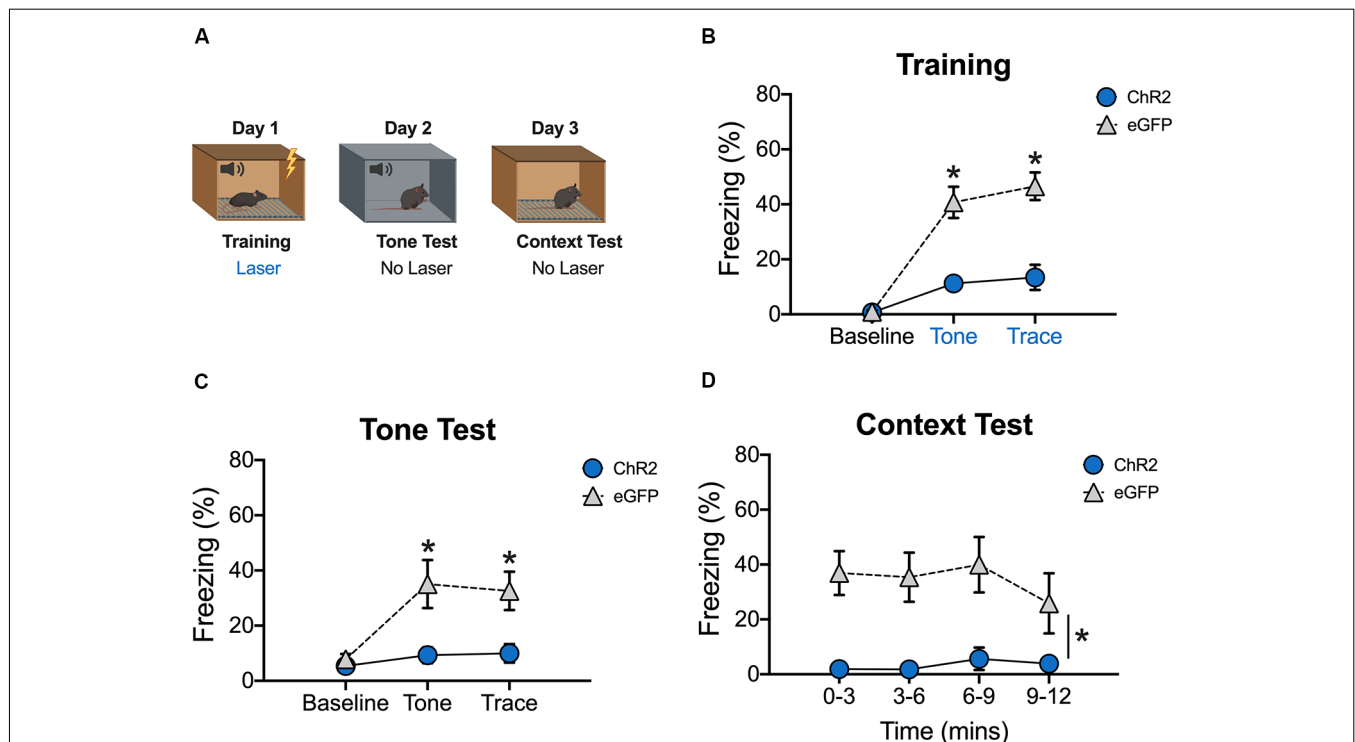


FIGURE 3 | Stimulation of dCA1 during trace fear encoding impairs memory acquisition. **(A)** Schematic of behavioral paradigm. On day 1, animals underwent trace fear conditioning with blue light (20 Hz) delivered to dCA1 during each training trial. The next day, mice underwent a tone memory test in a novel context with no laser stimulation. Twenty-four hours later, mice were placed back in the conditioning environment for a context memory test without light delivery. **(B)** Freezing during the training phase of trace fear conditioning (Mean \pm SEM). **(C)** Freezing during the tone test (Mean \pm SEM). **(D)** Freezing during the context test (Mean \pm SEM). Blue x-axis labels denote periods during which the laser was delivered. In all behavioral panels, blue represents the ChR2 group and gray represents the control group. * $p < 0.05$ relative to control.

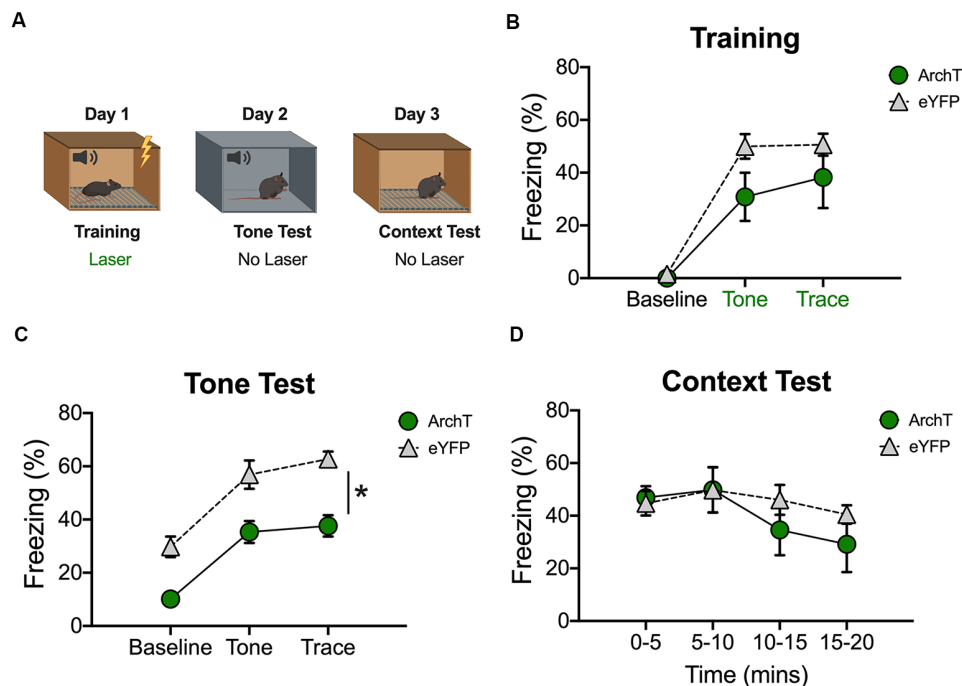


FIGURE 4 | Inhibition of dCA1 during trace fear encoding impairs memory acquisition. **(A)** Schematic of behavioral paradigm. On day 1, animals underwent trace fear conditioning with green light delivered to dCA1 during each training trial. The next day, mice underwent a tone memory test in a novel context with no laser stimulation. Twenty-four hours later, mice were placed back in the conditioning environment for a context memory test without light delivery. **(B)** Freezing during the training phase of trace fear conditioning (Mean \pm SEM). **(C)** Freezing during the tone test (Mean \pm SEM). **(D)** Freezing during the context test (Mean \pm SEM). In all behavioral panels, green represents the ArchT group and gray represents the control group. Green x-axis labels denote periods during which the laser was delivered. * $p < 0.05$ relative to control.

Twenty-four hours after the tone test, context memory was assessed by returning the mice to the training environment. Green light was not delivered during this session. The ArchT and eYFP groups froze at similar levels during this test indicating that dCA1 inhibition did not affect the formation of a context fear memory (No effect of group $F_{(1,10)} = 0.53$, $p > 0.05$; No effect of time $F_{(3,30)} = 2.41$, $p > 0.05$; No group \times time interaction $F_{(3,30)} = 0.74$, $p > 0.05$; **Figure 4D**).

These data are consistent with a recent report and suggest that reduced activity in dCA1 disrupts the acquisition of trace but not context fear memories (Sellami et al., 2017).

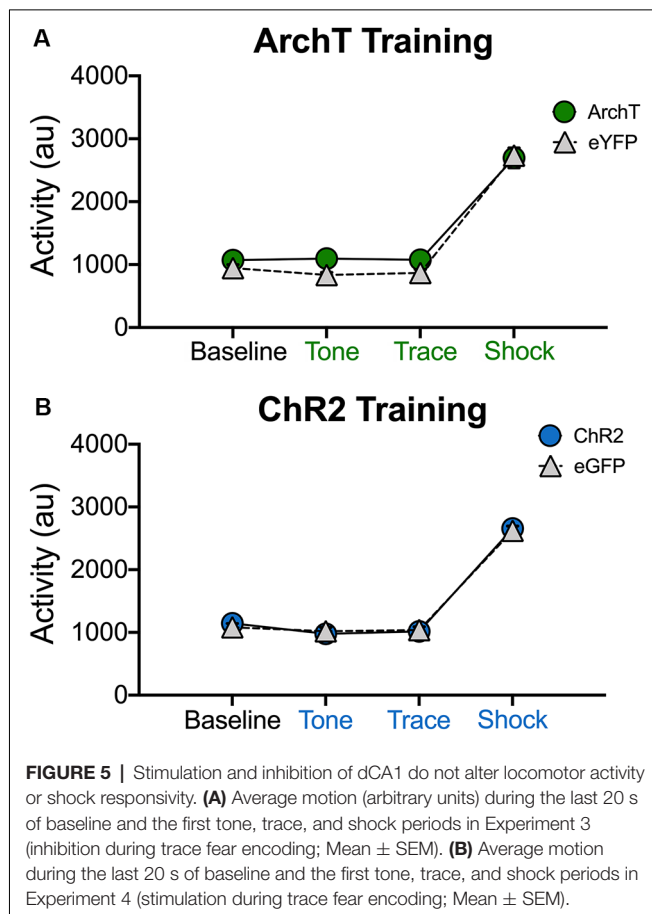
Altering dCA1 Activity Does Not Increase Exploration or Reduce the Response to Shock

It is possible that our manipulations impaired trace fear conditioning because they induced hyperactivity or disrupted the animals' ability to process shock. This is unlikely given that optogenetic inhibition of dCA1 does not impair delay fear conditioning or increase activity in the open field (Goshen et al., 2011). In addition, optogenetic activation of dCA1 increases the ability of aged mice to acquire trace fear conditioning (Sellami et al., 2017). Nonetheless, we addressed this issue by determining if laser stimulation altered exploration or shock reactivity during the first conditioning trial (**Figure 5**). Only the first trial was analyzed because mice were exploring naturally and had not yet

started freezing. In addition, endogenous opiates are released during fear conditioning and have been shown to reduce shock sensitivity (Fanselow and Bolles, 1979; Fanselow and Baackes, 1982). We quantified activity levels immediately before laser stimulation (BL) and then compared these to subsequent periods when the laser was on (tone, trace interval and shock). Analysis of our ArchT data revealed that activity levels were not altered when dCA1 was inhibited during the tone, trace interval or shock periods (No effect of group $F_{(1,10)} = 2.67$, $p > 0.05$; Main effect of stimulus period $F_{(3,30)} = 278.3$, $p < 0.05$; No group \times stimulus period interaction $F_{(3,30)} = 1.59$, $p > 0.05$; **Figure 5A**). Differences were also not observed when dCA1 was activated during these same periods *via* ChR2 stimulation (No effect of group $F_{(1,10)} = 0.03$, $p > 0.05$; Main effect of stimulus period $F_{(3,30)} = 330.2$, $p < 0.05$; No group \times stimulus period interaction $F_{(3,30)} = 0.31$, $p > 0.05$; **Figure 5B**). These results are consistent with previous reports and indicate that stimulation or inhibition of dCA1 does not impair trace fear conditioning by inducing hyperactivity or preventing the animals from processing shock.

DISCUSSION

In this set of experiments, we compared the effects of optogenetic inhibition and stimulation of the dorsal hippocampus on the encoding and retrieval of trace fear memories. Our results



demonstrate that intact dCA1 activity is required for the retrieval of both tone and context fear. This is true regardless of whether activity is decreased or increased. Although some previous work suggests that trace fear memories can be retrieved without the dorsal hippocampus (Yoon and Otto, 2007; Czerniawski et al., 2009; Cox et al., 2013), our results agree with previous studies that found lesions and pharmacological inactivation of this region impair trace fear expression (Chowdhury et al., 2005; Quinn et al., 2005; Raybuck and Lattal, 2011).

When dCA1 was inhibited during encoding, we found that tone fear memory was impaired, but memory for the training context remained intact. This is consistent with the fact that manipulations of the dorsal hippocampus during context fear learning often do not prevent memory formation (Maren et al., 1997; Frankland et al., 1998; Wiltgen et al., 2006). This finding is thought to reflect the ability of other brain areas (e.g., ventral hippocampus, prefrontal cortex) to compensate for the lack of dorsal hippocampus contributions to learning (Wiltgen and Fanselow, 2003; Rudy et al., 2004; Zelikowsky et al., 2013). In contrast, inactivation of the dorsal hippocampus after learning typically leads to robust retrograde amnesia for context fear (Kim and Fanselow, 1992; Maren et al., 1997; Anagnostaras et al., 1999; Matus-Amat et al., 2004), as seen in our retrieval experiments. Together, these data suggest that dCA1 is required for memory expression if this region is intact during learning (Moser and Moser, 1998; Wiltgen and Fanselow, 2003; Rudy et al., 2004).

Unlike inhibition, activation of dCA1 during training produced deficits in both tone and context fear memory. This more complete memory impairment suggests that the abnormal activity patterns induced by ChR2 stimulation disrupted encoding in brain regions that can normally compensate for the loss of the dorsal hippocampus. Consistent with this idea, stimulation of dCA1 has been shown to produce widespread increases in brain activity (Takata et al., 2015; Leebhardt et al., 2016). In contrast to our results, some studies have found that increases in CA1 activity during encoding enhance trace fear memory acquisition (Kitamura et al., 2014; Sellami et al., 2017). For example, Sellami et al. (2017) showed that direct stimulation of CA1 pyramidal cells during the trace interval attenuates trace fear conditioning deficits in aged mice. This discrepancy may be explained by differences in age between studies. Young mice show learning-related increases in CA1 intrinsic excitability following trace fear conditioning that are reduced with aging (Oh et al., 2010). It is possible that CA1 stimulation during the trace interval rescues this physiological impairment in old mice, ameliorating their trace fear conditioning deficits, but adds noise to the already-excitability hippocampus in younger animals. The effect of this noise on learning could be amplified by the higher stimulation frequency that was used in the current study (20 Hz vs. 5 Hz). Consistent with this idea, previous work showed that stimulation at 20 Hz could be used to induce freezing in the dentate gyrus but not in dCA1 (Ramirez et al., 2013). Our data are consistent with this observation and extend it by demonstrating that dCA1 stimulation at 20 Hz is actually disruptive to ongoing memory retrieval.

The current results support the idea that dCA1 is critically involved in forming and retrieving trace fear memories. Nonetheless, despite the extensive literature on this topic, the specific contribution of CA1 to these processes remains known. To better understand its role, future investigations will need to examine its unique physiological properties in more detail as well as characterize the type of information it receives from brain areas like the prefrontal cortex, entorhinal cortex and the nucleus reuniens.

DATA AVAILABILITY

All datasets generated for this study are included in the manuscript.

ETHICS STATEMENT

All experiments were reviewed and approved by the UC Davis Institutional Animal Care and Use Committee (IACUC).

AUTHOR CONTRIBUTIONS

JW and KP contributed equally to the design, implementation and analysis of experiments and to the writing of the manuscript. BW contributed to the design and analysis of experiments and to the writing of the manuscript.

FUNDING

This work was supported by National Institute of Neurological Disorders and Stroke (NINDS, NIH) RO1 (NS088053) to BW, National Institute of Mental Health (NIMH, NIH) T32 to JW (MH112507-01) and NIH T32 to KP (MH112507-02).

REFERENCES

- Anagnostaras, S. G., Maren, S., and Fanselow, M. S. (1999). Temporally graded retrograde amnesia of contextual fear after hippocampal damage in rats: within-subjects examination. *J. Neurosci.* 19, 1106–1114. doi: 10.1523/JNEUROSCI.19-03-01106.1999
- Chowdhury, N., Quinn, J. J., and Fanselow, M. S. (2005). Dorsal hippocampus involvement in trace fear conditioning with long, but not short, trace intervals in mice. *Behav. Neurosci.* 119, 1396–1402. doi: 10.1037/0735-7044.119.5.1396
- Cox, D., Czerniawski, J., Ree, F., and Otto, T. (2013). Time course of dorsal and ventral hippocampal involvement in the expression of trace fear conditioning. *Neurobiol. Learn. Mem.* 106, 316–323. doi: 10.1016/j.nlm.2013.05.009
- Czerniawski, J., Yoon, T., and Otto, T. (2009). Dissociating space and trace in dorsal and ventral hippocampus. *Hippocampus* 19, 20–32. doi: 10.1002/hipo.20469
- Eichenbaum, H. (2017). On the integration of space, time, and memory. *Neuron* 95, 1007–1018. doi: 10.1016/j.neuron.2017.06.036
- Esclassan, F., Coutureau, E., Di Scala, G., and Marchand, A. R. (2009). Differential contribution of dorsal and ventral hippocampus to trace and delay fear conditioning. *Hippocampus* 19, 33–44. doi: 10.1002/hipo.20473
- Fanselow, M. S., and Baackes, M. P. (1982). Conditioned fear-induced opiate analgesia on the Formalin test: evidence for two aversive motivational systems. *Learn. Motiv.* 13, 200–221. doi: 10.1016/0023-9690(82)90021-2
- Fanselow, M. S., and Bolles, R. C. (1979). Naloxone and shock-elicited freezing in the rat. *J. Comp. Physiol. Psychol.* 93, 736–744. doi: 10.1037/h0077609
- Frankland, P. W., Cestari, V., Filipkowski, R. K., McDonald, R. J., and Silva, A. J. (1998). The dorsal hippocampus is essential for context discrimination but not for contextual conditioning. *Behav. Neurosci.* 112, 863–874. doi: 10.1037/0735-7044.112.4.863
- Goshen, I., Brodsky, M., Prakash, R., Wallace, J., Gradinaru, V., Ramakrishnan, C., et al. (2011). Dynamics of retrieval strategies for remote memories. *Cell* 147, 678–689. doi: 10.1016/j.cell.2011.09.033
- Jimenez, J. C., Su, K., Goldberg, A. R., Luna, V. M., Biane, J. S., Ordek, G., et al. (2018). Anxiety cells in a hippocampal-hypothalamic circuit. *Neuron* 97, 670.e6–683.e6. doi: 10.1016/j.neuron.2018.01.016
- Kim, J. J., and Fanselow, M. S. (1992). Modality-specific retrograde amnesia of fear. *Science* 256, 675–677. doi: 10.1126/science.1585183
- Kitamura, T., Pignatelli, M., Suh, J., Kohara, K., Yoshiki, A., Abe, K., et al. (2014). Island cells control temporal association memory. *Science* 343, 896–901. doi: 10.1126/science.1244634
- Leibhardt, P., Hohenberg, C. C., Weber-Fahr, W., Kelsch, W., and Sartorius, A. (2016). Optogenetic fMRI in the mouse hippocampus: hemodynamic response to brief glutamatergic stimuli. *J. Cereb. Blood Flow Metab.* 36, 629–638. doi: 10.1177/0271678x15606455
- Liu, X., Ramirez, S., Pang, P. T., Puryear, C. B., Govindarajan, A., Deisseroth, K., et al. (2012). Optogenetic stimulation of a hippocampal engram activates fear memory recall. *Nature* 484, 381–385. doi: 10.1038/nature11028
- Maren, S., Aharonov, G., and Fanselow, M. S. (1997). Neurotoxic lesions of the dorsal hippocampus and Pavlovian fear conditioning in rats. *Behav. Brain Res.* 88, 261–274. doi: 10.1016/s0166-4328(97)00088-0
- Matus-Amat, P., Higgins, E. A., Barrientos, R. M., and Rudy, J. W. (2004). The role of the dorsal hippocampus in the acquisition and retrieval of context memory representations. *J. Neurosci.* 24, 2431–2439. doi: 10.1523/JNEUROSCI.1598-03.2004
- Moser, M.-B., and Moser, E. I. (1998). Distributed encoding and retrieval of spatial memory in the hippocampus. *J. Neurosci.* 18, 7535–7542. doi: 10.1523/JNEUROSCI.18-18-07535.1998

ACKNOWLEDGMENTS

We thank Yusuke Ota, Jamie Krueger, Jalina Graham, and Marrisa Lafreniere for their technical support and valuable conversations pertaining to this manuscript.

- Oh, M. M., Oliveira, F. A., and Disterhoft, J. F. (2010). Learning and aging related changes in intrinsic neuronal excitability. *Front. Aging Neurosci.* 2:2. doi: 10.3389/neuro.24.002.2010
- Quinn, J. J., Loya, F., Ma, Q. D., and Fanselow, M. S. (2005). Dorsal hippocampus NMDA receptors differentially mediate trace and contextual fear conditioning. *Hippocampus* 15, 665–674. doi: 10.1002/hipo.20088
- Ramirez, S., Liu, X., Lin, P.-A., Suh, J., Pignatelli, M., Redondo, R. L., et al. (2013). Creating a false memory in the hippocampus. *Science* 341, 387–391. doi: 10.1126/science.1239073
- Raybuck, J. D., and Lattal, K. M. (2011). Double dissociation of amygdala and hippocampal contributions to trace and delay fear conditioning. *PLoS One* 6:e15982. doi: 10.1371/journal.pone.0015982
- Raybuck, J. D., and Lattal, K. M. (2014). Bridging the interval: theory and neurobiology of trace conditioning. *Behav. Processes* 0, 103–111. doi: 10.1016/j.beproc.2013.08.016
- Rudy, J. W., Huff, N. C., and Matus-Amat, P. (2004). Understanding contextual fear conditioning: insights from a two-process model. *Neurosci. Biobehav. Rev.* 28, 675–685. doi: 10.1016/j.neubiorev.2004.09.004
- Ryan, T. J., Roy, D. S., Pignatelli, M., Arons, A., and Tonegawa, S. (2015). Engram cells retain memory under retrograde amnesia. *Science* 348, 1007–1013. doi: 10.1126/science.aaa5542
- Sellami, A., Abed, A. S. A., Brayda-Bruno, L., Etchamendy, N., Valério, S., Oulé, M., et al. (2017). Temporal binding function of dorsal CA1 is critical for declarative memory formation. *Proc. Natl. Acad. Sci. U S A* 114, 10262–10267. doi: 10.1073/pnas.1619657114
- Takata, N., Yoshida, K., Komaki, Y., Xu, M., Sakai, Y., Hikishima, K., et al. (2015). Optogenetic activation of CA1 pyramidal neurons at the dorsal and ventral hippocampus evokes distinct brain-wide responses revealed by mouse fMRI. *PLoS One* 10:e0121417. doi: 10.1371/journal.pone.0121417
- Taylor, K. K., Lowry, E., Tanaka, K., Levy, B., Reijmers, L., Mayford, M., et al. (2011). Characterization of NMDAR-independent learning in the hippocampus. *Front. Behav. Neurosci.* 5:28. doi: 10.3389/fnbeh.2011.00028
- Wiltgen, B. J., and Fanselow, M. J. (2003). “A model of hippocampal-cortical-amygdala interactions based on contextual fear conditioning,” in *The Neurobiology of Spatial Behaviour*, ed. K. J. Jeffery (New York, NY: Oxford University Press), 81–103.
- Wiltgen, B. J., Sanders, M. J., Anagnostaras, S. G., Sage, J. R., and Fanselow, M. S. (2006). Context fear learning in the absence of the hippocampus. *J. Neurosci.* 26, 5484–5491. doi: 10.1523/jneurosci.2685-05.2006
- Yoon, T., and Otto, T. (2007). Differential contributions of dorsal vs. ventral hippocampus to auditory trace fear conditioning. *Neurobiol. Learn. Mem.* 87, 464–475. doi: 10.1016/j.nlm.2006.12.006
- Zelikowsky, M., Bissiere, S., Hast, T. A., Bennett, R. Z., Abdipranoto, A., Vissel, B., et al. (2013). Prefrontal microcircuit underlies contextual learning after hippocampal loss. *Proc. Natl. Acad. Sci. U S A* 110, 9938–9943. doi: 10.1073/pnas.1301691110

Conflict of Interest Statement: The authors declare that the research was conducted in the absence of any commercial or financial relationships that could be construed as a potential conflict of interest.

Copyright © 2019 Wilmot, Puhger and Wiltgen. This is an open-access article distributed under the terms of the Creative Commons Attribution License (CC BY). The use, distribution or reproduction in other forums is permitted, provided the original author(s) and the copyright owner(s) are credited and that the original publication in this journal is cited, in accordance with accepted academic practice. No use, distribution or reproduction is permitted which does not comply with these terms.



Social Memory and the Role of the Hippocampal CA2 Region

Nikolaos Tzakis* and Matthew R. Holahan*

Department of Neuroscience, Carleton University, Ottawa, ON, Canada

The CA2 region of the hippocampus is a somewhat obscure area lacking in an understanding of its form and function. Until recently, the CA2 has been thought of as merely an extension of the CA3, with some referring to it as the CA3a region. Recent investigations into this area have not only delineated the CA2, but also defined it as a region distinct from both CA1 and CA3, with a unique set of cortical inputs and outputs and contributions to cognitive processes. One such process that has been shown to depend on the CA2 is the ability to recognize a novel or familiar conspecific, known as social recognition memory. Here, we review these findings and discuss the parallels between CA2 dysfunction and social impairments.

Keywords: CA2, social memory, hippocampus, social recognition, social neuroscience

OPEN ACCESS

Edited by:

Gregg Stanwood,
Florida State University, United States

Reviewed by:

Michael J. Schmeisser,
Johannes Gutenberg University
Mainz, Germany
Almira Vazdarjanova,
Augusta University, United States

*Correspondence:

Nikolaos Tzakis
NikolaosTzakis@gmail.com, carleton.ca
Matthew R. Holahan
matthew.holahan@carleton.ca

Specialty section:

This article was submitted to
Learning and Memory,
a section of the journal
Frontiers in Behavioral Neuroscience

Received: 01 May 2019

Accepted: 17 September 2019

Published: 01 October 2019

Citation:

Tzakis N and Holahan MR (2019)
Social Memory and the Role of the
Hippocampal CA2 Region.
Front. Behav. Neurosci. 13:233.
doi: 10.3389/fnbeh.2019.00233

SOCIAL NEUROSCIENCE

Social cognitive neuroscience is a burgeoning interdisciplinary field of research that aims to delineate the “why” and “how” of interactions between individuals. It aims to explore the relationship between cognitive processes and behavior in a social context. First described by Cacioppo and Berntson (1992), this field was developed to study mental and behavioral processes using an integrative, multimodal approach. This field of study is comprised of three levels of interaction: the social level, which focuses on the motivational and social factors that influence behavior and experience; the cognitive level, which focuses on the information-processing mechanisms that contribute to social-level processes; and the neural level, which focuses on the role of various brain regions and their involvement in cognitive level processing (Ochsner and Lieberman, 2001).

SOCIAL MEMORY

One of the processes that is paramount to the structure and stability of relationship networks that define societies is that of social memory (Kogan et al., 2000). Social memory reflects different cognitive and behavioral processes, such as the ability to recognize a familiar or novel conspecific, commonly referred to as social recognition, or the ability to learn from others, commonly referred to as social learning (van der Kooij and Sandi, 2012). For the purpose of this review, we will predominantly focus on the social recognition aspect of social memory.

The ability to recognize a familiar versus novel individual is the foundation on which social relationships are built. Memory for individual conspecifics is not only necessary to engage in meaningful relationships but is also required to express appropriate behavioral responses based on previous encounters (van der Kooij and Sandi, 2012; Jacobs et al., 2016). Social recognition memory in animals is essential for social hierarchy, mate and offspring recognition, territorial

defense, interspecies recognition, and for the general establishment and maintenance of groups (Ferguson et al., 2002; Jacobs et al., 2016). Social recognition depends on various sensory cues in order to establish the identity of an individual. Social recognition in humans and primates relies on the use of visual and auditory cues, with the right fusiform gyrus being responsible for coding information pertaining to the physical characteristics of an individual. Patients with lesions in the right fusiform gyrus are unable to recognize faces, an ailment known as prosopagnosia, while leaving all other visual and memory processes intact (Landis et al., 1986; Ferguson et al., 2002). While auditory and visual information may have important influences on social recognition in humans and other primates, chemosensory cues in the form of olfactory or pheromonal signals are more relied upon by most other mammals to encode social information (Ferguson et al., 2002). Chemically induced anosmia or removal of the vomeronasal organ in mice results in a decrease in individual recognition, providing evidence to suggest that intact olfactory processing is required for social recognition processes (Matochik, 1988; Bluthé and Dantzer, 1993; Kogan et al., 2000).

While social recognition is a common process across a variety of mammals, there are species and sex differences which may influence how it is expressed (van der Kooij and Sandi, 2012). Studies comparing social memory in mice and rats reported that the memory is much more resilient in mice than it is in rats. Recognition in rats was reported to only last about 30–60 min following acquisition as opposed to mice where it was reported to last for days. The opposite is true when comparing other types of memories, such as spatial memory, between the two species (Engelmann and Landgraf, 1994; Letty et al., 1997; Kogan et al., 2000; van der Kooij and Sandi, 2012). Differences in regional processing may account for the variations reported in these species. Following a social preference task, *c-Fos* expression in both the main and accessory olfactory bulb was significantly upregulated in mice where modest *c-Fos* expression was only observed in the accessory olfactory bulb in rats. This suggests that a difference in olfaction may account for the species-specific differences in social recognition (Noack et al., 2010; van der Kooij and Sandi, 2012).

Sex-differences have also been reported to exist in social recognition processes. In a social recognition task, female rats were reported to spend less time investigating a conspecific juvenile compared to males, yet females displayed stronger remote social recognition than males (Markham and Juraska, 2007; van der Kooij and Sandi, 2012). Based on these results, it is possible that estrogen activity may be a contributing factor that influences this behavior. Indeed, female mice lacking α and β estrogen receptors demonstrated impaired social recognition, while estrogen replacement in ovariectomized female mice improved social recognition (Choleris et al., 2003; Tang et al., 2005; van der Kooij and Sandi, 2012). Administration of an estrogen α receptor agonist impaired social recognition, while administration of an estrogen β receptor agonist prolonged it. Together, these results provide evidence to explain the presence of more robust social memory processes in females, which partly

relies on estrogen receptor activity (Clipperton et al., 2008; van der Kooij and Sandi, 2012).

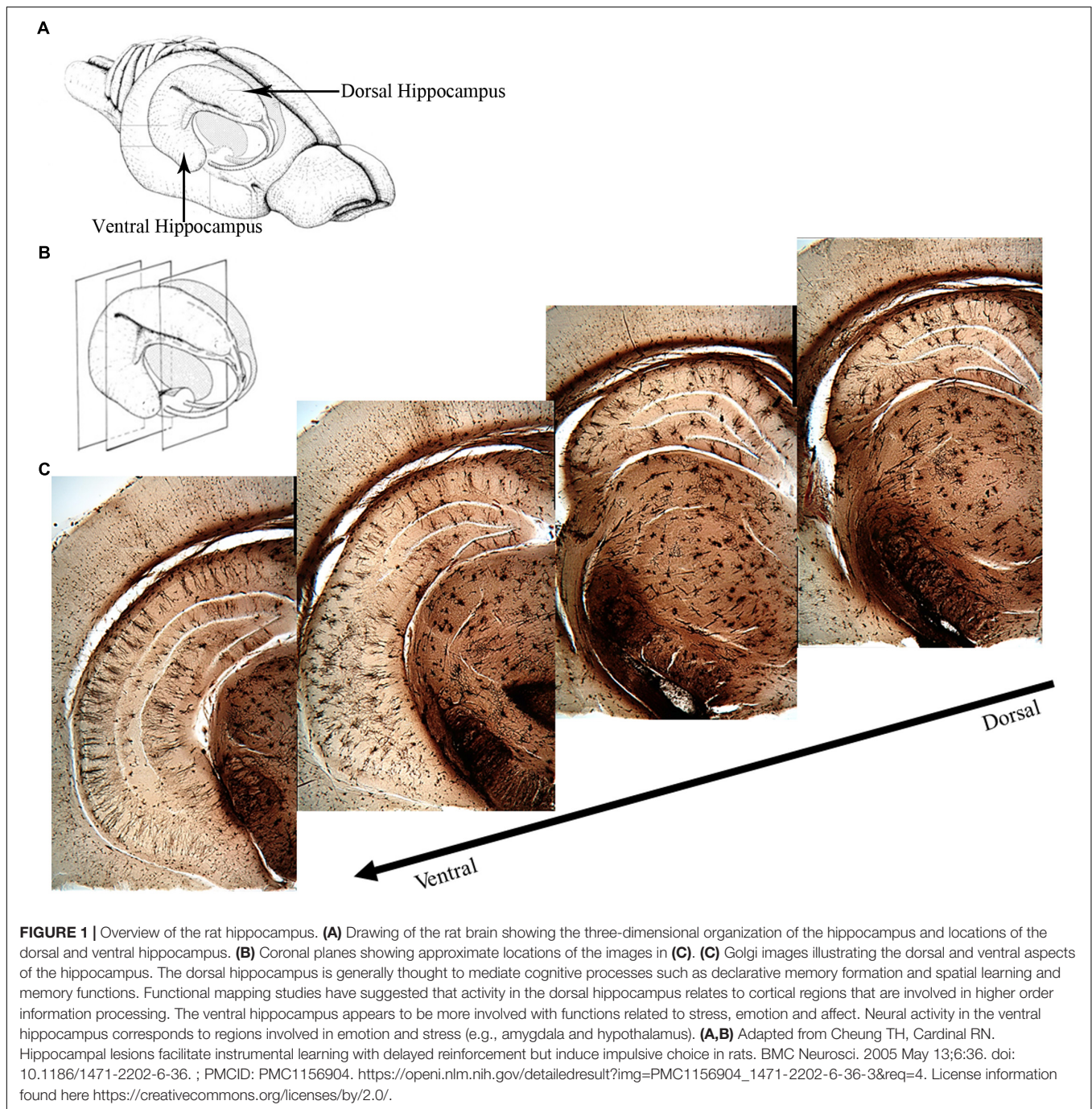
HIPPOCAMPUS AND SOCIAL MEMORY

Evidence suggests that the hippocampus is required for proper processing of social memories as data have shown that hippocampal lesions disrupt social recognition (Maaswinkel et al., 1996). Rats with hippocampal transections were introduced to a juvenile rat for 5 min then reintroduced 5 min later. On the following day, the rats were introduced to a novel juvenile rat and their behaviors were recorded (Maaswinkel et al., 1996). Lesioned rats spent less time engaged in social investigation than control rats and were unable to distinguish between a familiar and unfamiliar juvenile. While they were unable to determine the precise nature of the impairment in social memory, they postulated that the deficits resulted from a disruption in sequential behavior or conditional association formation (Maaswinkel et al., 1996).

Kogan et al. (2000) also provided evidence to suggest that the hippocampus plays a role in social memory. They induced hippocampal lesions using ibotenic acid in adult mice then exposed the mice to a social recognition task. For this task, the experimental mouse was introduced to a juvenile mouse for an initial interaction of 2 min. The experimental mouse was then exposed to either the same or a novel juvenile mouse following either a 30-s or a 30-min intertrial interval. Hippocampal-lesioned mice showed intact social memory when tested after a 30-s delay but impaired social memory when tested after a 30-min delay (Kogan et al., 2000). The authors concluded that immediate social recognition memory is not impaired by hippocampal lesions but that long-term social memory is dependent on hippocampal function. They further postulated that the role of the hippocampus in integrating complex stimuli, particularly those from the olfactory bulb, is crucial in the recognition process and may explain why intact hippocampal function is essential for social memory (Kogan et al., 2000).

FUNCTIONAL DIVISIONS OF THE HIPPOCAMPUS

The two major divisions of the hippocampus are the dorsal and the ventral hippocampus (**Figure 1**), each with their own distinct input and output connections and roles in memory processing (Swanson and Cowan, 1977; Moser et al., 1995; Moser and Moser, 1998; Fanselow and Dong, 2010). The dorsal hippocampus (**Figure 1**) receives input from the caudolateral band of the entorhinal cortex and sends excitatory projections to dorsal parts of the subiculum, presubiculum, and post-subiculum. Additionally, the dorsal hippocampus sends projections to the retrosplenial and anterior cingulate cortices, as well as the caudal and rostral part of the lateral septal nucleus, an area that has been found to regulate social behavior (Fanselow and Dong, 2010; Bredewold et al., 2015). The ventral hippocampus (**Figure 1**) receives input from the rostromedial band of the entorhinal



cortex and sends direct projections to the olfactory bulb, along with bi-directional projections to the amygdala (Saunders et al., 1988; Pitkanen et al., 2000; Cenquizca and Swanson, 2007; Fanselow and Dong, 2010).

The ventral hippocampus has been shown to be involved in emotional memory processes, like fear, and influences the fear memory processing of the amygdala, given that the ventral, but not the dorsal, hippocampus projects directly to the amygdala (Moser and Moser, 1998; Fanselow and Dong, 2010). The dorsal hippocampus contributes to spatial memory processes

due to the observation that place fields in this region are more compacted whereas place fields in the ventral hippocampus are more dispersed (Jung et al., 1994). A study reported by Moser et al. (1993) supports this hypothesis. After performing localized dorsal hippocampal lesions and testing rats in the Morris water maze, they noted impaired latencies during training, along with a reduction in the amount of time spent in the target quadrant during the probe test. Rats with ventral hippocampus lesions experienced no impairment in their spatial learning abilities. Based on these results, they concluded that

the dorsal hippocampus is more important for the encoding of new spatial information than the ventral aspect (Moser et al., 1993; Riedel and Micheau, 2001). Further evidence to support this hypothesis comes from studies completed by Moser et al. (1995) and Pothuizen et al. (2004), who also reported that hippocampal-dependent learning was impeded if the dorsal portion of the hippocampus was lesioned. They further noted that dorsal hippocampal lesions were just as effective as complete hippocampal lesions in disrupting spatial working memory, as opposed to lesions of the ventral hippocampus, which resulted in no disruption of spatial working memory.

SUBREGIONS OF THE DORSAL HIPPOCAMPUS

The dentate gyrus (Figure 2) receives multiple sensory inputs, including olfactory, auditory, and visual, from both the perirhinal and entorhinal cortices, along with spatially organized grid cells from the entorhinal cortex (Figure 2). These inputs allow the dentate gyrus to regulate, process, and represent both spatial and non-spatial information concurrently, commonly known as “conjunctive encoding” (Kesner, 2013).

The ability to organize and separate spatial events from one another, allowing an organism to temporally remember one place as distinct from another, is largely mediated by the dentate gyrus (Kesner, 2013). This spatial pattern separation is facilitated by mossy fibers (Figure 2) which form connections between granule cells in the dentate gyrus and pyramidal cells in the CA3 and CA2 regions and dictate which of these neurons will fire during learning based on activity in the dentate gyrus (O'Reilly and McClelland, 1994; Rolls, 1996; Kesner, 2013). Rats with dentate gyrus lesions were unable to discriminate object-place paired associates for reward; that is, they were impaired in their ability to distinguish between the same two objects placed in different locations (Lee and Solivan, 2010). Lesioned rats were able to discriminate between four different objects presented in the same location. Finally, using the same initial two objects, but placing them in remote locations, lesioned rats were initially impaired at discriminating the objects, but were able to relearn the task, showing no sustained deficits (Lee and Solivan, 2010). They concluded that the dentate gyrus is necessary for the ability to discriminate between object-place paired associates when object and/or spatial information overlaps but has less of an impact when that overlapping information decreases (Lee and Solivan, 2010). Other studies in the literature have corroborated these results suggesting that the deficits in spatial tasks resulting from dentate gyrus lesions may be a function of increased interference and impairment in spatial pattern separation (McDonald and White, 1995; Gilbert et al., 2001; Morris et al., 2012; Kesner, 2013).

The CA1, CA2, and CA3 regions are the principal pyramidal cell fields in the hippocampus (Figure 3) and are often the focus of research concerned with memory encoding and retrieval (McNaughton and Morris, 1987; Chevalyere and Siegelbaum, 2010). The CA regions are each composed of layers, or “strata”: the *stratum pyramidale*, the *stratum lacunosum-moleculare*, the

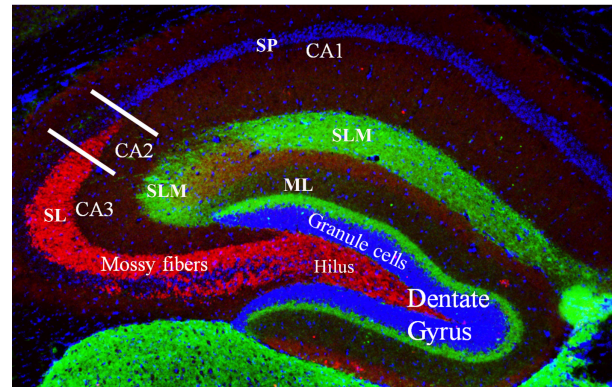


FIGURE 2 | Coronal cross section of the dorsal hippocampus showing the primary subdivisions. The granule cells (stained with DAPI) make up the major cell type in the dentate gyrus. These neurons project to the CA3 and CA2 regions via the unmyelinated mossy fibers (shown in red, stained with a zinc transporter antibody). The mossy fibers have large presynaptic terminals that enable synaptic connections to be made with CA3 and CA2 pyramidal cells and the mossy cells of the polymorphic layer (or, hilus). Each mossy fiber gives rise to several thin collaterals that synapse in the CA3 *stratum lucidum* (SL) and CA2 *stratum radiatum* (SR). The CA areas are all filled with densely packed pyramidal cells that make up the *stratum pyramidale* (SP; only labeled in CA1 but layer also present in CA2 and CA3). Green staining shows axonal terminal fields in the *stratum lacunosum moleculare* (SLM) of the CA1, CA2, and CA3 subfields and the molecular layer (ML) of the dentate gyrus. These terminals mainly arise from the entorhinal cortex.

stratum lucidum, the *stratum oriens*, and the *stratum radiatum*. The *stratum pyramidale* contains the cell bodies of pyramidal cells and various interneurons (Andersen et al., 2007). Pyramidal cell layers in the CA1 are more tightly packed than those in the CA2 and CA3 regions (Figure 3).

In the CA2 and CA3 regions, the *stratum lacunosum-moleculare* receives inputs from layers II and VI of the entorhinal cortex, while the *stratum lacunosum-moleculare* in the CA1 receives input from layers III and V of the entorhinal cortex (Witter and Amaral, 1991; van Groen et al., 2003; Figure 4). The *stratum lucidum*, which is found exclusively in the CA3 field between the pyramidal cell layer and the *stratum radiatum* (Figure 4), contains mossy fibers from the granule cells of the dentate gyrus (Witter and Amaral, 1991; Andersen et al., 2007). Axons from cells within the layer II of the entorhinal cortex synapse directly with the dendritic spines of granule cells in the dentate gyrus. Mossy fibers are formed by the axons of these granule cells and form synaptic connections with the proximal apical dendrites of pyramidal cells in the *stratum lucidum* of the CA3 via the hilus of the dentate fascia (Andersen et al., 1971; Sandler and Smith, 1991; Witter, 2007; Neves et al., 2008).

The *stratum oriens* is a deep, relatively cell-free layer containing the basal dendrites of the pyramidal cells and various interneurons, along with some of the myelinated Schaeffer collateral connections from CA3 to CA1 (Figure 4). The *stratum radiatum* possesses the majority of Schaeffer collateral connections (Andersen et al., 2007). Both the subiculum and the *stratum lacunosum-moleculare* of the CA1 also receive direct

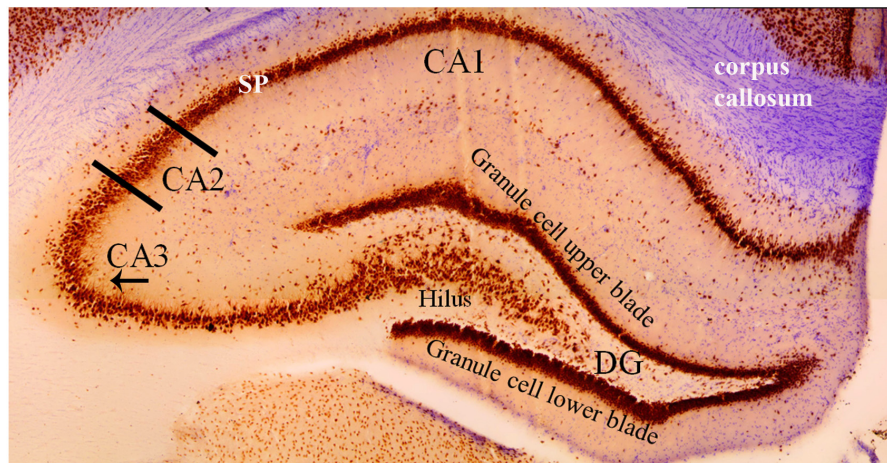


FIGURE 3 | Coronal cross section of the dorsal hippocampus stained with the neuron specific antibody, NeuN. Image more clearly shows the various cell types in each hippocampal subfield. The NeuN protein is localized in the nuclei and perinuclear cytoplasm of most neurons in the central nervous system. The hippocampus proper is defined by the dentate gyrus and Cornu Ammonis (CA). The dentate gyrus contains densely packed granule cells in both an upper and lower blade. The hilus (also referred to as the polymorphic layer) within the granule cell layers contains mossy cells. In this coronal plane, the NeuN stain shows the base of the apical dendrite protruding from the CA3 pyramidal cells (arrow under “CA3”). This pattern of staining is absent from the CA2 pyramidal neurons indicating (1) the CA2 apical dendrites are not in the coronal plane and (2) an anatomical distinction between CA2 and CA3 pyramidal cells. Comparison of the NeuN staining in CA2 and CA1 regions shows the CA1 *stratum pyramidale* (SP) layer to be more densely packed and narrower than the CA2 region. Purple stain from a cresyl violet counterstain shows the corpus callosum.

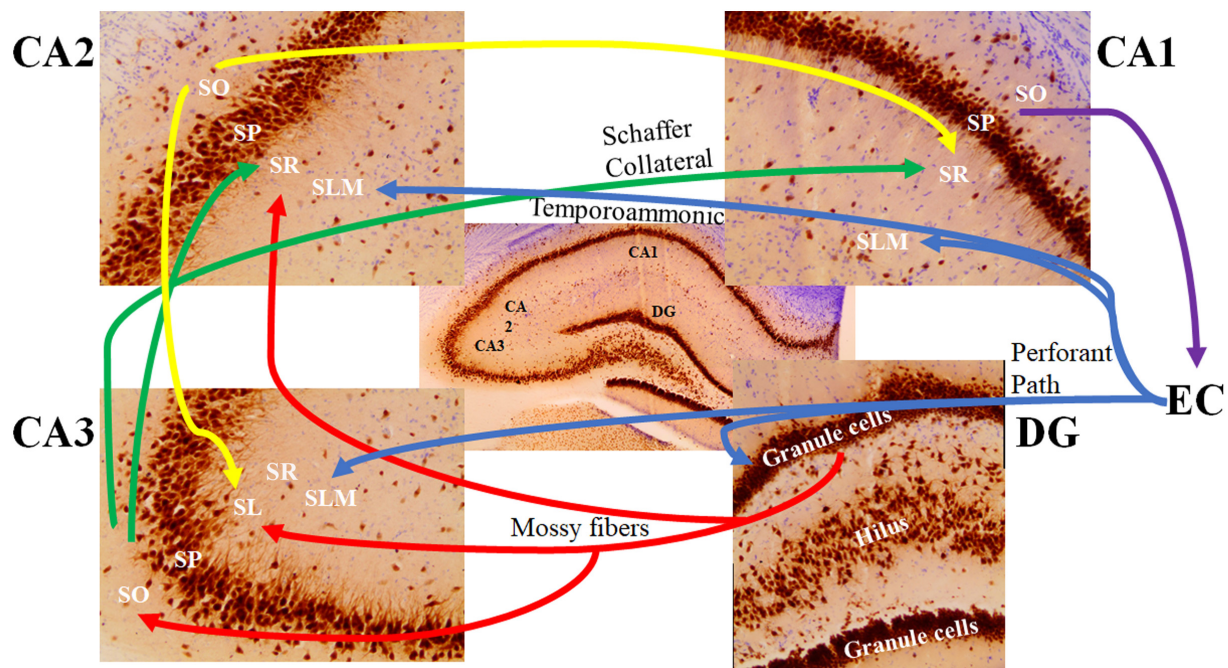


FIGURE 4 | The major signaling pathways through the hippocampal subfields. The most prominent afferent input to the hippocampus originates from the entorhinal cortex (EC). The axons forming the perforant path (blue) arise from layer 2 of the EC and show synaptic contacts in the granule cell molecular layer of the dentate gyrus (DG) and the *stratum lacunosum moleculare* (SLM) of the CA3 region. There are also distinct projections from layer 3 of the EC to the SLM of the CA1 and CA2 regions (referred to as the temporoammonic pathway; blue). Granule cells of the DG send their axons (mossy fibers; red) through the hilus to the CA3 *stratum lucidum* (SL) and the border of the CA2 *stratum radiatum* (SR) and SLM. The mossy fibers also show terminal fields in the *stratum oriens* (SO) of the CA3 pyramidal cells. Pyramidal cells of the CA3 region send their axons (the Schaffer Collateral pathway; green) to the CA1 and CA2 SR subfields. Pyramidal cells of the CA2 project back to the CA3 SL region and forward to the CA1 SR subfield (yellow). Pyramidal cells of the CA1 region send their axons to the subiculum (not shown) and back to the deep layers of the EC (purple). SP: *stratum pyramidale*.

projections from neurons in layer III of the entorhinal cortex (Kajiwaru et al., 2008; Maccaferri, 2011). Axons of CA1 pyramidal neurons project into the septum, hypothalamus, and contralateral hippocampus via the fimbria (Andersen et al., 1971). In addition to receiving input from cortical regions, layer V of the entorhinal cortex receives output from the CA1 via the subiculum, which then projects to other brain regions, such as the mamillary nuclei, the thalamus, and the nucleus accumbens (Amaral, 1993; Wible, 2013).

Norman and O'Reilly (2003) developed a computational model of recognition memory that provides insight into the interplay between the hippocampal subregions, which function to mediate the storage and retrieval of recognition memory and may be transferable to other forms of hippocampal-dependent memories. During acquisition, incoming information is relayed from the neocortex to the hippocampus via the entorhinal cortex. From the entorhinal cortex, activation is spread both directly, and indirectly, via the dentate gyrus, to the CA3. The representations within the CA3 and dentate gyrus are very sparse, allowing for only a few units of information to be active for a given stimulus. This gives rise to pattern separation, based on the notion that, if only a few units are active per input pattern, there is decreased overlap between the hippocampal representations of different items (Norman and O'Reilly, 2003). Here, the dentate gyrus facilitates pattern separation in the CA3. From there, representations in the CA3 link to active units in the CA1, which also contains re-representation of the original input pattern. The CA1 serves as a relay station between the CA3 back to the entorhinal cortex, linking the sparse representations in the CA3 with the overlapping representations in the entorhinal cortex. When recalling a stored memory, strengthened connections in the entorhinal cortex-CA3 pathway, along with strengthened CA3 recurrences, allow for a reactivation of the CA3 pattern corresponding to the original item. From there, activation spreads to the representation in the CA1, and back to the representation in the entorhinal cortex. This representation loop allows the hippocampus to retrieve the complete version of the original input in response to a partial cue (Norman and O'Reilly, 2003).

THE CA2 SUBREGION OF THE HIPPOCAMPUS

While the other subunits of the hippocampus have received extensive attention, the CA2 region has been largely neglected, poorly understood, and for the most part, unexplained (Chevalleyre and Siegelbaum, 2010; Caruana et al., 2012; Cui et al., 2013; Stevenson and Caldwell, 2014). Recent evidence has shed light on the obscurities of the CA2, characterizing it as a distinct subregion, with its own unique afferents and efferents, cellular composition, and contribution to hippocampal processes (Cui et al., 2013; Dudek et al., 2016; Mou, 2016).

Ramon y Cajal first described the hippocampus as a region with two distinct areas, which he divided based on the size of the pyramidal neurons that occupied the space: the *regio superior*, which was the top portion of the hippocampus and consisted

of small pyramidal neurons, and the *regio inferior*, which was the lower portion of the hippocampus and consisted of large pyramidal neurons (Caruana et al., 2012; Dudek et al., 2016). Upon closer examination, Lorente de No (1934) reported that a small area within the *regio inferior* differed enough in its cytoarchitecture and connectivity to warrant a distinction from the rest of the area. From there, the *regio superior* became known as the CA1 and the *regio inferior* was divided into the CA2 and CA3 regions (Lorente de No, 1934; Dudek et al., 2016).

The CA2 is situated between the CA3 and CA1 and is composed of a small population of large pyramidal neurons (Chevalleyre and Siegelbaum, 2010; Kohara et al., 2014). The cell bodies of the pyramidal neurons, like those of the CA3, are larger than those found in CA1 (Figures 5A,B). Unlike the CA3 pyramidal neurons, pyramidal neurons in the CA2 lack the specialized thorny excrescences on the apical dendrites associated with input from mossy fibers (Kohara et al., 2014; Dudek et al., 2016) yet receive mossy fiber input (Figure 5C). It was this morphological difference that prompted a separation of the *regio inferior* and was one of the first pieces of evidence that the CA2 was a distinct functional entity and not just an extension of the CA3 (Lorente de No, 1934; Amaral and Witter, 1989; Williamson and Spencer, 1994; Dudek et al., 2016; for additional differentiation, note PEP-19 staining in CA2 that is absent from CA3). In addition, unlike the dendrites of the CA3 pyramidal neurons, which extend along the longitudinal axis of the hippocampus, dendrites of CA2 neurons branch along the transverse axis of the hippocampus (Ishizuka et al., 1995; Chevalleyre and Siegelbaum, 2010; Figure 5B).

CA2 CONNECTIVITY

The CA2 has been shown to receive both intrahippocampal and extrahippocampal inputs (Figure 6). While the CA2 is often excluded from hippocampal circuit diagrams, it fits within the traditional trisynaptic loop circuit (Caruana et al., 2012). Pyramidal cells within the *stratum lacunosum-moleculare* of the CA2 receive strong spatial input from cells in layers II and III of the medial entorhinal cortex, along with non-spatial information from layers II and III of the lateral entorhinal cortex (Figure 6B). The CA2 then projects strong unitary inputs to the *stratum oriens*, and to a lesser extent the *stratum radiatum*, in the CA1, synapsing onto basal dendritic arbors of CA1 pyramidal cells (Chevalleyre and Siegelbaum, 2010; Jones and McHugh, 2011; Caruana et al., 2012; Kohara et al., 2014; Mankin et al., 2015; Dudek et al., 2016; Figure 6B). This forms a unique indirect pathway of information transfer from the entorhinal cortex to the CA1 via the CA2 that parallels the direct pathway to CA1. This furthers the point that the CA2 is much more than a transition zone between CA1 and CA3, as was previously thought (Mankin et al., 2015). Pyramidal cells in the CA2 region have also been reported to project back to layer II of the medial entorhinal cortex (Rowland et al., 2013). The constant relay and flow of information to and from the entorhinal cortex has been known to render the quality of information susceptible to accumulating error. Coupled with the fact that, prior to the discovery of

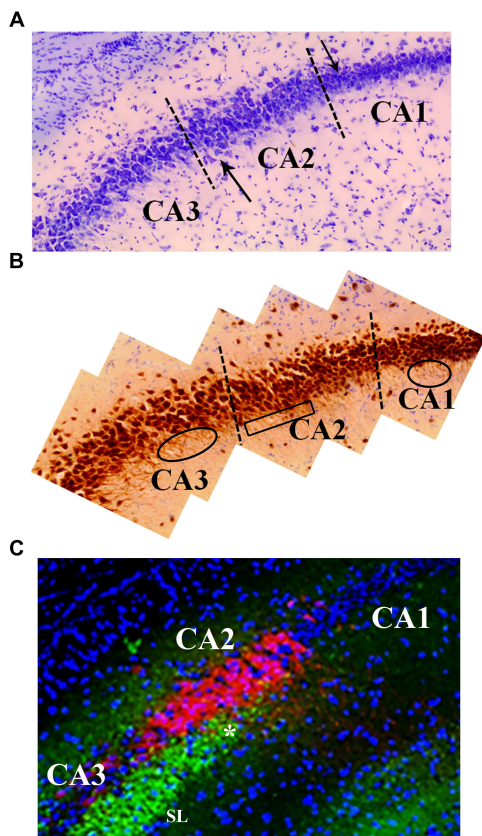


FIGURE 5 | Neuroanatomical features that distinguish the CA2 region from the CA3 and CA1. **(A)** Cresyl violet staining shows subtle differences between the CA2 and CA3 regions. Namely, cresyl violet-stained cells in the CA2 region are smaller in size and more densely packed than the CA3 cells. There is also a slight widening of the cell layer at the border of CA2 and CA3 (upward pointing arrow). The higher density of cells in CA1 is a characteristic that delineates the CA2 from CA1 (downward pointing arrow). **(B)** The neuron specific stain, NeuN, exemplifies the orientation of neurons in the CA3, CA2, and CA1 regions. Specifically, the base of the apical dendrites from CA3 and CA1 pyramidal cells can be seen in this image indicating a coronal plane orientation (ovals). The base of the apical dendrites protruding from the CA2 neurons is less clear (boxed area) suggesting these dendrites are not in the coronal plane. The NeuN stain also highlights the difference in the width of the cell layers between CA2 and CA1 (visible at dashed line). **(C)** The CA2 region contains a high density of PEP-19 protein (Purkinje cell protein 4, pcp4; red in image). PEP-19 is a small calmodulin (CaM)-binding protein. This is a clear indication of the CA2 boundaries and distinguishes the CA2 region from the CA1 and CA3 where PEP-19 staining is absent. Also shown in this image is the *stratum lucidum* (SL; green: synaptophysin staining) where the mossy fibers terminate (highlighted by the high density of synaptophysin staining in green). The most dorsal aspect of the mossy fiber projection (asterisk) is adjacent to the CA2, PEP-19 staining pattern. Blue is DAPI staining showing cell layers.

these direct, reciprocal CA2-entorhinal cortex inputs, the only known pathway between the entorhinal cortex and CA fields was a polysynaptic one, which could potentially lead to the loss of critical information necessary for recognition (McNaughton et al., 2006; Rowland et al., 2013). Given the importance of social recognition, particularly in terms of survival and social hierarchy,

compromising any incoming information about an individual and their features could result in difficulties differentiating friend from foe. As such, this direct flow of information between the CA2 and entorhinal cortex could ostensibly ensure that little information is lost, allowing for a more viable memory trace and more accurate recognition. Reciprocal, bilateral connections also exist between the CA3 and CA2 regions, whereby the *stratum radiatum* of the CA2 receives weak, converging input from the CA3 via Schaffer collaterals, and projects back to the *stratum oriens* of CA3 (Jones and McHugh, 2011; Caruana et al., 2012; Dudek et al., 2016; **Figure 6B**).

There is evidence that the mossy fiber terminals from the dentate gyrus may extend into the CA2 (**Figure 6B**) despite these neurons lacking dendritic thorny excrescences (Houser et al., 1990; Williamson and Spencer, 1994; Llorens-Martin et al., 2015). The absence of input from the dentate gyrus has been commonly used as an anatomical delineator between CA3 and CA2 regions. While this has been a common marker to distinguish the CA2 region from the CA3, it is not as reliable as the absence or presence of larger specialized post-synaptic markers (Dudek et al., 2016). Further investigations have also led to the understanding that the extent of dentate gyrus axon projection is species-specific (Dudek et al., 2016). The dentate gyrus has been reported to project axons to the *stratum radiatum* of the CA2 region in guinea pigs, cats, rats, and mice (McLardy, 1963; Hirama et al., 1997; Lavenex et al., 2009; Kohara et al., 2014; San Antonio et al., 2014; Dudek et al., 2016). Given the role of the dentate gyrus and its connectivity with the CA3 in spatial pattern separation, it is possible that the connections with CA2 mediate similar processes. Specifically, these connections may help the organism discriminate between a novel vs. familiar conspecific possessing similar features, especially considering that the dentate gyrus has been deemed necessary only when incoming information overlaps (i.e., may be similar) but has less of an impact when dissimilar information is processed (Lee and Solivan, 2010). Those same projections do not appear to occur in human and non-human primates (Lorente de No, 1934; Dudek et al., 2016). This may speak to the complexity of social recognition processing in human and non-human primate vs. other organisms; other organisms may rely on simple sensory input (smell, fur color, etc.) to discriminate between other individuals, which would potentially require simple circuitry to process the information. Social recognition in human and non-human primates is multi-factorial, involving the processing of emotion, context, etc., and not simply rely on the scent or singular physical feature of another to help recognize or discriminate between other organisms. As such, this processing would require more advanced circuitry and integration from other regions, and not rely solely on a dentate gyrus-CA2 connection to discriminate between all the different pieces of incoming information.

In addition to the intrahippocampal connections, the CA2 receives unilateral, extrahippocampal input from vasopressinergic cells in the paraventricular nucleus of the hypothalamus and the median raphe nucleus (**Figure 6B**). The CA2 also forms reciprocal, bilateral connections with the supramammillary nucleus, the medial and lateral septal nuclei, and the vertical and horizontal limbs of the diagonal band of

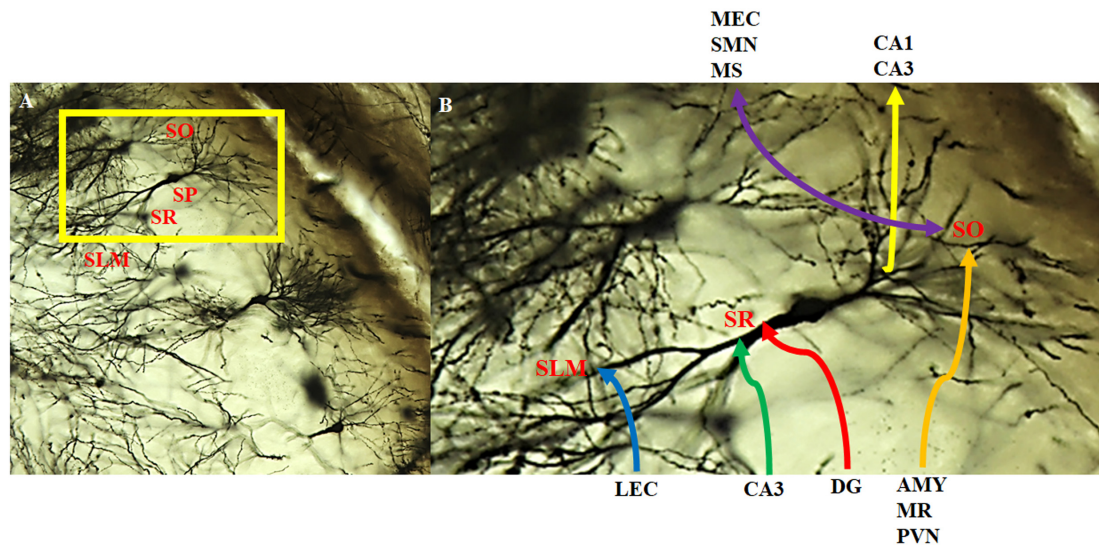


FIGURE 6 | Intra- and extra-hippocampal connectivity patterns of CA2 neurons. Neurons within the CA2 region visualized with the Golgi-Cox method and magnified at **(A)** 20x and **(B)** 40x. CA2 neurons receive direct innervation from the lateral entorhinal cortex (LEC) via the temporoammonic pathway (blue). This input terminates in the distal dendritic field making up the *stratum lacunosum moleculare* (SLM). Intra-hippocampal inputs arise from the CA3 (green) and the dentate gyrus (red; mossy fibers) that terminate on the more proximal dendritic field of the *stratum radiatum* (SR). CA2 neurons receive a substantial, extrahippocampal input (orange) from the amygdala (AMY), median raphe (MR), and paraventricular nucleus (PVN) that terminate on the basal dendritic field of the *stratum oriens* (SO). In addition, CA2 neurons make reciprocal, bilateral extrahippocampal connections (purple) with the medial entorhinal cortex (MEC), supramammillary nucleus (SMN) and medial/lateral septum/diagonal band of Broca (MS). There are also feedback projections to CA3 pyramidal cells and feedforward to CA1 pyramidal cells (yellow). SP: *stratum pyramidale*.

Broca (Cui et al., 2013; **Figure 6B**). While the contribution of this innervation is not entirely clear, it has been hypothesized to modulate hippocampal excitability and play a role in memory consolidation (Pan and McNaughton, 2004; Shahidi et al., 2004; Caruana et al., 2012). Oxytocin and arginine vasopressin are important for modulating social behavior in a species-specific fashion (Donaldson and Young, 2008). They are synthesized in the paraventricular and supraoptic nuclei of the hypothalamus, with vasopressin also synthesized in the suprachiasmatic nucleus and released from the pituitary, where they bind to receptors found throughout the central nervous system and periphery (Gimpl and Fahrenholz, 2001; Insel, 2010). Furthermore, oxytocin and vasopressin have both been considered to play a role in learning and memory (Gimpl and Fahrenholz, 2001). As such, the connectivity between the CA2 and these extrahippocampal regions may mediate the neurochemical underpinning of social memory through the release and subsequent activity of these neuropeptides on the target brain regions which may explain the contribution of the hippocampus to social memory processing.

LTP IN CA2

Long-term potentiation (LTP) has been widely accepted to be the cellular underpinning of synaptic plasticity, and memory acquisition, storage, and retrieval in the central nervous system (Caruana et al., 2012). High-frequency stimulation of CA3 region, activating the Schaffer collateral inputs to the CA1, creates

a robust potentiation within the CA1 region, inducing and sustaining LTP (Caruana et al., 2012). Similar induction of LTP is not observed within CA3-CA2 synapses. The inputs from CA3 via Schaffer collaterals amass a very large feedforward inhibition onto the CA2 neurons (Chevalleyre and Siegelbaum, 2010; Jones and McHugh, 2011). Zhao et al. (2007) used whole cell recording to test whether 100 Hz synaptic stimulation could induce LTP in CA2 neurons. Upon stimulation, they reported no potentiation of the synaptic currents, specifically in the *stratum radiatum* of the CA2. They used a variety of methods, including the use of a perforated patch clamp technique, to try to induce LTP within the CA2, but to no avail (Zhao et al., 2007).

The high expression of TREK-1 and TREK-2 potassium channels in CA2 relative to other hippocampal subregions was a likely candidate for the lack of LTP, given that these two-pore channels create a potassium-mediated leak current, significantly hyperpolarizing the resting membrane potential and requiring a greater depolarizing current to initiate LTP (Zhao et al., 2007; Caruana et al., 2012). Blocking potassium channels, including TREKs, with cesium in the electrode internal solution still inhibited LTP induction (Zhao et al., 2007; Dudek et al., 2016). LTP inhibition was linked to an abundance of STEP, a phosphatase that can dephosphorylate and inactivate ERK in response to NMDA receptor activation and can inhibit NMDA function (Zhao et al., 2007; Caruana et al., 2012). Application of okadaic acid, a protein phosphatase inhibitor, failed to induce LTP (Zhao et al., 2007). Induction of LTP was still absent when GABA_A inhibitory currents were blocked using picrotoxin, yet all of these protocols

consistently induced LTP in the CA1 (Zhao et al., 2007; Caruana et al., 2012).

Given that certain forms of LTP in the hippocampus are mediated by NMDA receptors, Zhao et al. (2007) compared the patterns of expression of NMDA receptor mRNA in the CA2 and CA3 and found that they were expressed evenly across both regions. They concluded that critical components of the LTP were missing in the CA2 and offered some molecular causes to explain the lack of LTP (Zhao et al., 2007). One possible explanation is the abundance of A₁ adenosine receptors, of which the population is denser in the CA2 region than other hippocampal regions (Zhao et al., 2007; Jones and McHugh, 2011). Adenosine is a well-known potent inhibitory modulator. It is a byproduct of both intracellular and extracellular ATP metabolism and is released with other neurotransmitters and metabolized by ectoprotein kinases (Wieraszko et al., 1989; Mitchell et al., 1993). Stimulation of adenosine A₁ receptors activates potassium channels and inhibits calcium channels, both of which result in a hyperpolarization of hippocampal neurons. The resulting hyperpolarization and reduction in calcium influx counteracts the post-synaptic depolarization that is required for LTP and suggests that the lack of LTP in the CA2 may be mediated by adenosine (Arai et al., 1990; de Mendonca and Ribeiro, 1990; Zhao et al., 2007).

Another explanation offered by Zhao et al. (2007) was that CA2 pyramidal neurons expressed calbindin, a calcium-binding protein found in inhibitory interneurons that can regulate synaptic plasticity. Since calcium signaling is important for the induction of LTP in other regions of the hippocampus, it is possible that the inhibition of LTP may reflect differences in local calcium handling in CA2 (Simons et al., 2009; Caruana et al., 2012). To test this hypothesis, Simons et al. (2009) loaded CA2 pyramidal neurons with a fluorescent calcium dye indicator and used two-photon confocal imaging to study the dendrites and spines of those neurons. They reported significantly smaller evoked calcium transients in CA2 compared to those in CA1 and CA3 (Simons et al., 2009). From there, they calculated a significantly higher endogenous calcium buffering capacity, along with significantly higher calcium extrusions, in the CA2 relative to CA1 and CA3. After raising the extracellular calcium levels of the preparation and using a higher frequency of tetanic stimulation, they managed to induce LTP at CA2 *stratum radiatum* synapses (Simons et al., 2009; Caruana et al., 2012; Dudek et al., 2016). They concluded that these observations could account for the lack of LTP propagation in the CA2 (Simons et al., 2009). This finding indicated that, while the CA2 contains a slew of proteins that may contribute to the failure of LTP induction, these synapses nonetheless possess the intracellular machinery necessary for LTP induction, but that higher calcium buffering and extrusion prevents plasticity (Simons et al., 2009).

The CA2 region possesses certain 'memory inhibiting' genes, of which one is RGS14. RGS14 is highly enriched in CA2, specifically in the *stratum lacunosum-moleculare* and *stratum radiatum* and has been shown to play a crucial role in the suppression of LTP induction (Lee et al., 2010; Dudek et al., 2016). It is a scaffolding protein that integrates G protein and

H-Ras/ERK/MAP kinase signaling pathways (Lee et al., 2010). Lee et al. (2010) created a transgenic mouse line, which lacked the RGS14. They reported a robust capacity for LTP within CA2 pyramidal neurons in the transgenic mice. They then evaluated the effect of RGS14 silencing on hippocampal-based spatial learning and memory. They reported that silencing of RGS14 resulted in marked improvements in both the Morris water maze and novel-object recognition task. They suggested that RGS14 may act as a natural brake to limit LTP and synaptic plasticity within the CA2 following stimulation. This may result from RGS14 binding to various kinases, inhibiting growth-factor directed MAP kinase signaling (Lee et al., 2010). They concluded that RGS14 regulates signaling pathways linking synaptic plasticity in CA2 to hippocampal-dependent memory processes, distinct from the trisynaptic pathway (Lee et al., 2010).

Given this lack of demonstrable LTP, it may be tempting to presume that the CA2 is a highly stable component of the hippocampal circuit, devoid of any plastic functions common to the hippocampus. However, investigations have provided evidence suggesting that the CA2 is, in fact, highly plastic, though highly selective for the type of stimulus that can induce LTP (Caruana et al., 2012). The abundance of adenosine vasopressin (AVPR) 1b and adenosine A₁ receptors have been shown to have powerful and selective effects on synapse within the CA2 region, inducing a long-lasting potentiation of synaptic transmission within the area following the release of vasopressin or oxytocin (Caruana et al., 2012). As such, the induction of LTP, and concurrent memory formation, within the CA2 occurs under very specific conditions, e.g., vasopressin and oxytocin receptor activation, which happen to be neuropeptides that highly regulate social memory and behaviors. This provides further support that LTP and synaptic plasticity at CA2 synapses play a role in social recognition, and provides further insight into the function of the aforementioned connectivity between the CA2 and extrahippocampal regions (Wersinger et al., 2002; Prediger and Takahashi, 2005; DeVito et al., 2009; Caruana et al., 2012).

CA2 FUNCTION

Though apparently resistant to plasticity, evidence exists to suggest that the CA2 plays an integral role in various memory processes. DeVito et al. (2009) assessed memory processes in AVPR1b-knockout mice. AVPR1b has been shown to play an important role in regulating social behaviors, but their role in hippocampal-dependent memory function has yet to be investigated. The highest level of expression of AVPR1b in the brain is in the CA2 subregion (Wersinger et al., 2002; Young et al., 2006; DeVito et al., 2009). DeVito et al. (2009) employed an object recognition task and found that the knockout mice spent the same amount of time exploring a recently observed stationary object as they did an older one. These results suggest an impairment in memories that involve a temporal component. They further concluded that the involvement of CA2, in particular AVPR1b within the CA2, might play a highly selective role in temporal processing that supports episodic memory (DeVito et al., 2009).

Further investigations into the contributions the CA2 makes in memory processes lead investigators to uncover a potential role in contextual learning. Wintzer et al. (2014) used compartment analysis of temporal activity fluorescence *in situ* hybridization (catFISH) imaging to compare cell ensembles in CA1, CA2, and CA3 subregions in mutant mouse lines lacking either NMDA receptors at the CA3 synapse (CA3-NR1 KO) or at the perforant path inputs from the entorhinal cortex to the dentate gyrus (DG-NR1 KO). This allowed the investigators to manipulate the quality of incoming information to CA2. CA3-NR1 KO leads to deficits in rapid encoding information and associative memory storage, making a familiar representation more novel, while DG-NR1 KO leads to deficits in context discrimination, making a novel representation more familiar (Nakazawa et al., 2002; McHugh et al., 2007; McHugh and Tonegawa, 2009; Wintzer et al., 2014). The mice were subjected to familiar, altered, and novel context environments. The investigators reported that cell ensembles in CA2 were particularly sensitive to subtle changes in familiar environments; that is, they observed a robust change in ensembles in the CA2 that were disproportionate to the magnitude of contextual change (Wintzer et al., 2014; Dudek et al., 2016). This results from a remapping in CA2, independent of what is observed in either CA3 or CA1, uncoupling the CA2 from both regions (Wintzer et al., 2014). They concluded that the CA2 functions to detect and encode changes in patterns of input, in effect detecting conflicts between what the hippocampus recalls and what the animal is experiencing. One of the attributes to this function may result from the extrahippocampal input the CA2 receives from the supramammillary nucleus, a region activated by novelty (Wintzer et al., 2014).

Mankin et al. (2015) recently investigated the role CA2 plays in processing spatial aspects of memories. They analyzed spatial firing patterns in rats that randomly foraged in highly familiar environments in the morning and, 6 h later, in the afternoon. A higher mean spatial firing rate without a difference in peak firing rate among all spatial locations was reported in the CA2 relative to the other regions. This suggests that the amount of spatial information per cell in the CA2 was lower compared to the other regions (Mankin et al., 2015). The CA2 was also reported to possess a higher number of place fields per cell, as well as a larger field size, compared to the other subregions. Mankin et al. (2015) suggested that the combination of a larger number of place fields per cell and an increase in field size accounted for the reduction of spatial information. Spatial firing patterns in the CA2 were as consistent as in the CA3 or CA1 when the rats visited the same box shape repeatedly. These same firing patterns in CA2 became less consistent for repeated sessions in the same box shape that were separated by an intervening session of another shape. These results indicate that place fields in the CA2 do not show a persistent code for space or for changes in context, but rather become increasingly dissimilar in response to the passage of time, suggesting a role in temporal coding. These results indicate that, while the CA2 plays some role in spatial processing, it is not equivalent to that played by the CA3 and CA1 (Mankin et al., 2015; Dudek et al., 2016).

According to Mankin et al. (2015), the unique inputs from CA2 converge with other inputs to CA1, differing the CA1

activity patterns from one time to another. This convergence of time-varying inputs would create a time-stamped neural code that differs between similar events at different times. In addition, there would be greater overlap within the neural code for events that occurred closer in time (Mankin et al., 2015). Therefore, while observing the CA2 at the individual cellular level may demonstrate properties consistent with a role in spatial coding, the population level points to more of a role in temporal coding and less of a role in spatial contextual coding (Mankin et al., 2015; Dudek et al., 2016). Contrary to the findings reported by Wintzer et al. (2014), which suggest that CA2 plays a crucial role in contextual coding, Mankin et al. (2015) reported that the CA2 showed weak discrimination between spatial contexts; that is, the place fields in this region showed less change in response to alterations in the shape of a context compared to other regions. As Dudek et al. (2016) pointed out in their review, both studies differed in how the context was changed. They noted that, while Wintzer et al. (2014) introduced a novel change to a familiar environment, the experimental protocol employed by Mankin et al. (2015) used a familiarized change in the shape of the box (Dudek et al., 2016). Taken together, results from both studies suggest that the CA2 is required when a context is being updated, in addition to temporal coding (Dudek et al., 2016).

The CA2 inputs into both CA3 and CA1 place the CA2 region in a good position to influence network physiology and information processing within the hippocampus (Boehringer et al., 2017). In order to assess the role of CA2 in hippocampal network function, Boehringer et al. (2017) silenced synaptic transmission of CA2 pyramidal cells both chronically, via the expression of the tetanus neurotoxin light chain, and acutely, via the activation of the G_i-coupled DREADD receptors. They reported that chronically silencing the CA2 lead to a hyperexcitability within the recurrent CA3 circuit during exploration. In addition, acute silencing caused “hotspots” of multi-unit activity resulting from an increase in the concentration of CA1 and CA3 pyramidal cell spiking (Boehringer et al., 2017). They then examined the chronic loss of CA2 output and its effect on hippocampal activity during periods of immobility. Chronic loss of CA2 output lead to the appearance of large-amplitude, short-duration epileptiform-like discharges, which were initially observed in CA3 and then CA1, indicating they were CA3-driven. They suggested that CA2 silencing lead to a replacement of normal ripples with epileptiform-like discharges due to abnormally strong CA3 input arising in CA2 (Boehringer et al., 2017). To assess acute CA2 silencing on memory processes, Boehringer et al. (2017) habituated mice to a single context, followed by a distinct novel context. They reported slower habituation in CA2-silenced mice, indicating that the CA2 is integral in contextual habituation (Boehringer et al., 2017). Taken together, these results suggest that CA2 acts as a regulator of network processing within the hippocampus, creating a balance between excitatory and inhibitory processes required for proper network function, and preventing the hippocampus from entering a state of pathological activity. In effect, the CA2 functions to prevent “overheating” of the entire hippocampal network (Boehringer et al., 2017).

Based on the presented investigations, the evidence supports the hypothesis that the CA2 plays an integral role in the temporal and contextual processing of information. In terms of social memory, one can deduce that the CA2 plays a role in delineating whether a conspecific was encountered recently or remotely, which may facilitate the recognition of another organism, especially one that was encountered recently. Additionally, the CA2 acts as a sort of hippocampal error detector, allowing for the differentiation between a novel context and one that is familiar but with slight variation. This can prove to be extremely useful in terms of social memory as it allows an organism to constantly adapt to changes within their surroundings, and those who surround them. Without this ability, any detectable change in the recognition cue of a familiar conspecific (scent, appearance, etc.) or the environment in which the conspecific was initially encountered could ostensibly create errors in recognition. Together with the temporal processing of information, the CA2 can be viewed as processing the general 'when, where, and what' aspects of social recognition.

CA2 PATHOLOGY

Investigations into the distinct physiology and unique cognitive contributions of CA2 have cultivated some novel insight into the role this region plays in a myriad of neuropsychological disorders. A postmortem study completed by Benes et al. (1998) was one of the first to point out the contribution of CA2 to neuropsychiatric disorders. In their investigation, there was a 40% reduction in the number and density of non-pyramidal neurons in the *stratum pyramidale* of CA2 in schizophrenic and manic-depressive patients compared to controls (Benes et al., 1998). Given that both schizophrenia and manic-depressive disorders present with different clinical presentations and unique pathophysiologies, there is unlikely to be a strictly genetic explanation for the reduction in non-pyramidal neurons observed, but perhaps an environmental one. Stress would seem to be a likely contributor to the non-pyramidal cell reduction, given that all forms of stress are associated with an increased release of glucocorticoids, which has been shown to have a particular affinity for the CA2 region and may potentially exert a more robust effect on neurons in this region (Benes et al., 1998). Glucocorticoids have been found to increase excitotoxicity in hippocampal neurons, which could have contributed to the decrease of non-pyramidal neurons in the CA2 (Benes et al., 1998).

Zhang and Reynolds (2002) reported a significant deficit in the density of parvalbumin-immunoreactive neurons in the CA2 of patients with schizophrenia. These GABAergic interneurons are directly involved in the inhibitory control of pyramidal cell output activity, and as such, a deficit may result in increased activity of excitatory pyramidal neurons (Zhang and Reynolds, 2002). These findings may point to neurodevelopmental etiology for schizophrenia, based on the observation that parvalbumin expression occurs substantially later than other calcium-binding proteins in the hippocampus. This creates a period of vulnerability, whereby immature GABAergic cells may be particularly susceptible to neurotoxic

events before the expression of parvalbumin can serve as protection (Zhang and Reynolds, 2002). Precisely how CA2 dysfunction contributes to positive, negative, or cognitive symptoms remains unclear, although the cognitive decline may be associated with a disruption in filtering of mnemonic information in the hippocampus (Jones and McHugh, 2011).

While both CA3 and CA1 pyramidal cells are extremely vulnerable to damage caused by epilepsy, CA2 pyramidal neurons are mostly spared (Sperk, 1994). After employing sustained electrical stimulation of the perforant path in rats, Sloviter (1983) observed large amplitude population spikes and epileptiform discharges from hippocampal granule cells, leading to a morphological damage in CA3 and CA1 pyramidal cells, while CA2 pyramidal cells were relatively unaffected. Based on these results, Sloviter (1983) hypothesized that the damage to CA3 pyramidal cells resulted from excessive excitation by granule cells in the dentate gyrus, while the damage to CA1 pyramidal cells was due to their sustained activation by the perforant path. The sparing of CA2 pyramidal cells seen in epileptic brains may result from their lack of dendritic thorns connecting with mossy fiber input from the granule cells, which means they would not be subjected to the same excitotoxic damage as would CA3 cells (Sloviter, 1983). Similarly, Williamson and Spencer (1994) reported that CA2, but not CA3 or CA1, cells appear to be resistant to damage caused by sustained epileptiform bursts found in patients with medial temporal lobe sclerosis, a common neuropathology found in temporal lobe epilepsy. They hypothesized that the calcium-binding proteins parvalbumin and calbindin-128D provide some form of neuroprotection against excitotoxic damage, given that the CA2 pyramidal cell possesses higher levels of these proteins than other populations of cells that are lost in medial temporal lobe sclerosis (Williamson and Spencer, 1994).

CA2 AND SOCIAL RECOGNITION

Investigations have implicated the CA2 as being a subregion paramount to social memory processes. Recent reports into the cellular components of the CA2 have provided further evidence for its role in social recognition. Young et al. (2006) performed *in situ* hybridization in mice brains and reported that the labeling of AVPR1b was the highest in the dorsal CA2 pyramidal cells and confirmed these findings with reverse transcriptase-polymerase chain reaction. They speculated that the CA2 field plays a role in the formation or retrieval of memories of social encounters, much like how other hippocampal pyramidal cells establish memories of place (Young et al., 2006). Expanding on this, Smith et al. (2016) used optogenetics to excite vasopressin terminals, originating from the paraventricular nucleus of the hypothalamus, in the CA2 to explore the involvement of AVPR1b-expressing neurons in the CA2. They observed enhanced social memory when optical stimulation occurred during memory acquisition, but not during retrieval. They then administered an AVPR1b antagonist directly into the CA2 and reported an impairment in the enhancement of social memory (Smith et al., 2016). These results suggest that direct stimulation

of vasopressin terminals that innervate CA2 enhances memory formation and extends social memories (Smith et al., 2016). In addition, this hypothalamic-CA2 pathway, along with its role in social recognition is reliant on AVPR1b signaling (Young et al., 2006).

The speculation that the CA2 region may integrate olfactory cues with social encounters in order to create an appropriate response becomes apparent when considering the direct inputs CA2 receives. For one, the CA2 receives non-spatial information from the entorhinal cortex (Chevalleyre and Siegelbaum, 2010; Jones and McHugh, 2011; Caruana et al., 2012; Kohara et al., 2014; Mankin et al., 2015; Dudek et al., 2016). The entorhinal cortex receives input from the olfactory bulb and piriform cortex, both areas that process olfactory information (Boeijinga and Van Groen, 1984). In addition, the CA2 is the only region within the hippocampus to receive vasopressinergic inputs from the paraventricular nucleus of the hypothalamus, which appear crucial to mediating social behavior (Cui et al., 2013; Zhang and Hernandez, 2013). Thus, it is possible that the CA2 incorporates both forms of input, e.g., social and olfactory, to create a memory trace that is reliant on the scent of the individual.

Recent advancements in genetic manipulation techniques have allowed for investigations into the role of CA2 in social cognition in a more precise and sensitive manner. Hitti and Siegelbaum (2014) used a Cre-expressing mouse line, known as *Amigo2-Cre*, to inactivate pyramidal neuron output from the CA2. They injected a Cre-dependent AAV into the dorsal hippocampus to express tetanus neurotoxin (TeNT) light chain in CA2 pyramidal neurons, which blocked neurotransmission. To test the efficacy of this method, they co-expressed channelrhodopsin-2 (ChR2) with either TeNT or yellow fluorescent protein (YFP) using Cre-dependent AAVs. From there, they used whole-cell current clamp recordings to determine the strength of synaptic transmission from CA2 to CA1 pyramidal neurons. Focal photostimulation over a wide range of intensities delivered to CA1 *stratum oriens* and *stratum radiatum* regions evoked robust monosynaptic potentials in the CA1 pyramidal neurons in slices in which ChR2 was co-expressed with YFP in CA2 pyramidal neurons. Slices in which ChR2 was co-expressed with TeNT in CA2 pyramidal neurons produced little to no synaptic response in CA1 neurons when CA2 neurons were illuminated (Hitti and Siegelbaum, 2014).

Given the efficacy of TeNT lesions, they then investigated the behavioral consequences of CA2 inactivation. A three-chamber social novelty test was used to compare performance between control mice, expressing YFP in CA2 pyramidal neurons, and CA2-TeNT mice. In this test, the amount of time that the experimental mouse spent interacting with a novel, unrelated mouse was compared to the time spent interacting with a familiar co-housed littermate in order to measure social recognition (Hitti and Siegelbaum, 2014). While the CA2-YFP control group showed a significant preference for the compartment containing the novel animal, the CA2-TeNT group did not. Additionally, the difference between the time spent exploring the novel mouse and the time spent exploring the familiar mouse was significantly less in CA2-TeNT mice compared to CA2-YFP mice (Hitti and Siegelbaum, 2014). Since neither a defined learning phase nor

a delay period was incorporated in this social novelty test, a direct interaction test was used to measure social memory (Hitti and Siegelbaum, 2014). The direct interaction test exposed the experimental mouse to an unfamiliar one in trial 1, and, after a 1-h inter-trial interval, either re-exposed the experimental mouse to the same mouse that it encountered in trial 1 or exposed it to a second, unfamiliar mouse (Hitti and Siegelbaum, 2014). The CA2-TeNT group demonstrated impaired social memory, given that there was no decrease in time that the CA2-TeNT mouse spent exploring a previously encountered mouse (Hitti and Siegelbaum, 2014).

A five-trial habituation/dishabituation social memory was used to confirm that CA2-inactivation resulted in impaired social memory. In this test, the experimental mouse was exposed to a stimulus mouse for four consecutive trials then introduced to a novel stimulus mouse on the fifth trial. The CA2-TeNT mice showed no significant habituation during the first four trials as evidenced by a lack of decreased exploration and no significant dishabituation to the novel mouse as shown by a lack of increased exploration (Hitti and Siegelbaum, 2014). The CA2-YFP mice showed both a marked habituation and dishabituation during the test, which confirmed the necessity of the CA2 for social memory (Hitti and Siegelbaum, 2014).

A three-chamber test of sociability was used to compare performance between CA2-YFP mice and CA2-TeNT mice. This test examined the normal preference of the experimental mouse for a chamber containing a littermate versus an empty chamber. Both the CA2-YFP and CA2-TeNT groups displayed a significant preference for the compartment containing their littermate, suggesting that CA2 inactivation did not alter sociability (Hitti and Siegelbaum, 2014). In their social novelty test, Hitti and Siegelbaum (2014) also reported that CA2-YFP and CA2-TeNT mice showed similar and unchanging exploration times during trials 1 and 2 when two novel mice were encountered in the two trials indicating that the sociability of the CA2-TeNT mice remained intact. Furthermore, CA2 silencing did not impair other hippocampus-dependent memory process, including novel-object-recognition and spatial memory, nor did it alter locomotor activity, anxiety-like behavior, or olfaction (Hitti and Siegelbaum, 2014). Thus, the impairment of the CA2 region and subsequent ablation of social recognition provides evidence for the crucial role the CA2 has in social cognition (Hitti and Siegelbaum, 2014).

Following up to the work by Hitti and Siegelbaum (2014) and Stevenson and Caldwell (2014) performed bilateral excitotoxic NMDA lesions of the CA2 region in mice to determine the effects on social recognition memory. To accomplish this, they employed two social memory test following surgical lesions of the CA2. In the first test, the experimental mouse was exposed to a stimulus mouse for 5 min, which was then removed, and reintroduced for the second trial 30 min later, along with a novel mouse. Control mice spent significantly more time investigating the stimulus mouse in the first trial than CA2-lesioned animals. In the second trial, the control mice spent significantly more time with the novel mouse than the familiar one, while CA2-lesioned rats demonstrated no difference in the amount of time spent investigating either mouse (Stevenson and Caldwell, 2014).

In the second test, the experimental animal was exposed to a stimulus mouse for 1 min, which was then removed for 5 min; this series of exposures with same familiar mouse occurred for a total of 10 trials with an inter-trial interval of 5 min. On the 11th trial, the experimental mouse was then exposed to a novel mouse. The CA2-lesioned mice spent significantly less time with the stimulus mouse presented throughout the 10 trials, as well as significantly less time investigating the novel mouse on the 11th trial, compared to control mice (Stevenson and Caldwell, 2014). Together, the results from both studies suggest an impairment in social recognition in CA2-lesioned mice. Stevenson and Caldwell (2014) went on to discuss the parallels between their results and the investigations into AVPR1b-knockout mice; social recognition deficits were noted in both cases. They suggested that AVPR1b within the CA2 may be important to display specific social behaviors, in particular the coupling of olfactory information with the “what” components of odor context. Therefore, inactivation of the CA2 would ablate the AVPR1b-driven associations between both components (Stevenson and Caldwell, 2014).

CONCLUSION

The CA2 is a dynamic region with a composition and connectivity unique to the hippocampus, and not just an extension of the CA3, as was previously believed. Given that research into this region is a relatively new endeavor, the precise role of the CA2 is not fully understood. Nevertheless, burgeoning research into this area has established the role of CA2 in social memory processes, with a particular focus on social recognition, and as such, dysfunction in

this area has been implicated in the social impairments common to a number of psychiatric diseases. Beyond these preliminary findings, little is known concerning the cellular pathways that regulate this brain region and how it mediates social recognition representations, while its contribution to neuropathologies is somewhat vague and inferential, at best. Further research into the cellular mechanisms that govern the CA2 may provide insight into the social deficits underlying certain neuropathologies, such as autism and schizophrenia, and potentially yield novel treatment strategies for these disorders.

AUTHOR CONTRIBUTIONS

NT wrote the initial and revised versions of the manuscript. MH commented and edited the manuscript. Both authors approved the final manuscript for submission.

FUNDING

The preparation of this review was made possible by an NSERC Individual Discovery Grant to MH (RGPIN-2018-05307).

ACKNOWLEDGMENTS

The authors acknowledge the insightful comments made by Dr. Hymie Anisman and Dr. Hongyu Sun. Kind thanks to Dr. Kyle Honegger for detonating a memory retrieval process and kindly donating the image of the PEP-19 staining.

REFERENCES

- Amaral, D. G. (1993). Emerging principles of intrinsic hippocampal organization. *Curr. Opin. Neurobiol.* 3, 225–229. doi: 10.1016/0959-4388(93)90214-j
- Amaral, D. G., Witter, M. P. (1989). The three-dimensional organization of the hippocampal formation: a review of anatomical data. *Neuroscience* 31, 571–91. doi: 10.1016/0306-4522(89)90424-7
- Andersen, P., Bliss, T. V. P., and Skrede, K. K. (1971). Lamellar organization of hippocampal excitatory pathways. *Exp. Brain Res.* 13, 222–238.
- Andersen, P., Morris, R., Amaral, D., Bliss, T., and O'Keefe, J. (2007). *The Hippocampus Book*. New York, NY: Oxford University Press, Inc.
- Arai, A., Kessler, M., and Lynch, G. (1990). The effects of adenosine on the development of long-term potentiation. *Neurosci. Lett.* 119, 41–44. doi: 10.1016/0304-3940(90)90750-4
- Benes, F. M., Kwok, E. W., Vincent, S. L., and Todtenkopf, M. S. (1998). A reduction of nonpyramidal cells in sector CA2 of schizophrenics and manic-depressives. *Biol. Psychiatry* 44, 88–97. doi: 10.1016/s0006-3223(98)00138-3
- Bluthe, R. M., and Dantzer, R. (1993). Role of the vomeronasal system in vasopressinergic modulation of social recognition in rats. *Brain Res.* 604, 205–210. doi: 10.1016/0006-8993(93)90370-3
- Boehringer, R., Polygalov, D., Huang, A. J. Y., Middleton, S. J., Robert, V., Wintzer, M. E., et al. (2017). Chronic loss of CA2 transmission leads to hippocampal hyperexcitability. *Neuron* 94, 642–655. doi: 10.1016/j.neuron.2017.04.014
- Boeijinga, P. H., and Van Groen, T. (1984). Inputs from the olfactory bulb and olfactory cortex to the entorhinal cortex in the cat. II. Physiological studies. *Exp. Brain Res.* 57, 40–48. doi: 10.1007/bf00231130
- Bredewold, R., Schiavo, J. K., van der Hart, M., Verreij, M., and Veenema, A. H. (2015). Dynamic changes in extracellular release of GABA and glutamate in the lateral septum during social play behavior in juvenile rats: implications for sex-specific regulation of social play behavior. *Neuroscience* 307, 117–127. doi: 10.1016/j.neuroscience.2015.08.052
- Cacioppo, J. T., and Berntson, G. G. (1992). Social psychological contributions to the decade of the brain. Doctrine of multilevel analysis. *Am. Psychol.* 47, 1019–1028. doi: 10.1037/0003-066x.47.8.1019
- Caruana, D. A., Alexander, G. M., and Dudek, S. M. (2012). New insights into the regulation of synaptic plasticity from an unexpected place: hippocampal area CA2. *Learn. Mem.* 19, 391–400. doi: 10.1101/lm.025304.111
- Cenquizca, L. A., and Swanson, L. W. (2007). Spatial organization of direct hippocampal field CA1 axonal projections to the rest of the cerebral cortex. *Brain Res. Rev.* 56, 1–26. doi: 10.1016/j.brainresrev.2007.05.002
- Chevalayre, V., and Siegelbaum, S. A. (2010). Strong CA2 pyramidal neuron synapses define a powerful disinaptic cortico-hippocampal loop. *Neuron* 66, 560–572. doi: 10.1016/j.neuron.2010.04.013
- Choleris, E., Gustafsson, J. A., Korach, K. S., Muglia, L. J., Pfaff, D. W., and Ogawa, S. (2003). An estrogen-dependent four-gene micronet regulating social recognition: a study with oxytocin and estrogen receptor- α and - β knockout mice. *Proc. Natl. Acad. Sci. U.S.A.* 100, 6192–6197. doi: 10.1073/pnas.0631699100
- Clipperton, A. E., Spinato, J. M., Chernet, C., Pfaff, D. W., and Choleris, E. (2008). Differential effects of estrogen receptor alpha and beta specific agonists on social learning and food preferences in female mice. *Neuropsychopharmacology* 33, 2362–2375. doi: 10.1038/sj.npp.1301625

- Cui, Z., Gerfen, C. R., and Young, W. S. III (2013). Hypothalamic and other connections with dorsal CA2 area of the mouse hippocampus. *J. Comp. Neurol.* 521, 1844–1866. doi: 10.1002/cne.23263
- de Mendonca, A., and Ribeiro, J. A. (1990). 2-chloroadenosine decreases long-term potentiation in the hippocampal CA1 area of the rat. *Neurosci. Lett.* 118, 107–111. doi: 10.1016/0304-3940(90)90260-g
- DeVito, L. M., Konigsberg, R., Lykken, C., Sauvage, M., Young, W. S. III, and Eichenbaum, H. (2009). Vasopressin 1b receptor knockout impairs memory for temporal order. *J. Neurosci.* 29, 2676–2683. doi: 10.1523/JNEUROSCI.5488-08.2009
- Donaldson, Z. R., and Young, L. J. (2008). Oxytocin, vasopressin, and the neurogenetics of sociality. *Science* 322, 900–904. doi: 10.1126/science.1158668
- Dudek, S. M., Alexander, G. M., and Farris, S. (2016). Rediscovering area CA2: unique properties and function. *Nat. Rev. Neurosci.* 17, 89–102. doi: 10.1038/nrn.2015.22
- Engelmann, M., and Landgraf, R. (1994). Microdialysis of vasopressin into the septum improves social recognition in Brattleboro rats. *Physiol. Behav.* 55, 145–149. doi: 10.1016/0031-9384(94)90022-1
- Fanselow, M. S., and Dong, H.-W. (2010). Are the dorsal and ventral hippocampus functionally distinct structures? *Neuron* 65, 1–25.
- Ferguson, J. N., Young, L. J., and Insel, T. R. (2002). The neuroendocrine basis of social recognition. *Front. Neuroendocrinol.* 23:200–224. doi: 10.1006/frne.2002.0229
- Gilbert, P. E., Kesner, R. P., and Lee, I. (2001). Dissociating hippocampal subregions: a double dissociation between dentate gyrus and CA1. *Hippocampus* 11, 626–636. doi: 10.1002/hipo.1077
- Gimpl, G., and Fahrenholz, F. (2001). The oxytocin receptor system: structure, function, and regulation. *Physiol. Rev.* 81, 629–683. doi: 10.1152/physrev.2001.81.2.629
- Hirama, J., Shoumura, K., Ichinohe, N., You, S., and Yonekura, H. (1997). Cornu ammonis of the cat: lack of a separate field of CA2. *J. Hirnforsch.* 38, 487–493.
- Hitti, F. L., and Siegelbaum, S. A. (2014). The hippocampal CA2 region is essential for social memory. *Nature* 508, 88–92. doi: 10.1038/nature13028
- Houser, C. R., Miyashiro, J. E., Swartz, B. E., Walsh, G. O., Rich, J. R., and Delgado-Escueta, A. V. (1990). Altered patterns of dynorphin immunoreactivity suggest mossy fiber reorganization in human hippocampal epilepsy. *J. Neurosci.* 10, 267–282. doi: 10.1523/jneurosci.10-01-00267.1990
- Insel, T. R. (2010). The challenge of translation in social neuroscience: a review of oxytocin, vasopressin, and affiliative behavior. *Neuron* 65, 768–779. doi: 10.1016/j.neuron.2010.03.005
- Ishizuka, N., Cowan, W. M., and Amaral, D. G. (1995). A quantitative analysis of the dendritic organization of pyramidal cells in the rat hippocampus. *J. Comp. Neurol.* 362, 17–45. doi: 10.1002/cne.903620103
- Jacobs, S. A., Huang, F., Tsien, J. Z., and Wei, W. (2016). Social recognition memory test in rodents. *Bio Protoc.* 6, e1804.
- Jones, M. W., and McHugh, T. J. (2011). Updating hippocampal representations: CA2 joins the circuit. *Trends Neurosci.* 34, 526–535. doi: 10.1016/j.tins.2011.07.007
- Jung, M. W., Wiener, S. I., and McNaughton, B. L. (1994). Comparison of spatial firing characteristics of units in dorsal and ventral hippocampus of the rat. *J. Neurosci.* 14, 7347–7356. doi: 10.1523/jneurosci.14-12-07347.1994
- Kajiwar, R., Wouterlood, F. G., Sah, A., Boekel, A. J., Baks-te Bulte, L. T., and Witter, M. P. (2008). Convergence of entorhinal and CA3 inputs onto pyramidal neurons and interneurons in hippocampal area CA1 – an anatomical study in the rat. *Hippocampus* 18, 266–280. doi: 10.1002/hipo.20385
- Kesner, R. P. (2013). An analysis of the dentate gyrus function. *Behav. Brain Res.* 254, 1–7. doi: 10.1016/j.bbr.2013.01.012
- Kogan, J. H., Frankland, P. W., and Silva, A. J. (2000). Long-term memory underlying hippocampus-dependent social recognition in mice. *Hippocampus* 10, 47–56. doi: 10.1002/(sici)1098-1063(2000)10:1<47::aid-hipo5>3.0.co;2-6
- Kohara, K., Pigatelli, M., Rivest, A. J., Jung, H. Y., Kitamura, T., Suh, J., et al. (2014). Cell type-specific genetic and optogenetic tools reveal hippocampal CA2 circuits. *Nat. Neurosci.* 17, 269–279. doi: 10.1038/nn.3614
- Landis, T., Cummings, J. L., Christen, L., Bogen, J. E., and Imhof, H. G. (1986). Are unilateral right posterior cerebral lesions sufficient to cause prosopagnosia? Clinical and radiological findings in six additional patients. *Cortex* 22, 243–252. doi: 10.1016/s0010-9452(86)80048-x
- Lavenex, P., Lavenex, P. B., Bennett, J. L., and Amaral, D. G. (2009). Postmortem changes in the neuroanatomical characteristics of the primate brain: hippocampal formation. *J. Comp. Neurol.* 512, 27–51. doi: 10.1002/cne.21906
- Lee, I., and Solivan, F. (2010). Dentate gyrus is necessary for disambiguating similar object-place representations. *Learn. Mem.* 17, 252–258. doi: 10.1101/lm.1678210
- Lee, S. E., Simons, S. B., Heldt, S. A., Zhao, M., Schroeder, J. P., Vellano, C. P., et al. (2010). RGS14 is a natural suppressor of both synaptic plasticity in CA2 neurons and hippocampal-based learning and memory. *Proc. Natl. Acad. Sci. U.S.A.* 107, 16994–16998. doi: 10.1073/pnas.1005362107
- Letty, S., Child, R., Dumuis, A., Pantaloni, A., Bockaert, J., and Rondouin, G. (1997). 5-HT₄ receptors improve social olfactory memory in the rat. *Neuropharmacology* 36, 681–687. doi: 10.1016/s0028-3908(96)00169-4
- Llorens-Martin, M., Jurado-Arjona, J., Avila, J., and Hernandez, F. (2015). Novel connection between newborn granule neurons and the hippocampal CA2 field. *Exp. Neurol.* 263, 285–292. doi: 10.1016/j.expneurol.2014.10.021
- Lorente de No, R. (1934). Studies on the structure of the cerebral cortex. II. Continuation of the study of the ammonic system. *J. Psychol. Neurol.* 46, 113–177.
- Maaswinkel, H., Baars, A. M., Gispen, W. H., and Spruijt, B. M. (1996). Roles of the basolateral amygdala and hippocampus in social recognition in rats. *Physiol. Behav.* 60, 55–63. doi: 10.1016/0031-9384(95)02233-3
- Maccaferri, G. (2011). Modulation of hippocampal stratum lacunosum-moleculare microcircuits. *J. Physiol.* 589(Pt 8), 1885–1891. doi: 10.1113/jphysiol.2010.201079
- Mankin, E. A., Diehl, G. W., Sparks, F. T., Leutgeb, S., and Leutgeb, J. K. (2015). Hippocampal CA2 activity patterns change over time to a larger extent than between spatial contexts. *Neuron* 85, 190–201. doi: 10.1016/j.neuron.2014.12.001
- Markham, J. A., and Juraska, J. M. (2007). Social recognition memory: influence of age, sex, and ovarian hormonal status. *Physiol. Behav.* 92, 881–888. doi: 10.1016/j.physbeh.2007.06.020
- Matochik, J. A. (1988). Role of the main olfactory system in recognition between individual spiny mice. *Physiol. Behav.* 42, 217–222. doi: 10.1016/0031-9384(88)90073-x
- McDonald, R. J., and White, N. M. (1995). Hippocampal and nonhippocampal contributions to place learning in rats. *Behav. Neurosci.* 109, 579–593. doi: 10.1037//0735-7044.109.4.579
- McHugh, T. J., Jones, M. W., Quin, J. J., Balthasar, N., Coppari, R., Elmquist, J. K., et al. (2007). Dentate gyrus NMDA receptors mediate rapid pattern separation in the hippocampal network. *Science* 317, 94–99. doi: 10.1126/science.1140263
- McHugh, T. J., and Tonegawa, S. (2009). CA3 NMDA receptors are required for the rapid formation of a salient contextual representation. *Hippocampus* 19, 1153–1158. doi: 10.1002/hipo.20684
- McLardy, T. (1963). Some cell and fibre peculiarities of uncus hippocampus. *Prog. Brain Res.* 3, 71–78.
- McNaughton, B. L., Battaglia, F. P., Jensen, O., Moser, E. I., and Moser, M. B. (2006). Path integration and the neural basis of the 'cognitive map'. *Nat. Rev. Neurosci.* 7, 663–678. doi: 10.1038/nrn1932
- McNaughton, B. L., and Morris, R. G. M. (1987). Hippocampal synaptic enhancement and information storage within a distributed memory system. *Trends Neurosci.* 10, 408–415. doi: 10.1016/0166-2236(87)90011-7
- Mitchell, J. P., Lupica, C. R., and Dunwiddie, T. V. (1993). Activity-dependent release of endogenous adenosine modulates synaptic responses in the rat hippocampus. *J. Neurosci.* 13, 3439–3447. doi: 10.1523/jneurosci.13-08-03439.1993
- Morris, A. M., Churchwell, J. C., Kesner, R. P., and Gilbert, P. E. (2012). Selective lesions of the dentate gyrus produce disruptions in place learning for adjacent spatial locations. *Neurobiol. Learn. Mem.* 97, 326–331. doi: 10.1016/j.nlm.2012.02.005
- Moser, E., Moser, M. B., and Andersen, P. (1993). Spatial learning impairment parallels the magnitude of dorsal hippocampal lesions, but is hardly present following ventral lesions. *J. Neurosci.* 13, 3916–3925. doi: 10.1523/jneurosci.13-09-03916.1993
- Moser, M. B., and Moser, E. I. (1998). Functional differentiation in the hippocampus. *Hippocampus* 8, 608–619. doi: 10.1002/(sici)1098-1063(1998)8:6<608::aid-hipo3>3.0.co;2-7

- Moser, M. B., Moser, E. I., Forrest, E., Andersen, P., and Morris, R. G. (1995). Spatial learning with a minislab in the dorsal hippocampus. *Proc. Natl. Acad. Sci. U.S.A.* 92, 9697–9701. doi: 10.1073/pnas.92.21.9697
- Mou, X. (2016). Hippocampal CA2 region: a new player in social dysfunctions. *J. Neurol. Neurophysiol.* 7, 1–4.
- Nakazawa, K., Quirk, M. C., Chitwood, R. A., Watanabe, M., Yeckel, M. F., Sun, L. D., et al. (2002). Requirement for hippocampal CA3 NMDA receptors in associative memory recall. *Science* 297, 211–218. doi: 10.1126/science.1071795
- Neves, G., Cooke, S. F., and Bliss, T. V. (2008). Synaptic plasticity, memory and the hippocampus: a neural network approach to causality. *Nat. Rev. Neurosci.* 9, 65–75. doi: 10.1038/nrn2303
- Noack, J., Richter, K., Laube, G., Haghighi, H. A., Veh, R. W., and Engelmann, M. (2010). Different importance of the volatile and non-volatile fractions of an olfactory signature for individual social recognition in rats versus mice and short-term versus long-term memory. *Neurobiol. Learn. Mem.* 94, 568–575. doi: 10.1016/j.nlm.2010.09.013
- Norman, K. A., and O'Reilly, R. C. (2003). Modeling hippocampal and neocortical contributions to recognition memory: a complimentary-learning-systems approach. *Psychol. Rev.* 110, 611–646. doi: 10.1037/0033-295x.110.4.611
- Ochsner, K. N., and Lieberman, M. D. (2001). The emergence of social cognitive neuroscience. *Am. Psychol.* 56, 717–734. doi: 10.1037//0003-066x.56.9.717
- O'Reilly, R. C., and McClelland, J. L. (1994). Hippocampal conjunctive encoding, storage, and recall: avoiding a trade-off. *Hippocampus* 4, 661–682. doi: 10.1002/hipo.450040605
- Pan, W. X., and McNaughton, N. (2004). The supramammillary area: its organization, functions and relationship to the hippocampus. *Prog. Neurobiol.* 74, 127–166. doi: 10.1016/j.pneurobio.2004.09.003
- Pitkanen, A., Pikkarainen, M., Nurminen, N., and Ylinen, A. (2000). Reciprocal connections between the amygdala and the hippocampal formation, perirhinal cortex, and postrhinal cortex in rat. A review. *Ann. N. Y. Acad. Sci.* 911, 369–391. doi: 10.1111/j.1749-6632.2000.tb06738.x
- Pothuizen, H. H., Zhang, W. N., Jongen-Relo, A. L., Feldon, J., and Yee, B. K. (2004). Dissociation of function between the dorsal and the ventral hippocampus in spatial learning abilities of the rat: a within-subject, within-task comparison of reference and working spatial memory. *Eur. J. Neurosci.* 19, 705–712. doi: 10.1111/j.0953-816x.2004.03170.x
- Prediger, R. D., and Takahashi, R. N. (2005). Modulation of short-term social memory in rats by adenosine A1 and A(2A) receptors. *Neurosci. Lett.* 376, 160–165. doi: 10.1016/j.neulet.2004.11.049
- Riedel, G., and Micheau, J. (2001). Function of the hippocampus in memory formation: desperately seeking resolution. *Prog. Neuropsychopharmacol. Biol. Psychiatry* 25, 835–853. doi: 10.1016/s0278-5846(01)00153-1
- Rolls, E. T. (1996). A theory of hippocampal function in memory. *Hippocampus* 6, 601–620. doi: 10.1002/(sici)1098-1063(1996)6:6<601::aid-hipo5>3.0.co;2-j
- Rowland, D. C., Weible, A. P., Wickersham, I. R., Wu, H., Mayford, M., Witter, M. P., et al. (2013). Transgenically targeted rabies virus demonstrates a major monosynaptic projection from hippocampal area CA2 to medial entorhinal layer II neurons. *J. Neurosci.* 33, 14889–14898. doi: 10.1523/JNEUROSCI.1046-13.2013
- San Antonio, A., Liban, K., Ikrar, T., Tsyganovskiy, E., and Xu, X. (2014). Distinct physiological and developmental properties of hippocampal CA2 subfield revealed by using anti-Purkinje cell 4 (PCP4) immunostaining. *J. Comp. Neurol.* 522, 1333–1354. doi: 10.1002/cne.23486
- Sandler, R., and Smith, A. D. (1991). Coexistence of GABA and glutamate in mossy fiber terminals of the primate hippocampus: an ultrastructural study. *J. Comp. Neurol.* 303, 177–192. doi: 10.1002/cne.903030202
- Saunders, R. C., Rosene, D. L., and Van Hoesen, G. W. (1988). Comparison of the efferents of the amygdala and the hippocampal formation in the rhesus monkey: II. Reciprocal and non-reciprocal connections. *J. Comp. Neurol.* 271, 185–207. doi: 10.1002/cne.902710203
- Shahidi, S., Motamedi, F., and Naghdi, N. (2004). Effect of reversible inactivation of the supramammillary nucleus on spatial learning and memory in rats. *Brain Res.* 1026, 267–274. doi: 10.1016/j.brainres.2004.08.030
- Simons, S. B., Escobedo, Y., Yasuda, R., and Dudek, S. M. (2009). Regional differences in hippocampal calcium handling provide a cellular mechanism for limiting plasticity. *Proc. Natl. Acad. Sci. U.S.A.* 106, 14080–14084. doi: 10.1073/pnas.0904775106
- Sloviter, R. S. (1983). “Epileptic” brain damage in rats induced by sustained electrical stimulation of the perforant path. I. Acute electrophysiological and light microscopic studies. *Brain Res. Bull.* 10, 675–697. doi: 10.1016/0361-9230(83)90037-0
- Smith, A. S., Williams Avram, S. K., Cymerbilt-Sabba, A., Song, J., and Young, W. S. (2016). Targeted activation of the hippocampal CA2 area strongly enhances social memory. *Mol. Psychiatry* 21, 1137–1144. doi: 10.1038/mp.2015.189
- Sperk, G. (1994). Kainic acid seizures in the rat. *Prog. Neurobiol.* 42, 1–32. doi: 10.1016/0301-0082(94)90019-1
- Stevenson, E. L., and Caldwell, H. K. (2014). Lesions to the CA2 region of the hippocampus impair social memory in mice. *Eur. J. Neurosci.* 40, 3294–3301. doi: 10.1111/ejn.12689
- Swanson, L. W., and Cowan, W. M. (1977). An autoradiographic study of the organization of the efferent connections of the hippocampal formation in the rat. *J. Comp. Neurol.* 172, 49–84. doi: 10.1002/cne.901720104
- Tang, A. C., Nakazawa, M., Romeo, R. D., Reeb, B. C., Sisti, H., and McEwen, B. S. (2005). Effects of long-term estrogen replacement on social investigation and social memory in ovariectomized C57BL/6 mice. *Horm. Behav.* 47, 350–357. doi: 10.1016/j.yhbeh.2004.10.010
- van der Kooij, M. A., and Sandi, C. (2012). Social memories in rodents: methods, mechanisms and modulation by stress. *Neurosci. Biobehav. Rev.* 36, 1763–1772. doi: 10.1016/j.neubiorev.2011.10.006
- van Groen, T., Miettinen, P., and Kadish, I. (2003). The entorhinal cortex of the mouse: organization of the projection to the hippocampal formation. *Hippocampus* 13, 133–149. doi: 10.1002/hipo.10037
- Wersinger, S. R., Ginns, E. I., O'Carroll, A. M., Lolait, S. J., and Young, W. S. III (2002). Vasopressin V1b receptor knockout reduces aggressive behavior in male mice. *Mol. Psychiatry* 7, 975–984. doi: 10.1038/sj.mp.4001195
- Wible, C. G. (2013). Hippocampal physiology, structure and function and the neuroscience of schizophrenia: a unified account of declarative memory deficits, working memory deficits and schizophrenic symptoms. *Behav. Sci.* 3, 298–315. doi: 10.3390/bs3020298
- Wieraszko, A., Goldsmith, G., and Seyfried, T. N. (1989). Stimulation-dependent release of adenosine triphosphate from hippocampal slices. *Brain Res.* 485, 244–250. doi: 10.1016/0006-8993(89)90567-2
- Williamson, A., and Spencer, D. D. (1994). Electrophysiological characterization of CA2 pyramidal cells from epileptic humans. *Hippocampus* 4, 226–237. doi: 10.1002/hipo.450040213
- Wintzer, M. E., Boehringer, R., Polygalov, D., and McHugh, T. J. (2014). The hippocampal CA2 ensemble is sensitive to contextual change. *J. Neurosci.* 34, 3056–3066. doi: 10.1523/JNEUROSCI.2563-13.2014
- Witter, M. P. (2007). Intrinsic and extrinsic wiring of CA3: indications for connectional heterogeneity. *Learn. Mem.* 14, 705–713. doi: 10.1101/lm.725207
- Witter, M. P., and Amaral, D. G. (1991). Entorhinal cortex of the monkey: V. Projections to the dentate gyrus, hippocampus, and subicular complex. *J. Comp. Neurol.* 307, 437–459. doi: 10.1002/cne.903070308
- Young, W. S., Li, J., Wersinger, S. R., and Palkovits, M. (2006). The vasopressin 1b receptor is prominent in the hippocampal area CA2 where it is unaffected by restraint stress or adrenalectomy. *Neuroscience* 143, 1031–1039. doi: 10.1016/j.neuroscience.2006.08.040
- Zhang, L., and Hernandez, V. S. (2013). Synaptic innervation to rat hippocampus by vasopressin-immuno-positive fibres from the hypothalamic supraoptic and paraventricular nuclei. *Neuroscience* 228, 139–162. doi: 10.1016/j.neuroscience.2012.10.010
- Zhang, Z. J., and Reynolds, G. P. (2002). A selective decrease in the relative density of parvalbumin-immunoreactive neurons in the hippocampus in schizophrenia. *Schizophr. Res.* 55, 1–10. doi: 10.1016/s0920-9964(01)00188-8
- Zhao, M., Choi, Y. S., Obrietan, K., and Dudek, S. M. (2007). Synaptic plasticity (and lack thereof) in hippocampal CA2 neurons. *J. Neurosci.* 27, 12025–12032. doi: 10.1523/jneurosci.4094-07.2007

Conflict of Interest: The authors declare that the research was conducted in the absence of any commercial or financial relationships that could be construed as a potential conflict of interest.

Copyright © 2019 Tzakos and Holahan. This is an open-access article distributed under the terms of the Creative Commons Attribution License (CC BY). The use, distribution or reproduction in other forums is permitted, provided the original author(s) and the copyright owner(s) are credited and that the original publication in this journal is cited, in accordance with accepted academic practice. No use, distribution or reproduction is permitted which does not comply with these terms.



Memory Performance Correlates of Hippocampal Subfield Volume in Mild Cognitive Impairment Subtype

Kathryn M. Broadhouse^{1,2*}, Loren Mowszowski^{3,4}, Shantel Duffy^{3,5}, Isabella Leung^{2,3}, Nathan Cross³, Michael J. Valenzuela^{2,6} and Sharon L. Naismith^{3,4,5}

¹ Sunshine Coast Mind and Neuroscience Thompson Institute, University of the Sunshine Coast, Sunshine Coast, QLD, Australia, ² Regenerative Neuroscience Group, Brain and Mind Centre, The University of Sydney, Sydney, NSW, Australia, ³ Healthy Brain Aging Program, Brain and Mind Centre, The University of Sydney, Sydney, NSW, Australia, ⁴ School of Psychology, Faculty of Science, The University of Sydney, Sydney, NSW, Australia, ⁵ Charles Perkins Centre, The University of Sydney, Sydney, NSW, Australia, ⁶ Sydney Medical School, The University of Sydney, Sydney, NSW, Australia

OPEN ACCESS

Edited by:

Martin Cammarota,
Federal University of Rio Grande do
Norte, Brazil

Reviewed by:

Sandhitsu Das,
University of Pennsylvania,
United States
Gianfranco Spalletta,
Santa Lucia Foundation (IRCCS), Italy

*Correspondence:

Kathryn M. Broadhouse
kbroadhouse@usc.edu.au;
kathryn.broadhouse@usc.edu.au

Specialty section:

This article was submitted to
Learning and Memory,
a section of the journal
Frontiers in Behavioral Neuroscience

Received: 29 May 2019

Accepted: 05 November 2019

Published: 21 November 2019

Citation:

Broadhouse KM, Mowszowski L,
Duffy S, Leung I, Cross N,
Valenzuela MJ and Naismith SL
(2019) Memory Performance
Correlates of Hippocampal Subfield
Volume in Mild Cognitive Impairment
Subtype.
Front. Behav. Neurosci. 13:259.
doi: 10.3389/fnbeh.2019.00259

The increased understanding that neuropathology begins decades before symptom onset, has led to the conceptualization and widespread utilization of Mild Cognitive Impairment (MCI) as an important transitional state between healthy aging and dementia. Further subcategorization to MCI subtype has led to more distinct prognoses and it is widely considered that amnesic and non-amnesic MCI (aMCI, naMCI) likely have distinct pathophysiologies. Yet, accurately classification remains contentious. Here, we differentiate hippocampal subfield volume between subtypes, diagnosed according to stringent clinical consensus criteria, where aMCI is characterized based on deficits in delayed recall (rather than encoding). We then identify memory performance correlates to subfield volume and associations with long-term cognitive performance and outcome. 3D T1-weighted structural MRI was acquired in 142 participants recruited from the *Healthy Brain Aging (HBA) Clinic* and diagnosed with aMCI ($n = 38$), naMCI ($n = 84$) or subjective memory complaints (SMC; $n = 20$). T1-weighted datasets were processed with the cortical and hippocampal subfield processing streams in FreeSurfer (v6.0). Subfield volumes, and associations with baseline and longitudinal objective memory scores were then examined. Subfield volumes were found to differentiate clinical profiles: subiculum, CA1, CA4 and dentate gyrus volumes were significantly reduced in aMCI compared to both naMCI and SMC. CA1 subfield volume was shown to predict concurrent memory performance in aMCI, while dentate gyrus volume significantly predicted longitudinal verbal learning and memory decline in the entire cohort. Our findings demonstrate that using a more stringent diagnostic approach to characterizing aMCI is well justified, as delayed recall deficits are strongly linked to underlying volumetric subfield reductions in CA1, CA4 and the dentate gyrus, subfields known to be associated with mnemonic processes. Further research is now warranted to replicate these findings in other MCI samples.

Keywords: mild cognitive impairment, hippocampus, subfields, memory, aging, neuroimaging

INTRODUCTION

Mild Cognitive Impairment (MCI), the transitional state between normal aging and dementia, is an important diagnostic entity in both clinical and research settings. Recent studies indicate that conversion rates to Alzheimer's Disease (AD) are as high as 15% over a 2 year period (Petersen et al., 2018) and almost 45% over 5 years (Gauthier et al., 2006; Duffy et al., 2014). Further subcategorization into the clinical phenotypes of amnesic and non-amnesic MCI (aMCI and naMCI) (i.e., depending on whether impairment is evident in memory or non-memory cognitive domains, respectively) has shown that aMCI is associated with the most pronounced risk of conversion to AD; approximately 50% within 5 years (Gauthier et al., 2006; Petersen et al., 2009). For those with naMCI, the disease trajectory is less well defined (Jungwirth et al., 2012), but appears to be linked to higher risk and more frequent conversion to other dementia types (e.g., vascular dementia) compared to those whom are cognitively intact (Csukly et al., 2016).

The aMCI and naMCI subtypes are believed to be underpinned by different underlying pathophysiologies and disease trajectories. As such, to enable the most appropriate clinical feedback for patients (particularly where modifiable risk factors play a role), accurate characterization of the clinical subtyping of MCI and accompanying neurodegeneration is particularly important (Hughes et al., 2011; Norton et al., 2014). Another pertinent cohort when investigating cognition in aging are those that present with subjective memory complaints (SMC) but who do not demonstrate objective impairment on testing. A recent meta-analysis has shown that approximately 2.3 and 6.6% of SMC will progress to dementia and MCI per year, respectively (Mitchell et al., 2014). Subsequently, it has been suggested that SMCs may be a "pre-MCI" stage in the evolution of normal aging to clinical AD (Steinberg et al., 2013). By definition SMCs perform within a "normal range" on standard psychometric measures and although the individuals themselves, close family or friends, report subtle decline in cognitive abilities, they are otherwise still healthy community dwelling older adults. They are therefore health seeking and as such make an appropriate control group when investigating disease progression in clinic-based settings.

Pathophysiologically, MCI and the early stages of AD are characterized by increased neurodegeneration of the hippocampus and entorhinal cortex (Frisoni et al., 2010; Mu and Gage, 2011). Imaging studies have shown that hippocampal atrophy, specifically within the CA1 region and subiculum, not only correlates with cognitive impairment severity (Jack et al., 2000; Morra et al., 2009), but is associated with increased risk of conversion from MCI to AD (Apostolova et al., 2006; Costafreda et al., 2011). Although there is increased recognition that aMCI and naMCI are different phenotypes, relatively few studies have investigated the underlying cortical and hippocampal differences between them. Subfield analysis in healthy controls, MCI and AD patients has highlighted the presubiculum and subiculum as possible predictors of memory

performance in MCI and suggests that prevalent atrophy of the presubicular-subicular complex is apparent from the early phases of AD (Carlesimo et al., 2015). Furthermore, significant reductions in whole hippocampal volume in aMCI relative to naMCI and controls has been shown (Csukly et al., 2016). However, a more in-depth subfield differentiation analysis, in particular with focus on association with objective memory performance has not been carried out in an early stage cohort or between MCI subtypes.

Regarding hippocampal-dependent memory deficits to categorize subtypes, we have observed that clinicians and researchers have utilized assessments of both new learning and delayed recall in characterizing aMCI (Bondi et al., 2014; Edmonds et al., 2015). However, our group has applied a more stringent criterion whereby only those demonstrating objective deficits in *delayed recall* are denoted as aMCI. Those with deficits in new learning, but not in delayed recall, or in other cognitive domains, are classified as naMCI. This deliberate methodological decision can be justified on both neuropsychological theoretical and evidence-based grounds. New learning is heavily dependent on sound and efficient encoding processes, which are frequently impacted by other cognitive skills including attention regulation and executive functions (e.g., with respect to strategic or effortful encoding strategies) that may in turn be linked to prefrontal cortex integrity. Delayed or episodic memory, however, is perhaps more specifically tied to hippocampal functioning and indeed delayed recall measures have been shown to be some of the most highly accurate predictors of progression to AD in both clinical and epidemiological samples (Gauthier et al., 2006). This more stringent approach to differentiating aMCI and naMCI may therefore be critical to ensuring more accurate diagnosis as well as exploring relationships with neuropathological markers of hippocampal functioning.

Accordingly, the aim of this study was to (a) determine entorhinal cortical and hippocampal subfield biomarkers that differentiate MCI subtypes and even those presenting with SMC; (b) identify whether our more stringent diagnostic approach is supported by whole hippocampal volumetric differences; and finally, (c) identify whether subfield volume is not only significantly associated with concurrent objective memory performance but also longitudinal memory decline.

MATERIALS AND METHODS

Participants were recruited from the *Healthy Brain Ageing (HBA) Clinic* at the Brain and Mind Centre, University of Sydney, Australia. The HBA clinic is a specialist early diagnosis and intervention research clinic that receives referrals from specialists and General Practitioners. Exclusion criteria for the clinic are: diagnosis of dementia or a Mini-Mental State Examination (MMSE) (Rovner and Folstein, 1987) score of less than 24, history of neurological illness, stroke or transient ischemic attack, head injury (with loss of consciousness >30 min), other medical conditions known to affect cognition, intellectual disability, insufficient English speaking skills for

neuropsychological testing and history of prior or current substance abuse. In addition, for this study, we excluded any participant with current DSM-IV major depression. This research was approved by the Human Research Ethics Committee of the University of Sydney.

Clinical Assessment

Using a semi-structured interview, a medical specialist (Neurologist, Psychiatrist or Geriatrician) recorded a full medical, clinical, psychiatric and medication history. For each participant, a Psychiatrist or research psychologist used the Mini International Neuropsychiatric Interview (van Vliet and de Beurs, 2007) to assess lifetime and current major depression. The 15-item Geriatric Depression Scale (GDS-15) (Greenberg, 2002) was also administered to measure depressive symptom severity. Clinician rated psychosocial functioning was assessed using the Social and Occupational Functioning Assessment Scale (SOFAS) (Rybarczyk, 2011) and severity of medical burden was measured using the Cumulative Illness Rating Scale – Geriatric Version (CIRS) (Linn et al., 1968) total score.

Neuropsychological Assessment

The tests reported in this study formed part of a broader assessment battery (Duffy et al., 2014). This study focuses specifically on two tests of verbal learning and memory:

- (i) The Logical Memory (LogMem) I and II subtests of the Wechsler Memory Scale (3rd edition) (Wechsler, 1997a) were used to measure encoding and recall of structured verbal material. Age-scaled scores (ASS) were computed according to normative data (Wechsler, 1997a).
- (ii) The Rey Auditory Verbal Learning Test (RAVLT) (Lezak, 1982) word list task was used to assess unstructured verbal learning over five trials (RAVLT 1-5) and memory after a 20-min delay (RAVLT A7). Standardized z-scores were calculated using age and education corrected normative data (Senior, 1999).

For descriptive purposes, we also report MMSE (Folstein et al., 1975) scores and estimated premorbid intellectual functioning using the Wechsler Test of Adult Reading (Wechsler, 1997a).

Group Diagnoses

Diagnosis was confirmed based on consensus rating of at least three clinicians. A clinical diagnosis of MCI was obtained using Winblad's criteria (Winblad et al., 2004) where cognitive decline was defined as a deficit of at least 1.5 SDs from estimated premorbid functioning on objective neuropsychological tests, relative to age- and education-adjusted normative data. Each participant was required to have subjective and objective cognitive decline, but with the general preservation of function (i.e., only minimal change, if any, in basic and complex activities of daily living). Within the HBA clinic aMCI was defined specifically by impairment on measures of delayed recall [assessed with the Logical Memory II total score (Wechsler, 1997b); Rey Auditory Verbal Learning Test (RAVLT) trial 7 total score (Schmidt, 1996)]. In cases where only new learning (e.g., Logical

Memory I total score or RAVLT 1-5) was impaired but delayed recall was intact, the individual was categorized as naMCI. SMC participants were identified as individuals who when recruited through HBA reported subtle decline in cognitive abilities on the Likert scale, yet upon neuropsychological testing, performed within the normal range. The five-point Likert scale identifies SMC by asking participants "In general, how would you rate your memory?." Those rating their memory as 'fair' or 'poor' but with intact cognition were defined as SMC (Ganguli et al., 2004; Purser et al., 2006).

MRI Acquisition and Analysis

A neuro-MRI protocol was acquired on a 3T GE Discovery MR750 Scanner (GE Medical Systems, Milwaukee, WI, United States), as described in Duffy et al. (2014). Entorhinal cortical thickness and hippocampal volumetric analyses were performed on a 3D T1-weighted, structural MRI sequence (1 mm isotropic resolution, matrix = 256 × 256, TR/TE/TI = 7.13/2.69/450 ms, flip angle = 12°) with the FreeSurfer(v6.0) cortical and hippocampal subfield processing stream (Reuter et al., 2010; Iglesias et al., 2015). All analysis was carried out on raw entorhinal cortical thickness measures (mm) and normalized subfield volumes and reported as percentage of intra-cranial volume (ICV). Whole-brain segmentations were visually inspected and manually adjusted where necessary before being processed through the subfield processing stream. Finally, subfield segmentations were then visually inspected to check for apparent errors in segmentation.

Statistical Analysis

T1-Weighted Subfield Segmentation Validation

Currently, the "gold standard" hippocampal subfield segmentation streams utilize a dedicated T2-weighted, high in-plane spatial resolution (0.4 mm in plane) acquisition (HighResT2) (Iglesias et al., 2015). This is important in aging studies as extensive atrophy can distort hippocampal canonical morphological relationships and diminish gray-white matter contrast. Continuous recruitment to the HBA clinic meant that initial MRI protocols did not include this HighResT2 scan. We therefore sought to internally corroborate the T1-weighted subfield segmentations against a the HighResT2 output in a more recent HBA cohort. Bivariate correlation analysis was used to compare FreeSurfer-based 3D T1-weighted and HighResT2 volumes. T1-weighted subfield segmentations with a Pearson's correlation of ≥ 0.9 with HighResT2 were deemed robust.

Group Analysis

Significant differences between age at MRI scan, years of education, and depressive symptomatology (GDS-15) was determined by a One-Way ANOVA. A Chi-Squared test was determined differences in female/male ratios across groups. A One-Way ANCOVA established statistically significant differences in normalized verbal learning and memory scores and cognitive performance between the clinical groups. Age, years of education, sex and GDS-15 were used as covariates. Finally, significant group differences in right and left entorhinal

cortical thickness, whole hippocampal and subfield volumes were assessed using a One-Way ANCOVA controlling for covariates.

MCI Subtype Criteria Validation

The legitimacy of the stringent (i.e., requiring deficits in delayed recall for aMCI) HBA subtype classification (“*stringent criteria grouping*”) was investigated; naMCI participants demonstrating deficits in new learning were recoded to aMCI following the general (i.e.,- deficits in memory OR learning accepted as aMCI) criteria (“*general criteria grouping*”). A stepwise, multiple discriminant analysis was used to investigate if any of the predictor variables (subfield volumes and demographics) differentiated between SMC, aMCI and naMCI groups using the “*stringent criteria*” grouping and “*general criteria*” grouping.

Association to Cognitive Performance

Relationships between concurrent delayed recall performance scores and left whole hippocampal and the subfield volumes were investigated on a group basis with partial regressions controlling for age and education in both MCI subtypes separately. Fisher *r*-to-*z* transformation was used to investigate the significance of the difference between partial regression correlation coefficients.

Longitudinal Cognitive Assessment Analysis

For a subset of 75 participants, longitudinal cognitive assessment data was available. A repeated measures ANOVA assessed significant differences in decline in cognitive performance between groups between baseline and follow up assessment. A backward stepwise multiple linear regression (MLR) sought to identify if any baseline subfield volume measures significantly predicted follow-up verbal learning and memory performance. Covariates, time between assessment and subfield volumes were entered into the initial model.

All statistical analyses were carried out in SPSS (IBM, Armonk, NY, United States. Release 24). To correct for multiple comparisons a *post hoc* Bonferroni multiple comparisons between groups were carried out for all ANOVA and ANCOVA analyses and results presented are corrected *p*-values.

RESULTS

Hippocampal Subfield Segmentation Corroboration

Segmentation corroboration was carried out in 79 participants recruited through HBA, diagnosed with SMC (*n* = 19), naMCI (*n* = 26), aMCI (*n* = 25) or AD (*n* = 8) [mean age = 69.0 years (SD = 8.4)]. Twenty-two of this cohort also had corresponding cognitive and MRI assessments, met diagnostic criteria and therefore their 3D T1-weighted data were also included in the principal analysis below. Five out of ten subfields met this criterion [subiculum, presubiculum, CA1, CA4 and dentate gyrus (Supplementary Figure 1)]. Accordingly, only these validated subfields were included in subsequent analyses. Examples of subfield delineation and the underlying 3D T1 and T2 -weighted data are given in Figure 1. These three examples were chosen at

random from the MCI subjects and T1 datasets were re-sliced onto T2 to provide visual validity of segmentations.

Sample Demographics and Neuropsychological Performance

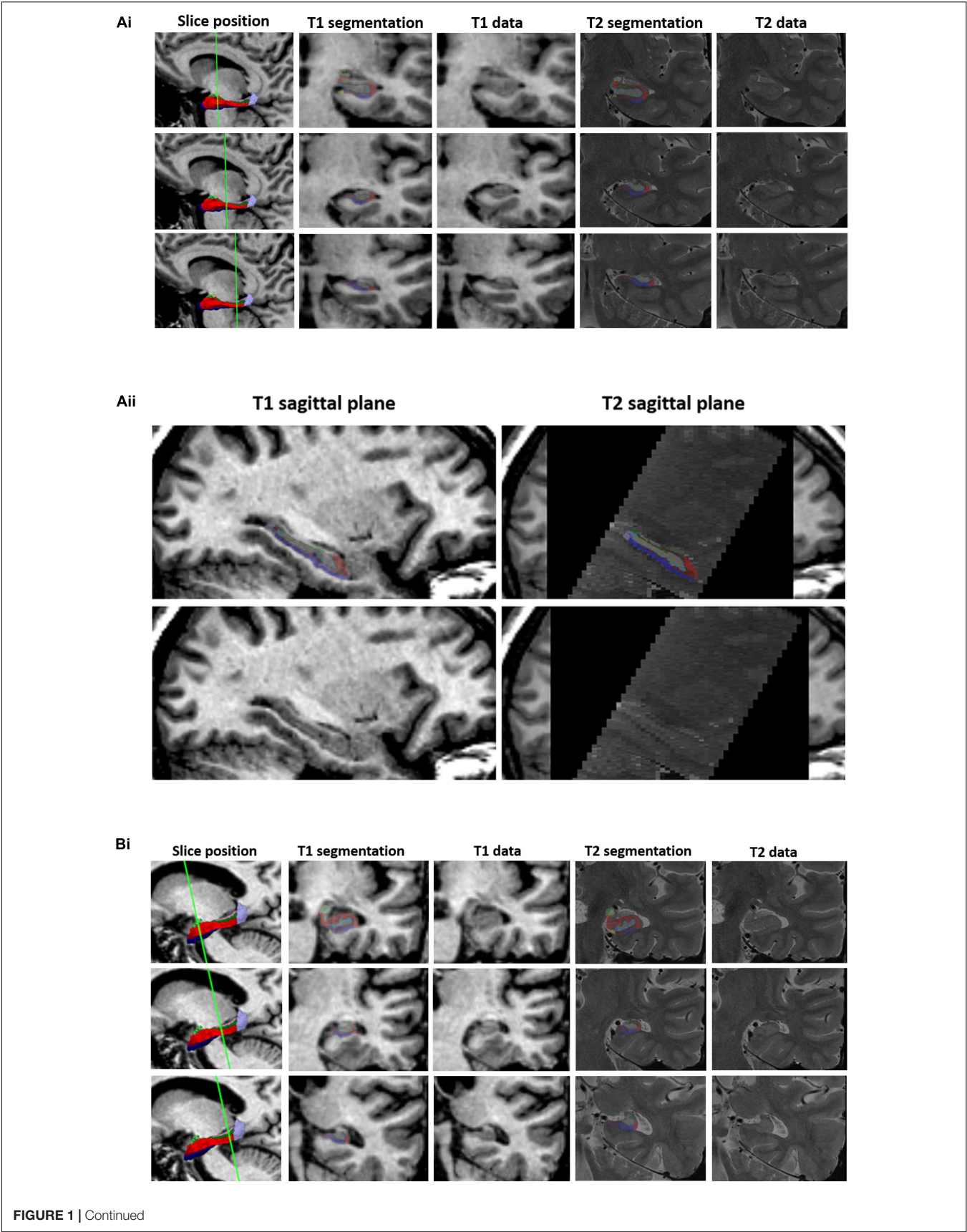
Of the total sample (*n* = 142), 20 had SMC, 38 were diagnosed with aMCI and 84 with naMCI. There was no significant difference in age, years of education and GDS-15 scores between groups. However, as all are important risk factors for cognitive decline these were still controlled for as covariates. There was a significant association between female/male ratio and group ($\chi^2 = 10.6$, *p* = 0.005) with more females in the SMC group. Considering our *stringent criteria* for aMCI, unsurprisingly this group demonstrated significantly reduced learning and delayed recall as well as and greater global cognitive impairment (MMSE) when compared to SMC and naMCI groups. SMC and naMCI group did not differ statistically in terms of their memory performance. Results shown in Table 1.

Subfield Volumes Differentiate MCI Subtypes

Both left and right whole hippocampal volumes were significantly reduced in aMCI compared to both SMC and naMCI (Left: *p* = 0.003, *p* = 0.002. Right: *p* = 0.022, *p* = 0.012, respectively). This pattern extended to the subfield analysis (Figure 2). All five analyzed subfields were significantly reduced in the aMCI compared to SMC groups and all but CA1 when compared to naMCI. This pattern was not as pronounced in the right, with only subiculum and presubiculum showing significant reductions when compared to naMCI. Cortical thickness analysis revealed that only the right entorhinal cortex was significantly reduced when comparing aMCI to SMC (*p* = 0.048). Full results given in Supplementary Table 1. As hippocampal differentiation was more prominent in the left and as entorhinal thickness did not differentiate between MCI subtype, all subsequent analyses were carried out with left subfield volumes only.

Stringent Criteria for Subtype Classification Is Supported by Subfield Volume

Recoding participants who had new learning deficits (*n* = 18) to aMCI in the “*general criteria*” grouping scheme led to 66 participants being re-coded as naMCI, and 56 re-coded as aMCI (SMC; *n* = 20). Preliminary exploration of our data revealed a clear separation of participants who were consistently classified as aMCI and naMCI in both grouping schemes. Supplementary Figure 2 shows RAVLT A7 *z*-scores plotted against presubiculum volume; where aMCI typically presented with smaller volumes correlating to poorer verbal delayed recall performance. The recoded participants, however, were spread throughout both aMCI and naMCI clusters. A stepwise multiple discriminant analysis revealed presubiculum volume as the sole significant variable that discriminates subtype in both grouping schemes. The “*stringent criteria*” grouping classification led to an overall increase in correctly classified participants (67.6% compared to 57.0%). More specifically, “*stringent criteria*”



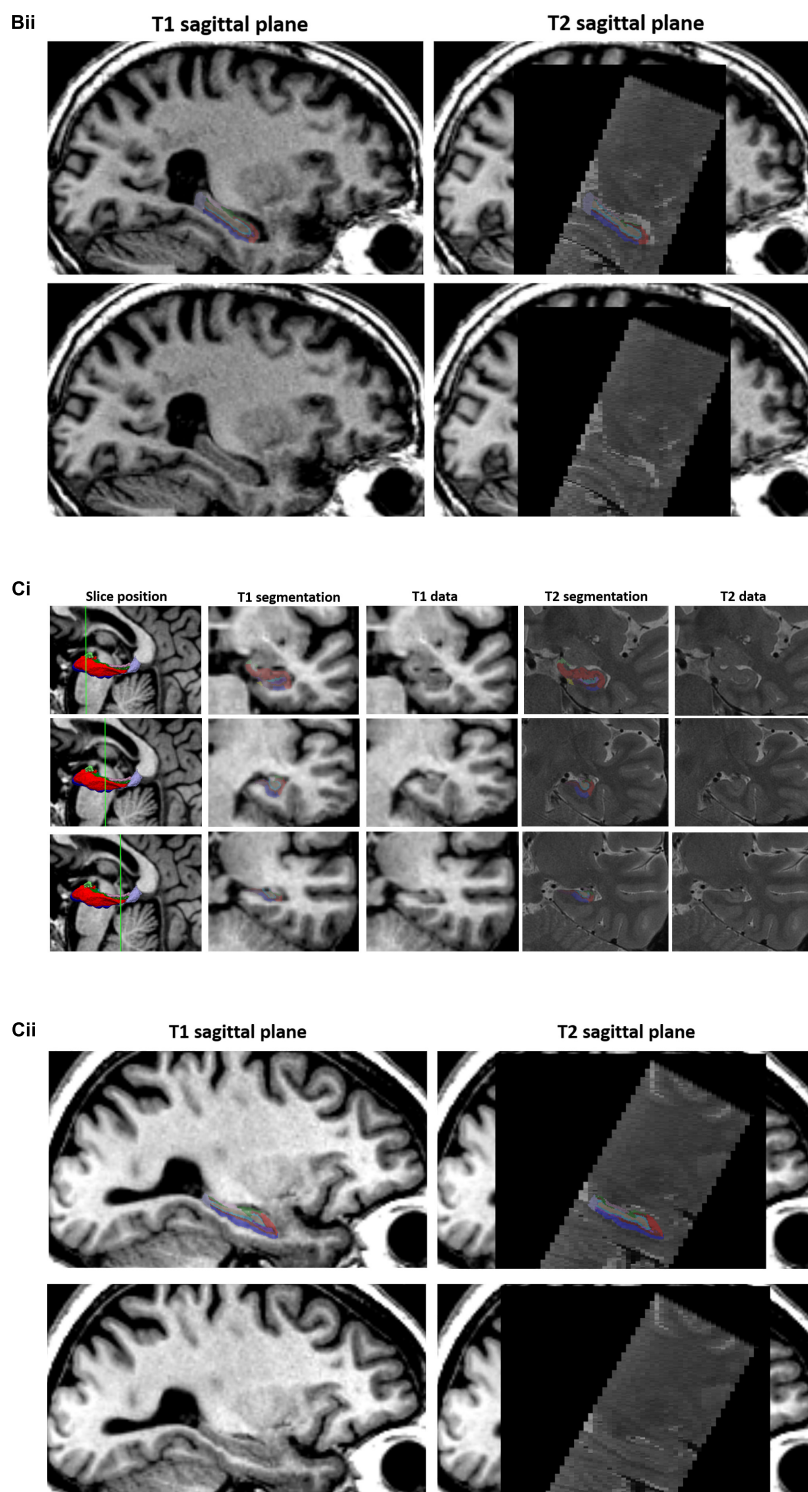


FIGURE 1 | T1 vs. T2 segmentations. 3D T1-weighted and T2-weighted segmentation outputs are given for three example participants (**A–C**) in the validation subset. (i) Three slices are shown through the hippocampus (1st column) with T1 segmentation and raw T1 data (2nd and 3rd column) and T2 segmentation and T2 raw data (4th and 5th column) of the equivalent slice. T1-weighted datasets have been re-sliced to T2 slice orientation. The left hippocampal segmentation has been removed to show the underlying T1 (3rd column) and T2 (5th column – data shown in native T2 space) data. (ii) Sagittal T1 (left column) and T2 (right column) structural scans are shown with (top) and without (bottom) the respective hippocampal segmentations. Segmentations opacity has been reduced to visualize the corresponding structural scan underneath. Internal structures/boundaries can clearly be seen in both the T1 and T2 raw data and overlays displaying the corresponding segmentation indicate that these boundaries have been adequately followed in both the T1 and T2 based segmentation streams.

TABLE 1 | Sample demographics and cognitive performance: mean (SD) values for individual groups and total sample.

	SMC	aMCI	naMCI	Total	F/X ²	Pairwise comparison
Number	20	38	84	142	–	–
Sex (M/F)	4/16	23/15	30/54	57/85	10.6***†	–
Education, years	13.5 (2.6)	14.3 (3.2)	13.5 (3.2)	13.7 (3.1)	0.8	–
Age at scan, years	67.6 (8.3)	67.6 (8.4)	66.5 (8.0)	66.9 (8.1)	0.3	–
GDS-15/15	2.8 (2.4)	3.7 (3.0)	4.5 (3.9)	4.0 (3.5)	2.2	–
MMSE/30	28.9 (0.4)†	27.6 (0.3)†	28.9 (0.2)†	–	9.4***	aMCI < naMCI < SMC
LogMem I ASS	12.2 (0.7)†	7.5 (0.5)†	10.3 (0.4)†	–	15.2***	aMCI < naMCI < SMC
LogMem II ASS	12.5 (0.7)†	7.0 (0.5)†	11.3 (0.3)†	–	34.0***	aMCI < naMCI < SMC
RAVLT 1-5, z-score	0.44 (0.2)†	–1.25 (0.1)†	–0.06 (0.1)†	–	33.6***	aMCI < naMCI < SMC
RAVLT A7, z-score	0.49 (0.2)†	–1.40 (0.1)†	0.11 (0.1)†	–	44.8***	aMCI < naMCI < SMC

†Indicates marginal means and standard error. Sex, age, years of education and GDS used as covariates. †Chi-squared. *** $p < 0.001$. GDS = Geriatric Depression Scale, 15-item; MMSE = Mini Mental State Examination; LogMem I ASS = Logical Memory I age-scaled score; LogMem II ASS = Logical Memory II age-scaled score; RAVLT 1-5 z-score = standardized z-score of the Rey Auditory Verbal Learning Test total score over 1-5 verbal learning trials; RAVLT A7 z-score = Standardized z-score for the Rey Auditory Verbal Learning Test A7 delayed (20-min) memory recall.

grouping led to 76.8% more accurate classification of aMCI participants than random assignment (40.6% with “general criteria” grouping) (Table 2).

CA1 Subfield Volume Predicts Memory Performance in aMCI

Partial regression analyses revealed that there was a clear differentiation between the significant predictors of delayed recall performance in both MCI subgroups. Specifically, smaller CA1, CA4 and dentate gyrus volumes were associated with poorer memory performance in aMCI. However, only presubiculum volume was significantly correlated with delayed recall performance (RAVLT A7 z-score) in the naMCI group (Table 3). The Fisher r -to- z transformation revealed that the association between CA1 and delayed recall performance (LogMem II ASS) was significantly larger in aMCI than naMCI ($z = 2.13$, $p = 0.03$) groups.

Dentate Gyrus Volume Predicts Longitudinal Auditory Learning and Memory Decline

Seventy-five participants (SMC = 15, aMCI = 14 and naMCI = 46) had a follow-up cognitive assessment at mean = 2.9 years (SD 1.3). There was no significant difference in follow-up time between groups. Participants diagnosed with aMCI at baseline had significant decline in global cognition, verbal learning and delayed recall performance at follow-up assessment compared to SMC and naMCI (MMSE: $p = 0.039$, $p = 0.030$, LogMem I ASS: $p < 0.0001$, $p = 0.001$, LogMem II ASS: $p < 0.0001$, $p < 0.0001$ and RAVLT 1-5 z-score: $p < 0.0001$, $p = 0.018$, RAVLT A7 z-score: $p < 0.0001$, $p < 0.0001$, respectively). Participants diagnosed with naMCI also had significant decline in RAVLT 1-5 z-scores compared to SMC ($p = 0.028$). Full results are given in **Supplementary Table 2**. Diagnoses at follow-up assessment (**Supplementary Table 3**) revealed that 11 and 7% of the aMCI and naMCI participants remained in the same diagnostic group, while the rest converted subtype, progressed to dementia or reverted to a “no MCI” diagnosis. A backward stepwise MLR

revealed that only dentate gyrus volume and age or years of education (where years of education were protective) were significant predictors of decline; smaller baseline dentate gyrus volume predicted decline in follow-up RAVLT verbal learning and delayed recall performance scores (Table 4).

DISCUSSION

This study provides further insight into the distinct structural and more specifically hippocampal pathophysologies that likely underpin memory decline in SMC and MCI subgroups. Consistent with previous studies (Winkler et al., 2014; Csukly et al., 2016) our findings show significant reduction of both right and left whole hippocampal volume in aMCI compared to naMCI and SMC. However, our work extends these previous findings, indicating that specifically focusing on the *delayed recall* characteristics of memory decline for defining MCI subtypes is not merely theoretical, but is supported by key neuroanatomical differences in subiculum and dentate gyrus subfields. These subfields are heavily implicated in mnemonic consolidation processes (O’Mara et al., 2000) and localized atrophy of these subfields are associated with risk of progression from MCI to AD (Apostolova et al., 2006, 2010).

Significantly, we have shown that hippocampal subfields in MCI are distinctly associated with verbal memory performance. Specifically, in those with aMCI, the dentate gyrus, CA1 and CA4 were associated with delayed memory recall performance. By contrast, in naMCI, the presubiculum was associated with delayed performance. Moreover, the association between CA1 and delayed recall performance was significantly stronger in aMCI than naMCI. This correlation was still present, but weaker ($R^2 = 0.34$) when following the “general criteria” grouping (results not included). These differential relationships may reflect the varied etiological mechanisms underpinning MCI subtypes. In addition, a recent study (Li et al., 2016) found significant atrophy in left subiculum and presubiculum subfields in a subcortical vascular MCI group (a prodromal stage of vascular dementia) compared to healthy controls.

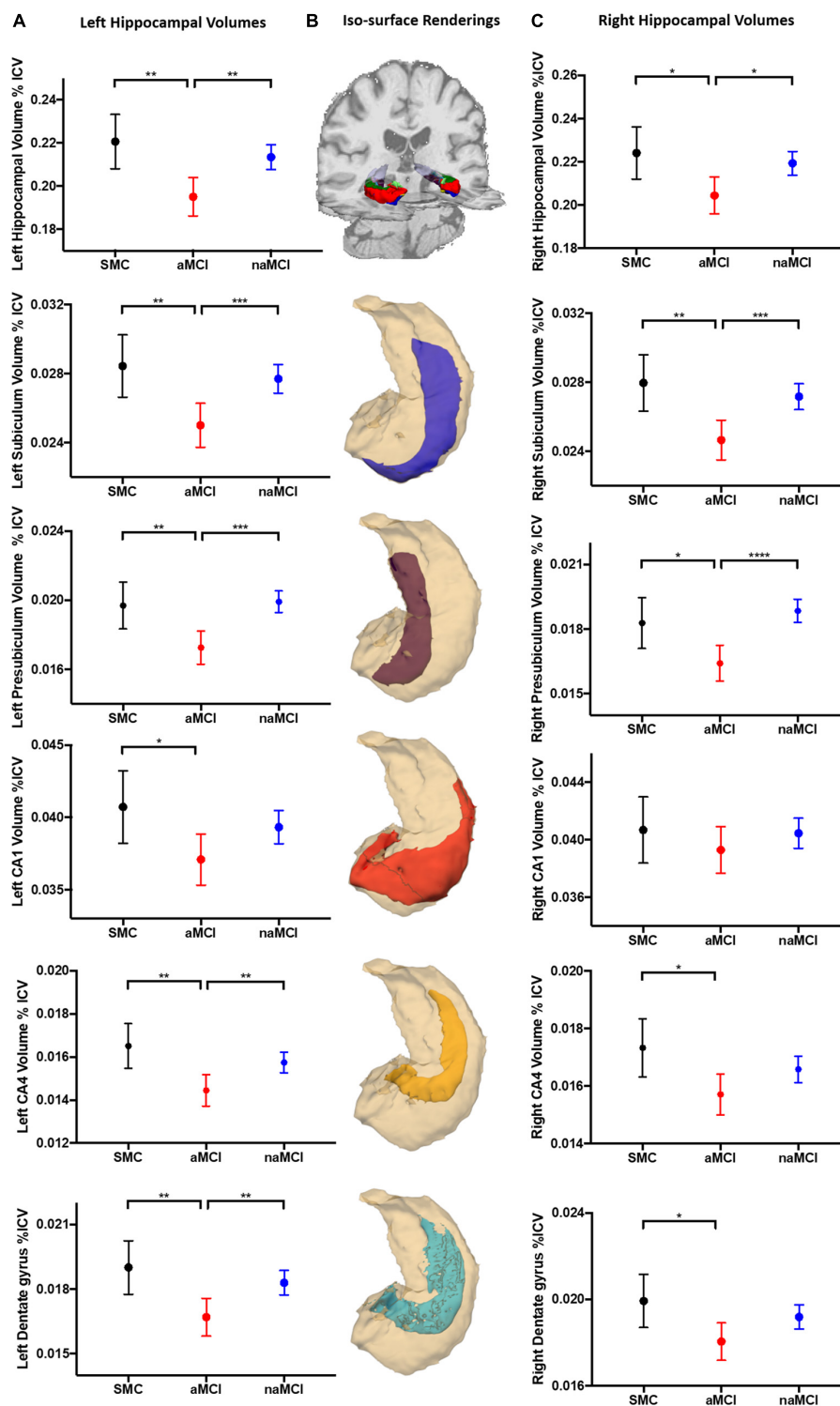


FIGURE 2 | Hippocampal volumetric analysis. Marginal mean (SD) plots of left (A) and right (C) whole hippocampal, and the memory associated subfields subiculum, presubiculum, CA1, CA4 and dentate gyrus volumes from SMC, aMCI and naMCI patient groups. Significant differences between patient groups from One-Way ANCOVA analysis are displayed (*) revealing that left hippocampal subfields are significantly atrophied in aMCI patients compared to SMC and naMCI groups. This pattern remains but is not as prevalent in the right hippocampus. Iso-surface renderings of an example whole hippocampal segmentation superimposed on coronal and axial planes of a structural 3D T1-weighted dataset (B) are displayed for reference purposes. Subsequent individual subfields of interest (blue = subiculum, magenta = presubiculum, red = CA1, yellow = CA4, cyan = dentate gyrus) shown in relation to the whole hippocampus (cream) are displayed below. Tests of between subject effects revealed that of the covariates, GDS-15 scores were significantly associated with left CA4 and dentate gyrus volume.

TABLE 2 | Stepwise multiple discriminant analysis results from (A) “stringent criteria” grouping and (B) “general criteria” grouping. Both analyses returned presubiculum volume as the sole discriminant function coefficient.

Prior probabilities for groups	Classification results					
	Prior%	Cases used	Predicted group membership%			
			SMC	aMCI	naMCI	Total
(A)						
“Stringent criteria” grouping						
SMC	4.1	20	0	20.0	80.0	100
aMCI	26.8	38	0	47.4	52.6	100
naMCI	59.2	84	0	7.1	92.9	100
(B)						
“General criteria” grouping						
SMC	14.1	20	0	30.0	70.0	100
aMCI	39.4	56	0	55.4	44.6	100
naMCI	46.5	66	0	24.2	75.8	100

A. 67.6% of original grouped cases correctly classified. B. 57.0% of original grouped cases correctly classified.

TABLE 3 | Partial correlation results showing association between verbal memory scores and subfield volume correcting for years of education and age.

Partial correlations		aMCI					naMCI				
		CA1	Subiculum	Presub	DG	CA4	CA1	Subiculum	Presub	DG	CA4
LogMem II ASS	R^2	0.40	0.25	0.26	0.35	0.33	−0.01	0.02	0.01	0.07	0.10
	Sig	0.016	0.146	0.130	0.039	0.050	0.945	0.883	0.90	0.543	0.373
RAVLT A7 z-score	R^2	0.45	0.24	0.13	0.38	0.37	0.14	0.23	0.40	0.20	0.19
	Sig	0.007	0.156	0.443	0.023	0.026	0.199	0.035	<0.001	0.074	0.090

LogMem II ASS = Logical Memory II age-scaled score; RAVLT A7 z-score = Standardized z-score for The Rey Auditory Verbal Learning Test A7 delayed (20-min) memory recall; presub = presubiculum hippocampal subfield; DG = dentate gyrus. Significant p values are indicated in bold.

TABLE 4 | Backward stepwise multiple linear regression result showing resultant significant predictors of follow-up verbal learning and delayed recall.

	Predictor variables	Overall R^2	Overall model significance
FU LogMem I ASS	Dentate gyrus: ($p = 0.061$, $R^2 = 0.05$) Education: ($p = 0.064$, $R^2 = 0.05$)	0.07	0.031
FU LogMem II ASS	Dentate gyrus: ($\beta = 0.25$, $p = 0.025$, $R^2 = 0.05$) Age: ($\beta = -0.23$, $p = 0.045$, $R^2 = 0.07$)	0.11	0.006
FU RAVLT 1-5 z-score	Dentate Gyrus: ($\beta = 0.26$, $p = 0.022$, $R^2 = 0.07$) Time between assessments: ($\beta = 0.26$, $p = 0.024$, $R^2 = 0.069$)	0.15	0.001
FU RAVLT A7 z-score	Dentate Gyrus: ($\beta = 0.27$, $p = 0.020$, $R^2 = 0.71$)	0.06	0.020

Overall model significance and correlation are shown as well as individual predictor partial variation. Standardized beta values are shown for significant predictors only. FU LogMem I ASS = Logical Memory I age-scaled score at follow up; FU LogMem II ASS = Logical Memory II age-scaled score at follow up; FU RAVLT 1-5 total z-score = standardized z-score of the Rey Auditory Verbal Learning Test total score over 1-5 verbal learning trials at follow up; FU RAVLT A7 z-score = standardized z-score for the Rey Auditory Verbal Learning Test A7 delayed (20-min) memory recall score at follow up. Significant p values are indicated in bold.

This coupled with our results, suggests that the presubiculum may be particularly sensitive to vascular pathologies, which may be more characteristic of naMCI.

Importantly, in this study, not only are the naMCI and SMC groups comparable on memory performance, but there were no measurable differences in whole hippocampal or subfield volume. Referring to **Supplementary Figure 2**, SMC participants did not form their own cluster in an extended upper quadrant along the linear trend line but fell within the boundaries of the naMCI participants. The lack of observable

and measurable difference supports the notion that cognitive change in naMCI is due to more diverse brain pathology, that is less likely attributable to early changes in Amyloid beta (A β). Alternatively, it is equally plausible that both groups may fall earlier in the cascade of dynamic biomarkers of AD, and may still exhibit preclinical AD, according to positron emission tomography (PET) and cerebrospinal fluid (CSF) biomarkers for AD (Coutinho et al., 2015; Dubois, 2018). Unfortunately, in this study, such measures necessary for future exploration were not available.

Various hippocampal subfields have been shown to play clear and distinct roles in mnemonic processes. Recent functional MRI studies in humans have found localized fMRI activity in the anterior CA2, CA3 and subiculum during learning, and in the CA1, and the posterior subiculum during retrieval of novel associations (Suthana et al., 2015). This idea of an encoding/retrieval gradient along the longitudinal axis of the hippocampus (Prince et al., 2005; Suthana et al., 2015) suggests that our results correlating the volume of retrieval-associated CA1 in aMCI may be functionally relevant. Furthermore, the earliest neurodegeneration seen in AD occurs in the entorhinal cortex and then progresses to the hippocampus. Future work should focus on combining both structural and functional data to investigate the association between not only hippocampal, but whole-brain atrophy patterns, corresponding functional signatures and cognitive performance, thus providing further insight into the underlying mechanisms differentiating MCI subtypes.

Improved understanding of the specific subfields that correlate with memory decline, will lead to more targeted treatments. Aerobic exercise has already been suggested as a possible promoter of hippocampal plasticity, with studies generally revealing attenuated whole hippocampal atrophy over the duration of intervention (Smith et al., 2010; ten Brinke et al., 2015). Furthermore, our recent work in an MCI sample found that hippocampal subfields susceptible to volume loss in AD were protected by progressive resistance training (Broadhouse et al., 2017 Abstract Supplement). Similarly, ongoing work in the field of cognitive training has demonstrated that these interventions can induce underlying neurophysiological alterations in healthy older adults and those with MCI (Belleville and Bherer, 2012; Suo et al., 2016).

Although AD sensitive subfields were significantly reduced in aMCI and these participants had statistically poorer performance at follow-up, subfield volume is clearly not the sole factor in determining outcome. It has, however, been postulated that the dentate gyrus plays a critical function in mediating processes such as recall of sequential information and short-term memory (Kesner, 2007). In this regard, our results showing larger dentate gyrus volume at baseline assessment was significantly associated with better follow-up cognitive and memory performance in all groups supports the notion that preserved dentate gyrus volume may be directly or indirectly associated with key neuroprotective factors implicated in preservation of memory function over time. It is in these early stage disease groups where modeling hippocampal volume trajectory preceding memory decline could be most relevant and informative. Further work incorporating both longitudinal MRI and cognitive assessment data is needed to fully understand the multifaceted, transient nature of MCI subtypes and SMC.

Several large-scale studies from the Alzheimer's Disease Neuroimaging Initiative (ADNI) have highlighted the need for the refinement of MCI diagnostic criteria and have suggested that improved methods may yield gains in biomarker and clinical trial study findings because of improvements in sample compositions of "true positive" cases and removal of "false positive" cases (Bondi et al., 2014; Edmonds et al., 2015). From a

clinical perspective, our results suggest that screening for MCI should always incorporate measures of delayed memory recall rather than simply relying on new learning or acquisition. Currently, gross screening tools do not incorporate such measures. Recent studies aiming to rate disease progression and score disease state have found that delayed recall is the earliest biomarker to become abnormal during transition from health to disease (Jedynak et al., 2012). Our findings suggest that further exploration of clinically useful neuropsychological tools that may detect very subtle memory impairment may be worth pursuing, particularly if they are sensitive to the earliest forms of memory decline. For example, tasks that utilize short-term memory binding (Fernandez et al., 2018) or accelerated forgetting (Weston et al., 2018) may be worth examining in preclinical and MCI periods, and in relation to AD biomarkers.

Limitations

Although the above reported results suggest a structural delineation between MCI subtypes there are several limitations to consider. Firstly, although we have limited our analyses to corroborated subfields to provide some confidence in our findings, it is important to note that although internally validated from high-field data, the FreeSurfer segmentations do not necessarily represent ground-truth in anatomy and must be interpreted with caution (Iglesias et al., 2015). FreeSurfer segmentations have not been validated against manual segmentation and without high-resolution T2 data there is a lack of internal information to guide the segmentation template and subfield labeling leading to uncertainty in subfield classification within the hippocampus. Due to the large user base, future studies validating FreeSurfer to manual segmentations would provide more confidence in T1 generated results. Though, as with all MR sequences there are tradeoffs. The improved gray/white matter contrast is achieved with a spin echo sequence – a gradient readout that is inherently longer and resultant contrast that provides less signal or "entropy" than the T1-weighted counterpart. Additionally, T2-weighted scans are much more affected by patient motion than the T1-weighted scans (Yushkevich et al., 2015). Furthermore, to achieve reasonable scan times the T2 sequence is not 3D and as a result has anisotropic resolution (typically $0.4 \times 0.4 \times 2$ mm). These factors need to be considered when carrying out subfield segmentation. In a cohort where hippocampal atrophy occurs along the anterior-posterior axis (along the *through-plane* direction where partial voluming effects will be greatest in the T2-weighted acquisitions) and speed to reduce motion artifacts is priority, the faster, 3D T1-weighted, isotropic resolution sequence may often be preferable. Future investigation of hippocampal subfields in MCI subtypes should implement a combined T1- T2- weighted segmentation method that takes full advantage of the isotropic T1 within the atlas-to-target registration and segmentation pipeline (Yushkevich et al., 2015). Furthermore, caution should be taken with any automated pipeline, T1- or T2-based, and investigators should always visually inspect their datasets for visible internal structures such as the leptomeningeal tissue in the

vestigial hippocampal sulcus that is often used as a segmentation landmark and make it suitable for subfield processing pipelines. Future advancements in imaging acquisition, shorter scan time and improved contrast, will also provide further improvements to segmentation pipelines.

Secondly, we cannot claim the HBA criteria represents the optimal method; we propose that it represents an important step toward improved clinical classification. Although **Supplementary Figure 2** provides a rudimentary visual inspection, this trend was apparent for all performance/subfield correlation plots (not included here). Deficits in delayed recall (aMCI) were linked with significant subfield atrophy, however, reduced subfield volume did not always lead to deficits in delayed recall (e.g., recoded participants). Although discriminant analysis indicated that “stringent criteria” grouping led to more participants accurately classified when considering hippocampal subfield volume alone, there is a clear need for further improvement. This lack of clear subgroup classification criteria for a subset of MCI subjects is most certainly due to the current modest understanding of disease etiology, and the poorly understood role of cognitive reserve in this population.

Finally, the lack of inclusion of a true “healthy control” group may limit our interpretation of results. However, by definition SMCs do not display objectively amnesic phenotypes. Although the individuals themselves report subtle decline in cognitive abilities, this is not detectable on conventional neuropsychological tests (which may lack sensitivity for detecting very subtle change) and the SMCs are otherwise still healthy community dwelling older adults. Recent evidence suggests that individuals with SMCs may be at increased risk of dementia and have a higher rate of progression to MCI than non-health seeking older adults (Schultz et al., 2015). Subsequently, it has been suggested that SMCs may represent a “pre-clinical” stage in the evolution of normal aging to clinical AD and might represent a potential target for intervention trials. Such individuals may indeed meet criteria for preclinical AD based on biomarker evidence (Gordon et al., 2018). As the field of AD has begun to increasingly focus on prevention, earlier detection and diagnosis of the disease has become paramount. Therefore, neurostructural comparison between SMCs and MCI subtypes may be more meaningful when investigating disease progression.

REFERENCES

- Apostolova, L. G., Dutton, R. A., Dinov, I. D., Hayashi, K. M., Toga, A. W., Cummings, J. L., et al. (2006). Conversion of mild cognitive impairment to Alzheimer disease predicted by hippocampal atrophy maps. *Arch. Neurol.* 63, 693–699. doi: 10.1001/archneur.63.5.693
- Apostolova, L. G., Mosconi, L., Thompson, P. M., Green, A. E., Hwang, K. S., Ramirez, A., et al. (2010). Subregional hippocampal atrophy predicts Alzheimer's dementia in the cognitively normal. *Neurobiol. Aging* 31, 1077–1088. doi: 10.1016/j.neurobiolaging.2008.08.008
- Belleville, S., and Bherer, L. (2012). Biomarkers of cognitive training effects in aging. *Curr. Transl. Geriatr. Exp. Gerontol. Rep.* 1, 104–110. doi: 10.1007/s13670-012-0014-5
- Bondi, M. W., Edmonds, E. C., Jak, A. J., Clark, L. R., Delano-Wood, L., McDonald, C. R., et al. (2014). Neuropsychological criteria for mild cognitive impairment

In summary, our data demonstrate that structural MRI can aid in the differentiation of MCI subtypes and reveals significant differences in whole hippocampal and subfield volumes between SMC, naMCI and aMCI which are in turn, strongly linked to verbal learning and memory performance. Of clinical significance, our findings further demonstrate that using a stringent diagnostic approach to characterizing aMCI based on predominant deficits in *delayed* recall (rather than merely encoding) is well justified, as such deficits are strongly and specifically linked to underlying volumetric subfield reductions in CA1, CA4 and the dentate gyrus.

DATA AVAILABILITY STATEMENT

The datasets generated for this study are available on request to the corresponding author.

ETHICS STATEMENT

The studies involving human participants were reviewed and approved by the Human Research Ethics Committee of the University of Sydney. The patients/participants provided their written informed consent to participate in this study.

AUTHOR CONTRIBUTIONS

KB, LM, SD, MV, and SN contributed to the conception and design of the study. KB and IL performed the image preprocessing and statistical analysis. NC organized the database. KB wrote the first draft of the manuscript. All authors contributed to the manuscript revision, read, and approved the submitted version.

SUPPLEMENTARY MATERIAL

The Supplementary Material for this article can be found online at: <https://www.frontiersin.org/articles/10.3389/fnbeh.2019.00259/full#supplementary-material>

improves diagnostic precision, biomarker associations, and progression rates. *J. Alzheimers Dis.* 42, 275–289. doi: 10.3233/JAD-140276

- Broadhouse, K., Suo, C., Fiatarone Singh, M., Gates, N., Wen, W., Sachdev, P., et al. (2017). What happens to the hippocampus 12-months after training? Longitudinal linear mixed effects model analysis of mild cognitive impairments in the SMART trial. *Alzheimer's Dement.* 13:P260. doi: 10.1016/j.jalz.2017.06.127
- Carlesimo, G. A., Piras, F., Orfei, M. D., Iorio, M., Caltagirone, C., and Spalletta, G. (2015). Atrophy of presubiculum and subiculum is the earliest hippocampal anatomical marker of Alzheimer's disease. *Alzheimers Dement.* 1, 24–32. doi: 10.1016/j.dadm.2014.12.001
- Costafreda, S. G., Dinov, I. D., Tu, Z., Shi, Y., Liu, C. Y., Kloszewska, I., et al. (2011). Automated hippocampal shape analysis predicts the onset of dementia in mild cognitive impairment. *Neuroimage* 56, 212–219. doi: 10.1016/j.neuroimage.2011.01.050

- Coutinho, A. M., Porto, F. H., Duran, F. L., Prando, S., Ono, C. R., Feitosa, E. A., et al. (2015). Brain metabolism and cerebrospinal fluid biomarkers profile of non-amnesic mild cognitive impairment in comparison to amnesic mild cognitive impairment and normal older subjects. *Alzheimers Res. Ther.* 7:58. doi: 10.1186/s13195-015-0143-0
- Csukly, G., Siraly, E., Fodor, Z., Horvath, A., Salacz, P., Hidas, Z., et al. (2016). The differentiation of amnesic type MCI from the non-amnesic types by structural MRI. *Front. Aging Neurosci.* 8:52. doi: 10.3389/fnagi.2016.00052
- Dubois, B. (2018). The emergence of a new conceptual framework for Alzheimer's disease. *J. Alzheimers Dis.* 62, 1059–1066. doi: 10.3233/JAD-170536
- Duffy, S. L., Lagopoulos, J., Hickie, I. B., Diamond, K., Graeber, M. B., Lewis, S. J., et al. (2014). Glutathione relates to neuropsychological functioning in mild cognitive impairment. *Alzheimers Dement.* 10, 67–75. doi: 10.1016/j.jalz.2013.01.005
- Edmonds, E. C., Delano-Wood, L., Clark, L. R., Jak, A. J., Nation, D. A., McDonald, C. R., et al. (2015). Susceptibility of the conventional criteria for mild cognitive impairment to false-positive diagnostic errors. *Alzheimers Dement.* 11, 415–424. doi: 10.1016/j.jalz.2014.03.005
- Fernandez, G., Orozco, D., Agamennoni, O., Schumacher, M., Sanudo, S., Biondi, J., et al. (2018). Visual processing during short-term memory binding in mild Alzheimer's disease. *J. Alzheimers Dis.* 63, 185–194. doi: 10.3233/JAD-170728
- Folstein, M. F., Folstein, S. E., and McHugh, P. R. (1975). "Mini-mental state". A practical method for grading the cognitive state of patients for the clinician. *J. Psychiatr. Res.* 12, 189–198.
- Frisoni, G. B., Fox, N. C., Jack, C. R. Jr., Scheltens, P., and Thompson, P. M. (2010). The clinical use of structural MRI in Alzheimer disease. *Nat. Rev. Neurol.* 6, 67–77. doi: 10.1038/nrneurol.2009.215
- Ganguli, M., Dodge, H. H., Shen, C., and DeKosky, S. T. (2004). Mild cognitive impairment, amnesic type: an epidemiologic study. *Neurology* 63, 115–121. doi: 10.1212/01.wnl.0000132523.27540.81
- Gauthier, S., Reisberg, B., Zaudig, M., Petersen, R. C., Ritchie, K., Broich, K., et al. (2006). Mild cognitive impairment. *Lancet* 367, 1262–1270. doi: 10.1016/S0140-6736(06)68542-5
- Gordon, B. A., Blazey, T. M., Su, Y., Hari-Raj, A., Dincer, A., Flores, S., et al. (2018). Spatial patterns of neuroimaging biomarker change in individuals from families with autosomal dominant Alzheimer's disease: a longitudinal study. *Lancet Neurol.* 17, 241–250. doi: 10.1016/S1474-4422(18)30028-0
- Greenberg, S. A. (2002). Geriatric depression scale [GDS]. *Occas. Pap.* 82:46.
- Hughes, T. F., Snitz, B. E., and Ganguli, M. (2011). Should mild cognitive impairment be subtyped? *Curr. Opin. Psychiatry* 24, 237–242. doi: 10.1097/YCO.0b013e328344696b
- Iglesias, J. E., Augustinack, J. C., Nguyen, K., Player, C. M., Player, A., Wright, M., et al. (2015). A computational atlas of the hippocampal formation using ex vivo, ultra-high resolution MRI: application to adaptive segmentation of in vivo MRI. *Neuroimage* 115, 117–137. doi: 10.1016/j.neuroimage.2015.04.042
- Jack, C. R. Jr., Petersen, R. C., Xu, Y., O'Brien, P. C., Smith, G. E., Ivnik, R. J., et al. (2000). Rates of hippocampal atrophy correlate with change in clinical status in aging and AD. *Neurology* 55, 484–489.
- Jedynak, B. M., Lang, A., Liu, B., Katz, E., Zhang, Y., Wyman, B. T., et al. (2012). A computational neurodegenerative disease progression score: method and results with the Alzheimer's disease neuroimaging initiative cohort. *Neuroimage* 63, 1478–1486. doi: 10.1016/j.neuroimage.2012.07.059
- Jungwirth, S., Zehetmayer, S., Hinterberger, M., Tragl, K. H., and Fischer, P. (2012). The validity of amnesic MCI and non-amnesic MCI at age 75 in the prediction of Alzheimer's dementia and vascular dementia. *Int. Psychogeriatr.* 24, 959–966. doi: 10.1017/S1041610211002870
- Kesner, R. P. (2007). A behavioral analysis of dentate gyrus function. *Prog. Brain Res.* 163, 567–576. doi: 10.1016/S0079-6123(07)63030-1
- Lezak, M. (1982). *Neuropsychological Assessment*, 2nd Edn. New York, NY: Oxford University Press.
- Li, X., Li, D., Li, Q., Li, Y., Li, S., et al. (2016). Hippocampal subfield volumetry in patients with subcortical vascular mild cognitive impairment. *Sci. Rep.* 6:20873. doi: 10.1038/srep20873
- Linn, B. S., Linn, M. W., and Gurel, L. (1968). Cumulative illness rating scale. *J. Am. Geriatr. Soc.* 16, 622–626.
- Mitchell, A. J., Beaumont, H., Ferguson, D., Yadegarfar, M., and Stubbs, B. (2014). Risk of dementia and mild cognitive impairment in older people with subjective memory complaints: meta-analysis. *Acta Psychiatr. Scand.* 130, 439–451. doi: 10.1111/a.12336
- Morra, J. H., Tu, Z., Apostolova, L. G., Green, A. E., Avedissian, C., Madsen, S. K., et al. (2009). Automated 3D mapping of hippocampal atrophy and its clinical correlates in 400 subjects with Alzheimer's disease, mild cognitive impairment, and elderly controls. *Hum. Brain Mapp.* 30, 2766–2788. doi: 10.1002/hbm.20708
- Mu, Y., and Gage, F. H. (2011). Adult hippocampal neurogenesis and its role in Alzheimer's disease. *Mol. Neurodegener.* 6:85. doi: 10.1186/1750-1326-6-85
- Norton, S., Matthews, F. E., Barnes, D. E., Yaffe, K., and Brayne, C. (2014). Potential for primary prevention of Alzheimer's disease: an analysis of population-based data. *Lancet Neurol.* 13, 788–794. doi: 10.1016/S1474-4422(14)70136-X
- O'Mara, S. M., Commings, S., and Anderson, M. (2000). Synaptic plasticity in the hippocampal area CA1-subiculum projection: implications for theories of memory. *Hippocampus* 10, 447–456.
- Petersen, R. C., Lopez, O., Armstrong, M. J., Getchius, T. S. D., Ganguli, M., Gloss, D., et al. (2018). Practice guideline update summary: mild cognitive impairment: report of the guideline development, dissemination, and implementation subcommittee of the american academy of neurology. *Neurology* 90, 126–135. doi: 10.1212/WNL.00000000000004826
- Petersen, R. C., Roberts, R. O., Knopman, D. S., Boeve, B. F., Geda, Y. E., Ivnik, R. J., et al. (2009). Mild cognitive impairment: ten years later. *Arch. Neurol.* 66, 1447–1455. doi: 10.1001/archneurol.2009.266
- Prince, S. E., Daselaar, S. M., and Cabeza, R. (2005). Neural correlates of relational memory: successful encoding and retrieval of semantic and perceptual associations. *J. Neurosci.* 25, 1203–1210. doi: 10.1523/JNEUROSCI.2540-04.2005
- Purser, J. L., Fillenbaum, G. G., and Wallace, R. B. (2006). Memory complaint is not necessary for diagnosis of mild cognitive impairment and does not predict 10-year trajectories of functional disability, word recall, or short portable mental status questionnaire limitations. *J. Am. Geriatr. Soc.* 54, 335–338. doi: 10.1111/j.1532-5415.2005.00589.x
- Reuter, M., Rosas, H. D., and Fischl, B. (2010). Highly accurate inverse consistent registration: a robust approach. *Neuroimage* 53, 1181–1196. doi: 10.1016/j.neuroimage.2010.07.020
- Rovner, B. W., and Folstein, M. F. (1987). Mini-mental state exam in clinical practice. *Hosp. Pract.* 22, 99,103,106,110.
- Rybarczyk, B. (2011). "Social and occupational functioning assessment scale (SOFAS)," in *Encyclopedia of Clinical Neuropsychology*, eds J. S. Kreutzer, J. DeLuca, and B. Caplan, (New York, NY: Springer), 2313–2313. doi: 10.1007/978-0-387-79948-3_428
- Schmidt, M. (1996). *Rey Auditory Verbal Learning Test: A handbook*. Los Angeles, CA: Western Psychological Services.
- Schultz, S. A., Oh, J. M., Kosik, R. L., Dowling, N. M., Gallagher, C. L., Carlsson, C. M., et al. (2015). Subjective memory complaints, cortical thinning, and cognitive dysfunction in middle-aged adults at risk for AD. *Alzheimers Dement.* 1, 33–40. doi: 10.1016/j.dadm.2014.11.010
- Senior, G. (1999). *Analysing RAVLT Learning and Serial Position Curves Using Mahalanobis Distance*. Toowoomba, QLD: University of Queensland.
- Smith, P. J., Blumenthal, J. A., Hoffman, B. M., Cooper, H., Strauman, T. A., Welsh-Bohmer, K., et al. (2010). Aerobic exercise and neurocognitive performance: a meta-analytic review of randomized controlled trials. *Psychosom. Med.* 72, 239–252. doi: 10.1097/PSY.0b013e3181d14633
- Steinberg, S. I., Negash, S., Sammel, M. D., Bogner, H., Harel, B. T., Livney, M. G., et al. (2013). Subjective memory complaints, cognitive performance, and psychological factors in healthy older adults. *Am. J. Alzheimers Dis. Other Dement.* 28, 776–783. doi: 10.1177/1533317513504817
- Suo, C., Singh, M. F., Gates, N., Wen, W., Sachdev, P., Brodaty, H., et al. (2016). Therapeutically relevant structural and functional mechanisms triggered by physical and cognitive exercise. *Mol. Psychiatry* 21:1645. doi: 10.1038/mp.2016.57
- Suthana, N. A., Donix, M., Wozny, D. R., Bazih, A., Jones, M., Heidemann, R. M., et al. (2015). High-resolution 7T fMRI of human hippocampal subfields during associative learning. *J. Cogn. Neurosci.* 27, 1194–1206. doi: 10.1162/jocn_a_00772

- ten Brinke, L. F., Bolandzadeh, N., Nagamatsu, L. S., Hsu, C. L., Davis, J. C., Miran-Khan, K., et al. (2015). Aerobic exercise increases hippocampal volume in older women with probable mild cognitive impairment: a 6-month randomised controlled trial. *Br. J. Sports Med.* 49, 248–254. doi: 10.1136/bjsports-2013-093184
- van Vliet, I. M., and de Beurs, E. (2007). [The MINI-international neuropsychiatric interview. A brief structured diagnostic psychiatric interview for DSM-IV en ICD-10 psychiatric disorders]. *Tijdschr Psychiatr.* 49, 393–397.
- Wechsler, D. (1997a). *Manual for the Wechsler Adult Intelligence Scale*. San Antonio, TX: The Psychological Corporation.
- Wechsler, D. (1997b). *Wechsler Adult Intelligence Scale-III*. San Antonio, TX: The Psychological Corporation.
- Weston, P. S. J., Nicholas, J. M., Henley, S. M. D., Liang, Y., Macpherson, K., Donnachie, E., et al. (2018). Accelerated long-term forgetting in presymptomatic autosomal dominant Alzheimer's disease: a cross-sectional study. *Lancet Neurol.* 17, 123–132. doi: 10.1016/S1474-4422(17)30434-9
- Winblad, B., Palmer, K., Kivipelto, M., Jelic, V., Fratiglioni, L., Wahlund, L. O., et al. (2004). Mild cognitive impairment—beyond controversies, towards a consensus: report of the International working group on mild cognitive impairment. *J. Intern. Med.* 256, 240–246. doi: 10.1111/j.1365-2796.2004.01380.x
- Winkler, A., Dlugaj, M., Mönninghoff, C., Huppertz, H.-J., Wanke, I., Erbel, R., et al. (2014). Role of hippocampal volume in identifying mci subtypes: results of a case-control study. *Alzheimer's Dement.* 10(4 Suppl.): 705. doi: 10.1016/j.jalz.2014.05.1295
- Yushkevich, P. A., Pluta, J. B., Wang, H., Xie, L., Ding, S. L., Gertje, E. C., et al. (2015). Automated volumetry and regional thickness analysis of hippocampal subfields and medial temporal cortical structures in mild cognitive impairment. *Hum. Brain Mapp.* 36, 258–287. doi: 10.1002/hbm.22627

Conflict of Interest: The authors declare that the research was conducted in the absence of any commercial or financial relationships that could be construed as a potential conflict of interest.

Copyright © 2019 Broadhouse, Mowszowski, Duffy, Leung, Cross, Valenzuela and Naismith. This is an open-access article distributed under the terms of the Creative Commons Attribution License (CC BY). The use, distribution or reproduction in other forums is permitted, provided the original author(s) and the copyright owner(s) are credited and that the original publication in this journal is cited, in accordance with accepted academic practice. No use, distribution or reproduction is permitted which does not comply with these terms.



Late Effects of $^1\text{H} + ^{16}\text{O}$ on Short-Term and Object Memory, Hippocampal Dendritic Morphology and Mutagenesis

Frederico Kiffer^{1,2}, Tyler Alexander^{1,2}, Julie Anderson^{1,2}, Thomas Groves^{1,2,3}, Taylor McElroy^{1,2}, Jing Wang^{1,2}, Vijayalakshmi Sridharan^{1,2}, Michael Bauer⁴, Marjan Boerma^{1,2} and Antiño Allen^{1,2,3*}

¹ Division of Radiation Health, University of Arkansas for Medical Sciences, Little Rock, AR, United States, ² Department of Pharmaceutical Sciences, University of Arkansas for Medical Sciences, Little Rock, AR, United States, ³ Neurobiology & Developmental Sciences, University of Arkansas for Medical Sciences, Little Rock, AR, United States, ⁴ Department of Biomedical Informatics, University of Arkansas for Medical Sciences, Little Rock, AR, United States

OPEN ACCESS

Edited by:

Aine Kelly,
Trinity College Dublin, Ireland

Reviewed by:

Antoine Besnard,
Harvard Medical School,
United States
Jesús Álvarez-Herms,
Ministerio de Educación Cultura y
Deporte, Spain

*Correspondence:

Antiño Allen
Aallen@uams.edu

Specialty section:

This article was submitted to
Learning and Memory,
a section of the journal
Frontiers in Behavioral Neuroscience

Received: 11 January 2020

Accepted: 22 May 2020

Published: 26 June 2020

Citation:

Kiffer F, Alexander T, Anderson J, Groves T, McElroy T, Wang J, Sridharan V, Bauer M, Boerma M and Allen A (2020) Late Effects of $^1\text{H} + ^{16}\text{O}$ on Short-Term and Object Memory, Hippocampal Dendritic Morphology and Mutagenesis. *Front. Behav. Neurosci.* 14:96. doi: 10.3389/fnbeh.2020.00096

The space extending beyond Earth's magnetosphere is subject to a complex field of high-energy charged nuclei, which are capable of traversing spacecraft shielding and human tissues, inducing dense ionization events. The central nervous system is a major area of concern for astronauts who will be exposed to the deep-space radiation environment on a mission to Mars, as charged-particle radiation has been shown to elicit changes to the dendritic arbor within the hippocampus of rodents, and related cognitive-behavioral deficits. We exposed 6-month-old male mice to whole-body ^1H (0.5 Gy; 150 MeV/n; 18–19 cGy/minute) and an hour later to ^{16}O (0.1Gy; 600 MeV/n; 18–33 Gy/min) at NASA's Space Radiation Laboratory as a galactic cosmic ray-relevant model. Animals were housed with bedding which provides cognitive enrichment. Mice were tested for cognitive behavior 9 months after exposure to elucidate late radiation effects. Radiation induced significant deficits in novel object recognition and short-term spatial memory (Y-maze). Additionally, we observed opposing morphological differences between the mature granular and pyramidal neurons throughout the hippocampus, with increased dendritic length in the dorsal dentate gyrus and reduced length and complexity in the CA1 subregion of the hippocampus. Dendritic spine analyses revealed a severe reduction in mushroom spine density throughout the hippocampus of irradiated animals. Finally, we detected no general effect of radiation on single-nucleotide polymorphisms in immediate early genes, and genes involved in inflammation but found a higher variant allele frequency in the antioxidants thioredoxin reductase 2 and 3 loci.

Keywords: Mars, brain, neuron, hippocampus, morphology, behavior, space, radiation

INTRODUCTION

NASA's efforts to extend manned spaceflight beyond low-earth orbit in the near future for the first time since the Apollo era dawns a new age in space exploration. Current plans involve lunar sortie missions followed by the deep-space gateway, where astronaut crews will be exposed to radiation, confinement, and microgravity for increasing durations-all leading to a manned mission to Mars,

targeted toward the late 2030s (Drake et al., 2010). This new age in space exploration brings new challenges for long-term life support as humans have never been exposed to the complex radiation environment of deep space for more than 13 days.

The interplanetary space within the solar system is host to high-energy charged particles that consist of galactic cosmic rays (GCR), and solar particle events (SPE), such as coronal mass ejections. Galactic cosmic rays originate from supernovas within our galaxy, and provide constant fluence of approximately 87% ^1H , 12% ^4He , and 1–2% high-mass ($Z > 2$) high-energy (HZE) particles at median energies of 1,000 MeV/n (Nelson, 2016). Of all HZE, ^{16}O is the most abundant particle, and is encountered at median energies of approximately 600 MeV/n (George et al., 2009). Similarly, solar particle events deliver almost exclusively ^1H and ^4He , but unlike the constant GCR fluence, SPE exposures are dependent upon the 11-year solar cycle, and greatly vary in energies (NCRP, 2006). In addition, the increased heliospheric magnetic fields observed during solar maximum act to “shield” incoming GCR-effectively reducing their fluence, by approximately one order of magnitude (Nelson, 2016). Because of these phenomena, predicting the exact dosage encountered on a mission to mars is not tangible. The dose estimates defined by the current Mars design reference architecture are between 0.25 and 0.5 Gy for GCR, with an additional 0.15–0.5 Gy for shielded exposures to SPE (Drake et al., 2010). Protons deliver approximately 50–60%, neutrons 10–20%, and HZE particles 10–20% of the relative total organ dose (Gy) from GCR (Nelson et al., 2016).

There is currently no feasible shielding capable of mitigating all high-energy charged particles. In addition, traditional aluminum shields may increase total body dosage due to particle fragmentation and back-scatter within the spacecraft (Cucinotta et al., 2012). The stochastic nature of particle interactions also adds uncertainty to dosage predictions. The central nervous system (CNS) may be particularly vulnerable to charged-particle radiation due to the discriminate regions in which neurogenesis occurs and the permanence of the G_0 phase in mature neurons. Recent *in silico* studies suggest that the dendrites of hippocampal neurons are particularly likely to undergo primary ionization events in response to charged-particle radiation, and have found that dendrites are 10-times more likely to be penetrated by charged-particles than the soma (Nelson et al., 2016). The added range in which incident δ -rays are capable of reaching-up to 1 cm-further exacerbates the likelihood of ionization events within dendrites (Alp and Cucinotta, 2018). NASA's concern for radiation-induced CNS insults include possible in-flight alterations to cognitive and motor function, and late neurological pathologies, including Alzheimer's disease, dementia, and premature aging (Nelson et al., 2016). Additionally, the National Council for Radiation Protection and Measurements recognizes that there may be subclinical CNS symptoms capable of compromising mission success (on Radiation Protection and (NCRP, 2016).

The effects of high-energy ^1H and HZE particles at doses below 1 Gy on hippocampus-dependent cognition have produced a body of literature describing cognitive-behavioral deficits in mice and rats (Kiffer et al., 2019b). High-energy ^1H exposures

have likewise been overwhelmingly known to induce deficits in hippocampus-dependent rodent behavior at low doses (Kiffer et al., 2019b). Recent particle accelerator advancements at NASA's Space Radiation Laboratory have allowed for multiple particle exposures, subsequently improving space radiation simulations. At this time few CNS studies have subjected animals to multiple space-relevant particle exposures (Raber et al., 2016, 2019; Kiffer et al., 2018; Krukowski et al., 2018). The study by Krukowski et al. (2018) observed that exposures of 0.1 or 0.5 Gy of $^1\text{H} + ^4\text{He} + ^{16}\text{O}$ resulted in dose- and sex-dependent deficits in hippocampus-dependent Novel Object Recognition (NOR), sociability, social memory, and anxiety. However, the recent study by Raber and colleagues reveals 0.5 or 2 Gy of $^1\text{H} + ^{16}\text{O} + ^{28}\text{Si}$ resulted in NOR deficits in male and female B6D2F1 mice (Raber et al., 2019). We have previously shown that a 0.6 Gy exposure to $^1\text{H} + ^{16}\text{O}$ within the same day induced short-term spatial memory deficits, as assessed by the Y-maze 3 months after exposure, and altered dendritic morphology in the hippocampus of male C57Bl/6J mice (Kiffer et al., 2018). The present study explores the effects on hippocampus-dependent behaviors 9 months after a 0.6 Gy exposure to $^1\text{H} + ^{16}\text{O}$.

MATERIALS AND METHODS

Animals and Irradiation

Male C57Bl/6J mice were acquired from Jackson Laboratories (Bar Harbor, ME, United States) and housed five per cage. Animals received water and standard low-soy rodent chow (2020X; Harlan® Laboratories Inc; Indianapolis, IN, United States) *ad libitum* and were housed on a 12:12 h light-dark schedule for the duration of the study. Mice were transported to Brookhaven National Laboratory, Upton, NY, by overnight airlift at 6-months of age. After 1-week of acclimation, mice received whole-body irradiation at the NASA Space Radiation Laboratory. During irradiation, mice were placed in individual well-ventilated Lucite holders, five at a time, and holders were mounted perpendicular to the beam direction. Animals first received 0.5 Gy of ^1H (150 MeV/n; 18–19 cGy/minute) and were placed back in their cages. Approximately 1 h later, mice were placed back in the Lucite holder and onto the beam line and exposed to 0.1 Gy ^{16}O (600 MeV/n; 18–33 cGy/minute). Dosimetry and beam properties were controlled by NASA Space Radiation Laboratory physicists. Sham-irradiated animals were placed on the beam line but did not receive charged-particle radiation. After irradiation, animals were transported back to the University of Arkansas for Medical Sciences (UAMS) by overnight airlift and given 2020X chow containing 150 ppm fenbendazole for 8 weeks, as a routine UAMS quarantine procedure. Mice remained housed five per cage with Enrich-o'Cob® (The Andersons, Inc) bedding. All animal procedures were approved by the Institutional Animal Care and Use Committees of UAMS and Brookhaven National Laboratory.

Y-Maze

Animal behavior was tested 9 months after irradiation ($n = 10$ per treatment). Mice were first tested via the Y-maze, which

relies on the animals' endogenous drive for exploring spatial novelty, not on negative or positive reinforcement (Dellu et al., 1992). The Y-maze is constructed out of opaque acrylic and consists of three similar arms (45 cm \times 15 cm \times 30 cm): start, familiar, and novel. The familiar and novel arms contain an object of different size and shape mounted at the end of the arm, with no other obvious environmental cues (other than the ceiling mounted camera). Animals are placed in the start arm facing away from the center of the maze, and the familiarization session consists of free exploration of the start and familiar arms. For the testing session, animals were again placed in the maze 3 h after the familiarization session, but this time with access to all arms. Allocation of arms (start, familiar, novel) was counterbalanced between and within each experimental group. Trials lasted for 5 min, and center and nose-points were recorded throughout each session. All experimental arenas were wiped clean with 20% EtOH solution after each trial. Behavioral experiments were recorded on a charge-coupled video camera, located above the maze for automatic behavioral analysis with EthoVision software version 11 (Noldus Information Technology).

Novel Object Recognition

NOR testing relies on animals' endogenous propensity for exploring novelty in their environment; unimpaired animals will spend significantly more time exploring the novel object. After the Y-maze testing, animals were tested for NOR, a 4-day procedure in which animals freely explore an arena for 10 min each day. The first 2 days serve as habituation days, in which mice are able to explore an empty arena, effectively serving as an open field test; locomotor activity is measured at this stage. Familiarization occurs on day three, when animals explore an arena containing two identical objects (cell-culture flasks filled with sand). Novel object recognition testing occurs on day four, when one of the now familiar objects is replaced by a novel object (large LEGO® blocks assembled to a similar size as the cell-culture flasks) (Leger et al., 2013). The arena is a 40 cm \times 40 cm \times 40 cm cube consisting of an aluminum floor, non-transparent acrylic walls, and an open ceiling. Animals were placed in the center of the arena parallel to the objects to ensure no bias. The tracking software was programmed to track animal-center points for the habituation trials and the animal-nose points during familiarization and testing trials.

Golgi Staining

Shortly after behavioral testing, animals were anesthetized with isoflurane, exsanguinated via the inferior vena cava, and their brains were extracted and dissected along the midsagittal plane. Golgi staining is a widely accepted and reliable method for assessing dendrite and dendritic spine dynamics in response to various treatments due to the low percentage of random neuron impregnation, which allows for low background noise, and resistance to fading or photobleaching over time (Mikolaenko et al., 2005; Giddabasappa et al., 2011). We adapted a staining protocol and used the reagents contained in the superGolgi kit (Bioenno Tech), as previously described (Groves et al.,

2017). All morphological and molecular experiments were performed in animals that underwent behavioral testing. A total of five brains from each treatment group, and the right hemispheres were stained.

Dendritic Morphology Quantification and Spine Analyses

We analyzed dendritic spines of coded, Golgi-impregnated dorsal and ventral hippocampus sections. Molecular layer dendrites from dorsal Dentate granular neurons were traced. We also examined dendrites in the apical (*stratum radiatum*) and basal (*stratum oriens*) divisions of pyramidal neurons of the dorsal CA1, and ventral CA3 subregions. Neurons meeting the following criteria were suitable for analyses: (1) presence of well-defined, non-truncated dendrites respective to the coronal plane, (2) consistently dark Golgi staining along the entire extent of the dendrite, and (3) relative isolation from neighboring neurons to avoid interference with analysis. Five dendritic segments (each at least 20 μm long) per granular, or pyramidal neuron were analyzed, and six to seven neurons were analyzed per brain (Titus et al., 2007; Magariños et al., 2011). Neurons that met staining criteria were traced using a 60 X objective, (100 X oil objective for spine analyses), a computerized oscillating stage for 3-dimensional imaging, and Neurolucida software (Ver. 11, Microbrightfield, Inc., Williston, VT, United States).

We quantified the morphology of the granular and pyramidal neurons contained in the hippocampal formation by Sholl analysis, total dendritic length, number of branch points, and dendritic complexity index (DCI) with the NeuroExplorer component of the Neurolucida program. Sholl analysis is used to assess the amount and distribution of the arbor at increasing radial distances from the cell body (Sholl, 1953). Radii were set to extend in 10 μm intervals from the soma. The length of each dendritic branch, within each progressively larger circle, was counted from the soma, with respect to three dimensions.

Next, we performed branch-point analyses, a method of quantifying the number of bifurcations and the order in which they occur (Morley and Mervis, 2013). Lower branch-point orders represent proximal regions of the arbor, whereas higher branch-point orders characterize distal regions. We used branch-point analysis to determine the complexity of dendritic arborization, because the complexity of the dendritic tree is an important phenotypic component of branching analysis and provides insight into circuit modulation. The DCI was determined by the following equation:

$$\text{DCI} = \sum \left((\text{branch tip orders} + \text{branch tips}) \times \left(\frac{\text{total dendritic length}}{\text{primary dendrites}} \right) \right)$$

In the *cornu ammonis* (CA) 1 and CA3 subregions of the hippocampus, apical and basal dendrites were analyzed separately. We traced five randomly stained neurons per subregion per animal. Morphological experiments were conducted blinded to treatment groups.

DNA Extraction and Quality Control

At the time of sacrifice, left brain hemispheres were dissected, and the hippocampi were promptly collected and fresh frozen in liquid nitrogen prior to storage in -80°C . gDNA was extracted with the All-Prep extraction kit by MIDSCI® in accordance to the manufacturer's protocol. Nucleic acid purity and concentration were determined by Nanodrop 2000™ spectrophotometry and Qubit™ fluorometry (Thermo Fisher Scientific™).

DNA Sequencing and Single-Nucleotide Polymorphism (SNP) Analyses

gDNA for all samples ($n = 10$) was normalized to 10 ng/μL and prepared for sequencing according to the Truseq custom amplicon low input library preparation protocol (Illumina® document 1000000002191 v04). Library qualities were assessed via Advanced Analytical™ fragment analyses (Agilent®). Pooled libraries were prepared for next-generation targeted sequencing in accordance to the manufacturer's protocol (Illumina® MiniSeq Denature and Dilute Guide, document 1000000002697 v00). PhiX v3 (Illumina®) was used as an assay control. Overall run quality and individual reads were evaluated and filtered based on the manufacturer's criteria, and *post hoc* quality filters: Variant is on target, loci or site genotypes were not in regions with conflicting indel calls, GQX (genotype quality minimum) and GQ (genotype quality) is greater than 30, Locus QD (quality by depth/variant confidence) is generally greater than two (in low QD instances, mapping quality is first checked and allelic depths are individually considered), and MQ (root mean square of the mapping quality of the call) is above 20.

A proportion of gene targets in our panel involved only coding regions (CDS) whereas a proportion involved full target regions, including untranslated regions (**Supplementary Table 1**). In all cases, known common SNPs in accordance with the NCBI37/mm9 genome assembly, as compiled by MGI dbSNP (build 142), were omitted from analyses. Previously unidentified SNPs, which were identical and present in all or most samples have likewise been omitted from analyses (**Supplementary Table 2**).

Statistical Analyses

We expressed data as a mean \pm the standard error of the mean (SEM). Analysis of behavioral data occurred throughout the length of each test. Discrimination ratios (DR) were calculated as:

$$\text{DR} = \frac{(\text{novel exploration} - \text{familiar exploration})}{(\text{novel exploration} + \text{familiar exploration})}$$

Behavioral assays comparing discrimination ratios or object exploration in individual treatment groups were analyzed via unpaired *t*-tests. We used a one-way analysis of variance (ANOVA) followed by *post hoc* multiple comparisons with Bonferroni corrections to evaluate statistical differences within sham and irradiated groups in measures of time spent in Y-maze arms. Sholl analyses were conducted via two-way ANOVA to test for effects of treatment and distance from the soma, with a *post hoc* multiple comparisons corrected by Fisher least-significant-difference (LSD), when appropriate. A Repeating

Measures ANOVA was used to assess main effects of radiation on habituation learning, with test day being the repeated measure, and a Tukey correction for *post hoc* multiple comparisons. We employed unpaired *t*-tests with Welch's corrections to evaluate differences in dendritic complexity index, spine density, and variant allele frequency between sham and irradiated mice. Statistical analyses for behavioral, morphological and sequencing assays were conducted with GraphPad Prism 8.0 software (La Jolla, CA, United States) and $P < 0.05$ was considered significant.

RESULTS

Behavior

Y-maze performance is contingent upon animals' ability to retain spatial memory encoded in the familiarization phase of the trial and recall it during the testing phase, effectively assaying short-term spatial memory (Dellu et al., 1997). Sham-irradiated animals displayed normal spatial recognition by exploring the novel arm during the testing session for a significantly longer period of time than they did the start and familiar arms [Main effect of arm expl.: $F_{(1.73,15.59)} = 22.56$; $P < 0.0001$; *post hoc* Mult. comp: Novel vs Fam $P < 0.001$; Novel vs Start $P < 0.01$; **Figure 1A**]. There was a significant main effect of treatment on arm exploration within the $^1\text{H} + ^{16}\text{O}$ -irradiated group [$F_{(1.84,16.57)} = 9.82$; $P < 0.01$; **Figure 1B**]. Multiple comparisons analyses reveal that treated animals spent significantly more time exploring the novel than the start arm ($P < 0.01$), but failed to distinguish the novel and familiar arms, by exploring both arms for approximately equal time ($P < 0.01$), indicating a deficit in spatial memory. Discrimination ratios indicate animals' ability to discern two objects presented in a behavioral paradigm, and can be ultimately interpreted as a measure of animals "remembering" or "forgetting" a novel object (Burke et al., 2010). Sham-irradiated animals displayed a positive discrimination ratio ($\mu = 0.33 \pm 0.05$). Irradiated animals also displayed a positive discrimination ratio ($\mu = 0.15 \pm 0.06$); however, the mean was less than half the discrimination displayed by control animals ($t = 2.40$, $P < 0.05$; **Figure 1C**). A measure of total distance moved was taken to ensure no bias in animal exploration due to gross locomotor deficits or other exploration-related issues. We detected no significant changes in mean total distance moved across treatment groups ($t = 0.44$, $P = 0.67$; **Figure 1D**).

The NOR task was used to assess non-spatial declarative object memory (Ran et al., 2016). Rodents naturally orient their head toward a novel stimulus, which provides a simple and effective method for quantifying visual recognition (Honey et al., 1998). In addition, mice rely on tactile exploration of objects in their environment, specifically under dimly-lit conditions (Hu et al., 2018). Therefore, contrasting proximity-dependent exploration of a novel versus a familiar object provides an index of object recognition and discrimination. First, the activity of the mice in the novel enclosure on training days one and two was analyzed. There was no effect of radiation on total distance moved across both habituation days [$F_{(1,17)} = 2.50$; $P = 0.13$]. Additionally, a main effect of habituation day was observed [$F_{(1,17)} = 70.0$; $P < 0.0001$], with both Sham and radiation groups resulting

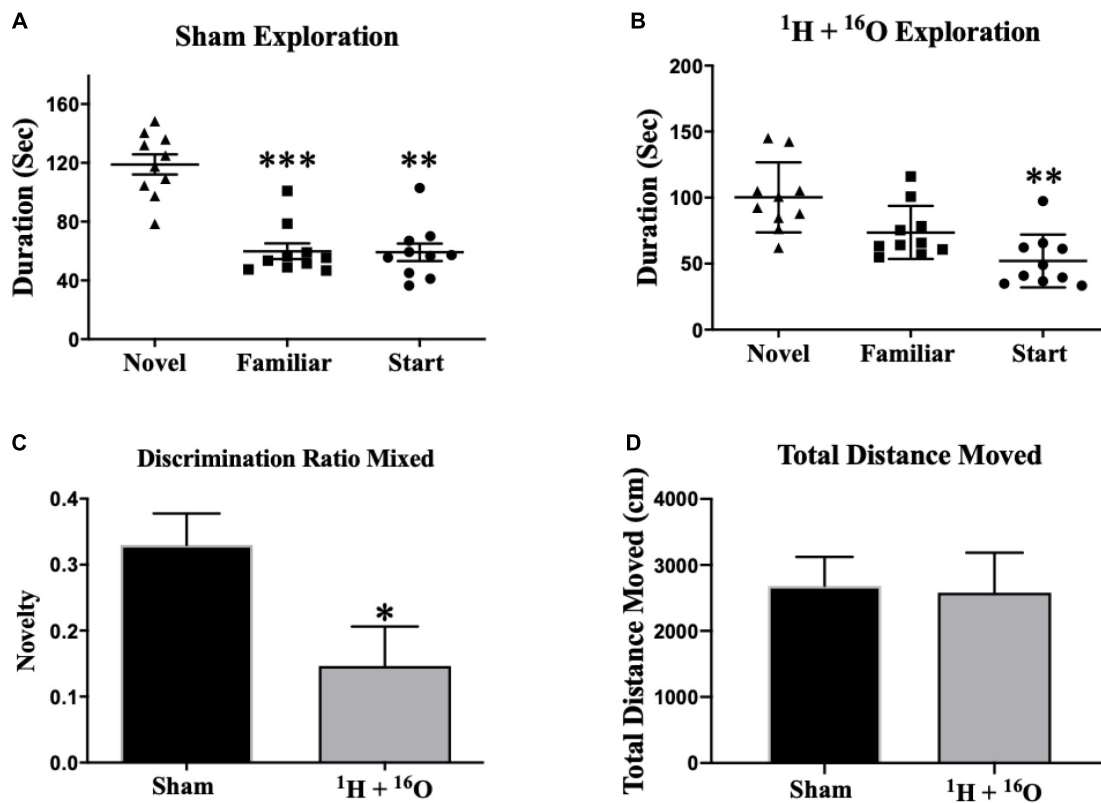


FIGURE 1 | Y-maze. **(A)** Sham-irradiated mice explored the novel arm for a significantly longer duration than the other arms during testing, indicating normal short-term spatial memory. **(B)** Irradiated animals spent more time exploring the novel than the start arm, but they were unsuccessful in exploring the novel arm for a longer duration than the familiar arm, implying spatial memory injury. **(C)** Discrimination ratios for both treatment groups reveal a marked decrease in novel arm discrimination for irradiated animals. **(D)** There was no effect of radiation on gross locomotor activity based on mean total distances moved. Average \pm SEM ($n = 10$); * $P < 0.05$, ** $P < 0.01$, *** $P < 0.001$.

in significantly lower cumulative movement across habituation days (Sham: $P < 0.001$; $^1\text{H} + ^{16}\text{O}$: $P < 0.0001$; **Figure 2D**). These data indicate that mice had neither a reduced exploratory drive nor gross motor symptoms during habituation. We next assessed potential effects of radiation on habituation learning, and we observed no differences between cohorts ($t = 1.84$; $P = 0.08$; **Supplementary Figure 1**). Next, the training session and a test session were conducted. During the training session (day 3), mice were placed in the open-field box with two identical objects. During testing (day 4), mice were subjected to a novel and a familiar object. Movement was tracked throughout the duration of the testing session to ensure no movement-related exploration bias. No difference in mean total distance moved was detected between groups ($t = 1.58$, $P = 0.13$; **Figure 2E**). Statistical analysis of total exploration time during the test session revealed that exposure to $^1\text{H} + ^{16}\text{O}$ significantly impaired mice, as they did not show preference for the novel object ($t = 0.82$, $P = 0.44$; **Figure 2B**). Sham-irradiated mice showed NOR by spending more time exploring the novel than the familiar object ($t = 5.36$, $P < 0.001$; **Figure 2A**). Discrimination ratios showed positive object novelty discrimination in sham-irradiated animals ($\mu = 0.11 \pm 0.02$), whereas irradiated animals produced low-to-negative discrimination ratios within the SEM ($\mu = -0.02 \pm 0.05$),

and the irradiated animals discrimination was significantly lower than sham-irradiated animals ($t = 2.15$, $P < 0.05$; **Figure 2C**).

Dendritic Morphology

Dentate Gyrus Granular Cells

Sholl analyses conducted in Golgi-impregnated neurons revealed differences in dendritic morphology between treatment groups. The granular cell layer of the dentate gyrus includes neurons whose dendrites extend unilaterally out of the soma into the molecular layer (*stratum moleculare*), receiving input from the entorhinal cortex and projecting to the Dentate polymorphic layer and *stratum lucidum* where an unmyelinated axon and its complex collateral plexus comprise mossy fibers that innervate the CA3 (Amaral et al., 2007). Our analysis, which was limited to the molecular layer dendrites, found that irradiation changed the distribution of the dendritic tree as a function of increasing 10 μm radial intervals from the soma. A significant main effect of radiation in dorsal dentate dendrites [$F_{(1,8)} = 16.12$; $P < 0.01$], as well as a significant interaction between radiation and distance from the soma [$F_{(23,184)} = 3.40$; $P < 0.0001$]. Multiple comparisons denote a significantly larger in dendritic length in irradiated animals (Fisher's LSD: 80–90 μm , 140–160 μm , $P < 0.05$; 100–130 μm , $P < 0.0001$; **Figure 3A**).

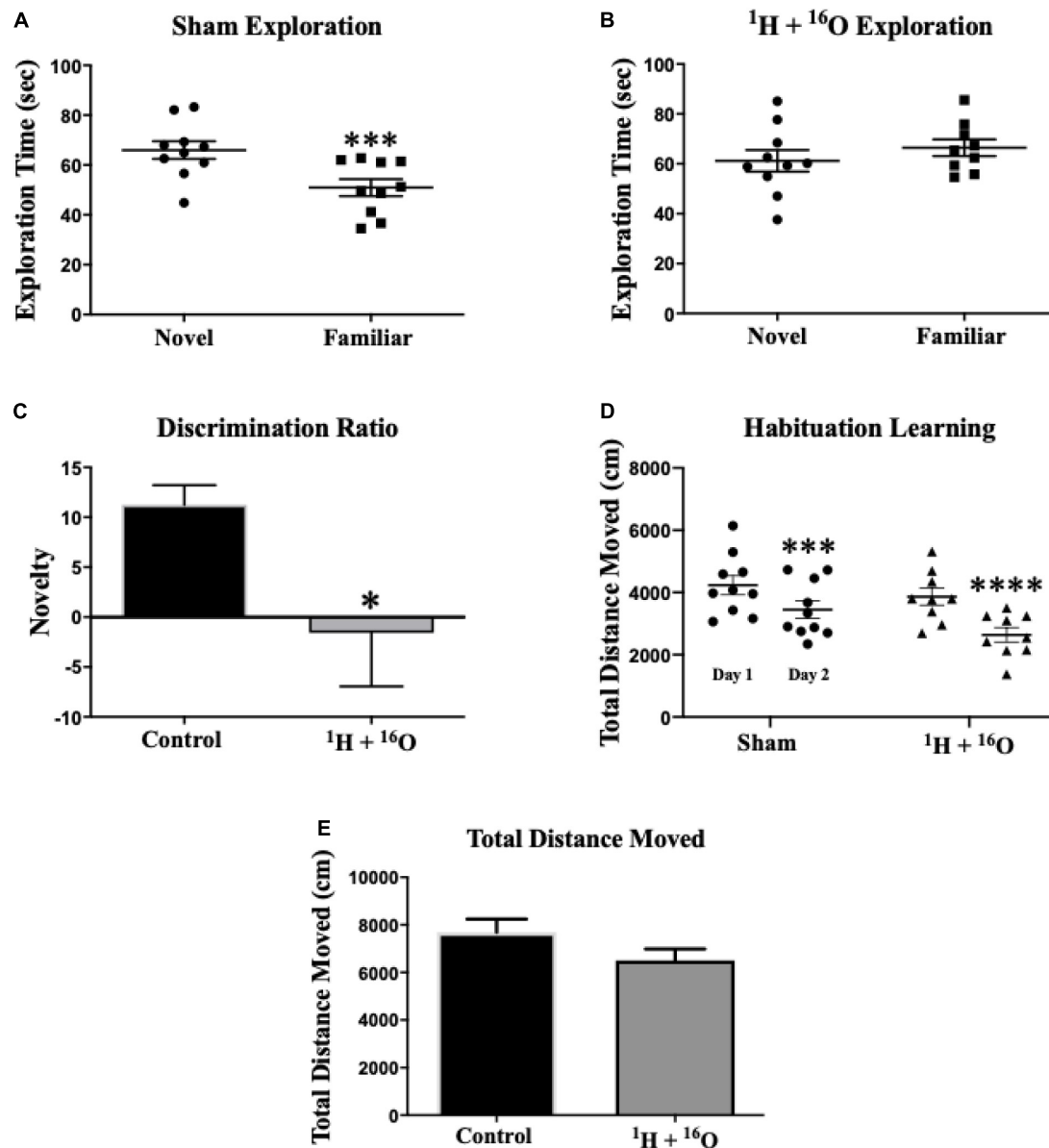


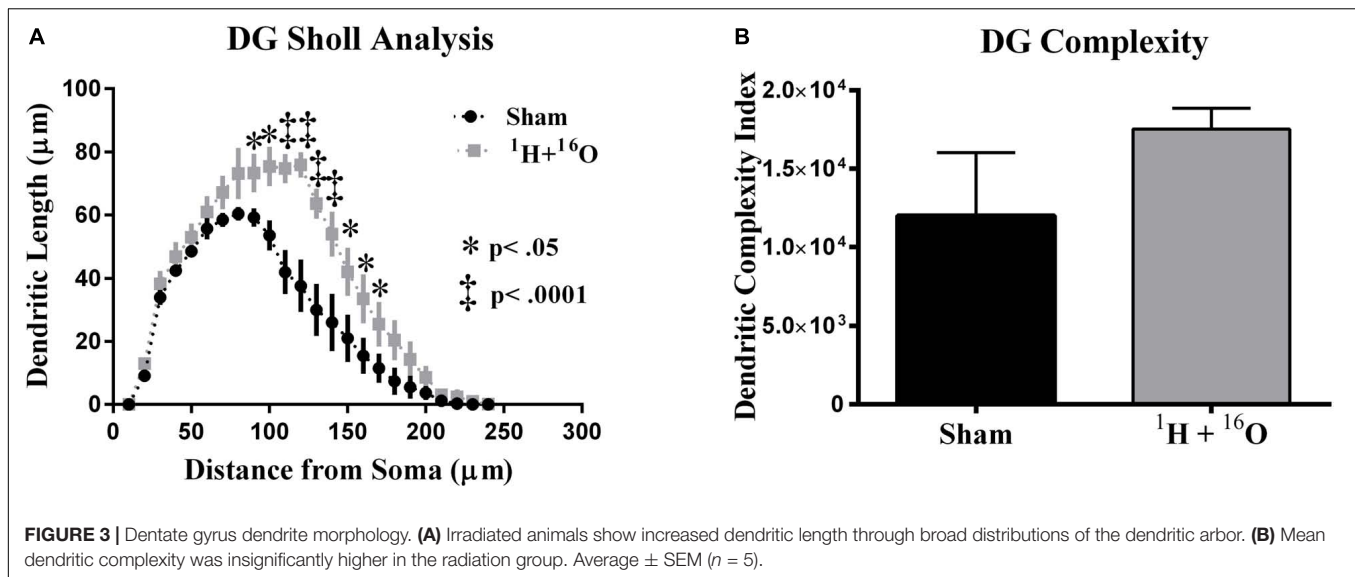
FIGURE 2 | Novel object recognition. **(A)** Sham-irradiated animals spent more time exploring the novel object than the familiar one. **(B)** Radiated animals spent approximately equal time exploring both the novel and familiar objects during testing, indicating an inability to remember the familiar object. **(C)** Animals who received radiation show profoundly low object discrimination relative to sham-irradiated animals. **(D)** Sham and irradiated mice displayed normal habituation to the empty testing arena, by attenuating cumulative exploration across both habituation days. **(E)** Locomotor activity was similar across radiation groups on testing day. Average \pm SEM ($n = 10$); * $P < 0.05$, *** $P < 0.001$, **** $P < 0.0001$.

To further quantify dendritic morphology, we assayed dendrite complexity (DCI), total bifurcations, dendritic ends, and dendritic length (Lom and Cohen-Cory, 1999; van der Velden et al., 2012). We observed a marked increase in total bifurcations ($t = 2.42$, $P < 0.05$; **Table 1**), dendritic ends ($t = 2.82$, $P < 0.05$; **Table 1**), and total dendritic length ($t = 4.02$, $P < 0.01$; **Table 1**) in irradiated animals. Despite an observed increase in nearly every parameter, we did not observe a significant increase in DCI ($t = 1.30$, $P = 0.25$; **Figure 3B**). However, we note that this was due to a high standard deviation in sham-irradiated animals

($\mu = 12,006$, $\sigma = 9,001$), as compared to irradiated animals ($\mu = 17,528$, $\sigma = 2,970$), and a low n of 5.

CA1 Pyramidal Neurons

Next, we compared dendritic morphology between cohorts in the CA1 subregion. The glutamatergic hippocampal network contains pyramidal neurons in the CA subregions that branch in two distinct arbors on opposite sides of the soma. The apical side branches through the *stratum oriens*, and the basal side through the *stratum radiatum*. A two-way ANOVA detected a



significant main effect of treatment between the irradiated group and sham-irradiated group in both the apical [$F_{(1,8)} = 130.1$; $P < 0.0001$] and basal [$F_{(1,8)} = 139.9$; $P < 0.0001$] divisions. Significant interactions between radiation and distance from the soma were also detected in the apical [$F_{(27,216)} = 8.15$; $P < 0.0001$] and basal [$F_{(20,160)} = 34.91$; $P < 0.0001$] CA1. *Post hoc* multiple comparisons reveal significant reductions in dendritic length far from the soma in the apical (Fisher's LSD: 40, 90–200 μm , $P < 0.05$; 50–80 μm , $P < 0.0001$; **Figure 4A**) and basal (Fisher's LSD: 40, 140 μm , $P < 0.05$; 50–130 μm , $P < 0.0001$; **Figure 4B**) subdivisions.

Further dendrite analysis showed a reduction in total bifurcations ($t = 4.81$, $P < 0.01$; **Table 2**), dendritic ends ($t = 4.64$, $P < 0.01$; **Table 2**), and dendritic length ($t = 11.21$, $P < 0.0001$; **Table 2**) in the apical division. Following suit, the basal division also showed marked reductions in bifurcations ($t = 4.93$, $P < 0.01$;

Table 2), ends ($t = 4.95$, $P < 0.01$; **Table 2**), and length ($t = 12.85$, $P < 0.0001$; **Table 2**). CA1 dendritic complexity was significantly lower in both the apical ($t = 7.21$, $P < 0.0001$; **Figure 4C**) and basal ($t = 3.24$, $P < 0.05$; **Figure 4D**) regions.

CA3 Pyramidal Neurons

Our final morphological analysis was conducted in the CA3. The CA3 relays information from the DG and onto several other hippocampal subregions, the most abundant of which is the CA1, via Schaffer collateral fibers. We detected a significant interaction between radiation and distance from the soma on apical [$F_{(23,184)} = 2.48$; $P < 0.001$; **Figure 5A**], but not on basal dendrites [$F_{(22,176)} = 0.65$; $P = 0.886$; **Figure 5B**]. *Post hoc* multiple comparisons on the apical CA3 reveal only a slight decrease at 70 μm from the soma (Fisher's LSD: $P < 0.01$) but predictably not in the basal CA3 (**Figure 5B**).

In accordance to our CA3 Sholl analyses, we did not observe significant changes in apical dendritic bifurcations ($t = 0.57$, $P = 0.59$; **Table 3**), ends ($t = 0.86$, $P = 0.42$; **Table 3**), and length ($t = 0.58$, $P = 0.58$; **Table 3**) or in basal dendritic bifurcations ($t = 0.81$, $P = 0.44$; **Table 3**), ends ($t = 0.54$, $P = 0.60$; **Table 3**), and length ($t = 0.44$, $P = 0.67$; **Table 3**). As expected, there were no changes in dendritic complexity due to radiation (apical, $t = 0.52$, $P = 0.62$; basal $t = 1.04$, $P = 0.33$; **Figures 5C,D**).

Dendritic Spine Density and Morphology

Golgi-stained sections were also used to examine hippocampal dendritic spines. We observed a minor, but significant decrease in spine density in the dentate gyrus of the irradiated group ($t = 3.53$, $P < 0.01$; **Table 1**). This was accompanied by a slight increase in thin spine density ($t = 2.90$, $P < 0.01$; **Table 1**), and a severe reduction in mushroom spine density ($t = 13.14$, $P < 0.0001$; **Table 1**) in the radiation group. We did not observe differences in stubby spines ($t = 0.96$, $P = 0.35$; **Table 1**).

We did not observe any changes in spine density in the apical ($t = 0.14$, $P = 0.89$; **Table 2**) or basal CA1 ($t = 0.59$, $P = 0.57$;

TABLE 1 | Effects of $^1\text{H} + ^{16}\text{O}$ irradiation on dendrite morphology in the DG.

Cell type and measurement	Sham (mean \pm SEM)	$^1\text{H} + ^{16}\text{O}$ (mean \pm SEM)	P-value
DG			
Thin spines	58.00 \pm 1.15	62.95 \pm 1.23	$P < 0.01$
Stubby spines	28.43 \pm 1.99	30.53 \pm 1.13	$P = 0.35$
Mushroom spines	15.16 \pm 0.60	6.355 \pm 0.36	$P < 0.01$
Overall density	24.28 \pm 0.57	22.18 \pm 0.24	$P < 0.01$
Total dendritic length (μm)	622.6 \pm 62.97	919.3 \pm 38.51	$P < 0.01$
Total # branch points	4.520 \pm 0.59	6.160 \pm 0.34	$P < 0.05$
Dendritic ends	6.160 \pm 0.48	7.840 \pm 0.35	$P < 0.05$
Dendritic complexity	12006 \pm 4025	17528 \pm 1328	$P = 0.25$

Radiation resulted in a marked decrease in spine density of dorsal dentate molecular layer dendrites. The shift in spine density is characterized by a minor increase in thin spine density, and major decrease in mushroom spine density in irradiated mice. Dendritic length, branch points and ends appeared to be higher in irradiated animals, despite no significant changes in dendritic complexity. Average \pm SEM ($n = 5$). Bold and italic values are statistically significant.

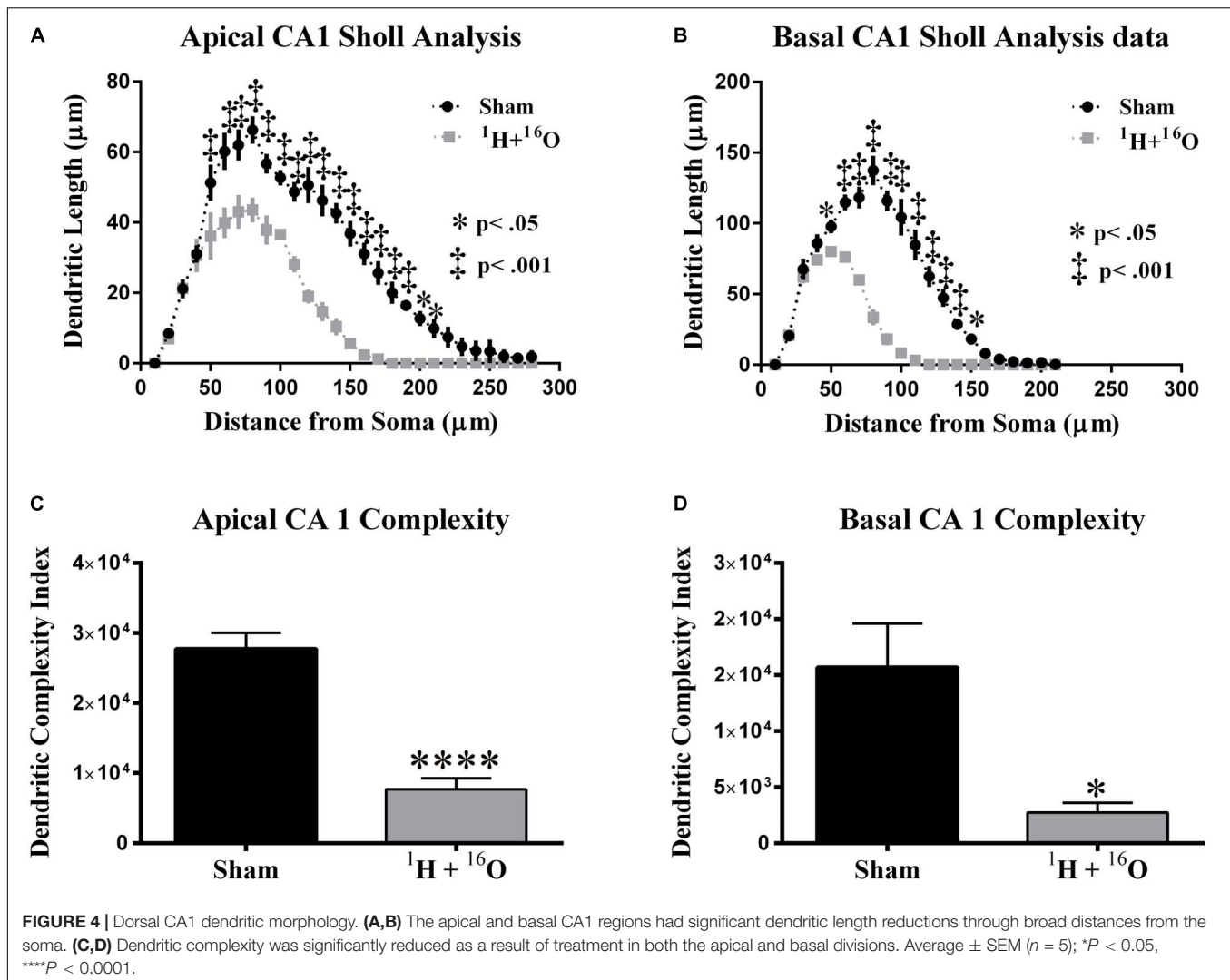


Table 2) subregions. The apical division revealed a slight increase in stubby spines ($t = 2.40$, $P < 0.05$; Table 2), no changes in thin spines ($t = 1.71$, $P = 0.12$; Table 2), and an explicit decrease in mushroom spines ($t = 7.61$, $P < 0.0001$; Table 2) in irradiated mice. However, differences between spines within the basal CA1 were similar to the dentate gyrus. Radiation resulted in a slight increase in thin spine density ($t = 2.94$, $P < 0.05$; Table 2), no changes in stubby spines ($t = 0.48$, $P < 0.64$; Table 2), and a substantial decrease in mushroom spines ($t = 7.59$, $P < 0.0001$; Table 2).

We then examined spine densities within the CA3. The apical region did not reveal changes in overall spine density ($t = 1.59$, $P = 0.15$; Table 3), though the basal region had a minor decrease in spine density in treated animals ($t = 2.50$, $P < 0.05$; Table 3). The apical and basal regions revealed no changes in thin (apical, $t = 0.68$, $P = 0.51$; basal, $t = 1.97$, $P = 0.08$; Table 3) or stubby (apical, $t = 1.66$, $P = 0.13$; basal, $t = 0.59$, $P < 0.57$; Table 3) spines. However, we again observed a sweeping decrease in mushroom spines of treated mice in the apical ($t = 6.92$, $P < 0.0001$; Table 3) and basal ($t = 6.45$, $P < 0.0001$; Table 3) regions of the

CA3, a constant change we observed throughout the regions of the hippocampus.

SNP Analysis of Hippocampal Lysates

Charged-particle radiation induces dense cores of ionization events in normal tissues, with a high mutagenic potential. We therefore expected a high number of SNPs in the DNA of homogeneous cell populations in the hippocampus even at a late time point from irradiation. We identified surprisingly few significant SNPs in immediate early genes, genes associated with oxidative stress elements, and genes involved in inflammation processes. Overall, we detected a significant difference in variant allele frequency between sham and irradiated samples in only 2 of 38 gene targets (Figure 6). The locus for thioredoxin reductase 2 was found to contain significantly higher SNPs in irradiated samples ($t = 2.99$, $P < 0.05$; Supplementary Table 2) with a mean VAF ranging from 7.9 to 9.3% in irradiated samples, and no SNPs detected in the sham group. Similarly, thioredoxin reductase 3 was also found to have a higher SNP rate, with 11.8–13.3% variant alleles ($t = 2.53$, $P < 0.05$; Supplementary Table 2). SNPs

TABLE 2 | Effects of $^1\text{H} + ^{16}\text{O}$ irradiation on dendrite morphology in the CA1.

Cell type and measurement	Sham (mean \pm SEM)	$^1\text{H} + ^{16}\text{O}$ (mean \pm SEM)	P-value
CA1 apical			
Thin spines	53.85 \pm 3.10	59.41 \pm 1.50	$P = 0.12$
Stubby spines	28.69 \pm 1.90	34.37 \pm 1.48	$P < 0.05$
Mushroom spines	17.47 \pm 1.52	6.218 \pm 0.50	$P < 0.0001$
Overall density	22.54 \pm 0.82	22.42 \pm 0.35	$P = 0.89$
Total dendritic length (μm)	774.8 \pm 17.23	375.6 \pm 31.17	$P < 0.0001$
Total # branch points	6.440 \pm 0.31	4.000 \pm 0.40	$P < 0.01$
Dendritic ends	7.440 \pm 0.31	5.040 \pm 0.41	$P < 0.01$
Dendritic complexity	27722 \pm 2289	7678 \pm 1575	$P < 0.0001$
CA1 basal			
Thin spines	54.99 \pm 1.54	62.60 \pm 2.08	$P < 0.05$
Stubby spines	30.03 \pm 0.66	30.91 \pm 1.70	$P = 0.64$
Mushroom spines	14.98 \pm 0.95	6.488 \pm 0.58	$P < 0.0001$
Overall density	21.75 \pm 0.73	22.23 \pm 0.37	$P = 0.57$
Total dendritic length (μm)	1110 \pm 51.67	440.3 \pm 6.835	$P < 0.0001$
Total # branch points	8.560 \pm 1.08	3.080 \pm 0.27	$P < 0.01$
Dendritic ends	11.72 \pm 1.03	6.440 \pm 0.29	$P < 0.01$
Dendritic complexity	15687 \pm 3901	2748 \pm 854.2	$P < 0.05$

The hippocampal CA1 of irradiated mice displayed altered densities of spine composition, but not in overall spine density compared to sham-irradiated animals in both apical and basal divisions. All parameters defining dendritic complexity were markedly lower in irradiated mice throughout dorsal CA1 pyramidal neurons. Average \pm SEM ($n = 5$). Bold and italic values are statistically significant.

generally occurred in unique locations across various genes. In addition, we detected 6 newly identified SNPs, which occurred on every sample that met testing criteria (Supplementary Table 3 and Figure 1). Variant allele frequencies (VAF) ranged from 0 to 56%, a surprising outcome considering the heterogeneous cell population in the whole hippocampus was sequenced, but perhaps explained by the old age of the mice.

DISCUSSION

We investigated the effects of whole-body $^1\text{H} + ^{16}\text{O}$ irradiation on hippocampus-dependent behavior and dendritic morphology of mice 9 months after radiation exposure. Irradiation elicited deficits in short-term spatial and object memory, as assayed by the Y-maze and NOR tests, respectively. We observed pronounced modulation in dendritic morphology in irradiated mice as compared to sham-exposed animals. Furthermore, we observed vast reductions in mushroom spine density throughout the hippocampus.

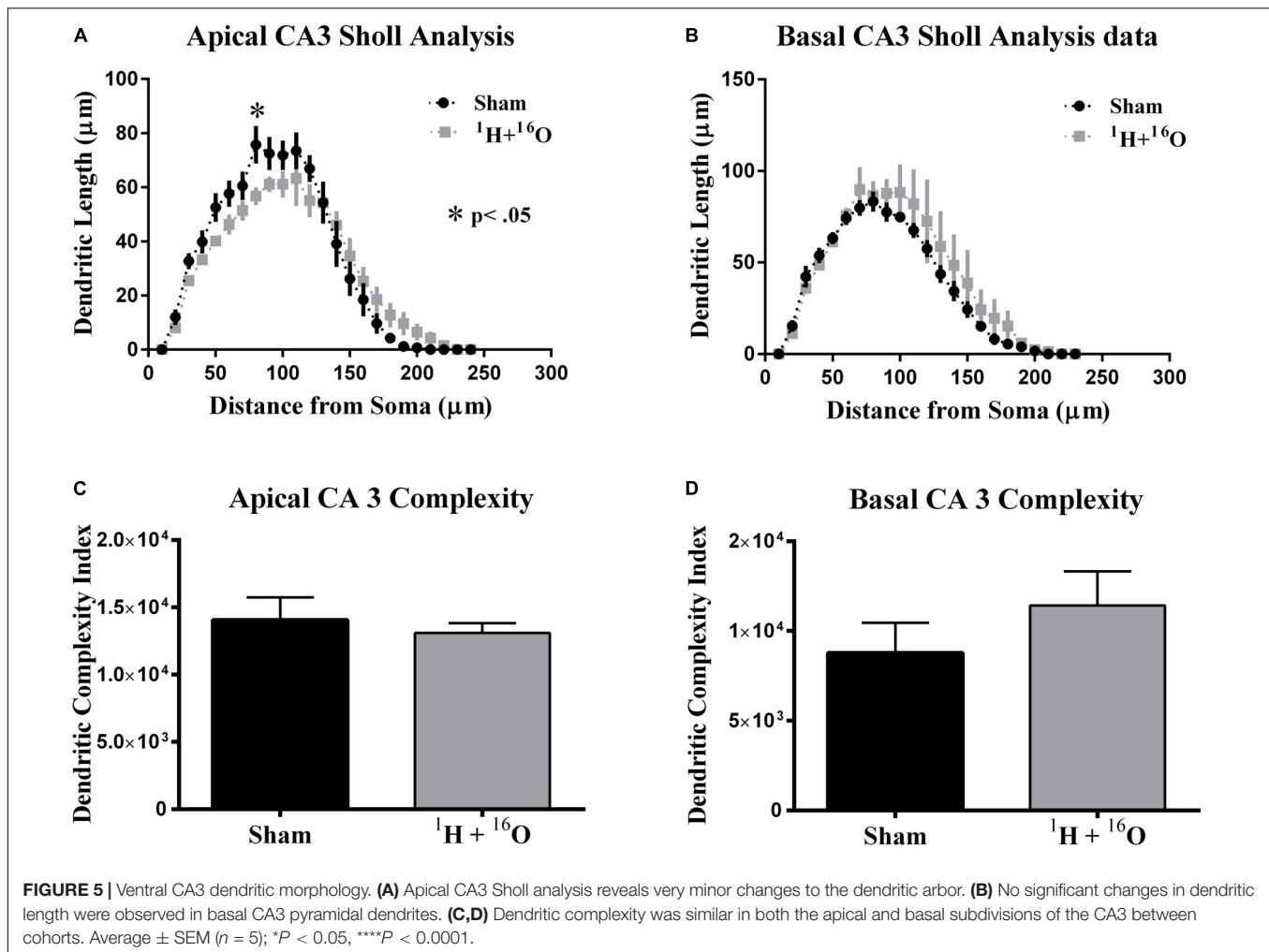
We have previously studied the effects of $^1\text{H} + ^{16}\text{O}$ on the hippocampus of mice at 3 months after exposure (Kiffer et al., 2018). Mice in the present study received exposure at the same time as the aforementioned study, but were housed in a different bedding: Enrich-o'Cob, which contains small cotton nesting material mixed with the bedding. Enrich-o'Cob requires mice to find and retrieve the nesting material that is interspersed with the bedding to form a weekly nest as cages are changed, effectively cognitively enriching mice. In our previous study, we observed a deficit in short-term spatial memory as assessed by

the Y-maze, similar to the present study; however, the deficit was more pronounced in the 3-month study, where irradiated mice displayed a negative discrimination ratio. The current study shows a lowered, but still positive, discrimination ratio in treated animals. Long-term housing under environmental enrichment has shown to improve cognition in rodents, and specifically, in those tested with the Y-maze (Chen et al., 2010; Hughes and Otto, 2013; Xing et al., 2016; He et al., 2017; Park et al., 2017). It is unclear whether these differences are due to time from irradiation or environmental enrichment.

Previous studies investigating the effects of whole-body exposure to ^{16}O on hippocampus-dependent behavior have shown deficits in NOR. Mice exposed ^{16}O showed reduced novel object exploration when tested 2–8 weeks (0.01, 0.5 Gy), and 9 months (0.05, 0.1, 0.25 Gy) postexposure (Rabin et al., 2014, 2015; Howe et al., 2019; Kiffer et al., 2019a). Six month-old transgenic Thy1-EGFP mice that received 0.3 Gy of ^{16}O showed a reduced discrimination index 6 weeks after irradiation (Parihar et al., 2015). ^1H -irradiation has also shown to induce cognitive-behavioral deficits in NOR. High-energy protons delivered to 2-month-old mice resulted in an inability to distinguish familiar and novel objects during NOR testing 3 months (0.1 Gy) after irradiation (Raber et al., 2016). Exposure to ^1H (60%) + ^4He (20%) + ^{16}O (20%) (totaling 0.15 or 0.5 Gy) resulted in NOR deficits in male mice (Krukowski et al., 2018). We currently show a drastically reduced discrimination ratio in irradiated animals who underwent NOR testing 9-months following ^1H (0.5 Gy) + ^{16}O (0.1 Gy) exposure, despite enriched housing.

Hippocampus-dependent spatial learning and object recognition relies on the tri-synaptic circuit of the hippocampus where dentate gyrus neurons receive cortical input via the perforant pathway, relay information unidirectionally through the CA3-CA1 subregions, and transmit processed information back to the entorhinal cortex directly and via the subiculum (Moser et al., 2008; Wojtowicz, 2012; Larkin et al., 2014; Roy et al., 2017). Recent publications suggest hippocampus-dependent episodic memories require rapid synaptic plasticity in engram cells (Rubin et al., 2015; Kitamura et al., 2017). However, CA1-CA3 engrams require high place-and-context specificity and are highly dynamic, whereas DG neurons require low specificity, but are capable of maintaining a spatial code for long durations (Hainmueller and Bartos, 2018). We previously observed a pronounced increase in dendritic length and complexity of dentate gyrus mossy fibers 3 months after $^1\text{H} + ^{16}\text{O}$ exposure. Our current findings show that dendrites in the DG showed increased length in irradiated mice, consistent with our previous observations. The observed increase in dendritic length as a function of distribution of the arbor (90–170 μm from the soma) was nearly identical as our previous study (80–180 μm from the soma), suggesting a highly organized, non-time-dependent response to radiation. We speculate this increase in dendritic length in the DG may be a compensatory response to radiation, given the role the DG plays in encoding spatial information.

The CA1, however, suffered a drastic decrease in dendritic length and complexity, which was consistent with our previous findings, but occurred at a much wider distribution of the arbor



in both the apical and basal regions. Although Golgi staining is functionally indiscriminate of specific neuronal populations due to its random impregnation, we assume the stochastic interactions between charged particles and cells suggests our findings include engram-specific neurons, though future work is needed to vet these assumptions. Interestingly, we did not observe pronounced changes in the dendrites of the pyramidal CA3 neurons, which we analyzed from the ventral region of the hippocampus. There is much debate as to whether the dorsal and ventral divisions of the hippocampus are involved in distinct processes. The dorsal hippocampus has recently been argued to be involved in cognitive information processing, whereas the ventral division is implicated in emotional and stress processing, with functionally distinct gene-expression (Fanselow and Dong, 2010; Lee et al., 2017).

Dendrites must reach respective input and output targets in order to functionally establish a computational circuit (Tavosanis, 2012). The sites where circuitry connections occur are dendritic spines, the bulbous protrusions along a dendritic shaft that host synaptosomes. The morphological characteristics of dendritic spines help dictate the stability of an individual synapse, and thus, the strength of a memory an individual synapse may

be involved in maintaining (von Bohlen and Halbach, 2009). Stubby spines contain a large, bulbous head, but no defined neck. Similarly, a mushroom spine contains a large bulbous head but instead has a pronounced neck, giving its characteristic stability, and association with maintaining memories (Matsuzaki et al., 2004). Inversely, thin spines contain a thin neck, and very small bulbous, head. Thin spines are capable of maturing into mushroom spines, or disappearing altogether, and due to this plasticity, they are associated with learning (Mancuso et al., 2013). We observed pronounced reductions in mushroom spine density in all hippocampal subregions, which together with dendritic modulation, suggest radiation-induced hippocampal modulation that may be un conducive to memory processes. Notably, even subtle adjustments in morphological parameters such as branch points within pyramidal neurons, result in profound changes in firing characteristics (Ferrante et al., 2013), and individual dendrites in these neurons are arguably considered independent computational units within the broader hippocampal network (Losonczy et al., 2008).

The mutagenic potential of charged-particle radiation has been extensively studied in cell cultures and *in vivo*, though relatively little attention has been devoted to studying mutagenic

TABLE 3 | Effects of $^1\text{H} + ^{16}\text{O}$ irradiation on dendrite morphology in the CA3.

Cell type and measurement	Sham (mean \pm SEM)	$^1\text{H} + ^{16}\text{O}$ (mean \pm SEM)	P-value
CA3 apical			
Thin spines	56.46 \pm 2.76	58.34 \pm 1.05	<i>P</i> = 0.51
Stubby spines	31.36 \pm 2.23	34.99 \pm 0.78	<i>P</i> = 0.13
Mushroom spines	12.23 \pm 0.71	6.673 \pm 0.44	<i>P</i> < 0.0001
Overall density	22.92 \pm 0.84	21.36 \pm 0.57	<i>P</i> = 0.15
Total dendritic length (μm)	753.6 \pm 59.95	708.4 \pm 49.30	<i>P</i> = 0.5764
Total # branch points	5.467 \pm 0.49	5.160 \pm 0.22	<i>P</i> = 0.5855
Dendritic ends	7.160 \pm 0.58	6.600 \pm 0.30	<i>P</i> = 0.4157
Dendritic complexity	14051 \pm 1694	13090 \pm 735.4	<i>P</i> = 0.6171
CA3 basal			
Thin spines	57.23 \pm 2.02	62.88 \pm 2.01	<i>P</i> = 0.08
Stubby spines	31.49 \pm 1.90	29.85 \pm 2.00	<i>P</i> = 0.57
Mushroom spines	11.40 \pm 0.47	7.267 \pm 0.44	<i>P</i> < 0.0001
Overall density	22.90 \pm 0.23	21.17 \pm 0.60	<i>P</i> < 0.05
Total dendritic length (μm)	818.8 \pm 24.64	858.8 \pm 86.74	<i>P</i> = 0.6689
Total # branch points	5.187 \pm 0.47	5.760 \pm 0.53	<i>P</i> = 0.4423
Dendritic ends	7.773 \pm 0.48	8.200 \pm 0.62	<i>P</i> = 0.6021
Dendritic complexity	8785 \pm 1671	11422 \pm 1894	<i>P</i> = 0.3271

Mushroom spine density was lower throughout the pyramidal CA3 neurons of irradiated mice, with lowered overall spine density in the basal CA3. No significant differences were observed in overall dendrite length, branchpoint, ends and complexity between irradiated and control mice. Average \pm SEM (*n* = 5). Bold and italic values are statistically significant.

effects on brain tissues (Gauny et al., 2001; Wiese et al., 2001; Yatagai, 2004; Bielefeldt-Ohmann et al., 2012; Sridharan et al., 2015). Previous *in vivo* work demonstrated that low doses of ^{56}Fe particles are capable of eliciting genome-wide SNPs, which played an important role in the loss of heterozygosity in explanted kidney epithelial cells (Turker et al., 2017). Protons have likewise been observed to induce loss of heterozygosity in explanted kidney epithelial cells at higher dosages (1–5 Gy), but not at a more mission-relevant dose (0.5 Gy) (Kronenberg et al., 2009; Turker et al., 2013, 2017). Whereas the role of charged-particle radiation on epigenetic remodeling of the hippocampus has recently placed attention on the genetic influence of radiation-dependent behavioral changes, no SNP analysis has yet been conducted on hippocampal tissues (Impey et al., 2016, 2017).

High-energy charged-particles are capable of inducing complex clustered DNA lesions that preferentially result in double-strand breaks (Brenner and Ward, 1992; Asaithamby et al., 2008). The dominant repair response to such damage involves non-homologous end-joining, which has been characterized as a relatively low-fidelity repair process, and is exacerbated by the complexity of lesions (Bétermier et al., 2014). Furthermore, the phenomenon of radiation-induced delayed genomic instability raises an increased possibility of mutations at a late time point following irradiation (Limoli et al., 2000). Based on these findings, we expected hippocampal cells that survived irradiation would carry a substantial mutational load despite the relatively low dose. Our results, which focused on mutations as compared to a relatively narrow gene array found that the few identified SNPs were not radiation dependent,

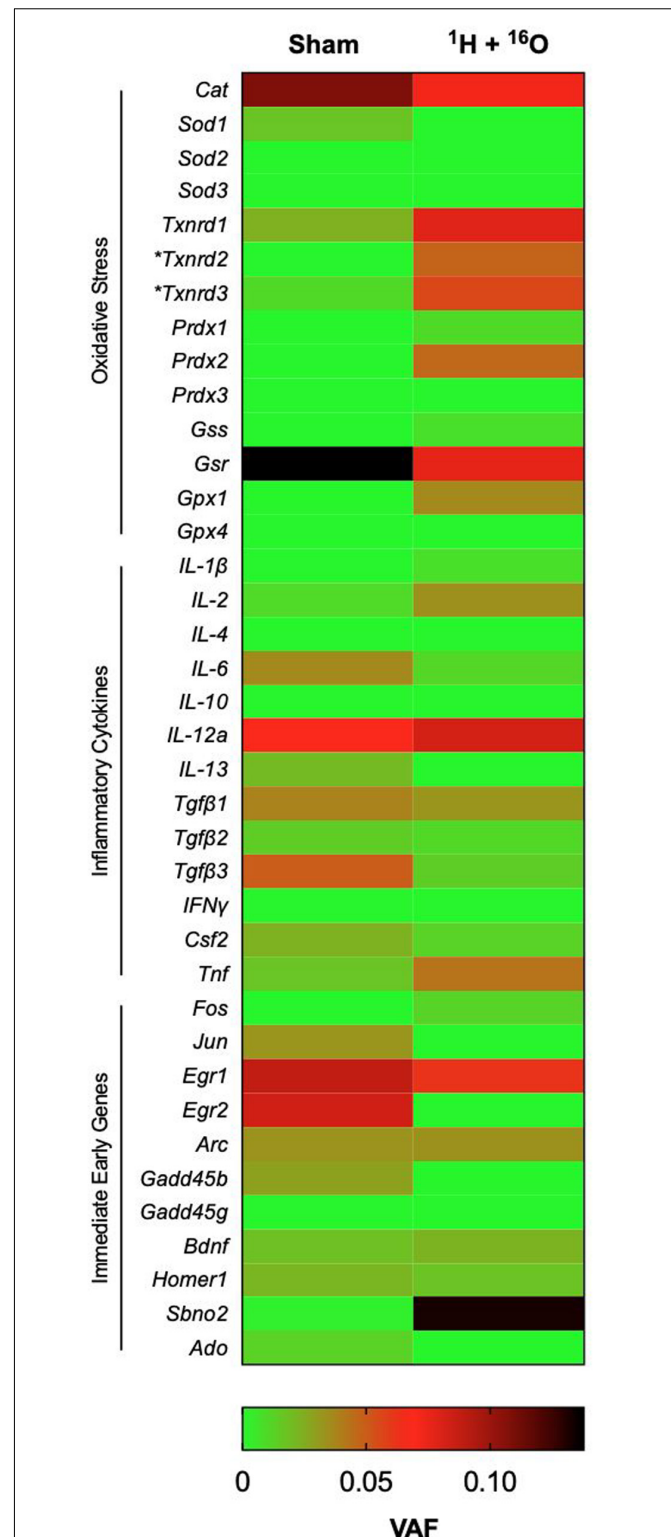


FIGURE 6 | Effects of $^1\text{H} + ^{16}\text{O}$ on SNPs in homogenous cell populations in the hippocampus. There were no significant effects of radiation on select genes for inflammatory cytokines, oxidative stress, and immediate early genes in the whole hippocampus. The only significant radiation-dependent increase in variant allele frequency occurred on oxidative stress elements Txnrd2 and Txnrd3 loci. Mean VAF (*n* = 10); **P* < 0.05.

and are commensurate to mutagenesis associated with aging (Enge et al., 2017). We only detected a significant change in SNPs between Sham and irradiated mice on the loci for mitochondrial ROS scavengers Thioredoxin 2 and Thioredoxin 3. Interestingly, Thioredoxin 2 is a major component of the mitochondrial apoptosis-signaling pathway and glutaredoxin system, and has been found to have an increased presence in the hippocampus of aged dogs, but is lowered in the CA1 region of aged Gerbils (Tanaka, 2002; Ahn et al., 2011; Lee et al., 2015). Conversely, little has been reported of Thioredoxin 3, which appears to have low expression in the mouse brain (Sun et al., 1999). Our findings support a line of evidence suggesting that charged-particle radiation elicits aging-like pathologies, which may be dependent on oxidative stress dysregulation (Joseph et al., 1993, 1999; Casadesus et al., 2005; Poulouse et al., 2011; Suman et al., 2013).

Charged-particle-induced DNA damage has been shown to occur preferentially on euchromatic regions, which is highly cell phenotype-dependent (Costes et al., 2007). In addition, the hippocampus consists of a variety of cell types, ranging from mature neurons, which are arrested at G_0 , to highly proliferating stem cell and stem cell-derived populations. To clearly establish the role of charged-particle radiation on possible polymorphisms in hippocampal tissues, future studies should include genome-wide sequencing experiments from homogeneous cell populations isolated from the irradiated hippocampus.

There is much to be learned as to how strategies currently used by astronauts, as well as other potential future countermeasures may be protective against spaceflight-related insults to the central nervous system. Physical exercise, for example appears to enhance hippocampus-dependent cognitive processes in rodents and humans (Chieffi et al., 2017). Previous rodent studies have demonstrated that antioxidant-rich diets are protective of hippocampus-dependent cognitive deficits following charged-particle exposure (Rabin et al., 2005a,b; Shukitt-Hale et al., 2013; Villasana et al., 2013; Poulouse et al., 2014, 2017). There is also a question as to whether cognitive enrichment can attenuate radiation-induced cognitive deficits. One study assessed whether rats that underwent the familiarization phase of NOR 2–4 h prior to exposure to either 25cGy of ^{56}Fe or 5 cGy of ^{16}O , and then were tested 24 h later, would have better recognition of the novel object, than rats that underwent familiarization 24 h and testing 48 h after radiation. In both cases, acute object recognition deficits occurred only in the group that underwent familiarization prior to irradiation (Rabin et al., 2015). However, a recent study involving an appetitive behavioral platform that depends on 1 month of near daily touchscreen training found that mice receiving 3 6.7 Gy fractions of ^{56}Fe improved hippocampus-dependent pattern separation on a number of tasks. This was also true of non-trained mice undergoing contextual fear conditioning 2 months following exposure to either ^{56}Fe or ^{28}Si , though it is not known if improvements in performance of such tasks is pathological behavior (Whoolery et al., 2020). Although our experiment, which to our knowledge is the first to test whether housing enrichment prior to, and after radiation would prevent hippocampal sequelae, suggests enrichment on its own was not sufficient to fully rescue radiation-induced

deficits. It is important to assess whether multiple factors such as diet, exercise and enrichment can together, prevent radiation-dependent alterations.

Mounting evidence highlights cognitive hazards associated with spaceflight. We show that a Mars-mission-relevant exposure to ^1H followed by ^{16}O an hour later results in object and short-term spatial memory deficits 9 months after exposure. Hippocampus-wide neuronal morphology alterations were observed in combination with drastic reductions in mushroom spine density. Surprisingly, radiation did not elicit noticeable widespread SNPs across select gene targets in the hippocampus when compared to sham-irradiated samples, with the exception of a higher VAF on loci for thioredoxin reductase 2 and 3 in irradiated samples. Future studies should elucidate mechanisms of dendrite dysmorphia in individual hippocampal subregions and address whether changes in dose-rate induce the same effects as single exposures. Future studies should also elucidate mutation rates on distinct cell populations in the hippocampus.

DATA AVAILABILITY STATEMENT

The datasets presented in this study can be found in online repositories. The names of the repository/repositories and accession number(s) can be found below: <https://www.ebi.ac.uk/ena/data/view/PRJEB38379>.

ETHICS STATEMENT

The animal study was reviewed and approved by University of Arkansas for Medical Sciences Animal Welfare Assurance number A3063-01.

AUTHOR CONTRIBUTIONS

AA and MBo: conceptualization, resources, and funding acquisition. FK: behavioral testing, DNA sequencing, and writing—original draft preparation. FK and TM: DNA isolation. TA, JA, and TG: software monitoring for behavioral testing. FK, TA, JA, and TG: Golgi staining. FK and AA: statistical analyses. JW: histological analyses. VS: animal husbandry and management. FK, TA, JA, TG, and VS: animal sacrifice and tissue collection. MBa and FK: DNA sequencing data curation. All authors contributed to the article and approved the submitted version.

FUNDING

This work was supported by the National Space Biomedical Research Institute (NSBRI) Grant RE03701 through NASA cooperative agreement NCC 9-58, and by the Translational Research Institute through NASA cooperative agreement NNX16AO69A. This work was also supported by core facilities of the Center for Translational Neuroscience IDeA program award P30 GM110702 and by the Center for Translational Pediatric Research Genomics Core supported by P20 GM121293.

The funders had no role in study design, data collection and analysis, decision to publish, or manuscript preparation.

ACKNOWLEDGMENTS

We thank Ms. DeAnn Hubberd and the UAMS Science Communication Group for grammatical editing the manuscript, Ms. Jill Castoe and Illumina for DNA sequencing support and

troubleshooting, and finally Dr. Stewart MacLeod, and his team for help with DNA fragmentation analyses.

SUPPLEMENTARY MATERIAL

The Supplementary Material for this article can be found online at: <https://www.frontiersin.org/articles/10.3389/fnbeh.2020.00096/full#supplementary-material>

REFERENCES

- Ahn, J. H., Choi, J. H., Song, J. M., Lee, C. H., Yoo, K.-Y., Hwang, I. K., et al. (2011). Increase in Trx2/Prx3 redox system immunoreactivity in the spinal cord and hippocampus of aged dogs. *Exp. Gerontol.* 46, 946–952. doi: 10.1016/j.exger.2011.08.004
- Alp, M., and Cucinotta, F. A. (2018). Biophysics model of heavy-ion degradation of neuron morphology in mouse hippocampal granular cell layer neurons. *Radiat. Res.* 189, 312–325. doi: 10.1667/rr14923.1
- Amaral, D. G., Scharfman, H. E., and Lavenex, P. (2007). “The dentate gyrus: fundamental neuroanatomical organization (dentate gyrus for dummies),” in *Progress in Brain Research*, ed. H. E. Scharfman (Amsterdam: Elsevier), 3–790. doi: 10.1016/s0079-6123(07)63001-5
- Asaithamby, A., Uematsu, N., Chatterjee, A., Story, M. D., Burma, S., and Chen, D. J. (2008). Repair of HZE-particle-induced DNA double-strand breaks in normal human fibroblasts. *Radiat. Res.* 169, 437–446. doi: 10.1667/rr1165.1
- Bétermier, M., Bertrand, P., and Lopez, B. S. (2014). Is non-homologous end-joining really an inherently error-prone process? *PLoS Genet.* 10:e1004086. doi: 10.1371/journal.pgen.1004086
- Bielefeldt-Olmann, H., Genik, P. C., Fallgren, C. M., Ullrich, R. L., and Weil, M. M. (2012). Animal studies of charged particle-induced carcinogenesis. *Health Phys.* 103, 568–576. doi: 10.1097/hp.0b013e318265a257
- Brenner, D. J., and Ward, J. F. (1992). Constraints on energy deposition and target size of multiply damaged sites associated with DNA double-strand breaks. *Int. J. Radiat. Biol.* 61, 737–748. doi: 10.1080/09553009214551591
- Burke, S. N., Wallace, J. L., Nematollahi, S., Upreti, A. R., and Barnes, C. A. (2010). Pattern separation deficits may contribute to age-associated recognition impairments. *Behav. Neurosci.* 124, 559–573. doi: 10.1037/a0020893
- Casadesus, G., Shukitt-Hale, B., Stellwagen, H. M., Smith, M. A., Rabin, B. M., and Joseph, J. A. (2005). Hippocampal neurogenesis and PSA-NCAM expression following exposure to 56Fe particles mimics that seen during aging in rats. *Exp. Gerontol.* 40, 249–254. doi: 10.1016/j.exger.2004.09.007
- Chen, Y., Mao, Y., Zhou, D., Hu, X., Wang, J., and Ma, Y. (2010). Environmental enrichment and chronic restraint stress in ICR mice: effects on prepulse inhibition of startle and Y-maze spatial recognition memory. *Behav. Brain Res.* 212, 49–55. doi: 10.1016/j.bbr.2010.03.033
- Chieffi, S., Messina, G., Villano, I., Messina, A., Esposito, M., Monda, V., et al. (2017). Exercise influence on hippocampal function: possible involvement of orexin-A. *Front. Physiol.* 8:85. doi: 10.3389/fphys.2017.00085
- Costes, S. V., Ponomarev, A., Chen, J. L., Nguyen, D., Cucinotta, F. A., and Barcellos-Hoff, M. H. (2007). Image-based modeling reveals dynamic redistribution of DNA damage into nuclear sub-domains. *PLoS Comput. Biol.* 3:e155. doi: 10.1371/journal.pcbi.0030155
- Cucinotta, F. A., Kim, M.-H. Y., and Chappell, L. J. (2012). *Evaluating Shielding Approaches to Reduce Space Radiation Cancer Risks*. Washington, DC: NASA. NASA Tech. Memo. 217361.
- Dellu, F., Fauchey, V., Le Moal, M., and Simon, H. (1997). Extension of a new two-trial memory task in the rat: influence of environmental context on recognition processes. *Neurobiol. Learn. Mem.* 67, 112–120. doi: 10.1006/nlme.1997.3746
- Dellu, F., Mayo, W., Cherkaoui, J., Le Moal, M., and Simon, H. (1992). A two-trial memory task with automated recording: study in young and aged rats. *Brain Res.* 588, 132–139. doi: 10.1016/0006-8993(92)91352-f
- Drake, B. G., Hoffman, S. J., and Beaty, D. W. (2010). “Human exploration of Mars, Design Reference Architecture 5.0,” in *Proceedings of the 2010 IEEE Aerospace Conference*, (Washington, DC: NASA), 1–24.
- Enge, M., Efsun Arda, H., Mignardi, M., Beausang, J., Bottino, R., Kim, S. K., et al. (2017). Single-cell analysis of human pancreas reveals transcriptional signatures of aging and somatic mutation patterns. *Cell* 171, 321.e14–330.e14. doi: 10.1016/j.cell.2017.09.004
- Fanselow, M. S., and Dong, H.-W. (2010). Are the dorsal and ventral hippocampus functionally distinct structures? *Neuron* 65, 7–19. doi: 10.1016/j.neuron.2009.11.031
- Ferrante, M., Migliore, M., and Ascoli, G. A. (2013). Functional impact of dendritic branch-point morphology. *J. Neurosci.* 33, 2156–2165. doi: 10.1523/jneurosci.3495-12.2013
- Gauny, S., Wiese, C., and Kronenberg, A. (2001). Mechanisms of mutagenesis in human cells exposed to 55 MeV protons. *Phys. Med.* 17(Suppl. 1), 235–237.
- George, J. S., Lave, K. A., Wiedenbeck, M. E., Binns, W. R., Cummings, A. C., Davis, A. J., et al. (2009). Elemental composition and energy spectra of galactic cosmic rays during solar cycle 23. *ApJ* 698:1666. doi: 10.1088/0004-637x/698/2/1666
- Giddabasappa, A., Hamilton, W. R., Chaney, S., Xiao, W., Johnson, J. E., Mukherjee, S., et al. (2011). Low-level gestational lead exposure increases retinal progenitor cell proliferation and rod photoreceptor and bipolar cell neurogenesis in mice. *Environ. Health Perspect.* 119, 71–77. doi: 10.1289/ehp.1002524
- Groves, T. R., Wang, J., Boerma, M., and Allen, A. R. (2017). Assessment of Hippocampal Dendritic Complexity in Aged Mice Using the Golgi-Cox Method. *J. Vis. Exp.* 124:55696. doi: 10.3791/55696
- Hainmueller, T., and Bartos, M. (2018). Parallel emergence of stable and dynamic memory engrams in the hippocampus. *Nature* 558, 292–296. doi: 10.1038/s41586-018-0191-2
- He, C., Tsipis, C. P., LaManna, J. C., and Xu, K. (2017). Environmental enrichment induces increased cerebral capillary density and improved cognitive function in mice. *Adv. Exp. Med. Biol.* 977, 175–181. doi: 10.1007/978-3-319-55231-6_24
- Honey, R. C., Watt, A., and Good, M. (1998). Hippocampal lesions disrupt an associative mismatch process. *J. Neurosci.* 18, 2226–2230. doi: 10.1523/jneurosci.18-06-02226.1998
- Howe, A., Kiffer, F., Alexander, T. C., Sridharan, V., Wang, J., Ntagwabira, F., et al. (2019). Long-term changes in cognition and physiology after low-dose ^{16}O irradiation. *Int. J. Mol. Sci.* 20:188. doi: 10.3390/ijms20010188
- Hu, X., Urhie, O., Chang, K., Hostetler, R., and Agmon, A. (2018). A novel method for training mice in visuo-tactile 3-D object discrimination and recognition. *Front. Behav. Neurosci.* 12:274. doi: 10.3389/fnbeh.2018.00274
- Hughes, R. N., and Otto, M. T. (2013). Anxiolytic effects of environmental enrichment attenuate sex-related anxiogenic effects of scopolamine in rats. *Prog. Neuropsychopharmacol. Biol. Psychiatry* 40, 252–259. doi: 10.1016/j.pnpbp.2012.10.009
- Impey, S., Jopson, T., Pelz, C., Tafessu, A., Fareh, F., Zuloaga, D., et al. (2017). Bi-directional and shared epigenomic signatures following proton and 56Fe irradiation. *Sci. Rep.* 7:10227.
- Impey, S., Pelz, C., Tafessu, A., Marzulla, T., Turker, M. S., and Raber, J. (2016). Proton irradiation induces persistent and tissue-specific DNA methylation changes in the left ventricle and hippocampus. *BMC Genomics* 17:273. doi: 10.1186/s12864-016-2581-x
- Joseph, J. A., Hunt, W. A., Rabin, B. M., Dalton, T. K., and Harris, A. H. (1993). Deficits in the sensitivity of striatal muscarinic receptors induced by heavy-particle irradiation: further “Age-Radiation”. *Parallels. Radiat. Res.* 135, 257–261.
- Joseph, J. A., Shukitt-Hale, B., McEwen, J., and Rabin, B. (1999). Magnesium activation of GTP hydrolysis or incubation in S-Adenosyl-L-methionine

- reverses iron-56-particle-induced decrements in oxotremorine enhancement of striatal release of dopamine. *Radiat. Res.* 152, 637–641.
- Kiffer, F., Alexander, T., Anderson, J. E., Groves, T., Wang, J., Sridharan, V., et al. (2019a). Late effects of 160-particle radiation on female social and cognitive behavior and hippocampal physiology. *Radiat. Res.* 191, 278–294. doi: 10.1667/RR15092.1
- Kiffer, F., Boerma, M., and Allen, A. (2019b). Behavioral effects of space radiation: a comprehensive review of animal studies. *Life Sci. Space Res.* 21, 1–21. doi: 10.1016/j.lssr.2019.02.004
- Kiffer, F., Carr, H., Groves, T., Anderson, J. E., Alexander, T., Wang, J., et al. (2018). Effects of $^1\text{H} + ^{16}\text{O}$ charged particle irradiation on short-term memory and hippocampal physiology in a murine model. *Radiat. Res.* 189, 53–63. doi: 10.1667/rr14843.1
- Kitamura, T., Ogawa, S. K., Roy, D. S., Okuyama, T., Morrissey, M. D., Smith, L. M., et al. (2017). Engrams and circuits crucial for systems consolidation of a memory. *Science* 356, 73–78. doi: 10.1126/science.aam6808
- Kronenberg, A., Gauny, S., Kwok, E., Connolly, L., Dan, C., Lasarev, M., et al. (2009). Comparative analysis of cell killing and autosomal mutation in mouse kidney epithelium exposed to 1 GeV/nucleon iron ions in vitro or in situ. *Radiat. Res.* 172, 550–557. doi: 10.1667/rr1804.1
- Krukowski, K., Grue, K., Frias, E. S., Pietrykowski, J., Jones, T., Nelson, G., et al. (2018). Female mice are protected from space radiation-induced maladaptive responses. *Brain Behav. Immun.* 74, 106–120. doi: 10.1016/j.bbi.2018.08.008
- Larkin, M. C., Lykken, C., Tye, L. D., Wickelgren, J. G., and Frank, L. M. (2014). Hippocampal output area CA1 broadcasts a generalized novelty signal during an object-place recognition task: generalized novelty signals in the hippocampus. *Hippocampus* 24, 773–783. doi: 10.1002/hipo.22268
- Lee, A.-R., Kim, J.-H., Cho, E., Kim, M., and Park, M. (2017). Dorsal and ventral hippocampus differentiate in functional pathways and differentially associate with neurological disease-related genes during postnatal development. *Front. Mol. Neurosci.* 10:331. doi: 10.3389/fnmol.2017.00331
- Lee, C. H., Park, J. H., Cho, J.-H., Ahn, J. H., Bae, E. J., and Won, M.-H. (2015). Differences in the protein expression levels of Trx2 and Prx3 in the hippocampal CA1 region between adult and aged gerbils following transient global cerebral ischemia. *Mol. Med. Rep.* 12, 2555–2562. doi: 10.3892/mmr.2015.3760
- Leger, M., Quiedeville, A., Bouet, V., Haelewyn, B., Boulouard, M., Schumann-Bard, P., et al. (2013). Object recognition test in mice. *Nat. Protoc.* 8, 2531–2537.
- Limoli, C. L., Ponnaiya, B., Corcoran, J. J., Giedzinski, E., Kaplan, M. I., Hartmann, A., et al. (2000). Genomic instability induced by high and low LET ionizing radiation. *Adv. Space Res.* 25, 2107–2117. doi: 10.1016/s0273-1177(99)01062-5
- Lom, B., and Cohen-Cory, S. (1999). Brain-derived neurotrophic factor differentially regulates retinal ganglion cell dendritic and axonal arborization in vivo. *J. Neurosci.* 19, 9928–9938. doi: 10.1523/jneurosci.19-22-09928.1999
- Losonczy, A., Makara, J. K., and Magee, J. C. (2008). Compartmentalized dendritic plasticity and input feature storage in neurons. *Nature* 452, 436–441. doi: 10.1038/nature06725
- Magariños, A. M., Li, C. J., Gal Toth, J., Bath, K. G., Jing, D., Lee, F. S., et al. (2011). Effect of brain-derived neurotrophic factor haploinsufficiency on stress-induced remodeling of hippocampal neurons. *Hippocampus* 21, 253–264. doi: 10.1002/hipo.20744
- Mancuso, J. J., Chen, Y., Li, X., Xue, Z., and Wong, S. T. C. (2013). Methods of dendritic spine detection: from Golgi to high-resolution optical imaging. *Neuroscience* 251, 129–140. doi: 10.1016/j.neuroscience.2012.04.010
- Matsuzaki, M., Honkura, N., Ellis-Davies, G. C. R., and Kasai, H. (2004). Structural basis of long-term potentiation in single dendritic spines. *Nature* 429, 761–766. doi: 10.1038/nature02617
- Mikolaenko, I., Rao, L. M., Roberts, R. C., Kolb, B., and Jinnah, H. A. (2005). A Golgi study of neuronal architecture in a genetic mouse model for Lesch–Nyhan disease. *Neurobiol. Dis.* 20, 479–490. doi: 10.1016/j.nbd.2005.04.005
- Morley, B. J., and Mervis, R. F. (2013). Dendritic spine alterations in the hippocampus and parietal cortex of alpha7 nicotinic acetylcholine receptor knockout mice. *Neuroscience* 233, 54–63. doi: 10.1016/j.neuroscience.2012.12.025
- Moser, E. I., Kropff, E., and Moser, M.-B. (2008). Place cells, grid cells, and the brain's spatial representation system. *Annu. Rev. Neurosci.* 31, 69–89. doi: 10.1146/annurev.neuro.31.061307.090723
- NCRP (2006). *Information Needed to Make Radiation Protection Recommendations for Space Missions Beyond Low-Earth Orbit*. Bethesda: National Council on Radiation Protection and Measurements.
- NCRP (2016). *on Radiation Protection, [ncrp] National Council, and (ncrp), M. Potential for Central Nervous System Effects from Radiation Exposure During Space Activities. Phase 1: Overview*. Bethesda: NCRP.
- Nelson, G. A. (2016). Space radiation and human exposures, a primer. *Radiat. Res.* 185, 349–358. doi: 10.1667/rr14311.1
- Nelson, G. A., Simonsen, L., and Huff, J. L. (2016). *Evidence Report: Risk of Acute and Late Central Nervous System Effects from Radiation Exposure*. Available at: <https://ntrs.nasa.gov/search.jsp?R=20160004368> (Accessed January 10, 2019).
- Parihar, V. K., Allen, B., Tran, K. K., Macaraeg, T. G., Chu, E. M., Kwok, S. F., et al. (2015). What happens to your brain on the way to Mars. *Sci. Adv.* 1:e1400256. doi: 10.1126/sciadv.1400256
- Park, J.-M., Seong, H.-H., Jin, H.-B., and Kim, Y.-J. (2017). The effect of long-term environmental enrichment in chronic cerebral hypoperfusion-induced memory impairment in rats. *Biol. Res. Nurs.* 19, 278–286. doi: 10.1177/1099800416686179
- Poulose, S. M., Bielinski, D. F., Carrihill-Knoll, K., Rabin, B. M., and Shukitt-Hale, B. (2011). Exposure to 160-particle radiation causes aging-like decrements in rats through increased oxidative stress, inflammation and loss of autophagy. *Radiat. Res.* 176, 761–769. doi: 10.1667/rr2605.1
- Poulose, S. M., Bielinski, D. F., Carrihill-Knoll, K. L., Rabin, B. M., and Shukitt-Hale, B. (2014). Protective effects of blueberry- and strawberry diets on neuronal stress following exposure to 56Fe particles. *Brain Res.* 1593, 9–18. doi: 10.1016/j.brainres.2014.10.028
- Poulose, S. M., Rabin, B. M., Bielinski, D. F., Kelly, M. E., Miller, M. G., Thanthaeng, N., et al. (2017). Neurochemical differences in learning and memory paradigms among rats supplemented with anthocyanin-rich blueberry diets and exposed to acute doses of 56Fe particles. *Life Sci. Space Res.* 12, 16–23. doi: 10.1016/j.lssr.2016.12.002
- Raber, J., Allen, A. R., Sharma, S., Allen, B., Rosi, S., Olsen, R. H. J., et al. (2016). Effects of proton and combined proton and 56Fe radiation on the hippocampus. *Radiat. Res.* 185, 20–30.
- Raber, J., Yamazaki, J., Torres, E. R. S., Kirchoff, N., Stagaman, K., Sharpton, T., et al. (2019). Combined effects of three high-energy charged particle beams important for space flight on brain, behavioral and cognitive endpoints in B6D2F1 female and male mice. *Front. Physiol.* 10:179. doi: 10.3389/fphys.2019.00179
- Rabin, B. M., Carrihill-Knoll, K. L., Carey, A., Shukitt-Hale, B., and Joseph, J. A. (2005a). Effect of diet on the disruption of operant responding at different ages following exposure to (56)Fe particles. *Age* 27, 69–73. doi: 10.1007/s11357-005-4000-0
- Rabin, B. M., Joseph, J. A., and Shukitt-Hale, B. (2005b). Effects of age and diet on the heavy particle-induced disruption of operant responding produced by a ground-based model for exposure to cosmic rays. *Brain Res.* 1036, 122–129. doi: 10.1016/j.brainres.2004.12.041
- Rabin, B. M., Poulose, S. M., Carrihill-Knoll, K. L., Ramirez, F., Bielinski, D. F., Heroux, N., et al. (2015). Acute effects of exposure to (56)Fe and (16)O particles on learning and memory. *Radiat. Res.* 184, 143–150.
- Rabin, B. M., Shukitt-Hale, B., Carrihill-Knoll, K. L., and Gomes, S. M. (2014). Comparison of the effects of partial- or whole-body exposures to 16O particles on cognitive performance in rats. *Radiat. Res.* 181, 251–257. doi: 10.1667/rr13469.1
- Ran, Y., Yan, B., Li, Z., Ding, Y., Shi, Y., and Le, G. (2016). Dityrosine administration induces novel object recognition deficits in young adulthood mice. *Physiol. Behav.* 164, 292–299. doi: 10.1016/j.physbeh.2016.06.019
- Roy, D. S., Kitamura, T., Okuyama, T., Ogawa, S. K., Sun, C., Obata, Y., et al. (2017). Distinct neural circuits for the formation and retrieval of episodic memories. *Cell* 170, 1000.e19–1012.e19.
- Rubin, A., Geva, N., Sheintuch, L., and Ziv, Y. (2015). Hippocampal ensemble dynamics timestamp events in long-term memory. *eLife* 4:e12247. doi: 10.7554/eLife.12247
- Sholl, D. A. (1953). Dendritic organization in the neurons of the visual and motor cortices of the cat. *J. Anat.* 87, 387–406.
- Shukitt-Hale, B., Lau, F. C., Cheng, V., Luskin, K., Carey, A. N., Carrihill-Knoll, K., et al. (2013). Changes in gene expression in the rat hippocampus following

- exposure to ^{56}Fe particles and protection by berry diets. *Cent. Nerv. Syst. Agents Med. Chem.* 13, 36–42. doi: 10.2174/1871524911313010006
- Sridharan, D. M., Asaithamby, A., Bailey, S. M., Costes, S. V., Doetsch, P. W., Dynan, W. S., et al. (2015). Understanding cancer development processes after HZE-particle exposure: roles of ROS, DNA damage repair and inflammation. *Radiat. Res.* 183, 1–26. doi: 10.1667/rr13804.1
- Suman, S., Rodriguez, O. C., Winters, T. A., Fornace, A. J. Jr., Albanese, C., and Datta, K. (2013). Therapeutic and space radiation exposure of mouse brain causes impaired DNA repair response and premature senescence by chronic oxidant production. *Aging* 5, 607–622. doi: 10.18632/aging.100587
- Sun, Q. A., Wu, Y., Zappacosta, F., Jeang, K. T., Lee, B. J., Hatfield, D. L., et al. (1999). Redox regulation of cell signaling by selenocysteine in mammalian thioredoxin reductases. *J. Biol. Chem.* 274, 24522–24530. doi: 10.1074/jbc.274.35.24522
- Tanaka, T. (2002). Thioredoxin-2 (TRX-2) is an essential gene regulating mitochondria-dependent apoptosis. *EMBO J.* 21, 1695–1703. doi: 10.1093/emboj/21.7.1695
- Tavosanis, G. (2012). Dendritic structural plasticity. *Dev. Neurobiol.* 72, 73–86.
- Titus, A. D. J., Shankaranarayana Rao, B. S., Harsha, H. N., Ramkumar, K., Srikumar, B. N., Singh, S. B., et al. (2007). Hypobaric hypoxia-induced dendritic atrophy of hippocampal neurons is associated with cognitive impairment in adult rats. *Neuroscience* 145, 265–278. doi: 10.1016/j.neuroscience.2006.11.037
- Turker, M. S., Grygoryev, D., Dan, C., Eckelmann, B., Lasarev, M., Gauny, S., et al. (2013). Autosomal mutations in mouse kidney epithelial cells exposed to high-energy protons *in vivo* or in culture. *Radiat. Res.* 179, 521–529. doi: 10.1667/rr3174.1
- Turker, M. S., Grygoryev, D., Lasarev, M., Ohlrich, A., Rwtambuga, F. A., Johnson, S., et al. (2017). Simulated space radiation-induced mutants in the mouse kidney display widespread genomic change. *PLoS One* 12:e0180412. doi: 10.1371/journal.pone.0180412
- van der Velden, L., van Hooft, J. A., and Chameau, P. (2012). Altered dendritic complexity affects firing properties of cortical layer 2/3 pyramidal neurons in mice lacking the 5-HT $_{3A}$ receptor. *J. Neurophysiol.* 108, 1521–1528. doi: 10.1152/jn.00829.2011
- Villasana, L. E., Rosenthal, R. A., Doctrow, S. R., Pfankuch, T., Zuloaga, D. G., Garfinkel, A. M., et al. (2013). Effects of alpha-lipoic acid on associative and spatial memory of sham-irradiated and ^{56}Fe -irradiated C57BL/6J male mice. *Pharmacol. Biochem. Behav.* 103, 487–493. doi: 10.1016/j.pbb.2012.09.021
- von Bohlen, A., and Halbach, O. (2009). Structure and function of dendritic spines within the hippocampus. *Ann. Anat. Anatomischer Anzeiger* 191, 518–531. doi: 10.1016/j.aanat.2009.08.006
- Whoolery, C. W., Yun, S., Reynolds, R. P., Lucero, M. J., Soler, I., Tran, F. H., et al. (2020). Multi-domain cognitive assessment of male mice shows space radiation is not harmful to high-level cognition and actually improves pattern separation. *Sci. Rep.* 10:2737.
- Wiese, C., Gauny, S. S., Liu, W. C., Cherbonnel-Lasserre, C. L., and Kronenberg, A. (2001). Different mechanisms of radiation-induced loss of heterozygosity in two human lymphoid cell lines from a single donor. *Cancer Res.* 61, 1129–1137.
- Wojtowicz, J. M. (2012). Adult neurogenesis. From circuits to models. *Behav. Brain Res.* 227, 490–496. doi: 10.1016/j.bbr.2011.08.013
- Xing, R., Zhang, Y., Xu, H., Luo, X., Chang, R. C.-C., Liu, J., et al. (2016). Spatial memory impairment by TRPC1 depletion is ameliorated by environmental enrichment. *Oncotarget* 7, 27855–27873. doi: 10.18632/oncotarget.8428
- Yatagai, F. (2004). Mutations induced by heavy charged particles. *Biol. Sci. Space* 18, 224–234. doi: 10.2187/bss.18.224

Conflict of Interest: The authors declare that the research was conducted in the absence of any commercial or financial relationships that could be construed as a potential conflict of interest.

Copyright © 2020 Kiffer, Alexander, Anderson, Groves, McElroy, Wang, Sridharan, Bauer, Boerma and Allen. This is an open-access article distributed under the terms of the Creative Commons Attribution License (CC BY). The use, distribution or reproduction in other forums is permitted, provided the original author(s) and the copyright owner(s) are credited and that the original publication in this journal is cited, in accordance with accepted academic practice. No use, distribution or reproduction is permitted which does not comply with these terms.

Advantages of publishing in Frontiers



OPEN ACCESS

Articles are free to read
for greatest visibility
and readership



FAST PUBLICATION

Around 90 days
from submission
to decision



HIGH QUALITY PEER-REVIEW

Rigorous, collaborative,
and constructive
peer-review



TRANSPARENT PEER-REVIEW

Editors and reviewers
acknowledged by name
on published articles

Frontiers

Avenue du Tribunal-Fédéral 34
1005 Lausanne | Switzerland

Visit us: www.frontiersin.org

Contact us: frontiersin.org/about/contact



REPRODUCIBILITY OF RESEARCH

Support open data
and methods to enhance
research reproducibility



DIGITAL PUBLISHING

Articles designed
for optimal readership
across devices



FOLLOW US

@frontiersin



IMPACT METRICS

Advanced article metrics
track visibility across
digital media



EXTENSIVE PROMOTION

Marketing
and promotion
of impactful research



LOOP RESEARCH NETWORK

Our network
increases your
article's readership